العوامل المؤثرة
في توقيع الأبنية الصناعية ضمن الموضع الصناعي

د. أمجد محمود عبد الله ألبدري
دكتوراه هندسة معمارية(مدرس)
جامعة بغداد – كلية الهندسة
قسم الهندسة المعمارية

الخلاصــة:

تمثل عمارة الابنية الصناعية ذات المقاسات الكبيرة، مرآة لتنوع الصناعة بمفرداتها وبمتطلباتها الوظيفية الواسعة، على اختلافات مفاهيمها وتعدد تصاميمها واحجامها وعلاقاتها بمكونات الموقع البنائية والعوامل المؤثرة على توقيعها ضمن الموقع والظروف المناخية المؤثرة عليها، تأميناً لكفاءة أداءها الحراري وباقل طاقة صناعية مستهلكة.

ولغرض توقيع المبنى الصناعي وفعاليات فضاءاته الاخرى ضمن الموقع العام، فان هذا يتطلب دراسة العلاقة المتبادلة مابين المبنى ومكونات الموقع الطبيعية والبنائية (العوامل الاقليمية) من جهة، وكذلك ظروف المناخ الموضعي للموقع (العوامل التخطيطية) من اخرى، ليرتبط كل ذلك بمفهوم التصميم المناخي للموقع والذي يهدف الى تحسين الاداء الحراري للمبنى بصورة اساسية، متمثلاً بمبدأ ترشيد استهلاك الطاقة على امتداد المدة الافتراضية لعمر المبنى، وتوفير بيئة داخلية مريحة للعاملين تتناعم مع متطلبات الراحة الحرارية والضوئية والبصرية والصوتية لفضاء المصنع، وهو ما يسعى اليه البحث.

Factors effecting locating Industrial Buildings in the Industrial Site

ABSTRACT:

Industrial building architecture of grand measures represent a reflection of industry diversity relating its items and functional vast requirements ;therefore, factories buildings should be recognized from their concept, various designs , location plus the factors effecting locating them within the location and effecting climate situations, to ensure adequacy of its their thermal performance with the minimum consumed industrial energy.

To locate the industrial building and other spaces activities within the location, this requires studying the relation exchanged between the building and constructive natural components of the location (Regional Factors) and the location atmosphere circumstances (Planning Factors). All this to relate with the location climate design concept, that aims at improving the building thermal performance basically. this is represented by the principle of rationing energy consumption on the hypothetical range of the building age and providing an internal environment comfortable for occupants that are consistent with requirements of thermal, light, visual, and sound comfort of the factors space. this what the research seeks at.

كلمـات رئيسيـة:
الموقع الصناعي – العوامل الاقليمية – العوامل التخطيطية– مكونات الموقع .

مشكلة البحث وهدفـه:

برزت مشكلة البحث في (عدم كفاية التصور بتأثير اساليب تخطيط وتصميم الموقع الصناعي على استجابة المبنى (المصنع) للظروف المناخية المؤثرة على ادائه البيئي العام (الضوئي - الحراري – الصوتي- وعلى صرفيات الطاقة فيه)، مما يجعل هدف البحث يكمن في دراسة العلاقة المتبادلة ما بين المبنى ومكونات الموقع الطبيعية والبنائية من جهة وظروف المناخ الموضعي للموقع من جهة اخرى، ليحقق مفهوم التصميم المناخي للموقع الصناعي الذي يهدف الى تحسين الاداء الحراري للمصنع ضمن مفاهيم حفظ الطاقة وتوفير البيئة الداخلية المريحة للعاملين داخل المبنى.

المقدمــة:

يطلق مصطلح الصناعة (Industry) على نشاطات مختلفة وعديدة، فالصناعة هي عملية تحويل او تغيير اي مادة او سلعة الى حالة او صورة اخرى، تصبح معها اكثر نفعاً او اشباعاً لحاجات ورغبات الانسان عن طريق العمليات الانتاجية بانواعها المختلفة (السماك ،1987، 20-p.19) وهي كل نشاط يتم في مؤسسة او معمل ويستخدم المكائن والالات سواء كانت يدوية او الية (حميد , p24,1979)، او هي النشاط الذي ينطوي على تحويل المواد الخام الى منتجات نهائية من الناحية اللغوية.(عمرو، 1965، p.154).

اما مفهوم الموقع الصناعي "Industrial site" فهو يتحدد من خلال تعريفه من انه "عبارة عن قطعة ارض يكون موقعها ضمن (أو خارج) النسيج الحضري مخصصة للصناعة يتم تقسيمها وتخطيطها بشكل مناسب وفق خطة شاملة تحقق التكامل في الهيكل الحضري وظيفياً وجمالياً وتقديم كافة الخدمات والتسهيلات التي تتطلبها المنطقة من اجل خلق بيئة صناعية مناسبة"(رياض، 1987، p.74).

او هي :- "قطعة من الارض تضم مجموعة من المباني الصناعية مزودة بكافة الخدمات والمرافق العامة، وتوزع قطعة الأرض هذه إلى أقسام صغيرة يخصص كل منها إلى مصنع او مشغل معين" (Duldley,1980,p.6)، والمناطق الصناعية هي احد أشكال استعمالات الارض الصناعية كالمساحات الصناعية (Industrial Areas) والنطاق الصناعي (Industrial Zone) والمتنزهات الصناعية (Industrial parks) وغير ذلك، والمنطقة الصناعية مكونة من عدد من القطع مقسمة ومفروزة لإنشاء أبنية صناعية، (أي عملية عقارية خالصة), اما **النطاق الصناعي** فهو ما يخصصه تصميم المدن من مساحات أو أجزاء من مدن للاستعمال الصناعي (James,1960,p.70).

نشأت المناطق الصناعية:

ان بداية المنطقة الصناعية بالعموم ترجع إلى مابين القرن الرابع عشر والثامن عشر خصوصاً في بريطانيا اذ كانت الصناعة بعيدة عن المناطق السكنية وتشمل أعمال الحديد في غابة (Dean) ومصانع النسيج في اكواخ (Lancashire) و (West Riding) اما مصادر الطاقة فهي المياه والرياح مما جعل الصناعة تكون بعيدة ومنعزلة ومشتتة ومقسمة الى وحدات صناعية صغيرة.

وبعد الثورة الصناعية تطورت مناطق المصانع لاعمال الحديد والنسيج بشكل خاص لتخلق الصناعة الحضرية، اذ كانت اول منطقة صناعية في (Trafford park) في (Manchester) عام (1896م) التي كان سبب نشوئها سهولة النقل ووجود الارض الصناعية الفنية ذات الايدي العاملة الماهرة، مع وجود قناة السفن لتربطها مع بحر ايرلندا والمحيطات والاسواق العالمية.

وفي عام (1920م) نشأت منطقة في Buckinghamshire، على محطة خدمات موجودة اصلاً ثم في (1924م) صممت المصانع القياسية التي قدمت الخدمات واحدثت الانتعاش لتزداد مساحة المنطقة الصناعية، بنشوء ثلاث مناطق لتجميع الصناعات ولاسباب سياسية وبضغط من الكتل العمالية على الحكومة البريطانية وهي (The Clyde)، (South Wales)، (Northeast-coast) التي جمعت الخدمات الملائمة بشكل استثمار وبعقود من المستأجرين ليكتمل الفعل الصناعي من التحولات التي رافقته الى حدود عام 1945 فانتجت الصناعة والمناطق الصناعية المعروفة حالياً (الديب,1973 p.5-6).

اما في امريكا فقد كانت منطقة (Clearing Industrial) في شياغوا عام (1899م) وكذلك مستعمرة نابولي في ايطاليا عام (1904م) وبعد عام (1950م) عرفت المناطق الصناعية في البلدان النامية كالهند وبورتوريكو وغيرها (Cherry, 1974, p.87).

الموقع الصناعي والنسيج الحضري:

ان موضوع الموقع الصناعي يمكن ان يقسم الى مستويين رئيسيين هما:-

الموقع الصناعي على المستوى القطري والاقليمي.

والموقع الصناعي في (أو خارج) منطقة حضرية معينة، كالمكان (Site) للصناعة المقترحة. (الحديثي،1971,p.44).

العوامل المؤثرة في اختيار الموقع الصناعي:

1- العوامل الاقتصادية:- أهم هذه العوامل هي كم ونوع العمل والمواد الاولية والوقود ومصادر الطاقة والسوق ورأس المال والدولة وسياستها والنقل ووسائل المواصلات والارض ومصادر المياه والبنى الارتكازية والمناخ.

2- العوامل الاجتماعية.

3- العوامل الستراتيجية "الأمنية" (William,1973, p.133).

ويجب ايجاد التكامل والترابط بين العوامل الاقتصادية والاجتماعية لانه لايوجد موقع مثالي للصناعة، وانما هنالك حلول مكملة بين وجهتي النظر الاقتصادية والاجتماعية. وعلى العموم هنالك ثلاثة عوامل تتفاعل مع بعضها بشكل ايجابي في تحديد الموضع الصناعي الافضل(Industrial site) , **وهي:-**

أ- امكان الوصول (Accessibility): حيث ان امكانية الوصول الى المواقع الصناعية له اهمية عظمى ليس لتمكين المنشآت الصناعية من تجميع المواد الخام بصورة اقتصادية فحسب،

بـل ايضـاً لتوزيـع منتجاتهـا، وتلعـب تكـاليف النقـل دوراً مهمـاً فـي هـذا المجـال (روبيـر, 1974،p.101).

ب- توفر الموضع المناسب (Site Availability), وتشمل:-

ب-1 - عوامل التربة التحتية للموضع "المكان": لها علاقة بالخصائص الجيوفيزياوية اذ من الضروري معرفة قوة تحمل التربة بشكل كافي للاثقال والمياه الجوفية ومدى تأثيرها على الهيكل الانشائي للمبنى او تصميمه (ناجي، 1982،p.22).

ب-2 - الخصائص السطحية للموقع: لها علاقة باستواء الارض او انحدارها والخدمات الفنية وبضمنها شبكة الشوارع.

ب-3 -- شكل الموضع : على اعتبار المحددات البيئية والوظيفية, فان الشكل المستطيل يمثل المخطط الرئيسي للمباني الصناعية، حيث ان الموقع المستطيل سيكون اكثر ملائمة من غيره بالاضافة الى توفير مساحات احتياطية للتوسع المستقبلي التي لاتتعارض مع اتجاهات النمو العمراني للمدينة (رمضان,1986,p.81).

ج - علاقات الموضع (Site relationships): مع الصناعات المجاورة والتي هي من العوامل الاقتصادية المهمة التي تؤثر على تحديد الموقع الصناعي كعامل الامكانات الخارجية (External economies) الناشئة عن علاقات الترابط والتكامل الصناعي. (Evans,1985,p.35).

توقيع المبنى الصناعي ضمن الموقع:

ان توقيع المبنى ضمن الموقع يتطلب دراسة:-

العوامل الاقليمية:

وهذه العوامل تحدد الظروف المناخية على مستوى الاقليم، وهي عبارة عن محددات بيئة طبيعية تفرض قوانينها على القوانين ككل كونها عوامل صعبة التغيير من قبل البشر للوصول الى بيئة ذات كفاءة حرارية. فيكون من السهولة التلاعب بالعوامل الاخرى التي تحقق نتائج افضل وبكلف اقل، على انه يمكن احياناً تغير هذه العوامل بدوافع اقتصادية وصناعية وزراعية، كعمل السدود او زراعة الغابات الكثيفة او المجمعات الصناعية، اكثر مما هي بيئية (فضيل،1992،p.7)، وبصورة عامة تتكون العوامل الاقليمية من :-

العوامل المناخية الرئيسية:

يعتبر المناخ العامل المهيمن في وضع المخطط العام للمدن التقليدية والمعاصرة وبضمنها المواقع الصناعية. ومن اهم العوامل المناخية التي تحدد البيئة الحرارية لاي موقع هي:-

الاشعاع الشمسي:- يعتبر الاشعاع الشمسي من اقوى العوامل المناخية تاثيراً واهم مصدر للطاقة والتي تصل من مصدرها بهيئة حزمة من اشعاع كهرومغناطيسي ينبعث من الشمس خلال الفضاء بدون الحاجة لوسط ناقل، فيسقط على سطح الارض وينعكس مرة ثانية منها والسطوح الاخرى اعتماداً على طبيعة السطح، وينتقل بالتوصيل الى داخل الفضاء او الى داخل الارض، وقسم منه يتم تبادله مع الهواء عن طريق الحمل، وهنالك الاشعاع الحراري الطويل الموجه المنبعث من السطوح بعد تسخينها والذي يزداد بارتفاع درجة حرارة السطح عن الهواء الملامس له.

ومن العوامل المحددة لتأثير الاشعاع الشمسي على المبنى هي:-

أ- خط عرض المنطقة او الاقليم.

ب- زاوية ارتفاع الشمس.

ج- الخصائص الفيزياوية للسطوح، من حيث الامتصاصية (Absorption)، الانعكاسية (Reflectivity).
د- الخصائص الحرارية للسطح، السعة الحرارية (Heat capacity) او الحرارة النوعية (Specific Heat).
هـ- مقدار وزمن التعرض، يعتمد على الاتجاه (Orientation) وزاوية ارتفاع اشعة الشمس (Altitude)، وزاوية السمت (Azimuth).

حركة ودرجة حرارة الهواء:- حيث ان تغير معدلات الارتفاع الشمسي ودرجة الحرارة يؤدي الى تغير في معدلات سرعة الريح خلال النهار، وهذه التغيرات تكون اكبر في المناطق ذات التباين العالي في شدة الاشعاع ودرجات الحرارة خلال النهار وخصوصاً المناطق الجافة والاقاليم الصحراوية (التنير,1978 p.26-29).

مكونات الموقع الطبيعية:
وتشمل بدورها كل من :

التضاريس "انحدار الموقع" : تلعب دوراً مهماً في تحديد ظروف مناخ الاقليم بناءاً على طبيعة سطح الارض من حيث الارتفاع او الانخفاض عن مستوى سطح البحر، وكذلك دوراً رئيسياً في تحديد الخصائص المناخية للمناخ والمناخ المحلي للموقع. وقد اثبتت الدراسات ان الموقع المنحدر بزاوية (15˚) والمتجه (15˚) شرق – الجنوب يستلم قدراً من الاشعاع الشمسي يقل 22% عن الموقع المسطح خلال الفترة الحارة من السنة ويزيد 4% عنه خلال الفترة الباردة منها, وهذا سيكون له تاثير ايجابي على مناخ ودرجات حرارة الموقع (U.N.,1989,p.323). ويؤثر مقدار زاوية ميل الموقع على شدة الطاقة الشمسية الساقطة عليه، اي كمية الاشعاع الساقطة على وحدة المساحة.

المساحات المائية : لها دور مهم في تحديد الخصائص المناخية للمناخ والمناخ المحلي او الموقعي، وذلك في خلق بيئة متوازنة حرارياً ضمن دائرة تأثيرها.

الغطاء النباتي: وهو يلعب دوراً هاماً في تحديد خصائص المناخ المحلي او الموقعي والمحيط بالمبنى، حيث تحجب الاشجار مقداراً معيناً من الاشعاع الشمسي الساقط عليها وبالتالي تساهم في تقليص تعرض السطوح المحيطة بها للاشعاع فتقلل الكسب الحراري لهذه السطوح، وذلك اعتماداً على مدى ارتفاعها وحجمها وكثافة وحجم وانعكاسية اوراقها.
وللنباتات القدرة على خفض درجة حرارة الغلاف الخارجي للمبنى بسبب حجبها للاشعاع الشمسي الساقط عليه بعدل (3-11) درجة مئوية صيفاً، وفي جميع الاحوال فانه يقلص ما لايقل عن (20%) من درجة حرارة السطح فيما لو كان غير مظلل، كما انها تقلص من الطاقة المستهلكة على مدار السنة . (Liem,2005,p111).

العوامل التخطيطية:
ان للعوامل التخطيطية دوراً كبيراً في تحديد ظروف المناخ الموقعي (الاشعاع الشمسي، درجة حرارة الهواء والرطوبة النسبية وحركة الهواء) وهناك امكانية لتحسينه بجعله اقرب الى حدود الراحة الحرارية، وان المناخ الموقعي يعتمد بدوره على التاثير الايجابي او السلبي لكل من (مكونات الموقع البنائية وعناصر تصميم الموقع وعلى الظروف المناخية للاقليم). ان اهمية تحسين المناخ الموقعي يؤدي بالنتيجة الى تحسين الاداء الحراري (Thermal

Performance) للمبنى بشكل غير مباشر وذلك باعتباره بمثابة الحاجز او المرشح الاول لتأثير الظروف المناخية على البيئة الداخلية، يليه دور غلاف المبنى . ولكي تساهم العوامل التخطيطية بشكل ايجابي في تحقيق المناخ الموقعي المطلوب، وبالتالي تحقيق كفاءة الاداء الحراري للمبنى بادنى استهلاك للطاقة، لابد من اعتمادها ضمن مراحل التصميم الاولى، وهذا يتطلب التطرق الى مراحل تخطيط الموقع الصناعي وهي كما يلي:-

التخطيط العمراني للمواقع الصناعية:

لايمكن القيام بالتخطيط العمراني للمواقع والمناطق الصناعية دون وجود برنامج تخطيطي واضح، تتم تهيئة واعداد هذا البرنامج وفقاً لما يلي (Perenyi, 1978, pp.70-77):-

تحديد السياسة العامة والاهداف المطلوب تحقيقها:

هنالك مدى واسع من الاهداف التي يمكن ان تحققها المناطق الصناعية بالنسبة للمجتمعات الحضرية، ان تحديد هذه الاهداف يجب ان يتم ابتداءً لانها تنعكس على البرامج التخطيطية للمنطقة الصناعية، فعندما يكون الهدف مثلاً توفير فرص عمل للسكان المحليين فان ذلك سيؤثر على اختيار نمط الصناعة الذي يحقق ذلك.

اجراء المسوحات الاولية:

تهدف هذه المسوحات أولا إلى بحث إمكانيات المواقع الممكنة في النسيج الحضري "Location" ثم دراسة الموضع نفسه (Site) من مختلف النواحي مثل هذه الدراسات تتطلب معلومات عن:-

- الموقع ضمن الهيكل العمراني الحالي للمدينة وضمن التطورات المستقبلية.
- معلومات عن السكان وأماكن العمل والموقع وشبكة النقل والاتصالات الحالية والمستقبلية ومعلومات عن المواد الوالية والأسواق.
- الخدمات التحتية الاجتماعية (Social infrastructure) والخدمات الصحية والمدارس .
- دراسة الاستعمالات المجاورة الحالية والمستقبلية .
- دراسة وتحديد حجم المنطقة الصناعية يعتمد على عوامل واعتبارات كثيرة اهمها:-

(مدى توفر الارض المناسبة، الموقع ضمن المدينة، سياسة تطوير الصناعة، نوع الصناعة) .

وكمثال عام فان النموذج المتبع في الهند يقسم المجمعات او (المناطق الصناعية) الى (جدول 1):-

أ - منطقة صناعية كبيرة: ما فوق (12) هكتار.
ب - منطقة صناعية متوسطة: مابين (4-12) هكتار.
ج - منطقة صناعية صغيرة: تحت (4) هكتارات.
د - المشاغل: تحت (0.8) هكتار .

جدول (1) يبين مساحة المواقع الصناعية في عدة بلدان (بالهكتار) (U N, 1962,p.67)

البلـــد	مساحة الموقع		
	صغير	متوسط	كبيـر
الولايات المتحدة	20-40	40-200	200-400 وما فوق
بريطانيا	الى 20	20-40	40-200 وما فوق
الهند	0.8-4	4-12	12 وما فوق

تحديد الفعاليات العامة:

اضافة الى الفعاليات الصناعية الاساسية هنالك فعاليات مكملة للعمل الصناعي ويعتمد حجمها ومدى حاجة المنطقة اليها على نوع ومتطلبات الصناعة المقترحة ومساحة المنطقة وحجم العمالة ومدى توفر هذه الفعاليات وامكانية احتمال توسع المنطقة ومن ضمنها الفعاليات الخدمية والترفيهية (Bharti, 1978, p.75-78).

دراسة وتحديد نوع الصناعات:

البرامج التخطيطية للمناطق الصناعية يجب ان تحدد نوع الصناعات المقترحة سلفاً، بسبب تأثيرها المباشر على التخطيط العمراني للمنطقة. وهناك مجموعة من العوامل تؤثر على اختيار نوع الصناعة منها:-

أ – تأثير نوع الصناعة على البيئة الحضرية المجاروة.
ب – موقع المنطقة الصناعية ضمن المنطقة الحضرية .
جـ- حجم المنطقة الصناعية الذي يؤثر في اختيار نوع وعدد المشاريع.
د – السياسة العامة الموضوعة للتنمية الصناعية.

وبعد ذلك يتم تحديد متطلباتها الوظيفية للابنية والارض (Gibberd, 1967, P.80).

طريقة ادارة واشغال المنطقة:

يجب تحديد الجهة التي ستعمل على تنفيذ وتشغيل ادارة المنطقة الصناعية، وبشكل عام يمكن تحديد ثلاثة اشكال لذلك (أ- حكومي/ ب- خاص/ جـ- تعاوني بدعم واسناد الحكومة من خلال توفير القروض طويلة الامد).(Ling,1967, p.36-37).

وضع المخطط الشامل للمواقع الصناعية:

يهدف المخطط الشامل الى تطوير وتنمية المنطقة الصناعية والسيطرة على استعمالات الارض فيها، ذلك لتجنب مشاكل الحركة والتوسع وعدم توافق الاستعمالات التي تزيد من كلف تطوير المنطقة فضلاً عن تأثر الاداء الصناعي. ان وضع المخطط الشامل الذي يحدد التوزيع العام للفعاليات وتحديد الاستعمالات لكل جزء من الموقع، يؤخذ بنظر الاعتبار النقاط الاتية (جمهورية العراق،1987،p.229-234):-

- حاجات ومتطلبات كل فعالية واهميتها النسبية هي الاساس في وضع التوزيع العام (Zoning).
- العلاقة بين الفعاليات والانطقة (Zones) المختلفة وطرق الربط بينهما.
- الاستعمالات المجاورة للارض الحضرية والتأثير المتبادل بينهما وبين الفعاليات الصناعية، ومدى الربط او العزل الفيزياوي المطلوب تحقيقه.
- امكانيات ومتطلبات المرونة والتوسع.
- توزيع الفعاليات (Zoning) ينبغي ان يتم بكفاءة عالية لاستخدام الارض ما دامت تقع ضمن المناطق الحضرية.
- توزيع الفعاليات سوف يتأثر بشكل كبير بالافكار التخطيطية والتصميمية لتلبية متطلبات الصناعة المختلفة.

على ضوء ما تقدم يتم تقسيم الفعاليات الى مجاميع توضع في انطقة (Zones) كخطوة اولى في وضع المخطط الشامل الذي سوف يحدد مايلي:-

انطقة الفعاليات الصناعية : (Industrial Facilites zones):

يمكن ان تضم نوعاً من الصناعة او لعدد من الصناعات المختلفة عن بعضها (اذا كانت صناعات مختلفة فهنالك عدد من المتطلبات لكل مجموعة من الصناعات فيما يخص الموقع والطاقة والفضاءات الخارجية والتي تتطلب ان توقع معاً في نطاق خاص).
وبشكل عام فان هذه الانطقة الصناعية هي (Walker,1980,p.75):-

أ - المنشآت ذات المتطلبات متشابهة المساحة Firms with similar space requirements:
يمكن ان تشغل ابنية او قطع اراضي قياسية ذات احجام موحدة (Standard building and plots)، اما في حالة انشاء معامل ذات مواصفات خاصة ويمكن ان يتم في نطاق اخر.

ب – نطاق المنشآت ذات المتطلبات متشابهة الموقع Firms with similar location needs:
فبعض الصناعات تميل الى ان توقع قرب شريان الحركة الرئيسي في المنطقة مثل خط سكة الحديد او ان تحتل المواقع المطلة على الطرق الرئيسية او مجاري الانهار.

جـ- نطاق الصناعات ذات المتطلبات الخاصة Firms with special requirements :
قد تتطلب عزل محدد عن المناطق المحاذية كان تكون مزعجة (الضوضاء) او يكون احتمال الحريق فيها اكثر من غيرها، عند ذلك يجب ان توضع في نطاق خاص اذا لم تكن هنالك ضرورة لرفعها نهائياً.

د – نطاق الصناعات ذات المتطلبات الخدمية الفنية العالية:
حيث يمكن تجميع الصناعات التي تستهلك كميات اكبر من الطاقة او المياه التي تنتج مخلفات سائلة معينة او التي ترتبط بعلاقة وثيقة بابنية الخدمات ومنشآت الخدمة (Utility plants)، يمكن ان تجمع هذه الصناعات بدلاً من توزيعها مع باقي الصناعات. عرض النطاق يتناسب مع حجم المنشآت الصناعية، لهذا فان النطاق يمكن ان يكون بشكل عدة صفوف او احزمة (Multi belted). لتحقق الحماية المطلوبة لكل منها. (الحديدي ، 1989، p.28).

انطقة الفعاليات الاخرى (Other Facilites zones):-

بالاضافة الى الفعاليات الصناعية فان المخطط ينبغي ان يحدد الانطقة (Zones) اللازمة للانشطة والفعاليات المكملة مثل المناطق الفاصلة (Buffer zones) والمناطق المفتوحة (Land-scaping) ومواقف السيارات، الابنية والخدمات الاخرى.

المخطط الشامل ينبغي ان يحدد الطرق المقترحة للسيطرة على تنمية وتطوير المنطقة من حيث تهيئة التعليمات والقوانين والمحددات.

تحديد مراحل التنفيذ وكيفية تعاقبها والهيكل العام لارتفاعات الابنية وتوزيع الكثافات البنائية (Building densities)، وتتراوح النسبة المخصصة للمصانع مابين (40%-55%) من مساحة المنطقة والشوارع والساحات المفتوحة (20%-40%) وللادارة والابنية الخدمية مابين (10%-20%) كما في (جدول 2). (Rudolf,1977,p.264-265).

(جدول 2) يبين النسب المئوية للفعاليات في المناطق الصناعية الهندية (Rudolf,1977,p.264-265)

التوصية	المصانع	الطرق والمناطق المفتوحة	الادارة والابنية الاخرى
1- توصيات التنظيم المركزي للصناعات الصغيرة (CSIO) منطقة كبيرة	**55**	**35**	**10**

منطقة متوسطة منطقة صغيرة	50 40	35 40	15 20
2- توصـــيات المـــؤتمرات للمنـــاطق الصناعية الهندية منطقة كبيرة منطقة متوسطة منطقة صغيرة	 65 55 40	 25 30 40	 10 15 20
3- نماذج مختارة من المشاريع القائمة	65-60	30	10-5

تصميم الموقع (Layout of site):-

ان عملية تنظيم العلاقة بين العناصر الاساسية الثلاثة التي تتكون منها البيئة الفيزياوية (Physical Environment) هي الابنية والطرق والمناطق المفتوحة، وان تحديد العلاقات المكانية بين الفعاليات المختلفة للبرنامج يتطلب دراسة:-

انظمة الطرق وتوجيهها وتنظيم القطع (Road Systems & Plots Layout):-

تشكل الطرق العامل الرئيس في تصميم الموقع الصناعي، لهذا يجب دراسة وتحليل انواع الحركة المتوقعة في المنطقة الصناعية والتي تتكون بشكل عام من:-

♦ حركة المواد والبضائع وسيارات نقل العاملين وحركة المشاة وحركة خطوط الخدمات. لهذا فان تحديد حجم كل نوع منها يعتمد على جملة عوامل منها متطلبات النقل وطبيعة عمل المنشآت الصناعية وحجم المنطقة وكثافة الابنية وعدد العاملين،سيكون الاساس في التوصل الى حلول ومعالجات مناسبة (كمونة، 1985، 28-25.p).

♦ ان من العوامل المهمة في نجاح المنطقة هو وضع تصميم وتخطيط جيد ومناسب للطرق من حيث جمع انواع الحركة المختلفة مع الاستعمالات الرئيسية الاخرى في المنطقة . (Bruyn,2002,p67),(Ling,1967, p.38-39).(شكل – 1).

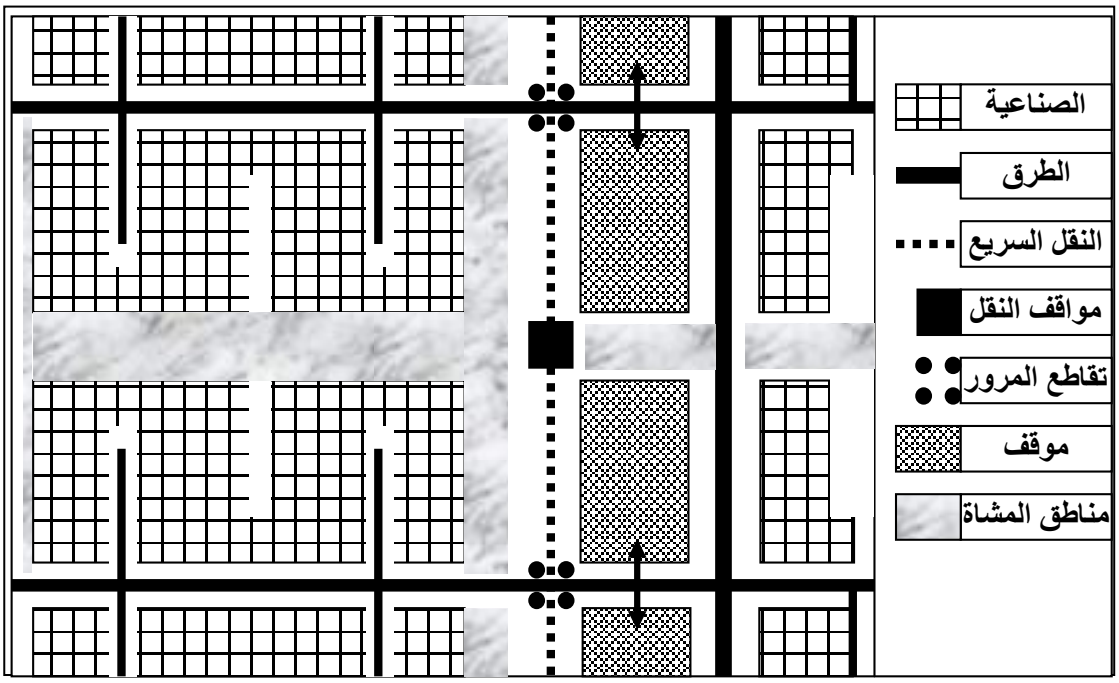

(شكل - 1) عملية الجمع بين أنواع الحركة مع الاستعمالات المختلفة للمنطقة الصناعية.
(Bruyn,2002,p67)

ان اختيار نمط الحركة وتوجيهها في المنطقة الصناعية يؤثر على تقسيم قطع الاراضي بشكل كبير، بالاضافة الى تاثير المناخ عليها، فهنالك عدة انظمة للحركة منها:-

نظام الحركة الشبكي (Grid Iron):- هذا النظام يقسم القطع الى اشكال مستطيلة، وبما ان اشكال الابنية وقطع الاراضي على الاغلب تتخذ شكلاً مستطيلاً (Gibberd, 1967,pp.230-231)، فان تصميم الموقع بشكل مستطيل (Rectangular Layout) سيكون افضل ما يناسب هذه القطع. وهذا النظام يتألف من شريان او طريق رئيسي تقع القطع الصناعية على جانبيه وفي هذه الحالة يسمى بالنظام الشبكي المفتوح (Open-Grid). (U.N.,1989,p.48-50),(Tony,2004,p334).(شكل – 2).

(شكل – 2) تخطيط المنطقة الصناعية المتكاملة وفقا للنظام الشبكي البسيط المعتمد على شريان الحركة الرئيس .(Tony,2004,p334).

النظام الشبكي التقليدي (Traditional Gridion):- ينتج عند مضاعفة النظام الاول (Open-Grid) الذي يقسم الموقع الى كتل مستطيلة (Rectangular blocks) مفصولة بطرق رئيسية، حجم هذه القطع يعتمد على نوع الصناعة وحجم الموقع ويفضل ان يكون بشكل مضاعفات اصغر قطعة صناعية، وهذا الاتجاه سائد في الولايات المتحدة الامريكية. (Gibberd, 1967,pp.253-255).

نظام الكتل (Super Blocks):- وهو ايضاً نظام شبكي ولكن يتألف من طريقين رئيسين واخرين ثانويين يكونان مناطق (Blocks)، كل (Block) يضم عدداً من الفعاليات العامة مثل الحوانيت والمركز الصحي ونظام الحركة الداخلي والمناطق المفتوحة ومواقف السيارات،كما ان الابنية الصناعية يمكن ان توقع جنباً الى جنب وبشكل قد يكون متقارباً في بعض الاحيان ويعتمد ذلك على نوع الصناعة، هذا النظام يوفر مرونة مناسبة عامة في المنطقة، ومرونة مناسبة ضمن البلوك نفسه بالنسبة لأحجام القطع المختلفة، وحجم البلوك يعتمد على حجم المصانع ومساحة المنطقة الكلية. وهذا النظام متبع في انكلترا. (U.N.,1989,pp.28-30),(Liem,2005,p253).(شكل - 3).

ان استخدام النظام الشبكي البسيط مع احجام القطع النموذجية المبنية على اساس وحدة قياسية (Module) تعتمد على طريق او شريان رئيسي واحد، تكون مناسبة في البلدان ذات الخبرة القليلة في انشاء المناطق الصناعية المخططة كحال بلدنا، وهناك اسلوب يسمى التجمعات الصناعية (Industrial clusters) يعتمد على ان قطعة الارض تقسم الى قطع قياسية وفق نظام معياري وبنظام شبكي للطرق، بعد ذلك تقسم هذه القطع القياسية او يتم الجمع بين عدد منها لاستيعاب مختلف الوحدات الصناعية، ويتميز هذا الاسلوب بقدرته على تكوين تجمعات متخصصة ومتكاملة، مع تشكيل نطاقات (Zones) او مناطق فرعية عند تجميع عدد من هذه التجمعات الصغيرة (جمهورية العراق،1987،p.231-236)، وهذا الاسلوب تم استعماله في تخطيط المنطقة الصناعية في مدينة الثرثار في العراق.(شكل – 4).

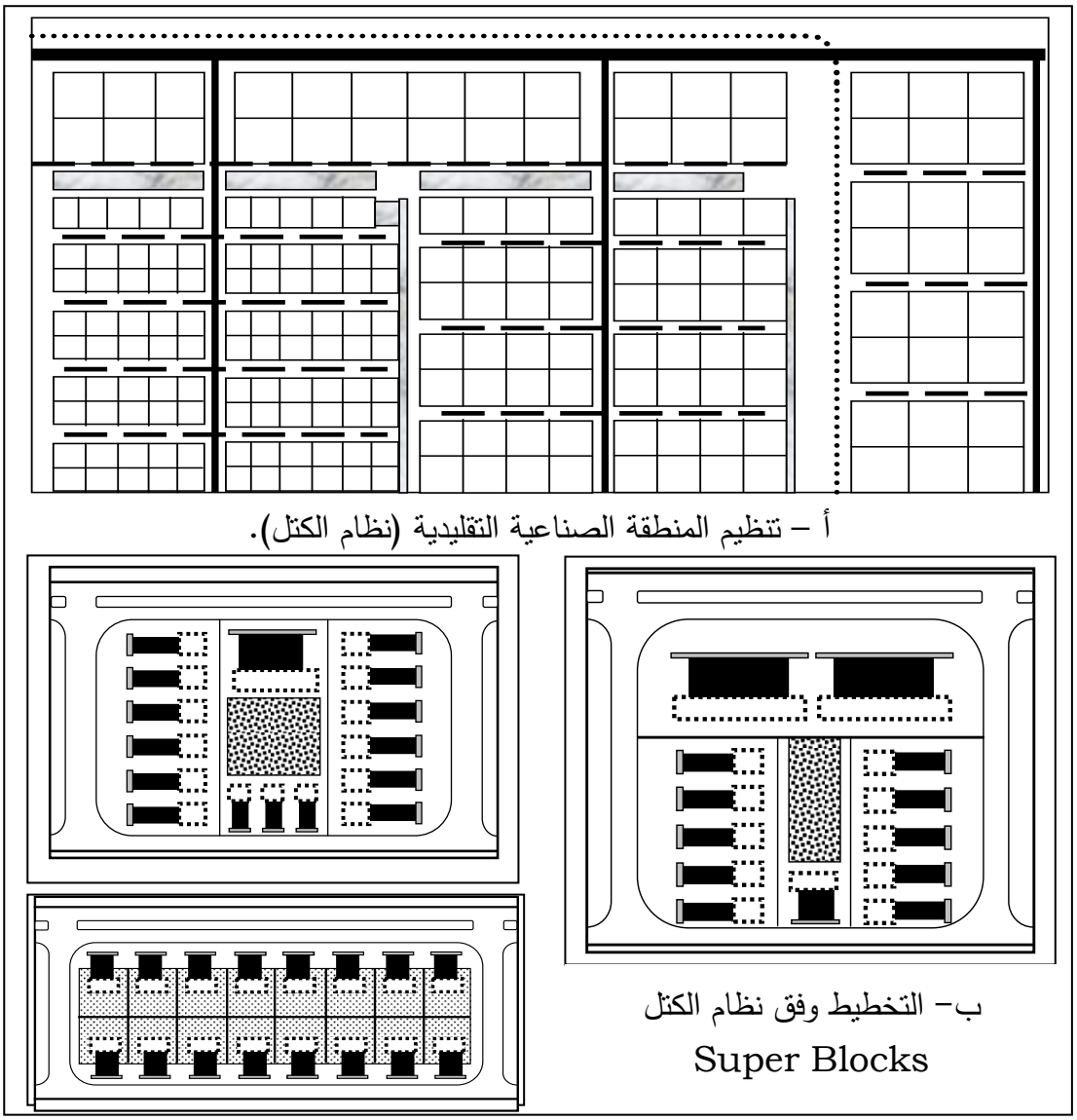

(شكل – 3) نظم الحركة في المواقع الصناعية .(Liem,2005,p253).

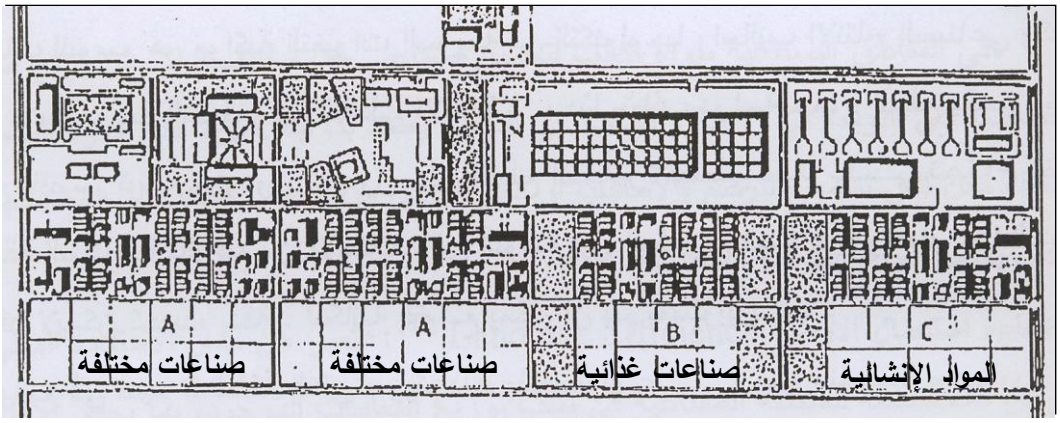

(شكل – 4) مخطط المجمع الصناعي لمنطقة الثرثار ذا النطاقات المتخصصة.
(جمهورية العراق,1987,ص 78).

توفير احجام متنوعة من قطع اراضي المصانع:-

ان مخطط المناطق الصناعية يجب ان يوفر احجاماً متنوعة من قطع الاراضي لتلبية المتطلبات الوظيفية للصناعات المختلفة، يعتمد حجم هذه القطع ومقدار تغطية الارض فيها (Coverage plot) على **(نوع الصناعة ومتطلبات الفضاءات المفتوحة وموقع المنطقة الصناعية بالنسبة للمدينة، وعدد الطوابق ونوع المنطقة الصناعية)** ، لذلك لاتوجد قاعدة للحجم المثالي للقطع الصناعية (Optimum plot size)، حيث ان القطعة الواحدة يجب ان تحتوي بالاضافة الى بناية المصنع على مساحات خارجية لخدمة مواقف السيارات وفضاءات التحميل ومساحات الفضاءات الخارجية (Landscape)، اضافة الى ترك مساحة للتوسع ضمن القطعة نفسها. لهذا فان نسبة مساحة البناء ضمن القطعة الصناعية الواحدة عامل مهم، وهذه النسب تختلف من بلد لاخر (U.N.,1989,pp.32-33) وكما يلي:-

- ففي الولايات المتحدة: تكون بعض المناطق الصناعية الحديثة تحدد مقدار الابنية بما لايتجاوز (1/3) مساحة القطعة، و التحديد العام هو ان الابنية يجب ان لاتغطي اكثر من (50%) منها.
- اما في الهند: فان الدراسات حول المناطق الصناعية حددت المساحة المغطاة من القطعة الواحدة (Coverage plot) بنسبة تتراوح بين (50%) للقطع الصغيرة و (66%) للقطع الاكبر.

اما احجام قطع الاراضي الصناعية فتتنوع بشكل كبير ويعتمد بالاضافة الى العوامل اعلاه على حجم البناية بشكل رئيس، وتتباين من قطر الى اخر، بل انها تتباين ضمن القطر الواحد ايضاً وكالاتي(Walker,1980,p.298):-

- ففي الولايات المتحدة: يكون الحجم الشائع (0.6) هكتار و (2) هكتاراً (جدول 3). هذه الابنية لاتحتاج الى خزن خارجي، مع امكانيتها للتوسع بمقدار (50%).

جدول (3) يوضح المساحات والابعاد التقريبية المناسبة للقطع الصناعية لمختلف حجوم الابنية في الميادين الصناعية الامريكية (Walker,1980,p.298).

مساحة بناية المصنع الاولية(م²) Initial building area	العمق المناسب للقطعة (م) Optimum Block depth	المساحة المناسبة للقطعة(م²) Optimum Block area
1000	60	4000

6000	80	2000
8000	95	3000
11200	110	4000
13600	120	5000
22000	145	8000
28000	160	10000
56000	220	20000
140000	330	50000

ان نسبة تغطية الارض تزداد بزيادة مساحة القطع والابنية فهي تتراوح بين (25%) و (35.7%)، وبعد التوسع المحدد بـ(50%) فان هذه النسب تتراوح بين (37.5%) و (53.5%).

- اما في المملكة المتحدة: وحيث ان التخطيط يكون وفقاً لنظام (Super Block) فان ابعاده تتراوح بين (150) و (200)م تقريباً، اما المسافة المحصورة بين الطريقين الرئيسين فتكون ضعفي هذا الرقم، هذه الابعاد تكون مناسبة لجذب المشاريع الكبيرة، ويمكن ان تقسم بشكل اقتصادي الى احجام اصغر غالباً ما تكون بمساحة (2000)م^2.

- وفي الهند: وهي من الدول النامية فان اغلب القطع الصناعية لا تزيد مساحتها عن حوالي (1500م^2) بينما اصغر القطع يمكن ان تصل مساحتها الى حوالي (200)م^2 فقط. كما في (جدول 4) (U.N.,1989,p31).

جدول (4) يبين مساحة القطع المعتمدة ومقدار تغطية الارض، وامكانية التوسع لاغلب الصناعات الصغيرة في الهند. (U.N.,1989,p31).

نوع	مساحة القطعة plot Size	مساحة البناء الاولية (م^2)	نسبة التغطية Plot coverage (%)	مساحة البناء الكلية بعد التوسع (م^2)	نسبة التغطية Plot coverage (%)
A	200	40	20	100	50
B	200	50	25	100	50
C	400	100	25	200	50
D	450	200	44	300	66
E	900	450	50	600	66
F	1150	500	43	750	65
G	1350	600	44	900	66
H	1500	800	53	1000	66
I	1500	900	60	1200	80

اما نسب توزع الاحجام المختلفة للقطع الكبيرة في المنطقة الصناعية في الهند فهو كما تم اقتراحه في مؤتمر بومباي 1977 المنعقد هنالك وفق (جدول 5).

جدول (5) يبين احجام القطع الكبيرة في منطقة صناعية في الهند) (U.N.,1989,p31).

المساحة الكلية للقطعة (م^2)	مساحة البناء الاولية (م^2)	مساحة البناء الكلية بعد التوسع (م^2)	نسبة التغطية %
2400	600	1200	25

4800	1200	1800	25
7200	1800	3600	15
9600	2400	4800	15
12000	مساحات متنوعة	مساحات متنوعة	20

من هذين الجدولين نلاحظ مدى صغر حجوم هذه القطع نسبة الى الدول الاخرى، وهذا يرتبط بنمط الصناعات السائدة في تلك البلدان، ثم ان نسبة تغطية الارض للقطعة الصناعية تزداد بشكل طردي مع زيادة مساحة القطع، لهذا فان من الضروري ان يكون هنالك تحديد مسبق لنوع الصناعة السائدة قبل تحديد مساحات الاراضي في المناطق الصناعية (U.N.,1989,p35).

اما في المجمعات الصغيرة فان مساحتها تراوحت مابين (90-420) م² وفق الجدول الاتي (جدول 6).(Bharti, 1978, p.159-161):

جدول (6) يوضح احجام قطع الارض الزراعية في المجمعات الصناعية الصغيرة (المتبع في الهند) (Bharti, 1978, p.159-161)

نوع	حجم القطعة (م²)	مساحة البناء الاولية (م²)	مساحة التوسع المستقبلي (م²)
A	100	20	40
B	100	25	50
C	200	40	100
D	200	50	100
E	400	100	200
F	450	200	300

- اما في العراق : فقد حدد المخطط الاساس لمدينة الثرثار الجديدة قطع الاراضي الصناعية بين (214-3600 م²) (جدول 7). (جمهورية العراق،1987،p.75).

جدول (7) يوضح احجام قطع الأراضي الصناعية في مدينة الثرثار الجديدة (الحديدي ، 1989، p.29)

نوع	الابعاد (م)	المساحة (م²)	الحد الاعلى لنسبة البناء (%)
قطع صغيرة			
S1	9×24	216	70
S2	12×24	288	70
S3	15×24	360	70
قطع متوسطة			
M1	18×24	432	70
M2	21×24	504	70
قطع كبيرة			
L1	24×42	1008	70
L2	24×45	1080	70
L3	24×60	1440	70
L4	60×60	3600	70

توفير امكانية التوسع المستقبلي Provision for future expansion:-

ان احد الفوائد الاساسية للمناطق الصناعية المخططة هي توفيرها إمكانية التوسع للأبنية الصناعية المشيدة على العكس من المواقع المفردة المتناثرة في المدينة، ان السبب لتخصيص مساحة للتوسع هو مواكبة التغيرات السريعة في التكنولوجيا وأساليب الإنتاج الصناعي وكذلك التغيرات السريعة المتوقعة في شاغلي الابنية. وهذا يتطلب دراسة حجوم القطع بالصورة التي تسمح باقصى توسع من دون التجاوز على القطع المجاورة ليعطي دليلاً على نجاح تخطيط المنطقة الصناعية بالرغم من الاختلاف في التوسع بين المشاريع الصناعية ومقدار هذا التوسع الذي قد يكون امراً لايمكن تحديده بدقة، لهذا فان امكانية التوسع يمكن ان يتم بمستويين هما:-

التوسع في حجم المنطقة الكلي:- ويتم ذلك بالحصول على ارض مناسبة مجاورة لتلبية الطلبات المستقبلية.

التوسع ضمن كل مشروع:- ويحدث عندما يكون التوسع الاول محدداً، لهذا يمكن ان يتحقق التوسع الثاني بعدة طرق هي :-

أ – توفير احجام متعددة من الابنية الصناعية:- بعض المناطق المخططة تعطي امكانية للصناعات ان تتحول الى ابنية اكبر ضمن المنطقة نفسها وللمشروع الصناعي نفسه.

ب – او ان يتم التوسع ضمن القطعة نفسها او على قطعة مجاورة متروكة لهذا الغرض وعند وصول التوسع الى اقصى حد ممكن له عند ذاك يلجأ الى ان ينتقل المصنع الى مكان اخر اكبر مساحة.

ففي المملكة المتحدة: يكون الاسلوب المتبع في كثير من المناطق الصناعية هو ترك (100%) من مساحة الارض لغرض التوسع، ومن خلال دراسة عدد من المجمعات البريطانية الصناعية، فقد تبين ان (1/5) فقط من مساحة هذه المناطق مشغولة بالابنية الصناعية. ان امكانية التوسع ينتج عنها كثير من الاحيان عدم الاستغلال الجيد لارض ذات قيمة صناعية طالما ان الصناعات لاتتوسع بالاسلوب نفسه وبالسرعة نفسها (U.N.,1989,p32).

اما في كندا وفي منطقة (Annacis Island): فقد كان التوسع من خلال الانتقال الى وحدة مضاعفة من مبنى ذي وحدة منفردة والانتقال الى مصانع خاصة يتم انشاؤها حسب المتطلبات الجديدة خصوصاً عند حالة وجود الجهة المسؤولة عن المنطقة الصناعية التي تقوم ببناء وايجار الابنية وليس ايجار او بيع الارض فقط.

وفي المملكة المتحدة: يكون التوسع الصناعي في مدينتي (Stevenage) و (Crawley) الجديدتين قد تحقق بالطرق الاتية:-

- توسع ضمن الموقع نفسه ويتم بتوسيع الابنية السابقة.
- انشاء بناية جديدة على موقع جديد مع استمرار عمل المنشأ السابق.
- التوسع على حساب معامل نموذجية ملاصقة للمنشأ الاصلي.
- اشغال معامل نموذجية في اجزاء اخرى من المنطقة وتشغيلها بالارتباط مع المنشأ الاصلي.
- الانتقال من مصنع صغير الى اخر كبير في مكان اخر من المنطقة الصناعية.

وفي المناطق الصناعية سواء اكانت تتضمن صناعات مختلفة او مشاريع صناعية متخصصة فان التوسع في الابنية والحاجة الى التوسع يعتمد بدرجة كبيرة على ادارة المشاريع او المنطقة

ككل التي تسمح بالتوسع بالاساليب او الطرق التي مرت انفاً وكذلك على التصميم المرن الذي يعكس نجاح المنطقة الصناعية (الحديدي ، 1989، p.29)

كفاءة استعمال الارض Land use Efficiency:

تعبر عن مدى الاستفادة المثلى للارض المخصصة للمنطقة الصناعية في نسب توزيع الفعاليات الموجودة بما يحقق الاداء الوظيفي لكل فعالية وبشكل تكاملي في المنطقة.

وتقاس كفاءة التصميم بنسبة تغطية المصانع من حجم الموقع الكلي، وهذه النسبة مهمة خاصة في البلدان التي تسعى لتطوير صناعتها بسرعة مع الحاجة الى مساحات مصانع اكثر من امكانياتها في توفير مناطق جديدة كما في البلدان النامية. وتختلف نسب التغطية من دولة لاخرى، ففي المملكة المتحدة تكون نسبة ما تغطيه يبلغ (1/3) من الموقع و (1/3) للطرق والسكك و (1/3) للمناطق المفتوحة.

وبشكل عام تزداد نسبة الاراضي المخصصة للمصانع بازدياد حجم المنطقة الصناعية وهي تتراوح بين (40%-65%) من المساحة الكلية للمنطقة كما في (جدول 1). وفي البلدان النامية تزداد هذه النسب لغرض زيادة نسبة الاراضي التي تستغلها الابنية الصناعية لتصل الى 80% احياناً (Liem,2005,p282),(U.N.,1989,pp.48-50).

وحيثما تكون زيادة نسبة تغطية الابنية على حساب المناطق المفتوحة او الخدمات العامة، فان هذا لاينطبق على شبكة الطرق التي يجب دراستها بحيث لاتكون اعرض من الحجم المناسب للمرور الكلي المتوقع.

قياس كفاءة تصميم الموقع:

تقاس كفاءة تصميم الموقع (Layout) وفقاً للمعايير الاتية:-

1- قابليته للتطور على مراحل.

2- امكانية التوسع المستقبلي.

3- ان يكون المخطط مرناً، قابل للتغير والتطوير و لا يكون المخطط جامداً (Rigid) وقابلاً لان يتصف بالمخطط المرن (Flexible layout), على اعتبار ان متطلب تغيير الاماكن والمتطلبات بالنسبة للمنشآت الصناعية يكون متوقعاً.

ان عاملي المرونة وامكانية التغيير (adaptaility) من المعايير المهمة في قياس كفاءة التصميم لتحقيق النجاح في ادائية المنطقة بشكل كفوء. وهنالك اساليب عديدة تحقق المرونة وهي:-

أ- تقسيم العمل الى مراحل.

ب- تقسيم الموقع الى اجزاء متكاملة.

جـ- التوقيع المرن للفعاليات والاعتماد على تصميم يحقق المرونة المطلوبة للاداء الصناعي.

د – الاعتماد على نظام وحدات قياسية تخطيطية في تصميم الموقع ككل وتصميم الفعاليات والاعتماد على نماذج قياسية standardization وبما ينسجم مع الفعاليات الصناعية (Walker,1980,p.303).

المحددات التخطيطية لتوقيع المبنى الصناعي:

بعد تحديد مراحل تخطيط المواقع الصناعية ووضع المخطط العام (Layout)، تبرز محددات تخطيطية في توقيع المبنى الصناعي ضمن الموقع وهي:-

أ- نسبة التغطية: (Plot coverage):-

حيث ان هنالك نسبة للتغطية مهما كبر او صغر الموقع من الابنية الصناعية وهذه النسبة تختلف من بلد لاخر فمثلاً (Walker,1980,pp.298-299).:-

- في الولايات المتحدة الامريكية تبلغ نسبة التغطية بعد التوسع النهائي 53.5% من مساحة الموقع والمساحة المتبقية هي للطرق والفضاءات المفتوحة وحسب نوع الصناعة التي قد تزيد او تنقص قليلاً عن هذه النسبة.

- اما في الهند فتبلغ نسبة التغطية من 20% للقطع الصغيرة الى 60% للقطع الكبيرة وتعتمد كذلك على مساحة قطعة الارض الصناعية ضمن الموقع وعلى نوع الصناعة المطلوبة، وتصل بعد التوسع النهائي الى 50% و 80% على التوالي من مساحة الموقع.

- وفي العراق حيث حدد المخطط الاساسي لمدينة الثرثار بان نسبة التغطية للموقع المخطط والمقسم الى قطع اراضي متدرجة في المساحة ولصناعات مختلفة ضمن الموقع، بان لاتتجاوز نسبة التغطية بعد التوسع النهائي عن 70% من المساحة الكلية (الحديدي ، 1989، p.35).

وتعود اسباب تحديد هذه النسب الى :-

1- نوع الصناعة او طبيعتها الوظيفية، وكونها ضارة او غير ضارة بحيث لاتؤثر على الابنية المجاورة.
2- عاملي المرونة والتغير في الاماكن ضمن الموقع واللذين يجب ان يتوفرا في تخطيط المنطقة الصناعية او المشروع الصناعي في نمط معين من الصناعة.
3- لمنع انتقال الحرائق والانفجارات والضجيج الى الابنية المجاورة.
4- توفير بيئة تقنية "بيئة داخلية مريحة حرارياً وبصرياً وصوتياً ووظيفياً".
5- توفير مناطق التحميل والتفريغ وسهولة الحركة بين الابنية الصناعية مما يتطلب وجود اكثر من مدخل.

مما يعني ومن هذه الاسباب بانه لايتم استغلال قطعة الارض او الموقع الصناعي, الا وفق معايير محددة ومتباينة وحسب طبيعة الصناعة ومتطلباتها والمحددات المتبعة في كل بلد.

علاقة المبنى الصناعي بالابنية المجاورة في المنطقة الصناعية:-

مبدئياً وقبل التطرق الى علاقة المبنى الصناعي بالابنية المجاورة له في الموقع الصناعي لابد من توضيح تكوين البيئة العمرانية (الصناعية والسكنية) بشكل عام والناتج عن اسلوب تقديم الكتل البنائية في المواقع، حيث يرجع له الاثر الكبير في تحديد ظروف المناخ الموقعي وبالتالي على ظروف البيئة الداخلية للمبنى، فهو اما ان يكون:-

التكوين المتضام: وتتميز به المدن التقليدية القديمة في المناطق ذات المناخ الحار الجاف، الذي يوفر اكبر قدر من الحماية من الاشعاع الشمسي بوجود الشوارع الضيقة التي تؤكد هذا المفهوم من ناحية وتوفر مسالك لحركة الريح من ناحية اخرى والمنازل ذات الفناءات الداخلية، وانخفاض الفضاءات المفتوحة فيه، اضافة الى ان نسب ابعاد هذه الفضاءات تكون متقاربة بين معدل ارتفاعها والابعاد الافقية او يزيد عنها، لهذا يقل تأثير الاشعاع الشمسي على هذه الفضاءات ويقتصر على فترة قليلة من النهار عندما تكون زاوية ارتفاع الشمس عالية، لهذا كلما كانت الابنية متقاربة ومتلاصقة، كان تأثير الاشعاع الشمسي على العناصر العمودية (الجدران والفتحات) قليلاً خاصة في فصل الصيف حيثما تزداد معدلات ارتفاع زوايا الشمس، لذا تقل اهمية توجيه الابنية ضمن هذا النوع من التكوينات (رمضان,1986,p82).

التكوين المتباعد: ويتميز به التكوين العمراني الحديث، حيث ان الكتل تؤدي الى خلق مساحات مفتوحة معرضة الى الاشعاع الشمسي فيصعب توفير ظروف بيئية مناسبة لها، لذا يكون من المستحسن زراعتها وتشجيرها، حيث ان الاشعاع الشمسي في المناطق الحارة الجافة

يكون مباشراً ومعروف الاتجاه، مما يجعل توجيه المباني مهماً بسبب الفضاءات المفتوحة والكبيرة فيه. ان هذا النمط لتجميع الكتل البنائية يستخدم للمصانع حيثما تكون كثافة التجميع وارتفاع الكتل (اي نوع تنظيمها) يتوقف على اساليب التخطيط المتبعة في المواقع الصناعية (بالاضافة الى نظام الحركة المتبع) وهي كما يلي (Evans, 1985,p.75):-

أ- وفق نظام الحركة الشبكي (Grid Iron):

ان هذا النظام يستخدم في تخطيط المشاريع الصناعية وابنيتها الصناعية في اغلب الاحيان ليعطي حرية توقيع المبنى وعلاقته مع الابنية الاخرى وفعاليات الفضاءات الخارجية ضمن الموقع المخصص لها ويمكن ان يكون من النوع المفتوح او التقليدي، ويساعد على تحقيق التوسع المستقبلي للتطور الصناعي السريع (Rudolf,1977,pp.274-276).

ب- وفق نظام الكتل (Super block):

يظهر هذا النظام اكثر من تصميم لتوقيع المباني الصناعية ولكنها تشترك جميعها بما يلي:-

أ – وجود مساحات خلفية غير مستغلة اضافة الى الارتداد الامامي (Setback).

ب- وجود فواصل جانبية بين الابنية تستعمل كطرق فاصلة او مناطق خضراء تقدر من (10-15)م، هذه المسافات تزداد في حالة الابنية الانتاجية التابعة لمشروع صناعي واحد، وهي موجودة بين الابنية المنفردة ضمن المنطقة الصناعية المخططة لصناعات متعددة، هذه المسافة تزداد او تقل حسب حجم المبنى وشكله.

ج- وفق اسلوب خاص هجين:

يستخدم فيه التخطيط وفق النظام الشبكي لمجموعة من المصانع التابعة لمشروع صناعي واحد، حيث يمكن ان تتوسع قسم من هذه المصانع وليس جميعها، وهذا الاسلوب اقتصادي اكثر في استغلال الموقع او نسبة التغطية. وفيه يتم ترتيب مجموعة من ابنية المصانع بحيث تكون هناك مسافة متروكة بين وحول الابنية (gaps) مساوية الى نصف عرض المصنع. هذا التخطيط يسمح لقسم من المباني بان تتوسع (3) اضعاف مساحتها الاولية، اما المعامل الواقعة على الجوانب فيمكن ان تتوسع بمقدار (125%) كحد اعلى او قد تتوسع معامل اخرى بنسبة (50%) من خلال المساحة الخلفية. ان توقيع الابنية الصناعية وبوجود هذه المسافة الفاصلة ولاسباب عديدة كما مر ذكرها، ستعطي صورة واضحة بان الكتل البنائية الصناعية ذات تنظيم متباعد (مفتوح) وليس متضام وذات كثافة بنائية قليلة بسبب تباعدها وبارتفاعات متباينة حسب نوع الصناعة ومتطلباتها (كمونة، 1985، p.25-28).

علاقة تنظيم كتل الابنية الصناعية والظروف المناخية:

ان لنوع التنظيم الكتلي اثراً كبيراً في تحديد ظروف المناخ المحلي في الموقع وبالتالي ظروف البيئة الداخلية للمبنى، وهذا الاثر يتمثل في تحديد مدى تعرض السطوح للاشعاع الشمسي وتحديد سرعة واتجاه الهواء ضمن الموقع.

وبما ان التنظيم المفضل للابنية الصناعية هو التنظيم المتباعد (او المفتوح) وليس المتراص، وعلى اعتبار ان الشكل المنفصل هو المستطيل (كما سبق شرحه), وبالاضافة الى انعدام تأثير التظليل المتبادل بين الكتل (Mutual shading)، فان هذا سيتطلب جملة من المعالجات تبدأ من المراحل الاولى للعملية التخطيطية والتصميمية، مضافاً الى ان حصول التظليل المتبادل يعتمد على العلاقة بين ارتفاع المبنى وعرض الفضاء الخارجي، فكلما زاد عرض الفضاء الخارجي قل تأثير التظليل او انعدم، وفقاً لمعيار زاوية التباعد (Spacing Angle) الذي يمكن بواسطته تحديد ارتفاعات الابنية والمسافة الفاصلة بينها، الا ان استعماله في تحديد ارتفاعات الابنية الصناعية ذو نطاق ضيق, بسبب ان ارتفاع وحجم المبنى يعتمد على طبيعة ونوع الصناعة- كما هو الحال عند الصناعات الضارة التي يجب فصل المباني فيها

بمسافات كبيرة تلافياً للمخاطر. كذلك وفي حالة تباعد الابنية تزداد اهمية التوجيه، على اعتبار ان التوجيه الجيد يقلل من تأثير الاشعاع الشمسي بشكل كبير(Evans,1985,pp.60-61).

الاستنتاجات:

- إن المباني الصناعية اصطلاح يطلق على المصانع وكذلك على ابنية المخازن المتميزة بكبر حجمها، وذلك لتوفيرها فضاءات عمل واسعة غير معاقة تحقق متطلبات العملية الانتاجية، بالإضافة إلى إن تصاميمها تسمح بامكانية تبادلها الوظيفي (توفيرها عامل المرونة)، لتلبي احتياجات التوسعات المستقبلية.
- حجوم هذه الابنية تختلف حسب نوع الصناعة وطبيعة المنطقة الصناعية وحجمها ونوع الاستثمار المحدد لاقامة مشاريع صناعية متعددة في الموقع او لخدمة مشروع صناعي واحد، وحسب طبيعة القوانين والأنظمة النافذة في البلد المعين.
- ان طبيعة المباني الصناعية يفضل ان تكون من النوع المنفصل بسبب مجموعة عوامل منها نسب التغطية للموقع، وامكانية التوسع المستقبلي ولكون اغلبها مبان انتاجية، ولاحتمال حدوث الحرائق او الاهتزازات العنيفة ولتسرب المواد الضارة، فيفضل فصل الابنية الصناعية مع اعتماد الأشكال الاستطالية كحجوم أثبتت كفاءتها البيئة والوظيفية.
- ان توقيع المبنى الصناعي ضمن الموقع وبعلاقات متباعدة مع الابنية الاخرى, سيعرض المبنى الى تاثير الظروف المناخية الخارجية بشكل كبير فيؤثر على ادائه الحراري وعلى توفير بيئة داخلية مريحة للعاملين فيه وبشكل خاص تاثير الاشعاع الشمسي المباشر, خصوصا تحت ظروف المناخ الحار الجاف الذي يمتاز به مناخ العراق , لذا يكون من الضروري الاستفادة من تجارب الدول المتقدمة صناعيا, خصوصا تلك التي يشابه مناخها العام مناخ العراق, لوضع اللبنة الأساس لمواقع صناعية ناجحة من الناحية التخطيطية والبيئية ولتوفر شروط ومتطلبات البيئة الداخلية المريحة للعاملين.
- عند الأخذ بعملية التنظيم المفتوح تعتبر مسألة توجيه الكتل البنائية في غاية الاهمية بسبب زيادة المساحة السطحية الى الحجم، اما في التنظيم المتضام (المتقارب)، فتقل نسبة زيادة المساحة السطحية الى الحجم وبالتالي تقل اهمية توجيه المبنى، لانها ستعمل جنباً الى جنب مع بقية الابنية في النسيج للتقليل من تأثير الاشعاع الشمسي، وهذا ما لايحصل في المواقع الصناعية.
- ولما كان اسلوب تجميع الكتل البنائية الأفضل للمباني الصناعية هو اسلوب التجميع المتباعد (على الرغم من اهمية مبدأ التراص الكتلي كمحدد لتوفير البيئة الداخلية المريحة في المناخ الحار الجاف) ، لذا فان دور التظليل المتبادل بين الكتل والتظليل الذاتي سيكون ضعيفاً ويصبح تأثير الظروف المناخية مؤثراً بشكل كبير على كفاءة أدائها الحراري وعلى صرفيات الطاقة المستخدمة لتحقيق متطلبات الراحة الحرارية للبيئة الداخلية فيها، ليصبح غلاف المبنى هو العامل الأساس في توفير الراحة داخل بيئة المصنع.

المصادر العربية:

- التنير, سمير ، "تصميم اولي للمجمع الصناعي",معهد الانماء العربي,بيروت,1978.
- الحديثي، د.حكمت عمر، "تطور نظرية اقتصاديات المواقع الصناعية"، مجلة عالم الصناعة، العدد الثالث، السنة الاولى، اب، 1971.
- الحديدي، تركي حسن علي، المتطلبات التخطيطية والمعمارية للمواقع الصناعية الحضرية،رسالة ماجستير غير منشورة، 1989.
- الديب، د.محمد محمود ابراهيم، "المستعمرات الصناعية تخطيطيا وانشاءاً",مكتبة الانجلو المصرية , الطبعة الاولى ,القاهرة ,1973.

- السماك، د.محمد ازهر، عباس علي التميمي، "اسس جغرافية الصناعة وتطبيقها"، الموصل، 1987.
- الفيروز ابادي، "القاموس المحيط"، الجزء الثالث، الطبعة الثانية القاهرة، 1952.
- جمهورية العراق، "هيئة المدن الجديدة، مدينة الثرثار الجديدة"، 1987، ج-أ 161 بغداد.
- حميد ، د.حميد جاسم حميد واخرون، "الاقتصاد الصناعي"، بغداد، 1979.
- رمضان, ثائر علي محمد "اثر العوامل المناخية في تخطيط وتصميم المستوطنات الحضرية في المناطق الصحراوية"، رسالة ماجستير، كلية الهندسة، جامعة بغداد، 1986.
- رياض، د.كمال رياض، "اسس التخطيط العمراني"، الطبعة الثانية القاهرة، 1987
- روبير, اوزاد، "فن تخطيط المدن"، ترجمة بيهج شعبان، بيروت. 1974.
- عمرو، د.حسين، "موسوعة المصطلحات الاقتصادية"، المكتبة الحديثة، القاهـــــرة، 1965.
- فضيل، فادي ، "اثر الشكل الهندسي للوحدة السكنية وتوجيهها على كفاءة ادائها الحراري في المناطق الحارة الجافة"، رسالة ماجستير، جامعة التكنولوجية 1992.
- كمونة، سعد عزيز، "معالجات تخطيطية ومعمارية للمناطق الصناعية في مدينة بغداد"، اطروحة ماجستير غير منشورة، جامعة بغداد، مركز التخطيط الحضري والاقليمي، بغداد، 1985.
- ناجي، عبد الصاحب، "الاسس التخطيطية لتوقيع الصناعات الملوثة وغير الملوثة في المدن العراقية"، اطروحة ماجستير، بغداد، 1982.

المصادر الاجنبية:

- De Bruyn, S. "Dematerialization and rematerializtoin as two recurring phenomena of industrial ecology," Ahadbook of Industrial Ecology, Edward Elgar press Northampton, U.S.A. 2002 .
- Duldley Hunt, "Encyclopedia at American Architectures", New York,1980.
- Evans, Martin; "Housing, climate and comfort" The Architecture press, 1985.
- Gibberd, Frederick, "Town design", fifth edition, Frederick A, Paregr, Inc, USA, 1967.
- James. F. Muncie, "Industrial Architecture" , New York,1960.
G.e. Cherry, "Urban Planning Problem", London, 1974.
- Liem, Andre/ supping, Li , "Anew Breed of leading Pragmatic and creative Designers - manage complex and innovative Environments from a human prespective," National Unversity of Singapore, 2005 .
- Ling, Arthur, "Runcorn Newtown", Midlands Engraving ltd, u.k.1967.
- Perenyi, Imre, "Town and environs" Budapest, 1978.
- R.K. Bharti, "Industrial Estates is Developing Economics", New Dothi, 1978.

- Ruodolf Herz, Friba,Dr Ing (Berlin),"Architects DATA", Ernst Neufert,Part,"Industrial Building", London,1977.
- Tony, Maggie - "The architecture of Ecological systems," Academy Editions - Wildfwl and wetland Canter – England 2004 .
- U.N. "The establishment of Industrial estates in developing countries", New York,1989
- U.N. "The Physical Planning of Industrial estates", New York,1962
- Walker, F. David,"Planning Industrial Development", London, John wiley and Sons, 1980
- William H. Clair, "Hand book on urban planning", New York, 1973

ستراتجيات العمارة الشمسية

دكتورة صبا جبار والمهندسة رنا مجيد ياسين
جامعه بغداد– كلية الهندسة

الخلاصة:–

تمثل عملية البناء الشكلي للعمارة الشمسية عملية منهجية تعتمد على ما وجود من اساليب تطورت على اساسها نظم وتفاصيل جديدة تحدد بنية الشكل المثالي الكفوء لحفظ الطاقة ، وتقترب من النظرية الوظيفية في البناء الشكلي كما تتاثر بالنظريات الاخرى ،وتتغير من مصمم الى أخر لتحقيق الابداع الشخصي في قضايا الشكل المتعلقة عادة بالحدس الذاتي والتركيز على استراتجية دون أخرى والاستفادة من المناورة التصميمية ضمن ماهو ممكن للوصول الى حلول مناسبة واحيانا مبدعة .

الا ان تاثر المصممين بالتقانة المعاصرة و تبني فكرة دمج التقانة الذكية بالعمارة الشمسية ضمن طرح سائد في اعتبارها دلالة الى تقانة منفصلة تربط بالمبنى سبب ظهور نماذج شكلية مختلفة ، وهو ما يعتبره البحث فكرة تحمل جانبا من المصداقية الا انها فكرة مجتزئة الحقيقة ، اذ ان التقانة في وقتنا المعاصر عنصر مهم يمثل البنية المتغيرة المستجيبة للتغيرات الحاصلة في البيئة المحيطة بالمبنى لتهئ ظرف راحة انسانية ،ولكي تكون فاعلة لابد ان تكون متكاملة مع الكيان المادي للمبنى ككل .

لذا ينطلق البحث من مشكلة معرفية تتناول دراسة ستراتجيات بناء الشكل المثالي للعمارة وتكامل النظم التقنية معه لتفعيل الاستفادة من الطاقة الشمسية ضمن العمارة بهدف تحديد ستراتجية البناء الشكلي للعمارة الشمسية في الوقت المعاصر عموما وضمن خصوصية المناطق الحارة الجافة خصوصا اذ توصل البحث الى فرضية مفادها ان للابنية الديناميكية اداء افضل من الابنية الساكنة، ولكي يحقق الاعتماد على الطاقة الذاتية فانه لابد ان يمتلك المبنى بنيتين متكاملتين تتميز البنية الاولى بالاستقرار تمثل ستراتجيات تصميم الشكل المثالي وحددها البحث " كبنية ثابتة " فيما تكون البنية الثانية مرحلة لاحقة لتصميم البنية الثابتة تعتمد عليها في حساباتها وتصميم نظمها تتميز بالحركة والتغير المستمر وفق ثلاث انواع من السيطرة تكون اما يدوية او ميكانيكة او كلايهما معا وهي ضمن العمارة المعاصرة تكون تقانة ذكية تملك استجابة ذاتية بسيطرة ميكانيكية ، حددها البحث " كبنية ديناميكية " .

ABSTRACT:

The research had dealt with a study about the solar architecture, and determined the development in its forming construction strategies, by entering the intelligent technology with architectural control systems to create a comfort interior environment and gaining solar energy.

The importance of the research came from being of contraction of using original design approaches which can be created solar architecture over ages ,against the appearing of wide use of intelligent technology integrated to solar architecture which is the reason of the appearance of different formal buildings types ,some designers have been effected by the contemporary technology signed to technological elements connected with building, to gain power from solar energy ,which the research consider it truth ,that have aside of credibility but it is a curtailed truth .

The purpose of this research is to state a “strategy of construction forming for the solar architecture “and determine its development with integrated technology to the solar energy gaining system and control system, and study the effect of using industrial intelligent technologies to gain it automation ability in the identity of response, and personified the effect by integrated it with the whole envelope of building.

While the general research problem is tended to find a knowledge to determined the effect of using solar energy in building to develop the strategies of forming construction in it, and find a knowledge to determine the effect of technology integrated to solar architecture to develop the strategies .and finally the research gained many result and reach many conclusion.

العمارة الشمسية :

تمثل العمارة الشمسية العمارة التي تتبنى توظيف الطاقة الشمسية كمرتكز اساسي للتصميم، مثل المباني الكفوءة الطاقة والتي توظف الطاقة الشمسية في تحقيق بيئة داخلية مريحة مسيطر عليها تتناسب وحدود الراحة الانسانية من متطلبات التكييف الحراري والانارة ،الى جانب اعتمادها طاقة ذاتية عن طاقة الاشعة الشمسية .

ان استخدام الطاقة الشمسية في العمارة لا يمثل فكرة القرن العشرين ولا توجه فكري لحركة معمارية ظهرت مع ظهور مشاكل الطاقة او غيرها ،وانما يمثل عملية منهجية لها اصول تصميمية تمتد الى بدايات تكون اولى الحضارات وبناء اول عمارة للانسان بالتعامل مع الظروف الطبيعية بتجنب اواكتساب هذه الطاقة ،لتتطور عنها مجموعة اساليب للتعامل مع المشاكل البيئية وتوظيف الطاقة الشمسية والتي تطورت بمرور الزمن الى مجموعة ستراتجيات تمثل تجارب الشعوب [Denholm, Paul L, 2004] .

مثلت هذه الاستراتجيات بنية الشكل المثالي ،والتي تقترب اكثر من النظرية الوظيفية في البناء الشكلي للعمارة كستراتجية اساس توجه العملية الفكرية لتكوين الحل ، الا ان الدافع الذي يوجه التغير نحو توظيف بدائل الطاقة[1] يرتبط بنظرية اخرى تعرف "بنظرية روح العصر" التي تهدف الى ايجاد معالجات فعالة لمشاكل سائدة ضمن تلك الفترة الزمنية ،وهو مايفسر التوجه الكبير لحل مشاكل الطاقة باعتبارها اهم

[1] في مقدمتها الطاقة الشمسية ضمن أفكار الاستدامة في العمارة

مشاكل العصر ،فيما تعنى النظرية الهندسية بتحقيق الشكل المثالي فيزيائياً، تتجسد في عدد كبير من الطروحات أبرزها لـ (رالف ناولز) في الشكل المثالي ونظرية الغلاف الشمسي،وطروحات(د.وأتسن ود.ماركوس ود.موريس) للشكل المثالي حراريا ،إلى جانب طروحات (اولجي) [Denholm, Paul L,2004].

بالرغم ان وظائف العمارة اقتصرت في السابق على تحقيق الراحة الحرارية [1] التي تتضمن تدفئة وتبريد الفضاءات [Bratati, 1994, p.2]، وفق معايير بسيطة بعيدة عن التعقيد تتماشى مع تكييف الإنسان ضمن بيئته بعيدا عن الترف بتصميم المبنى ليكسب قيمة اكبر تجعله متميزا عميق الارتباط مع بيئته [Schulz,1966,p.109-104-21],وهو ما يفسر الاختلاف في المباني التقليدية ضمن المناطق المختلفة في ظروفها البيئية ؛الحارة الجافة والحارة الرطبة والمناطق الباردة ولقد تطورت هذه الفكرة بواسطة المعالجات البيئية والتصميمية بأشكال عديدة .

إلى أن حدث التطور الحقيقي مع تطور مفهوم الآلة منذ بدايات الثورة الصناعية وتقدم وسائل السيطرة البيئة الذي يعكس التطور التقني في هذا المجال [Rush, Richard D ,1986,p.22].وهو ما طرحه ايزنمان من اسباب التغيير في النظرية المعمارية واوضح بان تقولب الوظيفة في اطار ما يسمى الشكل يتبع الوظيفة جاء نتيجة استحداث وظائف جديدة بسبب الماكنة والتصنيع خلفت العديد من التعقيدات التي لم تستطع الاطر النمطية ان تكون وافية لحل اشكالية التصميم فيها واوضح ايزنمان بان العمارة اصبحت فنا اجتماعيا والوظائف اصبحت اكثر تعقيدا و القدرة على اظهار الشكل النقي او النمط النقي اصبحت متاكلة ففي القرن التاسع عشر حتى العشرين اصبح نمو البرنامج اكثر تعقيدا و النمط الشكلي اصبح مقيسا كاهتمام قابل للادراك و التوازن[الدجيلي، عمار،1999،ص34].

ليتعدى التغير الى حالة اكثر عمقا تتمثل بتطور وتعقد متطلبات ونوعية الحياة (Life quality) كهدف يتضمن عامل المتعة (pleasure) ، والتي يوفرها المبنى من خلال عمله كمرشح للمناخ عن طريق المنشأ والخدمات. ومن المعلوم لغة أن المتعة شعورٌ أكمل وأتم من حالة الراحة ، وبالتالي فإن الراحة شيء والمتعة شيء آخر متفوق على الأول ولا يتم إلاّ به [رسول،هوشيار قادر ،2004].

يمتلك المعماريون الفرصة المناسبة ليوفوا بوقت واحد احتياجاتهم للتعبير الجمالي للهيئة والشكل والاداء الوظيفي اضافة للتدفئة والتبريد والإضاءة، فالتلازم بالعلاقة الوظيفة والخدمات (تدفئة ،تبريد،اضاءة) مع المعالم المعمارية جعل من السيطرة البيئية مانحة للشكل[2](form givers) في العمارة ومعززة الوجود الإنساني ضمنها [Norbert lechner,2001] ان المبنى الذي يجد فيه ساكنه ملجأ مريحا في جميع الفصول ويحميه مع ما يملك هو بلا شك أفضل المنازل وأجملها كما يعتقد سقراط (390-470 ق.م) [سلفر ناتان، 1978].

[1] إذ ان تأمين بيئة داخلية مسيطر عليها (Artificial Micro Climatic) هو الهدف الرئيس لإقامة المبنى [Schulz,1966,p.21].

[2] We can say that the environmental controls are form givers in architecture [Wiley&Sons,2001,p.9]

ان توسع متطلبات الراحة الإنسانية (Human Comfort) كمفهوم مرتبط بطبيعة الإنسان المعقدة المتجهة باتجاه التغير والتوسع والترف أفرزت تدريجيا وبنفس المعدل متطلبات أكثر تعقيدا وتوسعا.

ولعل مشاكل الطاقة كانت الاكثر من المحددات البيئية التي تتطلب التعامل مع العمارة ضمن مستوياتها المتعددة كي يكون الانتاج متوازنا في مضمونه ومظهره هو تخلي المعماري عن مهامه خلق عدد من المشاكل في مقدمتها مشكلة الطاقة.

إلا أنها مشكلة من نوع أخر ضمن قطاع ألمبان يبين رالف ناولز: حقيقة المشكلة كانعكاس لما قامت به المدارس المعمارية من تدريس أجيال من المعماريين اعتمادا على معان لا معمارية للتكييف البيئي (Environmental adaptation) والمشكلة في هذه المناهج تظهر للعيان ألان على هيئة معضلة استهلاك للطاقة(Energy Consumption Dilemma) لكنها من وجهة نظره "مشكلة تعبير معماري (Architectural Expression) انبثقت عن ذاك الأسلوب في التدريس[Norbert lechner,2001] .

ضمن هذا السياق يمكن تحديد جملة من التغيرات تسبب تزايد حاجة العمارة للطاقة وتظهر مدى عمق المطلب التصميمي لعمارة شمسية وفق ستراتجيات ثابتة وحيوية:

- ثورة في الوظائف العمارية الجديدة ،بعد الثورة الصناعية على الخصوص.
- التطور في معايير الراحة الانسانية الذي تعد هدفا للوصول الى شعور اكثر تمام يفوق شعور الراحة الى درجة المتعة.
- تقلص وتراجع اعتماد الاصول التصميمية التي افرزتها العمارة على مر العصور في تجنب او كسب الطاقة الشمسية لمعالجة مسالة تحقيق الراحة الحرارية والتي تمثل الجانب الاكبر المستهلك للطاقة ضمن العمارة ،وسببه التوجه الى الاعتماد على الطاقة الاحفورية التي اكتشفت كطاقة سهلة في تبريد وتدفئة واضاءة الفضاءات .
- تغيير الضغط الخارجية لعوامل البيئة المحيطة ،بسبب التغير العام للمناخ (climatic change) الذي فرض حملا اضافيا من الحرارة التي يتعرض اليها المبنى ،متطلبا جهد اكبر للسيطرة على البيئة الداخلية.

اذن العمارة اليوم تستهلك طاقة كبيرة الى حد يكفي لخلق مشكلة ، وان العمارة الشمسية لكي تكون عمارة مستدامة ناجحة تلبي التزايد في الحاجة الى الطاقة ضمن متطلبات الانسان في الوقت المعاصر فلابد من ان تستغل الطاقة الشمسية ضمن فترة الاشراق ليس لتكيف وانارة الفضاء نهارا فحسب وانما لتزويده بالطاقة المساعدة لتشغيل وادارة المبنى على مدار اليوم بالطاقة الذاتية وبما يسد حاجة التطور

التقني ونظم الادارة والسيطرة ضمن المبنى ، من خلال الاستجابة والتغير فيها للتعامل مع التغيرالمستمر في المعطيات المناخية[1] .

وبما إن العمارة ثابتة لابد من إن يكون هناك مستوى ثان من التعامل أكثر مرونة له خصائص احيائية يتعامل مع المعطيات المتغيرة للبيئة ويوفق بنها وبين التغير في المتطلبات المتغيرة للبيئة الداخلية المحتواة ضمن البنية الثابتة هذه الأجزاء تتغير استجابة لمؤشرات التغير في المحيط :الاتجاه ،الانفتاح والانغلاق ،الشفافية،البرامج الرقمية الذكية[الدراجي،رنا ،2006،ص31] .

الا ان اعتبار الشكل البنائي ثابت لصفة البناء ولا يمكن تغيره زمانيا ،يجعل التغير ينحصر ضمن قشرة المبنى مرتبطاً بالفضاءات الداخلية وتقنيات السيطرة والاتصال والادارة ضمن المبنى لتمرير ماهو ضروري من الاشعة الشمسية الى داخل الفضاءات وحجبها عند انتفاء الحاجة اليها او اكتسابها ضمن القشرة لتوليد الطاقة الذاتية .

لذا يفترض البحث ان الشكل المثالي في العمارة الشمسية لكي يحقق الاعتماد على الطاقة الذاتية فانه لابد ان يمتلك بنيتين متكاملتين تتميز البنية الاولى بالاستقرار تمثل ستراتجيات تصميم الشكل المثالي حددها البحث " كبنية ثابتة " فيما تكون البنية الثانية مرحلة لاحقة لتصميم البنية الثابتة تعتمد عليها في حساباتها وتصميم نظمها تتميز بالحركة والتغير المستمر وفق ثلاث انواع من السيطرة تكون اما يدوية او ميكانيكية او كلايهما معا وهي ضمن العمارة المعاصرة تكون تقانة ذكية تملك استجابة ذاتية بسيطرة ميكانيكية ، حددها البحث "كبنية ديناميكية" .

1.ستراتجيات العمارة الشمسية ضمن البنية الثابتة:

تشمل الاستراتجيات التصميمية للعمارة الشمسية تصميم المبنى لتحقيق الراحة الحرارية من تدفئة وتبريد إلى جانب توظيف الضوء الطبيعي ضمن نظم إنارة المبنى لتتجسد بـ: نظم التجنب الحراري (Heating Avoidance)والنظم الذاتية (Passive System) في التدفئة والتبريد والإضاءة[الدراجي،رنا ،2006،ص34].

حددت ستراتجيات تصميم العمارة الشمسية ضمن بنيتها الثابتة الى عدد من الاستراتجيات الخاصة التي تتفرع عن الاستراتجيات العامة والتي تصنف الى:

1. **ستراتجيات التجنب الحراري**(heating avoidance) والتي تتضمن عددا من الاستراتجيات الخاصة :

- **ستراتجات التوجيه** (orientation strategies): تمثل الإستراتجية الأولى في عملية تصميم العمارة الشمسية ، اذ ان التغير في التوجيه يسبب أختلاف كمية وزاوية الأشعة الشمسية الساقطة على أوجه المبنى ،مما يؤثر على ادائها الحراري بشكل كبير[Boyce, Newsham Myer ,2003,p.90] ،اذ ان التوجيه الجنوبي

[1] وهو ما يمثل ثروة تملكها المناطق الحارة الجافة التي تمتع بفترات اشراق طويلة على مدار اليوم والسنة وضمن مناخ صاف يحتفظ بالطاقة بدون تشتيت وامتصاص عن طريق الغيوم .

للمبنى يكسب السطح اكبر كمية إشعاع خلال الفترات التي تكون فيها درجة الحرارة تحت المعدل (شتاءاً) واقل كمية خلال الفترات التي ترتفع فيها درجة الحرارة فوق المعدل (صيفاً) مما يجعله التوجيه المثالي ،مع وجود مناورة تصميمية تعطي مرونة أكثر للتوجيه المثالي بزاوية ($22,5^{o}$) جنوب–جنوب شرقي مع نسبة سماح تصل إلى ($22,5^{o}$) جنوب شرق–جنوب غرب [Norbert lechner,2001,p.99]

- **ستراتجيات التظليل** (Shading Strategies):التي تمثل مفتاحا لتحقيق الراحة الحرارية الداخلية طبيعيا وجزءا أساسا من ستراتجية التجنب الحراري. يعتمد ستراتجيتين أساسيتين:. ستراتجية التظليل العام للمبنى .و 2. ستراتجية تظليل الفتحات.
- **ستراتجات الاضاءة الطبيعية** (sun lighting strategies): تصنف اعتماداً على محور توزيع الفضاءات نحو مصدر الأشعة لتحدد استراتجيتين اساس: 1.تنطيق الفضاءات على المستوى الأفقي بتنظم الفضاءات التي تتطلب مستويات عالية من الإضاءة الطبيعية قرب النوافذ ،وتوقيع النشاطات التي لا تحتاج إلى الكثير من الإضاءة بعيدا عن مصادرالإضاءة الطبيعية [Brown,G.Z.&Dekay&Mark,2001,p.167-168]. 2. تنطيق الفضاءات ضمن المستوى العمودي ضمن النسيج الحضري المزدحم توقع الفضاءات التي تحتاج إلى الضوء بشكل كبير يمكن إن توضع في الطوابق العلوية بينما التي تتطلب إضاءة اقل يمكن إن توضع قرب مستوى الأرض [Bratati,Biswas,1994,p.102] .
- **ستراتجيات العزل الحراري** (heating insulation strategies): استخدام العوازل الحرارية والتي هي مواد بسعة حرارية واطئة وذات ممانعة حرارية عالية يمكن بإضافتها تقليل السريان الحراري عبر قشرة المبنى والتي يفاد منها في المحافظة على درجة الحرارة الداخلية مستقرة على مدى ساعات اطول [البزاز ،إنعام،1990،ص102].
- **ستراتجيات اختيار الالوان** (color strategies) : يؤثر اختيار لون السطوح الخارجية على معامل الانعكاس والامتصاص [Brown,G.Z.& Dekay & Mark,2001,p.254].
- **ستراتجيات السيطرة على مصادر الحرارة الداخلية** (heating resources zoning strategies): تنتج بعض الفضاءات نسب عالية من الحرارة كالمطابخ والغرف الميكانيكية التي تضم مصدرا حراريا لذا فانها تدفأ و تبرد وتهوى بشكل منفصل عن الفضاءات المجاورة وتوضع جميعها لتشارك الغرف المجاورة بمدخل الحرارة الخاص بها وكإجراءات بديلة تنظم الفضاءات ضمن المبنى لتستخدم أو ترفض مصادر الحرارة الداخلية [Brown,G.Z.& Dekay & Mark,2001,p.161].
- **ستراتجيات التشجير**(Greening Strategies): تظليل ذو أهمية خاصة على مستوى تصميم الفضاءات الخارجية يتجسد بالبيئة المحيطة ،كالأبنية المجاورة الأشجار التي تحدث تظليل متجدد ومستمر [الدراجي،رنا ،2006،ص38] وفيما يلي جدول باهم استراتجيات التجنب الحراري لاحظ الجدول[1].
- **ستراتجيات النظم الذاتية(passive system)**: يشير مصطلح النظم الذاتية* إلى النظام الذي يجمع ويخزن ويعيد توزيع الطاقة الشمسية من دون استخدام مراوح أو مضخات أو إي نظم مراقبة معقدة " [Norbert

* مصطلح النظام الذاتي (Passive system) استخدم إثناء الحرب العالمية الثانية من قبل Naser (وكالة الفضاء الأمريكية) لوصف أدوات السيطرة على الهواء المحيط بالأرض (Aerospace) بدون استخدام المراوح وأجهزة السيطرة الميكانيكية إلا إن استخدامه في العقد السابع من القرن العشرين كان لتوضيح مفهوم (sky therm) والذي يعتمد سقف المبنى كنظام طبيعي للطاقة [Cook, Jefferey,1980,p.10]

[lechner,2001,p.146] من اجل حفظ الطاقة و تهيئة الراحة بأبعاد وإزالة الحرارة الشمسية الغير مرغوب بها [Inger Andresen,2000,p.28] بواسطة الطرق المدمجة في تصميم البناية وعناصرها الرئيسية العمودية والأفقية ،تتضمن استراتجيتين اساسيتين :

- **ستراتجيات التبريد الذاتي** (cooling passive system): تتضمن عدد من الاسترتجيات الخاصة من التبريد بالتهوية ،الاشعاع ، التبخيري ،التبريد الارضي وستراتجية ازالة الرطوبة بالتجفيف لاحظ جدول [2].
- **ستراتجيات التدفئة الذاتية** (heating passive system): تتضمن عدد من الاستراتجيات الخاصة من ستراتجيات التدفئة بالكسب المباشر ، وستراتجيات الكسب غير المباشر ونظم العزل التي تتضمن استخدام الافنية والفضاءات الصيفية والشتوية بالاعتماد على مبدء الهجرة بين الفضاءات لاحظ الجدول [3] .

جدول [1] ستراتجيات التجنب الحراري [الدراجي،رنا ،2006،ص46]

ستراتجيات التوجيه العام للمبنى	تحديد الهدف من توجيه المبنى	توجيه المبنى إلى الجنوب كتوجيه مثالي
		الاستطالة بالمبنى مع المحور شرق – غرب لتجنب الكسب الحراري
		الاستطالة بالمبنى مع المحور جنوب– شمال لرفع الكسب الحراري
	توجيه المنفذ الشمسي توجيها مغايراً	الدوران حول محور عمودي
		الدوران حول محور افقي
	تجزئ المبنى إلى وحدات منفصلة	
ستراتجيات التظليل	التظليل العام للمبنى	استخدام السقوف المظلية (parasol roof) لتظليل المبنى كاملا
		استخدام المظلة الأفقية لحماية الفناء الداخلي
		استخدام المظلة الافقية لتظليل الواجهات
	تظليل الفتحات	الكاسرات الشمسية sun breaker
		استخدام طبقة التظليل الداخلية
		توظيف الرفوف الضوئية ضمن الفتحات
ستراتجيات الإضاءة الطبيعية	تنطيق الفضاءات على المستوى الأفقي	التنظيم الشريطي للحصول على منفذ ضوئي لكل فضاء
		استخدام الإضاءة السقفية في المباني ذات الطابق الواحد
		استعارة الفضاءات الصغيرة للإضاءة الطبيعية عن الفضاءات الكبيرة الداخلية
		استخدام السطوح الأفقية الخارجية لعكس الأشعة إلى الفضاءات الداخلية
		توظيف الإضاءة الجانبية الكبيرة
		تفعيل علاقة ارتفاع النافذة مع عمق الغرفة
		رفع معامل الانعكاس لقشرة المبنى الخارجية
	تنطيق الفضاءات ضمن المستوى العمودي لتوفير الإضاءة الطبيعية	
إستراتجيات العزل الحراري	توظيف الكتلة الحرارية كعازل حراري	
	توظيف العازل الحراري ليحيط الكتلة الحرارية من الخارج	
	دمج العازل الحراري ضمن تجاويف الكتلة الحرارية	
	تغليف العازل الحراري للسطوح الداخلية للكتلة الحرارية	
ستراتجيات اختيار الألوان	التحكم بلون طلاء السطوح لرفع أو تقليل قابلية الانعكاس	استخدام الألوان الساطعة لزيادة معامل الانعكاس لسطح قشرة المبنى
		استخدام الألوان المعتمة لتقليل معامل الانعكاس لسطح قشرة المبنى

السيطرة على مصادر الحرارة الداخلية	تنظيم الفضاءات عموديا	استخدام البرج الخدمي المركزي في الأبنية متعددة الطوابق
	التنظيم المخطط الأفقي	استغلال مصادر الحرارة الداخلية في التدفئة أو عزلها لتقليل أثرها في زيادة أحمال التبريد
التشجير	استخدام الأشجار الكبيرة والمتوسطة الحجم	استخدام النباتات الدائمة الخضرة للتظليل طوال السنة
	استخدام النباتات المتسلقة	توظيف النباتات المتسلقة كعازل حراري يحيط السطح الخارجي لقشرة المبنى

جدول [2] ستراتجيات نظم التبريد الذاتية [الدراجي،رنا ،2006،ص52]

التبريد بالتهوية	التهوية المريحة	تصميم مسارات تهوية أفقية	استخدام المنافذ المباشرة لمنطقة هبوب الريح
			توظيف الافنية الوسطية لخلق اظطراب هوائي
		تصميم مسارات تهوية عمودية	توظيف ملاقط الرياح
			استخدام أنابيبDucts التحكم
			تنظيم البعد بين الفتحات العمودية
			دمج ستراتجيات التهوية والإضاءة والكسب الحراري
	التبريد بالتدفق الليلي		استخدام الأحواض الحرارية (heat sink)
التبريد بالإشعاع	التبريد بالإشعاع المباشر		
	التبريد بالإشعاع الغير مباشر		
التبريد ألتبخيري	التبريد بالتبخير المباشر		
	التبريد بالتبخير غير المباشر		
التبريد الأرضي	الارتباط المباشر بالأرض	استخدام الملاجئ الأرضية	احاطة الأرض لجوانب المبنى
			طمر المبنى في التربة مع ابقاء منافذ خارجية للرؤية والتهوية
			المبنى في الارض كليا
	ستراتجية الارتباط الأرضي الغير مباشر	استخدام القنوات الأرضية	النظام الحلقي – المفتوح Open – Loop system
			النظام الحلقي المغلق system closed – Loop
ستراتجية إزالة الرطوبة بالتجفيف	استخدام المواد المجففة لامتصاص الرطوبة من الجو الداخلي		استخدام المواد الكيماوية:جبل السيلكا والالمومينا الفعالةكلورا يد الكالسيوم

جدول [3] ستراتجيات نظم التدفئة الذاتية [الدراجي،رنا ،2006،ص63]

ستراتجيات التدفئة بالكسب المباشر	الكسب المباشر عن الواجهات	استخدام الواجهة الجنوبية المزججة
		ستراتجية التحكم بتوجيه النوافذ
		ستراتجية التحكم بحجم النوافذ
		التنظيم الشريطي للفضاءات لتوفير منفذ شمسي مباشر لكل منها
		استخدام الفضاءات لتتداخل مع المقطع العمودي للمبنى
		الكسب المباشر عن السقوف
		توظيف التدفئة السقفية في السطوح المنشارية المواجهة للجنوب
	توظيف كتلة المبنى للكسب الحراري	توظيف جدار الخزن الحراري لرفع الكسب الشمسي
		ستراتجية المناورة بمعامل (S/F) بتجميع الفضاءات
		تنطيق الفضاءات مع المحور العمودي للمبنى
		توظيف المناطق الفاصلة (Buffer Zones)
ستراتجيات	استخدام جدار الحراري	دمج نظام الكسب المباشر وجدار الجدار الحراري
		استخدام منافذ تهوية أعلى الجدار الحراري

الكسب الغير مباشر		استخدام العازل الحراري بين الجدار الحراري وطبقة الزجاج
		ترطيب الجدار الحراري بتصميمه من الحقائب المائية
	استخدام البركة السقفية roof pond	
ستراتجيات نظم العزل	الهجرة migration بين الفضاءات	
	ستراتجية توظيف الكتل الحرارية لتقليل التذبذب بدرجات الحرارة للفضاء الشمسية	
	ستراتجية استخدام الكتل الحرارية لتساهم في التبريد والتدفئة	

وان استخدام هذه الاستراتجيات في توفير بيئة داخلية مريحة حراريا هو امر اساس في تصميم اي مبنى ، بالرغم من ذالك قد يكون الجهد المتحد للتجنب الحراري والتبريد الذاتي غير كاف في بعض الظروف المناخية الأكثر تعقيداً ، مما يتطلب الخطوة الثالثة من طرق التصميم بتدخل المعالجات الميكانيكية لتكمل مالم تستطيع النظم الطبيعية إن تنجزه وفي هذه الحالة ستكون المعالجات الميكانيكية متواضعة وتستعمل مقدارا قليلا من الطاقة ممكن إنتاجها بالطرق الفعالة [Baker,Fanchiotti, Steemers, 1993,p.2] .

2.ستراتجيات العمارة الشمسية ضمن البنية الديناميكية

ستراتجيات تصميم البنية الديناميكية للعمارة الشمسية التي تتعامل مع تقانة الطاقة الشمسية ضمن مفاهيمها المعاصرة من اكتساب الصفات الاحيائية في الاستجابة الذاتية لمتغيرات البيئة الخارجية لتكوين ردود الافعال في تحقيق السيطرة على ظروف البيئة الداخلية.

ان كل ستراتجية تصميمية ضمن العمارة الشمسية تملك نوعا من المناورة وتاتي بمعالجات ثابتة على مستوى الشكل والذي يعرف (بالشكل المثالي) ليكون ملائما لاكبر فترة من السنة الا انها لاتلائم جميع ايامها[Norbert lechner,2001]. لذا تظهر فكرة دمج التقانة الذكية بالعمارة الشمسية لحل المشكلة ضمن محورين : الاول يمضي في اتجاه خلق الشكل المثالي القابل على التغير مع تغير ظروف البيئة الخارجية المستمرة. فيما يتجه الثاني في تحقيق اكتفاء العمارة بالاعتماد على الطاقة الذاتية عن كسب طاقة الاشعة الشمسية كشكل من اشكال الطاقة المستخدمة ضمن الانظمة الميكانيكية والتي تكون ضمن ادنى حدود الاستخدام بسبب استنادها الى ما صممت عليه العمارة الشمسية ضمن البنية الثابتة . ان التوسع في استخدام التطبيقات الخاصة بتقانة السيطرة في هذا السياق قاد الى ظهور مصطلح الابنية الذكية وقشرة المبنى الذكية لوصف بناء الشكل الذي يمكن ان يلبي هذه المطالب بنسب نجاح متباينة.

لذا فان الابنية الشمسية المعاصرة تعتبر ساكنة فيماعدا بعض الاجزاء الديناميكية فيها، من خلال سلوك اجزاء المبنى المكونة لقشرته باستجابة ذكية للمتغيرات كجزء من قابلية تكيفه مع البيئة الذي يتطلب تطوير ثلاث عمليات احيائية تدمج بالعمارة : الادراك (Perception) والتعقل (Reasoning) والفعل (Action) .وهي خصائص احيائية تكتسبها العمارة بدمج تقانة الذكاء الصناعي الى اجزاءها الداخلية والخارجية .الا

ان الاثر الواضح للتقانة في تغير بنية الشكل يتركز في تقانة الفعل والمتضمنة نظم الطاقة الذاتية ونظم القشرة المزدوجة والكاسرات المتحركة لتشكل العناصر المتحركة المكونة للقشرة الذكية ضمن المبنى الشمسي ، حدد البحث ستراتجيات البنية الديناميكية ضمن ثلاث مستويات :

1.**ستراتجيات توظيف تقانة الادراك** (Perception-Stratgies) : بمماثلة خاصية الادراك للكائن الحي وتطوير توظيفها ضمن البنية الديناميكية للعمارة على مستويين هما: ادراك الحالة البيئية؛ومتطلبات الشاغلين من خلال توظيف تقنيات متعددة منها تقنية المتحسس الضوئي ،الماسح الضوئي ، توظيف بيانات القمر الصناعي ، شريحة السطح البيني ومتحسس الاشغال وتقنية السطح البيني الحركي ووحدة البطاقة الذكية .

- **ستراتجيات توظيف تقانة التعقل** (Reasoning-Stratgies): يماثل الخاصية الاحيائية للكائن الحي بالتفكير بالحلول وفق ما معطى من ظرف ومتطلب ، والتي تتمثل باستخدام الانظمة التالية ،الانظمة الخبيرة ، منظومة الشبكات العصبية الاصطناعية ، الانظمة الضبابية ، الخوارزميات التطويرية ، النظم الهجينة [الدراجي،رنا ،2006،ص83].
- **ستراتجيات توظيف الفعل الصناعي** (Action-Stratgies): يماثل الاستجابة الذاتية للكائن الحي بتكوين رد الفعل ، والذي يتضمن توظيف كل من الانظمة المنتجة للطاقة من مجمعات ومكثفات الطاقة والواح الخلايا الضوئية ، الى جانب استخدام نظم القشرة المزدوجة وادوات التظليل المتحركة لاحظ الجدول[4].

جدول [4] ستراتجيات البنية الديناميكية للعمارة الشمسية[الدراجي،رنا ،2006،ص63]

ستراتجيات البنية الديناميكية للعمارة الشمسية		
	ادراك الحالة البيئيةِ	توظيف تقنية المتحسس الضوئي Photo sensor
		توظيف الماسح الضوئي للسماء Sky scanner

ستراتيجية الادراك الصناعي (الفهم)				توظيف بيانات القمر الصناعيGeostationary satellite
	فهم متطلبات الشاغليين			توظيف تقنية السطح البيني لنظام المستخدم
		توظيف تقنية متحسس الاشغال		متحسس الحركةِ
				متحسس الاشعة الحمراء
				توظيف تقنية السطح البيني الحركيTEmotion لبيانات المستعمل
				توظيف وحدة البطاقة الذكية
ستراتيجية التفكير الصناعي	تقنية البرامج الكومبيوترية			توظيف الأنظمة الخبيرة Expert systems
				توظيف منظومة شبكات عصبية إصطناعية Artificial neural networks
				توظيف الأنظمة الضبابية Fuzzy systems
				توظيف الخوارزميات التطوّريةEvolutionary algorithms
				توظيف النظم الهجينة Hybrid systems
ستراتيجية الفعل	ستراتيجيات استخدام الانظمة المنتجة	استخدام مجمعات الطاقة الشمسية		توظيف نظم شمسية ذات الوسط الحراري السائل
				توظيف نظم شمسية ذات الوسط الحراري الهوائي
				التدفئة المسبقة لهواء التهوية
				دمج نظم الطاقة الشمسية الفعالة / الذاتية
				انتاج الطاقة الكهربائية عن قوة حركة الهواء المسخن شمسيا
				توظيف هيكل المبنى لالتقاط وخزن الحرارة عن طاقة الاشعة الشمسية
				تضخيم مبدء عمل المجمع الشمسي الكبير
		مكثفات الطاقة الشمسية		استخدام الاشكال المختلفة للمكثفات الشمسية
				تضخيم مبدء عمل المكثف الشمسي
				التخزين الحرارة الظاهرة
				التخزين الكيمائي
		محولات الطاقة المباشرة منظومة الخلايا الضوئية		النظام المنفصل
				نظم المتصلة بالشبكة
			دمج منظومة الخلايا الضوئية ضمن العمارة	تغليف السطوح بالفوتوفولتك
				الواجهات المغلفة مع الفوتوفولتك
				التزجيج والفوتوفولتك
				ادوات التظليل الفوتوفولتك
				القشرة المزدوجة
				ادوات او وسائل التظليل المتحركة

حدد البحث (ستراتجية تصميمية للعمارة الشمسية) تم تسميتها بـ **(ستراتجية البناء الشكلي في العمارة الشمسية)** .تمتلك هذه الاستراتجية مرحلتين اساس تعتمد الثانية على الاولى كقاعدة لنجاح العملية التصميمية ككل ،لتشكل وتوضح البنية الشكلية للعمارة . تتمثل المرحلة الاولى في **(ستراتجية تصميم البنية**

الثابتة للعمارة الشمسية) اذ ان العمارة الشمسية هي ساكنة فيماعدا بعض الاجزاء النشطة و الديناميكية فيها والتي تملك القدرة على الاستجابة والتكيف التي تمثل المرحلة الثانية من ستراتجيات البناء الشكلي للعمارة الشمسية الذي تم تسميته ب **(ستراتجية تصميم البنية الديناميكية للعمارة الشمسية)** ، تمثل التطور التقني لاستغلال الطاقة الشمسية في العمارة تملك الاثر في تغير البنية الشكلية للعمارة سلسلة من العمليات التحولية .

سيتم اختبار توظيف ستراتجات العمارة الشمسية هذه ضمن ثلاث مشاريع تمثل الحالة الدراسية تقارن بين نموذج يوظف واخرى بنية بالعلاقة بينهما يدوية فقط ، فيما يتناول النموذج الثالث دراسة التكامل بين البنية الثابتة والديناميكية وفق سيطرة وادارة الاستجابة للتغير من خلال توظيف تقانة ذكية باستجابة ذاتية .

الحالة الدراسية :

سيتم في هذه الفقرة مناقشة المفردات المستخلصة ومناقشتها في مشاريع منتخبة من العمارة بدءاً من العمارة الشمسية التقليدية وصولا الى نماذج من العمارة المعاصرة . لاستقراء اثر توظيف التقانة المعاصرة للطاقة الشمسية في تغيير البنية الشكلية للعمارة في ثلاث مشاريع يمثل الاول بداية توظيف النظم الذاتية في التدفئة الذاتية والذي يمثل جزء اساس من بدايات تصميم الشكل المثالي فيما يمثل النموذج الثاني تطورا لاستخدام البنية الديناميكية على المستوى المبنى ككل وعلى مستوى عناصر قشرة المبنى الا انها تقانة بدائية بتحكم يدوي وليس ذاتي فيما يمثل النموذج الثالث تطور ستراتجيات تصميم ستراتجية البنية الثابتة بعلاقة مرتبطة الى بنية ديناميكية بسيطرة وادارة تقانة ذكية ذاتية ، المشاريع الثلاث :

1- القصر البلوري لجوزيف باكستن

القصر البلوري ، هو مبنى ضخم ، بني في عام 1851 في (Hyde Parke) في لندن ، ليكون أول معرض عالمي ، صممه (Joseph Paxton) شكل [1].

ستراتجية البناء الشكلي المتبعة في تصميم القصر البلوري تتضمن التعامل مع البنية الثابتة فقط متجسدة باستطالة المبنى مع المحور جنوب– شمال لرفع الكسب الحراري كستراتجية التوجيه العام للمبنى الى جانب استخدام الاضاءة الطبيعية المباشرة عن السطوح المزججة الافقية والعمودية كما تتضمن ستراتجيات التبريد الذاتي بالاعتماد على اسلوب التبريد بالتهوية بتصميم مسارات تهوية أفقية الى جانب الافادة من الكسب المباشر عن السطوح الافقية والعمودية في التدفئة الذاتية جدول [5].وفيما يخص البنية الديناميكة فلم تكن موجودة كخطة فكرية وتطبيقية في تصميم المبنى الشمسي انذاك .

شكل [1] القصر البلوري لجوزيف باكستن

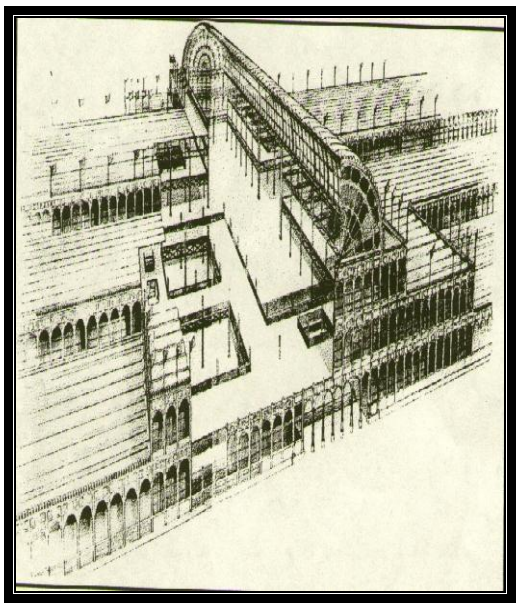

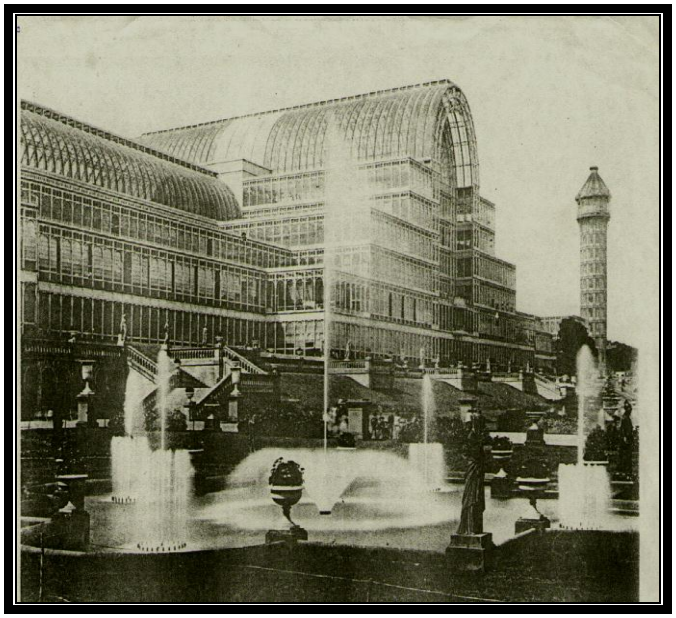

جدول [5] ستراتجيات البناء الشكلي للقصر البلوري [الباحث]

مناخ بارد	ستراتجية البناء الشكلي في العمارة الشمسية		
	ستراتجية تصميم البنية الثابتة للعمارة الشمسية		ستراتجية تصميم البنية الديناميكية للعمارة الشمسية
التجنب الحراري	التوجيه العام للمبنى	الاستطالة بالمبنى مع المحور جنوب–شمال لرفع الكسب الحراري	لايملك بنية متحركة
	الإضاءة الطبيعية	الاضاءة الطبيعية المباشرة عن السطوح المزججة الافقية والعمودية	
التبريد الذاتي	التبريد بالتهوية	تصميم مسارات تهوية أفقية	
التدفئة الذاتية	التدفئة بالكسب المباشر	الكسب المباشر عن السطوح الافقية والعمودية	

2– البيت الدوّار للمعمار روجرز (Revolving house)

البيت الدوار هومنزل المعمار رجرد فوستر في ولتن Wilton صممه سنة 1967،يمثل اولى محاولات تصميم المبنى المتحرك الكفوء للطاقة شكل [2].

يملك المنزل مخططا دائريا لتنظيم الفضاءات ضمن مستوى واحد ، المبنى مرفوع الى مسند مركزي مشيد من الكونكريت بسمك يختلف قرب القاعدة عنه قرب ارضية الفضاءات الداخلية المعلقة ، يخترق هذا المسند محور الحركة العمودية (الدرج)الحلزوني .

يملك المنزل صفة المبنى الديناميكي من خلال تصميمه للقاعدة المتحركة ضمن جزء وسطي منها يخترق سمك الارضية الكونكريتية للفضاءات الداخلية الذي يمثل سكة ملتفة حول الجزء العلوي من المسند الكونكريتي تسحب عناصر افقية تمتد قطريا الى محيط الفضاءات الى الخارج لتولد نوعين من الحركة : تشمل الاولى المبنى ككل بجعله يدور خلف الاشعة الشمسية لتفعيل الكسب المباشر شتاءاً . اما الحركة

الثانية فتشمل تحريك جزء من الواجهة الاسطوانية حول المحور الافقي اذ ان العناصر الافقية الممتدة قطرياً ترتبط بواجهة تمثل جزء من الاسطوانة الخارجية المكونة للقشرة الخارجية للمبنى تنزلق هذه الواجهة متحركا بسب ارتباطها المرن مع المنشأ لتمثل واجهة متحركة تعمل للتظليل من الحمل الحراري صيفا ،تزاح هذه الواجهة عن مسار الاشعة المباشرة المتوجهة نحو الفضاءات الداخلية لرفع الكسب الحراري شتاء،تعمل الواجهة المتحركة على تكوين نظام الجلد المزدوج الذي يعتمد وجود فجوة هوائية بين السطح الداخلي للواجهة المتحركة والسطح الخارجي لواجهة المبنى الذي يسخن عن الطاقة الحرارية المكتسبة عن الاشعة الشمسية المباشرة وغير المباشرة للواجهة المتحركة والتي تشعها ثانية الى هذه الفجوة الهوائية . توجد فتحات في الاعلى والاسفل من الجدارن الداخلية تعمل على توليد حركة هوائية air) movement)لان الهواء الساخن يرتفع ويصرف اعلى من منافذ تهوية مرتبطة بفجوة الحائط اما الهواء البارد يستخدم لتبريد الفضاءات الداخلية.

شكل [2] البيت الدوّار للمعمار رجرد فوستر

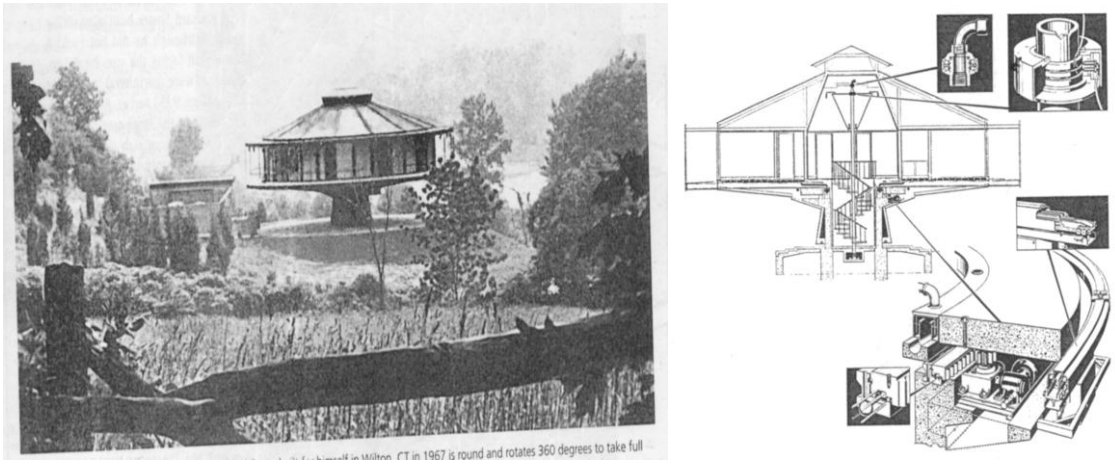

واستخدم في التكييف (الأرضية المعلقة raised floor) كنظام للتوزيع، جميع الهواء المضخ إلى الفضاء والخارج منه ، يتم عن طريق أجهزة وفتحات موجودة في هذه الأرضيات والنظام المستخدم هو نظام (الحجم المتغير + الحرارة الثابتة) ، فعند حدوث اختلاف في الكسب الحراري يتم تجهيز حجم متغير مع حرارة ثابتة من الهواء فضلا عن استغلال الماء كتبريد أولي في نظام التكييف كـ (Condenser coolant) ويضخ إلى أعلى المبنى باستخدام وحدات دفع الهواء تابع الجدول [6].

تتحدد ستراتجية البناء الشكلي في البيت الدوار بوجود بنية ثابتة واخرى ديناميكية الا انها لا تمتلك التحكم الذكي بوجود تقانة التحسس و الاستجابة والسيطرة الذاتية ضمن التطبيقات العملية للمباني الشمسية انذاك .

الاستراتجيات الثابتة ترتبط مع البنية الديناميكية وفق سيطرة وتحكم يدوي اذ انها لاتملك تقانة فهم صناعي مستعاض عنها بالتحكم اليدوي عن فهم الانسان للحالة البيئة والمتطلبات الانسانية كما لا تملك

تقانة تفكير صناعي مستعاض عنها بالتحكم اليدوي عن تفكير الانسان بالحلول الملائمة تبعا لفهمه الحالة البيئة اما تقانة الفعل الصناعي مستعاضا عنها بالتحكم اليدوي لاحظ الجدول [7] .

جدول [6] ستراتيجيات تصميم البنية الثابتة للبيت الدوّار [الباحث]

	المناخ حار جاف		
التجنب الحراري	ستراتيجيات التوجيه	توجيه المساحة السطحية المتضمنة المنفذ الشمسي توجيها مغايراً	الدوران حول محور عمودي
	ستراتيجيات التظليل	التظليل العام للمبنى	السقف المظلي
		تظليل الفتحات	الكاسرات الشمسية
			طبقة التظليل الداخلية
	ستراتيجيات الإضاءة الطبيعية	توظيف الإضاءة الجانبية الكبيرة	
	ستراتيجيات العزل الحراري	توظيف الكتلة الحرارية كعازل حراري	
		توظيف العازل الحراري ليحيط الكتلة الحرارية من الخارج	
		دمج العازل الحراري ضمن تجاويف الكتلة الحرارية	
		تغليف العازل الحراري للسطوح الداخلية للكتلة الحرارية	
	ستراتيجيات اختيار الألوان	استخدام الألوان المعتمة لتقليل معامل الانعكاس لسطح قشرة المبنى	
التبريد الذاتي	تصميم مسارات تهوية أفقية	استخدام المنافذ المباشرة لمنطقة هبوب الريح	
		التهوية الافقية للارضية برفعها عن الارض	
	تصميم مسارات تهوية عمودية	توظيف ملاقط الرياح	
		دمج ستراتيجيات التهوية والإضاءة والكسب الحراري	
التدفئة الذاتية	التدفئة بالكسب المباشر	الكسب المباشر عن الواجهات	استخدام الواجهة الجنوبية المزججة
			التحكم بتوجيه النوافذ
			التحكم بحجم النوافذ
			التنظيم الشريطي للفضاءات لتوفير منفذ شمسي مباشر لكل منها
		توظيف كتلة المبنى للكسب الحراري	توظيف جدار الخزن الحراري(THERMAL STORAGE WALL)
	الكسب الغير مباشر	ستراتيجية استخدام الجدار الحراري Trombe wall	دمج نظام الكسب المباشر والجدار الحراري Trombe wall
			استخدام العازل الحراري بين الجدار الحراري وطبقة الزجاج

جدول [7] ستراتيجيات تصميم البنية الديناميكية للبيت الدوّار [الباحث]

الارتباط مع ستراتيجيات البنية الثابتة	ستراتيجيات البنية الذكية		
	تقانة الفهم	تقانة التفكير	تقانة الفعل

تغير مستمر (تحكم يدوي)	لايملك تقانة فهم صناعي مستعاض عنها بالتحم اليدوي عن فهم الانسان للحالة البيئة والمتطلبات الانسانية	لايملك تقانة تفكير صناعي مستعاض عنها بالتحم اليدوي عن تفكير الانسان بالحلول الملائمة تبعا لفهمه الحالة البيئة والمتطلبات الانسانية	لايملك تقانة فعل صناعي مستعاض عنها بالتحم اليدوي

3- مركز جنزايمي الجديد (new genzimi center)

من الابنية كفوءة الطاقة التي تستخدم الانظمة المنتجة للطاقة الذاتية مبنى مكون من تسع طوابق ،تُخفّضُ إستراتيجياتُ التصميمِ الإضافيةِ وان إستعمالِ الطاقةِ اقل من خلال الاندماج مع الطبيعية باستخدام ستراتجيات التجنب الحراري بشكل مدروس وفق انظمة التصميم الكومبيوتري كحسابات للاشكال اعطت امكانية تحقيق اقل ما يمكن من فائدة لالستراتجيات التجنب الحراري ،الى جانب التصميم بنفس الاسلوب لاستخدام النظم الذاتية في التبريد ، ويظهر هذا الاندماج من خلال محاورته مع الطبيعة والإخضاع لأحكامها واستعمال رموز وعلاقات في عمارته – وإن كانت هذه الرموز والعلاقات هي غير واضحة ومبهمة ، الا انها اساس التنظيم المورفولجي للعمارة.

المبنى يعتمد كليا على الطاقة الذاتية بمعالجة ما يتطلب حاجة المبنى الى الطاقة من خلال توليد الطاقة الذاتية باستخدام النظم المنتجة للطاقة .

تعتمد منظومة تشغيل الية تعتمد وجود متحسسات ترتبط بالمنظومة تتحسس بوجود الانسان ضمن الفضاء وزخم وجوده وطبيعة فعاليته ضمن الفضاء ، اذ تمنحها البيانات على مدار اليوم ،من ثم تقوم هذه المنظومة بتزويد الفضاء بانارة ملائمة للفاعلية التي تتم داخل الفضاء والتي تتغير تبعا لتغير هذه الفعالية .

استخدم نظام هيكلي من الأعمدة والجسور والجدران الحاملة في بعض الأماكن ، ونظام الـ (Truss) في هيكل المظلات في الواجهة الخارجية فضلا عن الجدران الستائرية الحديدية مع الإملائيات الزجاجية ، وذلك نظراً لكتلية المبنى من جهة ، ومتطلبات الحركة التموجية للشكل الخارجي والتعامل مع الأنظمة المنشئية الجديدة من جهة أخرى .(الشكل3)

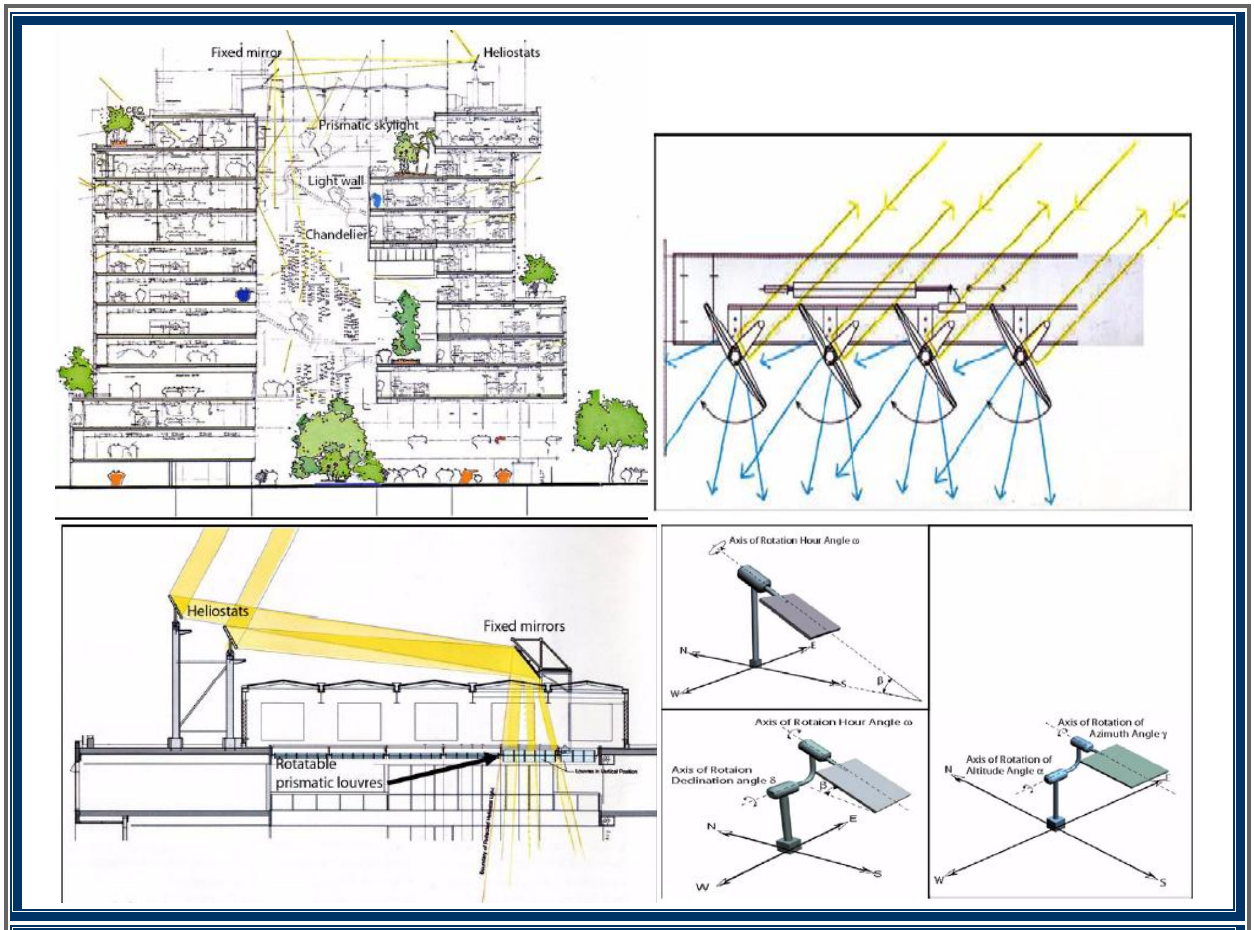

شكل [3] مركز جنزيوم يمتلك المتحسسات الضوئية في التي تكتسب بيانات التغير في زاوية وشدة الاشعة الشمسية لاعطاء الايعاز الى نظم ادارة حركة العواكس للحركة بالوضع المطلوب

استخدام هذه المواد وهذه الأنظمة المنشئية ، تتطلب الكثير من التمفصلات والتفاصيل ، هذه فضلا عن الاستخدامات الرمزية لتفاصيل (High-tech) جعلت من المبنى نموذجا معاصرا لافكار توظيف الانظمة المنتجة للطاقة خلال اوقات السنة من خلال حركة العواكس والكاسرات لتركيز الاشعة الى وحدات الكسب الشمسي من اجل تكثيف الاشعة وتوليد الحد الاعظمي للطاقة لادارة واكفاء حاجة المبنى المكون من تسع طوابق . استخدم المصمم مواد متنوعة في الهيكل والإنهاء، من استخدام جدران ستائرية من الزجاج والحديد في الواجهة .هذا فضلاً عن المظلات حديدية .

فيما تتحدد ستراتجية البناء الشكلي بوجود بنية ثابتة واخرى ديناميكية تمتلك التحكم الذكي بوجود تقانة التحسس و الاستجابة والسيطرة الذاتية ضمن التطبيقات العملية للمباني الشمسية انذاك لاحظ الجدول [9]الذي يحدد استراتجيات البنية الديناميكية .الى جانب الجدول [8]الذي يحدد ستراتجيات تصميم البنية الثابتة للعمارة الشمسية.

[8]ستراتجيات تصميم البنية الثابتة لمركز الجنازيوم الجديد [الباحث]

	مناخ حار جاف		
التجنب الحراري	ستراتجيات التوجيه	**تحديد الهدف من توجيه المبنى**	توجيه المبنى إلى الجنوب كتوجيه مثالي
	ستراتجيات التظليل	التظليل العام للمبنى	استخدام المظلة الأفقية لحماية الفناء الداخلي
		تظليل الفتحات	الكاسرات الشمسية
			طبقة التظليل الداخلية
			توظيف الرفوف الضوئية ضمن الفتحات
	ستراتجيات الإضاءة الطبيعية	التنظيم الشريطي للحصول على منفذ ضوئي لكل فضاء	
		استخدام الإضاءة السقفية في المباني	
		استخدام السطوح الأفقية الخارجية لعكس الأشعة إلى الفضاءات الداخلية	
		رفع معامل الانعكاس لقشرة المبنى الخارجية	
		تنطيق الفضاءات ضمن المستوى العمودي لتوفير الإضاءة الطبيعية	
	ستراتجيات العزل الحراري	توظيف الكتلة الحرارية كعازل حراري	
		توظيف العازل الحراري ليحيط الكتلة الحرارية من الخارج	
		دمج العازل الحراري ضمن تجاويف الكتلة الحرارية	
		تغليف العازل الحراري للسطوح الداخلية للكتلة الحرارية	
التبريد الذاتي	تصميم مسارات تهوية أفقية	استخدام المنافذ المباشرة لمنطقة هبوب الريح	
		توظيف الافنية الوسطية لخلق اظطراب هوائي يمثل منطقة ضغط عالي للهواء	
	تصميم مسارات تهوية عمودية	استخدام أنابيبDucts التحكم	
		دمج ستراتجيات التهوية والإضاءة والكسب الحراري	
التدفئة الذاتية	التدفئة بالكسب المباشر	الكسب المباشر عن الواجهات	استخدام الواجهة الجنوبية المزججة
			التحكم بتوجيه النوافذ
			التحكم بحجم التوافذ
			التنظيم الشريطي للفضاءات لتوفير المنافذ للشمسية المباشرة
		توظيف كتلة المبنى للكسب الحراري	توظيف جدار الخزن الحراري(Thermal storage wall)
	الكسب غير مباشر	ستراتجية استخدام الجدار الحراري Trombe wall	دمج نظام الكسب المباشر والجدار الحراري Trombe wall
			استخدام العازل الحراري بين الجدار الحراري وطبقة الزجاج

[9]ستراتجيات تصميم البنية الديناميكية لمركز الجنازيوم الجديد [الباحث]

	ستراتجيات البنية الذكية	
ستراتجية الادراك الصناعي (الفهم)	ادراك الحالة البيئيةِ	تقنية المتحسس الضوئي
		الماسح الضوئي للسماء
		بيانات القمر الصناعي
	فهم متطلبات الشاغلين	تقنية متحسس الاشغال
		تقنية السطح البيني
		وحدة البطاقة الذكية
ستراتجية التفكير الصناعي	تقنية البرامج الكومبيوترية	توظيف النظم الهجينة Hybrid systems
ستراتجية الفعل	منظومة الخلايا الضوئية	نظم المتصلة بالشبكة

المناقشة السابقة نجد ان التقانة المعاصرة تملك الاثر في تغيير بنية الشكل في العمارة الشمسية وستراتجياته ،من خلال أنماط التحولات التي تجرى على الشكل الديناميكي، وفق فعل معين بضوابط وقواعد التي بالإمكان إعادتها تكراراً . هذا المفهوم هو ما يعرف بالآلية (Mechanism) .

وان نوع الالية هي الية (التحول بالحركة)، بذلك تكون آليات متعددة ومتنوعة وقد تكون هناك آليات أخرى في عمليات التحول ، تعتمد على مهارة المصمم في تجربته التحولية . ويترك دور المصمم في الإقرار والاختيار النهائي لما يراه مناسباً مع الأنظمة الأخرى من جهة ونظام العمارة ككل من جهة أخرى من اجل تفعيل المبنى للاعتماد علة الطاقة الذاتية بنسبة اكبر ، فالأشكال المتجسدة عن البنية الثابتة للعمارة الشمسية والتي تمثل الشكل المثالي حتى وان كانت من الأجسام الأفلاطونية ، تملك قشرة ذكية ديناميكة ترفع من هذه النسبة اذا ما صممت وفق ستراتجيات تصميم البنية المتحركة ضمن المرحلة الثانية من تصميم العمارة الشمسية في الوقت المعاصر . تدمج البنيتين الى بعض لتوجد العناصر المتحركة نوعا من التغير من خلال المعالجة في أبعادها ، أو بإضافة عناصر أو الاقتطاع من هذه العناصر مع تغير هذه المعالجة مع الزمن

الاستنتاجات والتوصيات :

- توصل البحث الى تحديد ستراتجية تصميمية للعمارة الشمسية تم تسميتها ب (ستراتجية البناء الشكلي في العمارة الشمسية) ،والتي تمتلك هذه الاستراتجية مرحلتين اساس تعتمد الثانية على الاولى كقاعدة لنجاح العملية التصميمية ككل ،لتشكل وتوضح البنية الشكلية للعمارة . تتمثل المرحلة الاولى في (ستراتجية تصميم البنية الثابتة للعمارة الشمسية) اذ ان العمارة الشمسية هي ساكنة فيما عدا بعض الاجزاء النشطة والديناميكية فيها والتي تمتلك القدرة على الاستجابة والتكيف التي تمثل المرحلة الثانية من ستراتجيات البناء الشكلي للعمارة الشمسية الذي تم تسميته ب (ستراتجية تصميم البنية الديناميكية للعمارة الشمسية) ،تمثل التطور التقني لاستغلال الطاقة الشمسية في العمارة وتملك الاثر في تغير البنية الشكلية للعمارة من خلال سلسلة من العمليات (process) التحولية :
- **البنية الثابتة في العمارة الشمسية :** تتضح (البنية الثابتة) في العمارة الشمسية في العلاقة التي تربط (العمارة) مع (المناخ) و (امكانية الموقع) من خلال (الاستجابة التصميمية) .
- **البنية الديناميكية في العمارة الشمسية :** هو كل ما يتم إجراؤه (العمليات الاحيائية) للتقانة الذكية المتمثلة بثلاثية (الادراك والتفكير والعمل) مع التركيز على العناصر المادية المتجسدة بالعملية الاحيائية (العمل) ضمن تقانة الذكاء الصناعي والمتمثلة (بالتفاصيل المعمارية –التقنية) المتحركة كاستجابة للتغير في متطلبات الانسان تبعا للتغير في بيانات المحيط الخارجي.

- الالية: وهو مفهوم يتعلق بما تملك التقانة المعاصرة الاثر في تغيير بنية الشكل في العمارة الشمسية وستراتجياته ، من خلال انماط التحولات التي تجري على الشكل الديناميكي ، وفق فعل معين بضوابط وقواعد التي بالامكان اعادتها تكرارا.

لذا يوصي البحث بالاتي :

- تغيير النظر الى العمارة الشمسية كوجود مادي ثابت وساكن دائم ياخذ من حجمه المادي معيارا للمفاضلة والاختيار ، نحو التحول في التاكيد على القدرة على توفير المحيط الفيزيائي الملائم و المحفز الفكري للخلق و الابداع اساسا في التصميم بجميع اشكال وجودة التي تتعدى ما الفناه من ظهور ضمن موضوعة العمارة .
- اعتماد البنية الثابتة للعمارة كقاعدة اساسية لبناء العمارة الشمسية تتكامل اليها البنية المتحركة ضمن سياق الارتباط الجذري من اجل بناء عمارة مبدعة وناجحة، انسانية كهدف للظهور .
- ادخال مادة العمارة الشمسية كموضوع اساس ضمن الدراسة الاكاديمية في قسم العمارة وضمن محور البيئة يخصص له المنهج الكامل في الطرح والتقديم .
- البدء وبشكل مباشر في تاسيس مراكز للمعلومات في الاقسام الهندسية تكون مصدرا مباشرا في النشر المعرفي وتوليد لبنة اولية نحو الانتقال من الوسائل التقليدية في المعالجة و الطرح نحو الوسائل المتطورة .

المصادر :

I. الدجيلي، عمر عبد الصاحب علي علي (1999) : "الشكل والوظيفة في العمارة " اطروحة دكتوراه مقدمة الى كلية الهندسة \الجامعة التكنولوجيا .

II. الدراجي ، رنا مجيد (2006) : " ستراتجيات العمارة الشمسية ضمن البنية الثابتة والديناميكية لها " اطروحة ماجستير \كلية الهندسة المعمارية \جامعة بغداد .

III. رسول ، هوشيار قادر (2003):"العمارة والتكنولوجيا " اطروحة دكتوراه ،قسم الهندسة المعمارية ،كلية الهندسة ،جامعة بغداد.

IV. رزوقي،غادة(1996)"فكر الابداع في العمارة "،اطروحة دكتوراه،قسم الهندسة المعمارية ،كلية الهندسة ،جامعة بغداد .

V. سلفر ناتان (1978):"هندسة معمارية بدون مبان " في معنى المدينة ترجمة د.عادل العوا وزارة الثقافة والارشاد القومي، دمشق، سوريا.

VI. الكيالي ،عبد الواحد.الزهيري،كامل :"الموسوعة الساسية "

VII. نوبلر،ناثان(1987)حوار الرؤية –مدخل الى تذوق الفن والتجربة الجمالية "،ترجمة : فخريخليل،مراجعة جبرا ابراهيم جبرا،بغداد،دار المامون للترجمة والنشر.

VIII. هيك،وولتر &س.ك.كامبل(2000):"رؤية بيئية حول التنمية المستدامة"، بحث منشور ضمن دراسة تحت عنوان :"مبادئ التنمية المستدامة "–تحرير :ف.دوجلاس موستشيت – ترجمة : بهاء شاهين، الدار الدولية للاستثمارات الثقافية،القاهرة .

IX. Ably,D.F(2004):"Chapter 7- Promoting sustainable human settlement development" UN department of economic & Social Affairs, NY, الرابط الالكتروني لجهة النشر www.umich.edu/nppcpub/resources.html

X. Andersen ,Inger(2000):"AMulti criteria decision –Making Method for solar building design "thesis doctoral of science in architectural studies<the university of science and technology faculty of architecture.

XI. Bratati,Biswas(1994): "*Sensitivity Analysis Energy Responsive –Design*" thesis master of science in architectural studies, New Jersey Institute of technology.

XII. Denholm, Paul L(2004): "*Environmental and policy analysis of renewable energy enabling technologies*" thesis master of science in architectural studies of Wisconsin university.

XIII. Norbert lechner (2001) : "*heating, cooling lighting*" design Methods for architect, Wiley, john; and sons, Newyork, Inc., second edition.

XIV. Rush, Richard D.(1986): "*The building systems integration hand book*" the American institute of Architects, John Wiley & Sons, Yew York.

COUPLED FINITE ELEMENT ANALYSIS OF A DAM-RESERVOIR SYSTEM UNDER DYNAMIC LOA*DING*

Omar al-Farouk Salem Al-Damluji
Assiatant Professor and Head
Department of Civil Engineering,
University of Baghdad, Iraq.

Akram Younis Thannon Al-Sa'aty
Professor,
Department of Achitecture,
University of Mosul, Iraq.

Rafi' Mahmoud Sulaiman Al-Nu' aimi
Formerly Postgraduate Student,
Department of Civil Engineering,
University of Baghdad, Iraq.

ABSTRACT

This investigation presents a coupled analysis of a dam-reservoir problem which includes all aspects of fluid-structure interaction (*class I coupling*) and soil-pore fluid–structure interaction (*class II coupling*) under earthquake excitations using the finite element method. The analysis involves the compressibility of water, the flexibility of the dam, the earthquake excitation, the structural damping and the material nonlinearity on the response.

An efficient computer program in FORTRAN is developed for this analysis from the original computer code named MIXDYN. The new software for predicting and analyzing the coupled behaviour is established using *the pressure formulation* for modelling of fluid and the *u-p formulation* for modelling of soil-pore fluid behaviours. Also, the program prepared is provided with post-processing routines to plot the original and deformed meshes of the problem.

A staggered partitioned solution technique for coupled field problems is implemented and used in the computer code. This scheme is incorporated in terms of sequential execution of single-field analyzers. The Drucker Prager model is used to simulate the behaviour of the soil and concrete. Implicit-Implicit Newmark's scheme with a predictor-corrector algorithm is employed for time integration of the equations of motion. The capability and efficiency of the model are found to be very useful when applied on a dam-reservoir system.

الخلاصة :

يقدم هذا البحث تحليلاً مزدوجاً لمسألة سد مع خزان و الذي يتضمن كافة اوجه التفاعل المتبادل مابين المائع و المادة الصلبة (ازدواج من الصنف الاول) فضلاً عن تفاعل متبادل ما بين التربة و مائع المسام و المادة الصلبة (ازدواج من الصنف الثاني) تحت تأثيرات هزة ارضية باستخدام طريقة العناصر المحددة. يتضمن التحليل انضغاطية الماء و قابلية تكيف السد و الهزة الارضية و الاخماد الانشائي و لا خطية المادة من خلال تأثيرها على الاستجابة.

لقد تم تطوير برتامج حاسوبي باستخدام لغة فورتران خاصة بهذا التحليل من برنامج MIXDYN الحاسوبي. لقد تم التحقق من البرامجيات المستحدثة من خلال توقع و تحليل التصرف المزدوج باستخدام معادلة الضغط لتمثيل المائع و معادلة u-p لتمثيل التربة مع مائع المسام. لقد تم تحضير خوارزميات ما بعد المعالجة لرسم التقسيمات الاصلية و ما بعد التشوه للمسألة. لقد تم تضمين و استخدام طريقة حل التقسيم المتعرج لحل مسائل الوسط المزدوج في البرنامج الحاسوبي المطور. لقد تم اضافة هذه الطريقة بدلالة التنفيذ المتناوب لتحليلات الاوساط المنفردة. لقد تم استخدام طريقة دروكر بريكر لتمثيل تصرف التربة و الخرسانة. كما تم استخدام طريقة نيومارك الضمنية – الضمنية مع خوارزمية التوقع– التصحيح للتكامل الزمني لمعادلات الحركة. لقد وجد ان امكانية و كفاءة النموذج عالية جداً عند تطبيقها على نظام سد مع خزان.

KEYWORDS
coupled analysis, dam-reservoir, finite element method, u-p formulation.

INTRODUCTION

The dynamic analysis of soil-fluid-structure interaction includes all aspects of both fluid and solid mechanics (i.e., fluid-structure interaction (*class I coupling*) and soil-pore-fluid interaction (*class II coupling*)). In a fluid-phase, the viscosity of the fluid, the magnitude of the gradient of the velocity field throughout the flow and whether the fluid is (*compressible or incompressible*), depending on whether density variations are large or small, play a key role in choosing the kind of formulation to be used. However, in the solid-phase, the time scale and the solver algorithm to be used depend on the loading rate and the permeability of the porous medium. *Traditionally, fluid problems can be classified into two categories: (i) non-flow problems, such as impounded water in a reservoir, tank, etc. and (ii) flow problems, such as free surface flow, flow around an airfoil etc...*

In this study, the former type of problems is considered. The second class of problems to be considered here lies between the undrained and drained extremes where dynamic loading is applied and transient pore fluid motion is significant (Simon et al. [36]). The undrained analysis is possible when relatively rapid loads are applied and permeability is low, i.e., where the load rate is greater than the pore fluid diffusion rate. Otherwise, drained analysis is possible for situations with a relatively slow loading and high permeability, i.e., where the load rate is less than the pore fluid diffusion rate. *Consequently, the problem to be solved in this research is a triple interaction: fluid-structure-soil pore fluid.*

Fluid-Structure Interaction (Class I Coupling):

The dynamic interaction between an elastic structure and a fluid has been the subject of intensive investigations in recent years, e.g. ([10], [11], [21], [22], [32] and [35]). Since analytical solutions procedures are available only for very simple problems, numerical approaches, which can be formulated in the time or frequency domains, had to be employed, e.g. ([15], [17], [19], [27], [33] and [34]).

Many researchers have attempted to derive variational functionals for different classes of fluid-structure interaction problems. The size of the coupled fluid-structure interaction problem is generally large. That is why attempts were made to reduce the problem size in different ways

Out of all the works done in the area of developing a finite element method for fluid-structure interaction problems, two approaches predominate. The *first approach* is the displacement-based method where the displacements are the nodal variables in both the fluid

and the structure. Bathe and Hahn [3], Belytschko [4], Belytschko and Kennedy ([5] and [6]), Chopra et al [9] and Nitikitpaiboon and Bathe [24] described the method in detail. This approach is not well suited for problems with large fluid displacements. Another difficulty with this method is that special care must be taken to prevent zero-energy rotational modes from arising. In the *second approach*, the potential-based method, displacements remain the nodal variables in the structure, while velocity potentials or pressures are the unknowns in the fluid. Everstine [12], Everstine and others ([13] and [14]), Hamdi et al. [16], Morand and Ohayon [23], Ohayon and Valid [25], Olson and Bathe ([26] and [28]) and Zienkiewicz and others ([38], [39] and [42]) demonstrated techniques for formulating finite elements using potential-based methods. In all these works, only a linearized version of the problem has been considered.

Several finite element studies have considered the gravity and free surface effects along with the fluid structure interaction.

SOIL-PORE FLUID-STRUCTURE INTERACTION (CLASS II COUPLING):

Soils are multiphase materials exhibiting a strong mechanical coupling between the solid skeleton and the fluid phase. This coupling can be particularly strong in the case of saturated soils of low permeability and under fast transient or dynamic loading, where the pore pressure plays a significant role. The first successful attempt to develop a model for solid skeleton-pore fluid interaction was due to Biot [7 and 8] for linear elastic materials. This work was followed by further development at Swansea University, where Zienkiewicz and others ([41], [43], [44], [45], [46] and [47]) extended the theory to non-linear materials and large deformation problems.

Zienkiewicz [37] described extensively several kinds of coupled problems and their numerical solutions with some applications. The analysis of coupled soil-pore fluid interaction during an earthquake shock applied to a dam shows that the non-linear soil response causes a pore pressure build up and failure of the actual structure.

Park and Felippa [30] reviewed several developments of computational procedures for solving coupled field problems with emphasis on stabilization of partitioned analysis. It was found that the resulting matrices after semi-discretization are not symmetric. The non-symmetry in the coefficient matrices often induces *conditional stability* of partitioned solutions and, therefore, stabilization at the differential equation level before attempting to implement a partitioned solution procedure is necessary.

The behaviour of multiphase flow in deforming porous media is of interest in engineering problems such as the simultaneous flow of three immiscible fluids; e.g. gas, oil and water through a tar sand formation during the bitumen recovery process, with environmental studies, etc.. For most cases of fluid transport in soil, two or more fluid phases are present simultaneously in the pores and are separated from one another by interfaces. Li and Zienkiewicz [20] developed a numerical procedure for modelling the behaviour of porous media interacting with the flow of multiphase immiscible fluids based on Biot's theory and the principle of effective stress. The displacement of the solid, pressure and saturation of the wetting fluid were taken as primary unknowns of the model. Unconditionally stable direct and staggered solution procedures were used for the time domain while the numerical solution of the coupled finite element equations were set with u-p_w-S_w form and discreteized by Galerkin's method.

Fluid Formulations:

Various formulations are generally used for inviscid fluid fields. The most common formulations for non-flow problems are the *displacement, displacement potential, velocity potential and pressure formulations.* In finite element analysis, the displacement formulation gives rise to two or more variables compared with one in the other formulations (Paul, [31]). Therefore, in this work, the *pressure formulation* is used because it results in fewer unknowns.

PRESSURE FORMULATION:

Governing Equation of Motion:

The equation governing fluid motion is the well-known wave Equation (Joseph [18]):

$$\nabla^2 P + \xi' \nabla^2 \dot{P} = \ddot{P}/c^2 \quad \text{(Linearized-Navier-Stokes Equation)} \quad (1)$$

where: $\xi' = 4\mu'/3\rho_f c^2$, μ' = the dynamic viscosity of fluid and $c^2 = K/\rho$.

For an inviscid fluid, Equation (1) reduces to:

$$\nabla^2 P = \ddot{P}/c^2 \quad (2)$$

Boundary Conditions:

(i) At moving boundaries (at interface with solid) where the fluid has a normal acceleration, $\ddot{u}_n$, **n** being the direction of the unit normal to the boundary, the pressure gradient can be expressed as:

$$\partial P/\partial \mathbf{n} = -\rho_f \ddot{u}_n \quad (3)$$

At fixed boundaries; $\partial P/\partial \mathbf{n} = 0$.

(ii) At a free surface with surface waves (considering only primary waves):

$$P = \rho_f g u_y \quad \text{or} \quad \partial P/\partial y = \ddot{p}/g \quad (4)$$

At a free surface without surface waves: P = 0.

(iii) At radiating boundaries, the condition for no reflection of pressure waves can be expressed as:

$$\partial P/\partial \mathbf{n} = -\dot{P}/c \quad (5)$$

where: **n** = the direction of the unit normal at the radiating boundary.

Fluid Isoparametric Element:

The fluid domain is usually represented by finite elements in Cartesian coordinates. The number of nodes may be variable (4-9) in two dimensions, with one degree of freedom per node inside the fluid domain. This degree of freedom is the value of the pressure P at the nodes. At the free surface, the element has an extra translational degree of freedom to accommodate the free surface motion. This element enforces the continuity (equilibrium in solids) equation along the mesh domain. The applied forces represent the water pressure (unit volume per second) at this node. The positive pressure is in-pressure and the negative one is out-pressure. For global equilibrium, the in-pressure must equal to the out-pressure. At the boundaries, only the normal velocity may be specified because the tangential velocity does not affect the pressure. The nodal equilibrium is satisfied if the sum of the water pressure increments at the node is equal to the total applied pressure.

Fluid-Structure Interaction (Pressure Formulation):

The structure and fluid are together idealized as a two dimensional system subjected to support excitations both in the horizontal and vertical directions and the equations of motion

can be expressed, after spatial discretization, by two sets of second order coupled differential equations. The fluid can be modeled using any of the various formulations mentioned before. However, in this study, only the *pressure formulation* is used in which the coupled fluid-structure equations can be expressed as:

$$\underline{M}_s \ddot{\underline{u}} + \underline{C}_s \dot{\underline{u}} + \underline{K}_s \underline{u} = \underline{f}_s - \underline{M}_s \ddot{\underline{d}} + \underline{L}\, \underline{P} \quad \text{.....(6)}$$

$$\underline{M}_f \ddot{\underline{P}} + \underline{C}_f \dot{\underline{P}} + \underline{K}_f \underline{P} = \underline{f}_f - \rho_f \underline{L}^T (\ddot{\underline{u}} + \ddot{\underline{d}}) \quad \text{.....(7)}$$

where:

$$\underline{M}_s = \int_\Omega \underline{N}_u^T \rho \underline{N}_u d\Omega \quad \text{.....(8a)}$$

$$\underline{C}_s = \alpha\, \underline{M}_s + \beta\, \underline{K}_s \quad \text{.....(Rayleigh Damping).....(8b)}$$

$$\underline{K}_s = \int_\Omega \underline{B}^T \underline{D}_T \underline{B} d\Omega \quad \text{.....(8c)}$$

$$\underline{f}_s = \int_{\Gamma u} \underline{N}_u^T \underline{t}\, d\Gamma + \int_\Omega \underline{N}_u^T \rho\, \underline{b}\, d\Omega + \int_\Omega \underline{B}^T \underline{D}^T d\underline{\varepsilon}^o d\Omega \quad \text{.....(8d)}$$

$$\underline{L} = \int_\Omega \alpha_c \underline{B}^T \underline{\delta}\, \underline{N}_p d\Omega \quad \text{.....(8e)}$$

$$(\underline{M}_f)_{ij} = \int_{\Gamma F} \underline{N}_{pi}\, 1/g\, \underline{N}_{pj}\, d\Gamma + \int_{\Omega F} \underline{N}_{pi}^T\, 1/c^2\, \underline{N}_{pj}\, d\Omega \quad \text{.....(8f)}$$

$$(\underline{C}_f)_{ij} = \int_{\Gamma R} \underline{N}_{pi}^T\, 1/c^2\, \underline{N}_{pj}\, d\Gamma \quad \text{.....(8g)}$$

$$(\underline{K}_f)_{ij} = \int_{\Omega F} (\nabla \underline{N}_{pi})^T (\nabla \underline{N}_{pj})\, d\Omega \quad \text{.....(8h)}$$

$$(\underline{L}^T)_{ij} = \int_{\Gamma I} \underline{N}_{ui}^T\, n\, \underline{N}_{pj}\, d\Gamma \quad \text{.....(8i)}$$

and $\underline{N}_p$ and $\underline{N}_u$ are the shape functions used for pore pressure and solid skeleton, respectively. α and β are Rayleigh damping constants, Ω is the domain, Γ is the boundary surface, $\underline{B}$ is the strain-displacement matrix and t is the surface traction.

Pore Fluid–Solid Interaction (u-p Formulation):

When the seepage velocity relative to the solid skeleton is small compared with the motion of the solid skeleton or if the permeability is low, the relative acceleration of the fluid with respect to the solid can be neglected. With this approximation (i.e., neglecting the $\ddot{\mathbf{w}}$ term) and replacing the unknown w with the pressure P, the equilibrium equation of the fluid can be rewritten as (Paul [31]):

$$\dot{\underline{w}} = -k \underline{\nabla} P + k\rho \underline{b} - k\rho \ddot{\underline{u}} \quad \text{.....(9)}$$

which can be used to eliminate w from the continuity equation. Upon discretization, it is possible to write:

$$\underline{u} = \underline{N}_u \underline{u} \quad \text{.....(10)}$$

$$\underline{P} = \underline{N}_p P \quad \text{.....(11)}$$

and using the standard Gelerkin method, the resulting equations can be expressed as:

$$\underline{M}_s \ddot{\underline{u}} + \underline{C}_s \dot{\underline{u}} + \underline{K}_s \underline{u} = \underline{f}_s - \underline{M}_s \ddot{\underline{d}} + \underline{L}\, \underline{P} \quad \text{.....(12)}$$

$$\underline{C}_P \dot{\underline{P}} + \underline{K}_P \underline{P} = \underline{f}_P - \underline{L}^T \dot{\underline{u}} + \hat{\underline{M}} \ddot{\underline{u}} \quad \text{.....(13)}$$

where:

$$\underline{M}_s = \int_\Omega \underline{N}_u^T \rho \underline{N}_u d\Omega \quad \text{.....(14a)}$$

$$\underline{C}_s = \alpha\, \underline{M}_s + \beta\, \underline{K}_s \quad \text{.....(Rayleigh Damping).....(14b)}$$

$$\underline{K}_s = \int_{\Omega} \underline{B}^T (\underline{D}_T + \alpha_c^2 \delta.Q.\delta^T) \underline{B}.d\Omega \quad (14c)$$

$$\underline{f}_s = \int_{\Gamma u} \underline{N}_u^T \underline{t}\, d\Gamma + \int_{\Omega} \underline{N}_u^T \rho\, \underline{b}\, d\Omega + \int_{\Omega} \underline{B}^T\, \underline{D}^T d\underline{\varepsilon}^o\, d\Omega \quad (14d)$$

$$\underline{L} = \int_{\Omega} \alpha_c\, \underline{B}^T\, \underline{\delta}\, \underline{N}_p\, d\Omega \quad (14e)$$

$$\underline{C}_p = \int_{\Omega} \underline{N}_P^T\, 1/Q\, \underline{N}_p\, d\Omega \quad (14f)$$

$$\underline{K}_p = \int_{\Omega} (\nabla \underline{N}_P)^T\, k\, (\nabla \underline{N}_p)\, d\Omega \quad (14g)$$

$$\underline{f}_p = \int_{\Gamma p} \underline{N}_P^T\, P\, d\Gamma + \int_{\Omega} (\nabla \underline{N}_P)^T\, k\, \rho_f\, \underline{b}\, d\Omega \quad (14h)$$

$$\underline{L}^T = \int_{\Omega} \alpha_c\, \underline{N}_p^T\, \underline{\delta}\, \underline{B}\, d\Omega \quad (14i)$$

$$\hat{\underline{M}} = \int_{\Omega} (\nabla \underline{N}_P)^T\, k\, \rho_f\, \underline{N}_u\, d\Omega \quad (14j)$$

In this study, this formulation is implemented and used in the computer program.

Staggered Solution for Coupled–Field Problems:

Many engineering problems involve two or three fields, such as soil-structure interaction, fluid-structure interaction, soil-fluid-structure interaction, etc…Such problems are generally partitioned into well defined fields which are distinct in behaviour, material model or solution technique. These fields are linked continuously together through two-way interaction with other fields. Each field may be coupled (totally or partially) with all the other participating fields or with only few of them (at interfaces via the contact boundaries only).

The concept of staggered solution can be organized in terms of sequential execution of single-field analyzers. This leads in the nodal based implicit-explicit partitioning of time stepping, to a complete solution of the explicit scheme independently of the implicit one and then using the results to progress with the implicit partition. This approach offers several advantages over the field elimination and simultaneous solution approaches as follows:
(1) Completely different methodologies could be used in each part of the coupled system. (2) Independently developed codes dealing effectively with single systems could be combined. (3) Parallel computation with its inherent advantages could be used. (4) The time step size restrictions can be excluded from consideration. (5) In systems of the same physics, efficient iterative solvers could easily be developed. (6) This approach permits decoupling of high frequency and low frequency components of a single system, so that an alternative time marching algorithm can be used in each part (Zienkiewicz and Taylor [40]). Finally, (7) it turns out to be unconditionally stable with a predicted (approximate) value of u at $t+\Delta\mathbf{t}$ and with suitable integration formulae for each set of equations of motion (Li and Zienkiewicz [20]. *Therefore, in the present study, the staggered partitioned solution scheme for a coupled field problem as shown in Figure (1) is implemented and used in the computer code.*

NUMERICAL ALGORITHM:

Based on the procedures and equations described, a coupled dynamic finite element algorithm is developed from the original uncoupled code MIXDYN (Owen and Hinton [29]) by the name DCAPII (Al-Nu'aimy [1]). It is also an extension of the computer code DCAPI

developed by Al-Shereffi [2] under the supervision of al-Damluji. DCAPII includes classes I and II couplings presented above.

Numerical Example: Dam-Reservoir System:

The Koyna concrete gravity dam-reservoir system (India) is analyzed with all the aspects of fluid-structure interaction (*class I coupling*) and soil-pore fluid interaction (*class II coupling*). The shape and dimensions of this dam-reservoir system are shown in Figure (1). The material properties of the system are taken from Paul [31] and listed in Table (1). The analysis involves the compressibility of water, the flexibility of the dam, the structural damping, the earthquake excitations and structural nonlinearity on the response. *This problem*

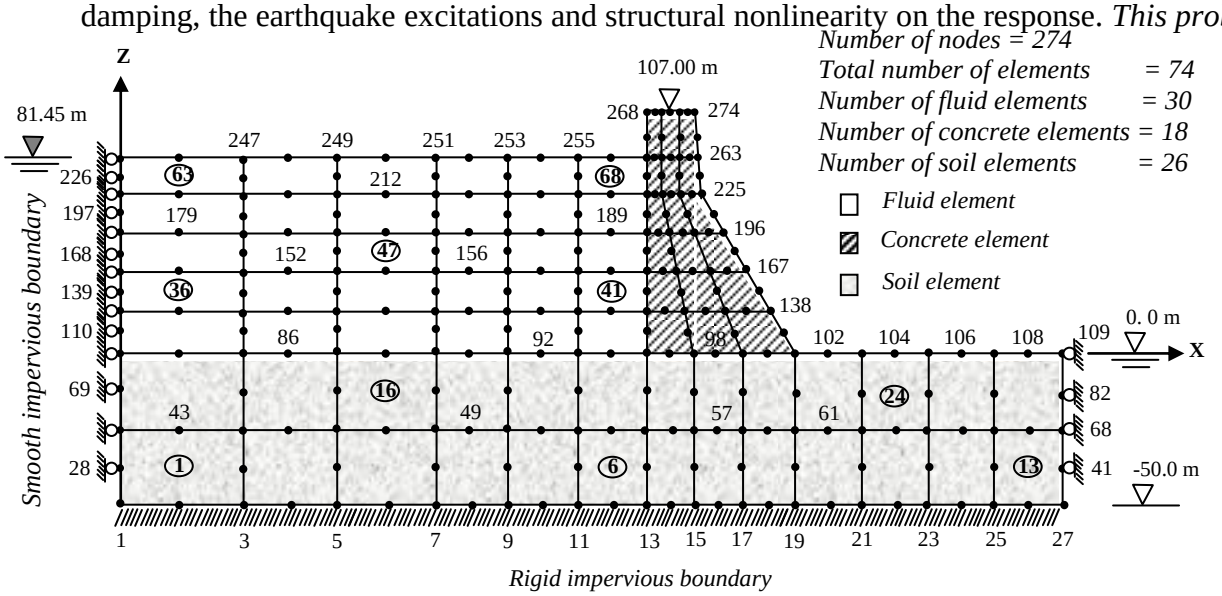

Figure (1): Koyna dam-reservoir system (India).

Table (1): Dimensions and properties of Koyna dam-reservoir system (from Paul, [31]).

Material and Property	***Value***
1. Dam (concrete)	
Height of dam above foundation (m).	107.00
Depth of reservoir (m).	81.45
Young's modulus of concrete, E_c (T/m^2)	3164000.0
Poisson's ratio of concrete, υ_c	0.20
Density of concrete, ρ_c (T/m^3)	2.690
2. Soil (rock)	
Young's modulus of soil, E (T/m^2)	1800000.0
Poisson's ratio of soil, υ_s	0.20
Density of soil, ρ_s (T/m^3)	1.830
3. Fluid (water)	
Compressibility of water, c (m/sec)	1439.0
Density of water, ρ_f (T/m^3)	1.000

The ratio of fundamental periods of reservoir to the dam: $\gamma_T = (T_f)$ reservoir/ (T_f) dam	0.566

is solved by Paul [31] as a fluid-elastic structure interaction (i.e., with class I coupling) only. The eight node isoparametric element is adopted for both the solid and fluid phases as shown in Figure (1). The boundary conditions are as depicted in the figure.

RESULTS AND DISCUSSION:

Effect of Water Compressibility:

For this study, the rigid Koyna dam is subjected to a horizontal Heaviside unit base excitation. The velocity of water is taken as a measure of water compressibility ($K = c^2 \rho_f$). Figure (2) shows the pressure distribution for cases with *incompressible* and *compressible* water. It is observed that as the velocity of water is increased from 1c to 4c, the peak hydrodynamic force does not change significantly. But, there is a shift in the occurrence of the peak force. The ratio of the peak hydrodynamic pressure to the hydrostatic force is 0.15 for the compressible water (at 1c) when compared with the incompressible one. This implies that the compressibility of water has a significant effect on the distribution of pressure on the rigid dam.

EFFECT OF DAM FLEXIBILITY:

Again, the rigid Koyna dam is subjected to a horizontal Heaviside unit base excitation. The pressure distribution for several cases of dam-foundation flexibilities are shown in Figure (3). For the case of dam on a flexible foundation, as the flexibility of the dam system increases (by decreasing its modulus of elasticity), the hydrodynamic force or the pressure distribution on the face of the dam also increases. The maximum effect is obtained when both the dam and the foundation are most flexible. Conversely, when the dam is rigid, foundation flexibility is not so important.

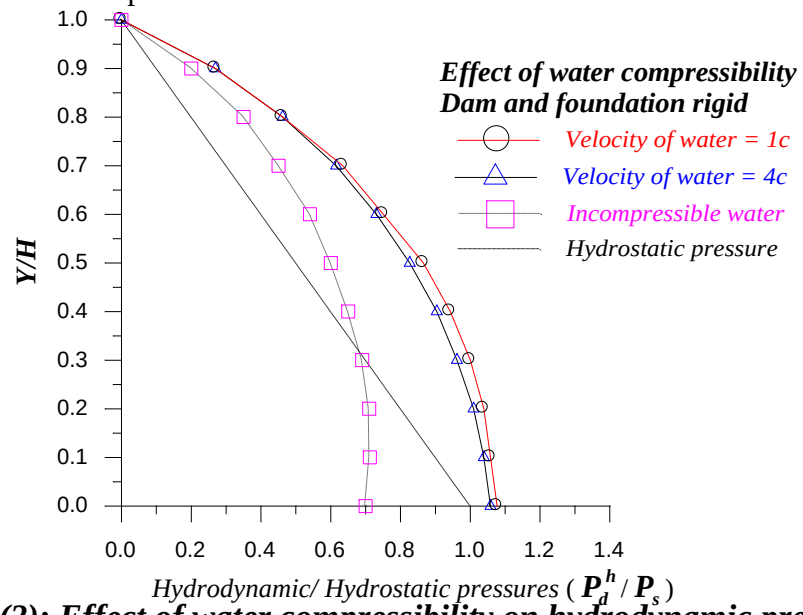

Fig (2): Effect of water compressibility on hydrodynamic pressure distribution due to a Heaviside unit base excitation.

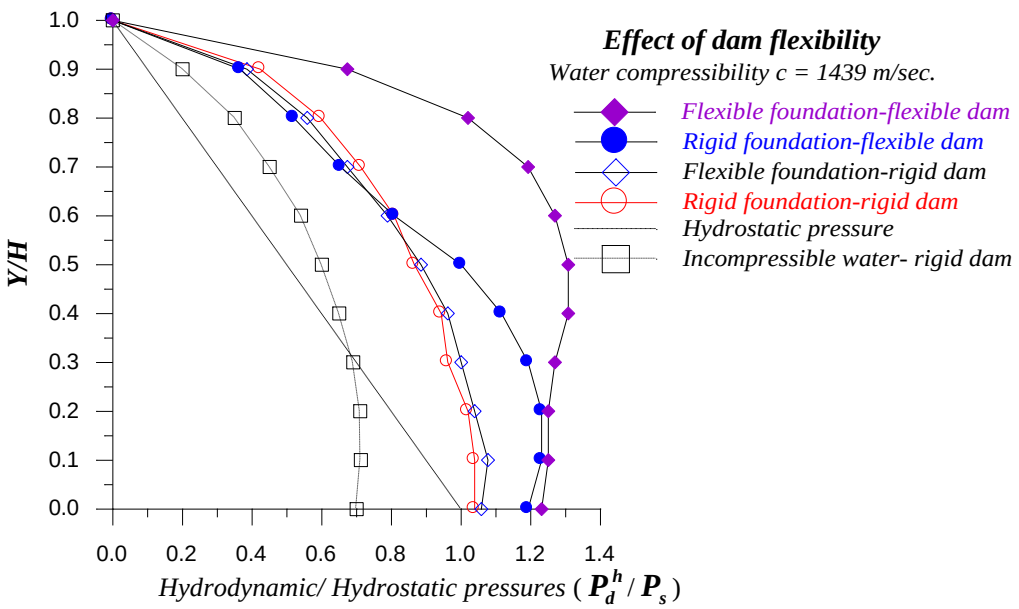

Fig (3): Effect of dam flexibility on hydrodynamic pressure distribution due to a Heaviside unit base excitation.

The peak hydrodynamic force is given in Table (2). This table shows that as the flexibility increases, the response also increases.

Table (2): Effect of dam flexibility on hydrodynamic pressure distribution due to a Heaviside unit base excitation.

Response Description	***Fexible Foundation***	***Rigid Foundation***			
	$\bar{E}$ = 1E	$\bar{E}$ = 1E	$\bar{E}$ = 2E	$\bar{E}$ = 4E	$\bar{E}$ = ∞
P^h_d/P_s	1.360	--	0.505	0.500	0.395

EFFECT OF EARTHQUAKE EXCITATION:

For this study, three different earthquakes each with different ground motion characteristics are considered as shown Figure (4a-e).

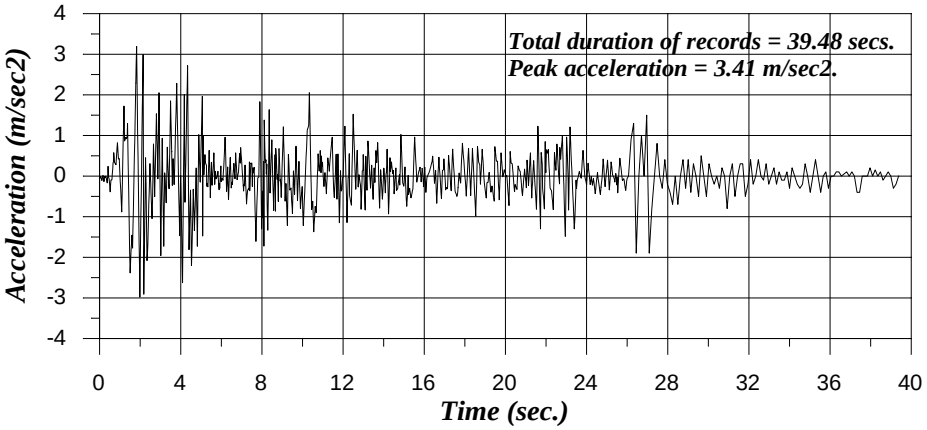

(a) Transverse component of El-Centro earthquake of May 1940.

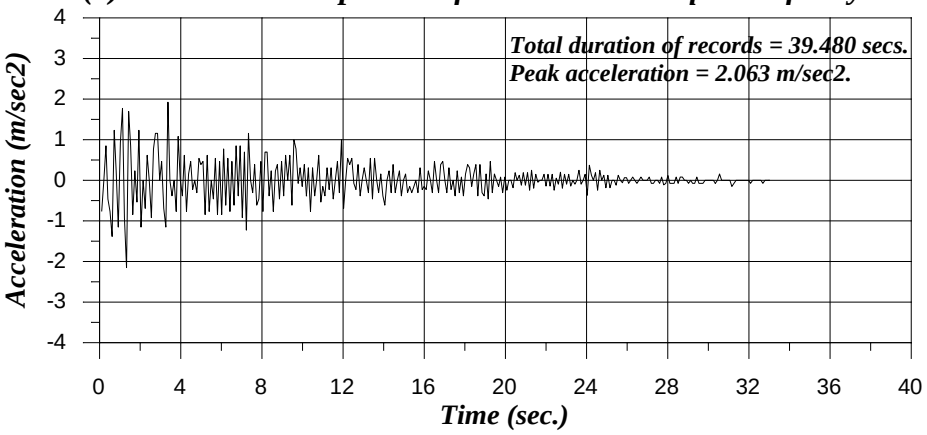

(b)Vertical component of El- Centro earthquake of May 1940.

Fig (4): Earthquakes (from Paul, [31]).

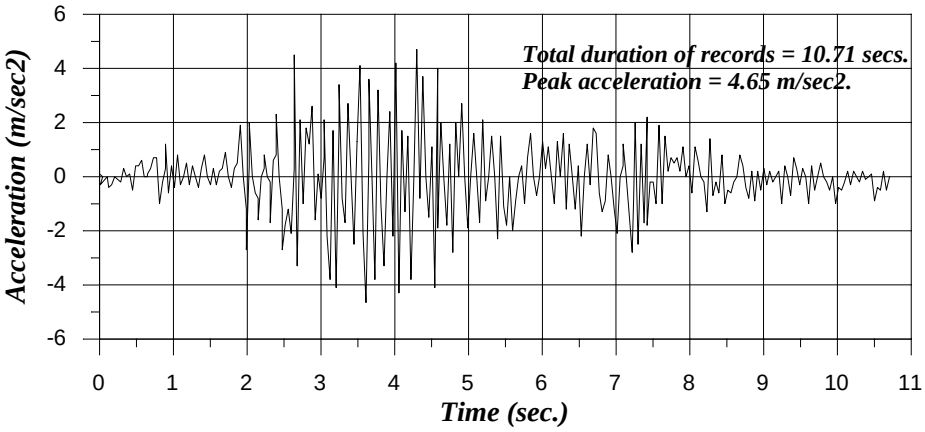

(c) Transverse component of Koyna earthquake of Dec., 1967.

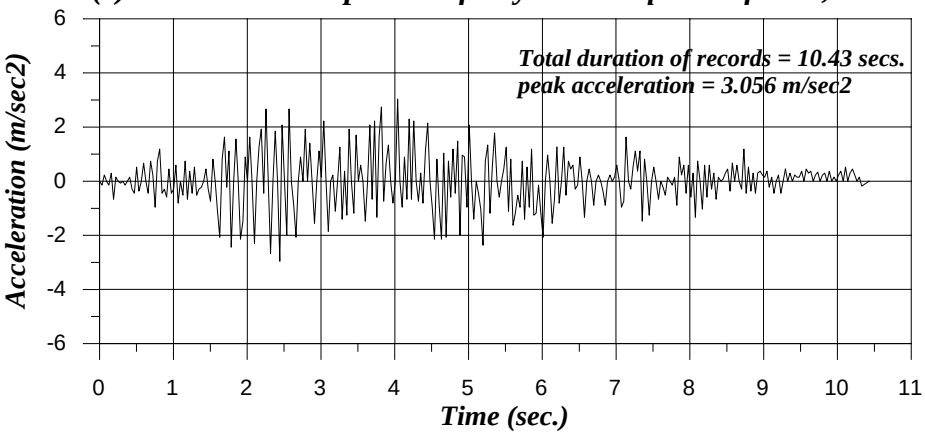

(d) Vertical component of Koyna earthquake of Dec., 1967.

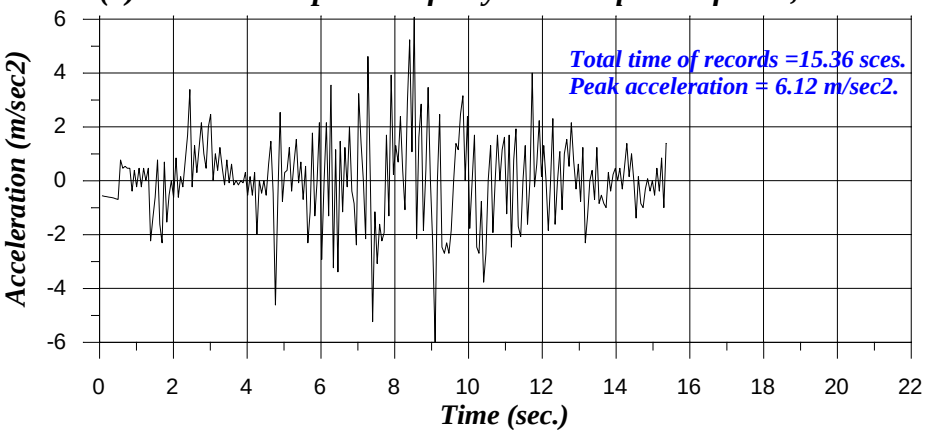

(e) San-Fernando earthquake N18E component Feb., 1971.

Figure (4): Continued

The undamped response (0 % damping) of the crest displacement (element 72), the stress at the dam heel (element 33) and the hydrodynamic pressure at the base of the dam (elements 33, 34 and 35) when subjected to both transverse and vertical components of either the El-Centro or Koyna or San Fernando earthquakes, simultaneously are shown in Figures (5), (6) and (7), respectively. It is noticed that the response characteristics are very much dependent on the type of earthquake excitation. This is because of the strong interaction between the impounded water and the foundation when the vertical component of the earthquake is considered in comparison with that due to only the transverse component of earthquake. The peak responses of the dam for various earthquake (transverse and vertical) excitations are summarized in Table (3).

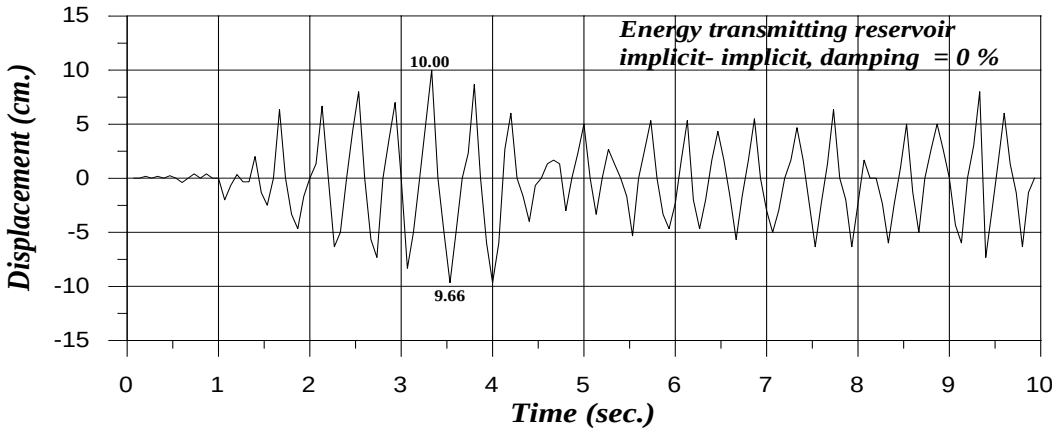

(a) El-Centro earthquake.

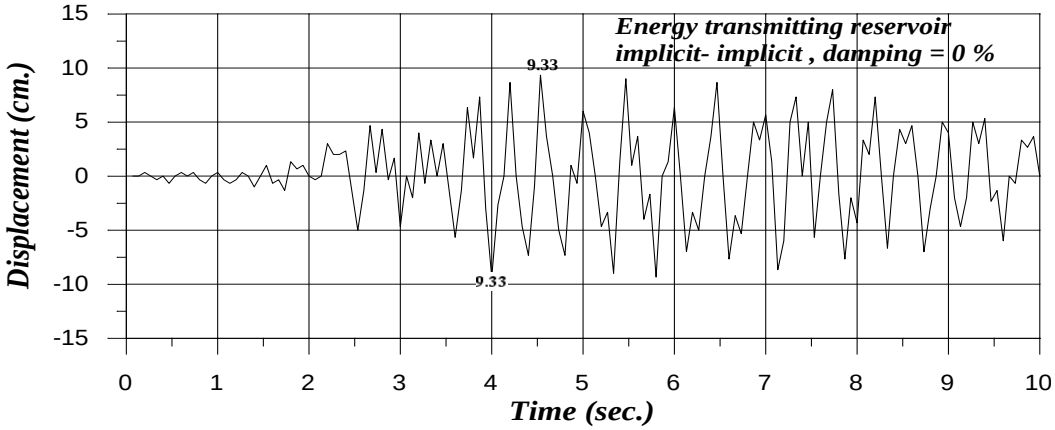

(b) Koyna earthquake.

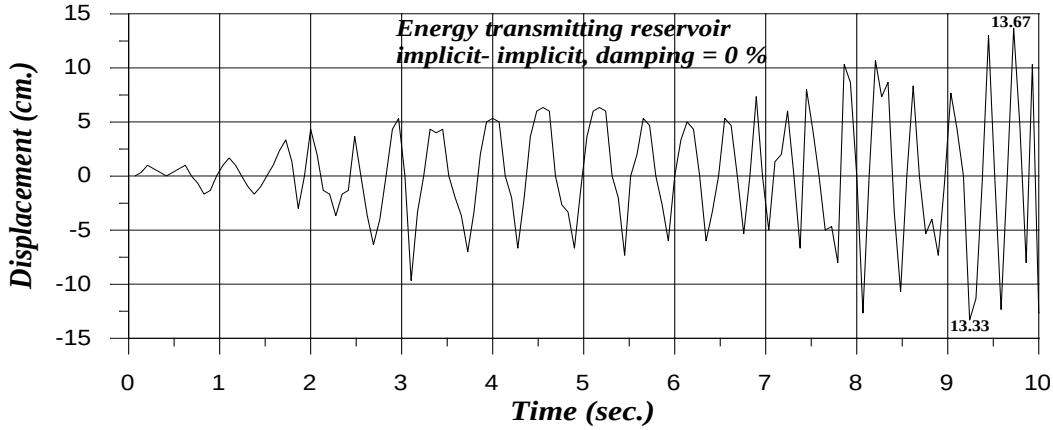

(c) San-Fernando earthquake.

Note : 1cm = 10 mm.

Figure (5): Response of dam crest displacement when subjected to various earthquakes (transverse and vertical) excitations.

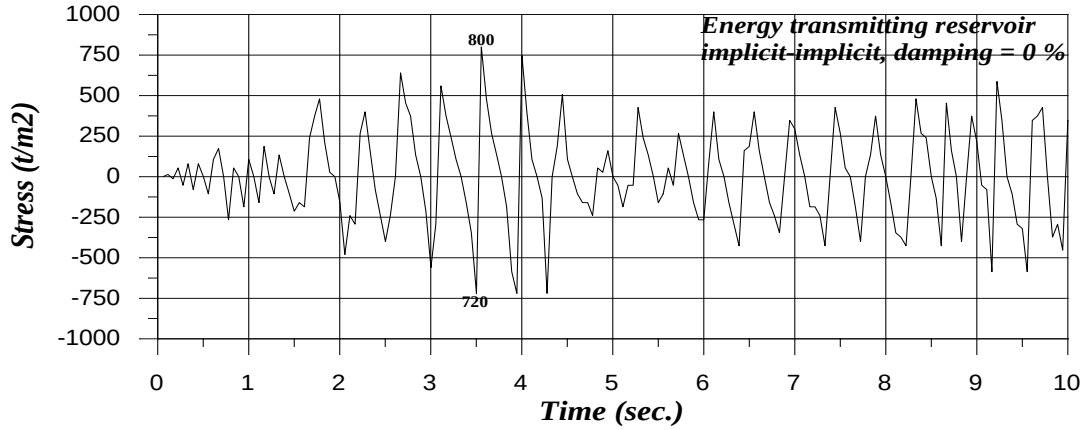

(a) El-Centro earthquake.

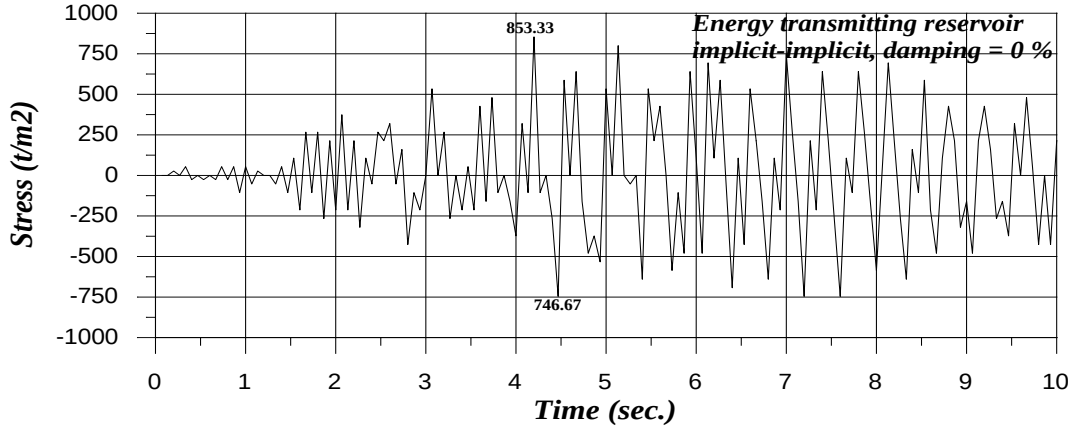

(b) Koyna earthquake.

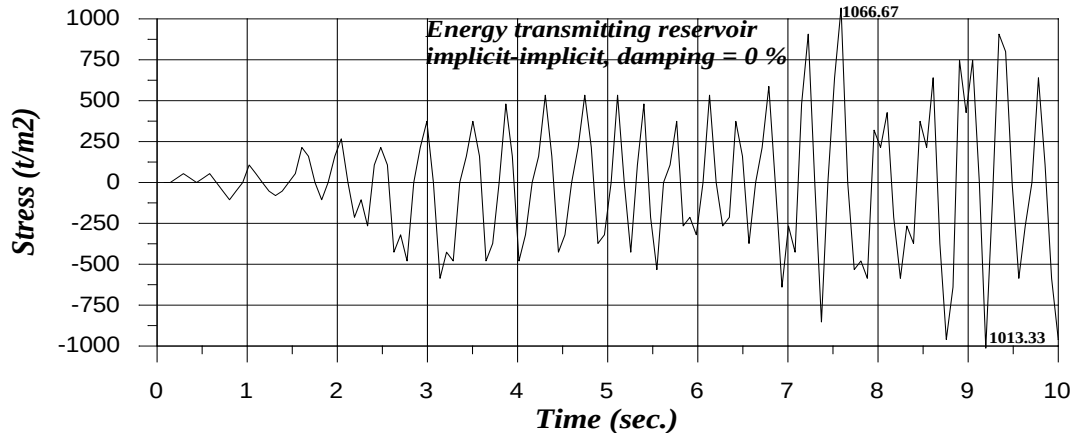

(c) San-Fernando earthquake.

Note: 1 t/m2 = 9.81 kN/m2

Figure (6): Response of normal stress at the dam heel when subjected to various earthquake (transverse and vertical) excitations.

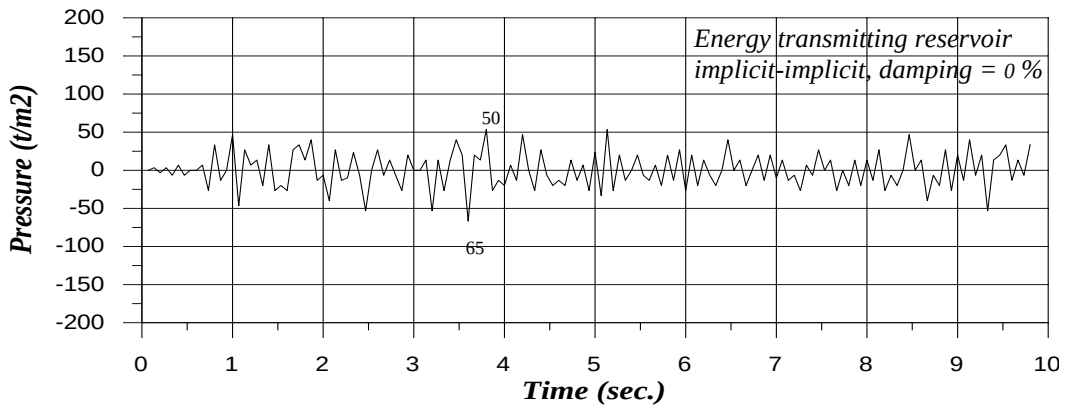

(a) El-Centro earthquake.

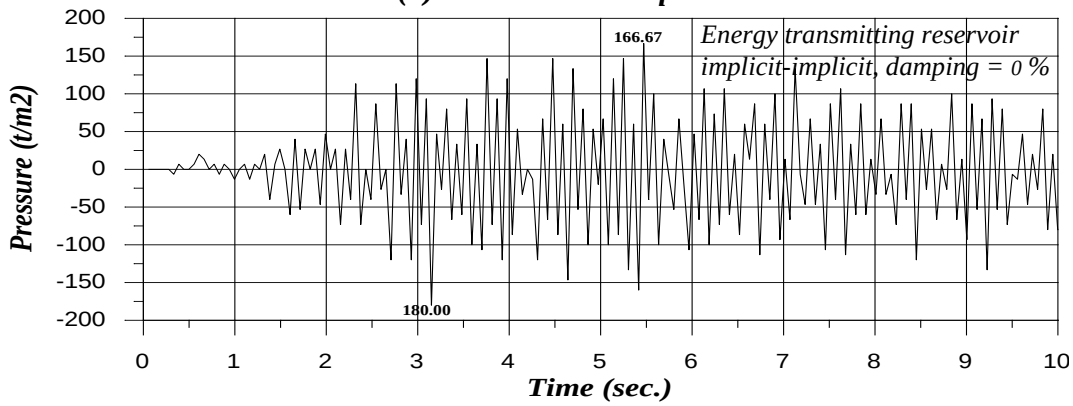

(b) Koyna earthquake.

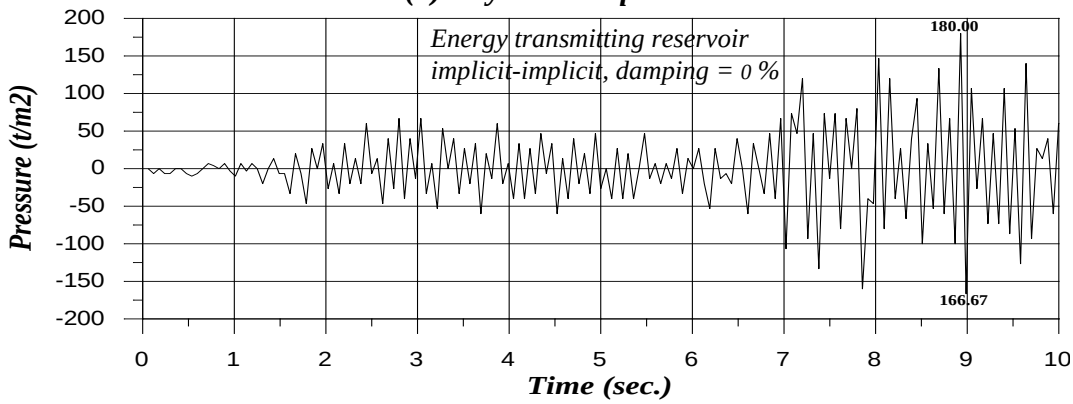

(c) San-Fernando earthquake.

Note: 1 t/m2 = 9.81 kN/m2

Figure (7): Response of pressure at the dam base when subjected to various earthquakes (transverse and vertical) excitations.

Table (3): Comparison of peak responses of dam for various earthquakes (transverse and vertical) excitations.

Response Description	*El-Centro Earthquake*	*Koyna Earthquake*	*San-Fernando Earthquake*
Dam crest displacement (cm)	*10.00 at 3.33 sec.*	*9.33 at 4.53 sec.*	*13.67 at 9.72 sec.*
	-9.66 at 3.53 sec.	*-9.33 at 4.00 sec.*	*-13.33 at 9.24 sec.*
Stress at the dam heel (T/m^2)	*800 at 3.55 sec.*	*853.33 at 4.20 sec.*	*1066.67 at 7.59 sec.*
	-720 at 3.50 sec.	*-746.67 at 4.47 sec.*	*-1013.33 at 9.19 sec.*
Pressure at the	*50 at 3.85 sec.*	*166.67 at 5.47 sec.*	*180.00 at 8.92 sec.*

Dam base (T/m^2)	*-65 at 3.60 sec.*	*-180.00 at 3.15 sec.*	*-166.67 at 8.98 sec.*

EFFECT OF STRUCTURAL DAMPING:

The responses of Koyna dam when subjected to the transverse component of the Koyna earthquake for 0%, 5% and 10% damping are shown in Figures (8), (9) and (10), respectively. It is observed that the effect of structural damping is significant and, therefore, estimation of damping in the evaluation of the response should be made carefully. The peak responses of the dam for different damping ratios are given in Table (4).

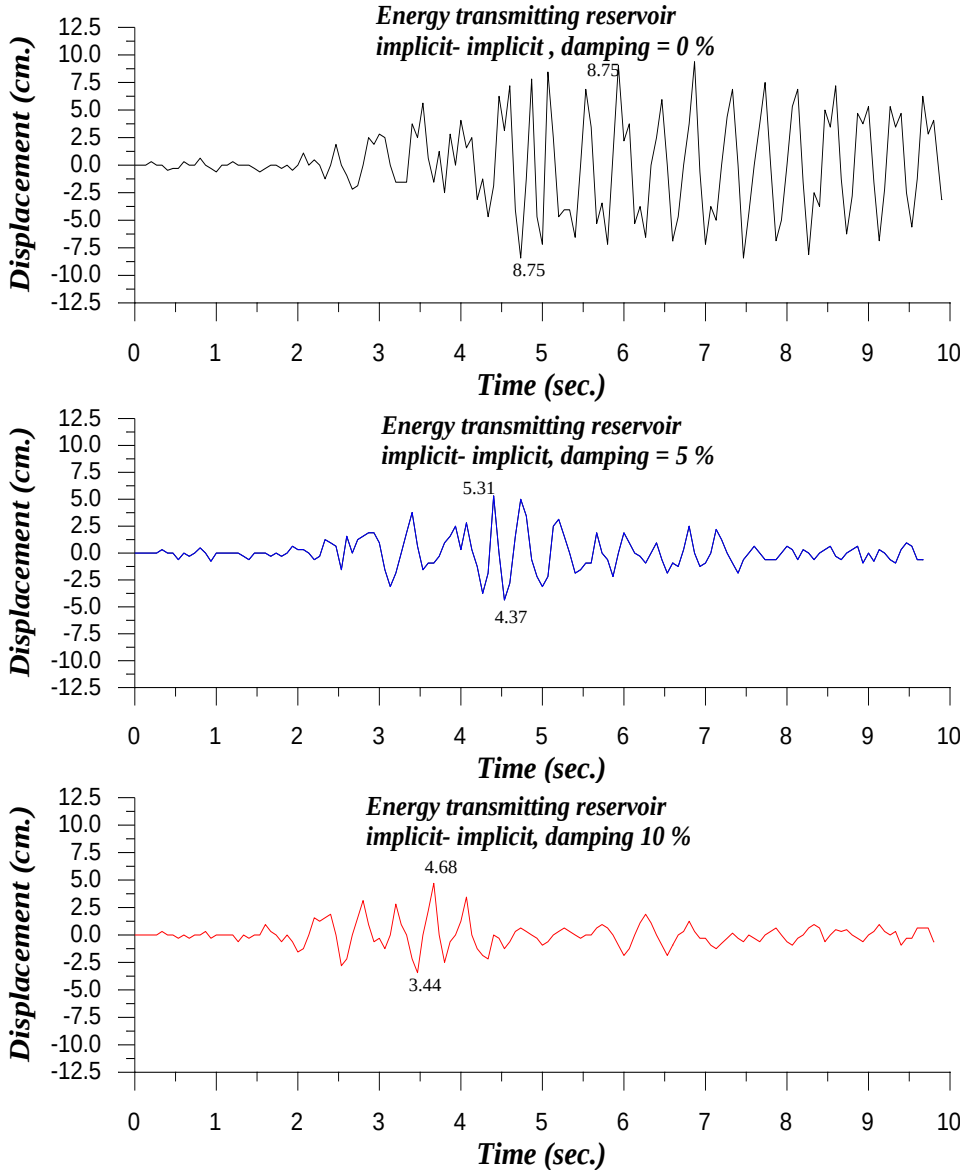

Note : 1cm = 10 mm.

Figure (8): Response of dam crest displacement when subjected to transverse component of Koyna earthquake.

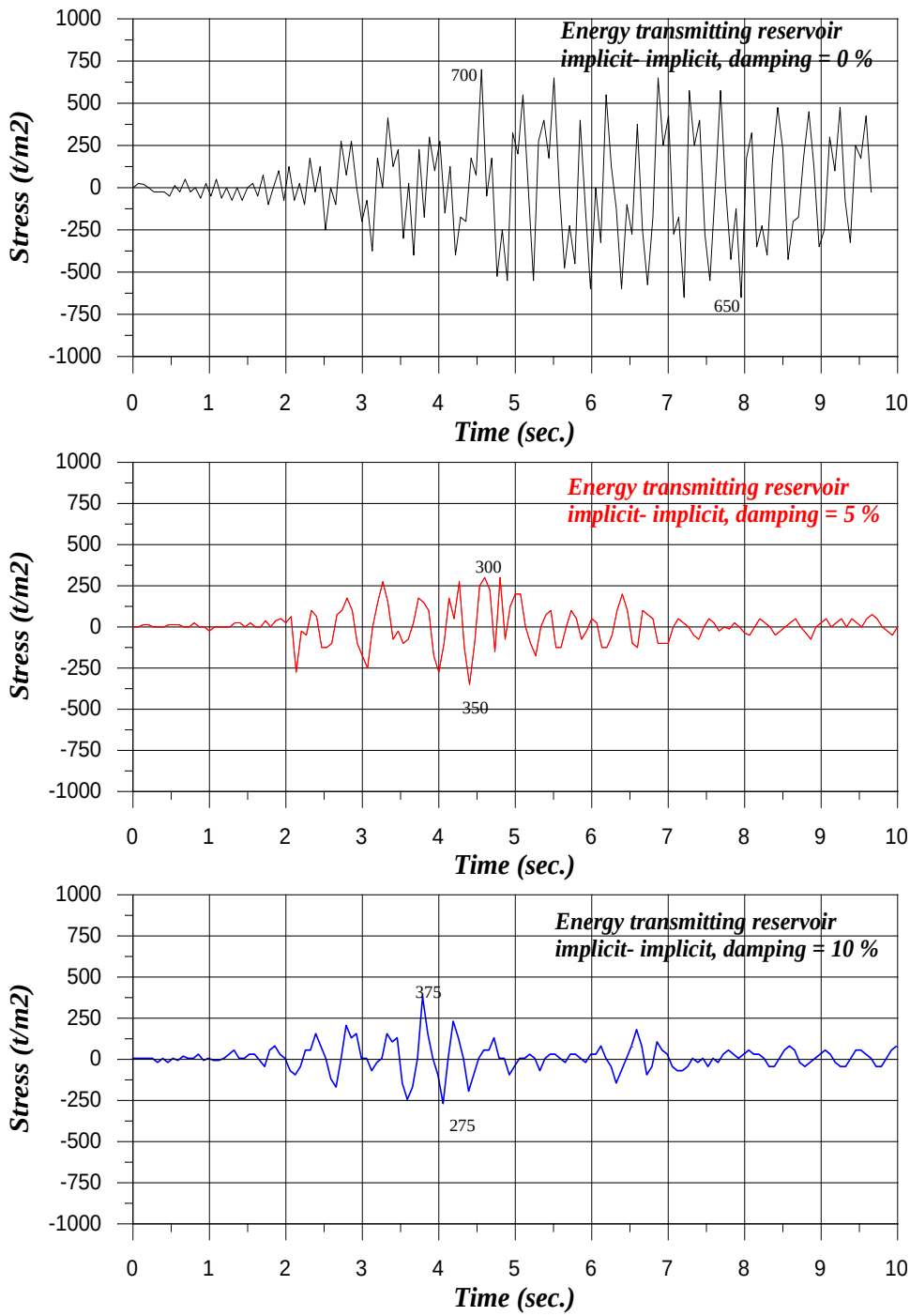

Note: 1 t/m2 = 9.81 kN/m2

Fig (9): Response of normal stress at the dam heel when subjected to a transverse component of Koyna earthquake.

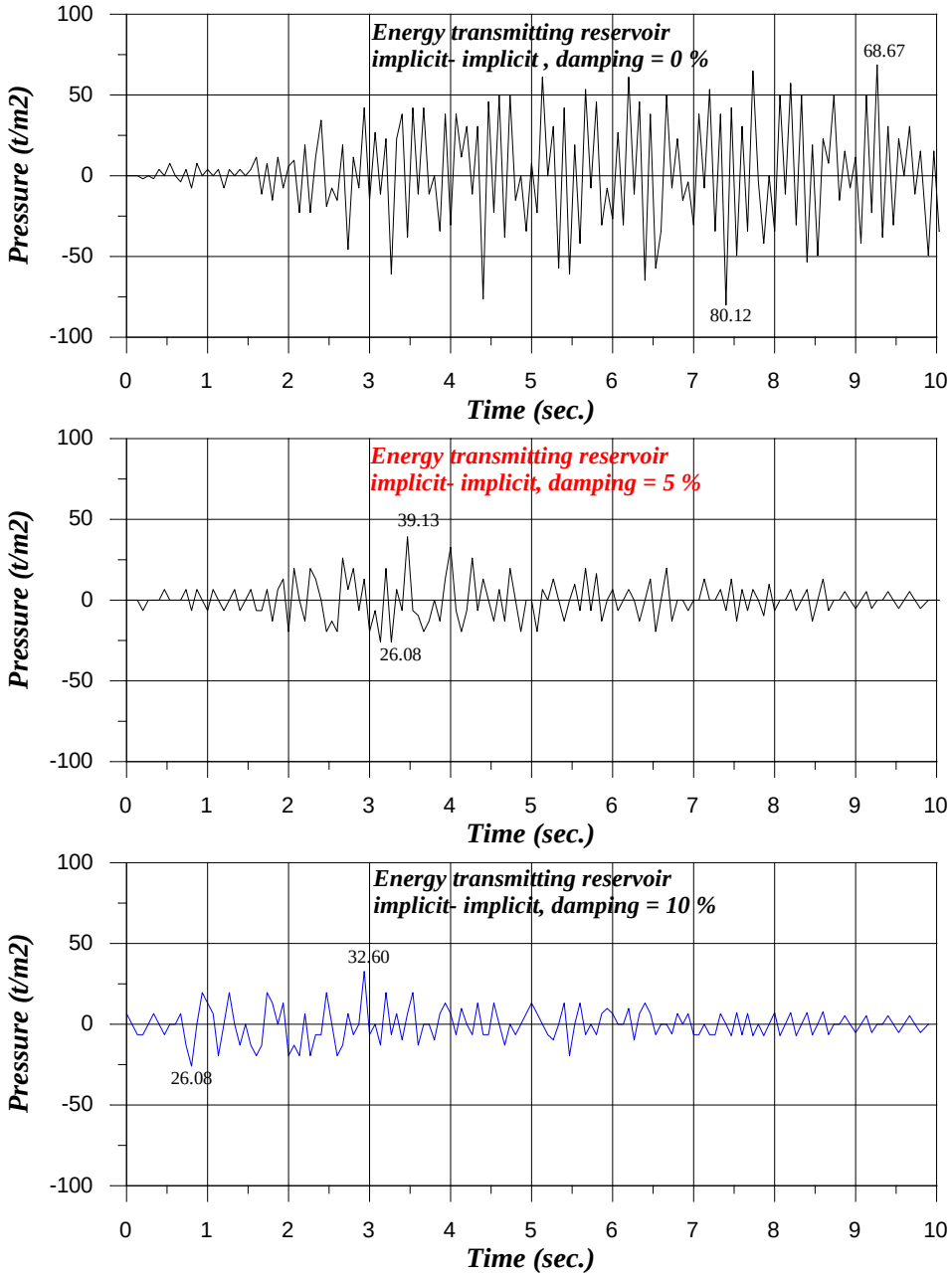

Note: 1 t/m2 = 9.81 kN/m2

Fig (10): Response of pressure at the dam base when subjected To a transverse component of Koyna earthquake.

Table (4): Effect of structural damping on the response of dam when the transverse component of Koyna earthquake is applied.

Response Description	*0 % damping*	*5 % damping*	*10 % damping*
Dam crest displacement (cm)	*8.75 at 5.8 sec.*	*5.31 at 4.4 sec.*	*4.68 at 3.66 sec.*
	-8.75 at 4.8 sec.	*-4.37 at 4.5 sec.*	*-3.44 at 3.46 sec.*
Stress at the dam heel (T/m^2)	*700 at 4.55 sec.*	*300 at 4.6 sec.*	*375 at 3.8 sec.*
	-650 at 7.95 sec.	*-350 at 4.4 sec.*	*-275 at 4.07 sec.*

Pressure at the Dam base (T/m^2)	*68.67 at 9.26 sec.*	*39.13 at 3.5 sec.*	*32.60 at 2.93 sec.*
	-80.12 at 7.4 sec.	*-26.08 at 3.26 sec.*	*-26.08 at 0.8 sec.*

EFFECT OF MATERIAL NONLINEARITY:

The nonlinear response of the Koyna dam when subjected to transverse and vertical Koyna earthquake components is shown in Figure (11). The concrete and foundation-rock-soil are represented by the Drucker-Parger yield criterion (Owen and Hinton [29]). The yield stress values of the concrete and the foundation rock are taken equal to be 323.94 T/m2 and 257.75 T/m2, respectively (1T/m2=9.81kN/m2). It is found that the effect of material nonlinearity is significant and when the nonlinearity in the dam structure is considered, the response reduces appreciably.

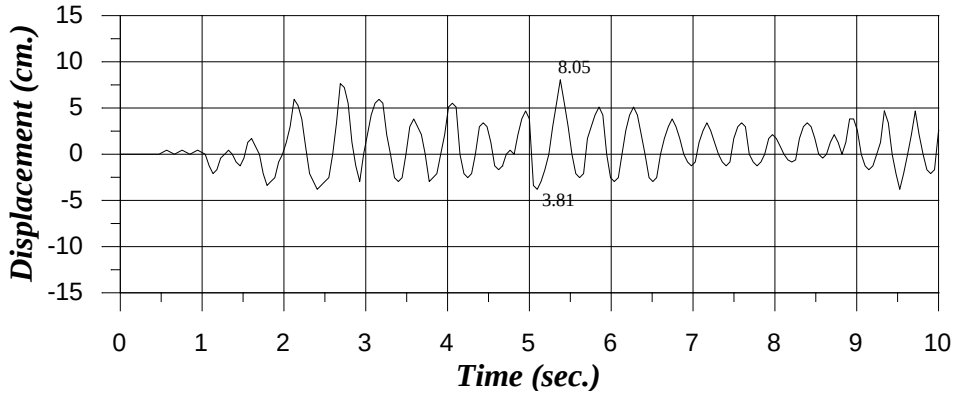

(a) Response of dam crest displacement.

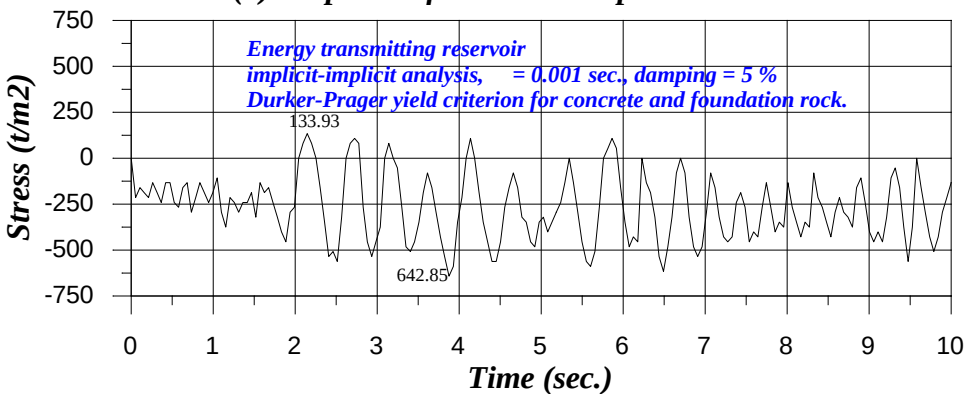

(b) Response of normal stress at the dam heel.

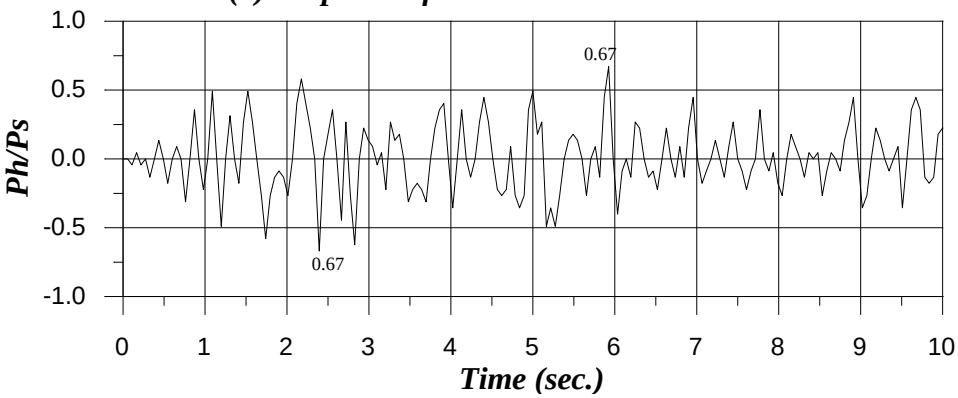

(c) Response of hydrodynamic force on dam.

Note : 1cm = 10 mm and,

1 t/m2 = 9.81 kN/m2.

Fig (11): Nonlinear response of dam when subjected to transverse and vertical components of Koyna earthquake.

CONCLUSIONS:

From this investigation, the following points can be drawn:

- The computer code developed is found to be very useful and can be used for a wide range of applications in many soil-fluid-structure interaction problems.
- The partitioned solution scheme in which the fluid, structure and soil-pore fluid is integrated in a staggered fashion is found to be very efficient.
- Two-phase materials subjected to dynamic loadings can be formulated with approximate numerical solutions and acceptable degrees of accuracy.
- Analysis of the actual behavior of constructions during dynamic loading exemplify the fact that the soil-structure interaction and, in the case of hydraulic structures, the fluid-structure interaction are phenomena which may have an important influence on the structural seismic response.
- The compressibility of water has a significant effect on the distribution of pressure on the rigid dam.
- As the flexibility of the dam system increases, the pressure distribution on the face of the dam also increases. The maximum effect is obtained when both the dam and the foundation are most flexible. Conversely, when the dam is rigid, foundation flexibility is not so important.
- The response characteristics of the dam-reservoir are very much dependent on the type of earthquake excitation, structural damping and material nonlinearity.

Aknowledgement: The authors wish to express their gratitude to Baiji Oil Refinery for supporting this research work.

REFERENCES:

- Al-Nu'aim, Rafi' M.S., (2004), "Non-Linear Analysis of Coupled Soil- Fluid- Structure Interaction Under Dynamic Loading", Ph.D. Thesis, Department of Civil Engineering, University of Baghdad.

- Al-Sherefi, M. H., (2000), "Non-Linear Dynamic Response of Soils", M.Sc. Thesis, College of Engineering, University of Baghdad, Iraq.

-. Bathe, K., and Hahn, W., (1979), "*On Transient Analysis of Fluid-Structure Systems"*, Journal of Computers and Structures, Volume 10, pp. 383-391.

- Belytschko, T., (1980), "*Fluid-Structure Interaction"*, Journal of Computers and Structures, Volume 12, pp. 459-469.

- Belytschko, T., and Kennedy, J., (1978),"*Computer Models For Subassembly Simulation"*, Journal of Nuclear Engineering and Design, Volume 49, pp. 17-38.

- Belytschko, T., and Kennedy, J., (1976), "*A Fluid-Structure Finite Element Method For the Analysis of Reactor Safety Problems"*, Journal of Nuclear Engineering and Design, Volume 38, pp. 71-81.

- Biot, M. A., (1955), "*Theory of Elasticity and Consolidation for a Porous Anisotropic*

Solid", Journal of Applid Physics, Volume 26, pp. 182-185.

- Biot, M. A., (1941),"*General Theory for Three-Dimensional Consolidation",* Journal of Applid Physics, Volume 12, pp. 155-164.
- Chopra, A., Wilson, E., and Farhoomand, I., (1969), "*Earthquake Analysis of Reservoir-Dam Systems"*, Proceedings of the 4th World Conference on Earthquake Engineering, Santiago, Chile.
- Dargush, G.F., and Banerjee, P. K., (1990), "*Development of an Integrated BEM for Fluid-Structure Interaction"*, Journal of Engineering for Gas Turbines and Power-Transactions of the ASME, Volume 112, No. 2, April, pp. 243-250.
- DiMaggio, F. L., and Sandler, I. S., (1971), *"Material Model for Granular Soils"*, Journal of Engineering Mechanics Division, ASCE, Volume 97, No.EM3, Proceedings Paper 8212, pp.935-950.
- Everstine, G. C., (1981), "*A Symmetric Potential Formulation For Fluid-Structure Interaction"*, Journal of Sound and Vibration, Volume 79, pp. 157-160.
- Everstine, G. C., and Henderson, F. M., (1990), "*Coupled Finite Element Boundary Element Approach for Fluid Structure Interaction"*, Journal of the Acoustical Society of America, Volume 87, No. 5, pp. 1938-1947.
- Everstine, G. C., Marcus, M. S., and Quezon, A. J., (1983), "*Finite Element Analysis of Fluid-Filled Elastic Piping System"*, Proceedings of the Eleventh NASTRAN Users' Colloquium, NASA Conference Publication, pp. 141-160.
- Fan, D., and Tijsseling, A., (1992), "*Fluid-Structure Interaction with Cavitation in Transient Pipe Flows"*, Journal of Fluids Engineering-Transactions of the ASME, Volume 114, No. 2, June, pp. 268-274.
- . Hamdi, M., Ousset, Y., and Verchery, G., (1978), "*A Displacement Method For the Analysis of Vibrations of Coupled Fluid-Structure Systems"*, International Journal for Numerical Methods in Engineering, Volume 13, pp. 139-150.
- Jeans, R.A., and Mathews, I.C., (1990), " *Solution of Fluid-Structure Interaction Problems Using a Coupled Finite Element and Variational Boundary Element Technique"*, Journal of the Acoustical Society of America, Volume 88, No.5, November, pp. 2459-2466.
- Joseph, H.S., (1997), *"Fluid Mechanics"*, Springer, Chapters 2 and 3.
- Kock, E., and Olson, L., (1991),"*Fluid Structure Interaction Analysis by the Finite Element Method- a Variational Approach"*, International Journal for Numerical Methods in Engineering, Volume 31, No. 3, March, pp. 463-491.
- . Li, X. and Zienkiewicz, O. C., (1992), *"Multiphase Flow in Deforming Porous Media and Finite Element Solutions"*, Computers and Structures, Volume 45, No.2, pp. 211-227.
- . Lui, A., and Lou, J., (1990), "*Dynamic Coupling of A Liquid-Tank System Under Transient Excitations"*, Journal of Ocean Engineering, Volume 17, No. 3, pp. 263-277.
- Luzzato, E., (1990), "*Analysis of Linear Dynamic-System Interaction- Application to Fluid-Structure Coupling"*, Journal De Physique, Volume 51 NC3, September, pp. 177-186.
- . Morand, H., and Ohayon, R., (1979), "*Substructure Variational Analysis of the Vibrations of Coupled Fluid-Structure Systems. Finite Element Results"*, International Journal of Numerical methods in Engineering, Volume 14, pp. 741-755.

- . Nitikitpaiboon, C., and Bathe K. J., (1993)," *An Arbitrary Lagrangian-Eulerian Velocity Potential Formulation for Fluid Structure Interaction"*, Journal of Computers and Structures, Volume 47, No. 4-5, June, pp. 871-891.

- Ohayon, R., and Valid, R., (1981),"*True Symmetric Formulation of Free Vibration of Fluid-Structure Interaction-Applications and Extensions"*, Proceedings of the International Conference of Numerical Methods for Coupled Problems, University College, Swansea, September.

- Olson, L. G., and Bathe, K. J., (1983), "*A Study of Displacement-Based Fluid Finite Elements For Calculating Frequencies of Fluid and Fluid-Structure Systems"*, Journal of Nuclear Engineering and Design, Volume 76, pp. 137-151.

- Olson, L., and Vandini, T., (1989), "*Eigenproblem from Finite Element Analysis of Fluid-Structure-Interactions"*, Computers and Structures, Volume 33, No. 3, pp. 679-687.

- Olson, L.G., and Bathe, K.J., (1985), "*Analysis of Fluid-Structure Interactions. A Direct Symmetric Coupled Formulation Based on the Fluid Velocity Potential"*, Journal of Computers and Structures, Volume 21, No. 12, December, pp. 21-32.

- Owen, D. R. J., and Hinton, E., (1980), "Finite Elements in Plasticity-Theory and Practice", Pineridge Press Ltd., Swansea.

- Park, K.C., and Felippa, C. A., (1984), "*Recent Developments in Coupled Field Analysis Methods",* Chapter 11, Numerical Methods in Coupled Systems (edited by R. W. Lewis, P. Bettes, and E. Hinton, John Wiley & Sons), pp. 327-351.

- Paul, D. K., (1982), "*Efficient Dynamic Solutions for Single and Coupled Multiple Field Problems"*, Ph.D. Thesis, University College, Swansea.

- Romano, A. J., Williams, E. G., Russo, K. L., and Schuette, L. C., (1992), "*On the Visualization and Analysis of Fluid-Structure Interaction from the Perspective of Instantaneous Intensity"*, Journal De Physique III, Volume 2, No. 4, April, pp. 597-600.

- Sauve, R.G., Morandin, G.D. and Nadeau, E., (1993), "*Impact Simulation of Liquid-Filled Containers Including Fluid-Structure Interaction .1. Theory"*, Journal of Pressure Vessel Technology, Transactions of the ASME, Volume 115, No. 1, February, pp.68-72.

- Sauve, R. G., Morandin, G. D., and Nadeau, E., (1993), "*Impact Simulation of Liquid-Filled Containers Including Fluid-Structure Interaction .2. Experimental Verification"*, Journal of Pressure Vessel Technology, Transactions of the ASME, Volume 115, No. 1, February, pp.73-79.

- Shawky, A. and Maekawa, K., (1996), *"Nonlinear Response of Underground RC Structures Under Shear",* Journal of Material, Concrete Structures and Pavements, JSCE, Volume 31, 538, pp. 195-206.

36. Simon, B. R., Wu, J. S. S., Zienkiewicz, O. C. and Paul, D. K., (1986), *"Evaluation of u-w and u-π Finite Element Methods for the Dynamic Response of Saturated Porous Media Using One-Dimensional Models"*, International Journal for Numerical and Analytical Methods in Geomechanics, Volume10, pp.461-482.

- Zienkiewicz, O. C., (1984), *"Coupled Problems and Their Numerical Solution"*, Chapter One, Numerical Methods in Coupled Systems (edited by R. W. Lewis, P. Bettess, and E. Hinton, John Wiley & Sons), pp. 35-58.

- Zienkiewicz, O. C., and Bettess, P., (1982), *"Soils and other Saturated Media under*

Transient, Dynamic Conditions: General formulation and the Validity of the Various Simplifying Assumptions", in Soil Mechanics: Transient and Cyclic Loads, Edited by G. N. Pande and O. C. Zienkiewicz, Wiley New York, Chapter One.

- Zienkiewicz, O. C., Chang, C. T., and Bettess, P., (1980), "*Drained, Undrained Consolidating and Dynamic Behaviour Assumptions in Soils, Limits of Validity",* Geotechnique, Volume 30, pp.385-395.
- Zienkiewicz, O. C. and Taylor, R. L., (2000),*"The Finite Element Method"*, Fifth Edition Published by Butterworth-Heinemann, Volume 3: Fluid Dynamics.
- Zienkiewicz, O. C., and Shiomi, T., (1984),*"Dynamic Behaviour of Saturated Porous Media: The Generalized Biot Formulation and Its Numerical Solution"*, Journal of Numerical Analytical Methods in Geomechanics, Volume 8, pp.71-96.
- Zienkiewicz, O.C., and Bettess, P., (1978), "*Fluid-Structure Dynamic Interaction and Wave Forces. An Introduction of Numerical Treatment"*, International Journal of Numerical Methods in Engineering, Volume 13, pp. 1-16.
- Zienkiewicz, O. C., Bettess, P. and Kelly, D. W., (1978), *"The Finite Element Method for Determining Fluid Loading on Rigid Structures, Two-and Three Dimensional Formulations"*, Numerical Methods in Offshore Engineering, Chapter Four, edited by O. C. Zienkiewicz, et al., John Wiley and Sons, pp. 141-184.
- Zienkiewicz, O. C., and Newton, R., (1969), "*Coupled Vibrations of a Structure Submerged in a Compressible Fluid"*, Symposium on Finite Element Techniques, Stuttgart.
- Zienkiewicz, O. C., Chan, A. H. C., Pastor, M., Paul, D. K., and Shiomi, T., (1990), *"Static and Dynamic Behaviour of Soils: A Rational Approach to Quantitative Solutions. I. Fully Saturated Problems"*, Proceedings of the Royal Society of London, Volume 429, pp. 285-309.
- Zienkiewicz, O. C., Pastor, M., Chan, A. H. C., and Xie, Y. M., (1991), *"Computational Approaches to the Dynamics and Statics of Saturated and Unsaturated Soils"*, In Advanced Geotechnical Analysis, Eds. P. K. Banerjee and R. Butterfield, Elsevier, Oxford, Chapter One, pp.1-46.
- Zienkiewicz, O. C., Xie, Y. M., Scherefler, B. A., Ledesma, A., and Bicanic, N., (1990), "*Static and Dynamic Behaviour of Soils: A Rational Approach to Quantitative Solutions. II. Semi-Saturated Problems"*, Proceedings of the Royal Society of London, Volume 429, pp. 311-321.

LIST OF SYMBOLS:

$\underline{b}$ = Displacement of fluid relative to the solid skeleton.
B = Strain –displacement matrix.
c = Speed of sound.
$\underline{C}_s$ = Rayleigh damping matrix.
$\underline{C}_f$ =Compressibility matrix.
C_{ijkl} = Components of the elasticity tensor.
D_t = Constitutive matrix.
E = Modulus of elasticity specified by Table (1).
$\bar{E}$ = Adopted modulus of elasticity in analysis.
g = Gravitational acceleration.

G = Shear modulus.
$\bar{h}(L)$ = Heaviside step function defined as 1 for $l > 0$ and 0 at $l \leq 0$.
H = Dam height.
$\hat{H}$ = Positive shape hardening scalar function of σ_{ij} and q_n .
$\hat{i}$, $\hat{j}$, $\hat{k}$ = Unit vectors in x, y and z directions, respectively.
k = Permeability coefficient.
K = Bulk modulus .
$\underline{K}_s$ = Stiffness matrix.
$\underline{K}_f$ =Flow matrix.
K_f = Bulk modulus of the fluid.
K_S= Bulk modulus of the solid phase.
K_T = Total bulk modulus of the solid skeleton.
$\underline{L}$ = Coupling matrix .
L = Loading index.
L_{ij} = Loading direction.
$\underline{M}_s$ = Solid skelton mass matrix.
$\underline{M}_f$ =Fluid mass matrix.
n = Porosity.
n = the direction of the unit normal at the radiating boundary.
$\underline{N}_p$ = Shape functions for pore pressure.
$\underline{N}_u$ = Shape functions for solid skeleton displacements.
P_f = Mass density.
P = Pressure above the hydrostatic value.
P_d^h = Hydrodynamic pressure.
P_s = Static pressure.

$$1/Q = \left[\frac{n}{K_f} + \frac{\alpha_c - n}{K_s} \right]$$

t = Surface traction.
T = Time.
$\underline{u}$ = Solid phase translation.
$\dot{u}_x$, $\dot{u}_y$ and $\dot{u}_z$ = Velocity of solid phase components in x, y and z directions, respectively.
$\underline{\dot{w}}$ = Fluid velocity.
Y = Rise from dam base.
α and β are Rayleigh damping constants.
$\alpha_c = 1 - K_T / K_S$.
$\underline{\varepsilon}^o$= Autogenous strains.
ε_{ij} = Strains due to stresses and the superscripts.
Γ = Boundary surface.
μ' = The dynamic viscosity of fluid.
ρ = Solid phase density.
ρ_f = Fluid density.
σ_{ij} = Stress tensor.
Ω = The domain.
$\langle\ \rangle$ = Macauley brackets defining the operation $\langle L \rangle = \bar{h}(L)L$.
A superposed dot indicates the rate.

NONLINEAR ANALYSIS OF RENFORCED FIBROUS CONCRETE VIERENDEEL TRUSS

Prof. Kalid Shaker Mahmod **Aalaa Whaleed Hameed**

ABSTRACT:

A Vierendeel truss is a hyper static frame composed of a series of rectangular or trapezoidal panels with out diagonal members. The end conections of all members are rigid and designed to take moment. In this work, the use of fiber reinforced concrete in construction of Vierendeel trusses with nonlinear material behavior is researched. The addition of randomly dispersed discrete steel fibers to concrete improves many engineering properties of the material such as fracture toughness, fatigue resistance, impact resistance and flexural strength. Several parameters that affected the behavior of the structure like fiber volume fraction, aspect ratio, and the position of the portion in structure that used fibrous concrete are studied. All these studies are hold out by developing a program, named (P3DNFEA).

الخلاصة:

مسنم فرنديل هو هيكل مستقر يتألف من سلسلة من الفضاءاتالمستطيلة أو المعينية المنحرفة وبدون عوارض قطرية. مناطق الاتصال لاعضاء المسنم تصمم لان تكون جاسئة وتتحمل عزوم. خلال هذا البحث, يتم استخدام الخرسانة المسلحة و المحتوية على الياف فولاذية في انشاء المسنمات الفرنديلية مع الاخذ بنظر الاعتبار التصرف الاخطي للمواد. ان اضافة الالياف الفولاذية الموزعة بشكل عشوائي في الخرسانة يحن عدد من الصفات الهندسية للمادة (الخرسانة) مثل مقاومة الكسر, مقاومة الكلل, مقاومة الصدمات و مقاومة الالتواء. العوامل التي تؤثر على تصرف المنشأ مثل نسبة تواجد الالياف, طول الليف وقطره, و الموقع من المنشأ الحاوي على خرسانة مسلحة بالالياف قد أخذت بنظر الاعتبار. كل هذه الدراسات تمت من خلال تطوير برنامج اسمه P3DNFEA.

KEYWORD

Finite element, fibrous concrete.

INTRODUCTION

The Vierendeel truss, in spite of its designation, is not a truss in the conventional sense of being an assemblage of connected triangular unit, but a rigid frame. The diagonals are omitted and the chords and web members are made fully continuous to obtain stability. In addition, Vierendeel truss: offers some esthetic qualities, has simple details because of the limited number of members at a joint, is easier to form and place, and can be pre-casted or cast in place.

Both steel and reinforced concrete have been used as material construction. Moreover, Vierendeel girders are used in structures where free unobstructed space is required between the top and bottom chords. Fig. (1) show an arc-welded steel truss of this type.

Fig. 1 Bent-Leg spandrel columns with Vierendeel bracing, Hoover Support Team.

FINITE ELEMENT

20-nodes brick elements have been used for representing concrete element, as n Fig. (2). In each twenty-nodes, three degrees of freedoms (translation) u, v and w are along the Cartesian coordinate X, Y and Z, respectively.

While for reinforcement bar the embedded representation is used. In this type of representation, the reinforcement bars are assumed as line element, which is capable of transmitting axial force only.

The idealization of fibers effect were perform in the tension-stiffening model used as a result of fiber addition. That was in (P3DNFEA) program, while in the ANSYS program the effect of fibers were introduced by concerning fibers as bar.reinfocement with small fraction.

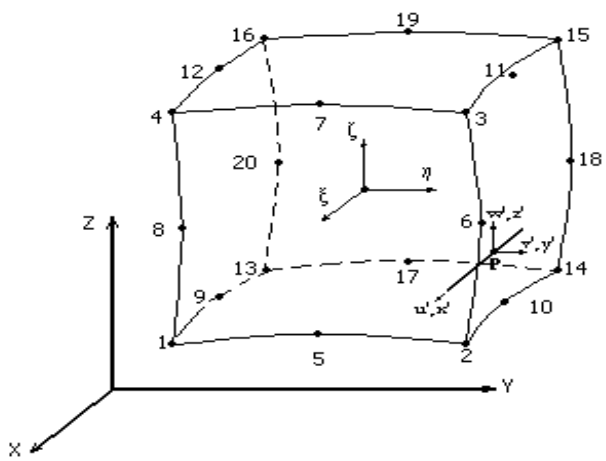

Fig. 2 20-node element in global and local coordinates with the definition of steel bar location.

Numerical Integration

One of the most accurate and convenient methods is "Gaussian quadrature", and which is used here. Gaussian quadrature is suited for numerical integration of polynomials for finite elements where dimensionless parameters (such as ζ, η and ξ) are used, and the origin is located at the center, Fig. 3.

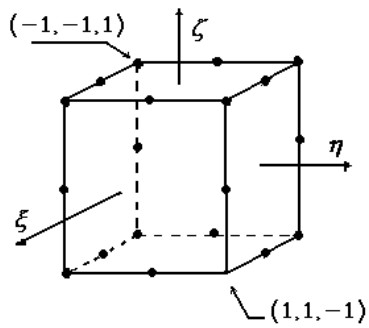

Fig. 3 Local coordinate system.

Nonlinear Solution Techniques

An incremental-iteration procedure is used through this work, Fig. 4. here, the load is applied incrementally, but after each increment successive iterations are performed.

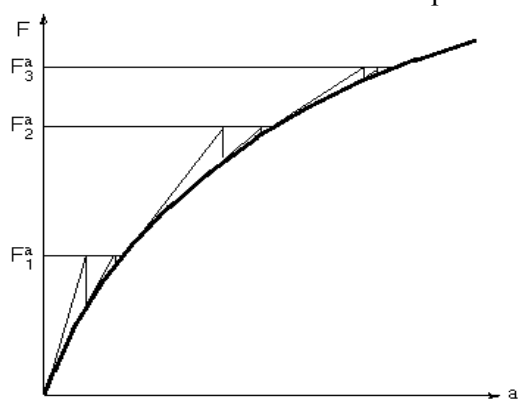

Fig. 4 The incremental-iteration procedure.

MATERIALS PROPERTIES

The main feature of plain concrete is its high compressive strength compared to its low tensile strength and low energy absorption capacity, as well, the brittleness behavior of failure mode. Therefore, to overcome these shortcomings, one may incorporate high-strength, small diameter fibers into the composites, and a new material can be gained, called fiber concrete or fibrous concrete.

Uniaxial Compression Behavior

The addition of fibers is shown to increase toughness much more than the first crack strength. In Fig. (5 and 6), which are the stress-strain curves in compression for SFR mortar (ACI committee 544), one can recognize a substantial increase in the strain at peak stress, and the slope of the decending portion is less steep than that of control specimens without fibers. This is an indication of substantially higher toughness, where toughness is a measure of ability to absorb energy during deformation.

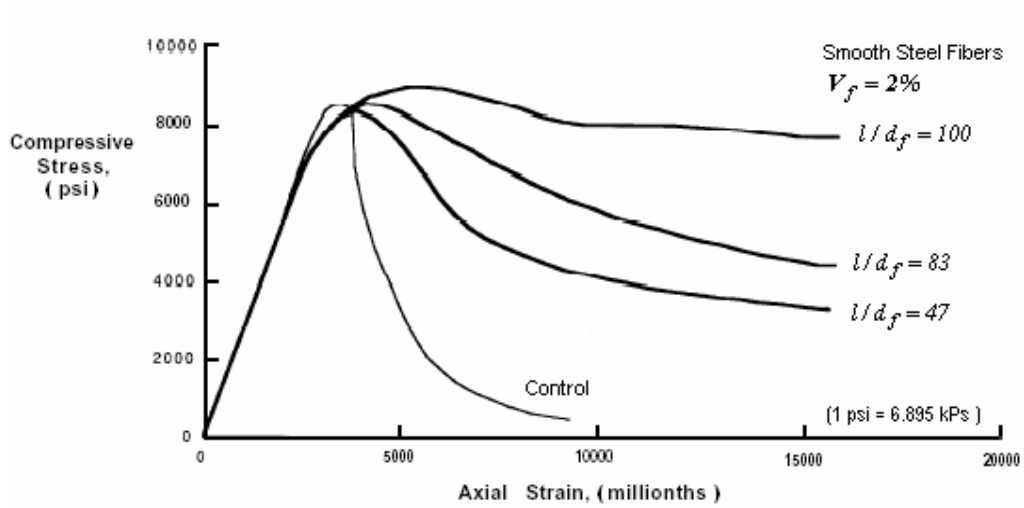

Fig. 5 Influence of the aspect ratio on the stress-strain curve, ACI committee 544.

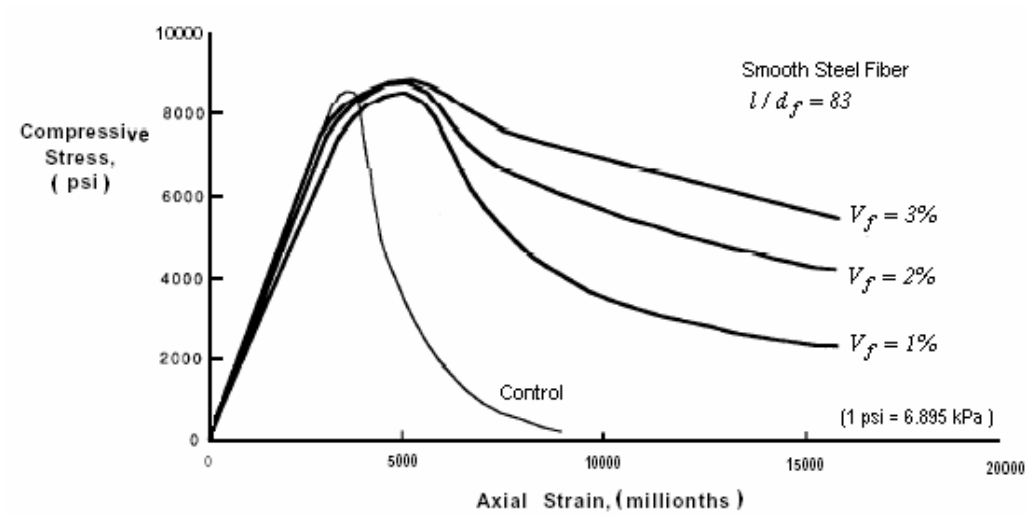

Fig. 6 Influence of te volume fraction of fibers on the compressive stress-strain curve[1].

Uniaxial Tensile Behavior

The strength mechanism of the fibers involves transfer of stress from the matrix to the fibers by interfacial shear, or by interlock between the fibers and the matrix if the fibers surfaces are deformed. Stress is, thus, shared by the fibers and the matrix in tension until the matrix crakes. Then the total stress is progressively transferred to the fibers. In tension, SFRC fails only after the steel fiber breaks or is pulled out of the cement matrix.

Multiaxial Behavior

The biaxial strength of fiber concrete is significantly greater than that of plain concrete. Fig. 7 shows a biaxial strength envelopes for plain and fiber concrete.

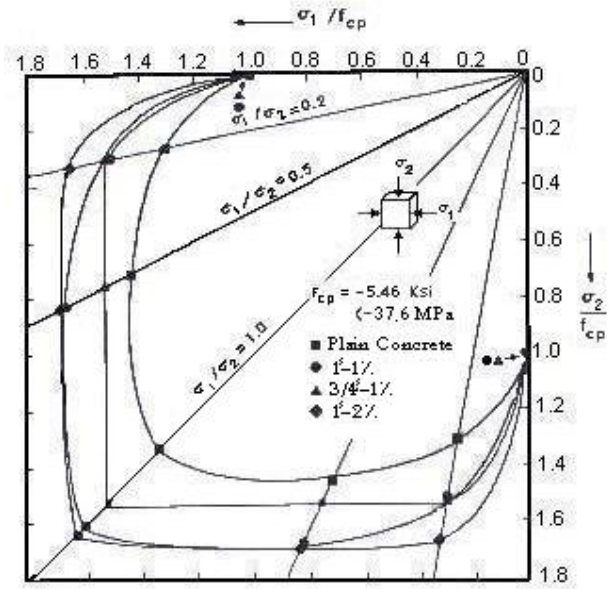

Fig. 7 Biaxial strength envelops for plain and fiber concrete[10].

The mechanical behavior of steel fiber reinforced concrete subjected to multiaxial loading may be assumed to be similar to that of plain concrete, its strength and ductility increase with the increase of confining pressure.

In this study the formulation presented by Soroushian and Lee for obtaining the stresses and strains in both compression and tension is used:

* For compression:

$$f_{cf}' = f_c' + 3.6 \times (V_f \cdot L_f)/d_f \quad (1)$$

$$\varepsilon_{pf} = 0.0021 + 0.007(V_f \cdot L_f)/d_f \quad (2)$$

* For tension:

$$f_{tf} = f_t\left(1 + 0.016 N_f^{1/3} + 0.05\pi \cdot d_f \cdot L_f \cdot N_f\right) \quad (3)$$

$$\varepsilon_{tf} = \varepsilon_t\left(1 + 0.35 N_f \cdot d_f \cdot L_f\right) \quad (4)$$

Where:

N_f : Number of fibers per unit cross-section area

MATERIAL MODELING

Modeling of Concrete

Behavior of Concrete in Compression

In the present study, the behavior of concrete in compression is simulated with an elastic-plastic work hardening model followed by perfect plastic response, which is terminated at the onset of crushing. The plasticity model can be illustrated in terms of the following constructions:

1. The Yield Criterion.

2. The Hardening Rule.
3. The Flow Rule.
4. The Crushing Condition.

The Yield Criterion

In the present work, a yield criterion based on two stress invariants has been adopted, and this is given by:

$$f(\sigma) = f(I_1, J_2) = [\alpha \cdot I_1 + 3\beta \cdot J_2]^{1/2} = \sigma_o \quad (5)$$

The Hardening Rule

The hardening rule defines the motion of the subsequent yield surfaces during plastic loading. A number of hardening rules has been proposed to describe the growth of subsequent yield surfaces for work-hardening materials, these are:

1. isotropic hardening rule.
2. kinematics-hardening rule.
3. mixed hardening rule.

Here, the isotropic hardening rule is adopted. The subsequent loading functions may be expressed as:

$$f(\{\sigma\}) = c \cdot I_1 + \left\{(c \cdot I_1)^2 + 3\beta \cdot J_2\right\}^{1/2} = \overline{\sigma} \quad (6)$$

The Flow Rule

So far, the loading surface alone is considered, mention has been made of the plastic stress-strain relations. The necessary connection between the loading function, ***f***, and the stress-strain relation for a work-hardening material will be made here by means of a flow rule. In plasticity theory the flue rule is defined so that the increments of plastic strain can be evaluated from a given stress state. An associated flow rule will be employed here. This means that the plastic deformation rate vector will be assumed to be normal to the adopted yield surface. The plastic strain increment is defined as:

$$d\{\varepsilon^p\} = d\lambda \cdot \frac{\partial f(\{\sigma\})}{\partial\{\sigma\}} = d\lambda \cdot \{a\} \quad (7)$$

The yield function derivatives with respect to the stress components define the flow vector as:

$$\{a\} = \left[\frac{\partial f}{\partial \sigma_x} \quad \frac{\partial f}{\partial \sigma_y} \quad \frac{\partial f}{\partial \sigma_z} \quad \frac{\partial f}{\partial \tau_{xy}} \quad \frac{\partial f}{\partial \tau_{yz}} \quad \frac{\partial f}{\partial \tau_{xz}}\right]^T \quad (8)$$

The Crushing Condition

The described hardening–plastic model governs the increase of the elastic deformation in concrete under compressive stress. Inelastic deformation continues in the concrete until crushing occurs. The crushing type of fracture is a strain-controlled phenomenon. A failure surface in the stress space must be defined so that this kind of fracture can be taken into account. Despite the lack of experimental data on concrete ultimate deformation capacity under multiaxial loading, crushing criterion is obtained by, simply, converting the yield criterion, equation 5 which is described in terms of stresses, directly into strains, thus:

$$cI_1' + \left\{(cI_1')^2 + 3\beta \cdot J_2'\right\}^{1/2} = \varepsilon_{cu} \quad (9)$$

Behavior of Concrete in Tension

Probably, the main feature of plain concrete material behavior is its low tensile strength, which results in tensile cracking at a very low stress compared with the failure stress in compression. However, the addition of steel fibers the mix will enhance the tensile strength and change the brittle failure to ductile one.

A smeared crack model will be adopted in this work. To understand and deal with such model, the following items have to be studied:

1. Cracking Criterion.
2. Tension Stiffening.
3. Shear Retention.

The Cracking Criterion

The tensile strength of uncracked concrete can be obtained from laboratory tests. Usually, concrete properties are deduced from the compressive strength. Simple criteria are, therefore, favored by most analysts to predict tensile fracture. Maximum tensile stress or maximum tensile strain criterion is, usually, used for this purpose. Here, the tensile type of fracture is the maximum tensile stress criterion (tension cut-off)[6]. For previously uncracked sampling point, the principal stresses and there directions are evaluated. if the maximum principal stress exceeds a limiting value, a crack is formed in a plane orthogonal to it. The limited tensile stress required defining the onset of cracking, which can be calculated for states of triaxial tensile stress and for combinations of tension and compression principal stresses as follows:

(a) For the triaxial tension zone $(\sigma_1 \geq \sigma_2 \geq \sigma_3 > 0)$

$$\sigma_i = \sigma_{cr} = f'_{tf} \qquad i = 1,2,3 \tag{10}$$

(b) For the tension-tension-compression zone $(\sigma_1 \geq \sigma_2 > 0, \sigma_3 \leq 0)$

$$\sigma_i = \sigma_{cr} = f'_{tf}\left[1 + \frac{0.75\sigma_3}{f'_{cf}}\right] \qquad i = 1,2 \tag{11}$$

(c) For the tension-compression-compression zone $(\sigma_1 > 0, \sigma_3 \leq \sigma_2 \leq 0)$

$$\sigma_i = \sigma_{cr} = f'_{tf} \cdot \left[1 + \frac{0.75\sigma_2}{f'_{cf}}\right] \cdot \left[1 + \frac{0.75\sigma_3}{f'_{cf}}\right] \tag{12}$$

Tension Stiffening Model

The reinforcement and the concrete are both subjected to tension, so that, large cracks are formed. The opening of cracks occurs at the same time as boned failure and relative movement between the bar and concrete takes place. The shear force at the contact surface feed tension stresses into the concrete between the crakes. The concrete hangs on the bare and contributes to over-all stiffness of the system. This stiffness effect is often called tension stiffening. The phenomenon is represented by the descending part of the stress-strain curve. The model proposed by Yin et. al.,1989, is used though this work, and it is defined as follows:

a) For $\varepsilon_{cr} \leq \varepsilon_n \leq \varepsilon_{tf1}$

$$\sigma_n = \alpha_2 \cdot \sigma_{cr} \tag{13}$$

b) For $\varepsilon_n \geq \varepsilon_{tf1}$

$$\sigma_n = 0 \tag{14}$$

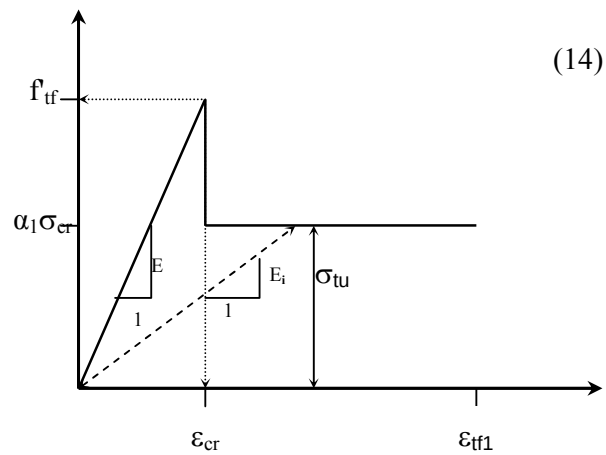

Fig. 8 Post-cracking model of steel fiber reinforced concrete.

Shear Retention Model

The shear stiffness at a cracked sampling point becomes progressively smaller as the crack widens. So the shear modulus of elasticity is reduced to βG, fig. 9. The following relations are used to account for the shear retention effect.

a) For $\varepsilon_n < \varepsilon_{cr}$

$$\beta = 1.0 \tag{15}$$

b) For $\varepsilon_{cr} < \varepsilon_n < \alpha_1 . \varepsilon_{cr}$

$$\beta = \frac{\gamma_2 - \gamma_3}{\gamma_1 - 1}\left[\gamma_1 - \frac{\varepsilon_n}{\varepsilon_{cr}}\right] + \gamma_3 \tag{16}$$

c) For $\varepsilon_n > \alpha_1 . \varepsilon_{cr}$

$$\beta = \gamma_3 \tag{17}$$

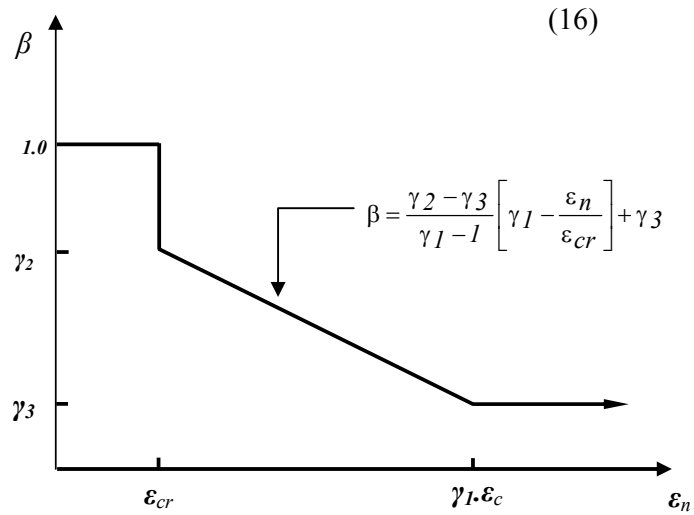

Fig. 9 Shear retention model for concrete.

Modeling of Reinforcement

Reinforcing steel is a homogenous material and has, usually, the same strength in tension and compression. In the present work, an elastic-linear work hardening model simulates the uniaxial stress-strain behavior of steel bars, as in fig 10

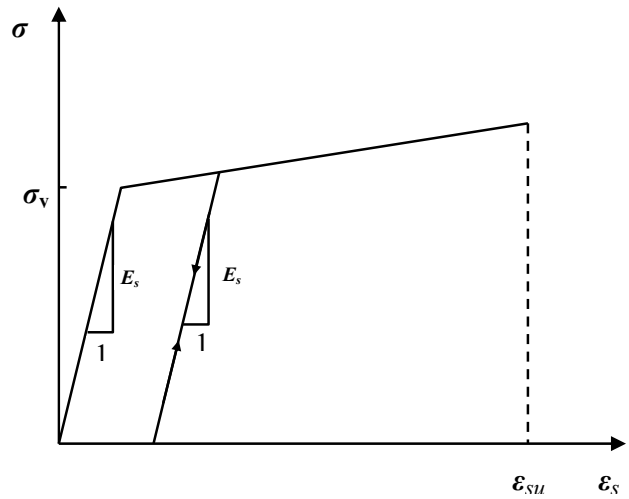

Fig.10 Stress-strain relationship of steel bars used in the analysis.

PARAMETRIC STUDY

Three Vierendeel structures are analyzed here. These structures have been tested by Alwash (1995). Each structure is subjected to a mid-span concentrated load applied at the upper chored. The details of geometry and arrangement of reinforcements for these structures are shown in figs. (11-a, b, c)

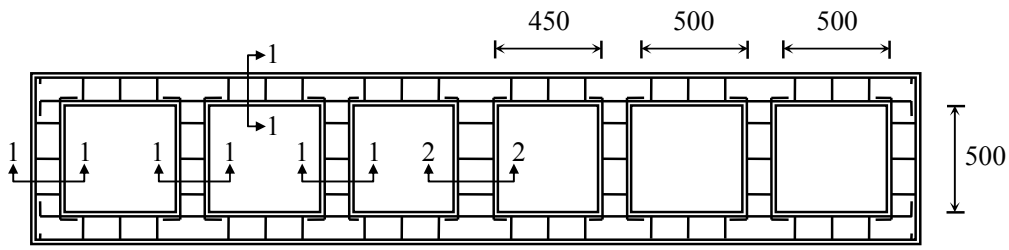

Fig. 11-a Geometry and arrangement of reinforcements for VER1.

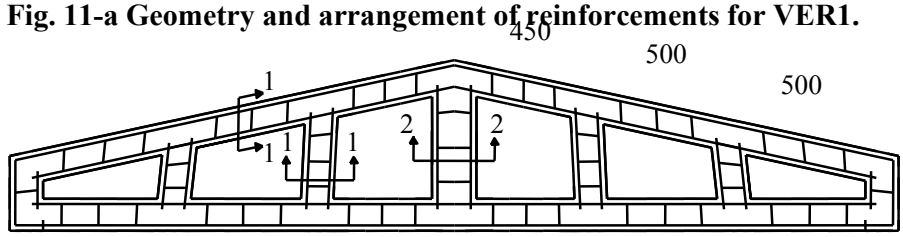

Fig. 11-b Geometry and arrangement of reinforcements for VER2.

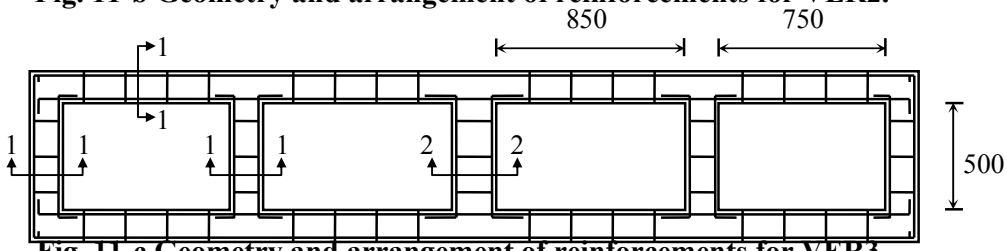

Fig. 11-c Geometry and arrangement of reinforcements for VER3.

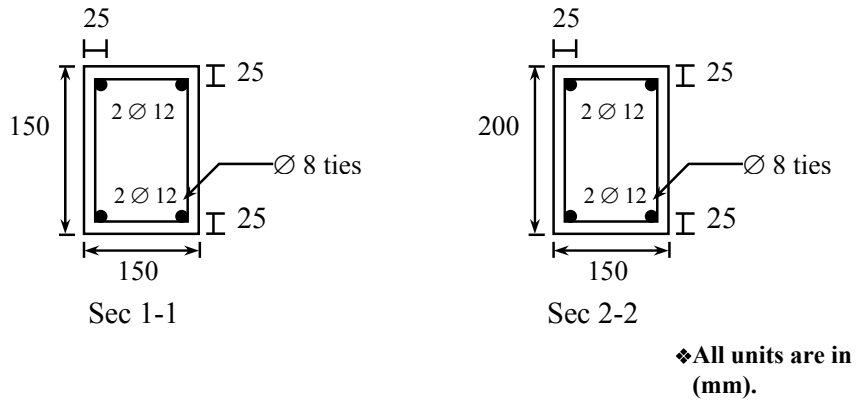

Fig. 11 Details of geometry and arrangement of reinforcements.

Structure shape

From thes three different shapesof Vierendeel trusses, two comparison cases are provided, one for voids number and size, and the other for the inclination of top chord.

Voids number and size

This comparison is carried out between VER1 and VER3. VER1 has six voids; their size varies from (500*500 mm) to (450*500 mm). On the other side, VER3 has four voids; their size varies from (750*500 mm) to (850*500 mm) here and after referring to Fig. 12, one can conclude that: when the number of voids is lessened on the expense of the increase in the voids size leads to a remarkable decrease (by 17.8%) in the structure rigidity and increase in the average deflection (by 14.1%).

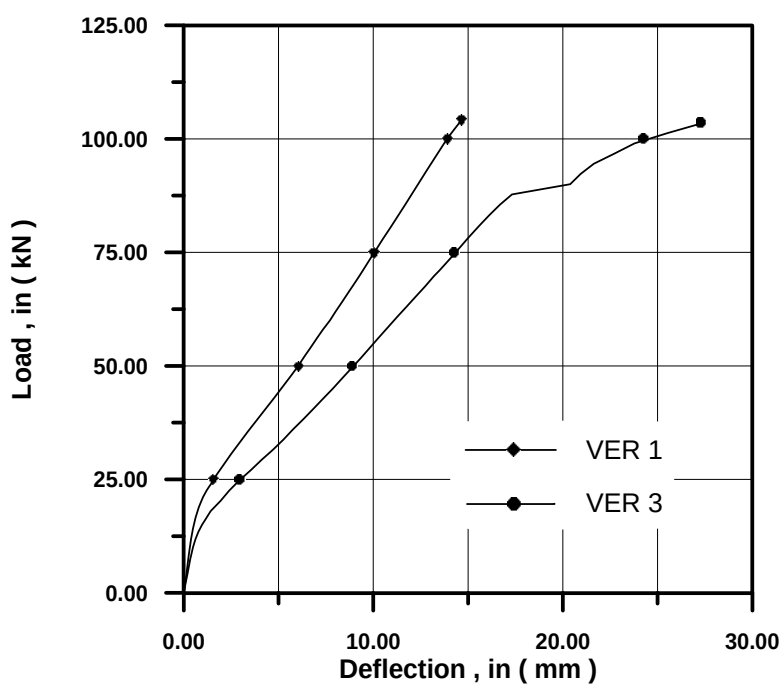

Fig. 12 Influence of voids number and size.

Inclination of top chord

By increasing the inclination of top chords from (inclination=0) to (inclination =12.4^o) structure strength increase with decreasing in its deflection, by (10.57%) and (36.71%), respectively, as in Fig. 13.

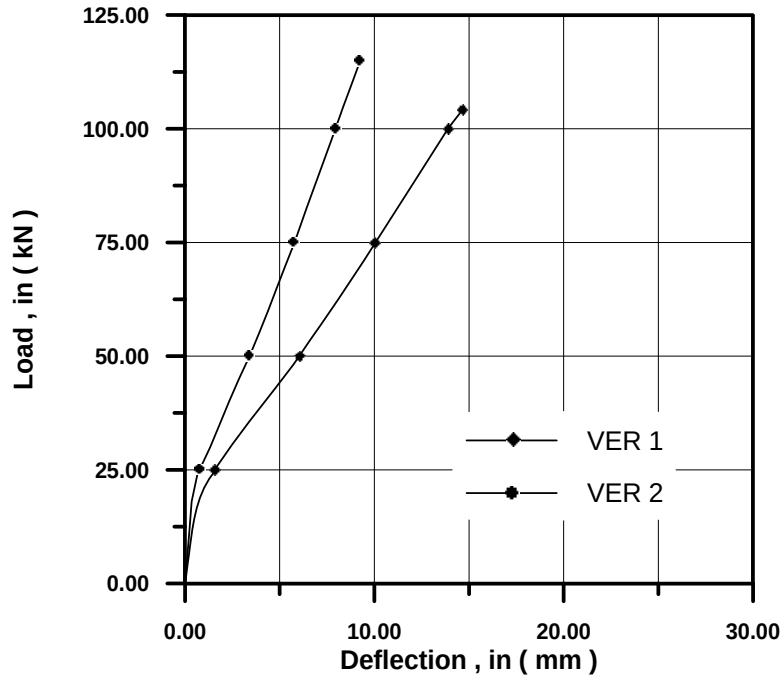

Fig. 13 Influence of inclination of top chord.

Fibers distribution

Three cases are searched to examine the influence of fibers distribution position through the structure. In the *first* case, fibers are distributed through the whole structure. While in the *second* case, fibers are distributed just in the bottom boom where the tensile stress is expected to be high. Finally, in the *third* case, fibers are distributed in both bottom boom (where expected high tensile stress) and vertical members (where the shear stress expected to be high and influential). The comparisons between these three cases are clearly shown in Figs. (14, 15, 16).

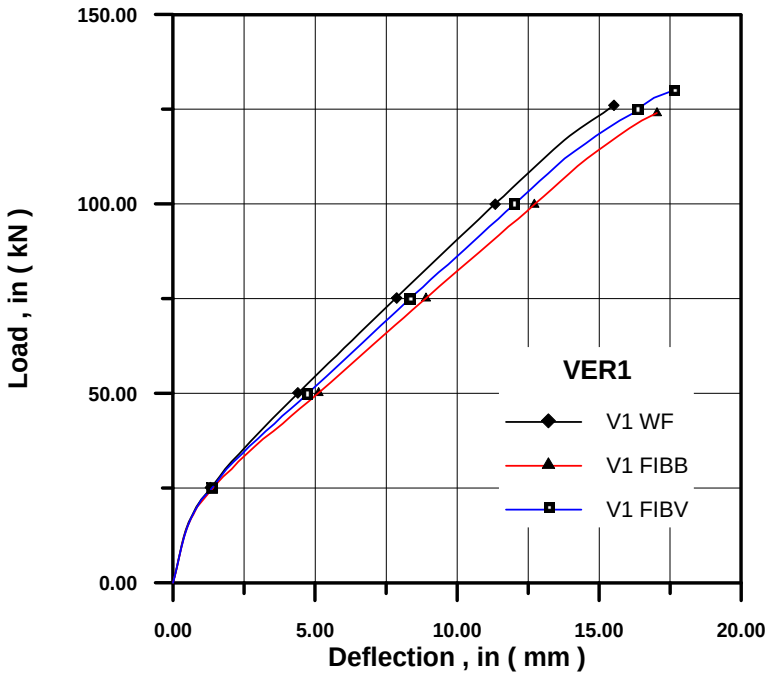

Fig. 14 The influence of fibers distribution in VER1.

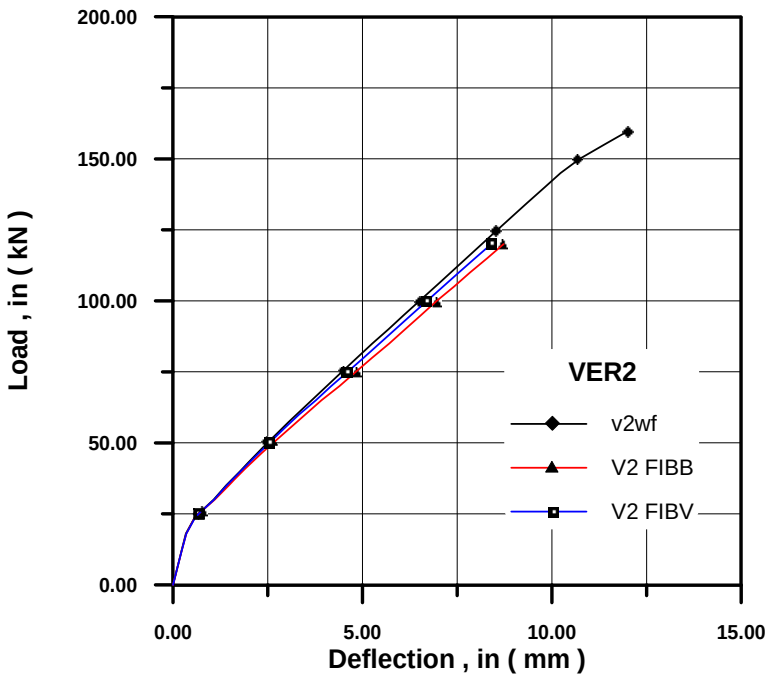

Fig. 15 The influence of fibers distribution in VER2.

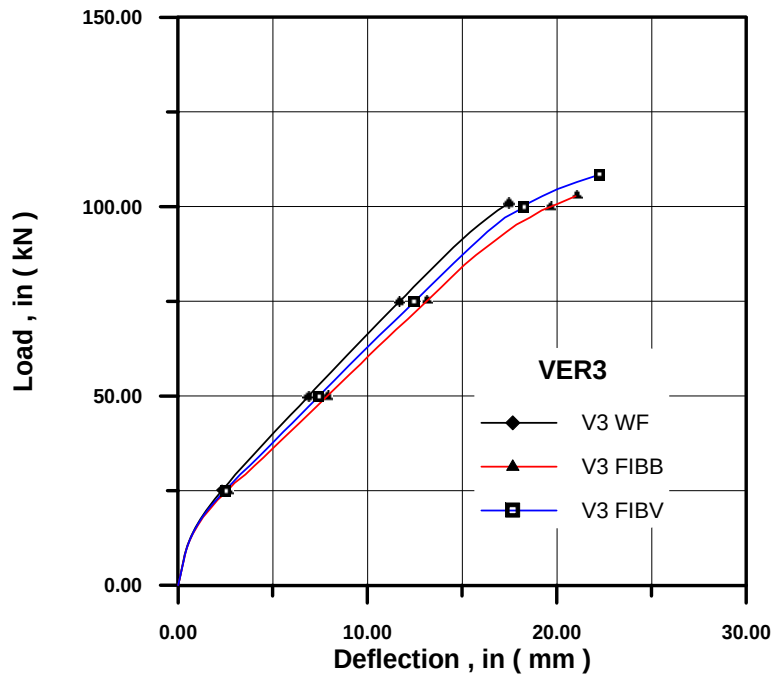

Fig. 16 The influence of fibers distribution in VER3.

When fiber geometries are changed like fiber length fiber diameter or fiber volume fraction, it seen to be affecting the response of structure which will be explained through the following notes:

1. When increasing V_f , a substantial increasing in structure rigidity is noticed, as in Fig 17. This is because of increasing in the crack arrestors. Therefore, delaying structure failure.

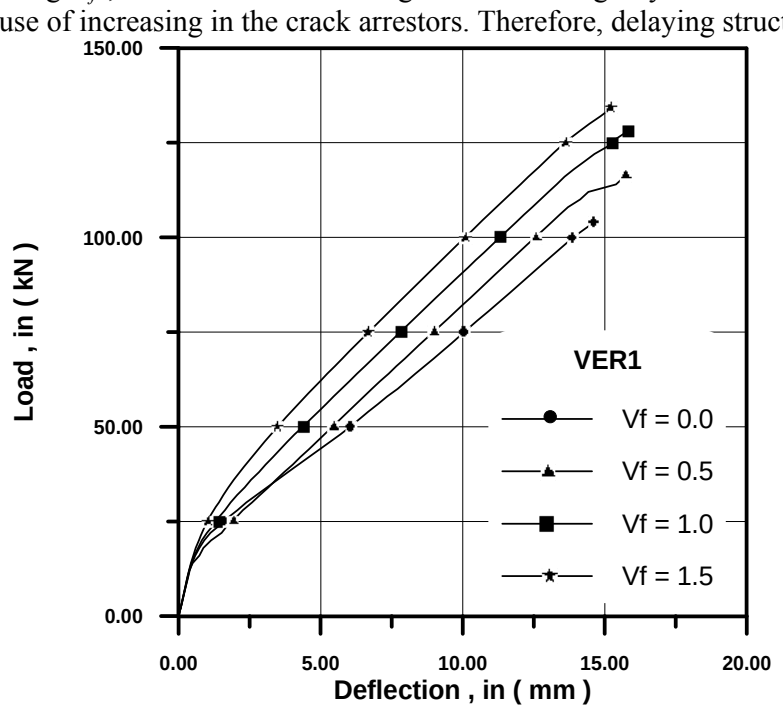

Fig. 17 Effect of V_f .

2. The matrix contains fibers distributed through it fail by two way. Either by fiber pull-out (this happened when fiber is short) or by fiber yield (this happened when fiber is long). The needed stress for the former type of failure is much more than the latter one. Therefore, when increasing L_f , an increasing in structure rigidity is observed.

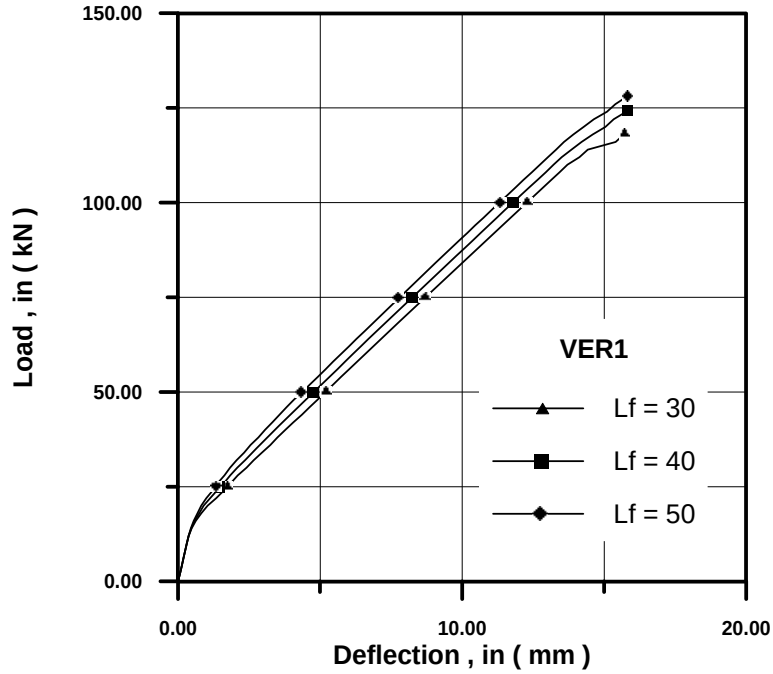

Fig. 18 Effect of L_f.

3. Here, the effect of d_f show a differ behavior than V_f and L_f, i.e., when increasing V_f, structure rigidity decreases.

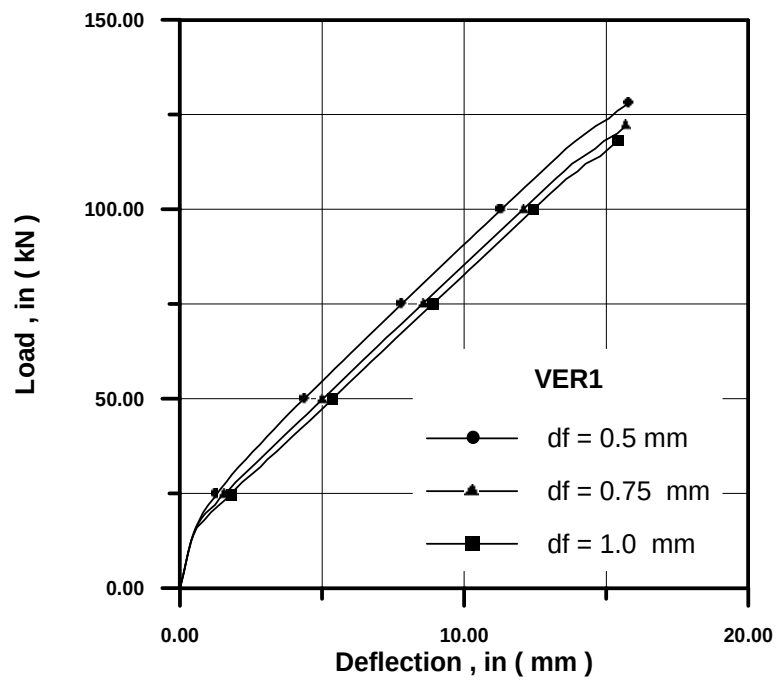

Fig. 19 Effect of d_f.

STRESSES STUDY

Here the stress distribution in Y-direction, with a sketch for the crack propagation through different load stages can be viewed. One can depend on this survey to decide on and through which portion fibers are to be distributed.

Stress distribution propagate in concrete

In Fig. 20 stress distribution in Y-direction for VER1 at mid-span

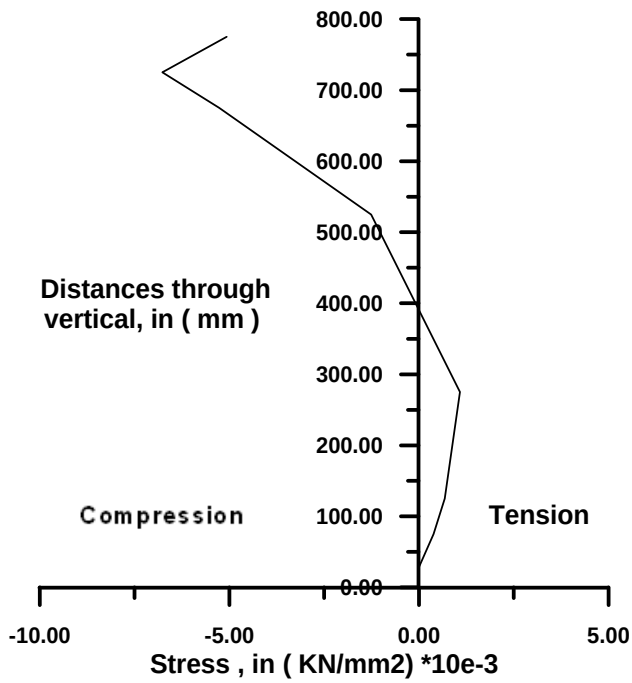

Fig. 20 Stress distribution in Y-direction for VER1 at mid-span.

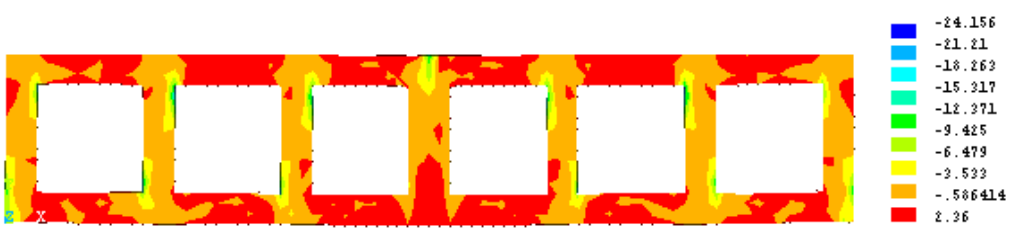

Fig. 21 Stress distribution in Y-direction for VER1, (N/mm^2).

Here and from Figs. 20 and 21, both distributions have similarity for half of the structure. The compressive and tensile zones are appearing clearly in these figures. By considering that the barrier between the compressive and tensile zones is a shear zone, the shear appears in the middle of verticals and near joints; while the tensile zone is more dominating in bottom booms.

Stress distribution through the longitudinal main bars

Fig. 22 shows the stress distribution and development for the bottom steel bars.

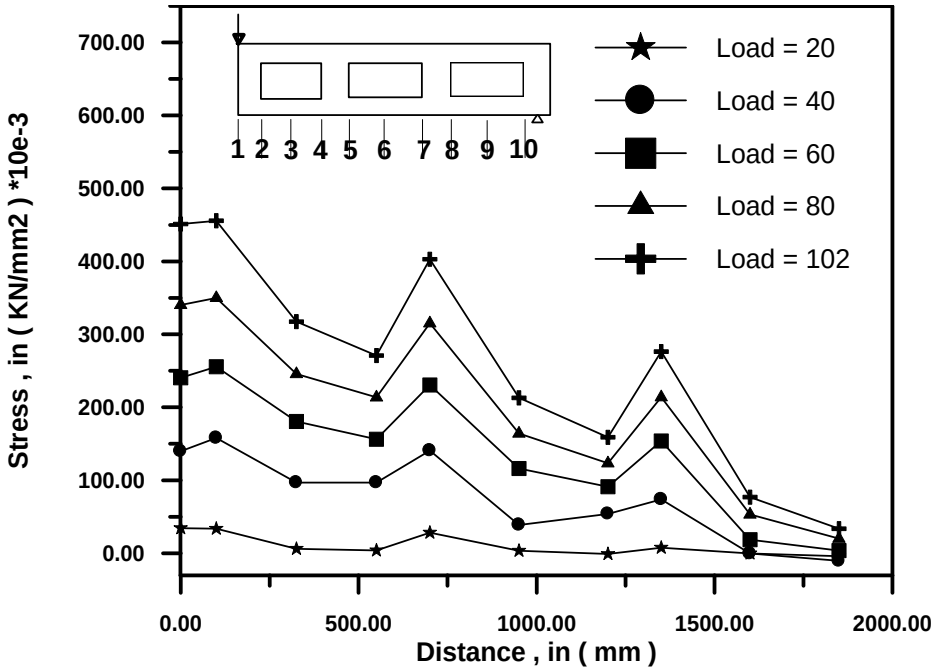

Fig 22 Stress distribution and development for the bottom steel bars of VER1.

This longitudinal stress reaches its maximum magnitude at mid-span, where maximum number of cracks exists, and decreases gradually as close from support, with some inflection points appear through structure holes. By increasing the applied load, the stress distribution magnitude increases indicating that the steel bars carry the stress release from the cracked concrete to achieve the equilibrium.

Crack pattern

Figs. (23-a, b, c and d) show the crack distribution and propagation through different load stages

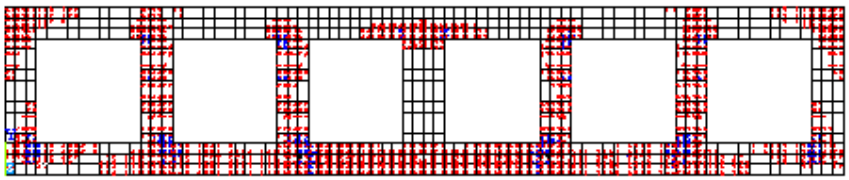

Fig. 23-a Crack pattern of VER1 at load (45 kN).

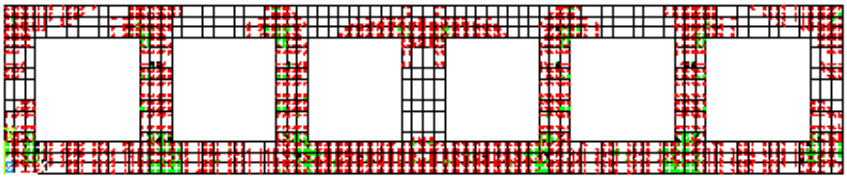

Fig. 23-b Crack pattern of VER1 at load (60 kN).

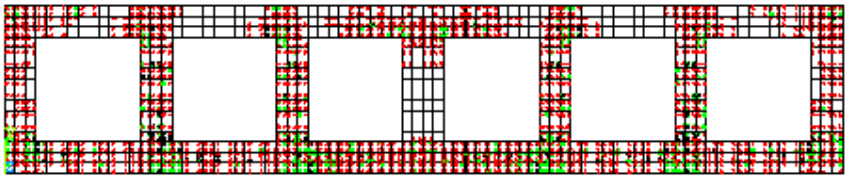

Fig. 23-c Crack pattern of VER1 at load (75 kN).

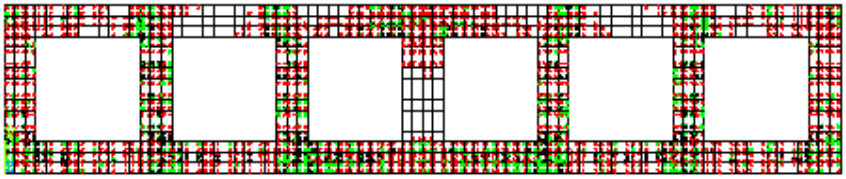

Fig. 23-d Crack pattern of VER1 at load (90 kN).

CONCLUSIONS

* The developed program has shown good agreement with experimental data of (Taan and Swamy) and ANSYS program in case of fibrous concrete.
* The use of inclined chords is recommended, because this inclination greatly reduces the bending stress.
* The use of steel fiber increases strength by (16.93 %) while deflection is decreased by (15.335 %) for the examples considered herein.
* The use of steel fibers is shown to increase the toughness much more than the first crack strength.
* The addition of steel fibers enhances the tensile strength, crack resistance, crack control.
* Fiber length, fiber diameter and fiber volume fraction influence the mechanical properties of steel fiber reinforced concrete.
* The usage of steel fibers may particularize in the tension and shear zones only for economical purposes.
* Tension zone is concentrated in central bottom chords with some fragmentary portions in structure, while shear zone is concentrated in verticals and middle of outer chords.
* Stress in steel bars has some inflection points because of change in stress distribution.

REFRENCES

- Al-Sha'arbaf (1990), "Three-Dimensional Nonlinear Finite Element Analysis of Reinforced Concrete Beams in Torsion" Ph.D. Thesis, University of Bradford, 1990.

- Alwash, N. A. K., "Nonlinear Finite Element Analysis of Reinforced Vierendeel Trusses", Ph.D. Thesis, University of Technology, 1995.

- Cervera, M., Hinton, E. and Hassan, O., "Nonlinear Analysis of Reinforced Concrete Plat and Shell Structures Using 20-Noded Isoparametric Brick Elements", computer and structure, Vol.25, No.6, p.p. (845-869), 1987.

- Chandrupatla and Belegundu, " Introduction to Finite Elements in Engineering", Prentice-Hall International, Inc.

- Chen, W.F., "Plasticity in Reinforced Concrete", McGraw-Hill Book company.

- Hannant, D. J., " Fiber Cement and Fiber Concrete", JOHN WILEY & SONS.

- Hoover Support Team, www.hoverdambypass.org, PDF file

- Jenn-Chuan Chern, et. al, "Behavior of Steel Fiber Reinforced Concrete in Multiaxial Loading" ACI materials journal, Vol. 89, No.1, January-February 1992, p.p. (32-40).

- Manual of concrete practice 1985, ACI committee 544, part5.

- Soroushain, P., and Lee, C. D., "Constitutive Modeling of Steel Fiber Reinforced Concrete under Direct Tension and Compression" Proceeding of the Inter. Conf. on the Recent Developments In Fiber Reinforced Cements And Concrete, 18-20 September 1989, Cardiff (U. K.), Eds. Swamy and Barr, p.p. (363-377).

- Traina, L. A., and Mansour, S. A., "Biaxial Strength And Deformational Behavior Of Plain And Steel Fiber Concrete" ACI material journal, Vol.88, No.4, July-Augost 1991, p.p. (354-362).

- Yin, W.S., et al, "Biaxial Tests of Plain and Fiber Concrete" ACI materials journal, Vol.86, No.3, May-June 1989, p.p. (236-243).

- Young D., "Analysis of Vierendeel Truss" ASCE transportation paper No. 1973, p.p (869-938).

NOTATIONS

$\{a\}$	Flow vector
d_f	Fiber diameter
$f(\sigma)$	Yield surface, yield function
f'_{cf}	Compressive strength of fiber reinforced concrete
f_{tf}	Tensile strength of fiber reinforced concrete
I_1	first invariant of the stress tensor
and J_2 J_3	second and third invariant of the deviator stress tensor
L_f	Fiber length
N_f	Number of fibers per unit cross-section area
V_f	Volume fraction of fiber

α_1	Rate of strain decay
α_2	Sudden loss in stress ration
β	Shear reduction factor
ε	Strain
ε_{cf}	The total strain
ε_{cu}	Ultimate strain value that can be extrapolated from the ultimate compressive test
ε_{tf}	Tensile strain of fiber reinforced concrete
γ_1	Rate of decay of shear stiffness as the crack widens
γ_2	Ratio of sudden loss in shear at the instant of cracking
γ_3	Ratio of the residual shear stiffness due to the dowel
$d\lambda$	A factor determining the size of the plastic strain increment
σ	Stress
σ_o	Equivalent effective stress at onset of plastic deformation
$\bar{\sigma}$	Effective stress or the equivalent uniaxial stress
σ_{cr}	Cracking stress
τ_u	Shear stress between the fiber and the concrete
ξ , η and ζ	Local coordinate

CHARACTERISTICS OF GYPSIES SOILS TREATED WITH CALCIUM CHLORIDE SOLUTION

Dr. Saad Farhan Al-Abdullah Highway Engineering Dept., Al-Mustansiria University
Nabeel Shaker Mahmood Al-Dulaimi (M.sc. Civil Engineering)

ABSTRACT

Gypseous Soils are distributed in many regions in the world including Iraq, which cover about (31.7%) of the surface area of the country. Existence of these soils, some times with high gypsum content, caused difficult problems to the buildings and strategic projects due to dissolution and leaching of the gypsum slates by the action of water flow through the soil mass.

In this study the effect of treatment with Dihydrate Calcium Chloride ($CaCl_2.2H_2O$) as water solution on compaction, compressibility, leaching, permeability and shear strength characteristics of Gypseous soil is investigated.

It is found that the maximum dry unit weight increases while optimum moisture content decreases with the increase in the concentration of calcium chloride in the molding water.

It is concluded that the engineering properties of the samples are highly improved when the samples are soaked in calcium chloride solution at (20%) concentration. Where, considerable reduction is observed in compressibility, collapsibility, coefficient of permeability, percentage of dissolved gypsum and leaching strain. Also, the treatment minimizes the reduction in cohesion component (c) upon soaking in water and slightly decreases the angle of internal friction (ϕ).

Analysis of the tests results showed that the using of calcium chloride solution in improvement the gypseous soil is more efficient than using it in any other form (powder).

الخلاصة

تتوزع الترب الجبسية في عدة مناطق من العالم ومن ضمنها العراق، حيث تغطي حوالي(31.7%) من المساحة السطحية للقطر. وإن وجود هذه الترب و بنسب جبس عالية في بعض المواقع قد سبب عدة مشاكل معقدة للمباني والمشاريع الستراتيجية، بسبب ذوبان وغسل الجبس بتأثير جريان الماء خلال كتلة التربة.

في هذا البحث تم دراسة تأثير المعالجة باستخدام كلوريد الكالسيوم المائي($CaCl_2.2H_2O$) كمحلول مائي على خصائص الرص، الانضغاط، الغسل، النفاذية ومقاومة القص للتربة الجبسية.

وقد وجد بان الكثافة الجافة العظمى تزداد وفي نفس الوقت المحتوى الرطوبي الأمثل يقل مع زيادة تركيز كلوريد الكالسيوم في الماء المستخدم في عملية الرص.

وقد تم استنتاج إن الخصائص الهندسية للنماذج تتحسن بصوره كبيرة بعد غمر النماذج بمحلول كلوريد الكالسيوم بتركيز (20%). حيث يلاحظ نقصان في كل من الانضغاطية ،الانهيارية، معامل النفادية، نسبة الجبس الذائب و انفعال الغسل. كذلك فان المعالجة تقلل النقصان في معامل التماسك(c)عند الغمر وتقلل بشكل طفيف زاوية الاحتكاك الداخلي للتربة المعالجة. كما إن

تحليل النتائج اظهر أن استخدام كلوريد الكالسيوم كمحلول مائي في تحسين التربة هو اكثر كفاءه من استخدامه باي شكل آخر (مسحوق).

INTRODUCTION

The development programs of many areas last years in Iraq was faced with a problem due to existence of various amount of gypsum in most of these areas as partially gypsum stratum or soil containing an amount of gypsum.

Many major projects suffered from several problems related to construction on or by gypseous soils such as cracks, tilting, collapse and leaching the soil. These problems could happen due to percolation of water into these soils causing dissolution of gypsum, which provides the cementing bonds between the soil particles. This process leads to collapse of soil structure and progressive compression, and the problem becomes more complicated if flow occurred causing continuous loss of soil mass and formation of serious cavities.

These considerable changes in the engineering properties of gypseous soils upon wetting or leaching necessitate geotechnical investigations of these soils and adopting more beneficial methods to improve their properties.

This study is an attempt to treat the gypseous soil adopted by using a water solution of dihydrat calcium chloride ($CaCl_2.2H_2O$) to improve its properties.

GYPSUM AND ITS SOLUBILITY

From chemical point of view, gypsum is calcium sulfate with two water molecules attached (CaSO4.2H2O), the two other natural forms of calcium chloride are anhydrate (CaSO4) and hemihydrate plaster of Paris (Bassanite) (CaSO4. 1/2H2O), alter to gypsum at the temperature and pressure normally found at the earth's surface (Nafie, 1989).

Saaed and Khorshid (1989), reported that the solubility of gypsum is of the order 2.41gm/1, while Saleam et. al.(1988), reported that the saturated solution may contains about 2.6 gm /1.

Seidell and Linke (1958), collected data from many references for the solubility of gypsum in water solutions of some salts. They showed that some salts such as [$Mg(NO_3)_2$, $Mgcl_2$, Kcl, $NaNO_3$, NaCl] increase the ionic strength and that lead to increase the solubility of gypsum. On the contrary to that, there are other salts like [$CaCl_2$, $MgSO_4$] cause an increase in common ions (Ca^{+2} or $S4^{-2}$), and thus decreasing the solubility of gypsum, see fig. (1).

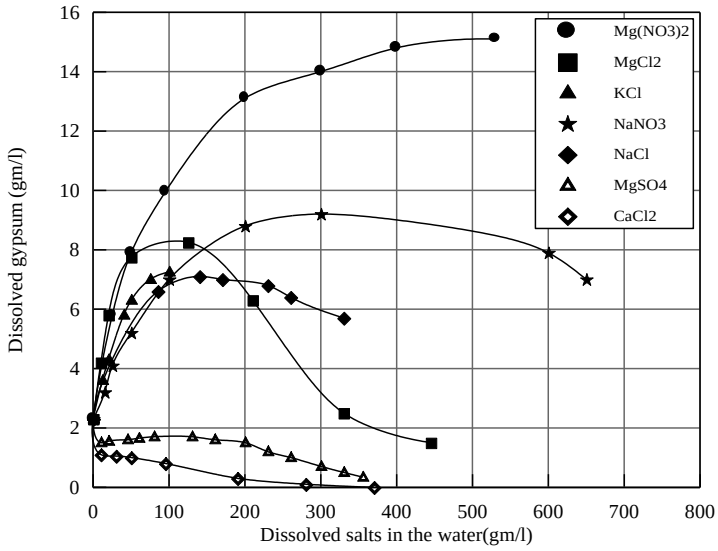

Fig. (1): Solubility of Gypsum at Different Salts Concentrations,

(Data Collected by Seidell and Linke, 1958).

EXPERIMENTAL WORK

Soil Properties

The soil of this investigation was taken from Heet site west of Iraq. Summary of physical and classification properties is presented in Table (1).

Table (1): Summary of physical and classification properties

Gypsum content %	53	$\gamma_{d\ field}$ (kN/m^3)	14.4
TSS (%)	52.39	L.L. %	31
SO_3(%)	26.6	P.L. %	16
pH	7.79	%Sand	82
G_s	2.43	%Fines	18
e_o	0.687	Soil Classification According to USCS	SC

Testing Program

Because of the difficulty of obtaining undisturbed samples for the engineering tests, the samples are prepared to satisfy dry unit weight by using static compaction method.

A series of engineering tests was conducted on the soil treated with a water solution of calcium chloride. This series including compaction, compressibility, leaching and shear strength tests.

Compressibility tests were performed using oedometer device. Shear strength parameters for both soaked and unsoaked samples were determined by using direct shear apparatus. Leaching tests were conducted using special oedometer cell called the Permeability-Consolation Cell.

Method of Treatment with Calcium Chloride Solution

The commercial product of Dihydrate Calcium Chloride ($CaCl_2$.2H2O), with purity from (94 to 97) %, was used in this study to improve the engineering properties of the gypseous soil taken from Heet area. The salt is white in color and crystalline solid in the hydrous state.

The procedure of treatment of gypsum with the salt could be summarized in following steps:

1. Preparing three concentrations (10, 20 and 30) %of calcium chloride solution by adding a specified weight of the salt to the distilled water to satisfy the required concentration. It should be noted that the adding of water to the salt causes an agglomeration of salt particles, and these will not dissolve easily. Therefore, the salt should be added to the water in small amounts with continuous mixing.
2. Preparing the samples at their field dry densities using static compaction method.
3. Soaking the samples in calcium chloride solution for about two hours.
4. After soaking period the samples were kept for (24) hours in nylon bags to insure homogeneous distribution of the solution through the samples. Then the samples were dried in the oven at (45°C) until the weights stabilize. These weights compared with their original dry weights lead to determine calcium chloride content as solids in the samples with respect to each concentration.

ANALYSIS AND DISCUSSION OF THE RESULTS

Effect of Treatment on Compaction Characteristics

Compaction curves for treated soil at different calcium chloride concentrations dissolved in molding water are shown in fig. (2). It can be seen that the maximum dry unit weight increases and

optimum moisture content decreases conjugate with the increase in concentration of the solution. This behavior may be attributed firstly to increase in fine particles and secondly to the lubrication between soil grains, where chlorides are considered as good lubricants when added to the soil (O'Flaharty, 1974).

Effect of Treatment on Compressibility Characteristics

The results of standard odometer tests of the soil treated with calcium chloride solution at different concentrations are shown in fig. (3). Also the tests results are listed in Table (2).

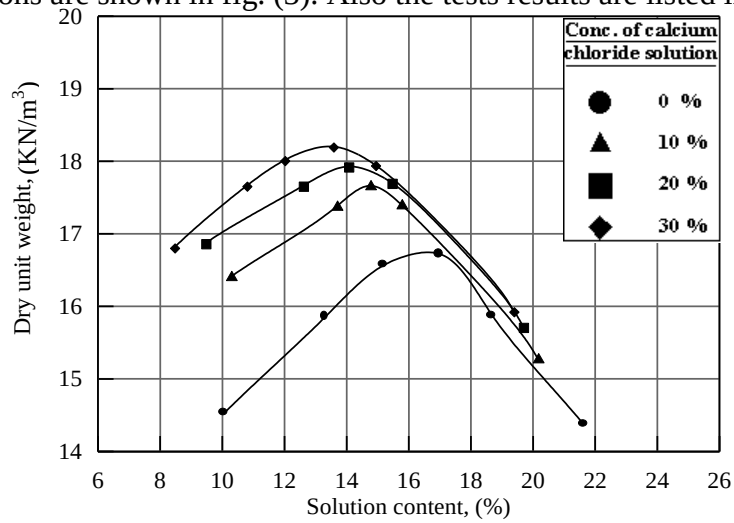

Fig. (2): Compaction Curves of Treated Soil at Different Solution Concentrations

In general the virgin compression and recompression curves are approximately linear. Also, the total volumetric strain at 800kPa ($\varepsilon v, _{800}$) decreases from (17.71 to 10.16) % and the compression index (Cc) decrease from (0.260 to 0.085), when the concentration of the used salt increases from (0 to 30) %. This behavior may be due to decrease of the dissolution of gypsum and increase of the cementing bonds between the soil particles.

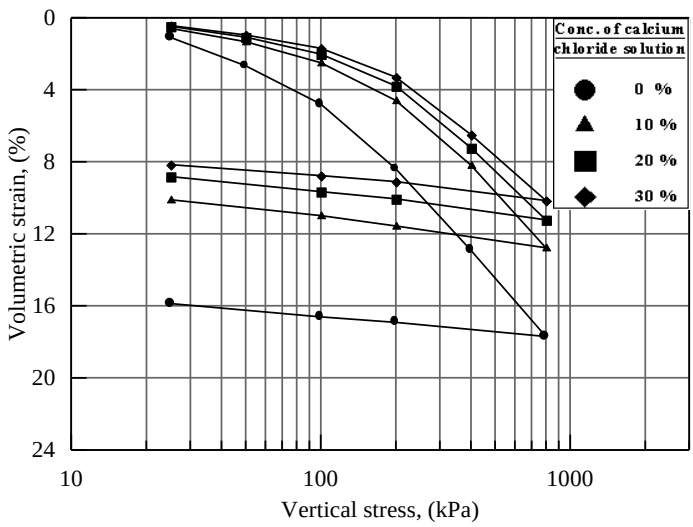

Fig. (3): Compression Test Results of Treated Soil

Table (2): Summary of Compression test Results of Treated Soil.

c.c.s* (%)	c.c.c** (%)	e_o	γ_d kN/m^3	$\varepsilon_{v,800}$ %	C_c	C_r
0	0	.687	14.13	17.71	.26	.022

10	1.95	.65	14.62	12.77	.139	.0251
20	3.64	.599	14.87	11.23	.137	.0260
30	5.14	.568	15.38	10.16	.085	.0260

* c.c.s: Concentration of Calcium Chloride Solution.
**c.c.c : Calcium Chloride Content as Solid in the Sample.

Collapsibility Characteristics

The results of collapse test are shown in fig. (4). It is obvious that the collapse potential highly decreased after treatment with calcium chloride solution.

Table (3) shows that the collapse potential of untreated soil is (5.28), where the degree of specimen collapse classified as a "Moderate" according to ASTM D5333, 2003. While this value decreases to (1.62) after treatment with the solution at (30%) concentration. Where the reduction in collapse potential is about (69.3%) and the degree of specimen collapse classified as a "Slight".

This reduction in collapse potential after treatment may be attributed to increase the common ion (Ca^{+2}), which decrease the solubility of gypsum (as explained in sec.2). In addition to that the used salt acts as a filler material in the pores of the soil and provides new commenting bonds between the particles. Also, It can be observed from Table (3) that collapse potentials obtained from the double oedometer test are greater than those obtained from collapse test

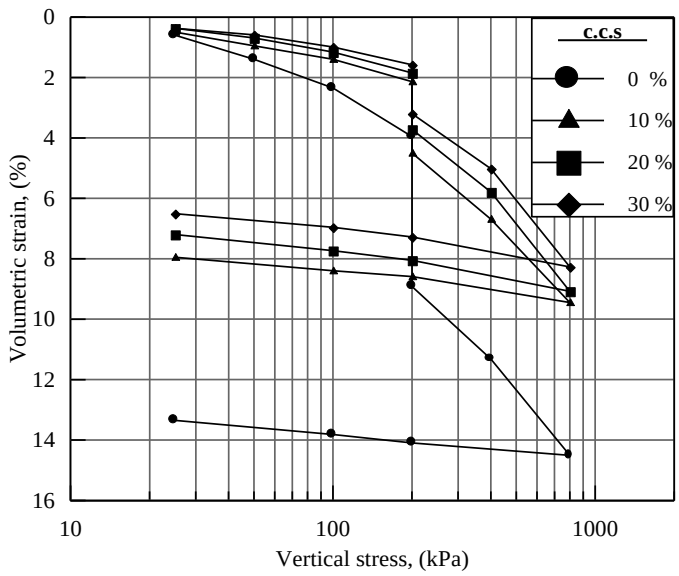

Fig. (4): Results of Collapse Test of Soil Treated with different (c.c.s)

Table (3): Collapsibility Tests Results of Treated Soil.

Soil Property	Concentration of Calcium Chloride Solution, %			
	0	10	20	30
c.c.c, %	0	1.98	3.63	5.12
e_o	0.687	0.65	0.599	0.568
γ_d (kN/m^3)	14.4	14.63	14.89	15.38

CT Collpse test	CP, %	5.28	2.36	1.87	1.62
	Reduction in CP, %	0	55.3	64.58	69.31
DOT Double Oedometer Test	CP, %	5.54	2.49	1.98	1.65
	Reduction in CP, %	0	55.05	64.26	70.21

Permeability and Leaching Characteristics

The effect of treatment on permeability and leaching characteristics of the soil was investigated. The oedometer permeability-leaching test (OPLT) was conducted under two leaching stresses (100 and 200) kPa with hydraulic gradient (i) equal to (20). A discussion of the effect of treatment on coefficient of permeability, leaching strain and dissolved gypsum could be as follows:

Permeability Characteristics

The variation of coefficient of permeability (k) with time at different concentrations of ($CaCl_2$) solution for each leaching stress level is shown in fig. (5).

It can be seen from this figure that the permeability decreases with the increase in concentration of the used solution up to 20%. But with higher concentration, i.e. (30) %, it begins to increase. Al-Busoda (1999), found similar results when treated the gypseous soil with 2.5 and 5 % calcium chloride powder. She attributed the decrease in permeability to increase in fine particles that filled the voids within soil structure. Moreover, the salt reduces the dissolved gypsum, and those decrease the construction of new voids or enlarging the original voids. While she attributed the increase in permeability with increase in calcium chloride content to hydration process of the additive to ($CaCl_2.6H_2O$) under certain conditions. This process generating a pressure tried to spread the particles from each other, therefore, the void ratio will increase. So, the coefficient of permeability will increase.

Also, it can be noticed that the permeability decreased with the increase in leaching stress level due to reduction in void ratio, which leads to the elimination of water paths. These results agree with the results obtained by Seleam (1988), Nashat (1990), Al-Busoda (1999), and Al-Qaisee (2001).

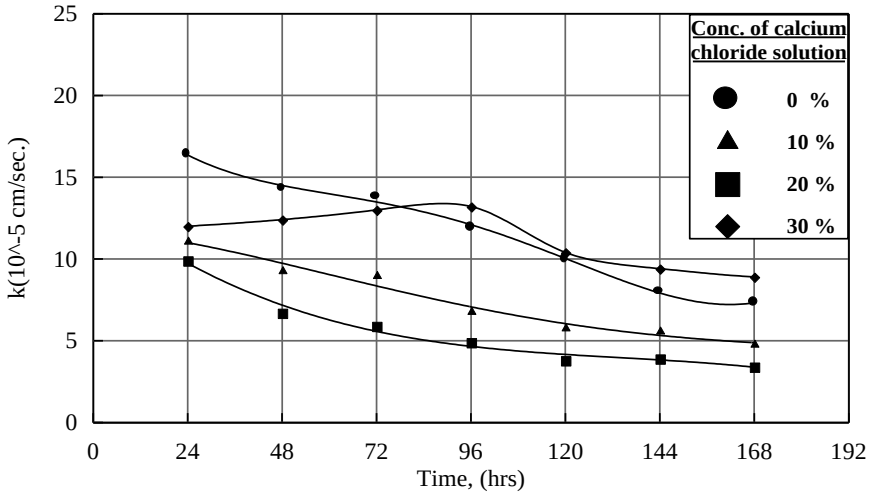

(a)

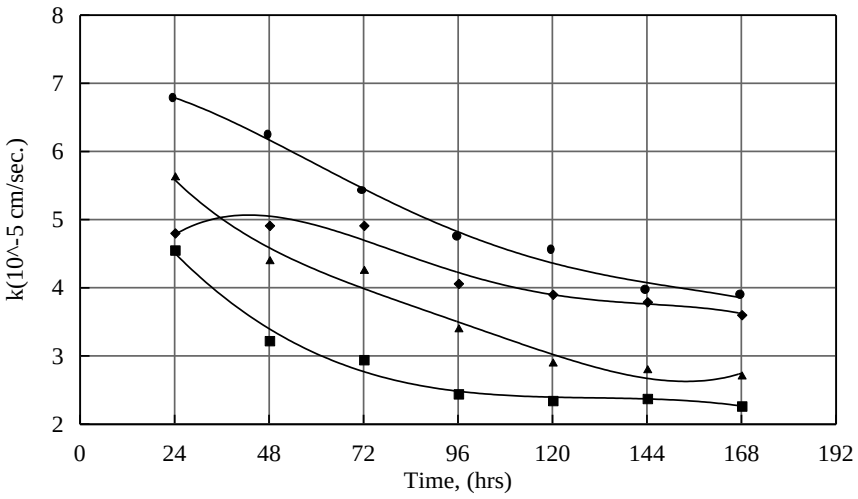

Fig. (5): Results of Oedometer-Permeability Leaching Test of Samples Treated with Different (c.c.s):
(a) Coefficient of Permeability (k) vs. Time Relation, σ_v=100 kPa
(b) Coefficient of Permeability (k) vs. Time Relation, σ_v=200 kPa

Leaching Characteristics

The variation of leaching strain and dissolved gypsum during leaching process at different $CaCl_2$ concentrations and leaching stresses are shown in figs. (6) and (7).

In general, it can be seen that the leaching strain increased with time as the leaching process continued. This behavior may be due to the continuous dissolution of gypsum that caused a continuous settlement. Also, the leaching strain increased with the increase in percentage of dissolved gypsum. Similar results are reported by many researchers such as Al-Khuzaie (1985), Seleam (1988), Al-Busoda (1999) and Al-Beiruty (2003).

Fig. (6) Shows significant reduction in leaching strain with time of the soil treated with (10 and 20) % concentrations. While with (30) % concentration the leaching strain begins to increase, but it remained below the leaching strain of untreated soil. The treatment with ($CaCl_2$,) leads to increase the calcium cations (Ca^{+2}) which represent the common ions with calcium cations of the gypsum, therefore, the amount of dissolved gypsum will decrease. So, the leaching strain decreases.

The increase in leaching strain which was observed for the specimens treated with (30) % concentration may be attributed to the increase in permeability (discussed previously in section 4.3.1) which will increase the dissolution of gypsum and calcium chloride and removal of it from soil skeleton. Hence additional leaching strain will take place due to the collapse of soil structure.

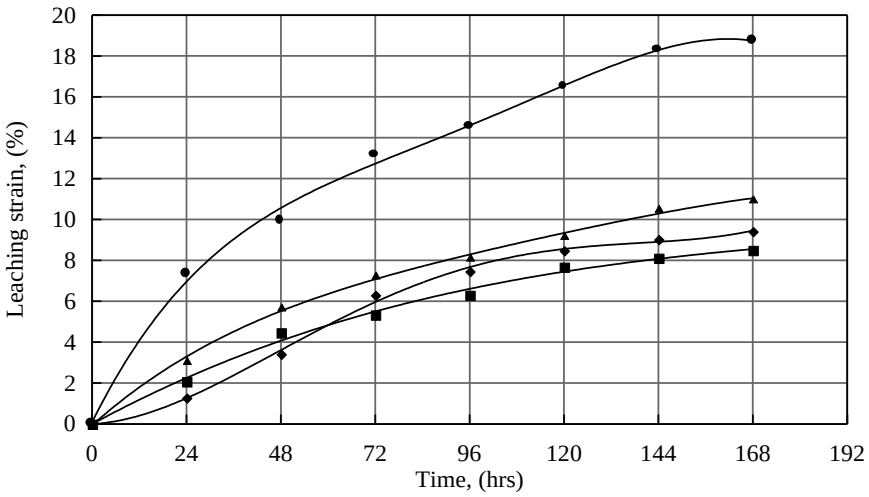

Fig. (6): Leaching Strain vs. Time Relation, σ_v=200 kPa

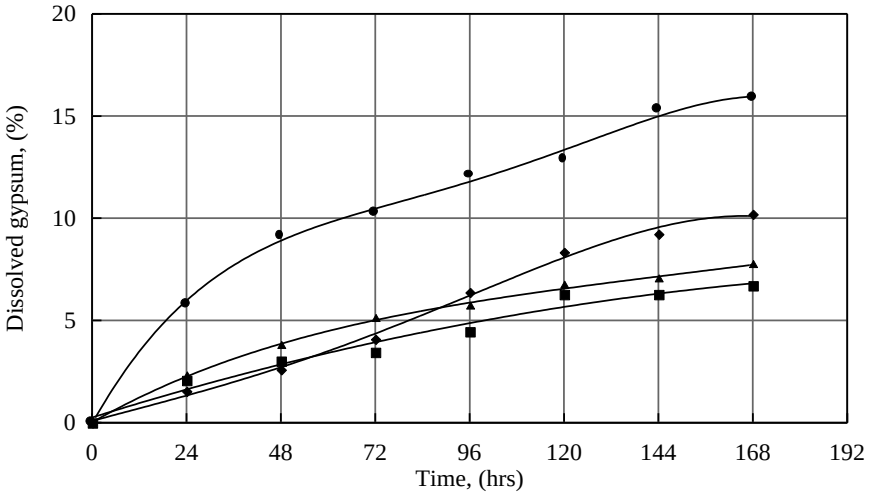

Fig. (7): Dissolved Gypsum vs. Time Relation, σ_v=200 kPa

Shear Strength Characteristics

To predict the shear strength parameters (c and ϕ), two types of tests were conducted on (6) samples treated in the same concentration, three of them tested in dry state, while the other three samples were tested after soaking in water for (2) hours.

Typical results of direct shear tests conducted on the samples treated with 20% concentrations of calcium chloride solution at dry state are shown in fig. (8)

For unsoaked samples, it can be observed that the cohesion (c) increases with increase concentration of calcium chloride solution. On the other hand, the treatment minimized the reduction in cohesion (c) that occurred due to soaking. This behavior may be attributed to the existence of calcium chloride as solids in the voids which act as binder material between the particles; moreover, it decreases the destruction of the gypsum bonds after soaking in water. Fig. (9) presents the values of shear strength parameters (c andϕ) in terms of isobar.

Also, a reduction in the values of angle of internal friction (ϕ) is observed after treatment especially for soaked samples. This could be attributed to that calcium chloride acts as lubricant when added to the soil. On the other hand, the soaking leads to hydration process of ($CaCl_2.2H_2O$)

which move the soil particles far from each other (as discussed previously), therefore, the inter particle friction will be reduced and as a result of that (ϕ) will decrease.

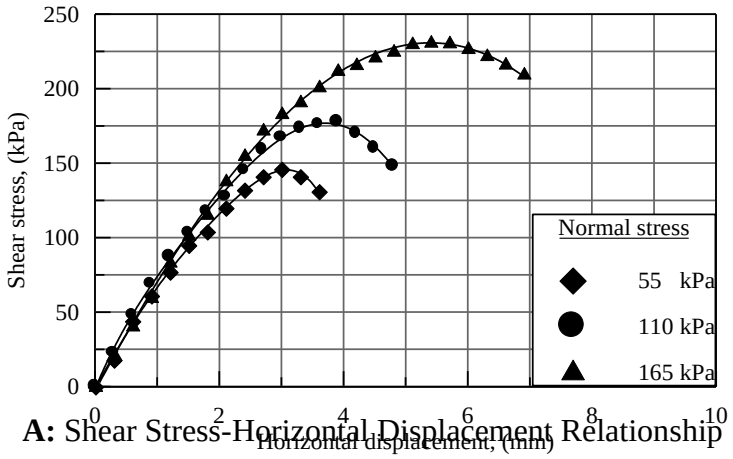

A: Shear Stress-Horizontal Displacement Relationship

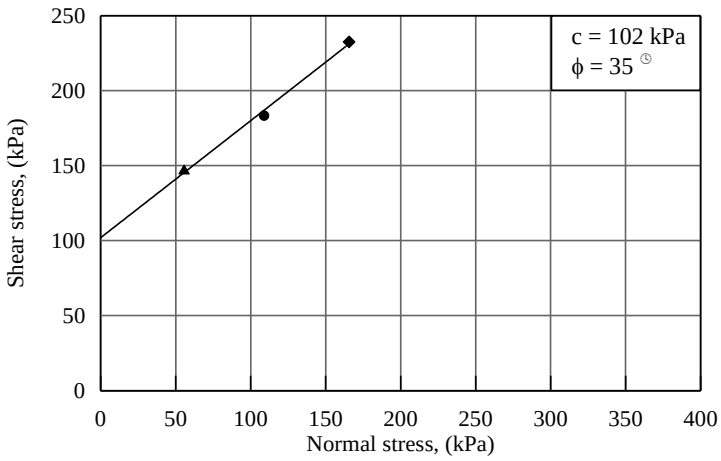

B: Shear stress –Normal Stress Relationship

Fig. (8): Direct Shear Test Results for Unsoaked Samples Treated with (20%) c.c.s

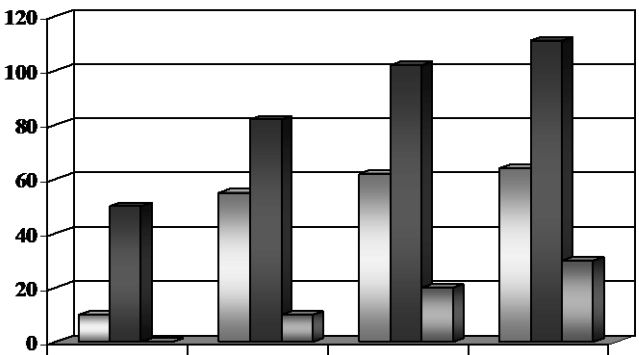

	1	2	3	4
con. Of (CaCl2) solution	0	10	20	30
c (unsoaked)	50	82	102	111
c (soaked)	10	55	62	64

A: Variation of Cohesion (c) with c.c.s of unsoaked and Soaked Samples

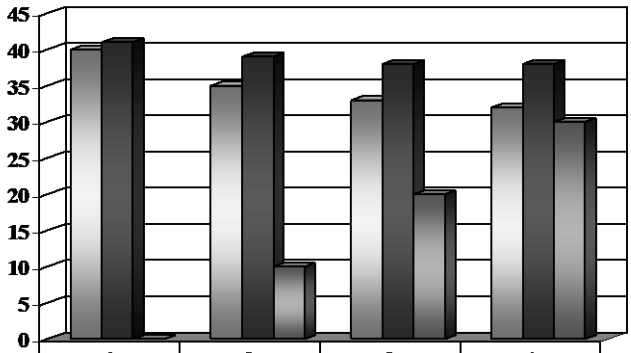

	1	2	3	4
con. Of (CaCl2) solution	0	10	20	30
(unsoaked)	41	39	38	38
(soaked)	40	35	33	32

B: Variation of Angle of Internal Friction (ϕ) with c.c.s of unsoaked and Soaked Samples

Fig. (9): Effect of Treatment on Shear Strength Parameters.

ANALYSIS OF TREATMENT RESULTS

From the results of the tests conducted on the samples after treatment with a water solution of ($CaCl_2.2H_2O$) at three concentrations (10, 20 and 30%) as explained previously, it can be concluded that (20%) is the optimum concentration of calcium chloride solution to be used in improvement.

The treatment at this concentration yields an increase in maximum dry density obtained from standard compaction test. Also it gives a significant reduction in compressibility, permeability and leaching characteristics see Table (4).

CONCLUSIONS

- The increase in concentration of calcium chloride ($CaCl_2.2H_2O$) in water used in compaction process of the gypseous soil causes an increase in the maximum dry unit weight which leads to decrease the optimum moisture content.
- The treatment by soaking the samples in calcium chloride solution at 20% concentration (optimum concentration) caused the following:
  a. Decrease in the compression index (Cc) and increase in the rebound index (Cr).
  b. Reduce values of the collapse potential obtained from collapse and double oedometer tests up to (64%).
  c. Decrease values of the coefficient of permeability (k).

d. Decrease the percentage of dissolved gypsum and leaching strain.
e. Minimize the reduction in cohesion component (c) upon soaking in water and slightly decrease the angle of internal friction (ϕ).

1. the calcium chloride solution can be used easily in compaction process or as a grouting material compared it as powder.

Table (4): Summary of Test Results of Untreated and Treated Samples with ($CaCl_2$, 2H2O) Solution of 20% Concentration (optimum concentration).

Characteristics			Untreated Soil	Treated with 20%	Increase or Reduction
Compression Characteristics	C_c		0.26	0.137	Red. 47.3%
	CP% ,	CT	5.28	1.87	Red. 64.6%
		DOT	5.54	1.98	Red. 64.2%
Permeability and Leaching Characteristics(at σ_v=200 kPa)	$k_{ave.}$ x10^{-5} (cm/sec.)		5.07	2.88	Red. 43.2%
	Total Leaching Strain% ,		18.75	8.49	Red. 54.72%
	Total Dissolved Gypsum,%		15.87	6.71	Red. 57.71%
Shear Strength	Unsoaked	c, kPa	50	102	Inc.100.04%
		ϕ, deg.	41	38	Red. 7.31%
	Soaked	c, kPa	10	62	Inc. 500.2%
		ϕ,deg.	40	33	Red. 17.5%

NOTATION

c : Cohesion Component of Strength, (kPa)
c.c.c : Calcium Chloride Content as Solid in the Sample, (%)
c.c.s : Concentration of Calcium Chloride Solution, (%)
Cc : Compression Index
CP : Collapse Potential
Cr : Rebound Index
Dr : Relative Density, (%)
e_o : Initial Void Ratio
Gs : Specific Gravity
i : Hydraulic Gradient
k : Coefficient of Permeability, (cm/sec)
kav. : Average coefficient of Permeability
L.L : Liquid Limit
SC : Clayey Sand
TSS : Total Soluble Salts
USCS : Unified Soil Classification System
$\varepsilon_{v,800}$: Volumetric Strain at (800 kPa) Stress, (%)
ϕ : Angle of Internal Friction, (degree)
γ_d : Dry Unit Weight
$\gamma_{d\ field}$: Field Dry Unit Weight , (kN/m^3)
σ_n : Normal Stress, (kPa)

REFERENCES

Al-Beiruty, M.Z.A. (2003): "Collapse Potential Determination of Gypseous Soil" M.Sc. Thesis, Civil Engineering Department, University of Baghdad.

Al-Busoda, B.S.Z. (1999): "Studies on the Behavior of Gypseous Soil and its Treatment During loading" M.Sc. Thesis, Civil Engineering Department, University of Baghdad.

Al-Khuzaie, H.M.A. (1985): "The Effect of Leaching on The Engineering Properties of Al-Jazirah Soil", M.Sc. Thesis, Civil Engineering Department, University Of Mosul.

Al-Qaisee, G.S.H. (2001): "Leaching Collapse of Gypseous Soils", M.Sc. Thesis, Civil Engineering Department, University of Baghdad.

Nafie, F.A. (1989): "The Properties of High Gypseous Soils and their Significant for Land Management", Ph.D. Thesis, University of London.

Nashat, I.H. (1990): "Engineering Characteristics of Some Gypseous Soils in Iraq", Ph.D. Thesis, Civil Engineering Department, University of Baghdad.

O'Flaherty, C.A. (1974): "Highway Engineering", 2nd Edition, London.

Saaed, S.A. and Khorshid, N.N. (1989): "Some Essential Characteristics of the Gypseous Soils of Al-Dour Area", Proceeding of the 5th Scientific Conference, Vol.4, part 2, Scientific Research Council, Baghdad.

Saleam, K., Al-Barazanji, A. and Wadei, B. (1986): "Effect of Type of Water on the Dissolution of Gypsum in Al-Dour", Symposium on Gypsiferous Soils and Their Effect on Construction and Agriculture Production, Water and Soil Research Institute, Baghdad.

Seleam, S.N.M. (1988): "Geotechnical Characteristics of a Gypseous Sandy Soil Including the Effect of Contamination with Some Oil Products", M.Sc. Thesis, Building and Construction Department, University of Technology, Baghdad.

Seidell, A. and Linke, W.E. (1958): "Solubilities, Inorganic and Metalorganic Compounds", Vol.1, 4th ed., American Chemical Society, D.Van Nostrand Co., Princeton, N.J.

ANALYTICAL SOLUTION FOR THE DEVELOPED HYDRODYNAMIC PRESSURES IN RESERVOIRS DUE TO VERTICAL EARTHQUAKES WITH SEDIMENT EFFECT

Prof. Dr. Rafa Al-Suhaili
Env. Eng. Dept. Univ. of Bagdad.

Ass. Lecturer Mohammad Rashid Al-Gadsawi
Computer Center, Univ. of Bagdad

ABSTRACT

In a typical reservoir a sediment layer of considerable depth may be deposited on the top of exposed bedrock foundation. In this research an analytical solution was proposed to solve the case of the vertical acceleration with infinite reservoir with existence of such sediment layer.

The results indicate that as the depth of sediment increases, the pressure increases also. The behavior is found to be affected by the change of the degree of saturation of the sediment layer. As this degree of sediment decreases the developed Hydrodynamic pressure increase. A comparison between the case of stiff and soft foundation indicates that the pressure values are always greater for the stiff foundation.

حل تحليلي لايجاد الضغوط الهيدرونيماكية فى خزانات السدود الناجمة عن التعجيل العمودى للهزات الارضية مع وجود الرسوبيات

الخلاصة

ان دراسة استقرارية السدود عند تعرضها للهزة الارضية موضوع ذو اهمية لا تنكر فهنالك العديد من الدراسات حول هذا الموضوع ولكن معظمها تفترض ارضية الخزان خلف السلد صلدة. ونظراً لوجود طبقة رسوبيات على هذه الارضية فليس من الواقع ان نفرض كونها صلدة.

يشمل البحث دراسة تأثير حركة الارض العمودية التي تعطي تعجيلاً عمودياً لارضية الخزان في كلا الحالتين اعلاه تم دراسة تأثير نوعية ارضية الخزان (Stiff) صلدة و (Soft) رخوة وخصائص الرسوبيات مثل ارتفاعها ودرجة تشبعها.

تم استنباط حل تحليلي لمعادلة الموجة احادية البعد وتم استخدام معادلات لمعاملي الاخماد لتعجيل الهزة ومعامل امتصاص موجة الضغط في الشروط الحدودية للمسألة وعلى سطح الرسوبيات. وقد بيّن الحل بأن معادلة الضغط تتكون من حدين حد حقيقي وآخر خيالي في حالة وجود الرسوبيات .

بينت نتائج الدراسة ان قيم الضغوط الهيدروديناميكية في الاحوال جميعا تكون اعلى في حالة اعتبار ارضية الخزان صلدة (Stiff) مما هي عليه في اعتبارها رخوة (Soft) اما بالنسبة لخصائص الرسوبيات مثل عمق الرسوبيات فقد اظهرت نتائج البحث بأنه يمكن القول بصورة عامة بأن الضغط يزداد بزيادة عمق الرسوبيات في حالة التشبع الكلي. اما بخصوص درجة التشبع فكانت الضغوطات المتولدة تزداد كلما قلّت درجة التشبع.

INTRODUCTION

The design of a new dam and safety evaluation of an existing dam should be carried out with a high level of accuracy. The failure of such structures, particularly during an earthquake may, be disastrous. Most failures recorded of such structures were due to earthquakes (**Okamoto, 1973**). During earthquakes, a pressure in excess of hydrostatic is exerted on the dam face, called hydrodynamic pressure. Hydrodynamic force was hence developed and may cause failure. The response of a dam to an earthquake is affected by the compressibility of water in the reservoir, and the absorption of pressure waves at the bottom of the reservoir. Therefore, an accurate analysis should consider these two factors, in addition to other factors, such as, earthquake acceleration intensity and frequency, with the geometrical factors.

Reservoir sedimentation is a complex process varying with sediment production rate, transportation, and deposition as mentioned by (**Chen and Hung,1993**), serious deposition of sediment in reservoirs built prior to (1935) were identified. One-third of these reservoirs lost between one-fourth and one-half of their original capacity. About (14%) of the reservoirs lost between (50-70%) of their original capacity, and 10% were completely depleted.

(**Chopra *et al*., 1980**) investigated the response of concrete gravity dams, including the dynamic effects of impounded water and flexible foundation rock, to the transverse (horizontal) and vertical components of earthquake ground motion. The system was analyzed under the assumption of linear behavior for the concrete, foundation rock and water. The complete system was considered as composed of three substructures: the dam, represented as a finite element system. The fluid domain, as a continum of infinite length in the upstream direction, and the foundation rock region as a viscoelastic halfplane

(**Hall and Chopra,1982**) developed an analysis procedure in the frequency domain for determining the earthquake response of two-dimensional concrete gravity and embankment dams including hydrodynamic effect; response of the elastic dams and compressible water are assumed linear. The dam and fluid domain are considered to behave linearly, and the water as compressible. The dam and fluid domain are treated as substructure and modeled with finite elements. The fluid domain model approximately accounts for the interaction between the fluid and the underlying foundation medium through a damping boundary condition applied along the reservoir bottom. The sediment at the bottom of the reservoir can be roughly represented by introducing a so-called absorbing boundary at the bottom of the reservoir.

(**Lotfi and Tassoulas,1986**) developed a finite element method for the two-dimensional problems of the dynamics of dam-reservoir-foundation systems, taking into account all interactions rigorously. In this study the dam-reservoir-foundation region is partitioned into three subregions: the neighborhood of the dam, the solid hyperelement and the fluid-solid hyperelement. This study indicates that including the sedimentary layer decreases the response to vertical ground motion significantly. However, the response to horizontal ground motion is very little reduced. A comparison

with the results obtained by the modified approximate treatment of reservoir-foundation interaction showed very good agreement.

(**Cheng,1986**) solved a simplified problem of a rigid dam impounded with water and subjected to vertical harmonic earthquakes. The reservoir bottom was modeled as a poroelastic sediment layer of finite extent sitting on the top of a semi-infinite elastic and impervious foundation. The reservoir bottom damping coefficients were obtained and explicitly expressed in terms of the earthquake excitation frequency and the material properties of the sediment.

(**Bougacha and Tassoulas,1991**) determined the response of a concrete gravity dam for a selected earthquake record in order to assess the potential significance of the sedimentary material accumulating on the reservoir bottom. The results were found to be sensitive to the direction of the horizontal ground motion. The significance of partially saturated sediment seems to be most pronounced when horizontal and vertical ground excitations are combined and less notable when only horizontal ground acceleration is applied. This study suggests that the reservoir bottom sediment may play a role in the response of dams to earthquakes. However, the importance of this role seems to hinge on the sediment properties, especially the pore-fluid compressibility.

(**Chen and Hung,1993**) used a two-dimensional model of poroelastic media to obtain the dynamic effect of reservoir sediment on the hydrodynamic pressure of an incompressible impounded water. The pressure wave equation for the pore water and the sediment is solved by an implicit finite difference method coupled with a fast Poisson solver. The sediment in this model has been treated as a fluid-filled mixture consisting of both solid and fluid phases. During the onset of ground acceleration, the ground rise of pore pressure associated with the compressibility of the pore water results in an incipient reduction of dynamic pressure in the impounded water. However, the dynamic pressure of the incompressible impounded water rises rapidly with the pore pressure associated with the pressure wave and inertia in the sediment.

(**Zhao,1994**) considered a simplified problem of a rigid dam impounded with water and subjected to vertical and harmonic earthquakes. The sediment of certain thickness at the bottom of a reservoir is assumed to be an elastic medium overlaying the top of a semi-infinite and impervious foundation. If the gravity dam is assumed to be rigid and the lateral scattering of reflected waves is negligible, a water-gravity dam-foundation system can be simplified as a one-dimensional wave problem.

(**Al-Suhaili,1997**) used a finite element model to investigate the transient pressures generated by earthquake in reservoirs, tunnels, and bottom outlets. Both infinite and finite reservoir cases were considered. The effect of tunnel diameter to reservoir height ratio, reservoir height to length of tunnel, and reservoir height to extent of reservoir ratio were studied. The effect of excitation frequencies was also investigated analytical solutions were also presented for two cases,namely dam-tunnel-reservoir with tunnel gate excited horizontally, and a reservoir and tunnel bottom excited vertically. All of those solutions were found to be simple and in good agreement with the verified finite elements results.

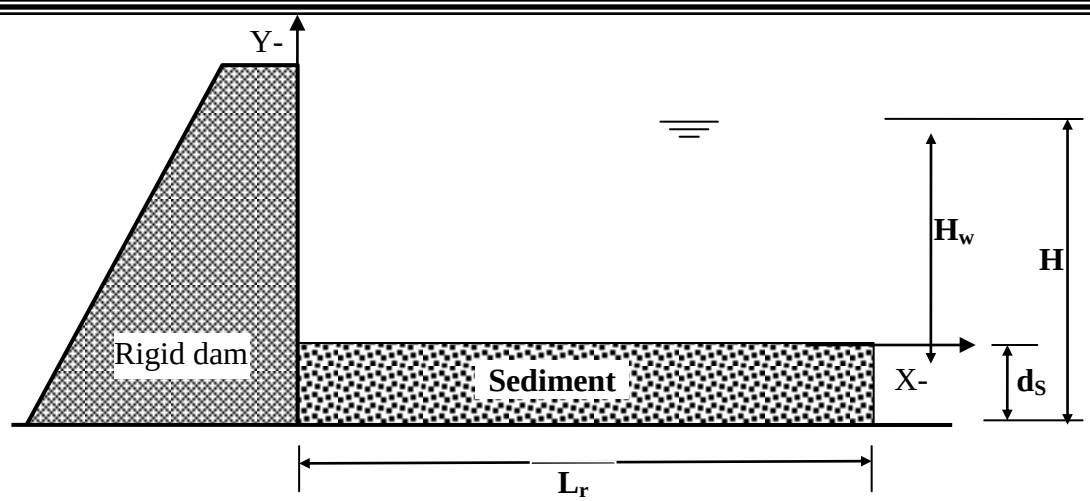

Bedrock foundation
Fig -1-

The proposed analytical Solution

For the case of infinite reservoir and with the existence of a sediment layer at the bottom of the reservoir i.e., (ds ≠ 0) depth of sediment layer fig (1), no analytical solution could be found in the literature. It is proposed to solve this problem using the one-dimensional wave equation and the following boundary conditions:

$$\frac{d^2\,\overline{P}}{d\,y^2}+\frac{\omega^2}{C_w^2}\overline{P}=0 \tag{1}$$

$$\overline{P}\left(H_w,\omega\right)=0 \tag{2}$$

$$\frac{d\,\overline{P}}{d\,y}\left(0,\omega\right)=-\left(\alpha_r+i\,\alpha_i\right)\rho_w\;ay+i\left(\frac{\omega}{C_w}\right)\left(\beta_r+i\beta_i\right)\overline{P}\left(0,\omega\right) \tag{3}$$

Where

Using the method of separation of variables, the solution is:

$$\overline{P}\left(y,\omega\right)=A\,sin\left(\frac{\omega}{C_w}y\right)+B\,cos\left(\frac{\omega}{C_w}y\right) \tag{4}$$

Applying the boundary condition Eq. (2) gives:

$$B=-A\,tan\left(\frac{\omega}{C}H_w\right) \tag{5}$$

and the boundary condition Eq. (3) gives:

$$A\times\frac{\omega}{C}=-\left(\alpha_r+i\,\alpha_i\right)\,\rho_w\;ay+i\left(\frac{\omega}{C_w}\right)\left(\beta_r+i\beta_i\right)\overline{P}\left(0,\omega\right) \tag{6a}$$

$$A=-\left(\alpha_r+i\,\alpha_i\right)\;\rho_w\,ay\left(\frac{C_w}{\omega}\right)+i\,\left(\beta_r+i\beta_i\right)\overline{P}\left(0,\omega\right) \tag{6b}$$

$$A=\left(-\,\alpha_r\,\rho_w\,ay\left(\frac{C_w}{\omega}\right)-\beta_i\;\overline{P}\left(0,\omega\right)\right)+i\left(-\alpha_i\,\rho_w\,ay\left(\frac{C_w}{\omega}\right)+\beta_r\;\overline{P}\left(0,\omega\right)\right) \tag{6c}$$

Since $\overline{P}(0,\omega)=B$, Eq. (4) can be modified as:

$$A=\frac{-\,\alpha_r\,\rho_w\,ay\left(\frac{C_w}{\omega}\right)-i\,\alpha_i\,\rho_w\,ay\left(\frac{C_w}{\omega}\right)}{1+i\beta_r\;tan\left(\frac{\omega}{C_w}H_w\right)-\beta_i\;tan\left(\frac{\omega}{C_w}H_w\right)} \tag{6d}$$

After substituting Eqs. (5), and (6d) in Eq. (4), the following equation will be obtained :

$$\overline{P}\left(y,\omega\right)=\frac{-\,\alpha_r\,\rho_w\,ay\left(\frac{C_w}{\omega}\right)-i\,\alpha_i\,\rho_w\,ay\left(\frac{C_w}{\omega}\right)}{1+i\beta_r\;tan\left(\frac{\omega}{C_w}H_w\right)-\beta_i\;tan\left(\frac{\omega}{C_w}H_w\right)}\;sin\left(\frac{\omega}{C_w}y\right)\;-$$
$$\frac{-\,\alpha_r\,\rho_w\,ay\left(\frac{C_w}{\omega}\right)-i\,\alpha_i\,\rho_w\,ay\left(\frac{C_w}{\omega}\right)}{1+i\beta_r\;tan\left(\frac{\omega}{C_w}H_w\right)-\beta_i\;tan\left(\frac{\omega}{C_w}H_w\right)}\;tan\left(\frac{\omega}{C_w}H_w\right)\;cos\left(\frac{\omega}{C_w}y\right) \tag{7}$$

where :

$\overline{P}$ = steady state response hydrodynamic pressure (F/L^2);

ω = earthquake circular excitation frequency (1/T);

$C_w = (E_w / \rho_w)^{1/2}$ = pressure wave velocity of water (L/T);

E_w = Bulk modulus of elasticity of water (F/L^2);

ρ_w = mass density of water (M/L^3);

α and β are depended on the sediment and the foundation properties;

Results and Discussions

Tables (1), (2), (3) and (4) show the values of $(\overline{P}/\gamma H_w)$ calculated by Eq. (7) for infinite reservoir length, using $(\omega/\omega_1 = 0.5)$, for a wide range of properties of sediment, and for a unit vertical earthquake acceleration (1g).it is watch to mention is that the $(\overline{P}/\gamma H_w)$values for different acceleration (0.2g) can be obtained by multiply these values by(0.2g)

Table (1) hydrodynamic pressure found by the developed of analytical solution for standardized hydrodynamic pressures, $(\overline{P}/\gamma H_w)$, for unit earthquake vertical acceleration, (1g), with stiff foundation (Hw=112.5m), $(\omega/\omega_1 = 0.5)$, dS= 12.5m, (ρs/ρw=1.5)

Analytic solution for stiff foundation (L= ∞)			
Y / H	**Fully saturated sediment (S=100%)**	**Partially saturated sediment (S=99.5%)**	**Partially saturated (sediment S=99%)**
0.1	1.290	1.597	1.980
0.19	1.185	1.467	1.819
0.28	1.072	1.328	1.646
0.37	0.953	1.180	1.463
0.46	0.828	1.025	1.271
0.55	0.698	0.864	1.071
0.64	0.564	0.698	0.865
0.73	0.426	0.527	0.653
0.82	0.285	0.353	0.438
0.91	0.143	0.177	0.219
1	1.03E-19	1.04E-19	0

Table (2) hydrodynamic pressure found by the developed analytical solution for standardized hydrodynamic pressures, $(\overline{P}/\gamma H_w)$, for unit earthquake vertical acceleration (1g) with soft foundation (Hw=112.5m), $(\omega/\omega_1 = 0.5)$, dS= 12.5m, (ρs/ρw=1.5)

Analytical infinite solution for soft foundation			
Y/H	**Fully saturated sediment (S=100%)**	**Partially saturated sediment (S=99.5%)**	**Partially saturated sediment (S=99%)**
0.1	1.184	1.411	1.657
0.19	1.088	1.296	1.522
0.28	0.984	1.173	1.377
0.37	0.875	1.042	1.224
0.46	0.760	0.906	1.064

0.55	0.641	0.763	0.896
0.64	0.517	0.616	0.724
0.73	0.391	0.465	0.547
0.82	0.262	0.312	0.366
0.91	0.131	0.156	0.183
1	0.000	0.000	0.000

Table (3) Results of analytical solution for standardized hydrodynamic pressures, $(\bar{P}/\gamma H_w)$, for unit vertical acceleration, (1g), with stiff foundation (Hw=100m), $(\omega/\omega_1 = 0.5)$, dS=25m, (ρs/ρw=1.5)

Analytic solution for stiff foundation (L= ∞)			
Y / H	**Fully saturated sediment (S=100%)**	**partially saturated sediment (S=99.5%)**	**Partially saturated (sediment S=99%)**
0.2	1.331	2.73	8.04
0.28	1.222	2.511	7.389
0.36	1.106	2.272	6.688
0.44	0.983	2.020	5.945
0.54	0.854	1.75	5.165
0.6	0.720	1.47	4.354
0.68	0.581	1.19	3.516
0.75	0.439	0.902	2.656
0.84	0.294	0.604	1.77
0.92	0.147	0.303	.822
1	0	0	0

Table (4) Results of analytical solution for standardized hydrodynamic pressures, $(\bar{P}/\gamma H_w)$, for unit vertical acceleration, (1g), with soft foundation (Hw=100m), $(\omega/\omega_1 = 0.5)$, dS= 25m, (ρs/ρw=1.5)

Analytic solution for soft foundation (L= ∞)			
Y / H	**Fully saturated sediment (S=100%)**	**Partially saturated sediment (S=99.5%)**	**Partially saturated (sediment S=99%)**
0.2	1.188	1.949	2.72
0.28	1.091	1.790	2.50
0.36	.987	1.620	2.265
0.44	.878	1.440	2.013
0.54	.763	1.251	1.749

0.6	.643	1.055	1.474
0.68	.519	.851	1.190
0.75	.392	.643	.899
0.84	.262	.431	.602
0.92	.131	.216	.302
1	0	0	0

The developed solution (eq.7)can be used to investigate the effect of different factors on the values and distribution of hydrodynamic pressures developed due to earthquakes on dam faces. The effect of the type of reservoir bedrock foundation, degree of saturation of sediments, depth of sediments, density of sediments. The following sensitivity analysed is proposed to illustrate the effect of each of those parameters.

1- Effect of the Type of Reservoir Bedrock Foundation

To show the effect of the type of foundation on the hydrodynamic pressure, the relation between (Y/H) and the normalized hydrodynamic pressure are plotted as shown in Figs. (1), (2), and (3). These figures show that for the case of stiff foundation, the hydrodynamic pressures developed were always greater than those for the soft foundation. This result is in agreement with the results obtained by (**Cheng,1986**)

Changing the ratio of depth of sediments, (d_S), to depth of reservoir (H), in Figs. (4), (5), and (6) and the degree of saturation have no effect on this behavior. The reason for this behavior can be explained upon the terms incorporated into the boundary conditions. Since, for the stiff foundation, the coefficient of absorption of pressure wave is less than that for soft foundation. This is obvious from the value of the coefficient of absorption of pressure wave, which is lower for stiff foundation than that for soft foundation.

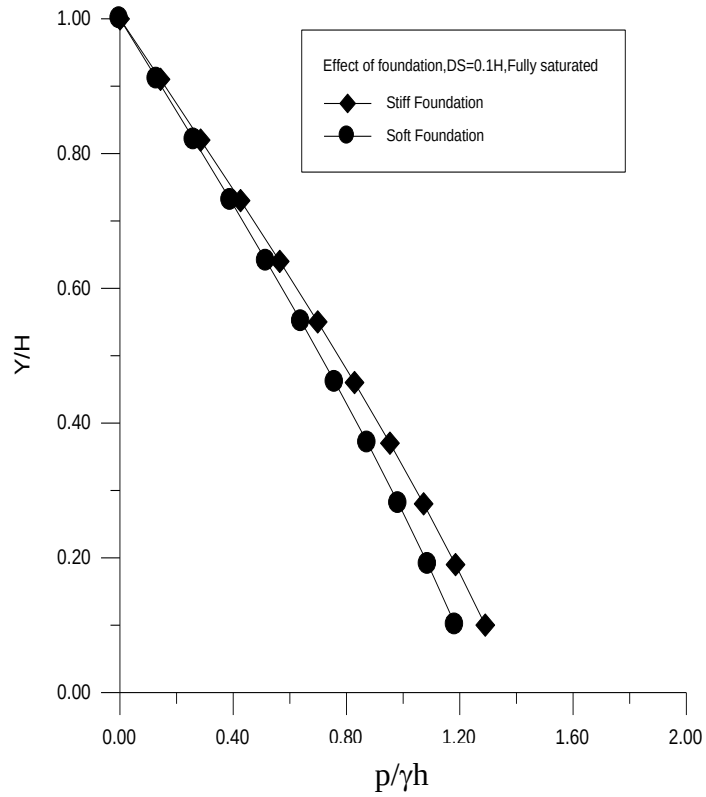

Fig.(1) Effect of the type of foundation on the hydrodynamic pressure developed due to vertical earthquake acceleration (1g) for ω/ω_1=0.5, with H_w=112.5m, d_S=12.5m, ρ_s/ρ_w=1.5,fully saturated sediments (100%)

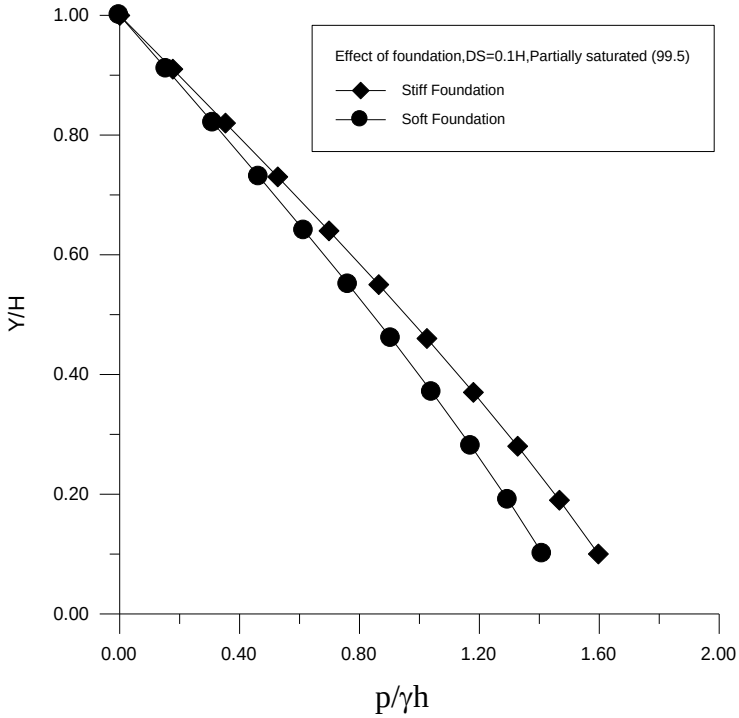

Fig.(2) Effect of type of foundation on hydrodynamic pressure developed due to vertical earthquake acceleration (1g) for ω/ω_1=0.5, with H_w=100m, d_S=25m, ρ_s/ρ_w=1.5,fully saturated sediments (100%)

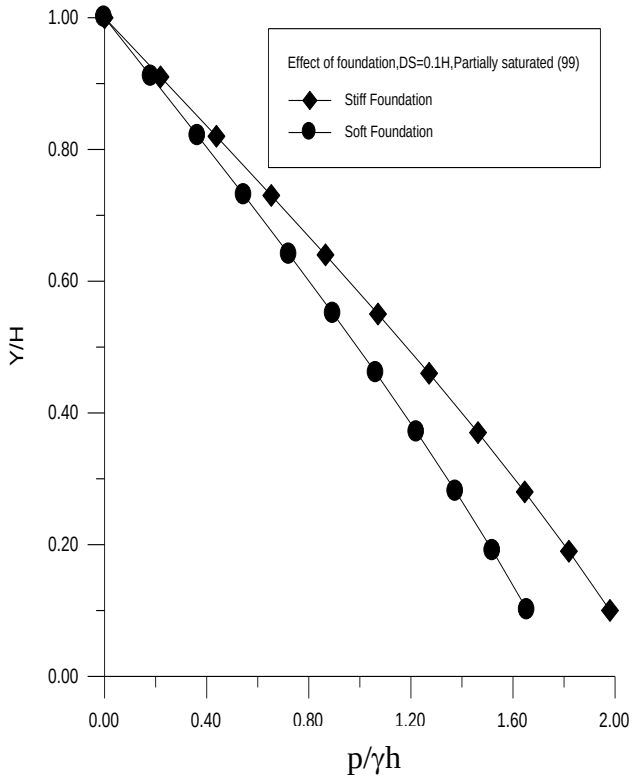

Fig.(3) Effect of type of foundation on hydrodynamic pressure developed due to vertical earthquake acceleration (1g) for ω/ω_1=0.5, with H_w=112.5m, d_S=12.5m, ρ_s/ρ_w=1.5,partially saturated sediments (99%)

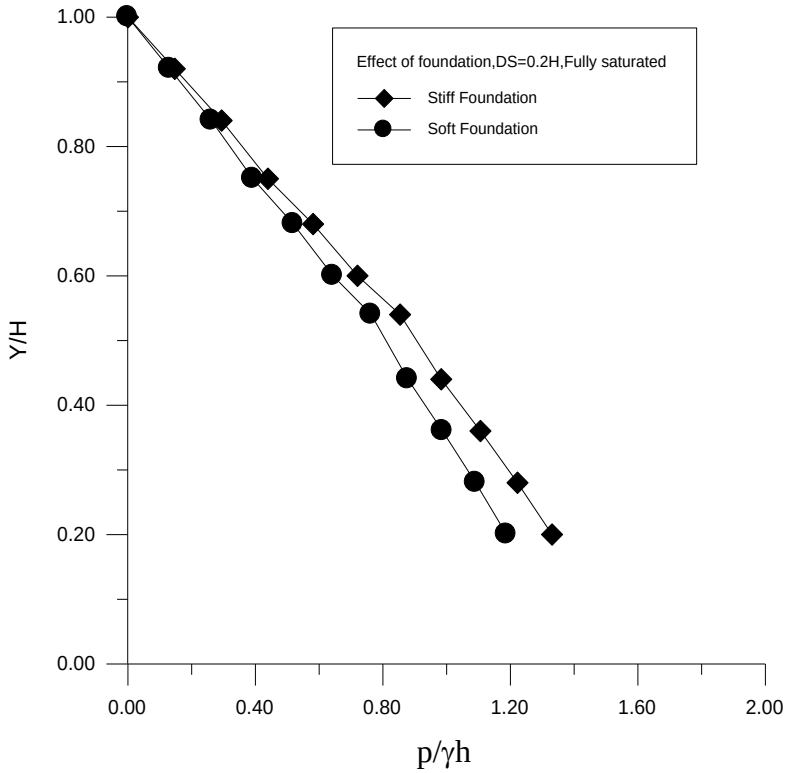

Fig.(4) Effect of type of foundation on hydrodynamic pressure developed due to vertical earthquake acceleration (1g) for ω/ω_1=0.5, with d_S=25m, ρ_s/ρ_w=1.5,fully saturated sediments (100%)

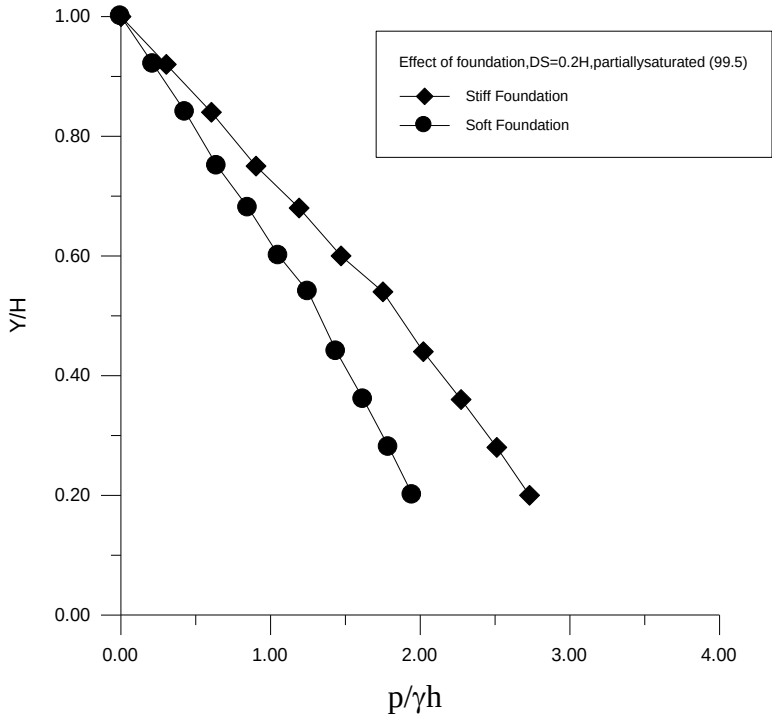

Fig.(5) Effect of type of foundation on hydrodynamic pressure developed due to vertical earthquake acceleration (1g) for ω/ω_1=0.5, with H_w=100m, d_S=25m, ρ_s/ρ_w=1.5,partially saturated sediments (99.5%)

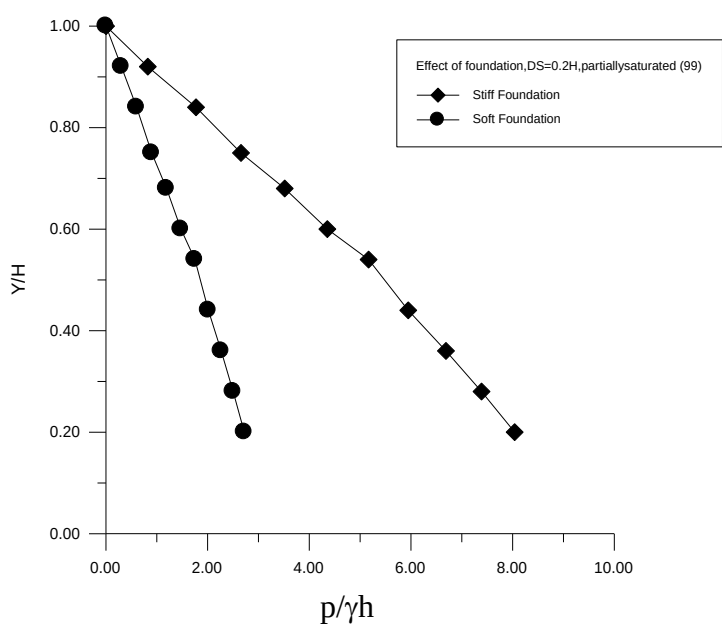

Fig.(6) Effect of type of foundation on hydrodynamic pressure developed due to vertical earthquake acceleration (1g) for ω/ω_1=0.5, with H_w=100m, d_S=25m, ρ_s/ρ_w=1.5,partially

saturated sediments (99%)

2- Effect of the Degree of Saturation of the Sediment

Figures (7), (8), (9) and (10) show the effect of the degree of saturation of the sediments on the hydrodynamic pressures developed due to vertical acceleration of (1g). It is shown that for (d_S/H) equals (0.1) and (0.2) the hydrodynamic pressure increases with the decrease of the degree of saturation. These results are in agreement with those found by (**Cheng,1986**), and (**Bougacha and Tassoulas,1991**).

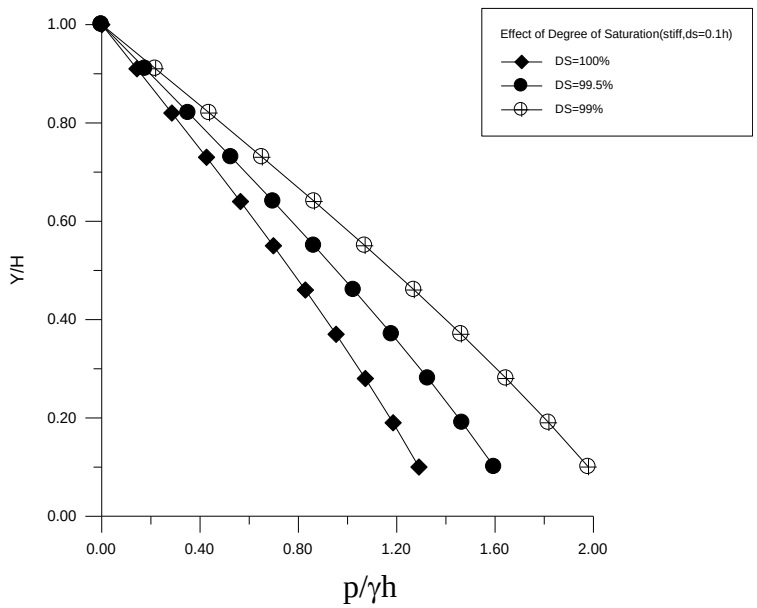

Fig. (7) Effect of the degree of saturation on the hydrodynamic pressures developed due to vertical acceleration (1g) for ω/ω_1=0.5, with H_w=112.5 m, d_S=12.5m, ρ_s/ρ_w=1.5, stiff foundation.

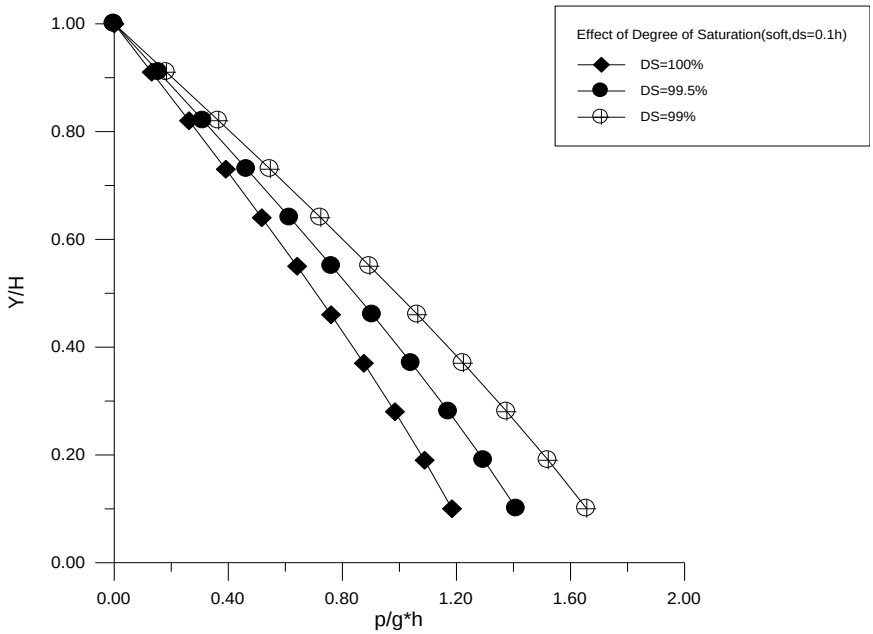

Fig. (8) Effect of degree p/γh on on hydrodynamic pressures developed due to vertical acceleration (1g) for ω/ω_1=0.5, with H_w=112.5 m, d_S=12.5m, ρ_s/ρ_w=1.5, soft foundation.

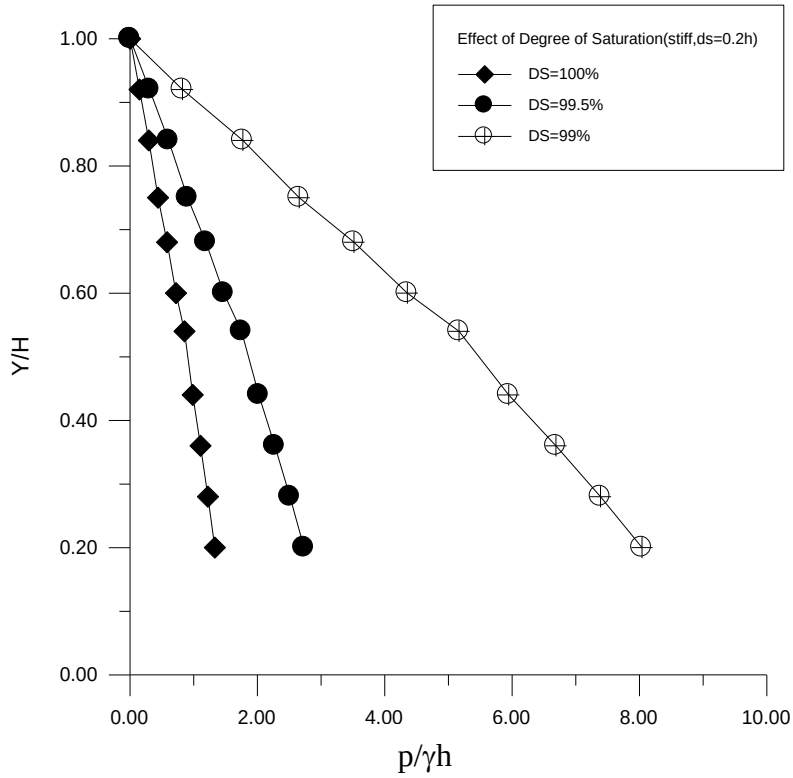

Fig. (9) Effect of degree of saturation on hydrodynamic pressures developed due to vertical acceleration (1g) for ω/ω_1=0.5, with H_w=100m, d_S=25m, ρ_s/ρ_w=1.5, stiff foundation.

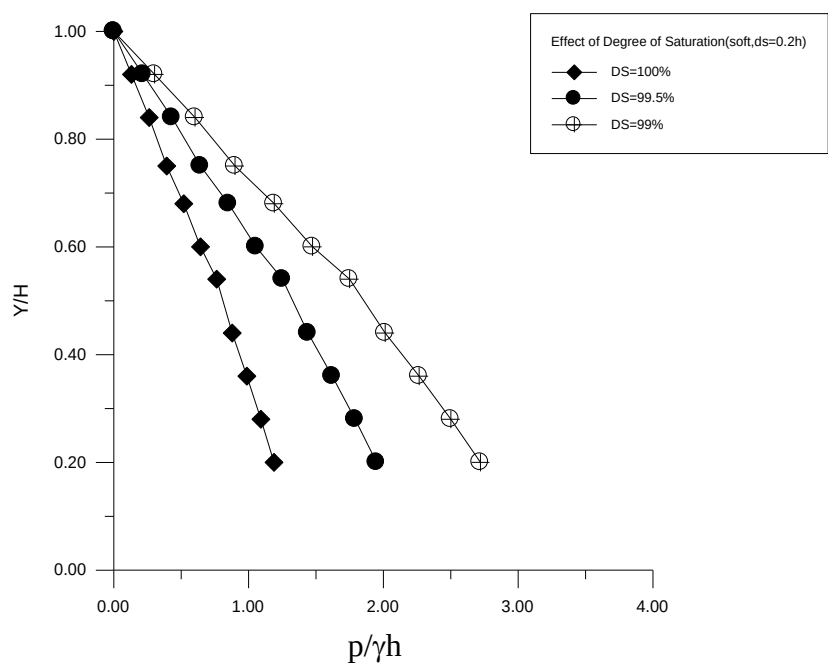

Fig. (10) Effect of degree of saturation on hydrodynamic pressures developed due to vertical acceleration (1g) for ω/ω_1=0.5, with H_w=100m, d_S=25m, ρ_s/ρ_w=1.5, soft foundation.

3- Effect of the Depth of the Sediment

Figures (11), (12), and (13) show the effect of the depth of sediments on the hydrodynamic pressure developed due to vertical earthquake acceleration of (1g). It is shown that for the two types of foundation the hydrodynamic pressure increases when the depth of sediment increases for (99.5%) and (100%) degree of saturation. Figures (14), (15), and (16)

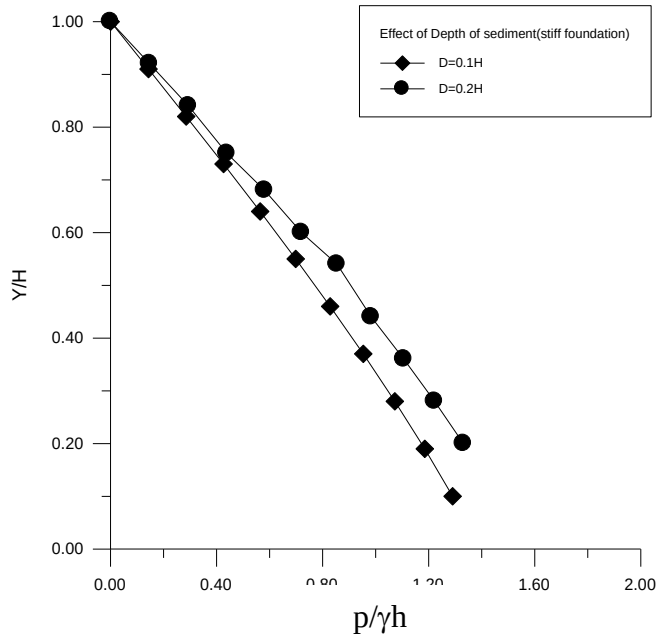

Fig. (11) Effect of the depth of sediment on the hydrodynamic pressures developed due to vertical acceleration (1g) for ω/ω_1=0.5, with H_w=112.5m, d_S=12.5m, ρ_s/ρ_w=1.5, stiff foundation,fully saturated sediments (100%).

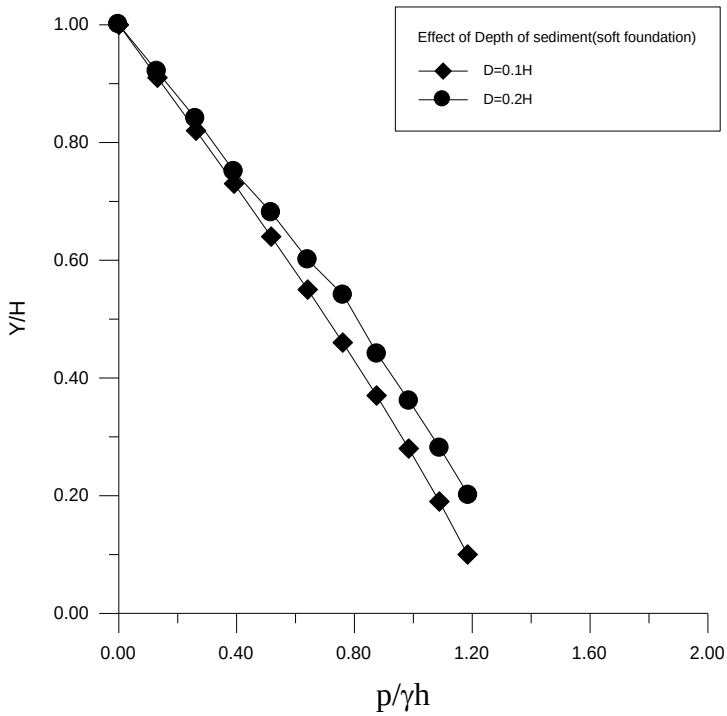

Fig. (12) Effect of the depth of sediment on the hydrodynamic pressures developed due to vertical acceleration (1g) for ω/ω_1=0.5, with H_w=100m, d_S=25m, ρ_s/ρ_w=1.5, soft foundation,fully saturated sediments (100%).

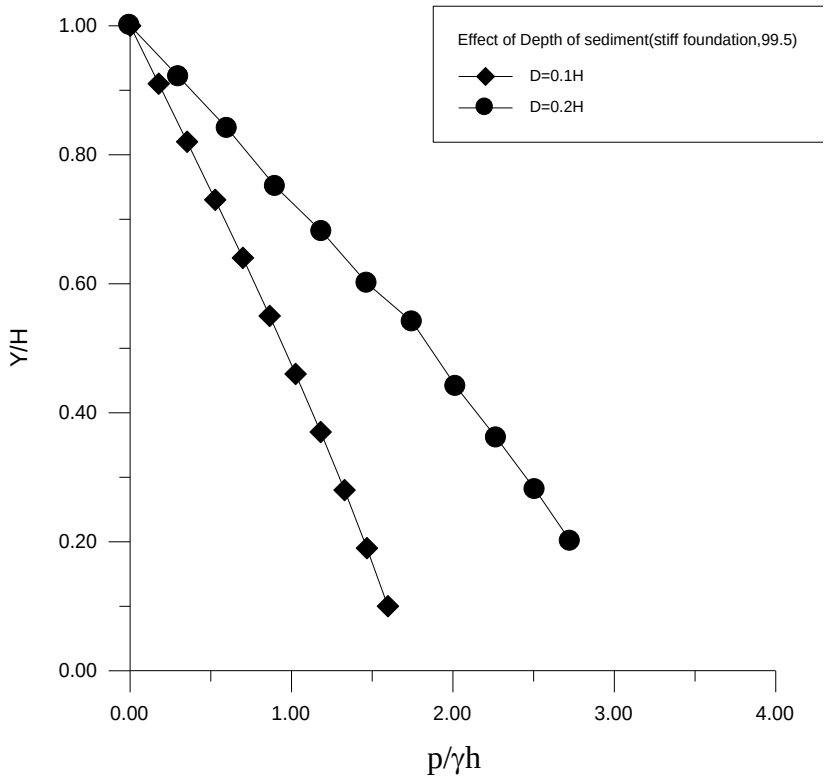

Fig. (13) Effect of depth the of sediment on the hydrodynamic pressures developed due to vertical acceleration (1g) for ω/ω_1=0.5, with H_w=112.5m, d_S=12.5m, ρ_s/ρ_w=1.5, stiff foundation,partially saturated sediments (99.5%).

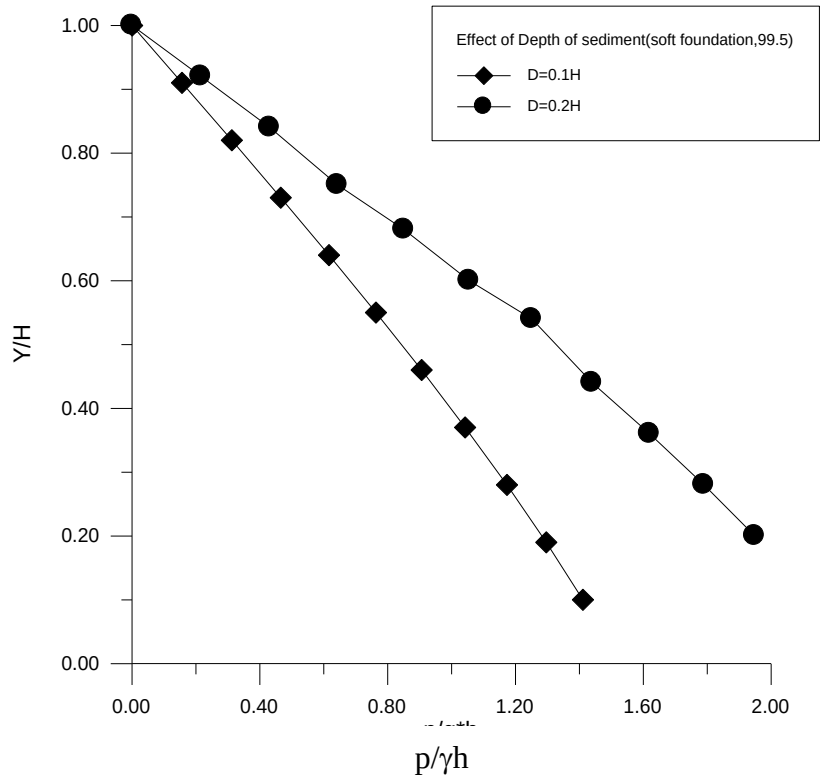

Fig. (14) Effect of the depth of sediment on the hydrodynamic pressures developed due to vertical acceleration (1g) for ω/ω_1=0.5, with H_w=100m, d_S=25m, ρ_s/ρ_w=1.5, soft foundation,partially saturated sediments (99.5%).

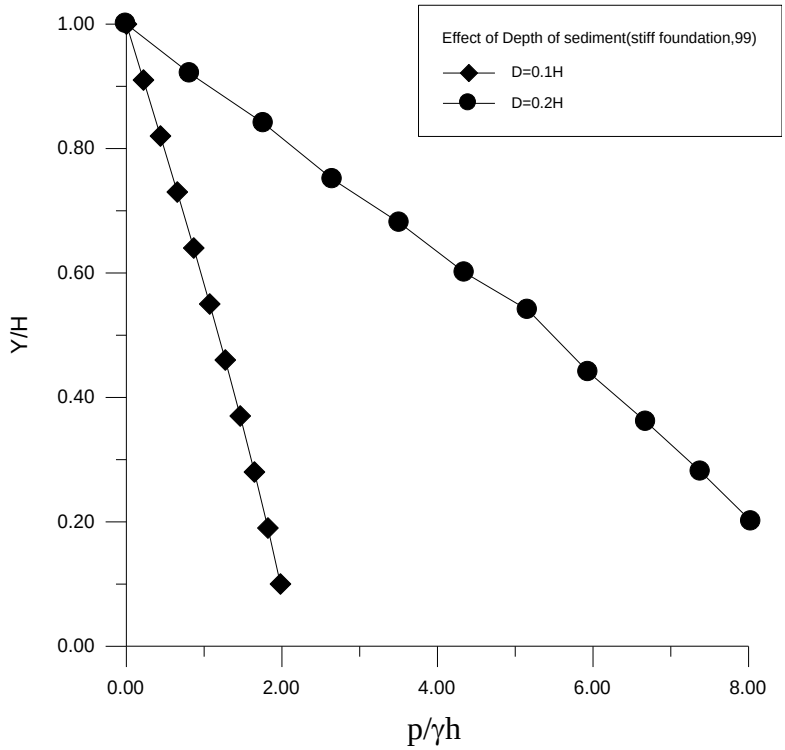

Fig. (15) Effect of the depth of sediment on the hydrodynamic pressures developed due to vertical

acceleration (1g) for ω/ω_1=0.5, with H_w=112.5m, d_S=12.5m, ρ_s/ρ_w=1.5, stiff foundation,partially saturated sediments (99%).

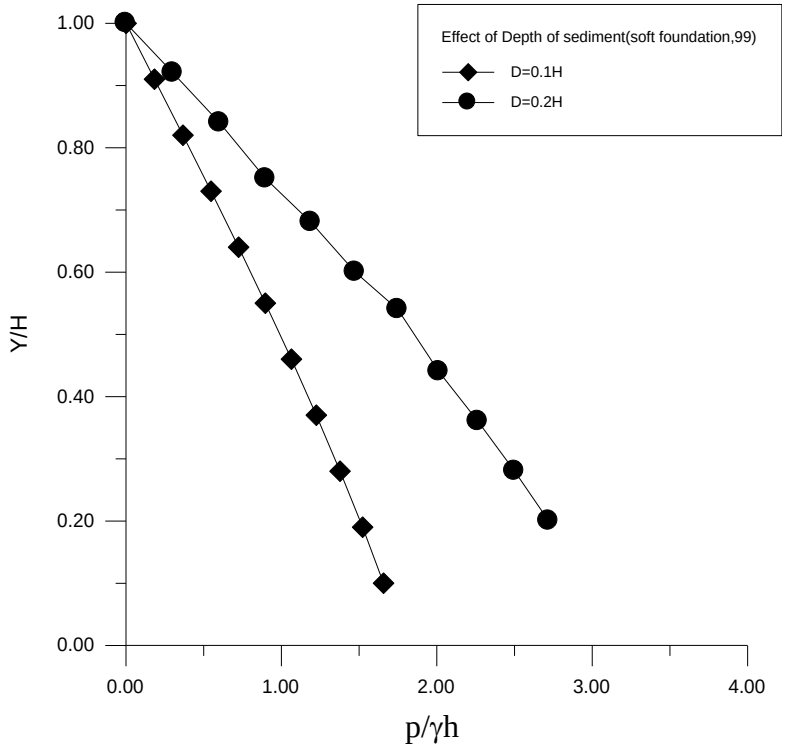

Fig. (16) Effect of the depth of sediment on the hydrodynamic pressures developed due to vertical acceleration (1g) for ω/ω_1=0.5, with H_w=100m, d_S=25m, ρ_s/ρ_w=1.5, soft foundation,partially saturated sediments (99%).

CONCLUSIONS

1. The values of the hydrodynamic pressure for the stiff foundation case are always larger than those for the soft foundation.

2. The hydrodynamic pressure increases with the decrease of the degree of saturation.

3. The hydrodynamic pressure increase when the depth of the sediment increase.

REFERENCES

Bougacha, S., and Tassoulas, J.L., (1991a): "Effects of sedimentary material on the response of concrete gravity dams." Earthquake Engng Struct. Dynamics Vol. 20, pp. 849-858, John Wiley & Sons, U.S.A.

Chen, B., and Hung, T., (1993): "Dynamic pressure of water and sediment on rigid dam." J. Engng Mech., ASCE, Vol. 119, pp.1411-1433.

Cheng, A. H., (1986): "Effect of sediment on earthquake–induced reservoir hydrodynamic response." J.

Engng Mech., ASCE, Vol. 112, pp. 654-663,.

Chopra, A. K., Chakrabarti, P., and, Gubta, S., (1980): "Earthquake response of concrete gravity dams including hydrodynamic and foundation interaction effects." Report No. UCB/EERC-80/01, Earthquake Engineering Research Center, Univ. of California, Berkeley.

Hall, J. F., and Chopra, A. K., (1982): "Two-dimensional dynamic analysis of concrete gravity and embankment dams including hydrodynamic effects." Earthquake Engng Struct. Dynamics Vol.10, pp. 305-332, John Wiley & Sons, U.S.A.

Okamoto, S., (1973): "Introduction to earthquake engineering" University of Tokyo Press.

Methods in Engineering, Vol. 21, pp. 1659-1669, John Wiley & Sons, U.S.A.

Al-Suhaili R.H., (1997): "Hydrodynamic pressures in dam-reservoir-tunnel system during earthquakes", Ph.D. Dissertation, College of Engineering, University of Baghdad.

Zhao, C., (1994): "Effects of reservoir bottom sediments on hydrodynamic pressure of gravity dams." Computers and Structures, Vol. 52, pp. 297-307, Pergamon, England.

Lotfi,v.,and Tassoulas,J.L..(1986):"analysis of the response of dams to earthquakes."report GR86-2,Geotechicnical Engineering

Research Cente,the University of texas,Austin.Texas.

EVALUATION OF THE PERFORMANCE OF SOME CHEMICAL INHIBITORS ON CORROSION INHIBITION OF COPPER IN ACID MEDIA

Dr. Aprael S. Yaro
University of Baghdad
College of Engineering
Chemical Eng. Department

Anees Abdullah Khadom
University of Daiyla
College of Engineering

ABSTRACT

The inhibition of copper corrosion by Naphthylamine (NA), Ethylenediamine (EDA), Tetraethylenepentamine (TEPA), Diethylenetriamine (DETA), and Phenylenediamine (PDA) in 5% HCl have been investigated by weight loss technique at different temperatures. The results were compared with Benzotriazole (BTA), the common inhibitor used for inhibition of copper corrosion in different environments. The BTA film formed on the copper surface obeys Langmuir Adsorption Isotherm. While NA, EDA, TEPA, and DETA appear to obey the Freundlich Adsorption Isotherm. In the other hand, the two-adsorption isotherms were unsuitable to represent the data of PDA. Results also showed that the Kinetic-Thermodynamic Model was suitable to fit the experimental data of the most inhibitors of the present study.

INTRODUCTION

Due to its good corrosion resistance in water and its excellent heat conductivity, copper and its alloy are used widely in heating systems and condensers. However, these systems should be regularly cleaned from carbonates and oxides that diminish their heating transmission. Diluted hydrochloric acid is used to clean these surfaces; a corrosion inhibitor is added to avoid the action of this acid on copper. Corrosion inhibitor

is a chemical substance which when added in small concentration to environment effectively checks, decrease or prevent the reaction of metal with environment [1]. It must be clearly understood that no universal corrosion inhibitor exists. Each inhibitor must be tailored to the specific corrosion problem that needs solution [2]. While the use of inhibitors for some types of corrosion can be similar to other, this similarity must be treated as coincidence. Most inhibitors have been developed by empirical experimentation. The corrosion mechanism can vary considerably depending on the corrosive factors that are present. Similarly, the mechanism of inhibition will vary depending on the chemical nature of the inhibitor and the factor causing corrosion [3]. The most widely accepted postulated involves the formation of surface layers or films, which reduce the ease of access of the corrosive materials to the metal surface. Such scale can be formed naturally, or can be induced to form [4].

An equation relates the amount of substance attached to surface to its concentration in gas phase or in solution at fixed temperature, is known as an *adsorption isotherms* [5]. The simplest isotherm was first obtained in 1916 by Irvan Langmuir [5]. This isotherm can be represented as;

$$\theta = \frac{KC}{1+KC} \qquad \ldots(1)$$

Systems that obey this equation are often referred to ideal adsorption. Systems frequently deviate significantly from Langmuir equation. This may be because the surface is not uniform, and also there may be interaction between adsorbed molecules, a molecule attached to surface may make it more difficult, or less difficult, for another molecules to became attached to a neighboring site, and this will lead to deviation from the ideal adsorption equation. Non-ideal system can sometimes be fitted to an empirical adsorption isotherm of Freundlich [6],

$$\theta = KC^{n} \qquad \ldots(2)$$

K, is equilibrium constant, C is inhibitor concentration, n is positive generally not integer constant, and (θ) is surface coverage. The surface coverage of inhibitor at a given concentration is calculated using the following equation:

$$\theta = \left\{1 - \left(\frac{W_{in}}{W_{un}}\right)\right\} \qquad \ldots(3)$$

Where the W_{in} and W_{un} are the weight loss corrosion rates with and without inhibitor respectively.

Recent researches have looked in to the action of adsorptive inhibitors from purely mechanistic kinetic point of view [7,8]. A kinetic-thermodynamic model for adsorption process at metal-solution interface has been suggested. This model has been tested on inhibition effect of number of open chain amines and one macrocyclic amine on the corrosion of steel in H_2SO_4 [8] and aluminum in HCL [9]. In this model, (y) is the number of inhibitor molecules occupying one active site. This model can be given by the following equation;

$$\left(\frac{\theta}{1-\theta}\right) = K`[C]^y \qquad \ldots(4)$$

Values of y>1 implies the formation of multilayers of inhibitor on the surface of metal. Values of y<1 mean a given inhibitor molecules will occupy more than one active site. K, corresponding to adsorption isotherm is given by;

$$K = K`^{\left(\frac{1}{y}\right)} \qquad \ldots \ (5)$$

The present work is an attempt to evaluate some corrosion inhibitors for copper in HCl. Some amines, which used in the past as corrosion inhibitors for another metals, such as Fe and Al, in another acids such as H_2SO_4, H_3PO_4 and HNO_3 are tested here for the corrosion of copper in HCl.

EXPERIMENTAL

The corrosion behavior of copper-nickel alloys, which used widely in many industrial equipments, was studied using weight loss in absence and presence of Benzotriazole (BTA), Naphthylamine (NA), Ethylenediamine (EDA), Tetraethylenepentamine (TEPA), Diethylenetriamine (DETA), and Phenylenediamine (PDA) in 5% HCl solution at different temperature (35, 45, and 55 C^o), and different inhibitor concentrations (1, 5, 10, and 15 g/l).

Locally produced hydrochloric acid supplied by AL-Furat Company for Chemicals Industries was used as a corrosive solution. The material of electrode was a copper-nickel alloy, which have the following analysis obtained by Specialized Institute of Engineering Industries shown in table (1) below: -

Table (1) Analysis of Cu-Ni alloy.

Compound	%	Compound	%
Sn	0.148	Ni >	2.4
Fe >=	0.2	Pb	0.0583
Zn	0.1374	Si	0.0202
Al	0.015	S	0.017
P	0.0003	As	0.0056
Sb >=	0.5	Cu	About 90

Ring shape specimen of Cu-Ni alloy with dimension (2.22 cm) outside diameter, (1.5 cm) width, and (0.13 cm) thickness, exposing a surface area of about (10 cm^2) to corrosive media. Specimens were cleaned by washing with detergent and flushed with tap water followed by distilled water, degreased by analar benzene and acetone, then annealed in vacuums to 600 C^o for one hour and cooled under vacuum to room temperature. Before each run, specimens of Cu-Ni were abraded in sequence using emery paper of grade number 220,320, 400, and 600, then washed with running tap water followed by distilled water then dried with clean tissue, degreased with benzene, dried, degreased with acetone, dried, and finally left in desicater over silica gel. Weighing the specimen was carried out using 4 decimals digital balance and its dimensions were measured with vernier.

The metal samples for weight loss runs were completely immersed in 250-cm^3 solution of corrodant contained in a conical flask. They were exposed for a period of three hour at a desired temperature, acid concentration, and inhibitor concentration. Weight losses were determined in absence and presence of inhibitors. The data are expressed as mass loss per unit time per unit area; in present work the units of corrosion rate were g/m^2.day (gmd).

RESULTS AND DISCUSSIONS

The corrosion rate increases with temperature increasing, generally, the addition of inhibitors reduces the corrosion rate, and the reductions depend on the type of inhibitor. Among all the inhibitors tested, *BTA* is the best one as shown in figure (1). As the concentration of BTA increased from (1 to 15 g/l) the corrosion rate decreased to a very low values. At 35 ^{o}C, the corrosion rate decreased from 12.5 gmd, when there is no inhibitor, to 0.0193 gmd at 15g/l-inhibitor concentration, with a maximum efficiency of 99.8 %. When the temperature increased, the corrosion rate also increased slowly. BTA still effective to less extent. Generally, efficiency of BTA decreased slightly with increasing in temperature.

The rest inhibitors, approximately, give the same behavior; the corrosion rate decreases with increasing the inhibitors concentrations, and increases with temperature increasing.

The order of inhibition of inhibitors evaluated by weight loss technique was as follows: -

BTA > NA > EDA > TEPA > DETA > PDA

The effect of temperature in presence of BTA is clear as shown in figure (2). The corrosion rate increase when the temperature increased, at any inhibitor used, and at inhibitor concentration.

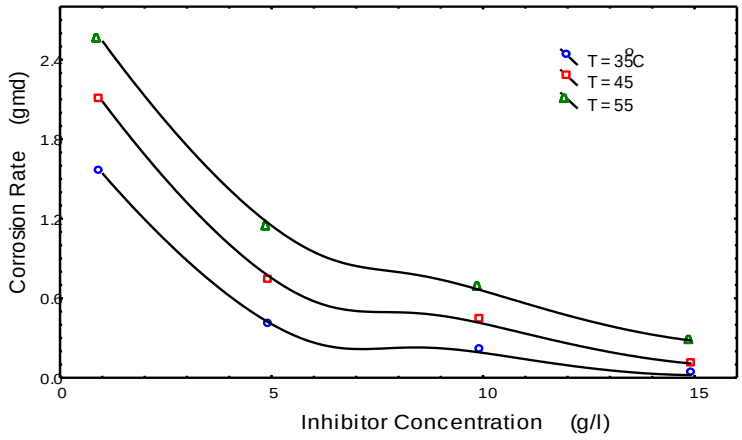

Fig. (1) **Effect of the Concentration of BTA on the corrosion of Cu-Ni**

Alloy in 5% HCl Acid.

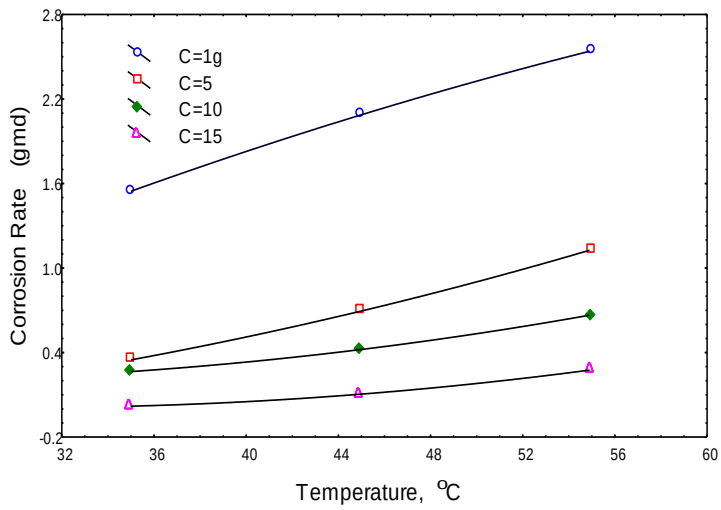

***Fig. (2)* Effect of Temperature on the Corrosion Rate of Cu-Ni alloy In Presence of BTA as Inhibitor in 5% HCl Acid.**

The corrosion rate data can be used to analyze the adsorption mechanism, by using the value of θ as a function of inhibitor concentration. Rearranging Langmuir isotherm equation will gives:

$$\frac{C}{\theta} = \frac{1}{K} + C \qquad \ldots (6)$$

Equation (6) can be plotted as $\left(\frac{C}{\theta}\right)$ vs. C, as shown in figure (3). The higher value of K indicates that the inhibitor is strongly adsorbed on the metal surface. From fig. (3) and table (2), we can see that BTA follows Langmair adsorption isotherm, values of K decreases from (5.586 to 4.762 l/g) when the temperature increased from 35C^o to 45 C^o, this may be due to the de-sorption of inhibitor, further increase in temperature to 55 ^{o}C, did not effect the value of K. It is clear that the highest value of K was 5.586 l/g at 35 ^{o}C, this suggest that at 35 C^o BTA gives the highest coverage at any concentration, and the lowest value was 4.762 l/g at 45 ^{o}C and 55 ^{o}C, which gives the lowest coverage, this similarity between the values of K at 45 ^{o}C and 55 ^{o}C due to the close range of the

surface coverage, which is ranged, from (0.868-0.99) at 45°C, and from (0.878-0.987) at 55°C. Langmuir adsorption isotherm fit the corrosion rate data of BTA strongly, and this is clear from the values of correlation coefficient, R, which has an average value of 0.9999 at different temperatures, this leads to suggest that BTA molecules form a monolayer on the metal surface. The values of y, (the number of inhibitor molecules occupying one active site in the metal surface), were approximately near unity, with an average value of 1.04, specially at 45 ^{o}C and 55 ^{o}C, which indicate that each molecule of BTA occupying one active site on Cu-Ni alloy surface, then it form a monolayer of inhibitor molecules.

The relation between surface coverage and the concentration of NA becomes linear when Freundlich adsorption isotherm is applied. This suggest that the corrosion rate data for NA is follow Freundlich adsorption isotherm, with K values of 0.1614, 0.1099, and 0.0895 l/g at 35,45and 55 C^{o} respectively, which in the same order and gives the same behavior as in Langmuir adsorption isotherm. The average value of (n) was 0.703 at different temperature, which is in agree with typical value of n= 0.6 [91]. Generally, values of K obtained from the two-adsorption isotherms were in a good agreed with the values obtained from kinetic-thermodynamic models (0.22, 0.151, and 0.123 l/g) at 35,45and 55 C^{o}, respectively. The values of y at different temperatures were near unity (1.19 to 1.154), which indicate that NA molecules were attached to one active site of Cu-Ni alloy.

For EDA, there is a good agreement between the adsorption isotherms and kinetic-thermodynamic model, as it is shown from the values of K obtained from different models. The best fit was obtained by Freundlich adsorption isotherm, the values of K approximately constant with increasing of temperature.

For TEPA, the best fit to the data was by using Freundlich adsorption isotherm with an average value of correlation coefficient of 0.995,as shown in fig. (6). The values of equilibrium constant were increased slightly with temperature, which indicate, that there is some improvement in surface coverage with increasing in temperature. Values of K obtained from kinetic-thermodynamic model are differing from that obtained from adsorption isotherm, which indicate that this model did not represent the corrosion rate data of TEPA.

Again, in the case of DETA, Freundlich adsorption isotherm fit the corrosion rate data with an average correlation coefficient of 0.9854, which is more than the average correlation coefficient of Langmuir adsorption isotherm, (i.e., 0.8948). Also, there is some increasing in the values of K with increasing in temperature. The values of K obtained from the two-adsorption isotherm were in the same order, while the values that obtained from kinetic-thermodynamic model were lower, and y<1. Fig. (8).

Non of the adsorption isotherm used in present work are represent the corrosion rate data of PDA, this may be due to a low surface coverage of this inhibitor and low ability to form a layer on the metal surface. Kinetic-thermodynamic model slightly fit the corrosion rate data with K values in the same order as the values obtained from the adsorption isotherms. Generally, the values of K are approximately constant with an average value of 0.021 l/g.

From the values of equilibrium constants, which obtained from different isotherms, the values of heat of adsorption, ΔG_{ads}, can be obtained using the following equation [10]:

$$K = \left(\frac{1}{55.55}\right)\exp\left(-\frac{\Delta G_{ads}}{RT}\right) \qquad \ldots (7)$$

The value of (55.5) is the water concentration in solution expressed in M, (i.e., ~1000 g/l). R and T are the gas constant and absolute temperature respectively.

The values of ΔG_{ads}, heat of adsorption of BTA, were obtained using the values of K from adsorption isotherm and kinetic-thermodynamic models. These values are given in tables (2), (3), and (4). According to Langmuir adsorption isotherm the values of ΔG_{ads}, were around (-22 kJ/mol.), this indicates that the process under study is spontaneous, and the inhibitor is chemically adsorbed on the metal surface, because the values of ΔG_{ads} for BTA on Cu-Ni alloy in 5% HCL in the range of chemical adsorption processes for organic inhibitor in aqueous media, which lies between –21 to –42 kJ/mol. [10].

The values of ΔG_{ads} for the last five inhibitors, as shown in tables (2), (3), and (4), were in the range of (-3.418 to -14.28 kJ/mol.), which indicate the weak adsorption of these inhibitors to the metal surface, also, these values are much lower than the values obtained with BTA. The values of K were also much lower these obtained with BTA.

Table. (2) Adsorption Constants, and heats of adsorption from Langmuir *Isotherm Models*.

Inhibitor	T (°C)	K (l/g)	ΔG_{ads} (kJ/mol.)	R
BTA	35	5.586	-22.093	0.99993
	45	4.762	-22.389	0.999923
	55	4.762	-23.093	0.99989
NA	35	0.1603	-13	0.9851
	45	0.106	-12.329	0.9725
	55	0.089	-12.24	0.99109
TEPA	35	0.115	-12.15	0.95489
	45	0.143	-13.121	0.9727
	55	0.18	-14.161	0.97755
PDA	35	0.02	-7.671	0.98296
	45	0.025	-8.510	0.2068
	55	0.0116	-6.683	0.6095

***Table. (3)* Adsorption Constants, Heats of Adsorption, and n From Freundlich Isotherm Models.**

Inhibitor	T (°C)	K (l/g)	n	ΔG_{ads} (kJ/mol.)	R
BTA	35	0.883	0.048	-17.37	0.9742
	45	0.87	0.049	-17.894	0.99017
	55	0.879	0.043	-18.485	0.9985
EDA	35	0.1698	0.532	-13.15	0.9967
	45	0.1954	0.460	-13.95	0.9971
	55	0.1496	0.526	-13.66	0.9994
TEPA	35	0.131	0.452	-12.484	0.99182
	45	0.148	0.455	-13.211	0.997246
	55	0.188	0.378	-14.279	0.99516
DETA	35	0.039	0.471	-9.381	0.99447
	45	0.054	0.546	-10.546	0.96312
	55	0.0656	0.672	-11.408	0.99861

***Table. (4)* Adsorption Constants, heats of adsorption, and y from**

Kinetic-Thermodynamic Models.

Inhibitor	T (^oC)	K (l/g)	y	ΔG_{ads} (kJ/mol.)	R
BTA	35	3.67	1.31	-21.018	0.89
	45	5.53	1.003	-22.784	0.9406
	55	8.803	0.813	-24.768	0.95529
NA	35	0.22	1.199	-13.811	0.9776
	45	0.151	1.176	-13.265	0.9861
	55	0.123	1.154	-13.122	0.9948
EDA	35	0.160	0.925	-12.996	0.9715
	45	0.152	0.793	-13.282	0.9789
	55	0.107	0.802	-12.742	0.9950
TEPA	35	0.0447	0.621	-9.73	0.9925
	45	0.065	0.652	-11.036	0.95252
	55	0.074	0.575	-11.737	0.9928
DETA	35	0.002	0.512	-1.775	0.99248
	45	0.0106	0.631	-6.241	0.95252
	55	0.0393	0.833	-10.011	0.99284
PDA	35	0.0038	0.722	-3.418	0.97802
	45	0.0444	1.168	-10.028	0.97838
	55	0.0325	1.319	-9.493	0.98551

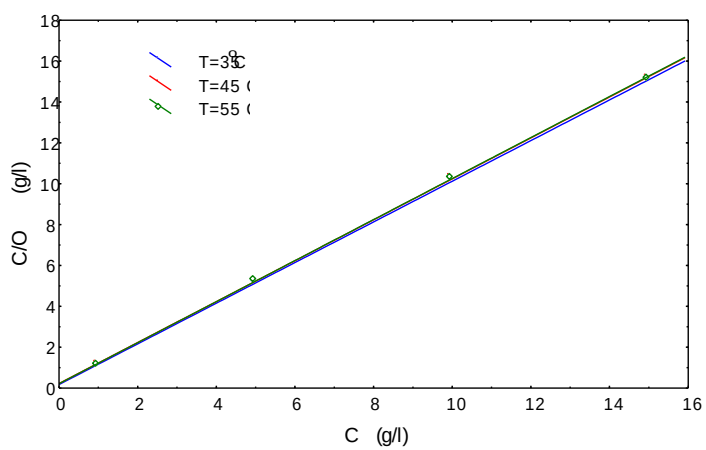

Fig. (3) Langmuir Adsorption Isotherm of BTA on Cu-Ni Alloy*In 5% HCl Acid.*

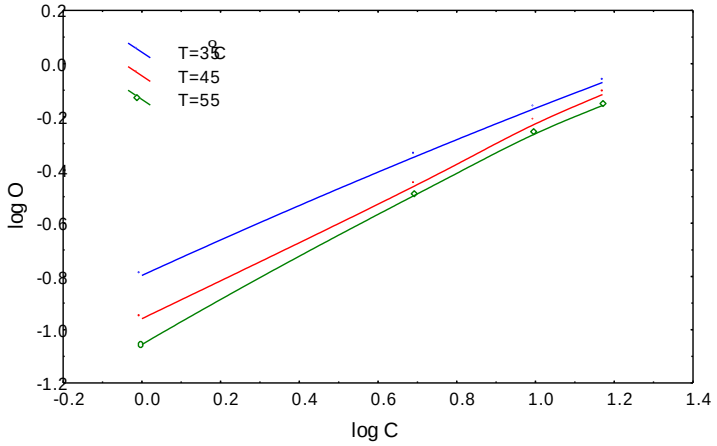

Fig. (4) Freundlich Adsorption Isotherm of NA on Cu-Ni AlloyIn 5% HCl Acid.

Fig. (5) Freundlich Adsorption Isotherm of EDA on Cu-Ni Alloy In 5% HCl Acid.

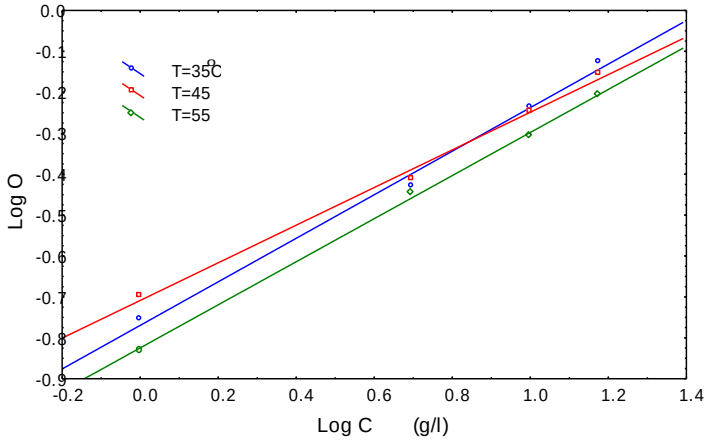

Fig. (6) Freundlich Adsorption Isotherm of TEPA on Cu-Ni Alloy in 5% HCl Acid.

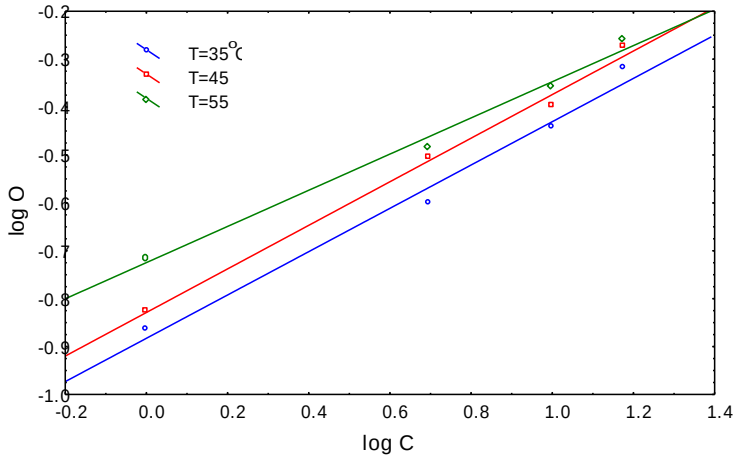

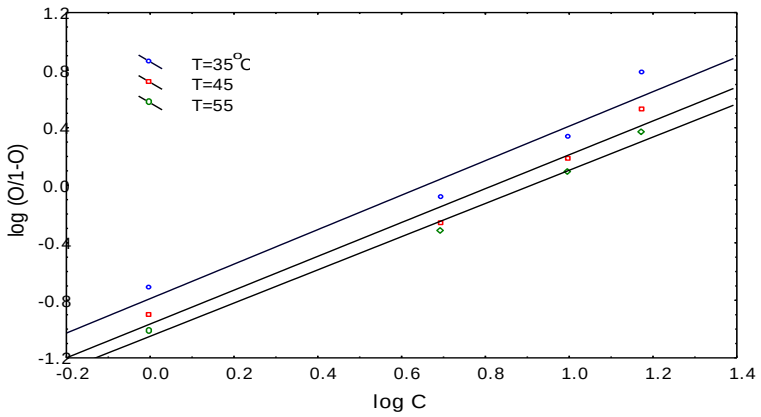

Fig. (7) Kinetic-Thermo. Model for the Corrosion of Cu-Ni Alloy in 5% HCl Acid in Presence of NA.

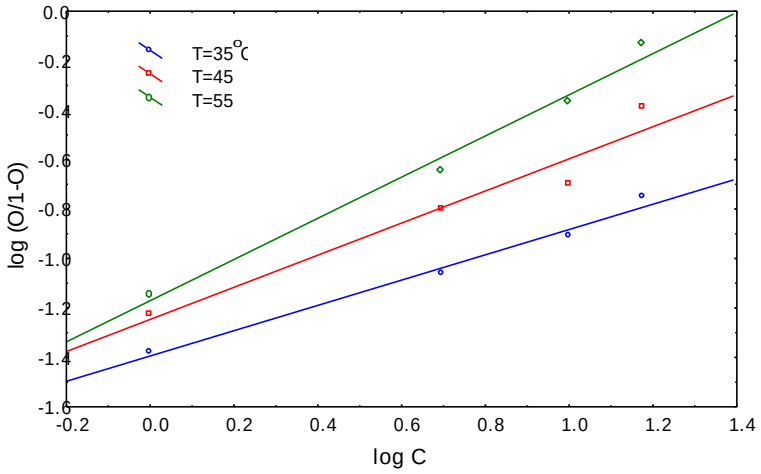

Fig. (8) Kinetic-Thermo. Model for the Corrosion of Cu-Ni Alloy in 5% HCl Acid in Presence of DETA.

CONCLUSION

The corrosion rate of Cu-Ni alloy in 5% HCl acid solution, increased with increasing of temperature, and decreased with increasing of inhibitor concentration. BTA is an effective inhibitor for copper in static hydrochloric acid solution. Maximum inhibitor efficiency is 99.8% at 15 g/l and 35 ^{o}C. Other chemicals (i.e. NA, EDA, TEPA, DETA, and PDA) were ineffective inhibitors even at high level of inhibitor concentration (i.e. 15 g/l). The BTA film formed on the copper surface obeys Langmuir Adsorption Isotherm

$\left(\theta = \frac{KC}{1+KC}\right)$. While NA, EDA, TEPA, and DETA appear to obey the Freundlich Adsorption Isotherm $\left(\theta = KC^{n}\right)$. In the other hand, the two-adsorption isotherms were unsuitable to represent the data of PDA. Results also showed that the Kinetic-Thermodynamic Model $\left(\frac{\theta}{1-\theta} = \mathrm{K}'C^{y}\right)$ was suitable to fit the experimental data of the most inhibitors of the present study. The values of y (i.e. the number of inhibitor molecules occupying one active site on the metal surface) obtained from the present work were near unity, which indicate the formation of monolayer on the metal surface.

Values of heat of adsorption $\left(\Delta G_{ads}\right)$ were higher in the case of BTA than the values of other inhibitors, which indicate the strong binding of BTA to the metal surface as compared with other inhibitors used. The order of inhibition of inhibitors evaluated by weight loss technique were as follows: -

BTA > NA > EDA > TEPA > DETA > PDA

REFERENCES

- Nathan, C.C., " ***Corrosion Inhibitors***", NACE (1973).
- George, G., **"*Corrosion Inhibitors*"**, NACE, Houston, Texas (1974).
- Bergman, J.I, **"*Corrosion Inhibitors***", The MacMillan Company, New York (1963).
- McDonald, H.J., ***Corrosion,*** Vol.4, Feb. (1948).
- Laidler, K.J. & Maeiser, J.H., **" *Physical Chemistry*"**, (1982).
- Clark, A., **" *The Theory of Adsorption and Catalyst*"**, (1970).
- El-Awady, A.A, Abd-El-Nabey, B.A. & Aziz, S.G., ***Int. J. Chem.***, 1, p.169 (1990).
- El-Awady, A.A, Abd-El-Nabey, B.A. & Aziz, S.G., ***J. Electochem.*** *Soc.,* 139, p.2, 153 (1992).
- El-Awady, A.A, Abd-El-Nabey, B.A. & Aziz, S.G., *J. Chem. Soc.* ***Faraday. Trans.***, 89,p.795 (1993).
- Damaskin, W.W., Pietrij, O.A. & Batrakow, W.W, **"*Adsorption of Organic Compounds on Electrode***", Plenum Press, New York (1971).

PREDICTION OF ZINC CONSUMPTION AS SACRIFICIAL ANODE IN CATHODIC PROTECTION OF STEEL IN SEA WATER USING ARTIFICIAL NEURAL NETWORK

APRAEL S. YARO
Chemical Engineering Department – College of Engineering – University of Baghdad

ABSTRACT
Corrosion has gained special attention due to its significance, when predicting corrosion rates. However, the complexity and variability makes it hard to model its effects. This study evaluates the usefulness of Artificial Neural Networks (ANN) to predict the corrosion rate as a function of several factors which have been related in previous studies to the protectiveness of low carbon steel in sea water, i.e. Temperature, Flow rate, pH, and time. Results showed that neural networks are a powerful tool and that the validity of the results is closely linked to the amount of data available and the experience and knowledge that accompany the analysis. Statistical analysis showed that the proposed correlation has an Average Absolute Relative Error (AARE) of 0.09% and Standard Deviation (S.D) 0.46%

KEYWORDS
artificial neural networks, corrosion prediction, cathodic protection

الخلاصة
ان ظاهرة التآكل تكتسب اهميه خاصة عندما يتعلق الأمر بالتنبؤ بمعدلات التآكل. من ناحية ثانية ان التعقيدات و المتغيرات اثناء حدوثها تجعل من الصعب نمذجة تأثيراتها. هذه الدراسه تقيم فوائد شبكة الأعصاب الأصطناعية للتنبؤ بمعدلات تآكل الحديد الكاربوني في عملية الحمايه الكاثودية في ماء البحر و بدلالة عدد من المتغيرات كدرجة الحرارة،سرعة جريان ماء البحر و حامضيته اضافة الى زمن تعرض النموذج للوسط. أظهرت النتائج ان تقنية شبكات الأعصاب الأصطناعيه اداة فعالة و ان صحة النتائج تربط و تعبر بقوة بين كمية النتائج المتوفرة و الخبرة المعرفة المرافقة لتحليل النتائج. التحليل الأحصائي اظهر ان العلاقة المقترحة في هذه الدراسة افرزت معدل الخطأ النسبي المطلق يساوي 0.09% و الأنحراف القياسي يساوي 0.46% .

INTRODUCTION

Corrosion is an electrochemical process in which a current leaves a structure at the anode site, passes through an electrolyte and reenters the structure at the cathode site. Current flows because of a potential difference between the anode and cathode that is the anode potential is more negative than the cathode potential, and the difference is the driving force for the corrosion current.The total system-anode, cathode, electrolyte and metallic connection between anode and cathode is termed a corrosion cell [1].

There are many methods for corrosion control as illustrated some of them in the [2]:

1. Cathodic protection.
2. Anodic protection.
3. Protective coating such as paint.
4. Corrosion-resistant metals and alloys.
5. Addition of inhibitors.
6. Very pure metals.

The selecting method depends on many factors such as cost, availability, contamination of environment with corroding metal …etc.

Cathodic protection is unique amongst all the methods of corrosion control in that if required it is able to stop corrosion completely, but it remains within the choice of the operator to accept a lesser, but quantifiable, level of protection. Manifestly, it is an important and versatile technique. In principle, cathodic protection can be applied to all the so-called engineering metals.

CATHODIC PROTECTION PRINCIPLES

It is possible to envisage what might happen if an electrical intervention was made in the corrosion reaction by considering the impact on the anodic and cathodic reaction. For example, if electrons were withdrawn from the metal surface it might be anticipated that the anodic reaction would speed up (to replace the lost electrons) and cathodic reaction would slow down because of the existing shortfall of electrons.It follows that the rate of metals consumption would increase. By contrast, if additional electrons were introduced at the metal surface, the cathodic reaction would speed up (to consume the electrons) and the anodic reaction would be inhibited; metal dissolution would be slowed down.This is basis of cathodic protection.[3]

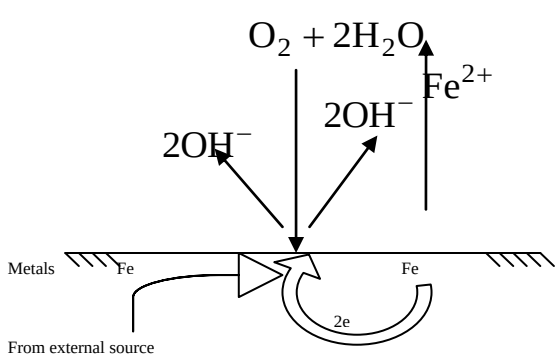

Fig.1 Schematic illustration of partial cathodic protection of steel in an aerated environmen

Artificial neural networks (ANNs) are simplified models of central nervous system. The network of highly inter connected neural computing elements that have the ability to respond to input stimuli and learn to adapt to environment.[4] As the term of artificial neural networks implies early work in the field of neural networks centered on modeling the behavior of neurons found in the human brain, engineering systems are considerably lees complex than the brain, hence from an engineering view point ANN can be viewed as non linear empirical models that are especially useful in representing input-output data. Making predication, classifying data, reorganization patterns, and control process. ANN which will be referred to as a node in this work and is analogous to a single neuron in the human brain. The advantages of using artificial neural network in construct with first principles models or other empirical models.[5]

1. ANN can be highly non linear.
2. The structure can be more complex and hence more representative than most other empirical models.
3. The structure does not have to be prespecified.
4. Quite flexible models.

THEORY AND MODELING OF ANN

Artificial Neural Networks (ANNs) have been increasingly applied to many problems in transport planning and engineering, and the feed forward network with the error back propagation learning rule, usually called simply Back propagation (Bp), has been the most popular neural network .[6]

Back propagation networks are among the most popular and widely used neural networks because they are relatively simple and powerful. Back propagation was one of the first general techniques developed to train multi-layer networks, which does not have many of the inherent limitations of the earlier, single -layer neural nets criticized by Minsky and Papert. These networks use a gradient descent method to minimize the total squared error of the output. A back propagation net is a multilayer, feed forward network that is trained by back propagating the errors using the generalized Delta rule.[7]

The input is the input to the hidden layer and the output layer is the output from the immediate previous layer, so it is called feed forward neural network. The number of the input units and the output units are fixed to a problem, but the choice of the number of the hidden units is somehow flexible as shown in figure 2. Too many hidden units may cause over fitting, but if the number of hidden units is too small, the problem may not converge at all. Usually a large number of training cases may allow more hidden units if the problem requires so.[8]

The conventional algorithm used for training a MLFF is the Bp algorithm, which is an iterative gradient algorithm designed to minimize the mean-squared error between the desired output and the actual output for a particular input to the network .[9]

Basically, Bp learning consists of two passes through the different layers of the network: a forward pass and backward pass as shown in figure 2.

During the forward pass the synaptic weights of the network are all fixed. During the backward pass, on the other hand, the synaptic weights are all adjusted in accordance with an error-correction rule.[10]

A MLFF consists of layers of interconnected denoted as the input layer, the hidden layer and the output layer. So the number of neurons in the hidden layer can be varied based on the complexity of the problem and the size of the input information.[10]

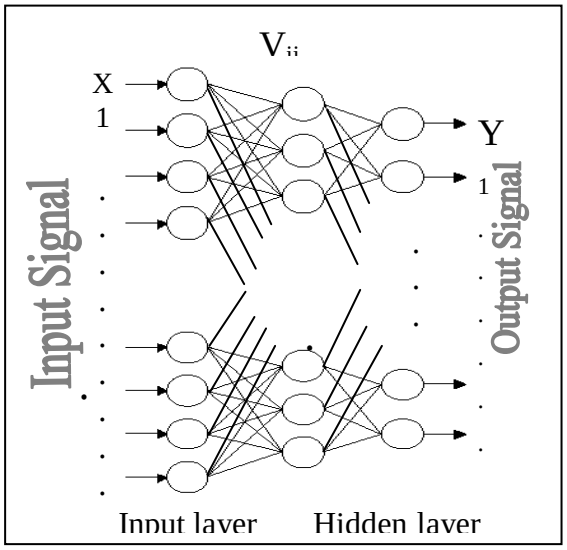

Fig.2 Multi- layer feed forward network (one hidden layer).

Two learning factors that significantly affect convergence speed as well as accomplish avoiding local minima, are the learning rate and momentum.

The learning rate (η) determines the portion of weight needed to be adjusted. However, the optimum value of η depends on the problem. Even though as small learning rate guarantees a true gradient descent, it slows down the network convergence process. If the chosen value of η is too large for the error value, the search path will oscillate about the ideal path and converges more slowly than a direct descent.

The momentum (α) determines the fraction of the previous weight adjustment that is added to current weight adjustment. It accelerates the network convergence process.

During the training process, the learning rate and the momentum are adjusted to bring the network out of its local minima, and to accelerate the convergence.

The algorithm of the error back-propagation training is given below [9]:

Step1: initialize network weight values.

Step2: sum weighted input and apply activation function to compute output of hidden layer.

$$h_j = f[\sum_i x_i w_{ij}] \quad (1)$$

Where

h_j: The actual output of hidden neuron j for input signals X.

X_i: Input signal of input neuron (i).

W_{ij}: Synaptic weights between input neuron hidden neuron j and i.

f: The activation function.

Step3: sum weighted output of hidden layer and apply activation function to compute output of output layer.

$$O_k = f\left[\sum_j h_j W_{jk}\right] \quad (2)$$

where

O_k: The actual output of output neuron k.

W_{jk}: Synaptic weight between hidden neuron j and output neuron k.

Step4: compute back propagation error.

$$\delta_k = (d_k - O_k) f'\left(\sum_j h_j W_{jk}\right) \quad (3)$$

where

f' :The derivative of the activation function.

d_k: The desired of output neuron k.

Step5: calculate weight correction term.

$(n-1)$

$$\Delta W_{jk}(n) = \eta \delta_k h_j + \alpha \Delta W_{jk}(n-1) \quad (4)$$

Step6: sums delta input for each hidden unit and calculate error term.

$$\delta_j = \sum_k \delta_k W_{jk} f'\left(\sum_i X_i W_{ij}\right) \quad (5)$$

Step7: calculate weight correction term.

$$\Delta W_{ij}(n) = \eta \delta_j X_i + \alpha \Delta W_{ij}(n-1) \quad (6)$$

Step8: update weights.

$$W_{jk}(n+1) = W_{jk}(n) + \Delta W_{jk}(n) \quad (7)$$

$$W_{ij}(n+1) = W_{ij}(n) + \Delta W_{ij}(n) \quad (8)$$

Step9: repeat step2 for given number of error.

$$MSE = \frac{1}{2p}\left[\sum_p \sum_k (d_k^p - O_k^p)^2\right] \quad (9)$$

where

p: The number of patterns in the training set.

Step10: END.

Bp is easy to implement, and has been shown to produce relatively good results in many applications. It is capable of approximating arbitrary non-linear mappings. However, it is noted that two serious disadvantages in the Bp algorithm are the slow rate of convergence, requiring very long training times, and getting stuck in local minima.

The success of Bp methods very much depends on problem specific parameter settings and on the topology of the network [Leonard 1990]. So in the next section the quick propagation will be presented.

MODELING CORRELATION OF ANN

In the current study, neural networks are used to fit a set of experimental points in order to provide a purely empirical model. The experimental points are called the training cases (or learning cases) and another are called testing cases. They consist of input vectors (values of input variables) associated with the experimental output value. To solve a problem with a back-propagation network, it is shown sample inputs with the desired outputs, while the network learns by adjusting its weights. If it solves the problem, it would have found a set of weights that produce the correct output for every input. This work includes computer simulation, implemented on a Pentium 4 computer using MATLAB**,** version7.

The modeling of ANN correlation began with the collection of large data bank following the learning file was made by randomly selecting about 70% of the data base to train the network. The remaining 30% of data is then used to check the generalization capability of the model. The last step is to perform a neural correlation and to validate it statistically. So that the steps of modeling are:-

Collection of Data**:** The first step in neural network modeling is collection of data. The data is necessary to train the network and to estimate its ability to generalize. In this model about 256 experimental points have been collected for corrosion rate used cathodic protection of low carbon steel in sea water [Khalid, 2006]. The data were divided into training and test sets: the neural network was trained on 70% (180) of the data and tested on 30% (76). The data includes a large range of temperature, flow rate, pH, and time. All of these parameters are input to neural network and there is one output; it is the corrosion rate.

THE STRUCTURE OF ARTIFICIAL NEURAL NETWORK

In this work, a multilayer neural network has been used, as it is effective in finding complex non-linear relationships. It has been reported that multilayer ANN models with only one hidden layer are universal approximates. Hence, three layer feed forward neural network are chosen as a correlation model. The weighting coefficients of the neural network are calculated using MATLAB programming. Structure of artificial neural network built as:-

1. Input layer: A layer of neurons that receive information from external sources and pass this information to the network for processing. These may be either sensory inputs or signals from other systems outside the one being modeled. In this work four input neurons in the layer and there is a set of (180) data points available of the training set.

2. Hidden layer: A layer of neurons that receives information from the input layer and processes them in hidden way. It has no direct connections to the outside world (inputs or output). All connections from the hidden layer are to other layers within the system. The

number of neuron in the first hidden layer consists of nine neurons and the second hidden layer consists of sixteen neurons. This gave best results and was found by trial and error. If the number of neurons in the hidden layer is more, the network becomes complicated. Results probably indicate that, the present problem is not too complex to have a complicated network routing. Hence, the results can be satisfactorily achieved by keeping the number of neurons in hidden layer at a best value with two hidden layer.

3. Output layer: A layer of one neuron that receives processed information and sends output signals out of the system. Here the output is the corrosion rate or Zn consumption as sacrificial anode in Cathodic protection of a steel in sea water.

4. Bias: The function of the bias is to provide a threshold for activation of neurons. The bias input is connected to each of hidden neurons in network.

The structure of multi layer ANN modeling is illustrated in figure.3

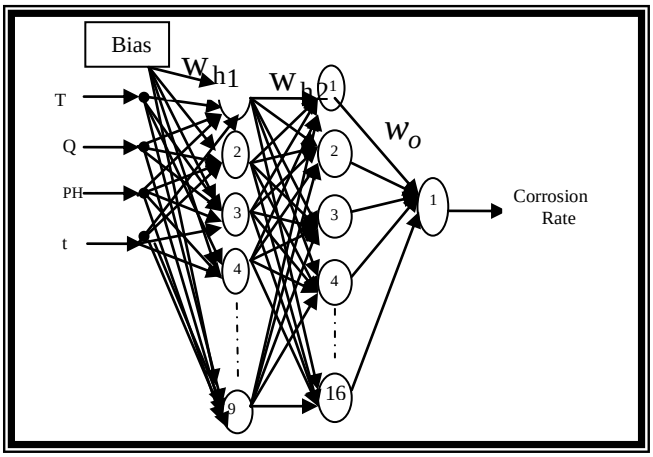

Fig.3Structure of a layer neural network

TRAINING OF ARTIFICIAL NEURAL NETWORK

Training is just the procedure of estimating the values of the weights and establishing the network structures and the algorithm used to do this is called a “learning” algorithm. Learning typically occurs through training or exposure to set of input, output data where the training algorithm iteratively adjusts the connection weights. These connection weights represent the knowledge necessary to solve specific problems (i.e. calculates the coefficients of correlation).

The training phase starts with randomly chosen initial weight values. Then a back-propagation algorithm is applied after each iteration, the weights are modified so that the cumulative error decreases. In back-propagation, the weight changes are proportional to the negative gradient of error. Back-propagation may have an excellent performance, this algorithm is used to calculate the values of the weights the following procedure is then used (called “supervised learning”) to determine the values of weights of the network:-

1. For a given ANN architecture, the value of the weights in the network is initialized as small random numbers.
2. The input of the training set is sent to the network and resulting outputs are calculated.

3. The measure of the error between the outputs of the network and the known correct (target) values is calculated.
4. The gradients of the objective function with respect to each of the individual weights are calculated.
5. The weights are changed according to the optimization search direction.
6. The procedure returns to step 2.
7. The iteration terminates when the value of the objective function calculated using the data in the test approaches experimental value. The trial and error to find the best ANN correlation model shown in table 1:-

Table (1)

Network parameters in ANN model

Structure	network Parameters				
	MSE	No.of iteration	Learning rate	Momentum coefficient	Transfer function
[4-16-1]	0.1	1340	0.7	0.9	Tan sigmoid
[4-18-1]	0.01	7654	0.65	0.9	Tan sigmoid
[4-9-16-1]	0.00001	929	0.9	0.9	Tan sigmoid

With reduced MSE the network is more accurate, because MSE is defined as:-

$$\text{MSE} = \frac{1}{2p}[\sum_{p}\sum_{k}(d_k^p - o_k^p)^2] \quad (10)$$

Where p: the number of patterns in training set

k=No. of iterations.

d_k^p =The desired output.

o_k^p =The actual output.

Learning rate: the main purpose of the learning rate is to speed up the rate at which the network learns. This is also accomplished by multiplying the learning rate by the change in weight factor from the previous iteration in order to determine the new weight factors.

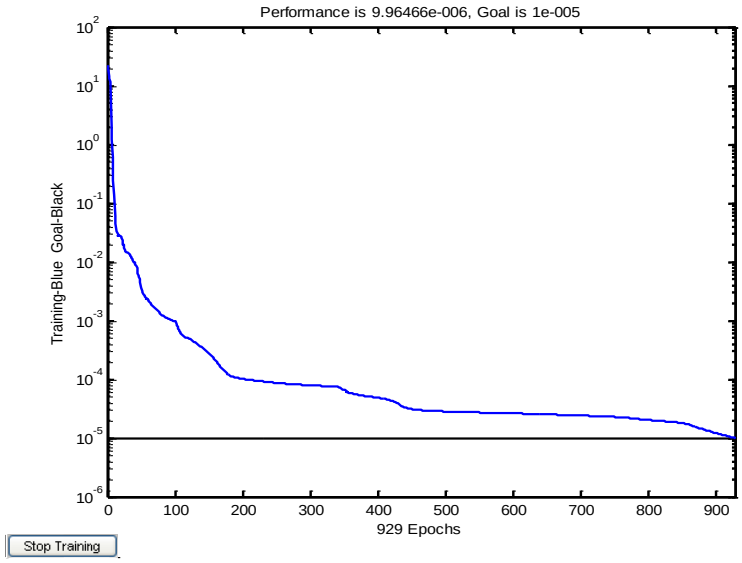

Fig.4 illustrates the number of epochs with MSE for corrosion rat

weight factors by multiplying by the change in the weight factor that was produced in last iteration.

The choice of transfer function is based on the function of the network being used. The tan-sigmoid function is appropriate for most types of network, especially prediction problems.

The learning process includes the procedure when the data from the input neurons is propagated through the network via the interconnections. Each neuron in a layer is connected to every neuron in adjacent layers. A scalar weight is associated with each interconnection.

Neurons in the hidden layers receive weighted inputs from each of the neurons in the previous layer and they sum the weighted inputs to the neuron and then pass the resulting summation through a non-linear activation function (tan sigmoid function).

Artificial neural networks learn patterns for this study can be equated to determining the proper values of the connection strengths (i.e. the weight matrices w_{h1}, w_{h2} and w_o illustrated in figure.3 that allow all the nodes to achieve the correct state of activation for a given pattern of inputs. The matrix, bias, and vector, given eq. (11), (12), (13) and (14) illustrate the result of coefficient weights for ANN correlation for this case where w_h is the matrix containing the weight vectors for the nodes in the hidden layer and w_o is the vector containing the weight for the nodes in the output layer.

$$w_{h1} = \begin{pmatrix} -0.2101 & -0.0522 & 0.5464 & 6.8392 \\ 0.0313 & 0.0006 & -0.2814 & 0.4433 \\ 0.2087 & -0.0050 & 1.0017 & -2.1666 \\ -0.0202 & -0.0010 & 0.3037 & 0.1873 \\ -0.0025 & -0.0077 & 0.7551 & 1.5166 \\ -0.0307 & -0.0023 & 0.2219 & -0.5138 \\ -0.1467 & -0.0169 & -3.8696 & 4.9871 \\ 0.0190 & 0.0001 & -1.7795 & 0.5599 \\ 0.0079 & 0.0009 & -0.0318 & -0.9718 \end{pmatrix} \quad \textbf{... (11)}$$

$$b = \begin{pmatrix} -4.9377 \\ -1.6042 \\ -1.7661 \\ -1.0162 \\ -5.5346 \\ 1.0628 \\ 8.9828 \\ 1.1397 \\ 0.2220 \end{pmatrix} \quad \ldots(12)$$

$$w_{h2} = \begin{pmatrix} 0.0406 & -0.3100 & -0.8888 & -0.3131 & -2.4295 & 0.5815 & 1.5191 & 2.2825 & -0.7296 \\ 8.7740 & -1.6365 & 1.5967 & -4.3531 & 1.2756 & -2.2288 & -1.5553 & -0.9756 & 7.6799 \\ 0.4378 & -0.4767 & 0.4341 & -1.2425 & -0.1427 & -0.8395 & -0.9642 & 1.6665 & -1.9187 \\ -3.5163 & -0.3959 & 1.7808 & -0.0079 & 3.7486 & -11.0608 & -1.7049 & -3.1292 & -0.6846 \\ -3.1893 & -1.5956 & 0.5030 & -1.9342 & 1.2678 & -3.5760 & -0.4841 & 4.5798 & 0.8413 \\ -0.2755 & -0.0541 & -4.7363 & -0.8619 & -6.6302 & 0.3583 & -5.6679 & -1.0520 & -3.6661 \\ 0.3525 & -2.6604 & -4.5104 & 1.6472 & -1.3579 & 0.3411 & -4.5446 & 0.3707 & 0.2862 \\ -1.6356 & -0.1007 & 2.6733 & -0.8482 & -3.0927 & 3.1922 & 2.1168 & -1.1799 & -1.2983 \\ -1.3712 & 0.0500 & 1.0391 & 4.8353 & 1.8285 & -1.3331 & 0.4950 & 0.0743 & 1.8176 \\ -6.8859 & -3.5244 & 6.0626 & -3.1854 & -3.5642 & -8.2899 & 1.0237 & 4.4005 & -1.8944 \\ -0.6302 & -1.4180 & -4.4862 & -1.1765 & -0.4018 & 0.1284 & -0.5081 & -0.3942 & -0.5212 \\ -0.2282 & 1.6494 & 0.0727 & -4.0256 & -1.6346 & 0.4222 & -0.9693 & 5.3954 & -6.9461 \\ 0.5453 & -0.2046 & -1.9745 & 0.5938 & -0.9798 & -0.0110 & 0.9162 & -0.9258 & -0.3238 \\ -0.0664 & -0.9405 & -1.2722 & 4.1727 & -8.6158 & 0.1517 & -3.5267 & 1.0009 & -10.2560 \\ 5.4313 & -0.1749 & 1.5971 & -4.8051 & -8.7707 & 7.6181 & -2.6448 & -0.4801 & -2.4320 \\ 0.0486 & 0.2388 & 0.3050 & 0.0095 & 0.9498 & -0.0550 & -0.2476 & 0.6169 & 0.3752 \end{pmatrix} \quad \ldots(13)$$

$$w_o = [4.3844 \quad -0.7402 \quad 2.7131 \quad 1.6743 \quad 1.8703 \quad 2.8731 \quad -1.7626 \quad 0.7479 \quad -2.5953 \quad 0.5427 \quad -1.5195 \quad 0.6907 \quad 4.0277 \quad 3.3468 \quad -0.6299 \quad 10.6241] \quad \textbf{...(14)}$$

RESULTS

The network architecture used for prediction corrosion rate for cathodic protection of low carbon steel in sea water in fig.3 consist of four inputs neurons corresponding to the state variables of the system, with hidden neurons and one output neuron. All neurons in each layer were fully connected to the neurons in an adjacent layer. The prediction of ANN correlation result is plotted in figure.5 compares the predicted of corrosion rate with experimental for training set.

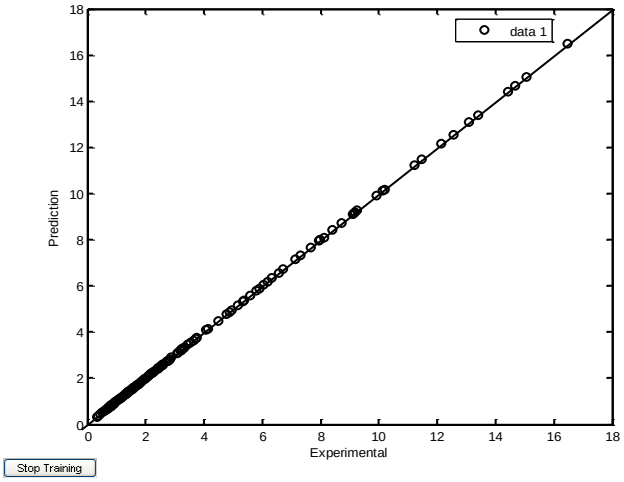

Fig.5 Comparison between experimental and prediction for Zinc consumption in training set

TEST OF THE PROPOSED ANN

The purely empirical model was tested on data that were not used to train the neural network and yielded very accurate predictions. Having completed the successful training, another data set was employed to test the network prediction corrosion rate. We made use of the same model to generate (76) new data values.

The result of prediction is plotted with experimental value as shown in figure.6.

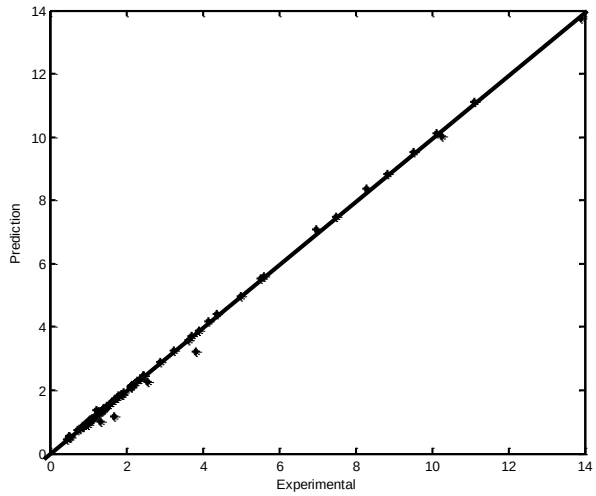

Fig(6) Comparison between experimental and prediction for Zinc consumption in testing set.

CONCLUSIONS

The ANN correlation shows noticeable improvement in the prediction of corrosion rate. The neural network correlation yields an AARE of 0.09% and standard deviation of 0.46%. The number of input units and output units are fixed to a problem, but the choice of the number of the hidden units is flexible. In this work it was started with a number of neurons in the hidden layer, but was found that two hidden layer the first layer consists of nine neurons and second consists of sixteen neurons gives butter results of prediction corrosion rate shown in table(2). Below two layer of hidden the network cannot to be trained.

Table (2) Gives the statistical information of neural networks models for prediction of corrosion rate.

ANN models	Structure	AARE%	S.D%	R
Case study	[4-9-16-1]	0.09	0.46	0.998

Acknowledgment

Partial support for this work was provided by Suhaiela A.Akkar.The author appreciate her valuable discussion.

NOMENCLATURE

d_k The desired of output neuron k

f The activation function

f' The derivation of the activation function

h_i The actual output of hidden neuron j

o_k The actual output of output neuron k

P The number of patterns in the training set

V_{ij} Weight on link from Xi to Zj

W_{ij} Synaptic weights between input and hidden neurons

W_{jk} Synaptic weight between hidden and output neuron

x_i Input signal of input neuron i

Y Target vector

Y_k Output unit

Z_i Hidden unit

GREEK SYMBOLS

SYMBOL	DEFINITION
δ_k	The error term
η	The learning rate

REFERENCES

- Shrier[1],LL,(1976)“Corrosion 1,matal/environment reactions", newness-Butter Worth,

- Bosich, F, G.,(1970) “Corrosion prediction for practicing engineering”, Barnes and Noble INC.

- Uhlig,H.H.(2000) “Corrosion handbook”, Edited by Winston, R., R., second Edition, John-Wiley and son.

- Patterson,H.(1996) “Artificial neural networks theory and applications”, Prentice Hall.

- David M.H.(2002), “Applications of artificial neural networks in chemical engineering”, Korean. J. Chem. Eng., 17, 373-392.

- Freeman, J.A and Skapura, D.M.,(1992) “Neural networks”, M.sc.thesis,Jordan University of Science and Technology.

- MATLAB, Version 7, June 2003, “Neural network toolbox”

- Sivanadam, S.N.,(2003) “Introduction to artificial neural networks”, Vikas Publishing House Pvt. Ldt.

- Lendaris, G.,(2004) “Supervised learning in ANN from introduction to artificial intelligence”, NewYork, April 7.

- Lippmann,R.P.,(1987) “An introduction to computing with neural nets”, IEEE Magazine, April, pp.4-22.

- Khalid,W.,Hameed.(2006)”Cathodic protection of low carbon steel in sea water”, Ph.D. thesis, Iraq, University of Baghdad.

APPENDIX

STATISTICAL ANALYSIS

Statistical analysis based on the test data is calculated to validate the accuracy of the output for pervious correlation model based on ANN. The structure for each model should give the best output prediction, which is checked by using statistical analysis. The statistical analysis of prediction is based on the following criteria:-

1. The AARE (Average Absolute Relative Error) should be minimum

$$AARE = \frac{1}{N}\sum_{1}^{N}\left|\frac{x_{prediction} - x_{\exp erimental}}{x_{\exp erimental}}\right|$$

Where N=Number of data points.

x=Corrosion rate.

2. The standard deviation should be minimum.

$$S.D = \sqrt{\sum_{1}^{N} \frac{[|(x_{prediction} - x_{experimental} / x_{experimental}| - AARE]^2}{N-1}}$$

3. The correlation coefficient R between input and output should be around unity.

$$R = \frac{\sum_{i=1}^{N} (x_{experimental}(i) - \bar{x}_{experimental})(x_{prediction}(i) - \bar{x}_{prediction})}{\sqrt{\sum_{i=1}^{N} (x_{experimental} - \bar{x}_{experimental})^2} \sqrt{\sum_{i=1}^{N} (x_{prediction} - \bar{x}_{prediction})^2}}$$

$\bar{x}_{experimental}$ =corrosion rate mean of experimental points

$\bar{x}_{prediction}$ =corrosion rate mean for prediction points

PREDICTION OF EXTRACTION EFFICIENCY IN RDC COLUMN USING ARTIFICIAL NEURAL NETWORK

Prof. Dr. Adil. A. A. Al-Hemiri and Chalak S. Omar

Chemical Engineering Department, College of Engineering, University of Baghdad

ABSTRACT

An application of neural network technique was introduced in modeling extraction efficiency in RDC column, based on a data bank of around 352 data points collected in the open literature. Three models were made, using back-propagation algorithm, the extraction efficiency was found to be a function of seven dimensionless groups: Weber number (we), (V_d / V_c), (μ_c / μ_d), (D_s / D_t), (D_r / D_t), (Z_c / D_t) and (Z_t / Z_c). Statistical analysis showed that the proposed models have an average absolute error (AARE) and standard deviation (SD) of 12.23% and 10.61% for the first model, 5.35% and 6.21% for the second model, 8.34% and 7.59% for the third model. The developed correlations also show better prediction over a wide range of operating conditions, physical properties and column geometry.

KEY WORDS

Rotating disc contactor, Extraction Efficiency, Artificial neural network, Back-propagation algorithm

INTRODUCTION

Liquid-liquid extraction has been emerging as a very important method for separation of liquid mixtures into its components by means of a solvent. The solvent used in the extraction process should be immiscible or partially miscible with one of the components of the mixture in order to facilitate the separation of the liquid phases (Laddha and Degaleesan, 1976).

The rotating disc contactor (RDC) has received considerable attention as liquid-liquid extraction equipment for refining of vegetable oils, processing of nuclear fuels, refining of crude petroleum and purification of vitamins. In common with other agitated columns it relies upon the application of mechanical energy to the contactor

contents to gain high mass transfer efficiency (Laddha and Kannappan, 1978). It consists of a vertical cylindrical shell divided into a number of compartments by a series of stator rings. A rotating disc supported on a central shaft driven by an electric motor is located in each compartment. The feed inlets, at each end of the column, are arranged tangentially in the direction of rotation. The outlets are usually through the top and bottom plates of the column. The dense phase is introduced into the top of the column and the light phase into the bottom, so that, counter current flow is established by gravity. One of the phases is dispersed by the action of the rotating discs. At the ends of the column there are settling zones for phase separation (Alders, 1959), as shown in fig. 1. The advantages of such device are the acheivement high efficiency per unit height and high throughput for a given flow area. The column is relatively free from plugging, and thus can be operate in the presence of small amounts of suspended solids or other impurities. Moreover it requires low driving power and has comparatively low operation and maintenance costs (Zhang et al, 1981).

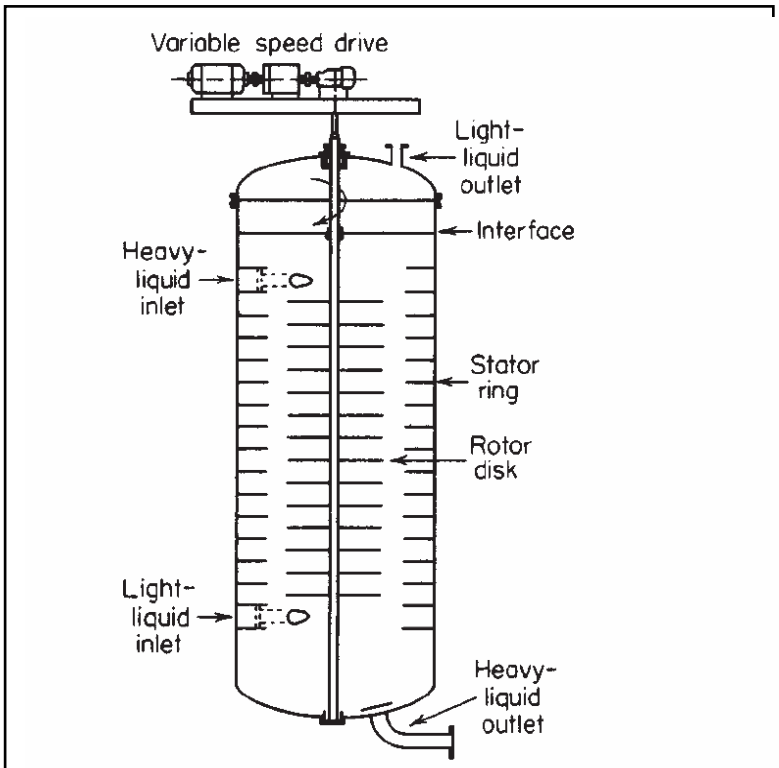

Rotating-disk (RDC) extractor. (*Courtesy of Glitsch Process Sys-*

COLUMN DESIGN VARIABLES:

The important column parameters that effect the performance of a rotating disc contactor for a given extraction system are;

Column diameter	(D_t)
Rotor disc diameter	(D_r)
Stator diameter	(D_s)
Compartment height	(Z_c)
Effective column height	(Z_t)
Speed of rotor disc	(N)

These dimensions are normally given as ratios with respect to (D_t). And may be varied slightly to provide flexibility in design. For the optimum design, the column dimensions should have the ratios (Remab and Olney, 1955; Logsdail et al, 1957).

$$(D_s/D_t) = 0.66 \text{ to } 0.75$$
$$(D_r/D_t) = 0.5 \text{ to } 0.66$$
$$(Z_c/D_t) = 0.33 \text{ to } 0.5$$

EXTRACTION EFFICIENCY:

Numerous studies have been made to obtain the effect of different parameters on RDC 's efficiency. Reman and Olney (1955) investigated the influence of column geometry and flow rates. Efficiency was found to increase with,

1. Decreasing stator opening.
2. Decreasing compartment height.
3. Increasing of dispersed flow rate at constant continuous flow rate.
4. Increasing rotor speed.
5. Increasing diameter of rotor discs.
6. Increasing specific load.

However, under certain conditions, increasing in rotor speed and specific load reduced the efficiency, due to back mixing.

Reman and Olney (1955) interpreted their results by plotting the efficiency, defined as the number of stages per foot column height, versus the energy input per unit volume ($N^3.R^5$ /$H.D^2$). Data for two column diameters, 4 inches and 16 inches correlated well.

Later Logsdail et al (1957), using the system toluene-acetone-water and butylacetate-acetone-water, the water being the continuous phase throughput, showed that the overall values of the mass transfer coefficient or H.T.U. , could be correlated by the expression;

$$\left[\frac{(H.T.U.)_{oc}}{V_c}\left(\frac{g^2.\rho_c}{\mu_c}\right)^{1/3}\right].x = \left[\frac{x}{K_{oc}.a}\left(\frac{g^2.\rho_c}{\mu_c}\right)^{1/3}\right] = K\left(\frac{\mu_c.g}{\overline{V}_N{}^3.(1-x)^3.\rho_c}\right)^{2m/3}.\left(\frac{\Delta\rho}{\rho_c}\right)^{2(m-1)/3} \quad ..(1)$$

Use of this expression for design purposes necessitates evaluation of the constant K, the exponent m, and the characteristic velocity $\overline{V}_N$

This may be determined from tests with the given system in a small-scale laboratory column. Alternatively for the case of transfer from an aqueous into solvent phase, i.e., a case of hindered coalescence, $\overline{V}_N$ may be evaluated using the equation below;

$$\frac{\overline{V}_N.\mu_c}{\sigma} = 0.012\left(\frac{\Delta\rho}{\rho_c}\right)^{0.9}\left(\frac{g}{D_r.N^2}\right)^{1.0}\left(\frac{D_s}{D_r}\right)^{2.3}\left(\frac{Z_c}{D_r}\right)^{0.9}\left(\frac{D_r}{D_t}\right)^{2.7} \quad .....(2)$$

THE BACK-PROPAGATION ALGORITHM:

Back-propagation is a supervised learning technique used for training artificial neural networks. It was first described by Paul Werbos in 1974, and further developed by David E. Rumelhart, Geoffery E. Hinton and Ronald J. Williams in 1986.

It is most useful for feed-forward networks (networks that have no feedback, or simply, that have no connections that loop). The term is an abbreviation for "backwards propagation of errors". Back-propagation requires that the transfer function used by the artificial neurons (or "nodes") be differentiable. Back propagation networks are among the most popular and widely used neural networks because they are relatively simple and powerful.

. The input is the input to the hidden layer and the output layer is the output from the immediate previous layer, so it is called feed forward neural network. The number of the input units and the output units are fixed to a problem, but the choice of the number of the hidden units is somehow flexible as shown in fig. 2. Too many hidden units may cause over fitting, but if the number of hidden units is too small, the problem may not converge at all. Usually a large number of training cases may allow more hidden units if the problem requires so (Sivanadam, 2003).

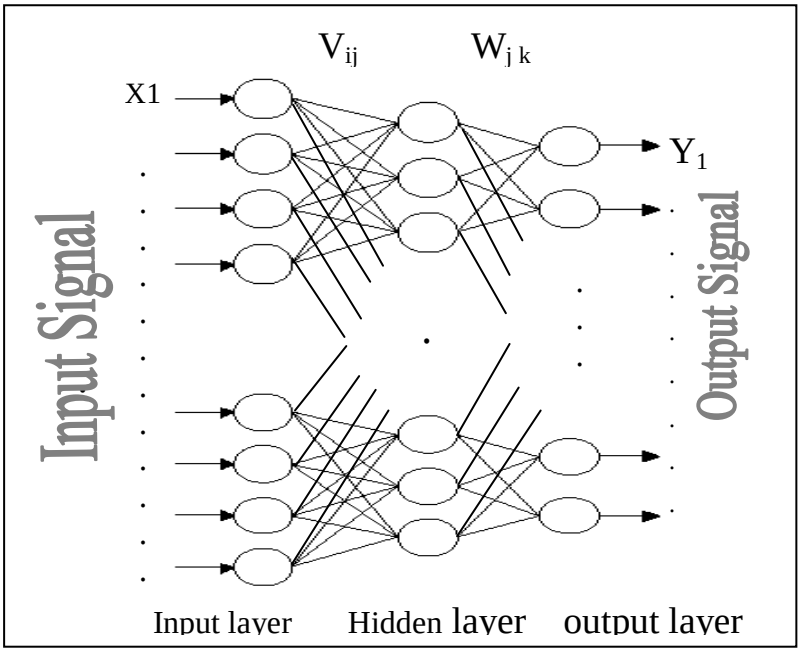

Fig. 2. Multi layer feed forward neural network

TRAINING A BACK-PROPAGATION NETWORK:

The conventional algorithm used for training a multi-layerd feed forward (MLFF) is the Bp algorithm, which is an iterative gradient algorithm designed to minimize the mean-squared error between the desired output and the actual output for a particular input to the network (Lendaris, 2004).

Two learning factors that significantly affect convergence speed as well as accomplish avoiding local minima, are the learning rate and momentum.

The learning rate (η) determines the portion of weight needed to be adjusted. However, the optimum value of η depends on the problem. Even though as small learning rate guarantees a true gradient descent, it slows down the network convergence process. If the chosen value of η is too large for the error value, the search path will oscillate about the ideal path and converges more slowly than a direct descent. The momentum (α) determines the fraction of the previous weight adjustment that is added to current weight adjustment. It accelerates the network convergence process. During the training process, the learning rate and the momentum are bring the network out of its local minima, and accelerate the convergence of the network.

The algorithm of the error back-propagation training for one hidden layer is given below (Lendaris, 2004):

Step1: initialize network weight values.

Step2: sum weighted input and apply suitable activation function to compute the output of the hidden layer.

$$h_j = f\left[\sum_i X_i W_{ij}\right] \qquad \ldots (3)$$

Where

h_j: The actual output of hidden neuron j for input signals X.

X_i: Input signal of input neuron (i).

W_{ij}: Synaptic weights between input neuron hidden neuron j and i.

f: The activation function.

Step3: sum weighted output of hidden layer and apply activation function to compute output of output layer.

$$O_k = f\left[\sum_j h_j W_{jk}\right] \qquad \ldots (4)$$

where

O_k: The actual output of output neuron k.

W_{jk}: Synaptic weight between hidden neuron j and output neuron k.

Step4: compute back propagation error.

$$\delta_k = (d_k - O_k) f'\left(\sum_j h_j W_{jk}\right) \qquad \ldots (5)$$

where

f' :The derivative of the activation function.

d_k: The desired output of neuron k.

Step5: calculate weight correction term.

$$\Delta W_{jk}(n) = \eta \delta_k h_j + \alpha \Delta W_{jk}(n-1) \quad \ldots (6)$$

Step6: sums delta input for each hidden unit and calculate error term.

$$\delta_j = \sum_k \delta_k W_{jk} f'\left(\sum_i X_i W_{ij}\right) \quad \ldots (7)$$

Step7: calculate weight correction term.

$$\Delta W_{ij}(n) = \eta \delta_j X_i + \alpha \Delta W_{ij}(n-1) \quad \ldots (8)$$

Step8: update weights.

$$W_{jk}(n+1) = W_{jk}(n) + \Delta W_{jk}(n) \quad \ldots (9)$$

$$W_{ij}(n+1) = W_{ij}(n) + \Delta W_{ij}(n) \quad \ldots (10)$$

Step9: repeat step2 for given number of error.

$$MSE = \frac{1}{2p}\left[\sum_p \sum_k (d_k^p - O_k^p)^2\right] \quad \ldots (11)$$

Where p: The number of patterns in the training set.

Step10: END.

COMPUTER SIMULATION RESULTS:-

COLLECTION OF DATA:

In this work about 352 experimental points have been collected from 11 sources spanning the years 1954-1986. These data were divided into training part (75%) and testing part (25%). 224 data points were used in the first model which is for mass transfer from continuous to dispersed phase ($c \rightarrow d$), 128 data points used in the second model for mass transfer from dispersed to continuous phase ($d \rightarrow c$) and over all 352 data points used in the third model for mass transfer for both directions ($c \rightarrow d, d \rightarrow c$). These data includes six chemical systems with a large range of rotary speed, velocity of both continuous and dispersed phase, column geometry, also the physical properties for each chemical system. Table 1 gives the detailed listing of data used for the present work.

Table 1. Details of data bank used for the present work.

Author	System ….Dispersed phase ….Continuous phase	Direction of solute transfer	No. of data
Ismail (1985)	Toluene Acetone Water	$(c \rightarrow d)$	57
Al-Hemiri (1973)	Toluene Acetone water	$(c \rightarrow d)$ $(d \rightarrow c)$	46
Al-Hemiri (1973)	Liquid paraffin Methyle ethyl ketone water	$(c \rightarrow d)$ $(d \rightarrow c)$	22
Korchinsky (1982)	Toluene Acetone water	$(c \rightarrow d)$	15
Zhang(1985)	Kerosene n-butyric acid water	$(c \rightarrow d)$ $(d \rightarrow c)$	30
Al-Aswad (1985)	Clairsol 350 Acetone water	$(c \rightarrow d)$ $(d \rightarrow c)$	22
Al-Husseini (1986)	Toluene Acetone water	$(c \rightarrow d)$	52
Cruz-pinto (1983)	Toluene Acetone water	$(c \rightarrow d)$	4
Chartres and Korchinsky (1978)	Toluene Acetone water	$(c \rightarrow d)$	7
Korchinsky and Cruz-pinto (1979)	Toluene Acetone water	$(c \rightarrow d)$	4
Vermijs and Kramers (1954)	Water Acetic Acid Methyl isobutyl ketone	$(c \rightarrow d)$	38
Krishnaiah (1967)	Benzene Acetic acid water	$(d \rightarrow c)$	55

CHOICE OF INPUT PARAMETERS:

In this study there are thirteen parameters used, these are: rotor speed (N), dispersed phase superficial velocity (V_d), continuous phase superficial velocity (V_c), dispersed phase density (ρ_d), continuous phase density (ρ_c), dispersed phase viscosity (μ_d), continuous phase viscosity (μ_c), interfacial tension (σ), rotor disc

diameter (D_r), stator diameter (D_s), column diameter (D_t), compartment height (Z_c) and column height (Z_t).

These parameters are input to the network as seven dimensionless groups that affect the efficiency of (RDC).

The main advantage of dimensionless group is to reduce the number of input parameters to the network.

The dimensionless group input to the network are:

1. Weber number: that consists the density difference of two phases ($\Delta\rho$), interfacial tension (σ), rotor disc diameter (D_r) and rotor speed (N)

$$We = \frac{\Delta\rho . D_r . (N . D_r)^2}{\sigma}$$

2. Ratio of dispersed to continuous phases velocities =(V_d / V_c) .
3. Viscosity ratio of the phases = (μ_c / μ_d).
4. Ratio of stator to column diameters = (D_s / D_t).
5. Ratio of disc to column diameters = (D_r / D_t).
6. Ratio of compartment height to column diameter = (Z_c / D_t).
7. Ratio of column to compartment height =(Z_t / Z_c).

This is number of compartment.

THE STRUCTURE OF ARTIFICIAL NEURAL NETWORKS:

The ANN structure is determined by trial and error. For the first model it consists of seven input neurons in the input layer, twenty one neurons in the hidden layer and one neuron in the output layer, for second case it has the same structure but different in number of neurons in the hidden layer it consists of twenty four neurons. The last case has the same structure of previous models but different in number of neurons with nineteen neurons in the hidden layer. And then the networks trained with back-propagation algorithm then calculate the weights and biases matrices.

The trial and error to find the best ANN correlation model for the case ($c \rightarrow d$), case ($d \rightarrow c$) and for over all two cases together are shown in tables (2), (3) and (4) respectively.

Table (2) Some of the trial and error attempts for finding the best ANN model for the case (c$\rightarrow$d).

Structure	MSE	No. of iteration	Learning rate	Momentum coefficient	Transfer function
[7-15-1]	0.01	2379	0.2	0.8	Tan sigmoid
[7-16-1]	0.005	1313	0.7	0.8	Tan sigmoid
[7-17-1]	0.008	1303	0.4	0.9	Tan sigmoid
[7-18-1]	0.003	1074	0.8	0.9	Tan sigmoid
[7-20-1]	0.002	2078	0.65	0.8	Tan sigmoid
[7-21-1]	0.001	2101	0.75	0.9	Tan sigmoid

Table (3) Some of the trial and error attempts for finding the best ANN model for mass transfer from ($d \rightarrow c$).

Structure	MSE	No.of iteration	Learning rate	Momentum coefficient	Transfer function
[7-15-1]	0.01	678	0.2	0.8	Tan sigmoid
[7-16-1]	0.008	721	0.5	0.8	Tan sigmoid
[7-17-1]	0.004	768	0.6	0.9	Tan sigmoid
[7-18-1]	0.003	362	0.7	0.9	Tan sigmoid
[7-24-1]	0.001	542	0.75	0.9	Tan sigmoid

Table (4) Some of the trial and error attempts for finding the best ANN model for mass transfer for all two cases.

structure	MSE	No.of iteration	Learning rate	Momentum coefficient	Transfer function
[7-15-1]	0.1	3180	0.5	0.9	Tan sigmoid
[7-16-1]	0.008	2352	0.6	0.9	Tan sigmoid
[7-17-1]	0.004	2718	0.7	0.8	Tan sigmoid
[7-19-1]	0.002	8320	0.75	0.9	Tan sigmoid

The weights and biases matrices for the three models are shown in equations below:

For the first model:

$$w_h = \begin{pmatrix} 0.6712 & -3.3673 & -1.9696 & 10.9379 & -15.2399 & 12.0679 & -0.5428 \\ -0.2061 & 0.0393 & -2.5898 & 5.9822 & 23.5954 & -4.8994 & 0.5979 \\ -0.0663 & -6.6292 & 2.4579 & 0.9583 & -39.1761 & 8.0865 & 0.2162 \\ -1.4236 & 9.1276 & -1.2101 & -1.0746 & -60.9264 & -0.1834 & 4.8962 \\ 0.2418 & -7.4610 & 11.5550 & -2.9587 & 23.0981 & -1.2386 & -0.4613 \\ 0.5020 & 6.7192 & -1.5953 & 5.5997 & -47.1539 & -1.1287 & -0.4449 \\ -0.1585 & 4.9900 & 2.8305 & -6.8283 & 35.0873 & 1.4067 & -0.5246 \\ 0.0117 & -6.6071 & 0.7065 & 1.2093 & -0.9628 & 6.0162 & -0.2302 \\ 0.0881 & -3.6348 & -0.5344 & -5.8485 & -37.5682 & -2.7069 & 0.0733 \\ -0.1074 & -0.4881 & 0.4455 & -9.2231 & -29.7618 & -2.9980 & 0.4807 \\ -0.0043 & -3.0572 & 1.4106 & -1.2227 & -31.5198 & -5.0645 & 0.0121 \\ 0.0049 & -1.3719 & 0.8255 & 15.8067 & -39.7171 & -8.2089 & -0.0138 \\ -3.1340 & -3.2529 & -0.1819 & -2.4573 & -30.3152 & 6.3427 & 0.1685 \\ -6.4694 & -20.1816 & 11.4064 & -4.6109 & 30.2074 & -1.0619 & 2.6669 \\ 0.0339 & 4.3099 & -3.1361 & 8.3781 & 12.1996 & 7.8483 & 0.0662 \\ -0.0617 & -7.1877 & 7.2925 & -3.4151 & 17.3276 & -6.9807 & -0.0961 \\ -0.0504 & 3.4739 & 3.5516 & 3.8803 & -15.4565 & -1.8829 & -0.0897 \\ 0.0011 & -6.8589 & 3.4766 & -10.6542 & 0.5341 & -4.1628 & 0.0705 \\ 0.1253 & 4.0017 & -3.8548 & 4.7763 & 38.7567 & -3.3763 & -0.1087 \\ 3.3161 & 8.4312 & -0.8098 & -3.1555 & 31.0113 & 8.4326 & -1.4653 \\ 0.0677 & -0.7855 & 0.8125 & 6.3748 & -8.6399 & -5.8645 & 0.2365 \end{pmatrix} \quad \ldots(12)$$

$$, \; b1 = \begin{pmatrix} 8.7672 \\ -23.9633 \\ 16.0111 \\ 33.8680 \\ 33.8680 \\ 24.9955 \\ -6.5297 \\ 1.0558 \\ 25.3744 \\ 13.1758 \\ 20.0840 \\ 12.9769 \\ 13.7197 \\ -17.5943 \\ -19.9880 \\ 3.2111 \\ 5.5152 \\ 9.1235 \\ -24.3990 \\ -17.2059 \\ 2.0656 \end{pmatrix} \quad \ldots(13)$$

$$b2 = [1.1006] \quad \ldots(14)$$

$$w_0 = [-3.4891 \quad -8.9789 \quad 6.1570 \quad -1.3785 \quad -2.6963 \quad 2.1895 \quad 10.3487 \quad -5.3463 \quad 10.0372 \quad 7.6532 \quad -11.0769 \quad 6.0423 \quad 6.2067 \quad -17.6195 \quad -8.3889 \quad -4.9637 \quad 1.2610 \quad 3.6164 \quad 7.3337 \quad -19.1532 \quad 1.7628] \qquad \ldots(15)$$

For the second model:

$$w_h = \begin{pmatrix} 0.1234 & 0.2889 & -0.2098 & 3.4187 & 35.7059 & 2.6383 & -0.1933 \\ -0.0357 & 0.7395 & -0.0531 & 4.1740 & -13.3786 & 3.6104 & 0.3944 \\ 0.0930 & -0.3501 & 0.0753 & 10.3319 & -23.1379 & 3.9859 & 0.0543 \\ -0.6547 & 0.0229 & 0.2226 & -3.9909 & 1.1249 & 5.5466 & 0.1787 \\ 0.0956 & -0.0465 & 0.0034 & -1.7553 & -60.4389 & 0.2748 & -0.0457 \\ -0.0011 & -1.4635 & 1.5229 & -0.6160 & 4.4112 & 5.8333 & -0.1594 \\ 0.1889 & -0.8623 & -0.1330 & 4.4915 & 35.6777 & 0.5701 & 0.0534 \\ -0.0900 & 0.5578 & -0.0051 & -7.9568 & -72.2110 & 2.3670 & 0.0189 \\ 0.1622 & 0.4424 & 0.0356 & -10.2791 & 42.3113 & 8.6717 & 0.1048 \\ -0.0716 & -0.1468 & -0.0947 & 6.5884 & 41.9295 & 6.5861 & -0.2150 \\ 0.0011 & -0.7969 & 0.1646 & 0.4433 & 37.0766 & -5.1581 & 0.1260 \\ -0.4757 & -0.4012 & -0.0098 & -9.3298 & -7.5400 & 2.5654 & -0.3187 \\ 0.1050 & 0.7325 & -0.1837 & -8.4602 & -54.0223 & -7.0581 & -0.1633 \\ 0.0316 & -0.5672 & -0.3076 & -7.5982 & 43.0925 & -4.9177 & 0.0049 \\ -0.2175 & -0.3830 & 0.0075 & -2.4090 & -48.6293 & 7.1045 & 0.0400 \\ -0.1616 & 0.6706 & -0.0360 & -2.3382 & -8.4124 & 3.8209 & -0.1280 \\ -0.0489 & 0.1188 & -0.1397 & -8.7265 & -57.7659 & -8.5403 & -0.1149 \\ -0.1628 & -0.2300 & -0.1223 & 12.8269 & -33.7744 & 1.6003 & -0.0373 \\ 0.0281 & 0.6424 & -0.1755 & -10.5666 & 68.4840 & -1.2927 & 0.0101 \\ 0.5449 & 0.0258 & 0.0105 & -2.9365 & 51.8078 & 9.2572 & -0.1245 \\ -0.1760 & -0.5069 & -0.3172 & -5.9202 & -31.6383 & -6.1096 & 0.1793 \\ 0.4355 & -0.5017 & 0.0074 & -6.3292 & 44.2235 & -7.4766 & 0.1543 \\ -0.1672 & 0.0926 & 0.4492 & 10.6306 & -3.2991 & -0.5583 & 0.6760 \\ -0.0400 & -1.8825 & 0.2747 & -4.7801 & 10.1719 & 11.9353 & -0.0195 \end{pmatrix} \ldots(16)$$

$$b1 = \begin{pmatrix} -22.4296 \\ -3.2096 \\ 6.9129 \\ -2.1792 \\ 37.2682 \\ -0.5794 \\ -17.6551 \\ 43.7335 \\ -18.8823 \\ -28.9934 \\ -19.2918 \\ 11.2014 \\ 37.5087 \\ -18.3603 \\ 23.8124 \\ 0.3039 \\ 36.8954 \\ 10.3930 \\ -28.2146 \\ -29.5656 \\ 21.5242 \\ -14.6105 \\ -7.9138 \\ -2.0174 \end{pmatrix} \ldots(17)$$

$$b2 = [0.0214] \qquad \ldots..(18)$$

$$w_o = [0.6345 \quad 0.4762 \quad -0.5996 \quad 0.1780 \quad 0.3690 \quad 1.3332 \quad 1.1331 \quad 1.0184 \quad 0.1551 \quad 0.7346 \quad 1.6231 \quad -0.0963 \quad 0.9227 \quad 0.6875 \quad 0.0962 \quad 0.2680 \quad -0.6648 \quad -0.6382 \quad -0.9553 \quad -0.8878 \quad -0.6872 \quad -0.0673 \quad 0.4206 \quad -0.7015] \qquad \ldots\ldots(19)$$

For the third model:

$$w_h = \begin{pmatrix} 0.0249 & 1.3648 & -0.4491 & 6.3232 & 14.8117 & 3.6421 & 0.1036 \\ -0.5099 & 6.1151 & -3.4781 & -2.5083 & -29.4055 & 8.2767 & 1.0769 \\ -0.2348 & 0.1972 & 0.1672 & 6.2039 & 33.9799 & -1.8162 & 0.1033 \\ 0.0389 & 0.1031 & -0.2641 & 6.1485 & 32.9483 & 6.0856 & -0.2337 \\ -0.0083 & 7.5839 & -0.1512 & 7.5159 & -24.7785 & -7.7478 & 0.2997 \\ 0.6398 & -2.2457 & -1.4695 & 6.8300 & 13.4595 & 3.5864 & -22.9526 \\ -0.1163 & -0.9637 & -0.0369 & -7.0662 & 23.4879 & -5.2558 & 0.0320 \\ -0.0034 & 11.6483 & -1.5612 & -9.4009 & 17.8948 & 2.6496 & -0.0233 \\ -0.0057 & -3.1547 & 0.0702 & -8.9703 & -5.5169 & 12.0045 & -0.5636 \\ 0.0155 & 1.8149 & 2.1384 & 3.6038 & -3.8340 & 3.4886 & -0.9107 \\ 0.4714 & 2.1124 & -3.7127 & -8.5942 & -4.6193 & 7.6501 & -1.0597 \\ -0.0031 & -1.1453 & 0.7689 & -13.9756 & 24.5252 & 4.0808 & 0.0316 \\ -0.0182 & -0.2930 & -5.5158 & 10.5766 & -1.3630 & 8.9686 & -0.0562 \\ 0.1329 & -5.2441 & -0.0645 & -11.1016 & -13.7026 & 8.0867 & -1.0243 \\ 0.1777 & 4.4825 & -0.6572 & 0.9513 & 2.4935 & 3.7738 & -0.5070 \\ -0.0015 & 0.0619 & 0.8831 & -3.2606 & 2.1586 & -7.8348 & 0.0943 \\ -0.0022 & -0.0247 & 3.2039 & 12.9280 & -31.2622 & -0.6524 & -0.2862 \\ -0.1088 & -1.7109 & 3.5722 & 10.5591 & 18.5896 & -5.4965 & 0.0918 \\ -0.9543 & 0.1094 & 0.0729 & -10.0114 & -5.1432 & -6.9029 & -0.0312 \end{pmatrix}, \quad b1 = \begin{pmatrix} -18.6431 \\ 17.0586 \\ -21.0471 \\ -18.3708 \\ 7.2773 \\ -15.4990 \\ -4.3358 \\ -5.8046 \\ 17.4021 \\ 8.6129 \\ -0.1512 \\ -4.3949 \\ -4.2431 \\ 9.2810 \\ 3.6552 \\ 1.8434 \\ 7.8422 \\ -20.6339 \\ 14.1979 \end{pmatrix}$$

…..(20) …(21)

$b2 =$[-1.4308] …..(22)

$w_o =$[1.5043 0.3633 -0.8227 -1.9027 -13.4247 -18.5098 1.8115 -0.5788
-7.8875 -0.8821 1.2929 0.9230 -5.8703 -4.1934 0.4554
-11.1639 7.4440 -1.5360 5.0601

……(23)

TEST OF THE PROPOSED ANNS:

The ANN models were tested using another data set to show the accuracy of the network for prediction extraction efficiency in (RDC). The first model was used to generate (60) new data values for mass transfer from (c$\rightarrow$d), the second model was used to generate (38) new data values for mass transfer from ($d \rightarrow c$) and the third model was used to generate (98) new data values for mass transfer from ($c \rightarrow d, d \rightarrow c$). The comparison between experimental and predicted efficiency for three cases were plotted in figures below:

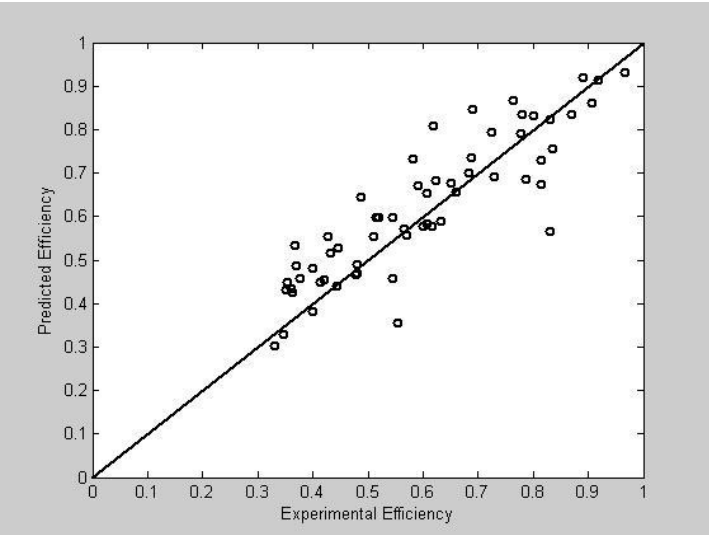

Fig. 3 .Comparison between experimental and predicted efficiency for the case ($c \rightarrow d$) in testing set.

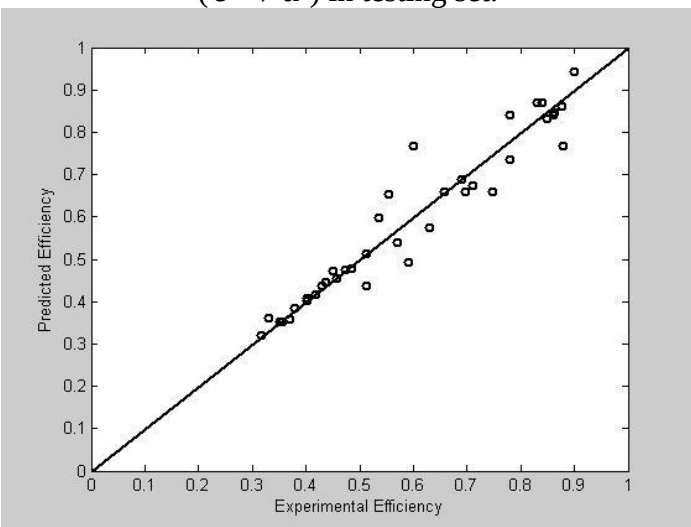

Fig. 4 . Comparison between experimental and predicted efficiency for mass transfer from ($d \rightarrow c$) in testing set.

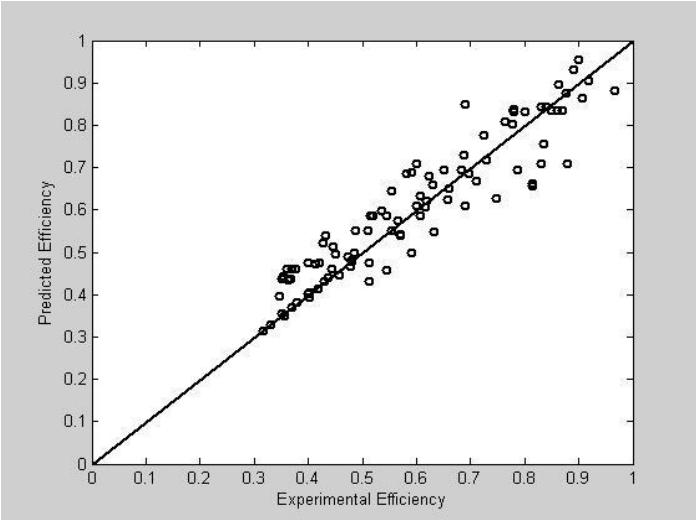

Fig. 5 . Comparison between experimental and predicted efficiency for all cases in testing set.

DISCUSSION

1- In the present work an attempt was made to correlate an ANN model for extraction efficiency prediction in (RDC). Three models were proposed, a model for mass transfer from ($c \rightarrow d$), mass transfer from ($d \rightarrow c$), and a model for the two cases together ($c \rightarrow d, d \rightarrow c$).

The accuracy of each model was validated by testing it with an experimental data not used in the training set and then compares the efficiency predicted from the ANN model with the experimental efficiency. Figures (3), (4) and (5) show the comparison between the predicted and experimental efficiency for ($c \rightarrow d$), ($d \rightarrow c$) and for ($c \rightarrow d, d \rightarrow c$) respectively.

Also the accuracy of these models was validated by statistical analysis (AARE, S.D and R). The model gives best output prediction based on AARE and S.D values respectively as shown in table 5.

Table 5. Statistical analysis information of three neural networks models

ANN models	Structure	AARE%	S.D%	R
Case 1 ($c \rightarrow d$)	[7-21-1]	12.23	10.61	0.879
Case 2 ($d \rightarrow c$)	[7-24-1]	5.35	6.21	0.962
Both cases	[7-19-1]	8.34	7.59	0.938

2. In this work back-propagation algorithm was used. This algorithm uses the (trainlm) training function, which appears to be the fastest method for training feed forward neural network.

3. The tansig (Hyperbolic tangent sigmoid) transfer function was used in the neurons in the hidden layer may be more accurate and is recommended for applications that require the hyperbolic tangent, especially prediction. Because the output from tan sigmoid varying from -1 to +1. The output neuron has a log sigmoid transfer function "logsig". Which is the best transfer function used in the output neuron for efficiency prediction. Because it generates outputs between 0 and 1.

4. Neural networks often encounter the well known 'overfitting' problem, which can make use of the ANN unreliable. To avoid 'overfitting' and make the ANN more useful, the following approach was used. The whole database was split into two parts, learning and generalization. The first part, called the 'learning file', was used to perform minimization using the ANN. The remaining part, called the 'generalization file', was used to validate the model

5. Third model concerning the two cases combined which cover cases of mass transfer from ($c \rightarrow d$) and from ($d \rightarrow c$) is found to be flexible and more comprehensive. Also it has optimum structure.

CONCLUSIONS:

It is very difficult to know which training algorithm will be the fastest for a given problem. It will depend on many factors, including the number of the experimental data points in the training set, the desired output (target) from the network, the relationship between the input and the desired output, the complexity of problem and the error goal. The number of neurons in the hidden layer was arrived at by trial and error starting from a minimum of fifteen neurons and according to the Hecht number.

ANN model can predict the extraction efficiency for a wide range of physical properties, operating parameters and column geometry. It has been demonstrated that the optimal model is a network that predicts for the two cases together ($c \rightarrow d, d \rightarrow c$) with one hidden layer.

NOMENCLATURE

a = Interfacial mass transfer area, m^2/m^3.

b = Bias.

d_k = The desired of output neuron k

D_r =Diameter of rotary disc, m.

D_s = Stator ring diameter, m.

D_t =Diameter of RDC column, m.

f = The activation function.

f' =The derivation of the activation function.

g = Acceleration due to gravity, m/s^2.

h_j = The actual output of hidden neuron j.

K_{oc} =Over all Mass transfer coefficient, m/s.

K= Constant (dimensionless).

N= Speed of rotor disc, rps.

o_k = The actual output of output neuron k.

P =The number of patterns in the training set.

R =Correlation coefficient.

V_c = Velocity of continuous phase, m/s.

V_d = Velocity of dispersed phase, m/s.

$\overline{V}_N$ = Characteristic velocity, m/s.
W_{ij}, w_h = Synaptic weights between input and hidden neurons.
W_{jk}, w_0 = Synaptic weight between hidden and output neuron.
We = Weber number (dimensionless).
x = Hold up.
x_i = Input signal of input neuron i.
Z_c = High of compartment, m.
Z_t = High of RDC column, m.

GREEK SYMBOLS
α = Momentum rate.
δ_k =The error term
η = The learning rate
ρ =Density, kg/m^3.
μ =Viscosity, kg/m.s.
σ = Interfacial tension, N/m.
$\Delta\rho$ =Difference in density, kg/m^3.

SUBSCRIPTS
c continuous phase.
d dispersed phase.

ABBREVIATIONS
AARE= Average Absolute Relative Error.
BP=Back Propagation.
H.T.U =Height Transfer Unit, m.
MLFF= Multi-Layer Feed Forward.
MSE=Mean Square Error.
S.D=Standard Deviation.

REFERENCES:

- Al-Aswad, K.K., Mumford, C.J. and Jeffreys, G.V., (1985), "The application of drop size distribution and discrete drop mass transfer models to assess the performance of a rotating disc contactor ", AICHE. J., 31, 9, 1488-1497.
- Alders, L., (1959), "liquid-liquid extraction", Elsevier publishing company.
- Al-Hemiri, A.A., (1973), "The effect of surface renewal on mass transfer in agitated contactors", Ph.D., thesis, University of Aston, UK.
- Al-Husseini, R. and Korchinsky, W.J., (1986), "liquid-liquid extraction (RDC) model parameters from drop size distribution and solute concentration measurements", J. Chem. Tech. Biotechnol, 36, 395-409.
- Charteres, R.H., and Korchinsky, W.J., (1978), "Drop size and extraction efficiency measurements in a pilot plant rotating disc contactor, Trans. I. Chem. Eng, 56, 91-95.
- Cruz-Pinto, J.J.C., and Korchinsky, W.J., (1983), "Exact solutions of the Newman, and the Handlos-Baron, model equation for counter current flow extraction", Comp. Chem. Eng, 7, 19-25.

- Ismail, A., (1985), "Evaluation of the hydrodynamic and mass transfer parameters in an extraction column (RDC)", Ph. D. thesis, Victoria, University of Manchester.
- Korchinsky, W.J., and Cruz-Pinto, J.C., (1979), "Mass transfer coefficients-calculation for rigid and oscillating drops in extraction columns", Chem. Eng. Sci, 34, 551-561.
- Korchinsky, W.J., Loke, C.T. and Cruz-pinto, J.J.C., (1982), "Optimization of drop size in counter current flow liquid-liquid extraction columns", Chem. Eng. Sci., 37, 5, 781-786.
- Krishnaiah, M.M., Pai, M.U., Rao, R. and Sastri, S.R., (1967), "Performance of a rotating disc contactor with perforated rotors", British chemical engineering, 12, 5, 719-721.
- Laddha, G.S., and Degaleesan, T.E., (1976), "Transport phenomena in liquid extraction", Tata Mc Graw-Hill publishing Co. Ldt, New Delhi.
- Laddha, G.S., and Kannappan, R., (1978), "Hydrodynamic and mass transport in rotating disc contactors", Can. J. Chem. Eng, 56, 137-149.
- Lendaris, G., (2004), "Supervised learning in ANN from introduction to artificial intelligence", New York, April 7.
- Logsdail, D.H., Thornton, J.D., and Pratt, H.R.C., (1957), "liquid-liquid extraction part XII: flooding rates and performance data for a rotating disc contactor", Trans. Inst. Chem. Eng., 35, 301-315.
- Reman, G.H, (1952), Proc.3rd world petrol congress, Hague, section III.
- Reman, G.H., and Olney, R.B., (1955), "The rotating-disc contactor- a new toot for liquid-liquid extraction", Chemical Engineering progress, 51, 3, 141-146.
- Sivanadam, S.N., (2003), "Introduction to artificial neural networks", Vikas publishing House Pvt. Ldt.
- Vermijs, H.J., and Kramers, H., (1954), "Liquid-liquid extraction in rotating disc contactor", Chem. Eng. Sci., 3, 55-64.
- Zhang, S.H., NI, X.D. and Su, Y.F., (1981), "Hydrodynamics axial mixing and mass transfer in rotating disc contactors", Can. J. Chem. Eng, 59, 573-583.
- Zhang, X.D., and Su, Y.F., (1985), "A model for liquid-liquid extraction column performance the influence of drop size distribution on extraction efficiency", Can. J. Chem. Eng, 63, 212-226.

IMPLEMENTATION OF A SECURITY SERVICE PROVIDER FOR INTRANETS

Hamid M. Ali **Wameedh N. Flayih**

ABSTRACT

Among the many branches of security, authentication and confidentiality are very important to be provided. This work studies authentication focusing on the authentication systems supported by Windows 2000 family, especially Kerberos. As a result of this study, some unconvincing points are found along with others that are considered as weaknesses, such as being subject to offline dictionary attacks and the lack of perfect forward secrecy. Hence, some protocols (for authentication and key agreement) are chosen to build an authentication system that takes into consideration the observations on Windows 2000 systems. Based on this system, a security service provider is developed. The proposed provider isolates the developer from the complexity of the underlying system.

KEYWORDS

: **security, security service provider, authentication, Kerberos, dictionary attacks, certificates.**

الخلاصة

يعتبر التصديق و الخصوصية من اهم فروع الامن التي يجب توفيرها. يقوم هذا البحث بدراسة التصديق مركزاً على انظمة التصديق المعتمدة في مجموعة انظمة التشغيل Windows 2000، وخصوصاً Kerberos . كنتيجة لهذه الدراسة وجدت بعض النقاط غير المقنعة و بعض مواطن الضعف، كالتعرض لoffline dictionary attacks و عدم توفير perfect forward secrecy . لذلك تم اختيار بعض البروتوكولات (للتصديق و الاتفاق على المفتاح) لبناء نظام تصديق ياخذ بنظر الاعتبار الملاحظات الماخوذة على الانظمة في Windows 2000 . و بالاعتماد على هذا النظام قد طور مزود خدمة امن. هذا المزود المقترح يعزل المطور عن تعقيدات النظام التحتي.

INTRODUCTION

Security is a must in today networks. For this reason, the software developers are facing a challenge in this field, because they must provide security for their applications, especially authentication and confidentiality. This is the role of security service providers (SSPs). They provide security services to the applications isolating them from the details. This leads to the fact that the security provided is dependent on the security protocols used by the SSP.

Passwords are the most common way to authenticate users. But they are considered weak keys; this means they cannot be used directly as encryption keys, because human users cannot remember long random numbers. This introduced the threat of dictionary attacks. An attacker carries ***offline dictionary attacks*** without direct interaction with the server. He eavesdrops and records messages exchanged between an authentic user and the server. These messages are constructed using

functions that take the password as input. Therefore, he applies the same functions on the entries in his dictionary and compares the result with the recorded messages, until they match. To slow down this attack, it is desirable to make the functions relatively slow such that the search operation takes more time, but in such a way not to annoy the users [MOV96]. A possible solution is the use of Diffie-Hellman based algorithms that reveal no information about the password, such as the Authentication via Memorable Passwords (AMP) protocol [Kwo01].

Another type of offline dictionary attacks is that against stored password file. It is common to store verifiers (hashes) of the passwords in a file on the server and not the passwords themselves. This prevents the compromise of passwords in case the file is stolen. But if it is stolen then the attacker can do the same previous procedure, but against the whole list, and not a specific user record. To slow down this attack, the password is salted before being hashed. Each password is attached with a random string (salt) and then hashed, so the hash and the salt are stored for each user.

In the evaluation of a key establishment protocol, the effect of compromise of long term keys should be considered. This is what ***perfect forward secrecy*** describes. *Perfect forward secrecy* is provided by a protocol, if compromise of long term keys does not compromise past session keys [MOV96]. For this reason, it is preferred to be provided by a protocol. All the transport protocols do not provide *perfect forward secrecy*. Also, symmetric techniques cannot provide this feature. The key agreement protocols based on public-key techniques (Diffie-Hellman) achieve this property.

IMPORTANCE OF THE WORK

In this work the authentication systems available in Windows 2000 through the Security Support Provider Interface (SSPI) are studied, taking into consideration the two concepts previously presented: *offline dictionary attacks* and *perfect forward secrecy*. This gives some unconvincing or weak points that must be noticed.

Then a Security Service Provider (SSP) is proposed taking into consideration the noticed points on Windows 2000 authentication, withstanding offline dictionary attacks and providing perfect forward secrecy.

SECURITY SUPPORT PROVIDER INTERFACE (SSPI)

Microsoft has given software developers the ability to develop software that makes use of some cryptographic functions and the authentication systems available in Windows 2000. This can be achieved through the use of Cryptographic Application Programming Interface (CryproAPI) and the Security Support Provider Interface (SSPI).

The CryptoAPI provides the basic cryptographic functions (encryption, hash, and public key signature). So it is suitable if the developer needs little cryptography for his applications, but as the requirements are extended to authentication systems then it is not a good choice.

On the other hand, SSPI provides a mechanism by which a distributed application can call one of several security providers to obtain an authenticated connection without knowledge of the details of the security protocol. This facilitates the way developers build their applications on the security of Windows 2000. A security provider is a Dynamic Link Library (DLL) that implements the SSPI and makes one or more security packages available to applications. A security package maps the SSPI functions to an implementation of the security protocol specific to that package, such as New Technology Local Area Network Manager (NTLM), Kerberos, or Secure Socket Layer (SSL). Security packages are sometimes referred to as Security Support Providers (SSPs) [Mic99a]. The

security strength provided by the SSPI is dependent on the three underlying authentication systems. As a result, a study on the authentication systems available in Windows 2000 is necessary.

WINDOWS 2000 AUTHENTICATION

Windows 2000 supports several protocols for verifying the identities of users, including protocols for authenticating dial-up connections and protocols for authenticating external users who access the network over the Internet. But there are only two choices for network authentication: Kerberos Version 5 and NTLM [Mic99b][TJ01].

SSL provides end-to-end encryption, integrity protection, and server authentication for the Web. It is also provided for applications through the SSPI. It makes use of certificates containing the public keys of the two parties. These certificates should be signed by a trusted Certificate Authority (CA). As a result, the next sections present NTLM, Kerberos, and certificates.

NTLM

The NTLM protocol was the default for network authentication in the Windows NT 4.0 operating system. It is retained in Windows 2000 for compatibility with down level clients and servers. NTLM is also used to authenticate logons to standalone (not domain members) computers with Windows 2000. It provides unilateral authentication. NTLM authentication was designed for a network environment in which servers were assumed to be genuine [Mic99b]. For this reason Kerberos v5 was used as the default system in Windows 2000.

Kerberos

Kerberos was developed at Massachusetts Institute of Technology (MIT) as a part of Project Athena in 1988 [MNS+87]. Symmetric cryptography and a trusted third-party are the basis of this authentication system. It is considered an authentication and key transport protocol. There have been two versions of the protocol in public use, namely Kerberos v4 and v5. The latter was chosen by Microsoft to be the default authentication system in Windows 2000 family [Mic99b]. The following points are noticed:

- It is subject to the offline dictionary attack [Wu99][KT03][BM91]. Since the client A sends the timestamp encrypted using the password hash, and the Authentication Server (AS) sends in the second message the timestamp encrypted using the A's password hash. This means that an eavesdropper which captures these messages can try to decrypt them using a dictionary of common passwords.

- The AS does not store a clear-text copy of the passwords. Instead, the password is encrypted using RSA MD4 algorithm, which takes a variable-length password and encrypts it using a secret key to produce a fixed-length result called the *message digest*. The result is the hash of the password using a secret key. Domestic versions of Windows 2000 use a 128-bit message digest, considered unbreakable by anyone but the National Security Administration (NSA), and only then with a great deal of expensive supercomputer time. Export versions of Windows 2000 are limited to a 40-bit message digest, considered easily crackable [Bos00].

- The Kerberos protocol does not provide *perfect forward secrecy*. This means that if long term secret of the client (password) is compromised then all session keys used by the client are compromised. This introduces a security risk, but depending on the requirements of the system it may be serious or not.

- The session key is controlled by the AS; this means that not only the two involved parties know the secret key, but the AS too. It is preferable that the secret be known to only the involved parties.

- An overhead introduced is that the client A needs to get a different ticket for each different service (application server). This requires from the client to contact the AS to get a new ticket. This also means an overhead in the storage of secret keys. A needs to store K_{AB}, K_{AC}, and K_{AD}, which represent the keys corresponding to tickets used to contact B, C, and D.

- In Windows 2000, Kerberos is the authentication system, but NTLM is used to authenticate previous versions of Windows. So, this weakens the security, because it is not totally based on Kerberos. To prevent this, all clients must be upgraded to Windows 2000, and then NTLM should be prevented.

CERTIFICATES

A certificate is a digital document (i.e. a formatted file) that binds a public key to its owner. A trusted Certificate Authority (CA) creates the certificate and digitally signs it using the CA private key. Using the CA public key, applications verify the issuing CA digital signature, and hence, the integrity of the contents of the certificate (most importantly, the public key and the identity of the owner).

Microsoft Certificate Services, included with Windows 2000 server family, provide a means for an enterprise to easily establish CAs. Windows 2000 supports the installation of stand-alone CAs or enterprise CAs.

Stand-alone certification authority does not require the use of Active Directory. By default, all certificate requests sent to the stand-alone CA are set to *pending* until the administrator of the stand-alone CA verifies the identity of the requester and Okays the request. This means there is no automated procedure in certificate granting.

Enterprise certification authority requires the use of Active Directory, which means there is a need to implement a domain. Here the requests are automatically serviced, and according to the user information in Active Directory, the certificate is issued or not [Mic00][TJ01].

The following points are noticed:

- In Windows 2000, the case of stand-alone CA is not practical because it puts the decision on the administrator. For this reason, the enterprise CA is considered the best choice. But this type will depend on the user information in the Active Directory. This means that when a user requests a certificate, then he is authenticated to the CA using the network authentication system available, which may be NTLM or Kerberos [Mic00][TJ01].

- Certificate Revocation List (CRL) may add overhead in the communication and management, and the need to protect the list from unauthorized change.

- Another very important point is that the certificate contains the public key, but the private key must be kept secret to the owner. So, in case the owner is a PC, there is no problem. But if the owner is a user, who needs to get access from different PCs, then he needs to store the private key on each PC, which is a security problem.

- Windows 2000 stores the private keys of users using the Cryptographic Service Providers (CSPs). This means the keys are stored in the PC at which the user requested the certificate.

So, for PCs that has several users, the CSP stores the keys according to the identity of the user. Each user is given access to keys corresponding to his identity. This makes us conclude that CSPs depend on the (username, password) pair to protect the keys. This gives (in theory) the attacker a chance to launch dictionary attack against the stored keys, assuming the attacker has access to the location where the keys are secured and knows how they are secured. In other words, dictionary attacks are possible if the only thing missing is the password. This may compose a serious threat because the keys of certificates are kept for long time, which gives the attacker the required time.

PROPOSED AUTHENTICATION SYSTEM

The proposed system will be based on a central authentication server (AS) hosting the clients' information. The system can be viewed to have two different participants: the authentication server (AS) and the clients (including application servers). Each client should contact the AS to authenticate itself, and the AS will grant it a ticket (certificate) that proves the client's identity, and binds it to the public key in the ticket. When a client wants to contact another client (usually an application server), the tickets are exchanged and the two parties agree on a session key. Some important objectives are that the system should be secure against offline dictionary attacks and stolen verifier file, and should provide perfect forward secrecy.

The authentication protocol used when the client contacts the AS is based on the AMP protocol. This will achieve security against dictionary attacks and stolen verifier file. The handshake protocol between two parties is based on Diffie-Hellman, providing perfect forward secrecy. RSA is used for digitally sign the tickets. Advanced Encryption Standard (AES) encryption is used as the symmetrical encryption algorithm. SHA-1 is the hash algorithm used. The ticket lifetime should be in hours or minutes.

SYSTEM PROTOCOLS

The details of the authentication protocol and ticket renewal protocol are presented next. Some important parameters used in the protocols are:

(Any arithmetic operation not specifying the modulus, means 'mod p')

- π: password
- hw: hardware id of the PC (for example: LAN card physical address or hard disk serial number).
- v= h(userid, π)
- V: password verifier = g^v
- x , g^x: private/public key pair of the PC.
- y , g^y: private/public key pair of the AS.
- V_{AS}: digital signature verification key of the AS.
- p , q: large prime numbers; as in AMP protocol.

The AS stores PC information (pcid, g^x, g^{hw}). It also stores the password verifiers in a file; each record is encrypted symmetrically using a secret key ***S*** and a salt $\boldsymbol{\tau}$. So, each record in the file is of the form :(userid, τ, $E_{S+\tau}(V)$). This makes the file secure against offline dictionary attacks when stolen.

A. AUTHENTICATION PROTOCOL

Fig. 1 shows the authentication protocol, assuming the user and PC are registered on the AS. The client A will be authenticated through H_1, while the AS will be authenticated to the client through G_3. At the end of the protocol the AS sends its digital signature verification key (V_{AS})

and its public exponential (g^y). Other values are also sent, such as the session duration and the session parameters (α and *n*). The public exponential will be used by clients later to communicate with the AS. g^{x1} will be used as the public key in the ticket.

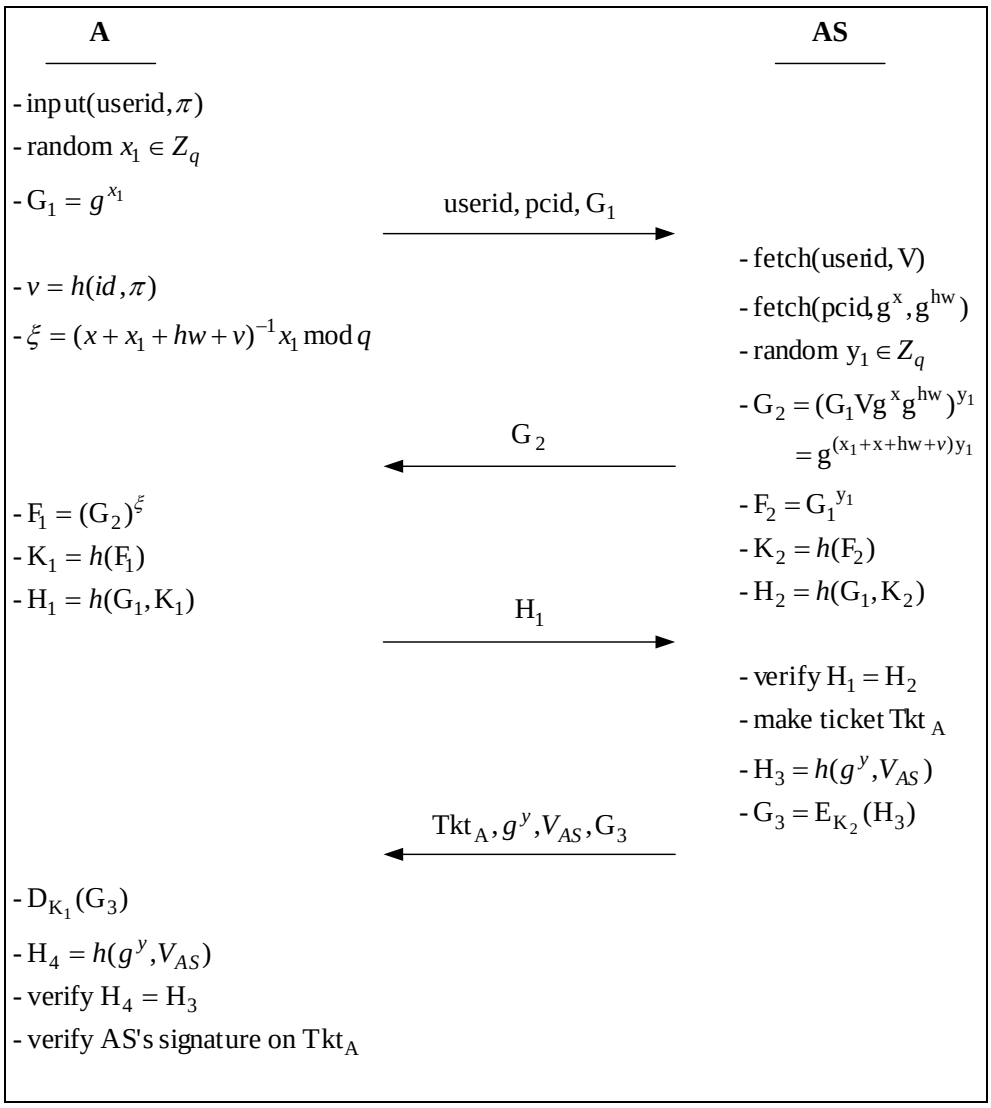

Fig. 1: Authentication Protocol

B. KEY AGREEMENT PROTOCOL

After the clients have been granted the tickets at the authentication phase, they can now communicate with each other. To communicate securely they must agree on a session key. The public exponentials included in the tickets are used to carry out a Diffie-Hellman key agreement. So, each client verifies the signature of the AS on the ticket of the other, and its validity. The details are shown in Fig. 2.

When A receives G_3 in step 2 it decrypts it using K_1 and checks α^{a1}, if it is correct then A is sure that the other party is really B. At step 3 A sends the hash of B's exponential (G_2). B checks it, and if it is correct then it is sure of the identity of A, because A is the only one that knows K_1 and so can decrypt G_3.

It is known that Diffie-Hellman states that: knowing the public exponentials only; it is hard to find the key α^{a1b1}. But here the case is more difficult, because α^{b1} is not public. It is encrypted

using K_1. Hence, the attacker must solve two such problems: one to find K_1 and then to find the session key K_2. For this reason the size of the number (n) can be reduced, this can improve the performance. So, 768 bits can be used in stead of 1024 bits used for (p).

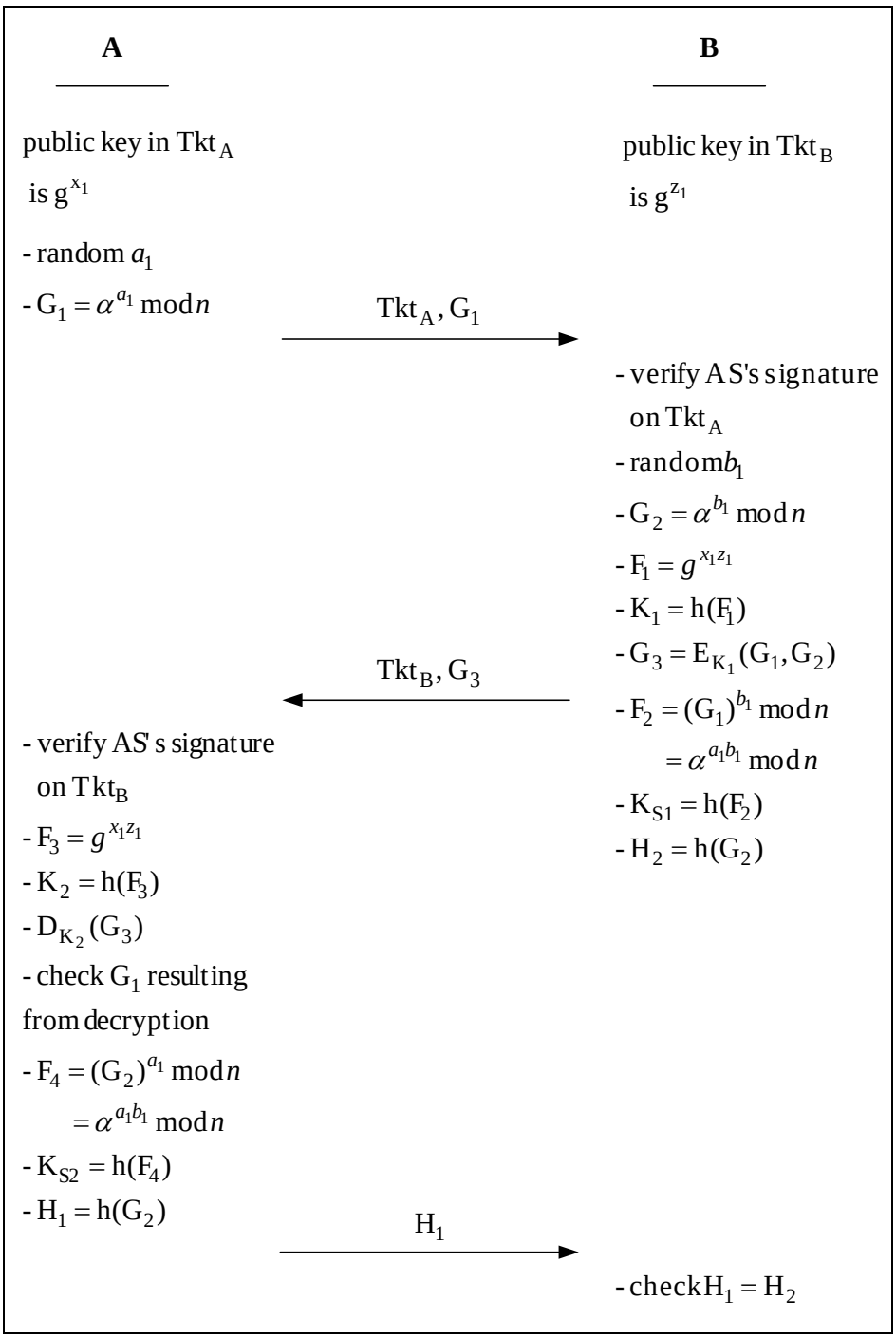

Fig. 2: Key Agreement Protocol

System Architecture

The system may be viewed to be composed of two parts: the Authentication Server (AS) and the Client's Security Service Provider (CSSP) as shown in Figure 3. The blocks representing the applications have discontinuous lines. This is to indicate that they are not part of the system, but the system will be used to provide services to these applications.

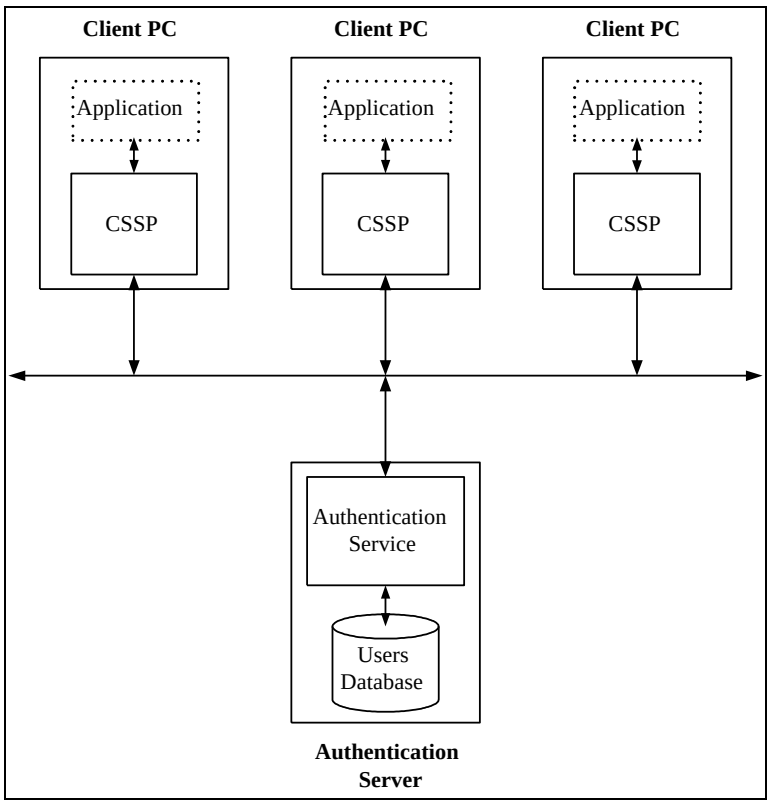

Fig. 3: System Components

A. Authentication Server Architecture

It is the part of the system hosting the tables containing information about the users, PCs, groups, and tickets granted. The AS is responsible for the authentication of clients, granting tickets, renewal of tickets, and consequently the administration of the system occurs here. The architecture is shown in Fig. 4.

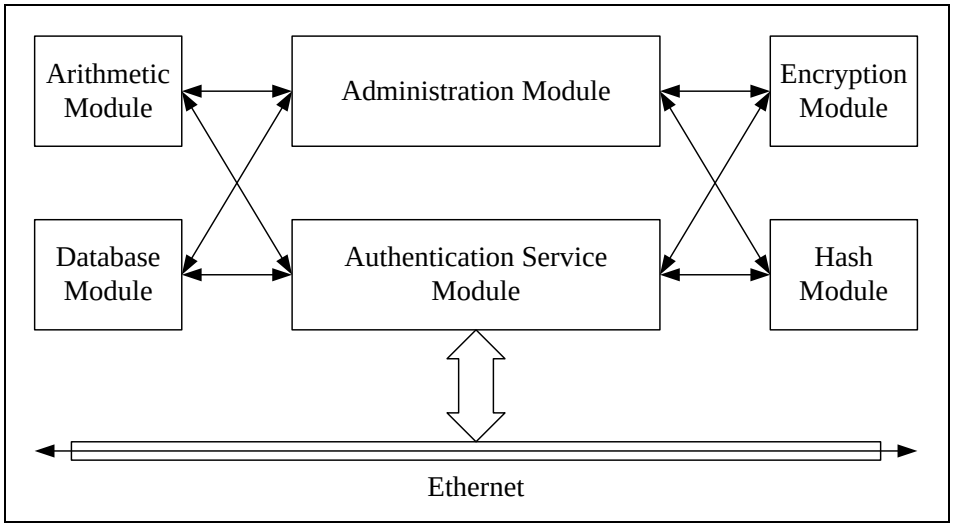

Fig. 4: The AS Architecture

B. Client's Security Service Provider

It represents the part of the system residing at the client PCs. It is considered as a gateway for the application built over it. Through it the application connects to the AS and to other instances of the applications on other PCs. The CSSP is not involved in the details of the information sent

between the applications. It just provides the secure communication channel between them. The CSSP is involved in the authentication, key agreement, and ticket renewal protocols. These protocols require several functionalities, and according to them the architecture of the CSSP will be build, as shown in Fig. 5.

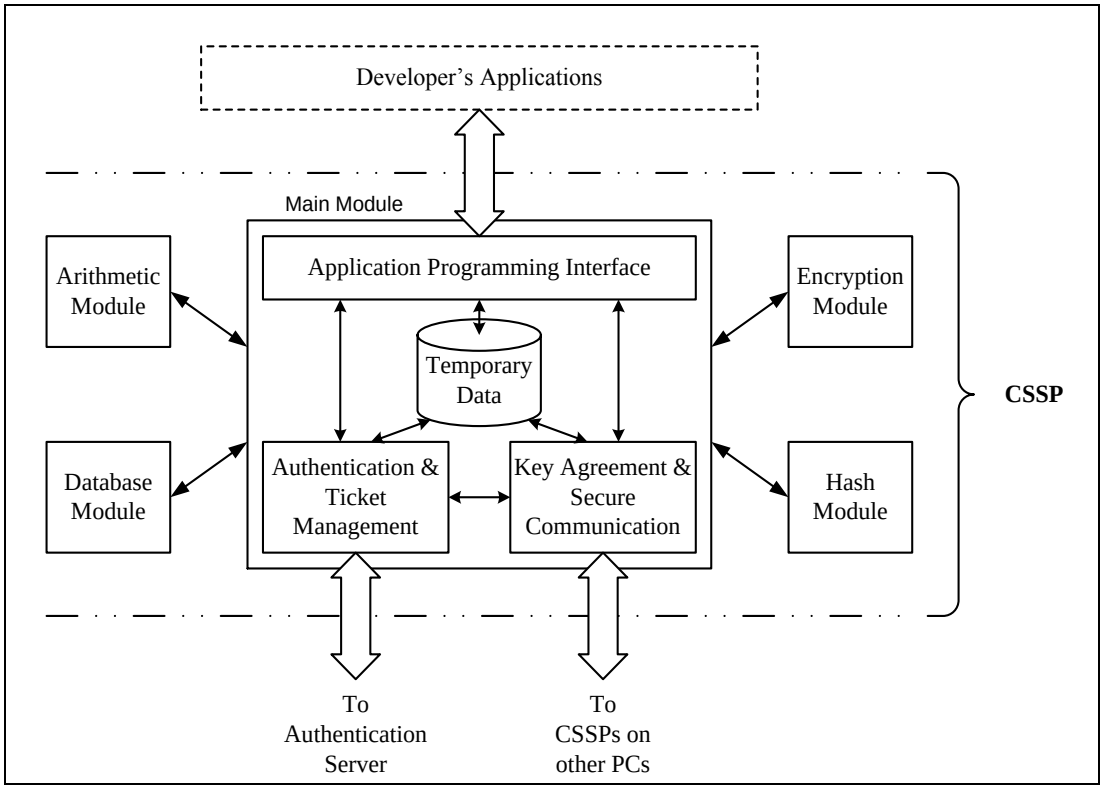

Fig. 5: CSSP Architecture

1. ***Application Programming Interface (API):*** it is the set of functions that the developer must deal with to link his application with the system. This part isolates the details of the system, providing the developer simple functions to interact with.
2. ***Authentication and Ticket Management:*** it includes the authentication protocol and ticket renewal protocol. This part communicates with the AS. So, it contains functions that provide network connectivity to the AS.
3. ***Key Agreement and Secure Communication:*** it communicates with other CSSPs (specifically with the Key Agreement and Secure Communication part). This part includes the key agreement protocol and provides the secure transfer of data between applications.

The steps carried out to establish a secure communication channel between two applications App_{1A} and App_{1B} are clarified through Fig. 6. App_{1B} acts as an application server that listens for client requests, and App_{1A} acts as a client to this application server.

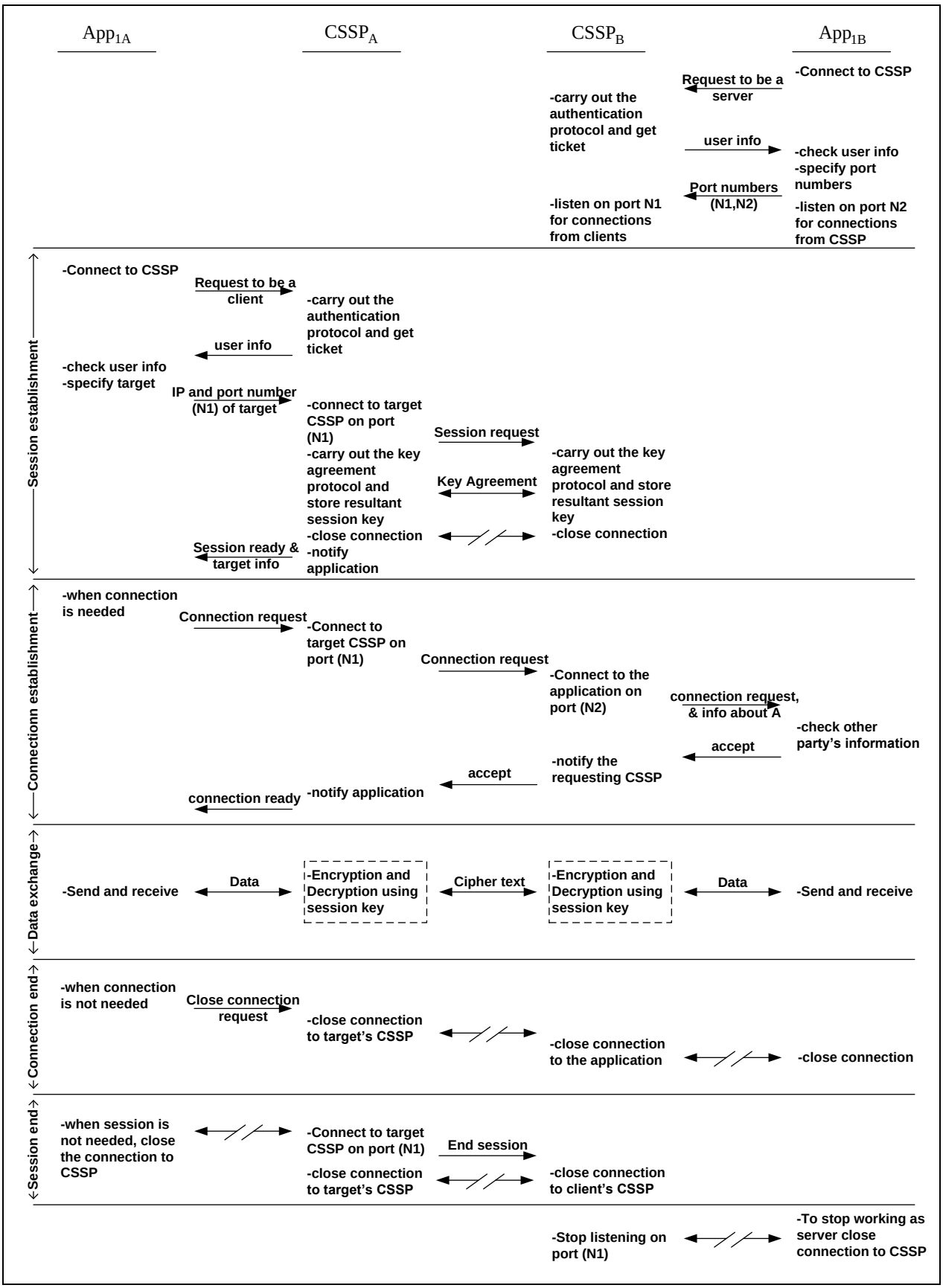

Fig. 6: CSSP Operation

IMPLEMENTATION AND PERFORMANCE

Visual C++ was the programming language used. Each module is a separate library (DLL) of functions. However, the parts of the main module of the CSSP are all integrated in one library (one DLL). The separation of the modules allows the modification of each module without affecting the others. The RSA operations are implemented using the CryptoAPI library. The connections between the applications and the CSSP will be using sockets programming (based on the *CAsyncSocket* class). The system works on Windows 2000 family and next versions. It is preferred to use NT File System (NTFS) to give access control to the files.

The system was tested on Pentium III with Windows 2000 Server operating system and 100 Mbps Fast Ethernet PCI Adapter. The authentication protocol starts and ends at the client side. Its average time has been found to be (**131.2 msecs**). This protocol starts at the CSSP acting as client, and ends at the other side (CSSP acting as server). Thus, the time will be taken for each side apart (i.e. the time each side participates in the protocol). The average time for the client side was (**91.6 msecs**) while for the server side was (**78.5 msecs**). Also, the effect of the protocols on the processor and network traffic was monitored using Windows 2000 Performance Monitor, and there was no high load.

CONCLUSIONS AND FUTURE WORK

The most important point is that Kerberos is subject to *offline dictionary attacks* and it does not provide *perfect forward secrecy* which may be considered important points, in addition to other notes. Also, it was shown that SSL supported by the SSPI depends on certificates, which are granted to clients through the network authentication system (Kerberos). This means that they suffer from the same weaknesses. This means that the SSPI provides a good level of security through Kerberos and SSL if their weaknesses are not considered serious. The seriousness of the weaknesses depends on the network environment in which the system is implemented.

In case the level of security provided by the SSPI is not considered enough, then the proposed protocols presented in section 5.1 solve the unconvincing points and weaknesses in Kerberos. This was done using the AMP authentication protocol and the Diffie-Hellamn key exchange. But this gave some disadvantages, because the proposed authentication system is slower than Kerberos because the latter is based on symmetric encryption techniques, while the AMP protocol is based on public key. Also, it adds overhead as compared to SSL, because the proposed system requires online trusted third part, while SSL requires offline trusted third party.

A very important point to be stated is that the proposed provider was implemented above the transport layer. This provides implementation flexibility and ensures that only the applications needing security use the system. But a disadvantage is that these applications must be modified (i.e. transparency is not provided). Transparency is provided if the security layer is implemented at the lower layers, network or data link layers, but at the cost of additional overhead and implementation complexity. The overhead results because not all the applications require the provided security.

A suggestion for the future is to extend the design to provide cross domain trust, such that a client under the control of AS1 can contact another client under the control of AS2 in case there is a trust relationship between AS1 and AS2. Also, it is possible to integrate the system with the SSPI, taking the advantages and disadvantages into consideration.

REFERENCES

[BM91] S. M. Bellovin and M. Merritt, *"Limitations of the Kerberos Authentication System"*, Proceedings of the Winter 1991 Usenix Conference, pp. 253-267, Dallas, January, 1991.

[Bos00] W. Boswell, *"Inside Windows 2000 Server"*, New Riders, 2000.

[KT03] K. Kasslin and A. Tikkanen, *"Attacks on Kerberos V in a Windows 2000 Environment"*, Research project for Helsinki University of Technology, 2003.

[Kwo01] T. Kwon, "*Authentication and key agreement via memorable passwords"*, Proceedings Network and Distributed System Security Symposium, San Diego, California, February 7-9, 2001.

[MOV96] A. Menezes, P. van Oorschot, and S. Vanstone, *"Handbook of Applied Cryptography"*, CRC Press, 1996.

[Mic99a] Microsoft Corporation, *"The Security Support Provider Interface"*, Windows 2000 White Paper, March, 1999.

[Mic99b] Microsoft Corporation, *"Windows 2000 Kerberos Authentication"*, Windows 2000 White Paper, 1999.

[Mic00] Microsoft Corporation, *"Windows 2000 Certificate Services"*, Windows 2000 White Paper, 2000.

[MNS+87] S. Miller, C. Neuman, J. Schiller, and J. Saltzer, *"Kerberos Authentication and Authorization System"*, M.I.T. Project Athena, Cambridge, Massachusetts, December 21, 1987.

[TJ01] C. Todd and N. L. Johnson, *"Hack Proofing Windows 2000 Server"*, Syngress Publishing, 2001.

[Wu99] T. Wu, *"A Real-World Analysis of Kerberos Password Security"*, Proceedings of the 1999 Internet Society Network and Distributed System Security Symposium, San Diego, CA, February, 1999.

ABREVIATIONS

AES	Advanced Encryption Standard
AMP	Authentication via Memorable Passwords
API	Application Programming Interface
AS	Authentication Server
CA	Certificate Authority
CRL	Certificate Revocation List
CryptoAPI	Cryptographic Application Programming Interface
CSP	Cryptographic Service Provider
CSSP	Client's Security Service Provider
DLL	Dynamic Link Library
MIT	Massachusetts Institute of Technology
NSA	National Security Administration

NT	New Technology
NTFS	NT File System
NTLM	New Technology Local Area Network Manager
SSL	Secure Socket Layer
SSP	Security Service Provider
SSPI	Security Support Provider Interface

DESIGN AND SIMULATION OF POWER FACTOR CORRECTION FOR AC/DC CONVERETER

Amina Mahmoud Shaker . Ass. Prof. Dr. Ali M. Salih Prof. Dr Kais S. Ismail

Al Nahrin University Baghdad University

ABSTRACT

One of the biggest problems in power quality aspects is the harmonic contents in the electrical system. Most of the current harmonics are due to the nonlinear operation of the power converters and arc furnaces . These harmonics cause overheating of the magnetic cores of transformers and motors beside their effect on the torque –speed of the later . These problems have lead to the creation of design standards for purpose of limiting the allowable harmonics on the power lines, and hence to improve the power factor.

This paper presents two types of power factor correction (PFC) for single phase AC/DC converter, the Boost converter and the Buck- Boost converter. The output of the Boost converter is fixed (400V , 3kW) while the output of the Buck – Boost converter is variable (150-400V, 3kW-1kW) and due to the discontinuous inductor current mode operation of the Buck mode of the Buck- Boost converter an average charge current control is used in the inner current loop control. From harmonic analysis the two types of converters has less harmonics as compared with the IEC1000-3-2 standards. The Buck Boost converter eliminates the problem of high inrush input current produced by the Boost converter type.

الخلاصة

ان واحدة من اهم المشاكل الموجودة في المنظومات الكهربائية هي توافقيات التيار (Current Harmonics) وان اكثر هذه التوافقيات هي نتيجة عمل مغيرات القدرة اللاخطية (Non –Linear Operation of Converters) . وافران الشرارة

تولد هذهالتوافقيات حرارة فائقة في القلب المغناطيسي للمحولات بالاضافة الى تأثيرها على خواص العزم _ السرعة (Torque _ Speed) للمحركات و هذه المشاكل أدت الى أيجاد حدود قياسية لتحديد هذه التوافقيات في المنظومات الكهربائية وبالتالي تحسين عامل القدرة.

هي احدى مصادر هذه التوافقيات غير (Single Phase Buck – Boost Converter) ان مغيرات المرغوب فيها وهي تستخدم في بعض التطبيقات التي تحتاج الى خرج متغير(Variable Output).

و فولتية الخرج (230V- 85)للفولتية ذو طور واحد بأدخال عام (Buck- Boost Converter)لقد تم اقتراح (Outer ويتم التحكم بفولتية الخرج بأستخدام حلقتين، حلقة الفولتية الخارجية (150- 400V)متغيرة من Voltage Loop) و حلقة التيار الداخلية (Inner Current Loop) بحيث يكون تيار الدخل وفولتية الدخل في طور واحد.

وعندما يعمل المغير كخافض للفولتية فأن التيار الداخل يكون متقطع لذا تم اقتراح طريقة تحسس معدل الشحنة في حلقة التيار الداخلية(Charge Average Current Sensing) ولقد تم ايجاد طريقة للتعديل في حلقة التيار . عندما تكون فولتية الخرج للمغير متغيرة.(Gain)الداخلية لتغيير الكسب

بأستخدام طريقة الكشف عن قمة فولتية الدخل (Inrush Current)كما تم اقتراح دائرة لتحديد تيار البدء (Peak Input Voltage Detection).

تم احتساب توافقيات الدائرة المقترحة ووجد بأنها اقل بالمقارنة مع المواصفات القياسية كما ان كفاءة الدائرة اعلى في حالة الدخل العالي من الدخل الواطي.

KEY WORDS

Boost converter, Buck – Boost converter, Power Factor Correction (PFC), current harmonics.

INTRODUCTION

Most modern electronic apparatus use some form of AC to DC power conversion within their architecture , and they draw pulses of current from the AC network during each half cycle of the supply waveform. The amount of reactive power drawn by a single apparatus may be small , but within a typical large number of these apparatus the amount of reactive power is large and hence the amount of current harmonics are also high.

The effect of power factor and harmonics generated by equipment that can be connected to the public mains network is a matter of concern today. These harmonics must be filtered and this has led to the creation of EN 61000-3-2 standards which is adapted by the European Community [1].

Boost , Buck – Boost converter is one type of AC/DC converter which is either for step up or step up- step down respectively. Many researchers have investigated in the field of power factor correction of AC/DC converter , a three phase Buck –Boost converter is presented in [2], the converter with an additional current loop and a circuit switches which switches between Buck and Boost stages using two transistors while a single phase Buck –Boost

converter with two current feedback loop is presented in [3] and [4] , the model used two transistors signal to generate the pulse width modulation (PWM) of the Buck – Boost switches . A single phase Buck – Boost with variable output is presented in [5]. A current programmed control for cascade two switches Buck- Boost converter is presented in [6]and its provided a variable output . A computer model for common switch mode control with average and conventional cycle by cycle switching operation mode for Buck – Boost is presented in [7]. A two switch Boost interleaved Buck- Boost converter is presented in [8] and it has the capability of producing both step-up and step down conversion with lower switches voltage stress.

POWER CIRCUIT DESIGN

This work presents a Boost converter with fixed output (400 V , 3kW) and a power factor preregulator (UC3854) is used in order to improve the power factor (as shown in figure 1) in such a way that the input current is forced to follow the sinusoidal input voltage . Two loops are used to control the output voltage and the input current , the outer voltage loop and the inner voltage loop [9].

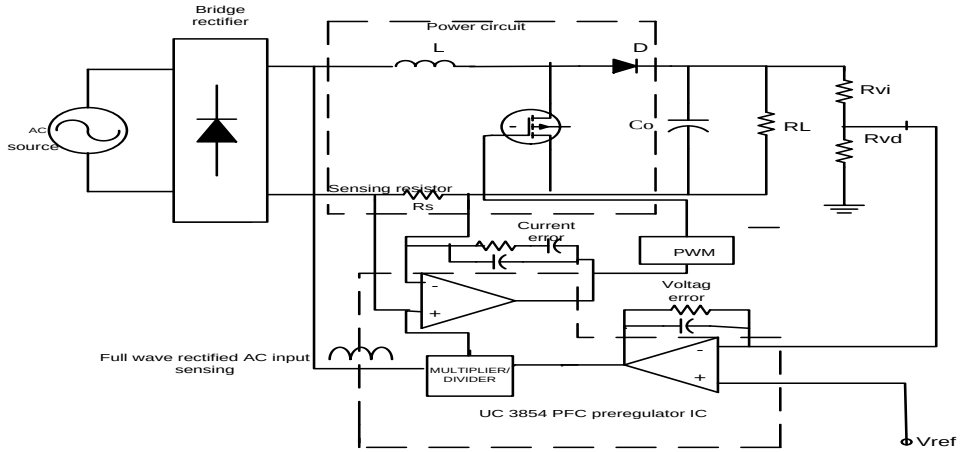

Fig(1) Power factor correction for Boost converter AC/DC Converter(UC3854)

The second converter is the Buck – Boost converter shown in figure 2 , the converter is either operate in boost mode in such away that the output voltage is higher than the maximum input voltage or in Buck Boost mode where the output voltage is lower than the maximum input voltage. Figure 3 shows the two operation mode of the Buck Boost converter .

The output inductor employed in the converter provides the energy storage and filtering . The current flowing through it has a triangular waveform . In selecting the inductance a compromise has to be found between high rating required for diminishing the ripple , and a low rating required for quick response to load changes.
The peak inductor current is the sum of the peak line current and half of the peak to peak high frequency ripple current. The inductor must be designed to handle this current level.

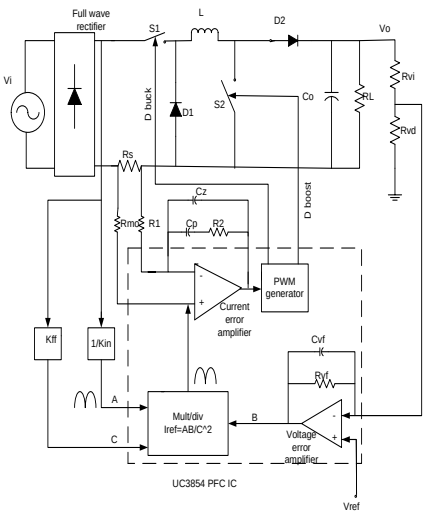

Fig (2) Power factor correction for Buck Boost Converter

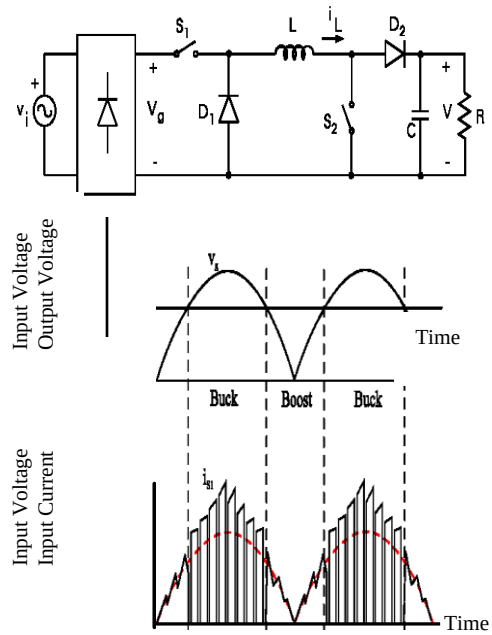

(Fig) The Buck Boost converter operation modes

- **BOOST CONVERTER INDUCTOR DESIGN:**

The Boost converter inductor is decided according to the minimum rms input voltage then

$$I_{peak} = \frac{\sqrt{2}P_{in}}{V_{i\,rms}} \qquad (1)$$

where I_{PEAK} is the maximum input current, P_{in} is the input power to the converter and $V_{i,,rms}$ is the root mean square of the input voltage.

Since in steady state the time integral of the inductor voltage over one time periods must be zero [10] , therefore

$$v_i t_{ON} + (v_i - V_o)t_{OFF} = 0 \qquad (2)$$

where v_i is the instantaneous value of the input voltage , t_{ON} is the on time of the switch , V_o is the output voltage of the converter and t_{OFF} is the off time of the switch.

Dividing both sides by T_s Where T_s is the switching frequency and rearranging terms yield

$$\frac{V_o}{v_i} = \frac{1}{1-d} \qquad (3)$$

where d is the duty cycle of the ON time of the boost switch.

During the ON period

$$V_L = L\frac{di_l}{dt} \quad (4)$$

where di_l is the inductor ripple current

$$dt = dT_S = (1-\frac{v_i}{V_o})T_S \quad (5)$$

then

$$L \geq \frac{V_{i,\max}T_S}{di_L}(1-\frac{V_{i,\max}}{V_o}) \quad (6)$$

- **BUCK- BOOST INDUCTOR DESIGN:**

The value of inductance is decided depending on the worst operating condition , i.e, when the ripple is X% and it is in continuous conduction during buck mode operation [5] . This occurs when the input voltage is at its maximum peak value and the output is at its minimum value then the peak input current is given by

$$I_{peak} = \frac{\sqrt{2}P_{in}}{V_{i,rms}(\max)} \quad (7)$$

$$\Delta i_L = \frac{X}{100}I_{peak} \quad (8)$$

where Δi_L is the peak to peak ripple of inductor current .

When the converter operates at buck mode , as the Buck switch is ON then,

$$V_L = v_i - V_o = L\frac{di_L}{dt} \quad (9)$$

$$dt = d_1 T_S$$

where d_1 is the duty cycle of the Buck switch , and as

$$d_{1\min} = \frac{V_2}{V_{i\max}} \quad (10)$$

then

$$L \geq \frac{V_o T_S}{\Delta i_L}(1-\frac{V_o}{V_{i\max}}) \quad (11)$$

- **OUTPUT CAPACITOR:**

The output capacitance selection depends on the following factors[10],[11]

- The switching frequency .
- The ripple current.
- The second harmonic ripple current.
- The output ripple.
- The output d.c. voltage .
- The hold up time of the capacitor.

It should be noted that for a given capacitance the capacitor value is proportional to the voltage rating and the maximum energy storage capability which is proportional to the square of the voltage rating. According to the above factors the capacitor with a certain hold up time is given by [10],[11]

$$C_O = \frac{2P_{out}t_{HOLD\,UP}}{V_o^{\,2} - V_{o\min}^{\,2}} \qquad (12)$$

where $t_{HOLD\ UP}$ is the time hold up by the capacitor and it is in the range of 16 to 50 ms[1].

BUCK BOOST CONVERTER CONTROL CIRCUIT :

Active PFC performs much better and is significantly smaller and lighter than the passive PFC circuit. The active PFC can be implemented with a single chip controller, making the circuit relatively simple with minimum number of components .

One of the most popular chip is the Unitrode UC3854 controller which accepts an ac input voltage of 75-275 rms voltage and a frequency of 50 – 400 Hz [9] .

The circuit has two control loop one of them is the fast acting internal current loop . It defines the input current shape to be sinusoidal and force it to be in phase with the input voltage .The second loop is the external voltage loop which regulates the output dc voltage.

The principle of operation of Boost PFC is as follows: The rectified sinusoidal input voltage is fed to a multiplier circuit , providing a current reference to the multiplier and a feed forward signal proportional to the rms value of the line voltage .The filtered DC voltage of Boost PFC is compared to a reference voltage V_{ref} and amplified. The error amplifier sense the variation between the output voltage and the fixed dc reference voltage. The error signal is applied to the multiplier .The multiplier output follows the shape of the input ac voltage. This signal is compared to the current signal sensed by R_s in a Pulse Width Modulation (PWM) circuit. The inductor current waveform follows the shape of the rectified ac line voltage. The gate drive signal controls the inductor current amplitude and maintains a constant output voltage.

A charge control scheme is adopted in this design of the current loop control of the Buck Boost converter since the input current to the converter is discontinuous and its one form of average current control [12-14].Charge control uses a reset integrator to control the average value of a pulsating circuit variable. Figure 4 show the input current for the two cases .

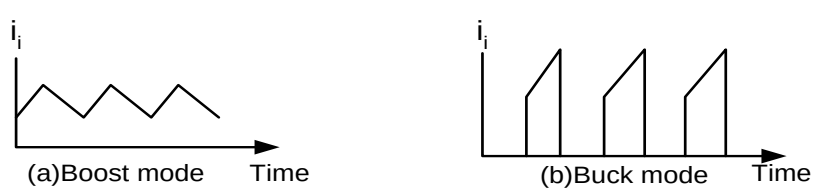

Fig(4) Input current for Boost and Buck mode

Figure 5 illustrates the circuit used in charge average current control used to sense the current in the PFC of the Buck- Boost converter. The i_{S1}/K is hall current sensor which is proportional to the instantaneous input current. Two capacitors C_1 and C_2 are used for integrating the input current alternatively . Transistor T_1 and T_2 employed to quickly discharge the capacitors. The four diode bridge Da-Dd allows i_{S1}/K to charge the capacitor with lower V_x to pick up the higher capacitor voltage which represents the average input current .

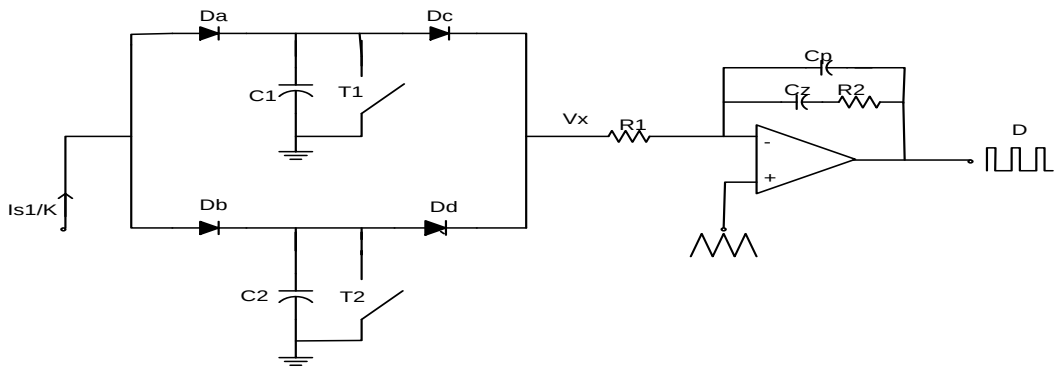

Fig(5) Charge average current sensing used in buck boost converter

SIMULATION RESULTS:

Using the package Orcad 10 **t**he simulation results for the Boost converter given in figure 6 is shown in figure 7(a, b, and c) when the input voltage is 230 V rms , line frequency 50 Hz , output voltage 400 V output power 3kW and the switching frequency is 20kHz . Figure 7 shows the input voltage input current , duty cycle of the boost switch , the output voltage and the input current harmonics. The input current at the first half cycle is 20-25 times the current of the converter. This problem is solved by using the Buck Boost converter shown in figure 8. Figures 9 ,10 and 11 show the input voltage , input current output voltage duty cycle of the buck and boost switch and input current harmonics when the output voltage of the converter is 400V ,250V and 150 V respectively.

The input current harmonics for these cases is shown in figure 12 and it shows that the current harmonics is lower than the EIC standards .

The problem of discontinuous input current in Buck mode operation is solved using average charge current control .

CONCLUSIONS :

A power factor correction control for AC/ DC Boost converter is presented and the input current harmonics is eliminated and it is lower than the standards ,the output voltage and output power is fixed in this type of converters .

The problem of high inrush input current is solved by using Buck Boost converter and also the output voltage and output power can be made variable in this type of converters

Since the input current in Buck mode of Buck Boost converter is discontinuous , a charge average current control is used to provide the error signal for the inner loop current amplifier. Also the input current harmonics is lower than the standard harmonics current and hence the power factor is within the range 0.993-0.998.

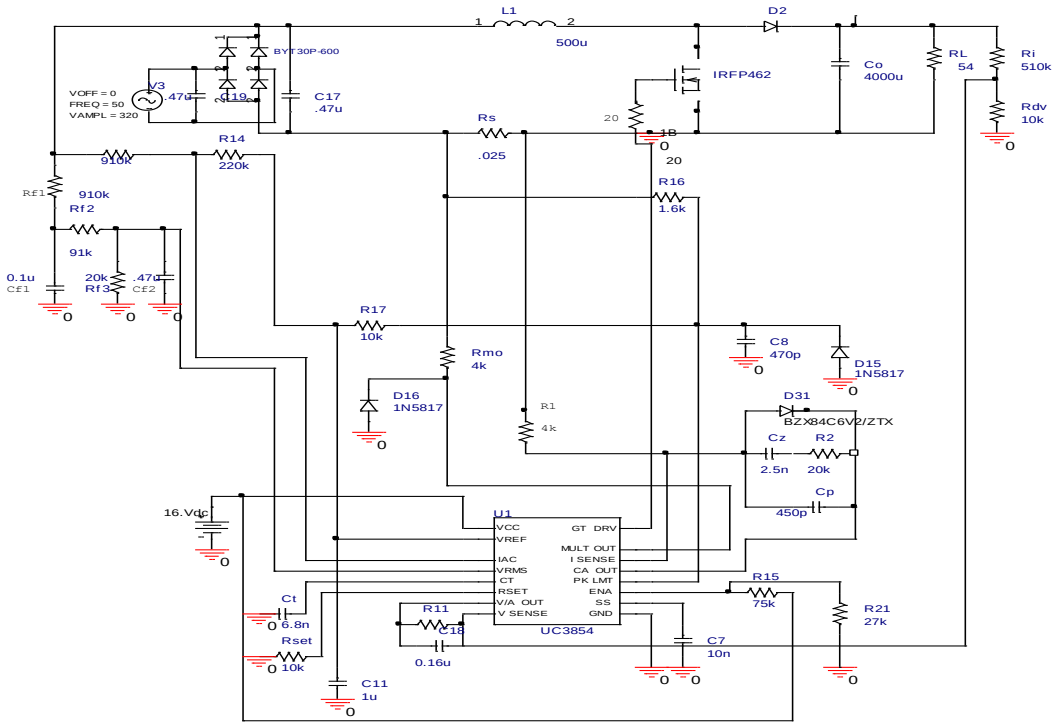

Fig(6) Single phase PFC boost converter schematic(UC3854)

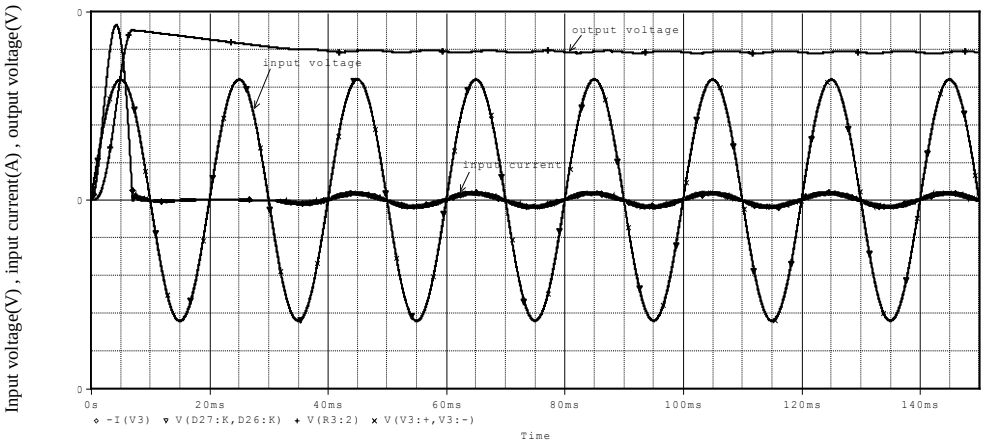

Fig(7)(a) Boost converter input voltage , input current and output voltage Vi=230Vrms,Vo=400V ,Po=3000W , f_S=20kHz

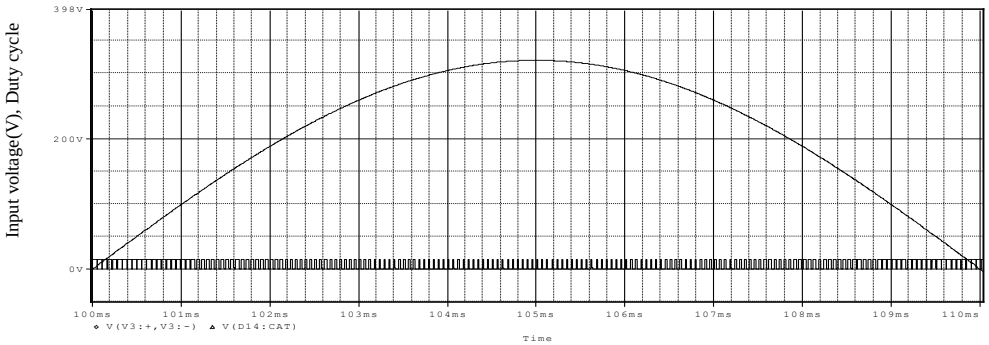

Fig 7(b)Duty cycle of Boost converter
Vi=230Vrms,Vo=400V Po=3000W , f_S=20kHz

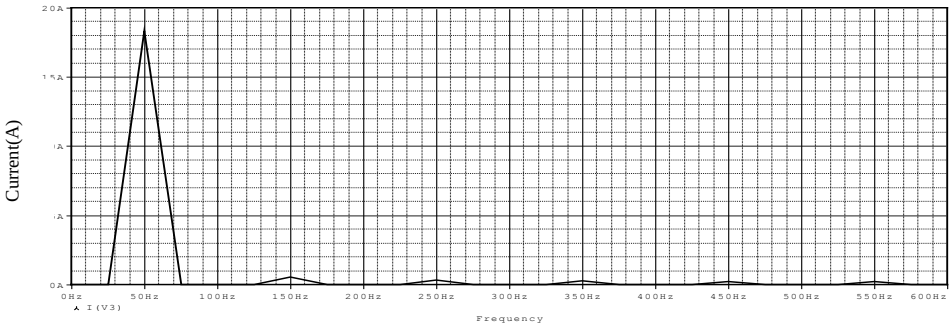

Fig7(c)Input current harmonics for Boost converter
Vi=230Vrms,Vo=400V Po=3000W , f_S=20kH

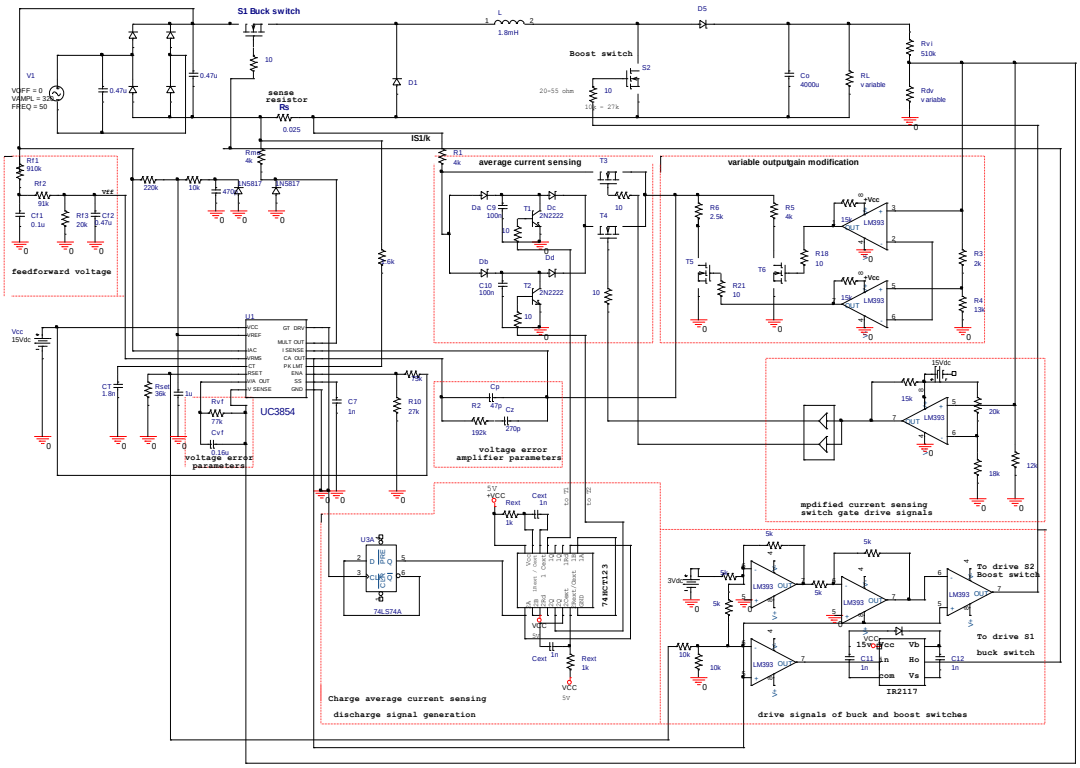

Fig8(a) The connection diagram for PFC single phase Buck Boost converter

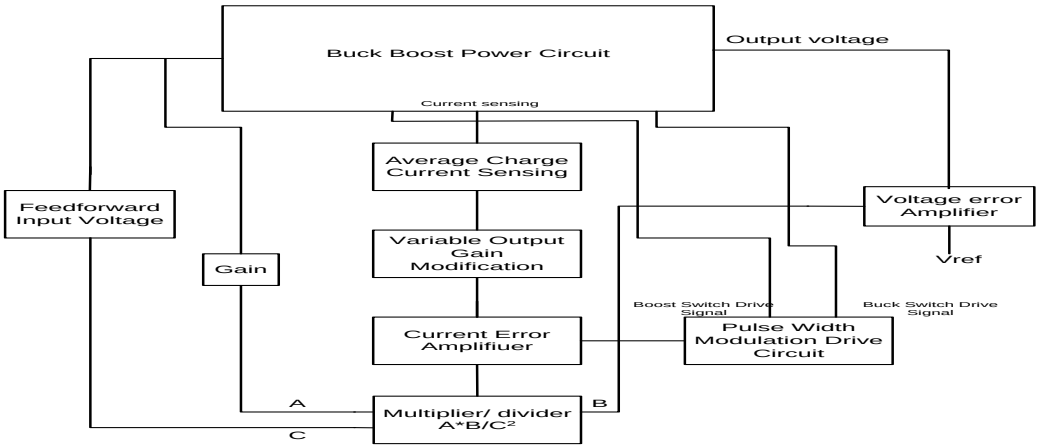

Fig8(b) Buck Boost Converter block diagram

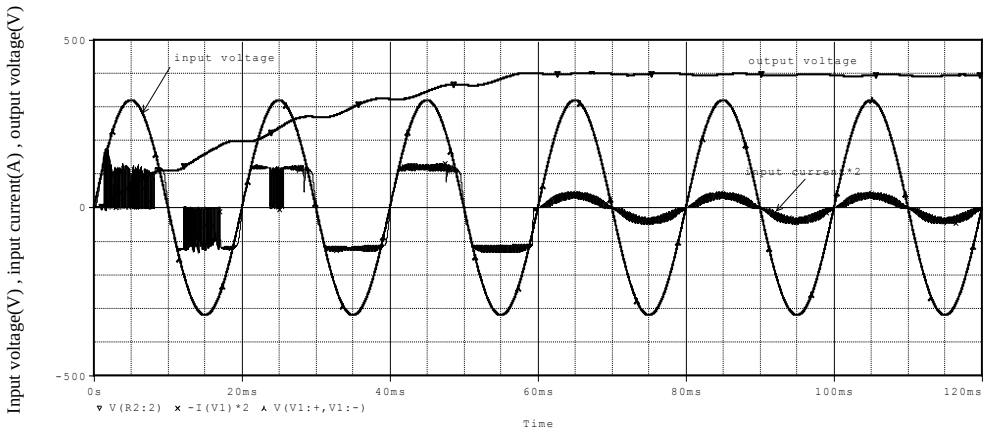

Fig9 (a) Buck –Boost converter input voltage , input current and out put voltage Vi=230Vrms,Vo=400V ,Po=3000W , f_S=20kHz

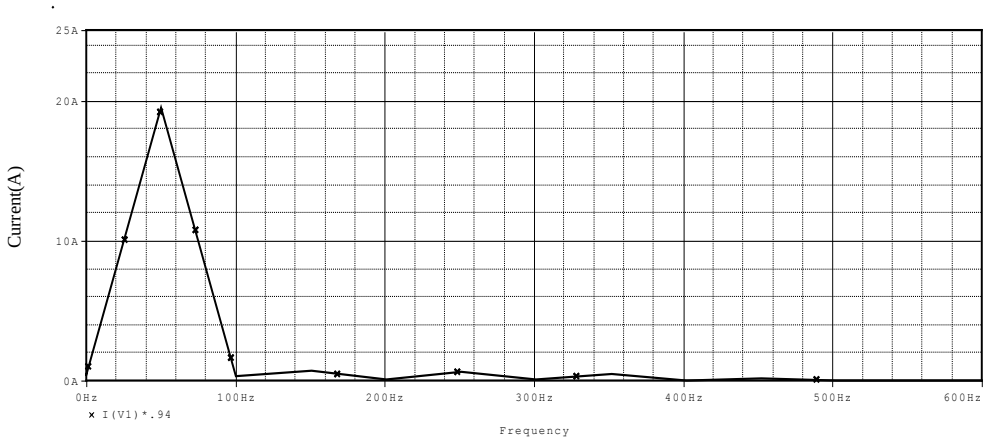

Fig9(b) Input current harmonics of Buck –Boost converter Vi=230Vrms,Vo=400V ,Po=3000W , f_S=20kHz

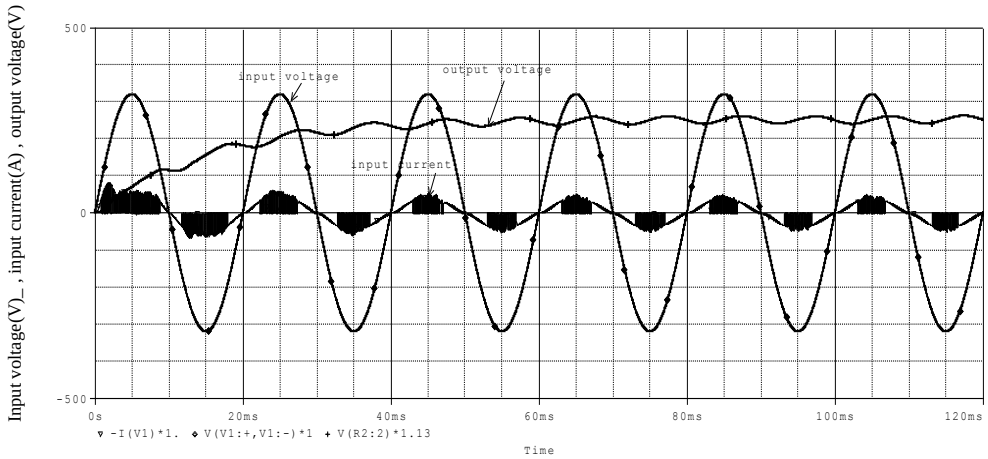

Fig 10(a) Buck- Boost converter input voltage , input current and out put voltage Vi=230Vrms,Vo=250V ,Po=2000W , f_S=20kHz

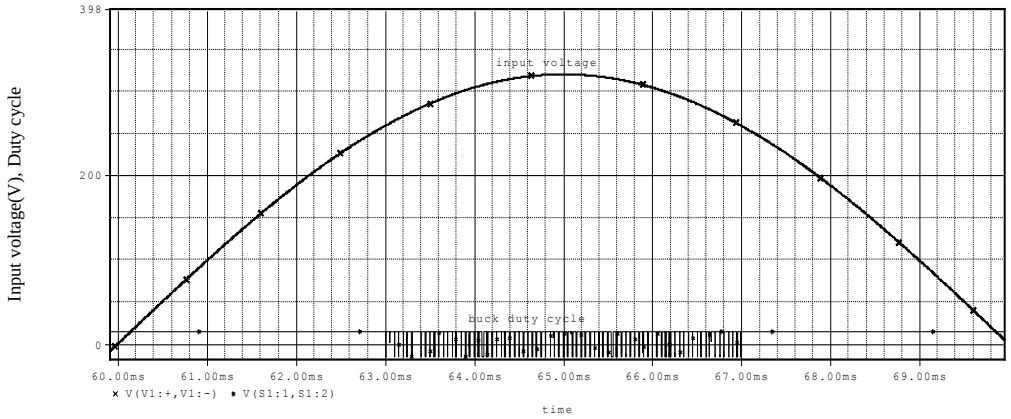

Fig 10(b) Buck switch duty cycle for Buck- Boost converter Vi=230Vrms,Vo=250V Po=2000W f_S=20kHz

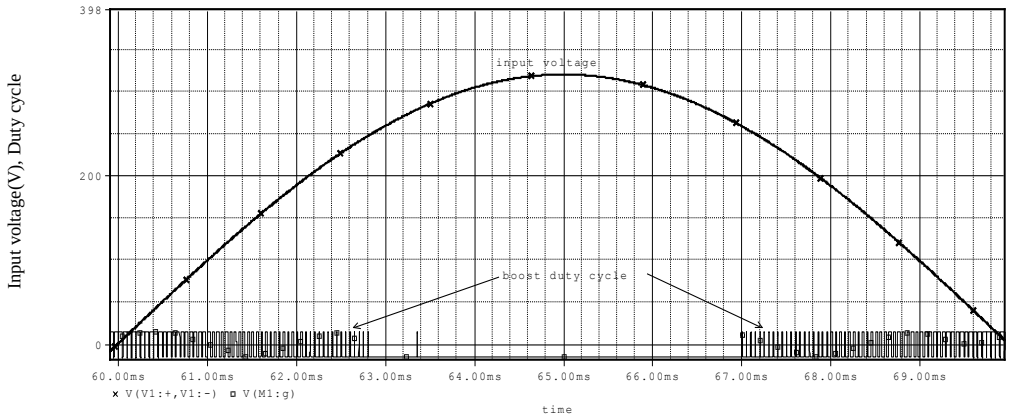

Fig 10(c) Boost switch duty cycle for Buck- Boost converter Vi=230Vrms,Vo=250V Po=2000W f_S=20kHz

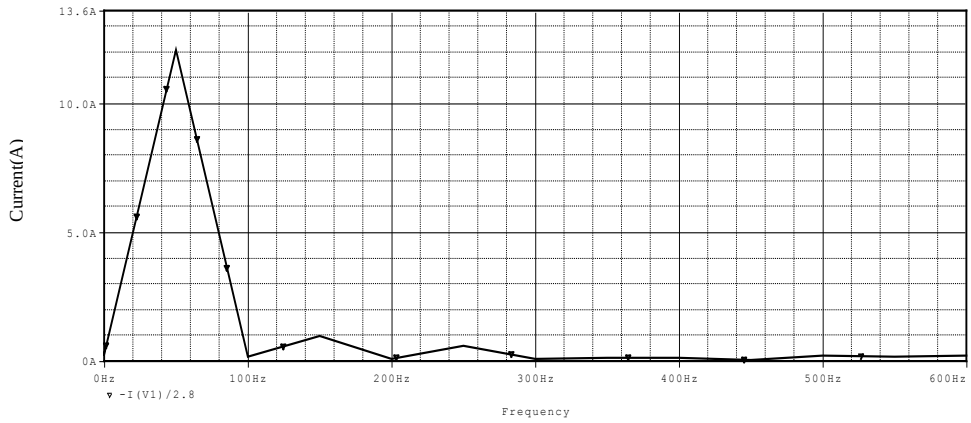

Fig10(d) Input current harmonics for Buck- Boost converter Vi=230Vrms,Vo=250V Po=2000W f_S=20kHz

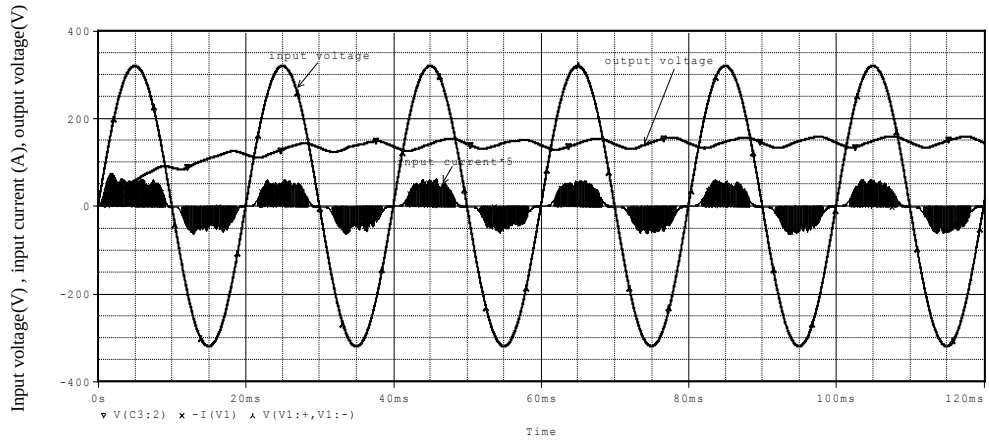

Fig11(a) Buck- Boost converter input voltage , input current and out put voltage Vi=230Vrms,Vo=150V ,Po=1000W , f_S=20kHz

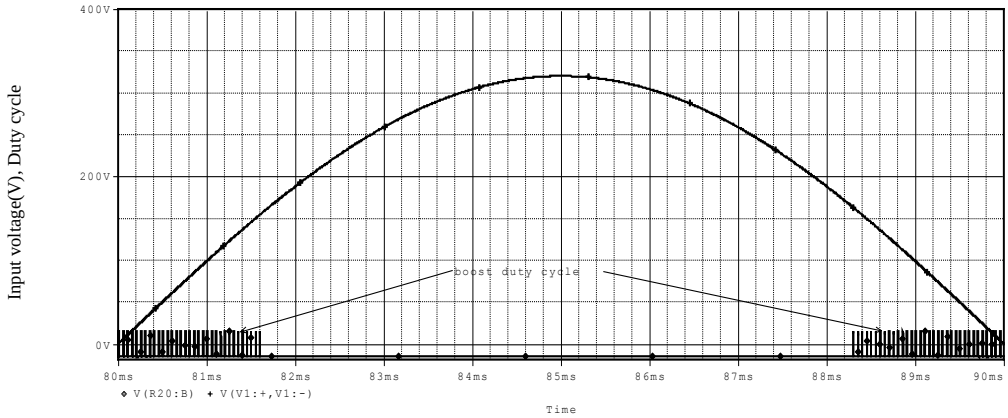

Fig 11(b) Boost switch duty cycle for Buck- Boost converter Vi=230Vrms,Vo=150V Po=1000W , f_S=20kHz

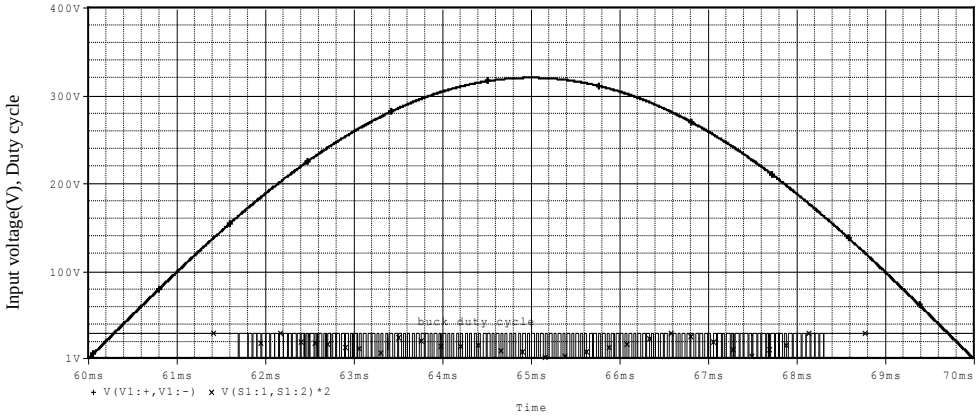

Fig11 © Buck switch duty cycle for Buck- Boost converter Vi=230Vrms,Vo=150V Po=1000W , f_S=20kHz

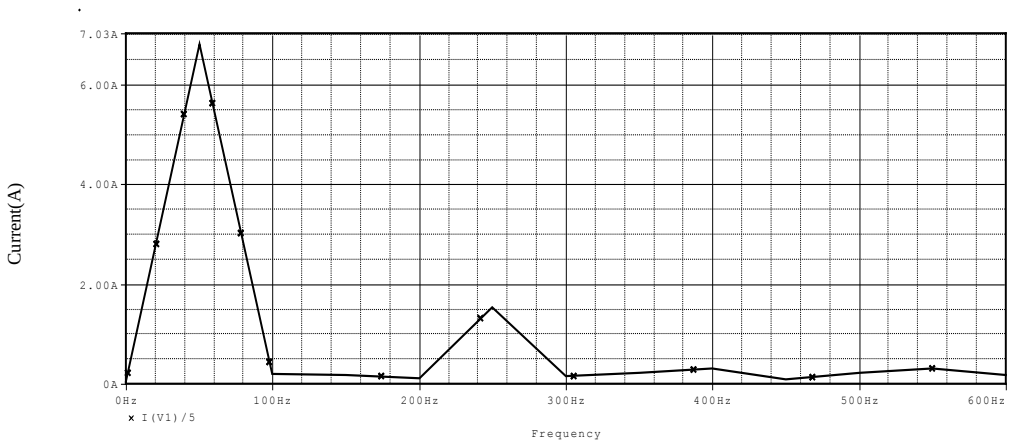

Fig 11 (d) Input current harmonics for Buck- Boost converter Vi=230Vrms,Vo=150V Po=1000W , f_S=20kHz

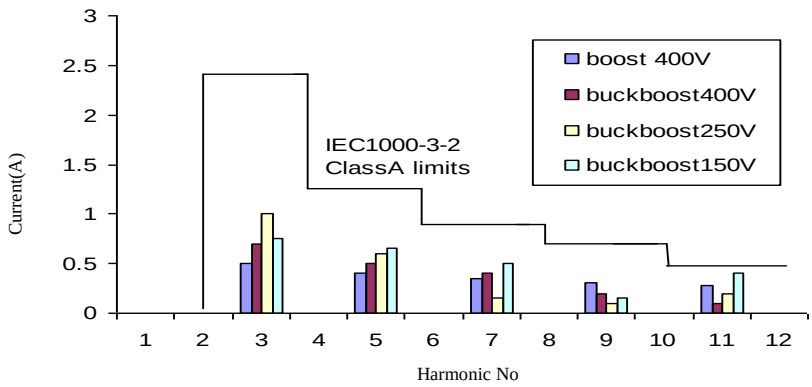

Fig` 12 Input current harmonics contents for the different cases

REFERENCES:

* IEC standard IEC 61000-3-2(2001-10)Ed2.1,"Electromagnetic compatibility (EMC) part 3-2 limits for harmonic current emissions", 2001.
* B. Flud, S. Kern and R.1993 Ridely "Combined buck and boost power factor controller for three phase input" IEEE, Poer Electronics and Applications ,1993, fifth European Conference Vol , Issue 13-16 , Sep , pp 144-148 vol .7.

* R. Ridely, S. Kern and B. Flud 1993" Analysis and design of a wide range PFC circuit for three phase application" IEEE , Applied power electronics conference , volume, issues 7-11 march, pp 299-305.
* M. Chanen, K. AL-Haddad and G.Roy1993, "A new single phase buck boost converter with unity power factor" , IEEE, Industry applications society , annual meeting , Volume , issue 2-8 Oct. 1993 pp 785-792 volume 1.2.
* Y. Zhao,1998"Single phase power factor correction with wide output voltage range" M.Sc. thesis ,Virginea University .
* G.K. Andersoen and F. Blaabjerg2001 "Current programmed control of a single phase two switch buck boost power factor correction", IEEE, Applied power electronics conference Volume issue 1 pp 350-356.
* G.G. Michael " Averaged and cycle by cycle switching model for buck , boost , buck boost and cuk converters with common average switching mode" Texas Tech University e mail Michael @ coez.coe.ttu.edu.
* J. Chen , D. Maksimovic and R. Erickson2006, " Analysis and design of a low stress buck boost converter in universal input PFC application" IEEE transaction on power electronics , Volume 21, No 2 march.
* C. Silva2001 "Power factor correction with the texas instrumentation catalogue UC3854" .
* N. Mohan , T.M. Undeland and W.P1995. Robbins "Powert electronics converters, applications and design" John wily and son, Inc . Second Edition , New York .

* M. O. Loughlin 2002“ UCC3819 , 250 W power factor correction (PFC) boost flower preregulater design , Texas Instrumentation Literature No.SLOA 296,.
* W. Jang , F.C Lee , R. B. Ridley and I. cohen1992 “ Charge control modeling analysis and design” IEEE PESC pp 503-511.
* V. Vorperian 1993“ the charge controlled PWM switch” IEEE PESC pp 533-543.
* W. Jang ,y. Jung , G.C .Hua andF.C Lee1993 “ Power factor correction with flyback converter imploying charge control” IEEE PESC pp 293-308 , 1993.

WATER PURIFICATION BY ELECTROCAGULATION PROCESS

Prof. Dr. Mohammad Ali Al-Hashimi –University of Technology, Dep. Of Building and construction
Amer Abdul-Amir Hussen – University of Baghdad, Environmental engineering Department
Mr. Jameel Yosif Abdel-Ridha – Iben Sina Institute Company –Technical manager

ABSTRACT

Electrocoagulation is an electrochemical method of treating polluted water.

Electrocoagulation and electroflotation are two techniques involving the electrolytic addition of coagulation metal ions directly from sacrificial electrodes by introducing an electrical current into the medium for the treatment of a wide range polluted water in an even wider range of reactor design, application of an electrical field prompts electrolysis of the water medium and generates particular quantities of hydrogen gas.

The process works best with water's pH in range 7.0-7.5 and will still often work less efficiently in the range 3.5 <pH<9.The effects of electrocoagulation process are in reduction water turbidity in relation to electrical current and operation period.

The Electrocoagulation process gives removal efficiency of turbidity by about 85% for batch process and by about 62% for continuous flow and removal efficiency of total suspended solid by about 96% for batch process and 66% for continuous process.

The optimum temperature was found to be at 35 C^0 to give high efficiency in removal of turbidity, total suspended solid and sulphate ions.

الخلاصه

تعتبر طريقة التلبيد الكهروكيمياوي إحدى الطرق الكهروكيمياويه لمعاملة الماء.

إن كلا من تقنيتي التلبيد الكهروكيمياوي (electrocoagulation) والتطويف باستخدام التيار الكهربائي (electroflotation) طريقه تتضمن إضافة ايونات المعادن المكونه للتكتيل والتلبيد بصوره مباشره من الأقطاب إلى داخل المحيط المائي لمعالجة مختلف أنواع الملوثات وباستخدام تصاميم مختلفه من المفاعلات .إن استخدام التيار الكهربائي يحفز تحلل الماء كهربائيا لينتج كميات من غاز الهيدروجين الذي يساعد على رفع وتطويف العوالق المائيه.

تعمل هذه الطريقه بصوره كفوءه لمعاملة الماء الذي تكون دالته الحامضيه ضمن المدى (7.0 – 7.5) ولكنها تعمل بصوره اقل كفاءه للمديات(9 > > 3.5) وباستخدام هذه الطريقه ترتفع الحامضيه بمقدار 0.25 - 1

لقد أظهرت الدراسة تأثيرات عملية التلبيد الكهروكيمياوي في اختزال عكورة الماء بالعلاقة إلى التيار الكهربائي المستخدم وزمن التشغيل . فقد أعطت عملية التلبيد الكهروكيمياوي كفاءة إزالة العكوره بحدود 85% لمفاعل الدفعه الواحدة (batch process) وحوالي 62% لمفاعل الجريان المستمر (continuous process) وكفاءة إزالة المواد العالقة بحدود 96% لمفاعل الدفعه الواحدة و 66% لمفاعل الجريان المستمر.
لقد وجد إن أفضل درجه حرارية تكون عندها أفضل النتائج عند $35C^0$ لتعطي أعلى كفاءة لازاله كل من العكوره,المواد ألصلبه العالقة والكبريتات.

General

At the turn of the last century, it was estimated that some 1.1 billion people (one-sixth of the worlds population) were without an improved water supply (WHO/ UNICEF/ 2000) while in the foreseeable future the demand for water is only expected to grow as human population and industrialization increases [(1)].

Coagulation and flocculation are traditional methods and most important physicochemical operation for the treatment of polluted water. In these processes coagulating agent (e.g. alum or ferric chloride) and other additives (e.g. poly electrolytes) are dosed to produce larger aggregates for smaller particles which then can be separated physically by sedimentation, filtration or flocculation.

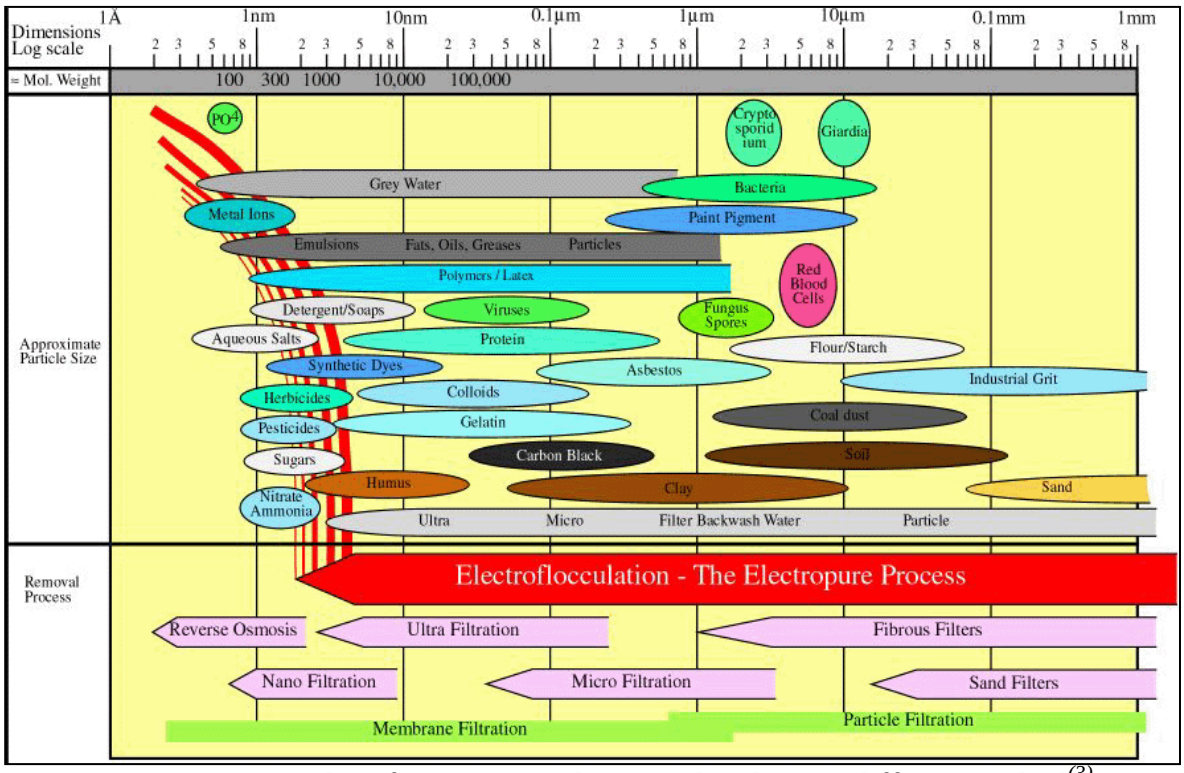

Fig.(1) Examples of some material removed with some different method[(3)]

The electrocoagulation technology introduces low concentrations of nontoxic aluminum hydroxide species into the aqueous media by the electrochemical dissolution of aluminum-containing electrode or pellets. The aluminum species

that are produced neutralize the electrostatic charges on suspended material and / or prompt the co-precipitation of certain soluble ionic species and thereby facilitate their removed [(2)].

Electrocoagulation has been demonstrated to enhance the filtration and dewatering rates for solids removed from an effluent, such enhancements are prompted by growth in the mean particle size from typically 0.3 µm in diameter to as much as 150 µm depending on the degree of electrocoagulation as shown in Fig (1)[(3)]. So that electrocoagulation process can handle most of the pollutants that can be handled by particle filtration, micro filtration, ultra filtration combined and dissolved air flotation. Significant reductions in the total suspended solids (TSS) loading of particulate slurries and in the concentrations of metals (lead, copper, zinc, chromium), fluorides and phosphates from aqueous streams under certain pH conditions. This is suitable for waste water that is largest problem associated with waste and byproduct production and great quantities of water are used to remove small amounts of pollutants, in additional many different techniques are required including a variety of filters, chemical dosing, reverse osmosis and similar operations. On the other hand many of these are either pollutant specific or more expensive than dumpling and using more water.

Electrocoagulation Theory: -

One of more common methods of treating polluted water has been to dose it with chemical coagulation agent such as aluminum sulphate or ferric chloride. The metal ions agglomerate the pollutants, causing them either to sink to the bottom or become sufficiently larger than they can be filtered out, or floated out using dissolved air flotation [(6)]. One of the difficulties associated with this progress is that the ionic contents of the water are increased by the addition of these salts. Although the metal ions are removed during the process, the salt content of the water has been greatly increased, often preventing the ability to use water in recycling or other applications. One method of overcoming, it has been to use a process known as electrocoagulation in which the metal ions are added electrolytically.

In electrocoagulation, sacrificial electrodes are used and the passage of an electric current through the water from the electrodes causes the metal to go into solutions as ions, via the anode reaction.

A current is passed through a metal electrode, oxidizing the metal (M) to its cation (M^{n+}) as in equation (1). Simultaneously, water is reduced to hydrogen gas and the hydroxyl ion (OH^-) as in equation (2).

Electrocoagulation thus introduces metal cations in situ, electrochemically, using sacrificial anodes, (usually aluminum or iron) inside a processing tank [(3)].

The reactions at the anode and cathode are respectively:

$M \rightarrow M^{n+} + ne^-$ …….. (1)

$2H_2O + 2e^- \rightarrow 2OH^- + H_2$ …….. (2)

So that;

$AI - 3e^- \rightarrow AI^{3+}$ …….. (3)

$Fe - 3e^- \rightarrow Fe^{3+}$ …….. (4)

The cation hydrolyzes in water forming a hydroxyl with the dominant species determined by solution pH.

Many other reactions forms may accrue as follows [(4)]:

$O_2 + 2H_2O + 4e^- \rightarrow 4OH^-$ …….. (5)

$O_2 + 4H^+ + 4e^- \rightarrow 2H_2O$ …….. (6)

$2H^+ + 2e^- \rightarrow H_2$ …….. (7)

The metal ions combine with (OH^-) ions from the water to form highly charged coagulants which adsorb pollutants to form insoluble floc particles; so that Al^{+3} reacts with H_2O to form Al $(OH)_3$. Thus, each mole of dissolved Al^{+3} is added to reduce one mole of Al $(OH)_3$.

Highly charged cations destabilize any colloidal particles by the formation of poly hydroxide complexes. These complexes have high adsorption properties forming aggregates with pollutants. Evaluation of hydrogen gas is aid in mixing and hence flocculation. Once the floc is generated, the electrolytic gas creates a flotation effect removing the pollutants to the floc-foam layer at the liquid surface [(10, 14)].

There are a variety of ways in which species can interact in solution [(3)]:-

1- Migration to an oppositely charged electrode (electrophoresis) and aggregation due to charge neutralization.

2- The anion or hydroxyl ion $(OH)^-$ forms a precipitate with the pollutant.

3- The metallic cation reacts with $(OH)^-$ to form a hydroxide, which has high adsorption properties thus bonding to the pollutant (bridge coagulation).

4- **The hydroxides from larger lattice-like structures and sweeps through** the water (sweep coagulation).

5- Oxidation of pollutants to less toxic species.

6- Removal by electroflotation and adhesion to bulk.

Aluminum Dosing: -

In electrocoagulation, the electrodes of the electrochemical cell are connected to an electrical power source. Faraday's law can be used to describe the relationship between current density (Amp cm^{-2}) and the amount of aluminum which goes into solution (gm Al cm^{-2}) [3,5].

$$W = I\,t\,m / z\,F \qquad \text{..... (8)}$$

Where:

w= aluminum dissolving (gm Al cm^{-2}) or may express as electrode consuming rate (Ec)

I= current density (Amp cm^{-2})

t= time (sec.)

m= molecular weight of Al (M=27)

z= number of electrons involved in the oxidation / reduction reaction (z=3)

F= Faraday's constant 96,500 (Colomb/g-eq.)

The theoretically calculated by Eilen [6] the amount of Al dissolved at various raw water temperatures is compared with the weighed values of Al dissolved; the correlation found was relatively good (r^2=0.94) and suggests making further experiments, the Al dose was calculated based on Faraday's law. The coefficient of dissolved metal can be calculated according to the formula [5]:

$$\eta = Q_\Gamma / Q \qquad \text{..... (9)}$$

where:

η = metal dissolubility coefficient;

Q_Γ = actual quantity of dissolved metal (Kg Al);

Q = theoretical quantity of dissolved metal (Kg Al) .

Electrode working time can be calculated as:

$T = S_a\, b\, \rho\, \eta_3 / (10 * Q)$ …….. (10)

where

T = working time (days);

S_a= total anode surface area (m^2);

b = electrode thickness (m);

ρ = specific weight of electrode material, (Kg/m^3)

η_3= electrode usage coefficient; η_3=0.8

Electrode Material :-

The electrode material impacts markedly on performance of the electrocoagulation reactor. The anode material determines the cation introduced into solution. Several researchers have studied the electrode material using a variety of theories according to the preference of a particular material. The most common electrodes are aluminum or iron plates .Do and Chen (1994) compare the performance of iron and aluminum electrodes for removing color from dye solution[(3)]. Their conclusion is that the optimal electrocoagulation conditions vary with the choice of iron or aluminum electrodes, which in turn is determined by:-

1.initial pollutant concentration.

2.pollutant type.

3.stirring rate.

Passivations:-

One of the greatest operational issues with electrocoagulation is electrode passivation [(3)]. Passivation is lack of a systematic approach to electrocoagulation reactor design / operation thus limiting electrode reliability and its implementation [(1)].

There are various methods for preventing and / or controlling electrode passivation including:-

1. Changing polarity of the electrode.
2. Hydro mechanical cleaning.
3. Introducing inhibiting agents.
4. Mechanical cleaning of the electrodes.

According to these researchers, the most efficient and reliable method of electrode maintenance is to periodically clean the electrodes which for large-**scale,** continuous processes is arduous issue. On other hand, to avoid electrode passivation and to ensure uniform electrode usage their polarity is periodically reversed (reversal period being not more than 1 day) [(5)].

SOME APPLICATIONS OF ELECTROCOAGULATION PROCESS [(8)]: -

* Clay Water / Suspended Solids
* Fats, Oils and Grease (FOGs)
* Sewage Treatment Plant and Effluent Aeration Treatment Units
* Removal of Heavy Metals
* Cyanide and Arsenic Removal
* Printing / Ink
* Textile Dye Plants
* Food Processing.

- Experimental work:

In order to achieve the goals of study, there was a plan to study a batch process by changing the current density, pH solution, temperature of water, and current concentration to get optimum conditions of these parameters, to reverse these conditions and compare the results with these of continuous process that has optimum condition. The effects of electrolytic cell in water treatment are evaluated in this study in different water conditions. It is decided to use the final turbidity, total suspended solid, calcium ions concentration as parameters of range of treatment. These parameters indicate the effective process of electrocoagulation in water treatment when comparison is made after and before treatments.

*** <u>Batch Process</u>: -**

It is divided two categories:-

4-1-A By using (111 mm L x 168 mm W x 1 mm) of one aluminum electrode as a node and two plates of stainless steel electrodes plot on two sides as cathode with 6 mm distance between electrodes and with total anode area used as 374 cm^2.These experiments were done to test the parameter changes along height level

of container; so the results show the pH; Calcium ions; Sulphate ions and Aluminum ions change at three levels: surface, middle and bottom level.

4-1-B By using ladder series of electrolytic cell which consists of four blades aluminum anodes, each of it is (110 mm L x 85 mm W x I mm thick) and five blades stainless-steel cathodes as shown in Fig. (2).

The two categories above use:

1- glass container with volume of 13 lit.

2- electrical device (power supply) that generates low voltage at maximum 32 volt with maximum D. C. current at 10 Amp.

The electrolytic cell is constructed to achieve a concentric gap of about 20mm between the central anode and the surrounding cathode. This arrangement allows the hydrogen bubbles to rise up, carrying all containments and water pollutants to the water surface.

Continuous Process: -

Pilot scale model consisting of raw water storage tank (T-101) is connected to packed bed by using centrifugal pump with 120 lit / min and (5.5 -40 m) head; Flow was adjusted by using Gate valves with Rotameter . The reactor formed from 10 cm diameter, Schedule 80, PVC pipe; 30 cm high, equipped with aluminum electrode as anode at inlet side and stainless-steel electrodes at outlet side and whose interior was filled with (0.8 cm O.D. x 0.55 cm I.D x 0.125 cm Thickness x 1 cm length) aluminum rushing ring with effective area 10245 cm^2 [12], as shown in Fig. (3).The total high of packed is 25 cm; the unit was powered at 0.5 – 10 Amp depending on the position of bed – vertical or horizontal.

Throughout the various phases of the experimental studies; samples of the treated effluent were collected and allowed to settle for 1 hour and then analyzed for turbidity ,TSS, (Ca, Mg, Al…etc) ions.

Study No. 1 Changing of (pH, Ca, Mg and Al) with time at three levels of reactor depths:-

This study considers the changes that may happen at three levels of containers; at the surface, middle and the base of the container. It was done by using 374 cm^2 of aluminum anode area; the results are shown in Fig (4A) to Fig (4E) .

The pH changing was studied with time; the result is shown in Fig. (4A).It is shown that pH value rises up about 0.25 unit; to a value of 7.69 during the five

minute of starting the operation; that results from the aluminum hydroxide formation and then falls down suddenly to a value below of 7.25, that is because aluminum hydroxide is consumed by water containments, then it gradually rises up to a value of primary magnitude

Study No. 2 Effects of Current Density Change on Removal Efficiency in Electrocoagulation Process:-

This study considers current density change effects by using 730 cm^2 aluminum electrode area with 6 liter volume of water at 19C°, under four electric current values namely (0.5, 0.9, 1.5 and 3) amp. Figs. (5A),(5B) and (5C) show the results of current density effects after 1 hr operation on (turbidity, TSS, SO_4, Ca, Al and conductivity) in which aluminum dosage varies with current changes.

A little change were shown between 1.5 Amp and 3 Amp to produce 2.64 NTU and 2.48 NTU respectively but a little effects shown with calcium ions, to produce 63.57 to 65.38 ppm respectively, while it has effects on removal of total suspended solid to point of 60 ppm and 21 ppm respectively

Study No. 3 Effects of pH Change on Removal Efficiency in Electrocoagulation Process:-

Another consideration in this study is the effect of pH in electro coagulation process which uses the current density at 1.5 Amp with different pH variation at (3, 6.35, 7.25 and 9) adjusting with HCl acid and NaOH base by using 730 cm^2 aluminum electrode anode area and 6 liter volume of water at 19C°; the results were plotted in Figs (6A,B,C) in which show that most effects of aluminum dosage at pH of raw water ranged from (6.35 to 7.24) Study No. 4 Effects of Temperature Change on Removal Efficiency in Electrocoagulation Process:-

The consideration of this experimental study is shown in Figs. (7 A,B,C), which show 730 cm^2 aluminum electrode and 6 lit volume of water at 1.5 Amp. The temperature values used are (2, 19, 35 and 65) C°; where the results are optimum at 35 C°; the final turbidity is 1.74 NTU while it is at high value 2.46 NTU at 2 C° and 1.98 NTU at 65 C° as shown in Fig. (7 B).

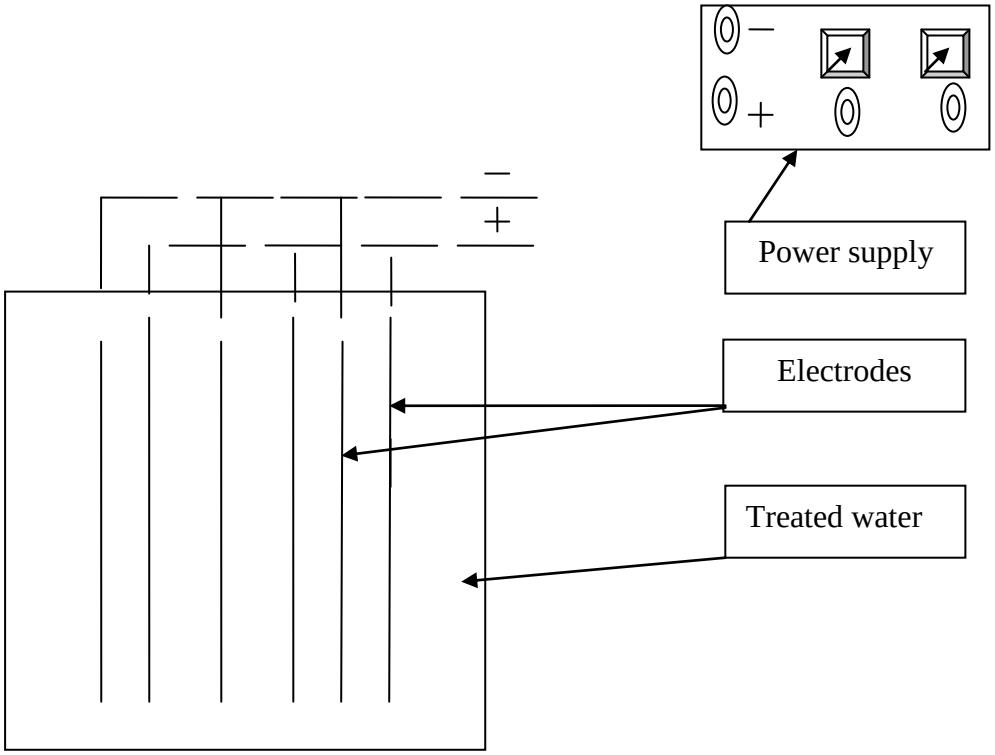

Fig (2) Batch process

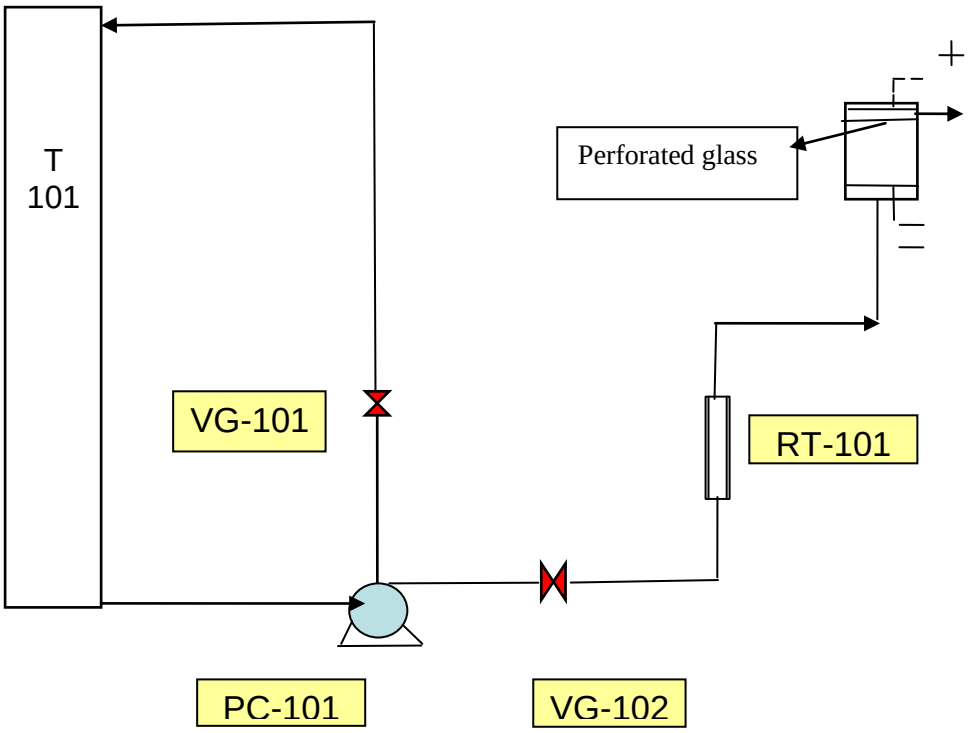

Fig (3) Continuous process flow diagram

Pc-101	Centrifugal pump
R-101	Packed bed reactor
RT-101	Rotameter
T-101	Storage Tank

VG-101	Gate valve
VG-102	Gate valve

Study No. (5) Effects of Water Volume Change on Removal Efficiency in Electrocoagulation Process (Effects of Current Concentration Changes):-

This group of experimental work considers the effects of changing volume of water treated on purification, 730 cm^2 aluminum electrodes are used as anode at 1.5 Amp and 20 C° Figs (8A,B,C), show that using of minimum volume gives an optimum condition of water treatment and it consider the volume of 6 lit water as a maximum volume which is suitable for 730 cm^2 aluminum anode area and this means the optimum current concentration is (166.7) Amp per m^3 of water treated and (8.11) m^3 of water per m^2 of aluminum anode area.

Study No. (6) Effects of Current Density Change at Continuous flow rate on removal efficiency in electrocoagulation Process:-

Figs (9A,B) show flow rate change in which D.C. electrical current changes (0.1, 0.5, 0.8, and 1.5) Amp with packed bed of (30 cm high x 10 cm diameter) with 25 cm packing high of rushing rings.

Study No. (7) Effects of Flow Rate Change on Removal Efficiency in Electrocoagulation Process:-

By using the D.C. electrical current at 1.5 Amp with flow rate values of (0.66, 23.4, 75.6 and 120) l/hr which indicate an optimum flow rate at 23.4 lit/hr; as shown in Figs. (10A,B).

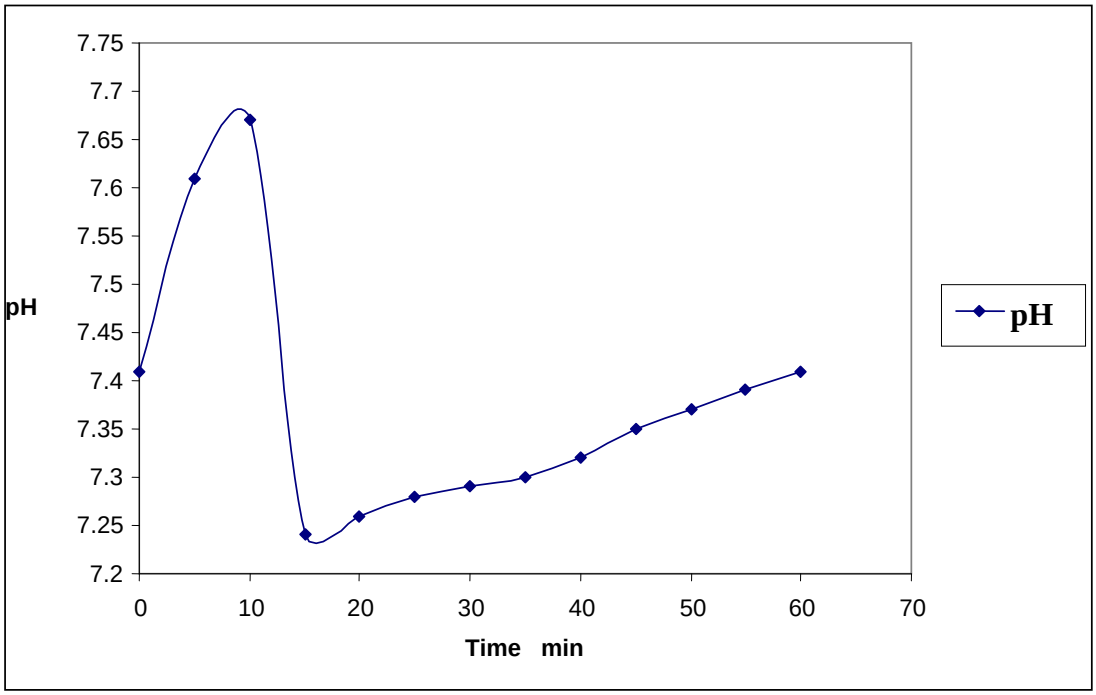

Fig. (4A) pH changing with time due to hydroxide formation

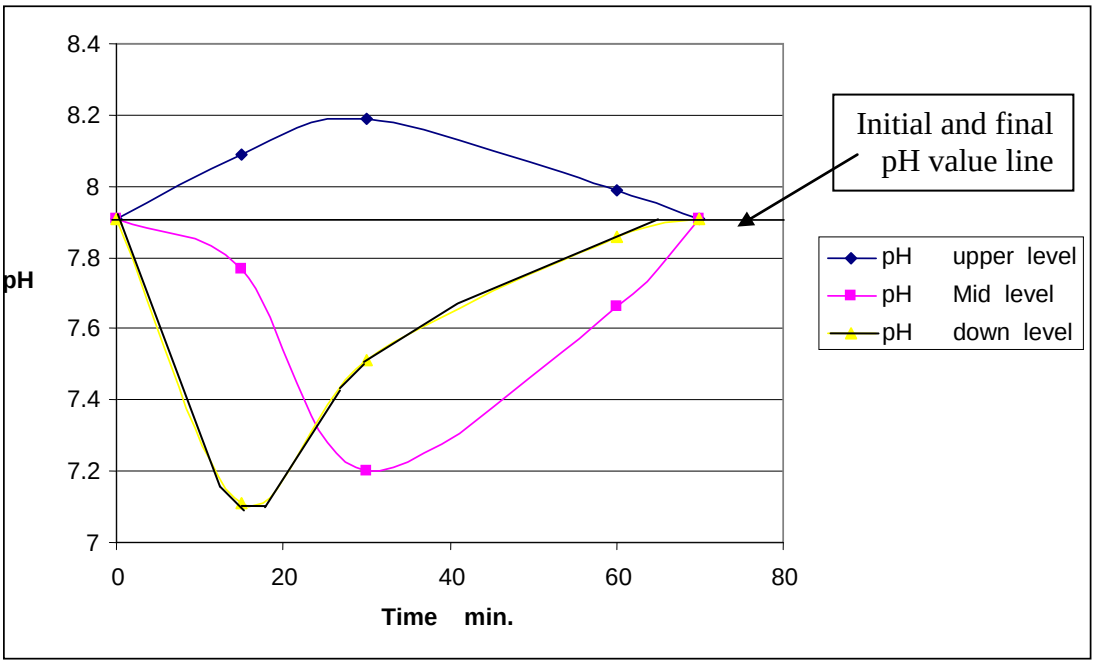

FIG (4B) pH changing with time at different levels of reactor

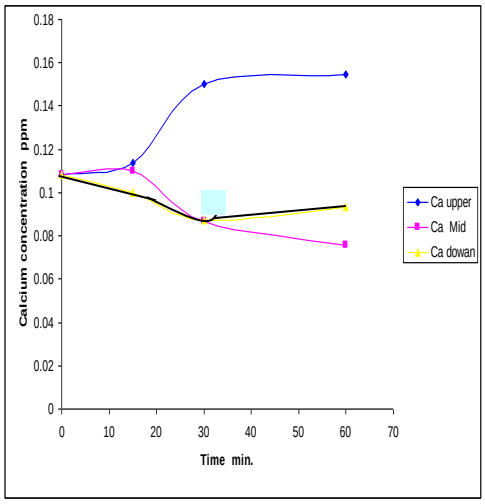

FIG (4C)

Calcium changing with time at different levels of reactor

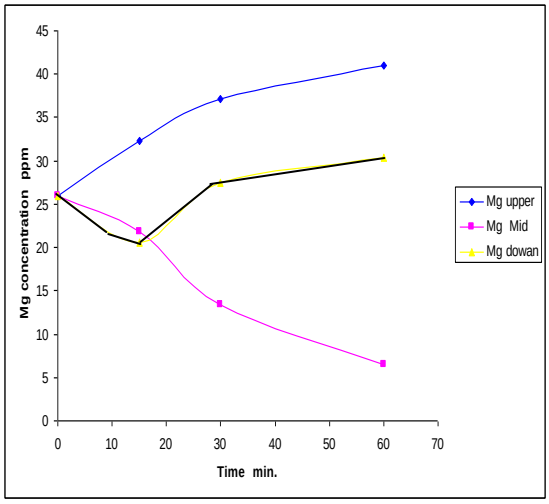

FIG (4D)

Magnesium changing with time at different levels Of reactor

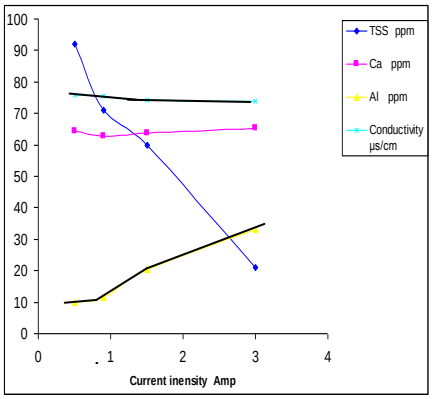

FIG.(4 E)

Aluminum changing with time at different levels of reactor

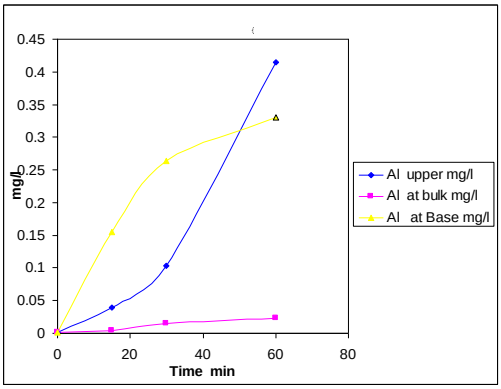

FIG (5A)

Current intensity changes effect on water quality

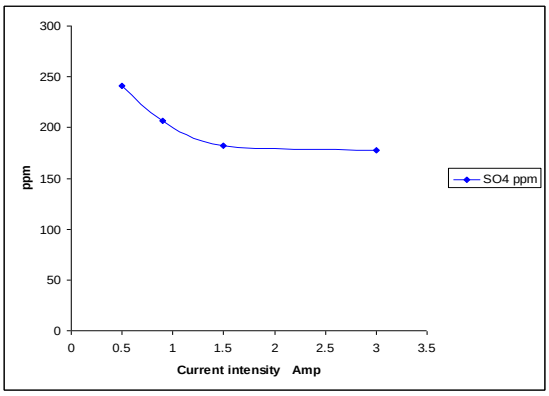

FIG (5C)

Current intensity changes effect on water quality

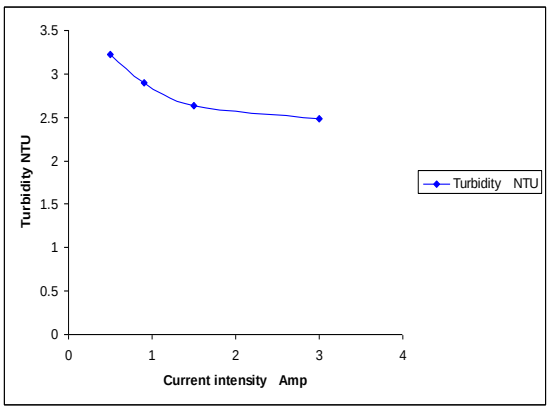

FIG (5B)

Current intensity changes effect on water quality

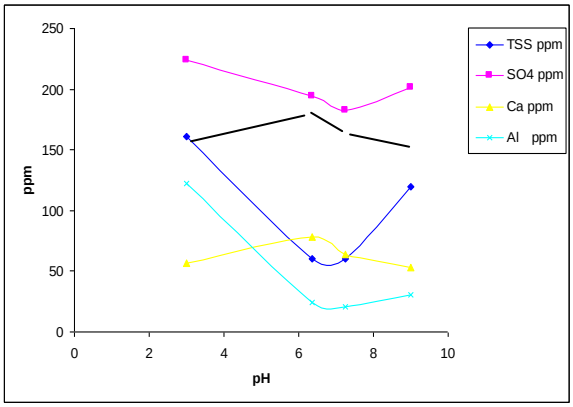

FIG (6A)
pH changes effect on water quality
*By using HCl adjusting

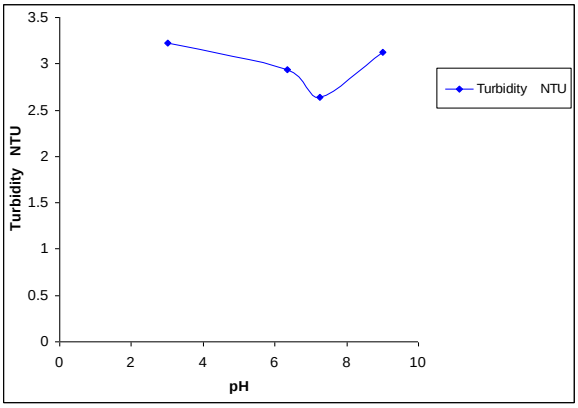

FIG (6B)
pH changes effect on water quality
*By using HCl adjusting

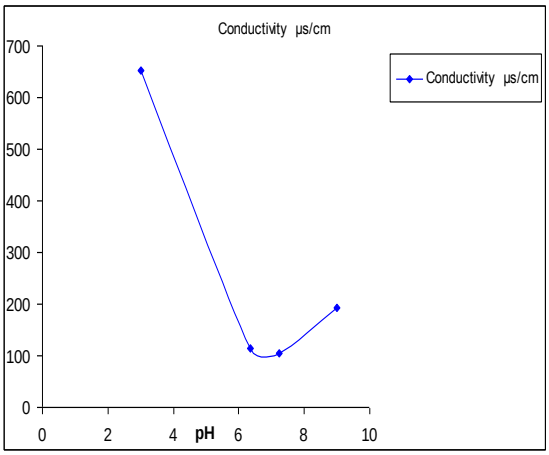

FIG (6C)
pH changes effect on water quality
*By using HCl adjusting

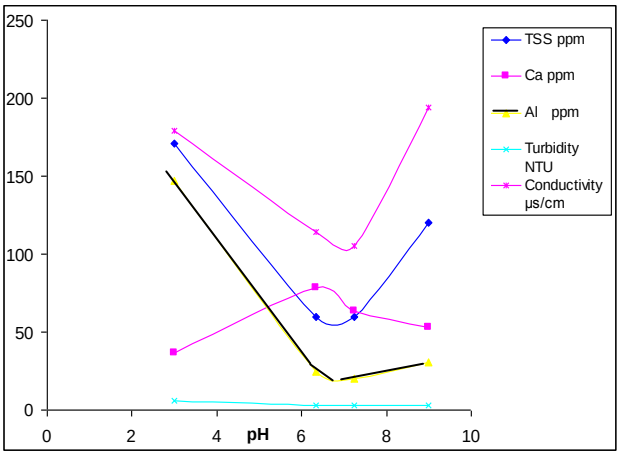

FIG (6D)
pH changes effect on water quality
* By using H_2SO_4 adjusting

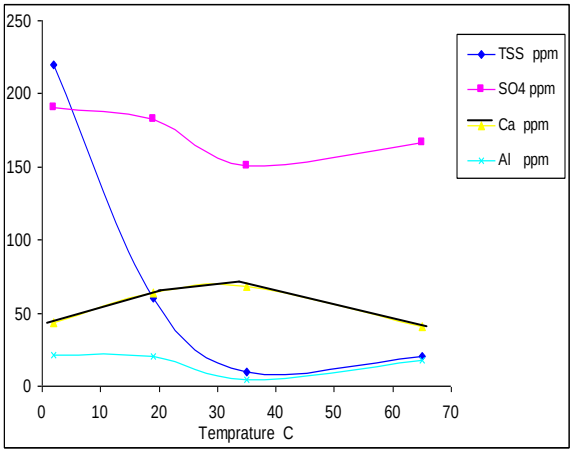

FIG (7A)
Temperatures change effect at constant current density

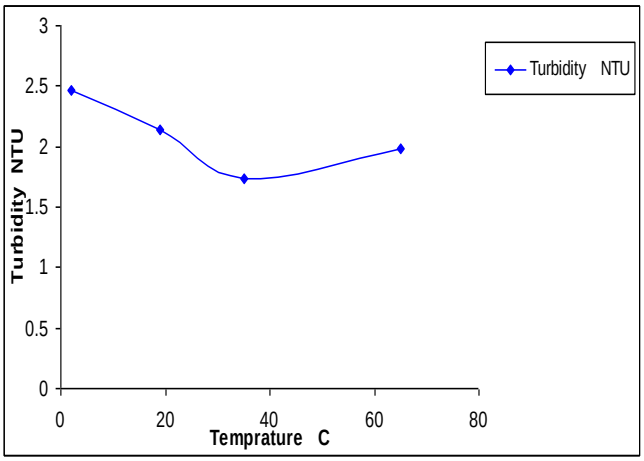

FIG (7B)
Temperatures change effect at constant current density

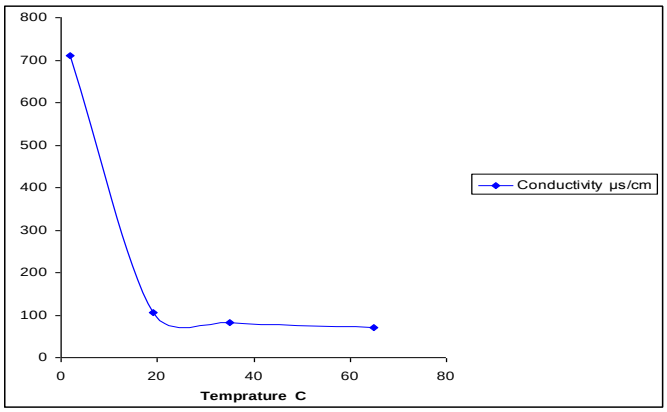

FIG (7C)
Temperatures change effect at constant current density

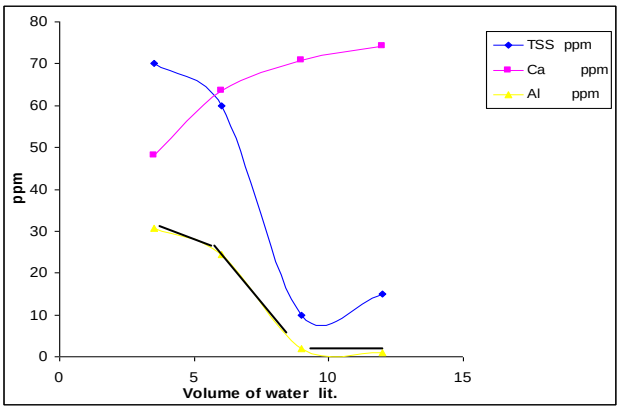

FIG. (8A)
Volume of water changes effect on water quality

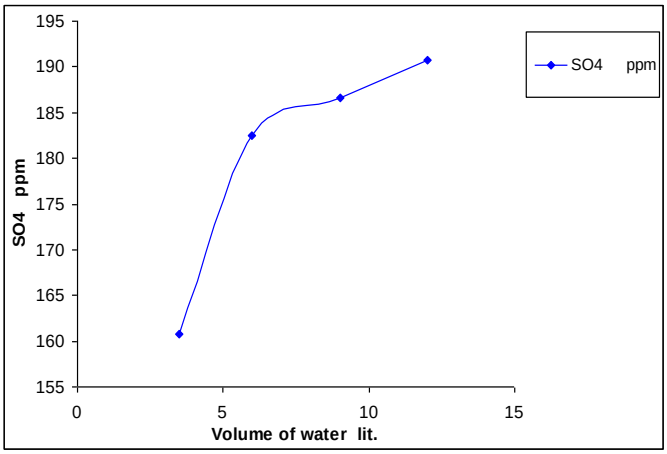

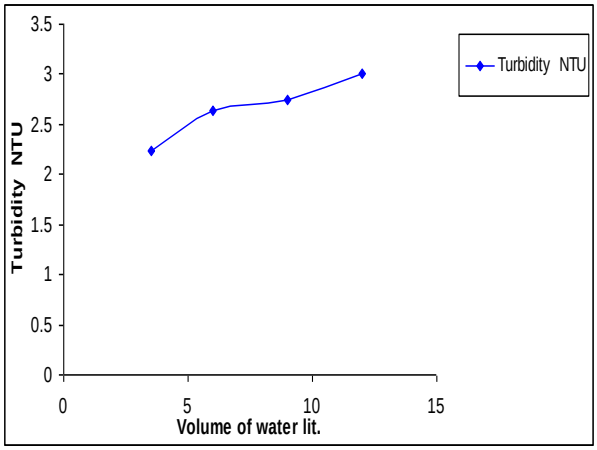

FIG. (8C)
Volume of water changes effect on water quality

water quality

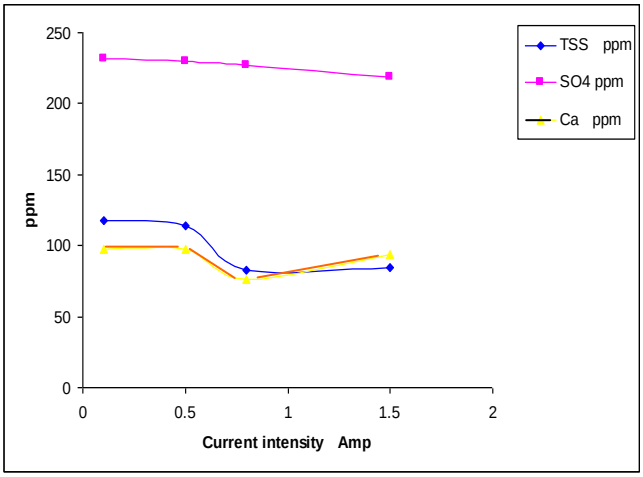

FIG (9A)
Current density changes effect at constant flow rate
(23.4 l./hr)

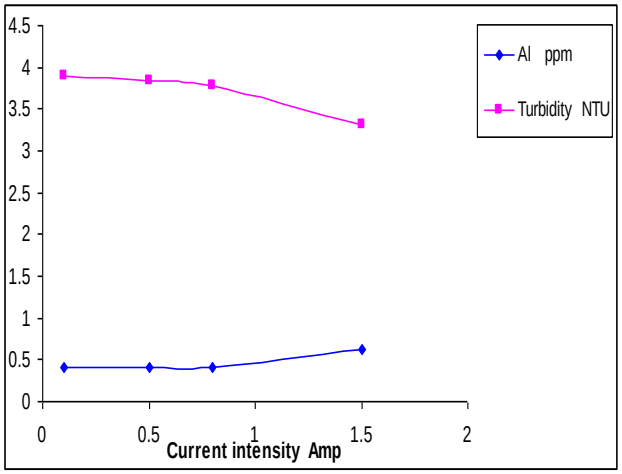

FIG (9B)
Current density changes effect at constant flow rate
(23.4 l./hr)

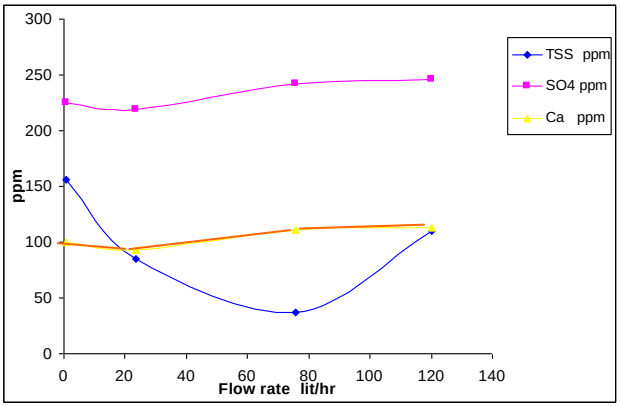

FIG (10A)
Flow rate Changes effect at constant Current density (1.5 Amp)

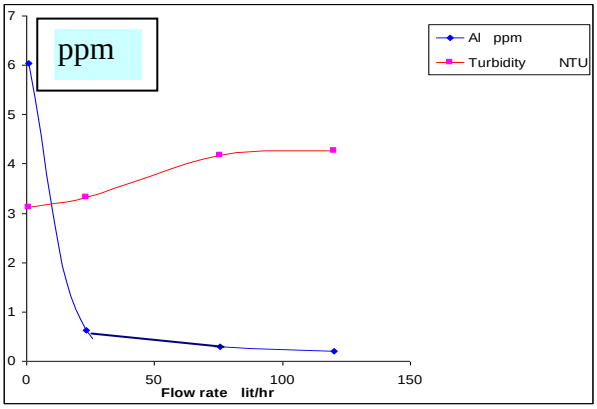

FIG (10 B)
Flow rate Changes effect at constant Current density (1.5 Amp)

CONCLUSIONS:-

* The removal efficiency of turbidity with electrocoagulation process is due to the dosage of aluminum in which production increases with current density increasing.
* It is shown that the optimum efficiency of electric current is at 0.9 Amp but in where the removal of others matters like calcium ions and sulfate ions and total suspended solids are taken in consideration, the electric current 1.5 Amp is the optimum current density to be adopted for an area equal to 730 cm^2 which is used in this investigation. By that is meant the optimum current density is 20.54 Amp/m^2
* By testing different value pH of water, the optimum pH lies at 7 – 7.5, while gives a higher effectiveness of electrocoagulation process.
* The optimum temperature used is at 35 C° while it is at lower or higher than the removal of other materials.
* The study shows the optimum current concentration at (166.7) Amp/m^3.
* The proportion of optimum aluminum area to volume of water used is at (8.11) m^2/m^3.
* It was found that packed bed unit must be used at a horizontal situation that will allow the hydrogen gas formation and other upper floating flock to rise without causing any obstruction between two electrodes.
* In compare with previous study by Naomi, It seems that rushing ring produce high quality water than fluidized bed, in addition to low current using in.
* The optimum current used in continuous flow rate for packed bed has effective area equal to 10245 cm^2 and at D.C. electrical current equal to 1.5 Amp. This achieves higher efficiency. That means the optimum current density is 1.46 Amp/m^2.
* The optimum flow rate of continuous flow used for packed bed is at (23 Lit / hr) which has achieved higher efficiency.

REFERENCES:

* Peter K. Holt, Geoffry W. Barton, Cynthia A.Mitchell
The future for electro coagulation as a localized water treatment technology
Department of chemical engineering,university of sydny (2004)
www.elsevier.com/locate/chemosphere
* Naomi P. Barkley, Clifton Farrell and Traacie Williams (1993)
Electro-pure alternating current electrocoagulation
Emerging technology summary
www.worldcatlibraries.org
* Peter K. Holt ; Geoffrey Barton and Cynthia Mitchell
Electrocoagulation as a waste water treatment
Department of chemical engineering, The University of Sydney, New South Wales.(1999)www.isf.uts.edu.au/publications
* Jerome Kruger
Electro chemistry Encyclopedia/ Electro chemistry of corrosion
The Johns Hopkins University (2001)
www.electrochem.cwru.edu
* Lucjan Pawlowski
Physicochemical methods for water and waste water treatment
Pergamon press (1979)
* Peter K. Holt ,G.W.Barton and C.A. Mitchell
Deciphering the science behind electro coagulation to remove suspended
Clay Particles from water.
Water science and technology, volume 50 No. 12 pp 177-184, 2004
www.iwaponline.com
* Fresh Patents .com
Track New Patents and Technologies
Novel cells and electrodes for electro coagulation treatment of waste water
www.freshpatents.com
* Robinson Vivian; BSc Phd (1999)
Electro pure Australia Limited
Electroflocculation in the treatment of polluted water
www.electropure.com.au
* Robinson Vivian; BSC, PhD. (2000)
Electro Pure Australia Limited
A new technique for the treatment of waste water
Internet: Electropure%20international%20pty%20ltd.htm
www.electropure.com.au
* Robinson Vivian;BSc Phd (2001)
Electro Pure Industrial Australia Pty Ltd
The treatment of storm water runs off from building sites-some case studies
www.electropure.com.au
* Electro Pure International Pty Ltd
What's electro-pure electro-flocculation?
www.electropure.com.au
* Coulson J.M. and Richardson J. F.
Chemical Engineering vol. 6
Pergamon press 1971
* Kaselco by Kaspar,(2000)
Waste water treatment Utilizing Electrocoagulation
Manufacturing qualify products since 1898
Internet: Electrocoagulation%20by%20kaselco.htm
www.kaselco.com
* Powell water systems. INC. Potable water
www.powellwater.com/appllications.htm
* Peter K. Holt , G.W.Barton and C.A.Mitchell
Mathematical Analysis of batch electro coagulation reactor
Internet water supply-25-6 (2002) 65 (IWA) www.iwaponline.com

SHORT TERM FORECASTING OF SULFATE CONCENTRATIONS IN BAGHDAD

Rafa H. Al-Suhaili
Prof. Dr. College of Engineering
Baghdad University

Shuwan J. I. Barzanjy
M.Sc. from College of Engineering
Baghdad University

ABSTRACT

Water quality control is an important protection issue. The analysis of the water quality parameters and the prediction of their changes in future, are important in the planning for water pollution control program. This analysis and prediction are the important steps and functions that the environmental engineer must perform.

In this study, time series analysis was applied to model a short term forecasting for the minimum and the maximum values for both raw and produced water of Sulfate concentrations at seven water treatment plants serving Baghdad city (Karkh, Sharq Dijlah, Karama, Wathba, Qadisiya, Dora, and Rasheed).

Holt-Winters' method was used for the modeling. Three years (2001-2003) were used for building the model and the year (2004) was used for the verification, to check the model acceptability. Comparisons by (t-test) and (F-test) between means and variances of the observed concentrations and these generated by the Holt-Winters' model had reflected the applicability of this model. Hence, in future for operation purposes, it can be use for forecasting Sulfate concentrations.

Visual Basic Application (VBA) software was built for this short-term forecasting model. This software was built in away, which allows an automatic updating of the model parameters. Adding additional observed data usually performs the updating of such model.

INTRODUCTIONT

The idea of using a mathematical model to describe the behavior of a certain physical phenomenon is well established. In particular, it is some times possible to derive a model based on physical laws. This model is enabling to calculate the value of some time dependent quantity nearly exactly at any instant of time. If exact calculation were possible such a model would be entirely deterministic. Probably no phenomenon is totally deterministic because of the unknown factors that contribute to its variation. So it is not possible to use a deterministic model to describe this phenomenon. In this case, it may be possible to derive a model that can be used to calculate the probability of a future value lying between two specified limits. Such a model is called a stochastic model **[1]**.

Stochastic analysis of water quality parameters is a useful treatment of its' data for making quantitative decisions, such as whether water quality is improving or getting worse over time. The

short-term forecasting can be useful for extrapolating the momentum that exists in the phenomena. As changes in established patterns are not likely over a short span, extrapolating them provides, most often, with accurate and reliable forecasters. Seasonality can also be predicted fairly well **[2]**.

Area and Objective of the Study

The Tigris River has a large importance in the present and in the future. This is because of the detrimental effect of pollutants resulting from human activities, industrial wastes, sewage wastes, and harmful effect of increasing drainage waters coming from agricultural lands upstream coupled with the decreasing in its discharge. So it has become necessary to make detailed studies and researches to evaluate the suitability of the river water for different purposes in a selected site of the river.

The reach of the river along Baghdad city and Sulfate concentration levels were chosen for this study. Time series analysis was applied to both raw water and treated water of the existing treatment plants that exists along the river in Baghdad. The running conventional water treatment plants are (Karkh, Sharq Dijlah, Karama, Wathba, Qadisiya, Dora, and Rasheed) as shown in Figure (1).

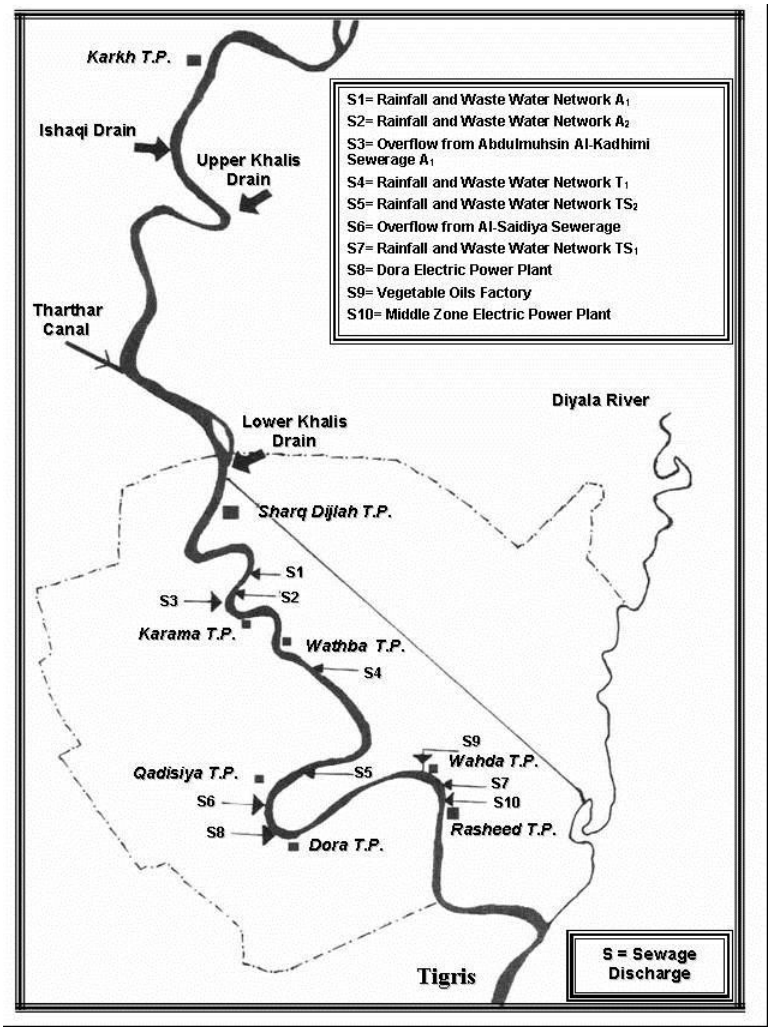

Figure (1) : Conventional water treatment plants and main sources of pollutions in Tigris River at Baghdad (from [3])

The main objective of this study is to arrive at a stochastic description of the time series of Sulfate water quality data for the (7) plants in Baghdad for both raw and treated water with its monthly maximum and minimum recoded values. This can be achieved by obtaining a short-term forecasting model, which can be used for operation purposes.

The analyzed time series for each plant is (3) years in length, during the period (2001-2003) of monthly maximum and minimum values for both raw and produced water. The records of year (2004) are used to check the model acceptability. The Sulfate concentration records were measured as SO_4 in (mg/L) units.

INTRODUCTION

Time series analysis is a major tool in assessing the state of pollution of water resources. A review of short-term forecasting models and related researches are presented here in historical sequence .

Brown **[4]** in (1956) developed an extension to the weighted moving average forecasting by exponentially decreasing weights which known as exponential smoothing procedures. A flat forecast function was used because single exponential smoothing works best for data, which have no trend, no seasonality. The smoothing was modified by a factor known as the damping factor.

Holt **[5]** in (1957) extended the single exponential smoothing to a linear exponential smoothing to allow forecasting of data with trends. Holt's method sometimes called double exponential smoothing. Two smoothing constant were modified, one for level and the other for trend.

Winters **[6]** in (1960) extended Holt's method to capture seasonality directly. The Holt-Winters' method was based on three smoothing equations, one for level, one for trend, and one for seasonality.

Harrison and Stevens **[7]** in (1976) developed a multi disturbance state space approach. They introduced, in the 'recipes' section of their papers, special cases that in today's terminology are called the local level, local trend and local seasonal models.

Snyder **[8]** in (1985) developed a state space framework based on a single source of error, with equations closely resembling those of exponential smoothing, was proposed. For the first time, a statistical framework with clear, direct links with exponential smoothing had been found.

Hyndman ***et. al.*** **[9]** in (2002) provided a statistical framework for the exponential smoothing. The framework incorporated stochastic models underlying the various forms of the exponential smoothing and enabled the calculation of maximum likelihood estimates of smoothing parameters.

Baki ***et. al.*** **[10]** in (2005) showed that the applications of exponential smoothing to forecast time series usually rely on three basic methods: simple exponential smoothing, trend corrected exponential smoothing and a seasonal variation thereof. A common approach to select the method appropriate to a particular time series was based on prediction validation on a withheld part of the sample using criteria such as the mean absolute percentage error. A second approach was to rely on the most appropriate general case of the three methods. For annual series this is trend corrected exponential smoothing: for sub-annual series it is the seasonal adaptation of trend corrected exponential smoothing. The rationale for this approach is that a general method automatically collapses to its nested counterparts when the pertinent conditions pertain in the data.

THEORY OF SHORT-TERM FORECASTING

Generally, a time series can be expressed as a linear combination of four components depending on the type of variable and the averaging time interval. These components are represented in the form:

$$X_t = J_t + T_t + P_t + D_t \quad \text{.....} \quad (1)$$

Where:

Xt : Time series observations at time t = 1,2,3 … N

Jt : Jump component.

Tt : Trend component.

Pt : Periodic component.

Dt: dependent stochastic component.

N: No. of observations

The first three components represent the deterministic part which is exactly determined by some mathematical function, while the fourth component represents the non-deterministic part (stochastic part) which is described only in terms of the probability distribution **[11]**.

Short-term forecasting is used in the water quality systems for operation purposes. Forecasting can be useful by extrapolating the momentum that exist in the phenomena because it provides, most often, an accurate and reliable forecasters. Seasonality can also be predicted fairly well **[2]**.

Exponential smoothing is a class of methods that imply exponentially decreasing weights as the observation get older. There are a variety of exponential smoothing methods, but they all have in common the property that recent values are given relatively more weight in forecasting than the older observations. Method of exponential smoothing takes the forecast for the previous period and adjusts it using the forecast error, then:

$$F_{1+1} = W\ X_t + (1-W)\ F_t \quad \text{.....} \quad (2)$$

Where:
Xt : Observation at time (t)
Ft : Forecast value at time (t)
Ft+1 : Forecast value at time (t+1)
W : Damped factor in exponential smoothing method (between 0 and 1)

The new forecast will include a substantial adjustment for the error in the previous forecast. Conversely, when (W) is close to zero, the new forecast will include very little adjustment **[2]**. To find the optimal value for (W), It must minimize the mean square error (MSE) between the observation and the forecasted values.

$$MSE = \frac{\sum_{t=1}^{N} (X_t - F_t)^2}{N} \quad \text{.....} \quad (3)$$

Exponential smoothing works best for data, which have no trend, no seasonality, or other underlying pattern.

Holt **[5]** extended the exponential smoothing to linear exponential smoothing to allow forecasting of data with trends. The forecast was found by using two smoothing factors (W1) for level and (W2) for trend. Each ranges between zero and one.

$$L_t = W1\ X_t + (1-W1)(L_{t-1} + T_{t-1}) \quad \text{.....} \quad (4)$$

$$T_t = W2(L_t - L_{t-1}) + (1-W2)T_{t-1} \quad \text{.....} \quad (5)$$

$$F_{t+1} = L_t + T_t \quad \text{.....} \quad (6)$$

Where:
Xt : Observation at time (t)
Lt : Level at time (t) in Holt's linear method
Tt : Trend at time (t) in Holt's linear method

Ft+1 : Forecast value at time (t+1)
W1 : Smoothing factor for level in Holt's linear method
W2 : Smoothing factor for trend in Holt's linear method

The initialization process requires two estimations: one for finding (L1) and the other for finding (T1). This can be done by use the assumptions suggested by Holt **[5]**:

$$L_1 = X_1 \quad (7)$$

$$T_1 = |X_2 - X_1| \quad (8)$$

To find the optimal values for (W1) and (W2), we must minimize the mean square error (MSE) between the observation and forecast values by using equation (3).

Holt's method was extended by Winters **[6]** to capture seasonality directly. The method is based on three smoothing equations, one for the level, one for trend, and one for seasonality **[2]**. The basic equations for the method are:

$$L_t = W1\frac{X_t}{S_{t-s}} + (1 - W1)(L_{t-1} + T_{t-1}) \quad (9)$$

$$T_t = W2(L_t - L_{t-1}) + (1 - W2)T_{t-1} \quad (10)$$

$$S_t = W3\frac{X_t}{L_t} + (1 - W3)S_{t-s} \quad (11)$$

$$F_{t+1} = (L_t + T_t)S_{t+1-s} \quad (12)$$

Where:
Xt : Observation at time (t)
Lt : Level at time (t) in Holt-Winters' method
Tt : Trend at time (t) in Holt-Winters' method
St : Seasonality at time (t) in Holt-Winters' method
Ft+1 : Forecast value at time (t+1)
W1 : Smoothing factor for level in Holt-Winters' method
W2 : Smoothing factor for trend in Holt-Winters' method
W3 : Smoothing factor for seasonality in Holt-Winters' method
s : Season interval (for monthly data: s=12)

To initialize the method, It needs initial values of the level (Lt), the trend (Tt), and the seasonal. To determine initial estimates of the seasonal indices it needs to use one complete season's data **[2]**. Therefore we initialize trend and level at period (s).

The level is initialized by taking the average of the first season:

$$L_s = \frac{1}{s}\left(X_1 + X_2 + \ldots.. + X_s\right) \quad (13)$$

To initialize trend, it is convenient to use two complete seasons as follows:

$$T_s = \frac{1}{s}\left[\frac{X_{s+1} - X_1}{s} + \frac{X_{s+2} - X_2}{s} + \ldots. + \frac{X_{s+s} - X_s}{s}\right] \quad (14)$$

Finally, the seasonal indices are initialized using the ratio of the first few data values to the mean of the first year, so:

$$S_1 = \frac{X_1}{L_s}, \qquad S_2 = \frac{X_2}{L_s}, \qquad \ldots\ldots \qquad S_s = \frac{X_s}{L_s} \quad \ldots\ldots\ldots\ldots\ldots\ldots\ldots\ldots (15)$$

To find the optimal values for (W1), (W2), and (W3) it must minimize the mean square error (MSE) between the observations and forecasted values by using equation (3) after two seasons **[2]**.

Modeling of the Sulfate Concentrations

The problem, which arises in the use of any statistical analysis, is the missing data values **[11]**. These gaps should be filled before starting the data analysis. Among many methods available to obtain a missing value, linear interpolation procedure was used for filling the gaps in the data series to complete the historical records of each station using the (SPSS) software. The parameters (W1, W2, and W3) of Holt-Winters' method are shown in Table (1). Were:

R : Raw water
S : Supply water
Min : Minimum
Max : Maximum

Table (1) : Holt-Winters' model parameters for sulfate parameter

Month	Prameters		Karkh T. P.	Sharq Dijlah T. P.	Karama T. P.	Wathba T. P.	Qadisiya T. P.	Dora T. P.	Rasheed T. P.
			Min	Min	Min	Min	Min	Min	Min
1	W1	R	0.5	0.3	0.3	0.9	1.0	0.8	0.3
	W2	R	0.0	0.0	0.0	0.0	0.0	0.0	0.3
	W3	R	0.2	0.1	0.4	1.0	0.0	0.4	0.4
2	W1	R	0.5	1.0	0.3	1.0	1.0	0.8	0.2
	W2	R	0.0	0.0	0.0	0.0	0.0	0.0	0.0
	W3	R	0.2	0.0	0.6	0.0	0.0	0.4	0.3
3	W1	R	0.5	0.3	0.3	1.0	0.6	1.0	0.3
	W2	R	0.0	0.0	0.0	0.0	0.0	0.0	0.0
	W3	R	0.9	0.4	0.8	0.0	0.9	0.0	0.1
4	W1	R	1.0	1.0	0.7	1.0	1.0	0.9	0.6
	W2	R	0.0	0.0	0.0	0.0	0.0	0.0	0.0
	W3	R	0.0	0.9	1.0	0.0	0.3	1.0	0.7
5	W1	R	0.6	1.0	0.6	0.9	1.0	1.0	0.7
	W2	R	0.0	0.0	0.0	0.0	0.0	0.0	0.0
	W3	R	1.0	0.2	1.0	1.0	0.0	0.0	0.7
6	W1	R	0.6	1.0	0.5	1.0	1.0	0.9	0.7
	W2	R	0.0	0.0	0.0	0.0	0.0	0.0	0.0
	W3	R	0.7	0.1	1.0	0.1	0.0	1.0	0.4
7	W1	R	0.6	0.5	0.5	0.7	0.8	0.8	0.6
	W2	R	0.0	0.0	0.0	0.0	0.0	0.0	0.0
	W3	R	1.0	0.7	1.0	0.8	1.0	0.0	0.7
8	W1	R	1.0	1.0	0.5	1.0	1.0	0.8	0.6
	W2	R	0.0	0.0	0.0	0.0	0.0	0.0	0.0
	W3	R	0.0	0.2	0.9	0.0	0.6	0.0	0.5
9	W1	R	0.9	0.9	0.5	1.0	1.0	0.7	0.5
	W2	R	0.0	0.0	0.0	0.0	0.0	0.0	0.0
	W3	R	1.0	1.0	0.9	0.0	0.0	0.0	0.4
10	W1	R	0.8	1.0	0.5	1.0	1.0	0.7	0.6
	W2	R	0.0	0.0	0.0	0.0	0.0	0.0	0.0
	W3	R	1.0	0.0	0.9	0.3	0.8	0.0	0.7
11	W1	R	0.8	1.0	0.5	1.0	0.8	0.5	0.9
	W2	R	0.0	0.0	0.0	0.0	0.0	0.0	0.0
	W3	R	1.0	0.2	0.8	0.0	1.0	0.4	0.1
12	W1	R	1.0	0.6	0.6	1.0	1.0	1.0	1.0
	W2	R	0.0	0.0	0.0	0.0	0.9	0.0	0.0
	W3	R	0.0	0.7	0.9	0.1	0.0	0.0	0.0

Month	Prameters		Karkh T. P.	Sharq Dijlah T. P.	Karama T. P.	Wathba T. P.	Qadisiya T. P.	Dora T. P.	Rasheed T. P.
			Max	Max	Max	Max	Max	Max	Max
1	W1	R	0.6	0.4	0.3	0.5	0.5	0.5	0.3
	W2	R	0.0	0.0	0.0	0.0	0.0	0.0	0.0
	W3	R	0.5	0.2	1.0	0.8	1.0	0.7	1.0
2	W1	R	0.5	0.5	0.3	0.5	0.9	0.5	0.4
	W2	R	0.0	0.0	0.0	0.0	0.0	0.0	0.0
	W3	R	0.4	0.1	1.0	0.9	1.0	0.6	1.0
3	W1	R	0.6	0.4	0.3	0.8	0.9	0.5	0.4
	W2	R	0.0	0.0	0.0	0.0	0.0	0.0	0.0
	W3	R	0.6	0.4	1.0	1.0	1.0	0.6	1.0
4	W1	R	1.0	0.3	0.3	0.7	0.8	0.5	0.3
	W2	R	0.0	0.0	0.0	0.0	0.0	0.0	0.0
	W3	R	0.0	0.7	1.0	1.0	1.0	0.5	1.0
5	W1	R	0.7	0.9	0.3	0.8	0.7	0.4	0.3
	W2	R	0.0	0.0	0.0	0.0	0.0	0.0	0.0
	W3	R	0.5	1.0	1.0	1.0	1.0	1.0	1.0
6	W1	R	0.6	0.6	0.3	0.6	0.9	0.7	0.4
	W2	R	0.0	0.0	0.0	0.0	0.0	0.0	0.0
	W3	R	0.2	0.7	0.9	1.0	1.0	1.0	1.0
7	W1	R	0.5	0.5	0.3	0.4	0.7	0.6	0.3
	W2	R	0.0	0.0	0.0	0.0	0.0	0.0	0.0
	W3	R	0.7	0.6	1.0	1.0	1.0	1.0	1.0
8	W1	R	1.0	0.6	0.3	0.5	0.7	0.5	0.4
	W2	R	0.0	0.0	0.0	0.0	0.0	0.0	0.0
	W3	R	0.0	0.8	1.0	1.0	1.0	1.0	1.0
9	W1	R	0.9	0.6	0.3	0.4	0.9	0.5	0.4
	W2	R	0.0	0.0	0.0	0.0	0.0	0.0	0.0
	W3	R	1.0	0.7	1.0	0.9	1.0	0.9	1.0
10	W1	R	1.0	0.6	0.3	0.4	0.8	0.5	0.4
	W2	R	0.0	0.0	0.0	0.0	0.0	0.0	0.0
	W3	R	0.0	0.8	1.0	0.8	1.0	0.7	1.0
11	W1	R	1.0	1.0	0.3	0.8	1.0	1.0	0.5
	W2	R	0.0	0.0	0.0	0.0	0.0	0.0	0.0
	W3	R	0.0	0.0	1.0	1.0	0.0	0.0	0.7
12	W1	R	0.8	1.0	0.5	1.0	1.0	0.3	0.6
	W2	R	0.0	0.0	0.0	0.0	0.0	0.0	0.0
	W3	R	1.0	0.0	1.0	0.0	0.0	0.6	0.6

Table (1) : Continued

Month	Prameters		Karkh T. P.	Sharq Dijlah T. P.	Karama T. P.	Wathba T. P.	Qadisiya T. P.	Dora T. P.	Rasheed T. P.
			Min	Min	Min	Min	Min	Min	Min
1	W1	S	0.7	0.3	0.3	0.9	1.0	0.7	0.3
	W2	S	0.0	0.0	0.0	0.0	0.0	0.0	0.0
	W3	S	0.0	0.1	0.8	1.0	0.0	0.7	0.4
2	W1	S	0.6	0.3	0.5	1.0	0.4	0.8	0.2
	W2	S	0.0	0.0	0.0	0.0	0.0	0.0	0.0
	W3	S	0.1	0.2	0.7	0.0	0.8	0.6	0.4
3	W1	S	0.5	0.3	0.3	0.9	0.3	0.8	0.3
	W2	S	0.0	0.0	0.0	0.0	0.0	0.0	0.0
	W3	S	0.4	0.4	0.7	1.0	1.0	0.7	0.5
4	W1	S	1.0	0.3	0.9	1.0	0.4	0.9	0.5
	W2	S	0.0	0.0	0.0	0.0	0.0	0.0	0.0
	W3	S	0.0	0.4	1.0	0.0	1.0	1.0	1.0
5	W1	S	0.6	1.0	0.8	0.9	0.4	0.7	0.7
	W2	S	0.0	0.0	0.0	0.0	0.0	0.0	0.0
	W3	S	1.0	0.0	1.0	1.0	1.0	1.0	1.0
6	W1	S	0.6	0.9	0.7	0.9	0.4	0.7	0.7
	W2	S	0.0	0.0	0.0	0.0	0.0	0.0	0.0
	W3	S	0.9	1.0	1.0	1.0	1.0	1.0	1.0
7	W1	S	0.5	0.6	0.6	0.7	0.4	0.5	0.6
	W2	S	0.0	0.0	0.0	0.0	0.0	0.0	0.0
	W3	S	1.0	1.0	1.0	1.0	1.0	0.8	1.0
8	W1	S	1.0	0.6	0.6	1.0	0.4	0.5	0.6
	W2	S	0.0	0.0	0.0	0.0	0.0	0.0	0.0
	W3	S	0.0	1.0	0.9	0.0	1.0	0.8	1.0
9	W1	S	0.8	0.7	0.7	1.0	0.4	0.4	0.6
	W2	S	0.0	0.0	0.0	0.0	0.0	0.0	0.0
	W3	S	1.0	1.0	1.0	0.0	1.0	0.6	0.8
10	W1	S	0.8	0.7	0.7	1.0	0.4	0.4	0.6
	W2	S	0.0	0.0	0.0	0.0	0.0	0.0	0.0
	W3	S	1.0	1.0	1.0	0.0	0.9	0.5	1.0
11	W1	S	0.7	0.7	0.7	1.0	0.4	0.4	0.7
	W2	S	0.0	0.0	0.0	0.0	0.0	0.0	0.0
	W3	S	1.0	1.0	1.0	0.6	1.0	0.7	0.8
12	W1	S	0.6	0.8	0.8	1.0	0.4	0.4	0.9
	W2	S	0.0	0.0	0.0	0.0	0.0	0.0	0.0
	W3	S	1.0	1.0	1.0	0.0	1.0	0.5	1.0

Month	Prameters		Karkh T. P.	Sharq Dijlah T. P.	Karama T. P.	Wathba T. P.	Qadisiya T. P.	Dora T. P.	Rasheed T. P.
			Max	Max	Max	Max	Max	Max	Max
1	W1	S	0.5	0.4	1.0	0.6	0.4	0.4	0.3
	W2	S	0.0	0.0	0.0	0.0	0.0	0.0	0.0
	W3	S	0.6	0.8	0.0	0.9	1.0	0.9	0.9
2	W1	S	0.5	0.4	0.3	0.6	1.0	0.4	0.3
	W2	S	0.0	0.0	0.0	0.0	0.0	0.0	0.0
	W3	S	0.4	0.5	0.8	1.0	0.0	0.8	0.8
3	W1	S	0.5	0.3	0.3	0.9	1.0	0.4	0.3
	W2	S	0.0	0.0	0.0	0.0	0.0	0.0	0.0
	W3	S	0.7	0.6	0.9	1.0	0.0	0.8	0.8
4	W1	S	1.0	0.3	0.3	0.9	1.0	0.5	0.3
	W2	S	0.0	0.0	0.0	0.0	0.0	0.0	0.0
	W3	S	0.0	0.6	0.9	1.0	0.0	0.7	0.9
5	W1	S	0.6	0.4	0.4	1.0	0.8	0.3	0.4
	W2	S	0.0	0.0	0.0	0.0	0.0	0.0	0.0
	W3	S	1.0	0.7	0.8	0.2	1.0	1.0	1.0
6	W1	S	0.6	0.5	0.3	0.7	1.0	0.6	0.5
	W2	S	0.0	0.0	0.0	0.0	0.0	0.0	0.0
	W3	S	0.8	0.6	0.7	1.0	0.6	1.0	1.0
7	W1	S	0.5	0.5	0.3	0.4	0.8	0.5	0.3
	W2	S	0.0	0.0	0.0	0.0	0.0	0.0	0.0
	W3	S	0.8	0.6	0.8	1.0	1.0	0.8	1.0
8	W1	S	0.7	0.6	0.2	0.5	1.0	0.4	0.5
	W2	S	0.0	0.0	0.0	0.0	0.0	0.0	0.0
	W3	S	1.0	0.8	0.7	1.0	0.0	1.0	1.0
9	W1	S	0.7	0.7	0.3	0.5	0.9	0.5	0.5
	W2	S	0.0	0.0	0.0	0.0	0.0	0.0	0.0
	W3	S	1.0	1.0	0.7	1.0	1.0	0.7	1.0
10	W1	S	0.7	0.8	0.3	0.5	0.7	0.4	0.4
	W2	S	0.0	0.0	0.0	0.0	0.0	0.0	0.0
	W3	S	1.0	1.0	0.7	1.0	1.0	0.5	0.9
11	W1	S	1.0	1.0	0.3	1.0	0.9	0.8	0.7
	W2	S	0.0	0.0	0.0	0.0	0.0	0.0	0.0
	W3	S	0.0	0.0	0.6	0.3	1.0	0.3	0.6
12	W1	S	0.6	0.9	0.4	1.0	1.0	0.2	0.6
	W2	S	0.0	0.0	0.0	0.0	0.0	0.0	0.0
	W3	S	1.0	1.0	0.7	0.0	0.0	0.8	0.4

Results and Discussion

For checking the Holt-Winters' model, the generated data are tested with those of the observed series (2004) using (t-test) and (F-test) at 95% level of significant as shown in Table (2).

Table (2) : Comparison between means and standard deviations of observed data and generated by Holt-Winters' model for sulfate parameter

		Karkh T. P.	Sharq Dijlah T. P.	Karama T. P.	Wathba T. P.	Qadisiya T. P.	Dora T. P.	Rasheed T. P.
		Min	Min	Min	Min	Min	Min	Min
t calculate	R	1.18	1.46	0.98	0.87	1.33	2.55	1.68
t tabulate	R	2.07	2.07	2.07	2.07	2.07	2.07	2.07
t-Test Result	R	Homog.	Homog.	Homog.	Homog.	Homog.	Not Homog.	Homog.
F calculate	R	3.63	1.36	1.47	1.05	3.75	1.66	3.29
F tabulate	R	2.82	2.82	2.82	2.82	2.82	2.82	2.82
F-Test Result	R	Not Homog.	Homog.	Homog.	Homog.	Not Homog.	Homog.	Not Homog.
		Max	Max	Max	Max	Max	Max	Max
t calculate	R	1.65	2.10	0.86	1.96	1.17	0.64	0.96
t tabulate	R	2.07	2.07	2.07	2.07	2.07	2.07	2.07
t-Test Result	R	Homog.	Not Homog.	Homog.	Homog.	Homog.	Homog.	Homog.
F calculate	R	2.83	3.18	1.30	2.62	5.56	1.30	1.05
F tabulate	R	2.82	2.82	2.82	2.82	2.82	2.82	2.82
F-Test Result	R	Not Homog.	Not Homog.	Homog.	Homog.	Not Homog.	Homog.	Homog.
		Min	Min	Min	Min	Min	Min	Min
t calculate	S	1.28	1.05	1.27	0.46	1.97	1.34	1.24
t tabulate	S	2.07	2.07	2.07	2.07	2.07	2.07	2.07
t-Test Result	S	Homog.	Homog.	Homog.	Homog.	Homog.	Homog.	Homog.
F calculate	S	1.63	1.59	1.87	1.03	1.29	1.15	2.36
F tabulate	S	2.82	2.82	2.82	2.82	2.82	2.82	2.82
F-Test Result	S	Homog.	Homog.	Homog.	Homog.	Homog.	Homog.	Homog.
		Max	Max	Max	Max	Max	Max	Max
t calculate	S	1.10	1.86	1.53	2.04	1.41	0.52	1.07
t tabulate	S	2.07	2.07	2.07	2.07	2.07	2.07	2.07
t-Test Result	S	Homog.	Homog.	Homog.	Homog.	Homog.	Homog.	Homog.
F calculate	S	2.41	3.61	2.59	2.22	4.85	1.31	1.65
F tabulate	S	2.82	2.82	2.82	2.82	2.82	2.82	2.82
F-Test Result	S	Homog.	Not Homog.	Homog.	Homog.	Not Homog.	Homog.	Homog.

Figure (2) shows the comparison between monthly observed and generated Sulfate concentrations by Holt-Winters' model. The figure indicates that the Holt-Winters' model is capable of preserving the monthly means for all Sulfate quality parameter.

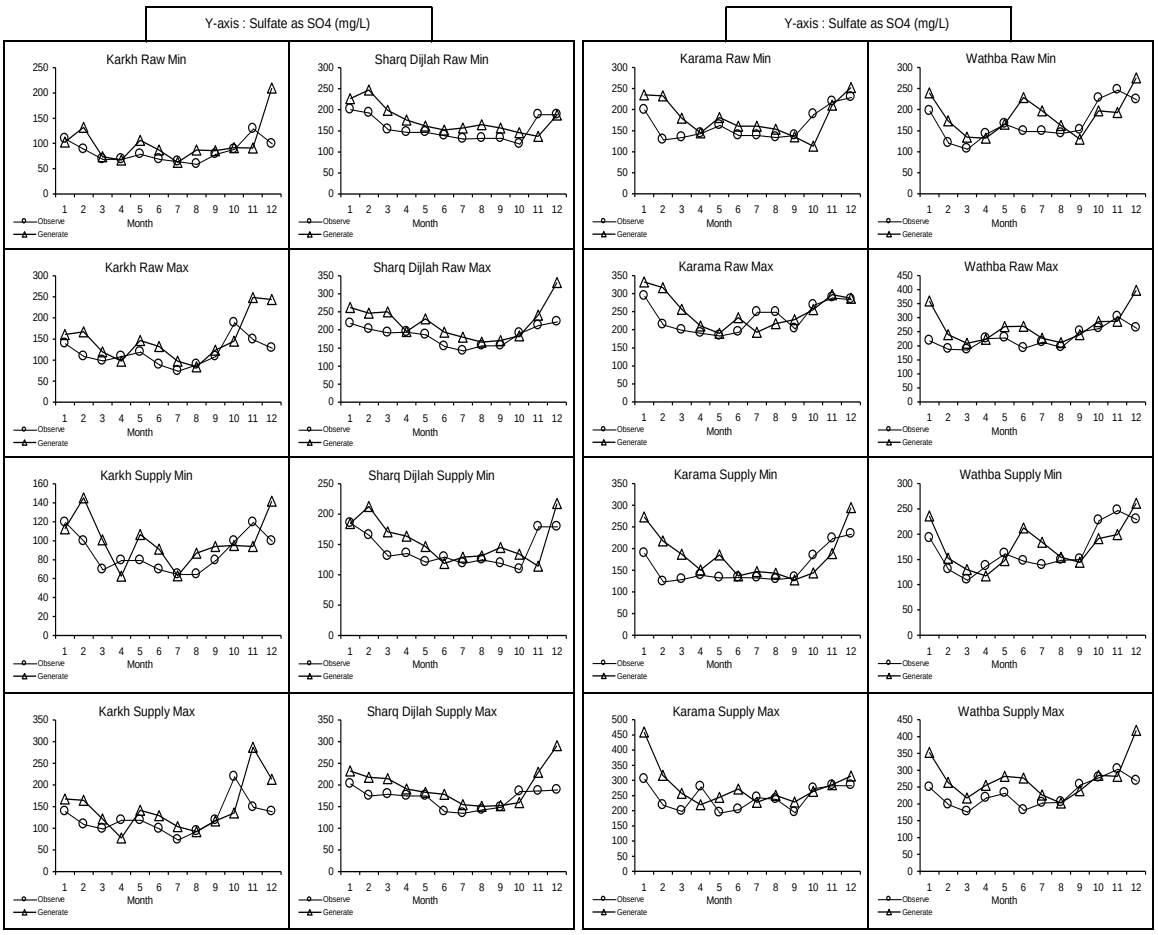

Figure (2) : Comparison between monthly observed data and generated by Holt-Winters' model for sulfate parameter

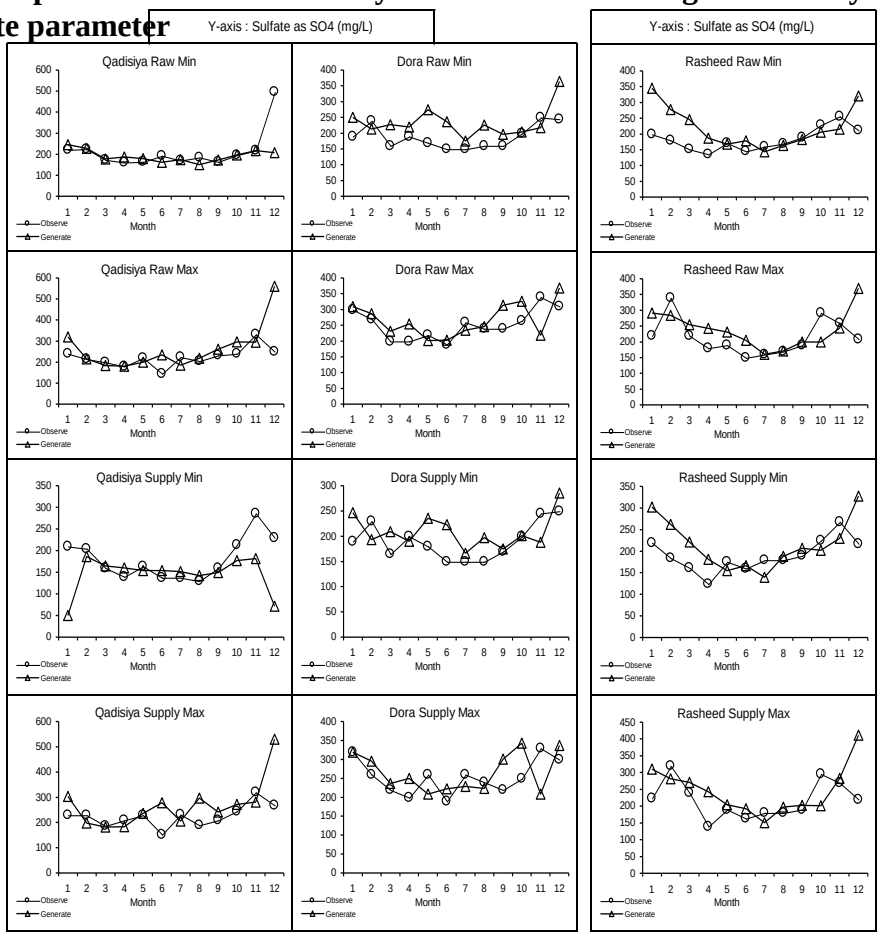

CONCLUSIONS

* Comparisons between means of observed data and generated series by Holt-Winters' model were reflected the applicability of this model for short-term forecasting, except the case of minimum records of Dora station and maximum records of Sharq Dijlah station due to the different sources of pollutions along the river which dispose their waste into it and change the concentrations in the water, therefore the randomness is increased.
* Comparisons between standard deviations of observed data and generated were reflected the applicability of this model for short-term forecasting, except some cases as shown in Table (3).

Table (3) : Failure cases of comparisons between standard deviations of observed and generated data.

Extreme Type	Water Type	Treatment Plant
Min	R	Karkh
Min	R	Qadisiya
Min	R	Rasheed
Max	R	Karkh
Max	R	Sharq Dijlah
Max	R	Qadisiya
Max	S	Sharq Dijlah
Max	S	Qadisiya

1. Most of the extreme values of the observed series and those of the generated series were found to exceed the allowable limits according to Iraqi and EEC specifications.

REFERENCES

- *Box, G.E.P.; Jenkins, G.M. and Reinsel, G.C.* : **"Time Series Analysis : Forecasting and Control"**. 3rd Ed., Englewood Cliffs, NJ: Prentice-Hall. 1994.

- *Makridakis, S.; Wheelwright, S.C. and Hyrdman, R.J.* : **"Forecasting : Methods and Applications"**. John Wiley & Sons, Inc., USA. 1998.

- *Abuhamdeh, M.R.M.* : **"Study of Tigris Water Quality and Treated Water at The Water Treatment Plants for Baghdad City"**. M.Sc. Thesis, College of Engineering, University of Baghdad. 2000.

- *Brown, R.G.* : **"Exponential Smoothing for Predicting Demand"**. New York: McGraw Hill.1956.

- *Holt, C.C.* : **" Forecasting Trends and Seasonal by Exponentially Weighted Averages"**. Office of Naval Research, Research Memorandom.1957.

- *Winters, P.R.* : **"Forecasting Sales by Exponentially Weighted Moving Averages"**. Management Science, 6, 324-342.1960.

- *Harrison, P.J. and Stevens, C.F.* : **"Bayesian Forecasting (With Discussion)"**. Journal of the Royal Statistical Society, Ser. B, 38, 205-247. 1976.

- *Snyder R.D.* : **"Recursive Estimation of Dynamic Linear Models"**. Journal of the Royal Statistical Society, Ser B, 47, 272-76. 1985.

- *Hyndman, R.J.; Koehler, A.B.; Snyder, R.D. & Grose, S.* : **"A State Space Framework for Automatic Forecasting Using Exponential Smoothing Methods"**. International Journal of Forecasting, 18, 439-454. 2002.

- *Baki B.; Maxwell L.K.; Ralph D.S. and Anne B.K.* : **"Exponential Smoothing Model Selection for Forecasting"**. Department of Econometrics and Business Statistics, MONASH University, Australia. Mar., 2005.

- *Al-Suhaili, R.H.* : **"Stochastic Analysis of Daily Streamflow of Tigris River"**. M.Sc. Thesis, College of Engineering, University of Baghdad. 1986.

PREDICTION OF TURBIDITY IN TIGRIS RIVER USING ARTIFICIAL NEURAL NETWORKS

Rafa H. Al-Suhaili Waleed M.S.Kassim Yousif M.Yousif
Department of Environmental Engineering / College of Engineering /
Baghdad University.

ABSTRACT

Over the past two decades, there has been an increased interest in a new class of computational intelligence systems known as Artificial Neural Networks (ANNs). In this work, (ANNs) technique was applied in an attempt to predict the turbidity at intake of Al-Wathba water treatment plant (WTP) in Baghdad. This prediction is useful in the planning, evaluation, management, and operation of such plants, which may produce water of better quality. The available records from (1991-2000) were used for predicting turbidity in Tigris River, based on monthly maximum values of the water quality parameters near intakes of the water treatment plants. Multi-layer perceptron trainings using the back-propagation algorithm were used in this work. The feasibility of ANNs technique for modeling this water quality parameter was investigated. A number of issues in relation to ANNs construction such as the effect of ANNs geometry and internal parameters on the performance of ANNs model were investigated. It was found that ANNs have the ability to predict the Turbidity at Al-Wathba WTP with a good degree of accuracy (the coefficient of determination (R^2) was 0.9687). The ANNs model developed to study the impact of the internal network parameters on model performance indicate that ANNs performance was relatively insensitive to the number of hidden layer nodes, momentum term, and learning rate.

INTRODUCTION

Water quality control and management have attached increasing attention from developing countries. The aspects of environmental protection are becoming a major obstacle for further and sustainable economic and social development. The use of raw water quality data cannot be over looked, since such data have considerable effect on the calculation of needed chemical, proper management, treatment, and assessing the potentialities of the use of furnished water supplies for different purposes, **(Barzanjy, 2007).**

Traditionally, there have been two main philosophical approaches for surface water quality modeling. Process based models, which consider the underlying physical processes directly, and statistical models, which determine relationships based on historical data sets. Recently, artificial neural networks (ANNs) have emerged as alternatives to traditional statistical models in a variety of fields, including water quality management, (Maier and Dandy, 2000).

ANNs are one of the modeling techniques that attempt to simulate the operation of the human brain and nervous systems. ANNs learn by 'example' in which an actual measured set of input variables and the corresponding outputs are presented to determine the rules that govern the relationship between variables. Consequently, ANNs are well suited to modeling complex problems where the relationship between the variables is unknown and when non-linearity is suspected. Although, the concept of artificial neurons was first introduced in 1943 by McCulloch and Pitts, research into applications of ANNs has blossomed since the introduction of the back-propagation-training algorithm for feed forward ANNs in 1986. ANNs may thus be considered a relatively new tool in the field of prediction and forecasting, (Shahin et. al. 2003).

AREA AND OBJECTIVE OF THE STUDY

The Tigris River has a large importance in the present and in the future. This is because of the detrimental effect of pollutants resulting from human activities, industrial wastes, sewage wastes, and harmful effect of increasing drainage waters coming from agricultural lands upstream coupled with the decrease in its discharge, **(Abu-Hamdeh, 2000).** So it has become necessary to make detailed studies and researches to evaluate the suitability of river water for different purposes in a selected site of the river.

Baghdad city was chosen for this study. Artificial neural network was applied to predict the turbidity at the intakes of the existing water treatment plants in Baghdad. The running conventional water treatment plants are (Karkh, Sharq Dijlah, Karama, Wathba, Qadisiya, Dora, and Rasheed) as shown in Fig. (1).

The records from (1991-2000) were used for predicting turbidity at Al-Wathba WTP of monthly maximum values for the water quality parameters near intakes of the water treatment plants.

The main objective of this study is the evaluation and management for some of the water quality parameters at intakes of the water treatment plants in Baghdad by using ANNs technique to predict the turbidity at intake of Al-Wathba water treatment plant in Baghdad.

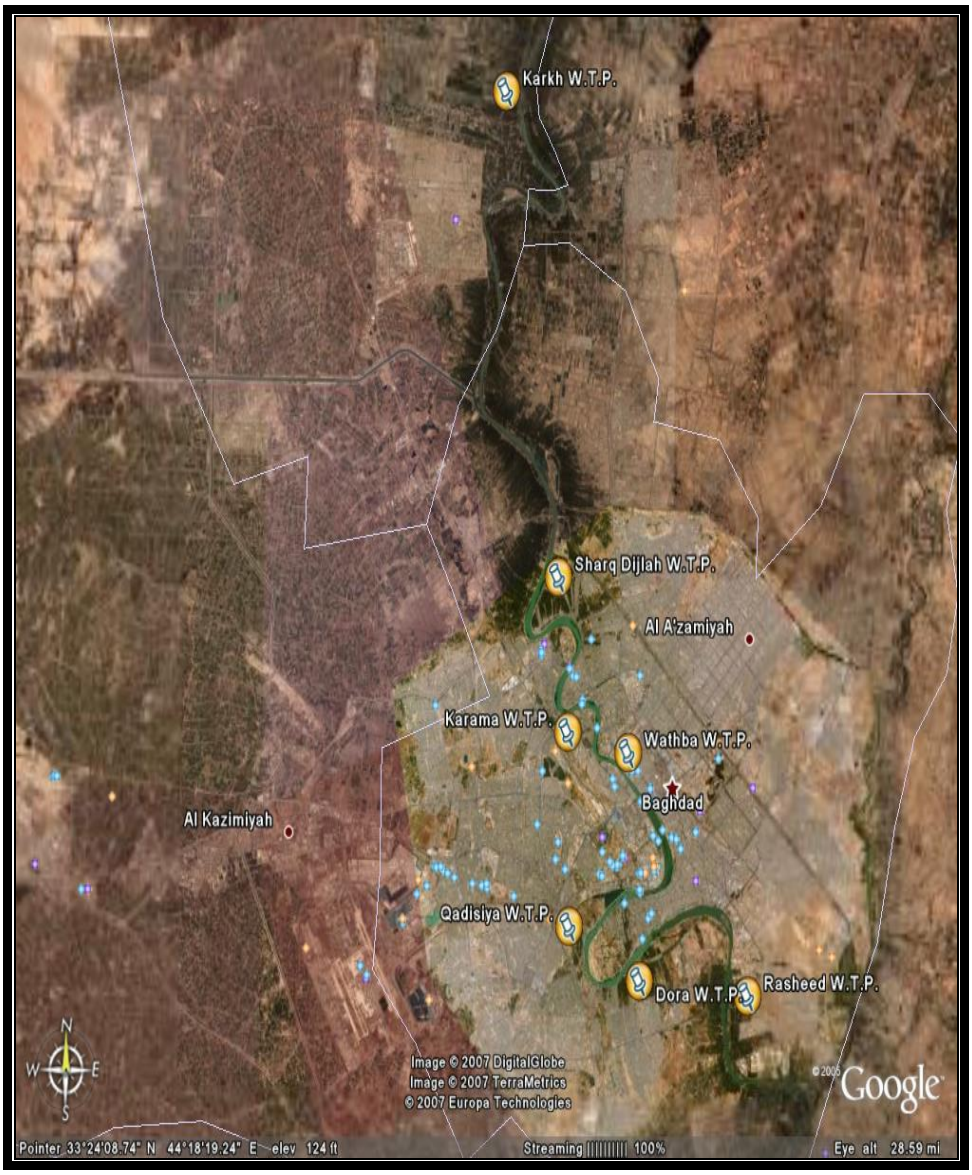

Fig. (1) View of the Study Area

DETERMINATION OF ARTIFICIAL NEURAL NETWORKS MODELS

Artificial neural networks (ANNs) models need to be in a systematic manner to improve its performance. Such an approach needs to address major factors such as, determination of model inputs, data division and pre-processing, determination of model architecture, model optimization (training), and model validation, **(Maier and Dandy, 2000).** These factors are explained and discussed below.

A PC-based commercial software system was used, called ***Neuframe*** program (Version 4.0) (Neusciences 2000, Neurosciences Crop., Southampton, Hampshire, U.K.). The optimal network architecture was determined by trail-and-error.

Determination of Model Inputs and Outputs

The selection of the model input variables that have the most significant impact on the model performance is an important step in developing ANNs models. Presenting as large a number of input variables as possible to ANNs models usually increases network size, resulting in a decrease in processing speed and a reduction in the efficiency of the network, **(Zaheer and Bai, 2003).**

Different approaches have been suggested to assist the selection of input variables. The approach that was adopted in this research based on priori knowledge, the appropriate input variables can be selected. This approach is usually utilized in the field of civil engineering, **(Maier and Dandy, 2000).**

The inputs of this model are:

- Flow of the river, Q.
- The Turbidity at Al-Karkh WTP, Tur-1.
- The Turbidity at Sharq Dijlah WTP, Tur-2.
- The Turbidity at Al-Karama WTP, Tur-3.
- Suspended Solid at Al-Karkh WTP, S.S-1.
- Suspended Solid at Sharq Dijlah WTP, S.S-2.
- Suspended Solid at Al-Karama WTP, S.S-3.
- The Distance between Al-Karkh and Al-Wathba WTP, D-1,4.
- The Distance between Sharq Dijlah and Al-Wathba WTP, D-2,4.
- The Distance between Al-Karama and Al-Wathba WTP, D-3,4.

The output of the model is the turbidity at Al-Wathba WTP**,** Tur-4.

DATA DIVISION AND PRE-PROCESSING

It is a common practice to divide the available data into three sets, training, testing, and validation. The training set is used to adjust the connection weights of the neural network. The testing set is used to check the performance of the network at various stages of learning, and training is stopped once the error in the testing set increases. The validation set is used to evaluate the performance of the model once training has been successfully accomplished. The way data are divided can have a significant effect on model performance, **(Al-Janabi, 2006**), and trail-and-error process was used to select the best division.

Once the available data have been divided into their subsets (i.e. training, testing and validation), it is important to pre-process the data in a suitable form before they applied to the ANNs. Data pre-processing is necessary to ensure all variables receive equal attention during the training process. Pre-processing can be in the form of data scaling, normalization and transformation. Thus, the logarithm of inputs and outputs of this model were taken (except the distances) before proceeding forward in the next steps.

DETERMINATION OF MODEL ARCHITECTURE

Determining the network architecture is one of the most important and difficult tasks in ANNs model development. It requires the selection of the optimum number of layers and the number of nodes in each of these layers. There is no unified theory for the determination of an optimal ANNs architecture. It is generally achieved by fixing the number of layers and choosing the number of nodes in each layer.

There are always two layers representing the input and output variables in any neural networks. It has been shown that one hidden layer is sufficient to approximate any continuous function provided that sufficient connection weights are given, **(Al-Neami, 2006).** The number of nodes in the input and output layers are restricted by the number of model inputs and outputs, respectively. There is no direct and precise way of determining the best number of nodes in each hidden layer. A trial-and-error procedure, which is generally used in civil engineering to determine the number and connectivity of the hidden layer nodes, can be used, **(Shahin et. al, 2002).**

(Resop, 2006) suggested that the upper limit of the number of hidden nodes in a single layer network may be taken as (2I+1), where I is the number of inputs. The best approach found by **(Nawari et. al, 1999)** was to start with a small number of nodes and to slightly increase the number until no significant improvement in model performance is achieved.

MODEL OPTIMIZATION (TRAINING)

As mentioned previously, the process of optimizing the connection weights is known as 'training' or 'learning'. This is equivalent to the parameter estimation phase in conventional statistical models. The aim is to find a global solution to what is typically a highly non-linear optimization problem. The method most commonly used for finding the optimum weight combination of feed-forward neural networks is the back-propagation algorithm, which is based on first-order gradient descent, **(Jun, 2002).** Ultimately, the model performance criteria, which are problem specific, will dictate which training algorithm is most appropriate. If training speed is not a major concern, there is no reason why the back-propagation algorithm cannot be used successfully.

MODEL VALIDATION

Once the training phase of the model has been successfully accomplished, the performance of the trained model should be validated. The purpose of the model validation phase is to ensure that the model has the ability to generalize within the limits set by the training data in a robust fashion, rather than simply having memorized the input-output relationships that are contained in the training data. The approach that is generally adopted in the research to achieve this is to test the performance of trained ANNs on an independent validation set, which has not been used as part of the model building process. If such performance is adequate, the model is deemed to be able to generalize and is considered to be robust. The training error and the testing error (carried out by ***Neuframe*** software) and the coefficient of correlation of validation set (r) are the main criteria that are often used to evaluate the prediction performance of ANNs models.

RESULTS AND DISCUSSION

The effect of data subsets divisions on performance of ANNs was investigated. Trail-and-error process was used to select the best division, the network that performs best with respect to testing error was used in this work. Using the default parameters of the software, a number of networks with different divisions were developed and the results are shown graphically in Fig. (2). It can be seen from Fig. (2) that the best division is 60 % for training set, 25 % for testing set, and 15 % for validation set, according to lowest testing error. Thus, this division was adopted in this model.

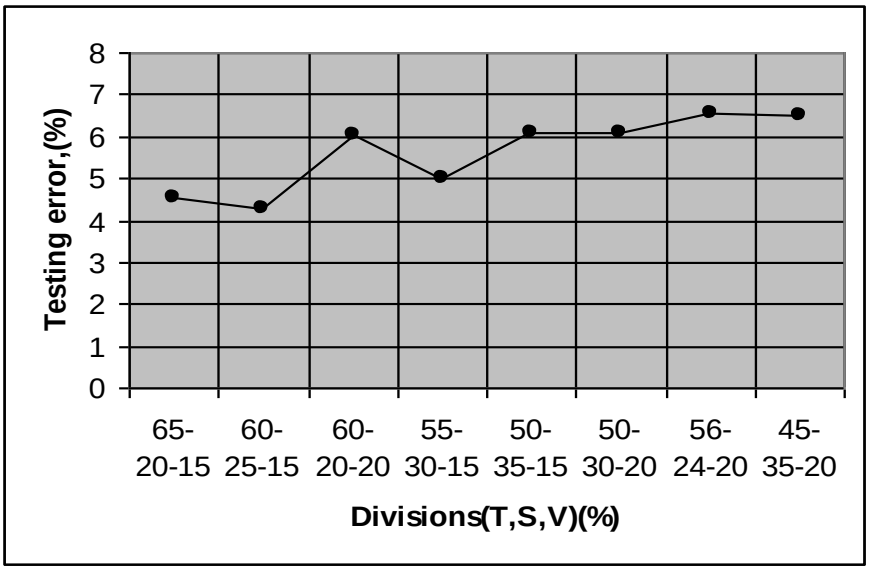

Fig. (2) Effect of data divisions on performance of ANNs

The effect of the number of hidden nodes on ANNs performance was investigated. A number of trials were carried out using the default parameters of the software used with one hidden layer and start with one hidden node and then slightly increasing the number of the nodes until no significant improvement in the model performance, was gained. a number of networks with different numbers of hidden layer nodes were developed and the results are shown graphically in Fig. (3). It can be seen from Fig. (3) that there are slightly differences in the testing error after 8 nodes. Therefore, the process was stopped at 10 nodes where no significant improvement in model performance, was found. Fig. (3) shows that the network with 3 hidden layer nodes has the lowest prediction error for testing test. However, it is believed that the network with 1 hidden layer node is considered optimal, as it is prediction error is not far from the network with 3 hidden layer nodes coupled with smaller number of connection weights. Therefore, 1 hidden layer node was chosen in this model.

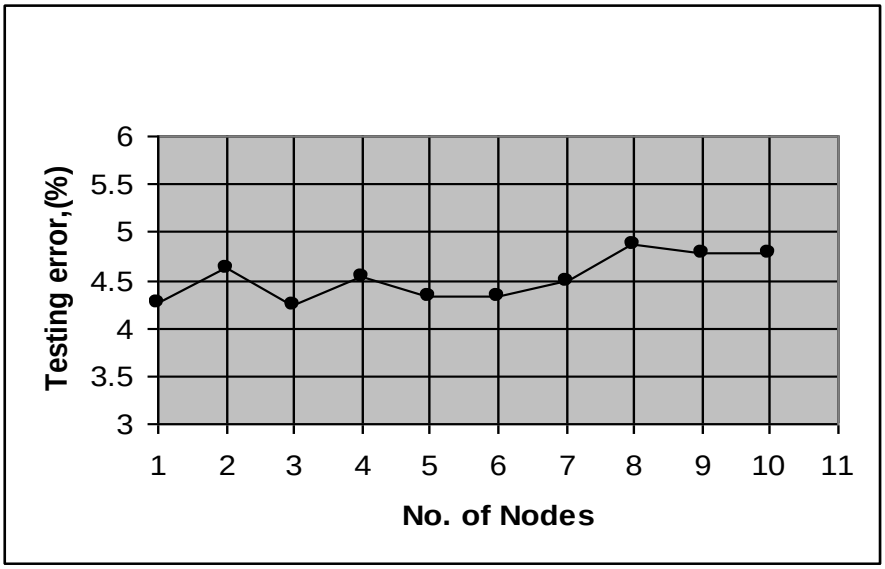

Fig. (3) Performance of ANNs model with different hidden layer nodes

The effect of the internal parameters controlling the back-propagation algorithm (i.e. momentum term and learning rate) on the model performance was investigated for the model with 1 hidden layer node. The effect of the momentum term on model performance is shown graphically in Fig (4). It can be seen that the performance of the ANNs model is relatively insensitive to the variation of the momentum term, particulary in the range 0.01 to 0.60. Then the testing errors slightly decrease at the range 0.80 to 0.95. Thus, the obtained optimum value for momentum term is 0.80, which have the lowest values of testing error and training error, hence it was used in this model.

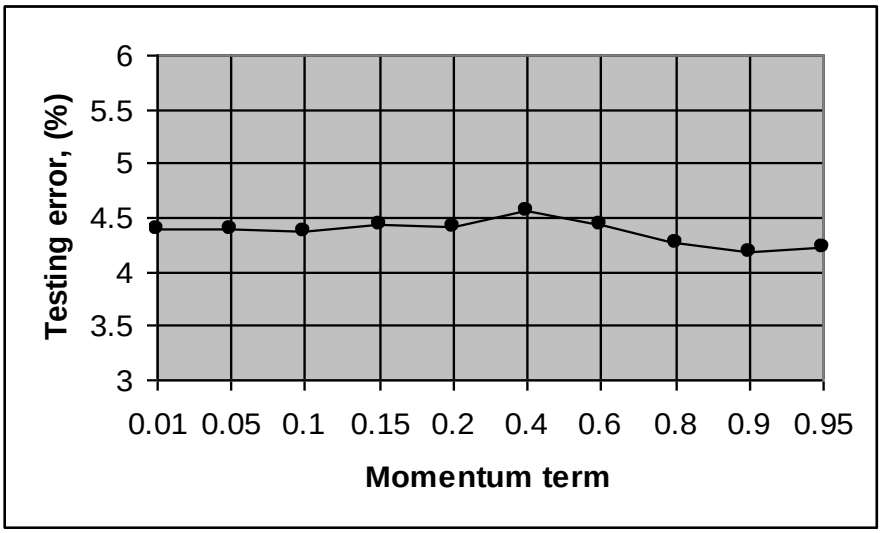

Fig. (4) Effect of various momentum term on ANNs performance

The effect of the learning rate on the model performance is shown graphically in Fig. (5). It can be seen that the performance of the ANNs model is relatively insensitive to the variation of the learning rate. The testing errors are slightly decreased at the range 0.10 to 0.40, while it is slightly increase at the range 0.60 to 0.99. Thus, the obtained optimum value for learning rate is 0.40, which has the lowest value of testing error, hence it was used in this model.

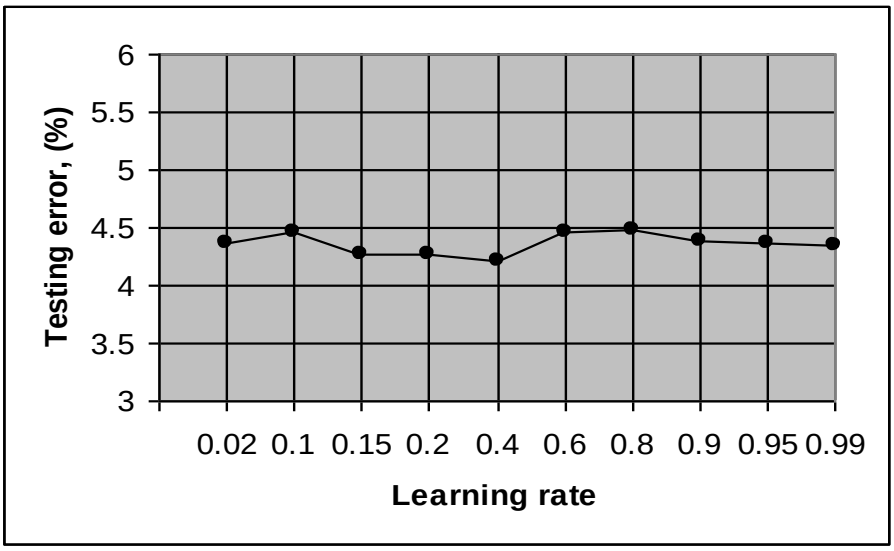

Fig. (5) Effect of various learning rate on ANNs performance

In an attempt to identify which of the input variables have the most significant impact on the

output predictions, a sensitivity analysis was carried out on the ANNs. A simple and innovative technique proposed by **(Garson, 1991)** was used to interpret the relative importance of the input variables by examining the connection weights of the trained network. The results indicate that the turbidity and suspended solid at Al-Karama WTP have the most significant effect on the predicted the turbidity at Al-Wathba WTP with a relative importance of 16.4 and 16.343 % respectively. The results also indicate that the turbidity and suspended solid upstream have a moderate impact on prediction, while the flow of the river and the distances between those water treatment plants have the smallest impact on the prediction, as shown in Fig. (6).

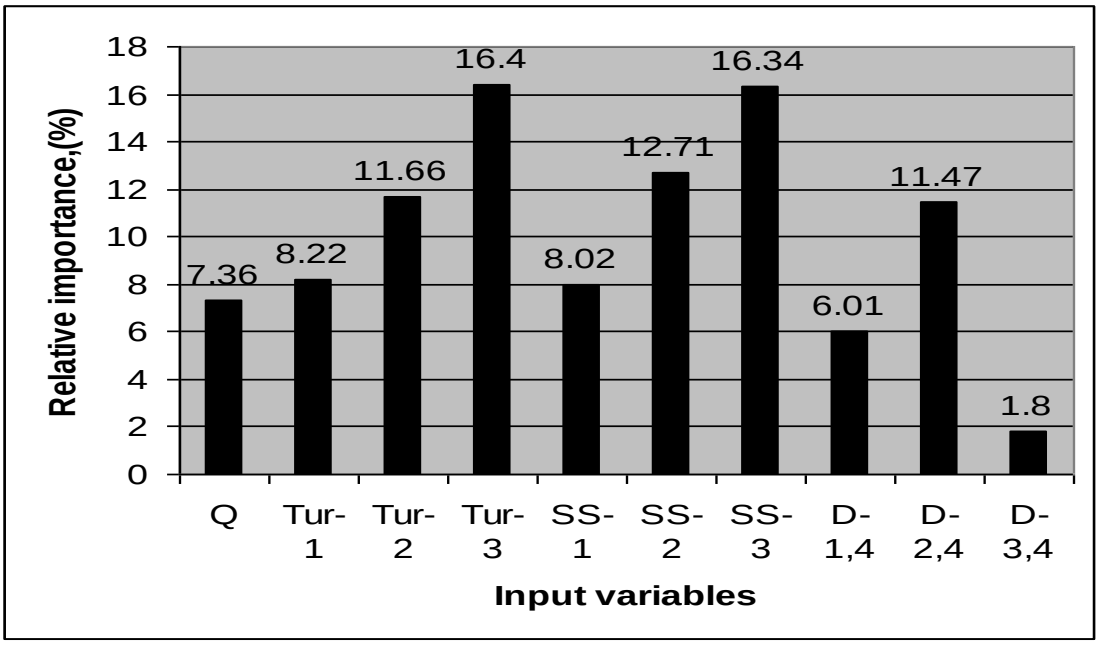

Fig. (6) Relative importance of the input variables

ANNS MODEL EQUATION

The small number of connection weights obtained by **Neuframe** for the optimal ANNs model enables the network to be translated into relatively simple formula. To demonstrate this, the structure of the ANNs model is shown in Fig. (7).

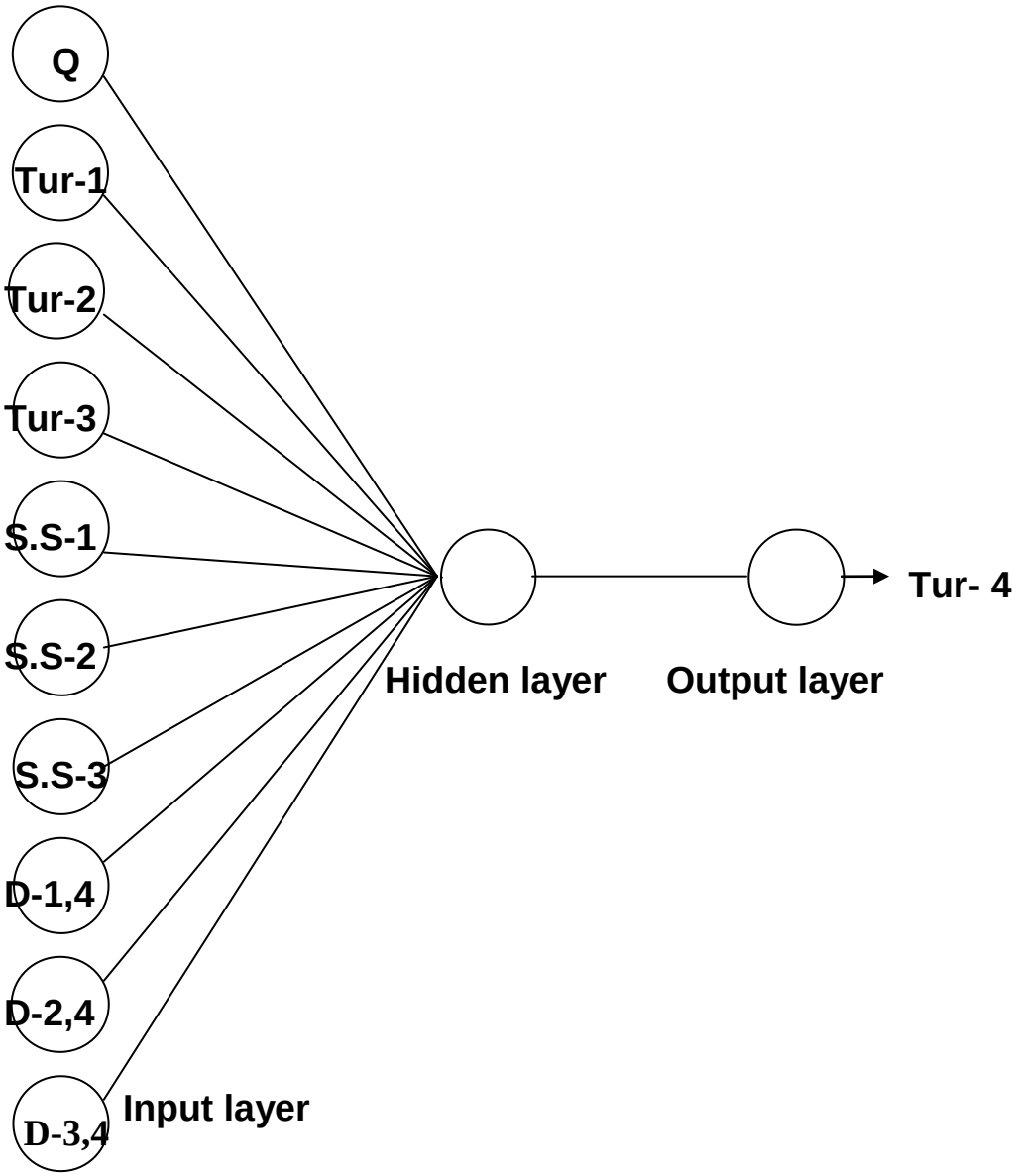

Fig. (7) Structure of the ANNs optimal model

The derived formula is as follows:

$$Tur-4 = \frac{2.699}{1+e^{(-1.7+5.595\tanh x)}} + 1.255 \quad \ldots\ldots\ldots\ldots\ldots\ldots\ldots\ldots\ldots\ldots\ldots (1)$$

Where:

x = 1.233 + 0.735Q - 0.139Tur_1 – 0.307Tur_2 - 0.22Tur_3 – 0.131S.S_1 -0.253S.S_2 – 0.339S.S_3 …… (2)

VALIDITY OF THE ANNS MODEL

To assess the validity of the ANNs model for the turbidity at Al-Wathba WTP (Tur-4), the predicted values of Tur-4 are plotted against the measured (observed) values of Tur-4 for validation data set, as shown in Fig. (8). It is clear from Fig. (8), the generalization capability of ANNs techniques using the validation data set. The coefficient of determination (R^2) is (96.87 %),

therefore it can be concluded that ANNs model show very good agreement with the actual measurements.

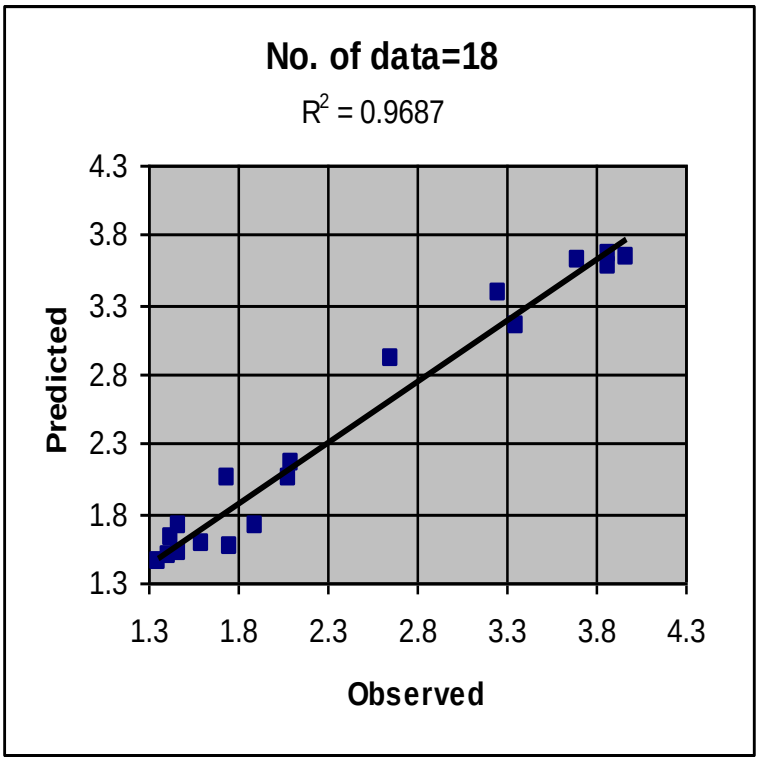

Fig. (8) Comparison of predicted and measured Tur-4 for validation data set

CONCLUSIONS

The results obtained from this work had yielded the following conclusions.

-ANNs have the ability to predict (Tur-4), with a very good degree of accuracy within the range of data used for developing ANNs models.

- The ANNs models developed to study the impact of the internal network parameters on model performance indicate that ANNs performance is insensitive to the number of hidden layer nodes, momentum terms, and learning rate (the optimal network usually achieved by trail and error process).

- The sensitivity analysis indicated that the parameters at Al-Karama WTP have the most significant effect on the prediction of the parameters at Al-Wathba WTP. The results also indicated that the parameters at further upstream of the river have a moderate impact on the prediction, while the flow of the river and the distances between those WTP have the smallest impact on the prediction.

- ANNs models could be translated into simple and practical formula from which (Tur-4) may be calculated.

REFERENCES

- Abu-Hamdeh, M.R.M., (2000), ***Study of Tigris Water Quality and Treated Water at the Water Treatment Plants for Baghdad City***, M.Sc. Thesis, Environmental Eng. Dept. University of Baghdad.
- Al-Janabi, K.R.M., (2006), ***Laboratory Leaching Process Modeling in Gypseous Soils Using Artificial Neural Network (ANN)***, Ph.D. Thesis, Building and Construction Eng. Dept. University of Technology.
- Al-Neami, M.A.M., (2006), ***Evaluation of Delayed Compression of Gypseous Soils with Emphasis on Neural Network Approach,*** Ph.D. Thesis, Building and Construction Eng. Dept. University of Technology.
- Barazanjy, S.J.I., (2007), ***Short and Long Term Forecasting of Water Quality Parameters in Baghdad,*** M.Sc. Thesis, Environmental Eng. Dept. University of Baghdad.
- Garson, G. D. (1991), ***"Interpreting Neural-Network Connection Weights."*** AI Expert 6(7), 47-51.
- Jun, H., (2002), ***Application of Artificial Neural Networks for Flood Warning Systems,*** Ph.D. - Thesis, Dept. of Civil and Environmental. Eng. University of North Carolina.
- Maier, H.R., and Dandy, G.C., (2000), ***Application of Artificial Neural Networks to Forecasting of Surface Water Quality Variables: Issues, Application and Challenges,*** Artificial Neural Networks in Hydrology, R.S. Govindaraju, and A.R. Rao, eds., Kluwer, Dordrecht, Nethrlands, 287-309.
- Nawari, N.O, Liarg, R. and Nussairat, J., (1999***), "Artificial Intelligence Techniques for the Design and Analysis of Deep Foundations",*** EJGE, Vol.4.
- Resop, J.P., (2006***), A Comparison of Artificial Neural Networks and Statistical Regression with Biological Resources Applications,*** M.Sc. Thesis, Faculty of the Graduate School of the University of Maryland, Collage Park.
- Shahin, M.A, Jaska, M.B. and Maier, H.R., (2002), "***Predicting Settlement of Shallow Foundations Using Neural Networks***", Journal of Geotechnical and Geoenviromental Engineering, ASCE, Vol.128, No.9, pp. 785-793.

Shahin, M.A., (2003), ***Use of Artificial Neural Networks for Predicting Settlement of Shallow Foundations on Cohesionless Soils,*** Ph.D. Thesis, Department of Civil and Environmental Eng., University of Adelaide.

- Shahin, M.A, Jaska, M.B. and Maier, H.R., (2003), ***"Application of Artificial Neural Networks in Foundation Engineering,*** Australian Geomechanics.
- Zaheer, I., and Bai, C., (2003), ***Application of Artificial Neural Networks for Water Quality Management,*** Lowland Technology International, Vol. 5, No. 2, 10-15.

PRELIMINARY DESIGN OF A MULTI- STAGE AXIAL COMPRESSOR

Prof. Dr.Munther I. Al-Druby
Mech. Eng. Dept.
College of Engineering
University of Baghdad
Baghdad - Iraq

Prof. Dr. Ihsan Y. Hussain
Mech. Eng. Dept.
College of Engineering
University of Baghdad
Baghdad - Iraq

Ruqeaa Ismail M. Al-Rubyee
Ministry of Science and Technology
Space & Aeronautics Research Center
Turbomachine Dept.
Baghdad - Iraq

ABSTRACT

A numerical calculations algorithm has been developed in the present work for a thermodynamics and aerodynamic design of an axial flow compressor. The design calculations were based on thermodynamics, gas dynamic, fluid mechanics, aerodynamic and empirical relations. A two- dimensional compressible flow is assumed with constant axial and rotor blade velocities. A free –vortex swirl distributions was used in the design. These calculations include; power of the compressor, thermodynamic properties of the working fluid, stage efficiency, number of rotor and stator blades, tip and hub diameters, blade dimensions (chord, length and space) for both rotor and stator, velocity triangles before and after the rotor, Mach number, solidity, degree of reaction, flow and blade angles (blade twist) and lift and drag coefficients along the blade and lift. A repeated stage calculation is made to calculate the above parameters along compressor stages. The twist of the blades can be calculated along the blade length at any required number of sections selected by the designers to obtain smooth blade twist profile. The developed algorithm was tested on a compressor cascade series type NACA 65(12)10 with circular camber angle of (30°). The results show that; the lift coefficient decreases as mean flow angle increases, the drag coefficient increases along blade length at a mean flow angle of (15°), the relative Mach number increases along blade length as mean flow angle increases, the ratio of total drag coefficient to lift coefficient increases when the mean flow angle increases, the drag coefficient decreases along blade length as the solidity increases, the cascade efficiency increases as the mean flow angle increase to (45°).

الخلاصة:

تم في هذا البحث تطوير خوارزمية حسابات عددية للتصميم الثرموديناميكي والايروديناميكي لضاغطة محورية. تم في هذه الحسابات التصميمية اعتماد معادلات الثرموديناميك, ديناميك الغازات, ديناميك الموائع, الايروديناميك و بعض العلاقات التجريبية بالاعتماد على الفرضيات التالية: اعتبار الجريان ثنائي البعد وانضغاطي, ثبوت السرعة المحورية وسرعة الريشة الدوارة والتوزيع الدوامي الحر لالتواء الريش. تم في هذه الخوارزمية ايجاد اهم الخواص واكثرها فاعلية في حسابات تصميم الضاغطة.

تم ايجاد قدرة الضاغطة وخواص المائع الحرارية للريش الدوارة والثابتة, كفاءة المرحلة الواحدة, عدد الريش الدوارة والثابتة, الاقطار عند قمة وقاعدة الريشة بثبوت قطر وسط الريشة, ابعاد الريشة الدوارة والثابتة (طول, عرض و وتر), مثلثات السرع قبل

وبعد الريشة الدوارة, رقم ماخ النسبي, النسبة الفراغية, درجة رد الفعل, زوايا الجريان وزوايا الريش الدوارة والثابتة (التواء الريش) ومعامل الرفع على طول الريشة. تم اجراء حسابات لتحديد التواء الريش عن طريق اختيار عدد من النقاط على طول الريشة(حسب رأي المصمم) والحصول على درجة التواء مقبولة. تم اعتماد أسلوب حسابات المرحلة المتكررة لتسهيل الانتقال من صف إلى آخر أو خلال مراحل الضاغطة. تم إجراء اختبار خوارزمية الحسابات العددية على متعاقبة من سلسلة الضواغط نوع NACA65(12)10ذات معدل تحدب دائري وزاوية تحدب (30) درجة. أظهرت النتائج إن معامل الرفع يقل بزيادة متوسط زاوية الجريان, يزداد معامل الكبح عند اقل متوسط زاوية جريان, ازدياد رقم ماخ عند زيادة متوسط زاوية الجريان, زيادة نسبة معامل الكبح الكلي الى معامل الرفع بزيادة متوسط زاوية الجريان, يقل معامل الكبح على طول الريشة عند زيادة النسبة الفراغية, تزداد كفاءة المتعاقبة عند زيادة متوسط زاوية الجريان وصولا الى زاوية مقدارها (45) درجة بعده تبدأ بالنقصان تدريجيا.

KEYWORDS
Axial Compressor, Multi-Stage, Preliminary design

INTRODUCTION

Axial compressor is one of the most common compressor types in use today. It finds its major application in large gas turbine engine like those of power today's jet aircraft, it derive its name from the fact that the air being compressed has very little motion in the radial direction, in contrast, the radial motion of the air in centrifugal compressor is much longer than the axial motion **(Yahya 1983)**. In general, the axial machines have much greater mass flow but much less pressure ratio per stage because of the boundary layer behavior, fundamentally, the axial compressor is limited by boundary layer behavior in adverse (positive) pressures gradients, each blade passage of compressor may be thought of as a diffuser, so that the boundary layer on all its wall are subject to a pressure increase unless this pressure gradient is kept under control, separation or stall will occur **(Peterson 1970)**. The compressor is made up of two major assemblies. The rotor with its blades and the casing with its stationary blades (stator) and this make one stage, the rotor increase the angular velocity of the fluid resulting increase in total temperature, total pressure and static pressure. The following stator decrease the angular velocity of the fluid, resulting in an increase in the static pressure and sets the flow up for the following rotor **(Mattingly 1996)**.

The axial compressor may be designed with constant tip diameter or with constant mean diameter or with constant hub diameter or with all varying; however the mean blade radius does not usually change very much. The blade length varies in order to accommodate the variation in air density so that the axial velocity component will be approximately uniform. **(Vincent 1950)**

THEORETICAL FORMULATION

A theoretical and empirical formulation of design calculations for a multi -stage axial flow compressor is developed. The formulation will be based on a thermodynamic, gas dynamic, fluid mechanics and aerodynamic relations. Besides; an empirical correlations and values for some design parameters will also be used. The design calculations include, in general, the number of stages, rotor and stator blades data (numbers, width, pitch, height and twist angles), annular area distribution along the compressor, the thermodynamic state along the compressor section and along the blade height at each section, lift and drag for both stator and rotor blades along the compressor, the degree of reaction along the blade height for each stage, the power required to drive the compressor, Mach numbers and the velocity diagram at the rotor inlet and outlet along the blade height.**(Al- Rubyee 2006)**

Power of the Compressor:

From the general momentum equation (Peterson 1970);

$$\Sigma F = \frac{d}{dt}\int_{cv} \rho V_u dv + \int_{cs} \rho V_u (V_u \cdot n) dA \quad (1)$$

It can be shown that the

$$P_{sh} = \dot{m} U (r_2 V_{2u} - r_1 V_{1u}) \quad (2)$$

Where $U = \omega * r$ & for the axial machines, ($r_2 = r_1$)

And, the power required to drive the compressor is calculated as;

$$\textbf{Power} = P_{sh} / \eta_c \quad (3)$$

Compressor Efficiencies:

By using the definition of the compressor efficiency: [Mattingly 1996]

$$\eta_c = \frac{h_{nss} - h_1}{h_n - h_1} = \frac{T_{nss} - T_1}{T_n - T_1} \quad (4)$$

$$\eta_c = \frac{(P_n/P_1)^{\frac{\gamma-1}{\gamma}} - 1}{(P_n/P_1)^{\frac{\gamma-1}{\gamma \eta s}} - 1} \quad (5)$$

Using the (h-s) diagram, the stage efficiency can be obtained as;

$$\eta_s = \frac{(T_{3ss}/T_1) - 1}{\frac{T_3 - T_1}{T_1}} \quad (6)$$

Radial Equilibrium:

For long blades, the variations of blade speed, static pressure and the axial velocity are considerable and the three – dimensionality must be taken into account. The basic assumption of the radial equilibrium type of design is that the radial velocity component is zero at entry and exit from a blade row. The basic equation of motion is (Peterson 1970);

$$\frac{1}{\rho}\frac{\partial P_o}{\partial r} = \frac{V_u^2}{r} + V_u \frac{\partial V_u}{\partial r} + V_x \frac{\partial V_x}{\partial r} \quad (7)$$

Using the exponential swirl distribution type of design, where the swirl velocity (V_u) at the inlet and exit to the rotor has the following general variation with radius (Dixon 1975);

$$V_{1u} = ar^n - \frac{b}{r} \quad \& \quad V_{2u} = ar^n + \frac{b}{r} \quad (8)$$

Where (a) and (b) are constants and the index (n) have any value, but in exponential swirl distribution the index is taken to be equal to zero (n=0**)**.

Note that, the axial velocity at the rotor inlet and exit is the same along the mean line, but at other section the axial velocity will be calculated at inlet and outlet as follows:

Differentiating **eq.(8)** and substitute the results in **eq.(7)** to get the variation of axial velocity as;

$$V_{x1}^2 = k_1 - 2a^2\left[\ln(r) + \frac{b}{ar}\right] \quad \& \quad V_{x2}^2 = k_2 - 2a^2\left[\ln(r) - \frac{b}{ar}\right] \quad (9)$$

(k_1) and (k_2) can be evaluated at constant axial velocity in the mean line section and taking the same for all blade section.

Thermodynamic Calculations:

The thermodynamic properties at stage inlet (rotor) are calculated from equations below (Mattingly 1996)**;**

$$P_1 = P_{o1} * \left(\frac{T_1}{T_{o1}}\right)^{\gamma/\gamma-1} \quad (10)$$

$$h_1 = C_P * T_1 \quad (11)$$

The isentropic stagnation and static temperature can be found from:

$$T_{o3ss} = T_{o1} * \left(\frac{P_{o3}}{P_{o1}}\right)^{\frac{\gamma-1}{\gamma}} \quad \& \quad T_{3ss} = T_{03ss} - \frac{V_3^{\,2}}{2C_P} \tag{12}$$

Also, the static isentropic enthalpy can be obtained as;

$$h_{3ss} = C_P \; * T_{3ss} \tag{13}$$

Now,

$$\Delta h_{is} = h_{3ss} - h_1 \quad \& \quad \Delta h_{rotor} = R_C * \Delta h_{is} \tag{14}$$

Where (R_C) is the degree of reaction.

Thus

$$h_{2is} = h_1 + \Delta h_{rotor} \tag{15}$$

$$T_{2is} = h_{2is} / C_P \tag{16}$$

Now, the pressure, temperature, density and enthalpy at rotor exit can be calculated as;

$$P_2 = P_1 * \left(\frac{T_{2is}}{T_1}\right)^{\frac{\gamma}{\gamma-1}} \quad \& \quad T_2 = \frac{h_2}{C_P}$$

(17)

$$\rho_2 = \frac{P_2}{R * T_2} \quad \& \quad h_2 = h_1 + 0.5 * \left(w_{1m}^{\,2} - w_{2m}^{\,2}\right) \tag{18}$$

Note that, the terms (w_{1m} and w_{2m}) in **eq.(18)** were calculated from velocity triangle at mean section, as will be explained later; the stagnation temperature loss at mean section can be calculated as;

$$\frac{\Delta T_o}{T_{o1}} = \left(\frac{U_m^{\,2}}{C_P * T_{o1}} * \frac{V_{xm}}{U_m} * \tan\beta_{1m}\right) - \left(\frac{V_{xm2}}{V_{xm1}} * \tan\beta_{2m}\right) \tag{19}$$

Degree of Reaction:

A useful term for turbomachine designers is the degree of reaction which is defined as the ratio of the static enthalpy increase across the rotor to the increase in static enthalpy for the stage.

$$R_c = \frac{\Delta h_{rotor}}{\Delta h_{stage}} = \frac{h_2 - h_1}{h_3 - h_1} \tag{20}$$

Or, using the notation for the axial flow stage as shown in **Fig.(1)** (Yahya 1983);

$$R_c = \frac{w_1^{\,2} - w_2^{\,2}}{2U(V_{2u} - V_{1u})} \tag{21}$$

Aerodynamic Calculations:

To evaluate the lift and drag forces, lift and drag coefficients must be calculated as shown below:

The mean relative velocity for rotor can be obtained as (Bathie 1995);

$$w_m = \frac{(w_1 + w_2)}{2} \quad \& \; w_{um} = \frac{(w_{1u} + w_{2u})}{2} \tag{22}$$

And mean angle **(β_m)** for rotor can be obtained from:

$$\beta_m = \tan^{-1}\left(\frac{w_{um}}{V_{xm}}\right) \tag{23}$$

Cascade Test:

From typical cascade test (Peterson 1970) for blade type NACA 65 (12) 10 at solidity equal one (c/s =1) and by using curve -fitting program, the equation relates the cascade angles to the stagger angle were obtained from:

$$\beta_{ii} = -25.3 + 0.228 * \beta_i + 0.929 * \lambda \quad (24)$$

This equation can be applied at (λ) values between (10° - 50°) and (β_i) between (30°-70°) to calculate the angle at cascade exit (β_{ii}) and these will be taken as the same for all stages.

For rotor: $\beta_i = \beta_1$, $\beta_{ii} = \beta_2$

For stator: $\beta_i = \alpha_2$, $\beta_{ii} = \alpha_3$

$$C_L = 2\frac{s}{c}\cos\beta_m\left(\tan\beta_i - \tan\beta_{ii}\right) - \frac{\Delta P_o}{\rho w_m^2/2} * \frac{s}{c}\sin\beta_m \quad (25)$$

$$C_D = \frac{\Delta P_o}{\rho w_m^2/2} * \frac{s}{c}\cos\beta_m \quad (26)$$

The total effective drag coefficients for the cascade (using the notations of the present work for length) may be written as;

$$C'_D = (C_D)_{cascade} + 0.02(s/L) + 0.018C_L^2 \quad (27)$$

Pressure Rise Limitations:

The limiting pressure coefficient can be expressed for a simple case in terms of blade angles, in which the blades may be either rotor or stator blades, since the axial velocity is constant at inlet and outlet to cascade, where many designers limit the static pressure rise in a given blade row to $C_P < 0.6$ (Peterson 1970), therefore :

$$C_P = 1 - \frac{\cos^2\beta_i}{\cos^2\beta_{ii}} \quad (28)$$

Compressibility Effects:

Compressibility limits the relative velocity at the inlet to any blade row, and this limitation is especially important for the first stage of the axial flow compressor. The relative Mach number at rotor entrance usually lies in the range of $0.6 < M_{1rel} < 0.85$ and it can be calculated as (Peterson 1970);

$$M_{1rel} = \frac{w_1}{\sqrt{(k * R * T_1)}} \quad (29)$$

Annular Area Distribution

Constant Mean Diameter(see Fig. 2-a):

By assuming the design radius of the compressor stage is at the mean line, this leads to:

$$D_m = D_{m1} = D_{m2} = D_{m\,n}$$

From equations below the area, mean diameter and length at stage inlet can be computed as;

$$A_1 = \frac{\dot{m}}{\rho_1 * V_{xm}} \quad \& \quad L_1 = \frac{A_1}{\pi * D_m}, \quad r_m = D_m / 2 \quad (30)$$

Thus, the tip and hub (root) diameter is obtained from:

$$D_{t1} = D_m + L_1 \quad \& \quad D_{r1} = D_m - L_1$$

Similarly, in the same way can be found all dimensions at rotor exit or at stage exit.

Constant Root Diameter (see Fig. 2-b):

The root diameter can be defined as;

$$D_r = D_{m1} - L_1$$

From assumption of constant root diameter: $D_r = D_{r1} = D_{r2} = D_{r3} = D_{r\,n}$

Now, the tip diameter at inlet to the stage is:

$$D_{t1} = D_r + 2L_1 \tag{31}$$

Again, by using the continuity equation the tip diameter at rotor exit can be calculated as;

$$\dot{m} = \rho_{m2} V_{xm} * \frac{\pi}{4}(D_{t2}^2 - D_r^2) \quad \& \quad D_{t2} = \sqrt{\frac{4\dot{m}}{\rho_{m2} V_{xm} * \pi} + D_r^2} \tag{32}$$

So, the length and mean diameter at rotor exit can be found from:

$$L_2 = \frac{D_{t2} - D_r}{2} \quad \& \quad D_{m2} = D_r + L_2 \tag{33}$$

Constant Tip Diameter (see Fig. 2-c):

The tip diameter can be defined as;

$$D_t = D_{m1} + L_1$$

Also, from assumption of constant tip diameter: $D_t = D_{t1} = D_{t2} = D_{t3} = D_{t\,n}$

Now, at inlet to the stage: $D_{r1} = D_t - 2L_1$

Again, by using the continuity equation, the tip diameter at rotor exit is;

$$\dot{m} = \rho_{m2} V_{xm} * \frac{\pi}{4}(D_t^2 - D_{r2}^2) \quad \& \quad D_{r2} = \sqrt{D_t^2 - \frac{4\dot{m}}{\rho_{m2} V_{xm} * \pi}} \tag{34}$$

So, the length and mean diameter at rotor exit can be found from:

$$L_2 = \frac{D_t - D_{r2}}{2} \quad \& \quad D_{m2} = D_t - L_2 \tag{35}$$

Number of Blades:

To specify the number of blades for both rotor and stator, suitable limit for aspect ratio and solidity must be assumed. The aspect ratio is defined as;

$$AR = \frac{L}{c} \tag{36}$$

The space can be obtained from equation of solidity (σ.) as;

$$\sigma = \frac{c}{s} \tag{37}$$

∴ The number of rotor blades can be evaluated as;

$$n = \frac{(2 * \pi * r_m)}{s} \tag{38}$$

The number of blades must be a whole number, if not an interpolation for the blades number must be and recalculate in the reverse order then yields a new space, chord and aspect ratio as (Cohen 1972);

$$s = \frac{(2 * \pi * r_m)}{n} \quad , \quad c = \sigma * s \quad \& \quad AR = \frac{L}{c} \tag{39}$$

The calculations of chord, space and number of blades for the stator is made in a similar procedure as mentioned above, but the solidity of the stator blades is usually less than that for the rotor blades (Vincent 1950).

Blade Twist

Blade Angle: The blade inlet angle will be known when chosen incidence angle at the design point, equal to zero, but the blade outlet angle can not be determined until the deviation angle (δ) has been determined (Cohen 1972) by using the Howells relations;

$$\delta = m\theta\sqrt{(s/c)} \quad , \quad \text{where : } m = 0.23(2\frac{a}{c})^2 + 0.1(\frac{\beta_2}{50}) \tag{40}$$

For circular arc camber (2a/c) =1(Cohen 1972), and (a) is the distance of point of maximum camber from the leading edge of the blade.

In terms of rotor blades;

$$\theta = \beta'_1 - \beta'_2 \quad \& \quad \delta = \beta_2 - \beta'_2 \tag{40a}$$

From **eq.(40a & 40)** and using zero incidences (i.e. $\beta_1 = \beta'_1$: $\alpha_1 = \alpha'_1$) can be get:

$$\theta = \frac{\beta_1 - \beta_2}{\left(1 - m\sqrt{s/c}\right)} \tag{41}$$

Velocity Triangle Calculation at Mean Section

It is important to be able to calculate the change in tangential velocity across the rotor (Dixon 1975). This is best accomplished by drawing velocity diagrams for a normal compressor stage as shown in **Fig.(1)**.

The velocity diagrams at the mean section may calculate as follows:

The inlet absolute velocity from:

$$V_{1um} = V_{xm} * \tan(\alpha_{1m}) \quad \& \quad V_{1m} = \sqrt{\left(V_{xm}^{\ 2} + V_{1um}^{\ 2}\right)}$$

And the inlet relative velocity as; (42)

$$w_{1um} = U_m - V_{1um} \quad \& \quad w_{1m} = \sqrt{\left(V_{xm}^{\ 2} + w_{1um}^{\ 2}\right)}$$

Where the V_{1um} & w_{1um} is the component velocity of V_{1m} & w_{1m} and by applying the set of equations below, the outlet absolute velocity can be calculated from:

$$w_{2um} = \sqrt{\left(w_{2m}^{\ 2} - V_{xm}^{\ 2}\right)}, \quad V_{2um} = U_m - w_{2um} \quad \& \quad V_{2m} = \sqrt{\left(V_{xm}^{\ 2} + V_{2um}^{\ 2}\right)} \tag{43}$$

Now, the flow angles related to the relative inlet and outlet velocity were calculated as:

$$\beta_{1m} = \tan^{-1}\left(w_{1um}/V_{xm}\right) \quad \& \quad \beta_{2m} = \tan^{-1}\left(w_{2um}/V_{xm}\right) \tag{44}$$

Also, the outlet flow angles related to the outlet absolute velocity can be calculated as;

$$\alpha_{2m} = \tan^{-1}\left(V_{2um}/V_{xm}\right) \tag{45}$$

The constants (a) & (b) is obtained by evaluating the **eq.(8)** at the mean radius as;

$$a_1 = \frac{V_{1um} + V_{2um}}{2} \quad \& \quad b_1 = \frac{r_m\left(V_{1um} - V_{2um}\right)}{2}$$

Also, the constants (k_1)& (k_2) can be calculated from **eq.(9)** at constant axial velocity in the mean section ;

$$k_1 = V_{xm}^{\ 2} + 2a^2\left(\ln r_m\right) + \frac{b}{ar_m} \quad \& \quad k_2 = V_{xm}^{\ 2} + 2a^2\left(\ln r_m\right) - \frac{b}{ar_m}$$

RESULTS AND DISCUSSION

A verification of the proposed theoretical formulation is made here through a comparison between the present work results and the published results of preliminary design of axial flow compressor (Al-Druby and Hussain 1995), the results of calculations for the present work and this case are summarized in **(Tables 2 to 9)** with the given input data listed in **Table (1).**

The length, root and tip diameters are shown in **Table (2)** at inlet, exit from rotor and stage exit at constant mean diameter. The root diameter increases from inlet to exit stage, whereas the tip diameter and length decreases from inlet to exit, these diameters forms the compressor stage geometry, the hub diameter and tip diameter are between (0.306-0.320) and (0.501-0.491), respectively. The number of blades, chord length, and space are shown in **Table (3)**, the calculated aspect ratio for rotor and stator blades is also tabulated. the aspect ratio were calculated after re-calculating the number of blades and space, calculated aspect ratio is less than the assuming value in the given data. The stage exit pressure and temperature, stage efficiency, stagnation temperature rise for one stage, compressor efficiency, pressure and temperature at compressor exit, and the

power required are shown **Table (4)**. The pressure, temperature and density along blade length are shown in **Table (5)**, all thermodynamic properties are increasing from hub to tip radius and the shadow lines represents the mean line data. The lift coefficient result along blade length are shown in **Table (6)** the shadow line represents the mean line data, the lift coefficient increases above the mean line and decreases below the mean line, the lift coefficient is proportional to solidity ratio were calculated. The twist angles at inlet and outlet from rotor and stator, camber angles and relative Mach number along the blade length are shown in **Table (7)**, all the angles increases except the camber angles for rotor which decreases along blade length, the values of relative Mach No. (0.55-0.70) and these value are in the limiting range. The variation of solidities for rotor and stator, degree of reaction along blade length are shown in **Table (8)**, the solidity decreases whereas degree of reaction increases along blade length, the shadow line represents the mean line data and these values is approximately equal to the input data, the solidity in the present work were calculated after re- calculating chord length and space values for the stator are higher than the rotor, thus; the solidity for rotor is less than for the stator along blade length. The results of cascade lift and drag coefficient and effective drag coefficient (total) on the mean line design are shown in **Table (9)**, by using the cascade test curve (Peterson 1970), were chosen the stagger angle of (40°) and inlet cascade angle of (50°) to obtain cascade outlet angle from equ.(24), then applying equ.(28) to find the pressure coefficient (C_P) equal to (0.51) and this value is less than the limiting range. the term (C_D) and (C_L) is for cascade where the term (C_{Dtotal}) is for actual compressor blades, by using the value of (C_{Dtotal}), the actual stagnation pressure (ΔP_O) for rotor and stator can be obtained to yield the lift and drag forces for actual compressor. The flow angles and the swirl velocity distribution at inlet and exit of the rotor for the present work are shown in **(Figs. 3 and 4)**. There is a significant variation with blade length of the swirl velocity and flow angles near the blade root and very little near the tip, the relative flow turns about (65°) at the hub and only about (39°) at the tip. The large radial variation in the rotor inlet flow angle for one stage requires that its rotor blade have a lot of twist in them. (Mattingly1996). The relative Mach No. along blade length are shown in **Fig.(5)**, the values of the Mach number are between (0.55- 0.7), and these values in the limiting range leads to efficient operation. The advantage of high Mach No. operation is that the mass flow per unit area and the pressure ratio per stage will both be high. Also a parametric case study will be made in different solidities and mean flow angle, the plot of lift and drag coefficients at three solidities (1, 1.33, and 2) along the blade length are shown in **(Figs. 6 and 7)**, the lift coefficient decrease as solidity increases, taking the solidity of one as a reference, the rate of change in lift curve slope for solidity of (1.33) is approximately half that change for solidity of (2), the difference is due to the interference of two opposing effects, the 1st, is that large blade spacing increase the lift, the 2nd , is that close blade spacing mean that the flow angle leaving a blade row exhibits smaller variation a cross the blade passage (Jassam1992), the drag coefficient increases at the tip diameter, then decreases at hub diameter, the drag coefficient increases as solidity decreases, the values of drag coefficient at solidity (1) are between (0.025-0.027) whereas at solidity (2) the values are between (0.037-0.042). A plot of lift and drag coefficients along the blade length at different mean flow angles (15°, 25° ,35° and 45°) are shown in **(Figs. 8 and 9),** where the lift coefficient decreases as mean flow angle increases, till it reaches 45°, the lift coefficient is nearly a straight line, on the other hand, the drag coefficient increases with mean flow angle, up to a value of (45°) then it decreases. The efficiency of compressor cascade with different mean flow angles (15° to 75°) as shown in **Fig.(10)** at varying ratio of (C_D/C_L) calculate from the following equation (Dixon 1975);

$$\eta = 1 - \frac{2C_D}{C_L \sin 2\alpha_m} \qquad (46)$$

The maximum efficiency of compressor cascade is obtained when the mean flow angle only a little less than 45° but the curve is rather flat for a wide range in mean flow angle.

CONCLUDING REMARKS

A suitable design calculations algorithm has been developed for a multi-stage axial flow compressor. The lift coefficient decreases along the blades length from hub to tip. The upper limit of lift coefficient is when the solidity equals one. The lift coefficient decreases as mean flow angle increases, approximately to optimum value at (45°) then the lift coefficient varied little along blade length. The drag coefficients reach higher limits along blade length when the mean flow angle is (15°). The relative Mach No. increases along blade length, but when mean flow angle increases the relative Mach No. decreases.

REFERENCES

Cohen, H. and Rogers, G. F. C., and Sravanamuttoo, H. I. H., "Gas Turbine Theory", Longman Group Limited, 2nd 1972.

Hill, P. G. and Peterson, C. R. "Mechanics and Thermodynamic of Propulsion", Addison – Wesley Publishing Company, Third Addition, 1970.

Jack D. Mattingly, "Elements of Gas Turbine Propulsion", McGraw- Hill Book, Inc. 1996.

M. I. AL- Durby and I. Y. Hussain "Preliminary Design Calculations for Axial- Flow Turbines and Compressors"; University of Baghdad /Collage of Engineering /Mechanical Department, Technical Report, 1995.

Nayef, T. Jassam, "Parametric Study of Deviation in Axial Flow Compressor", M.Sc., Thesis, Baghdad University, 1992.

Ruqeaa Ismail M. Al- Rubyee, " Preliminary Design of A Multi- Stage Axial Compressor" M.Sc., Thesis, Baghdad University / College of Engineering /Mechanical Dept. , 2006.

S L., Dixon, "Fluid Mechanics, Thermodynamics of Turbomachinery", 2nd Edition, 1975. S M Yahya,., "Turbines, Compressors and Fans", TATA McGraw- Hill, 1983.

S. M Yahya,., "Turbines, Compressors and Fans", TATA McGraw- Hill, 1983.

Vincent, E. T., "The Theory and Design of Gas Turbines and Jet engines", McGraw- Hill Book Company, Inc. 1950.

William W. Bathie, "Fundamentals of Gas Turbines", John Wiley and Sons, Inc., 2nd Edition, 1995.

NOMENCLATURE

Latin Symbols

Greek Symbols

Symbol	Description	Units
α	Stator Flow Angle	degree

ά	Stator Blade Angle	degree
β	Rotor Flow Angle	degree
β′	Rotor Blade Angle	degree
γ	Ratio of Specific Heat	----
δ	Deviation Angle	degree
ε	Strain	
λ	Stagger Angle	degree
ρ	Density	kg/m^3
σ	Solidity	----
θ	Camber Angle	degree
Δ	Change per Stage	----
ω	Rotating Speed	r.p.m
∏	Pressure ratio	----
η	Efficiency	----

Symbols	Descriptions	Units
a	constant	----
A	Area	m^2
AR	Aspect Ratio	----
b	constant	----
c	Chord	m
C_D	Drag Coefficient	----
C_L	Lift Coefficient	----
C_p	Specific Heat at Constant Pressure	J/kg.K
D	Diameter	m
h	Enthalpy	kJ/kg
i	Incidence Angle	degree
L	Length (height)	m
M	Mach No.	----
$\dot{m}$	Mass flow rate	kg/s
n	No. of Blade	----
P	Pressure	Pascal
U	Blade Velocity	m/s
r	Radius	m
R	Gas Constant	kJ/kg.K
R_c	Degree of reaction	----
s	Space	m
T	Temperature	K
V, w	Fluid Velocity, Relative Velocity	m/s
The compressor inlet temperature (T_{o1})		294K

Table 1: The Main Input Data (Al-I

The compressor inlet pressure (P_{o1})	101325 Pa
The compressor inlet velocity (V_1)	146 m/s
The mean axial velocity (V_X)	122 m/s
The compressor pressure ratio (P_{o3}/P_{o1})	1.23
The overall compressor pressure ratio	4
The mass flow rate ($\dot{m}$)	18.144 kg/s
The rotor blade velocity (U)	244 m/s
The angular velocity	11500 r.p.m
The blade aspect ratio (AR)	3
The solidity (σ)	1
The air inlet angle (α_1)	33°

Design Calculations:

Table 2: Stage Geometry

	D_r (m)	D_m (m)	D_t (m)	L (m)
Rotor inlet	.3064730	.4052223	.5018698	9.728426 E-02
Rotor exit	.3138668	.4052223	.5003454	9.023113 E-02
Stage exit	.3207271	.4052223	.4910624	8.501962 E-02
Comp. exit	.3605752	.4052223	.4502072	4.264601 E-02

Table 3: Blade Dimension

	Blades No.	Chord Length (m)	Space (m)	AR
Rotor	39	3.242809E-02	3.637267E-02	2.93
Stator	34	4.722581E-02	4.106592E-02	2.25

Table 4: Stage Data

Stage Exit	125411.8 (Pa)	314.9377(K)
Stage Efficiency %	88	------
ΔTo/To1 for stage	.069875	------
Compressor Efficiency %	84	
Compressor Exit	357452.5(Pa)	460 (K)
The Power Required	3083.518 (kW)	

Table 5: Thermodynamics Properties along the Blade

D (m)	P_2 (Pa)	T_2(K)	ρ_2 (kg/m^3)
.305738	103930.24	296.576	1.22533
.3255473	1074035	299.6945	1.240205
.3505473	108585.5	300.5109	1.255302
.3755473	110460	303.0857	1.269312
.405223	**111877.7**	**303.4635**	**1.289135**
.4255473	113897.6	304.6796	1.291372
.4505473	115272	305.7607	1.307121
.4755473	115622.7	307.7281	1.310012
.5005473	116281.7	307.5991	1.332690

Table 6: Lift Coefficient along the Blade

D (m)	C_L
.305738	.5902831
.3255473	.5810574
.3505473	.5707791
.3755473	.5391446
.405223	**.505476**
.4255473	.4580317
.4505473	.3832497
.4755473	.2800809
.5005473	.2030155

Table 7: Blade Angles

D (m)	α^o_1	α^o_2	β^o_1	β^o_2	θ^o_{rotor}	θ^o_{stator}	M_{1rel}
.30	24.27	47.13	39.12	1.33	38.82	-22.77	.55
.33	26.24	48.19	42.16	8.68	35.56	-21.85	.56
.35	28.11	49.35	46.22	15.99	31.90	-21.15	.57
.38	29.90	50.65	51.20	23.45	27.09	-20.66	.58
.40	**33.0**	**53.65**	**53.5**	**32.30**	**20.96**	**-20.35**	**.59**
.43	35	55.4	56.77	41.64	15.85	-20.30	.61
.45	36.71	57.39	59.36	48.22	11.91	-20.58	.65
.48	38.41	59.55	61.81	54.40	7.43	-21.09	.68
.50	40.43	63.61	64.45	60.57	3.31	-21.88	.70

D (m)	σ_{rotor}	σ_{stator}	% R_c
.30	1.31	1.56	17.68
.33	1.23	1.45	27.26
.35	1.15	1.36	35.87
.38	1.05	1.28	44.00
.40	**.99**	**1.01**	**50.05**
.43	.94	1.03	56.02
.45	.89	.98	60.47
.48	.85	.93	64.93
.50	.81	.9	68.72

Table 8: Solidity and Degree of Reaction along Blade

At: λ = 40° , β_i = 50°

Table 9: Cascade Aerodynamic Forces

$C_{L\ cascade}$	$C_{D\ cascade}$	$C_{D\ total}$	Lift (N)	Drag (N)
1.32	0.049	0.0546	568	21

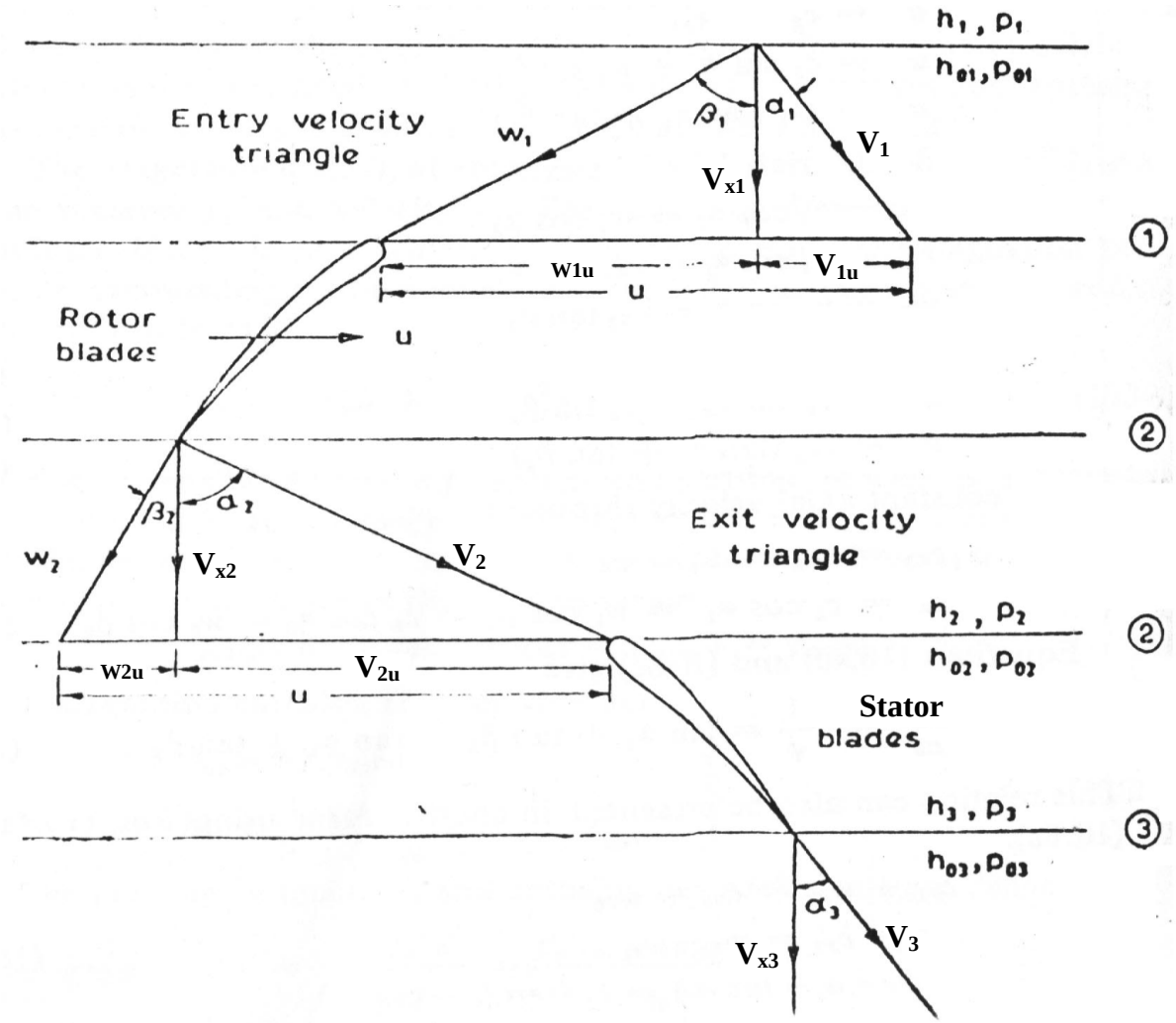

Fig. 1: Velocity Triangle for Compressor Stage [Yahya 1983]

1 2 3 n

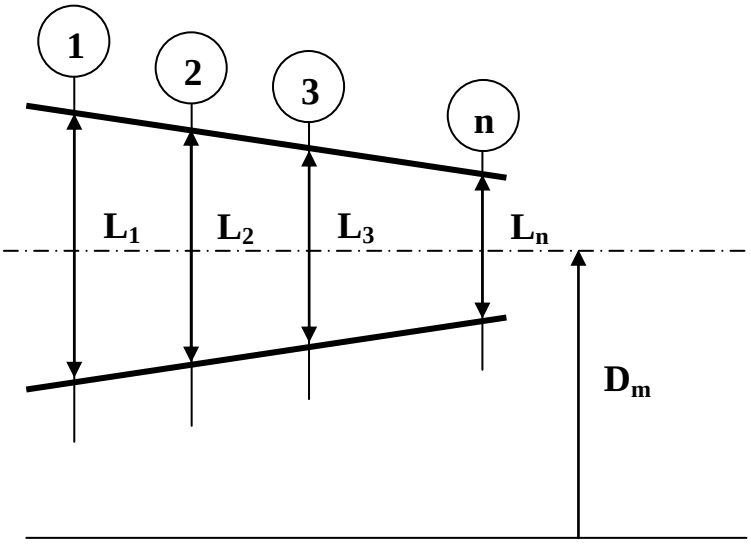

(a)

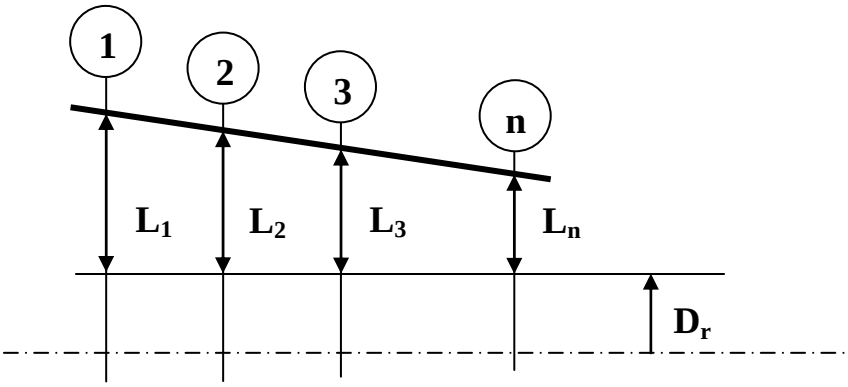

(b)

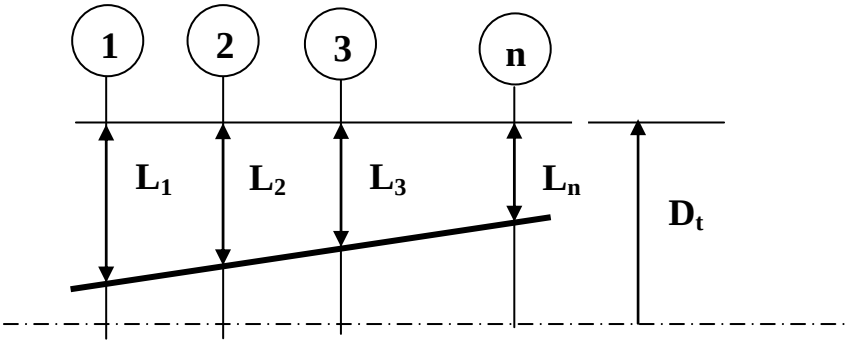

(c)

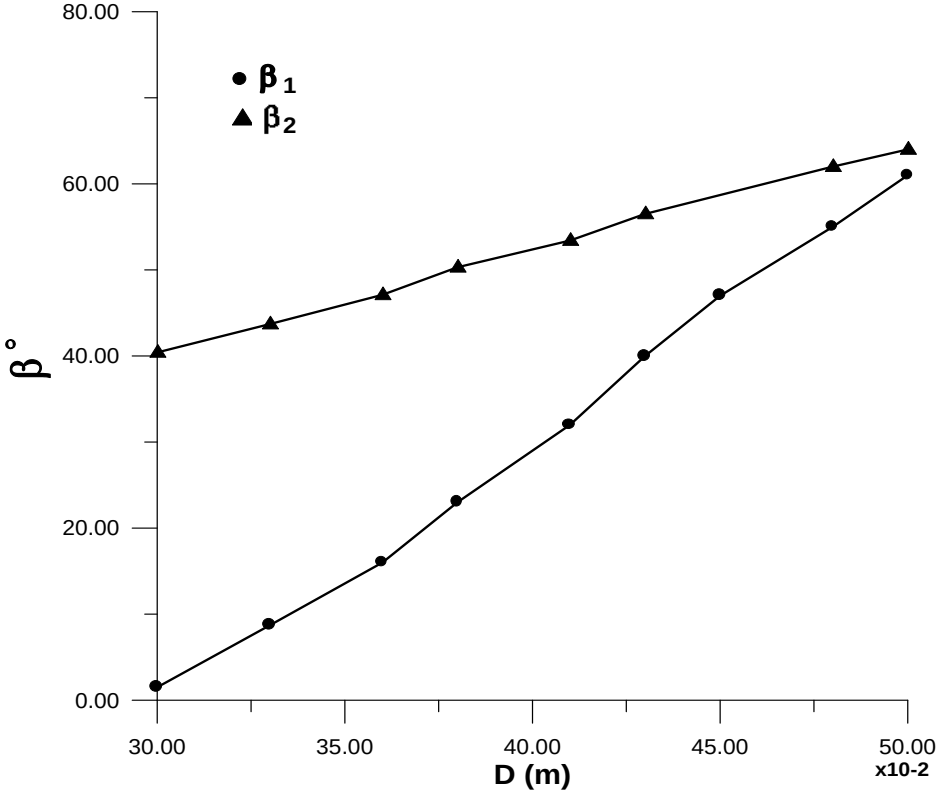

Fig. 3: Twist of Rotor Angles along Blade Length

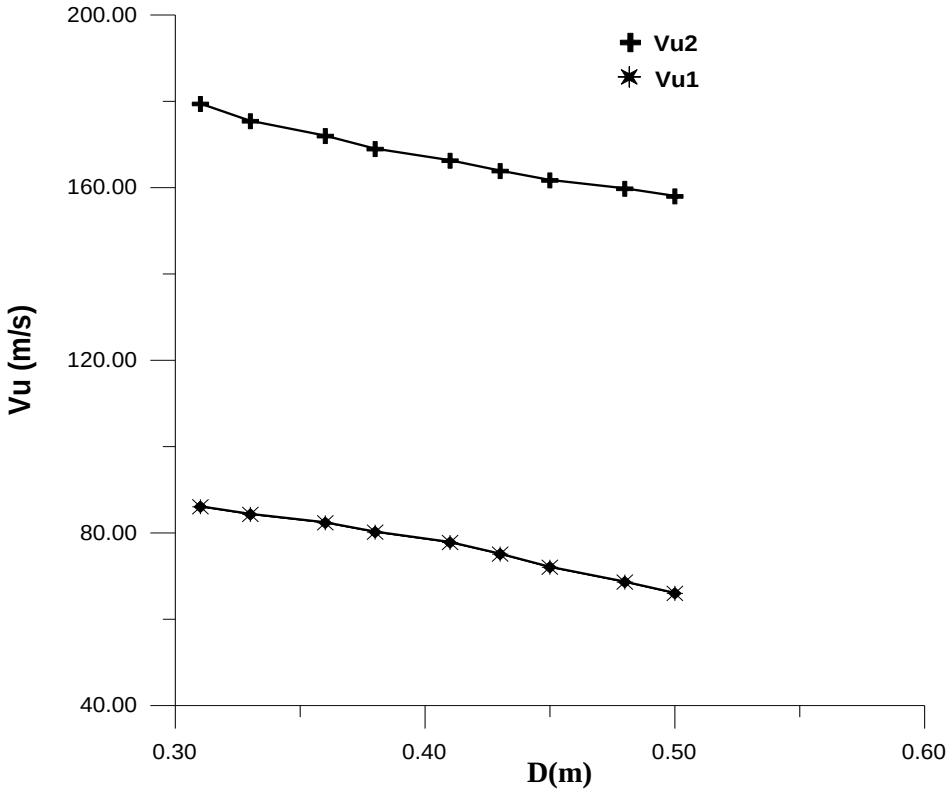

Fig. 4: Variation of Swirl Velocity along Blade Length

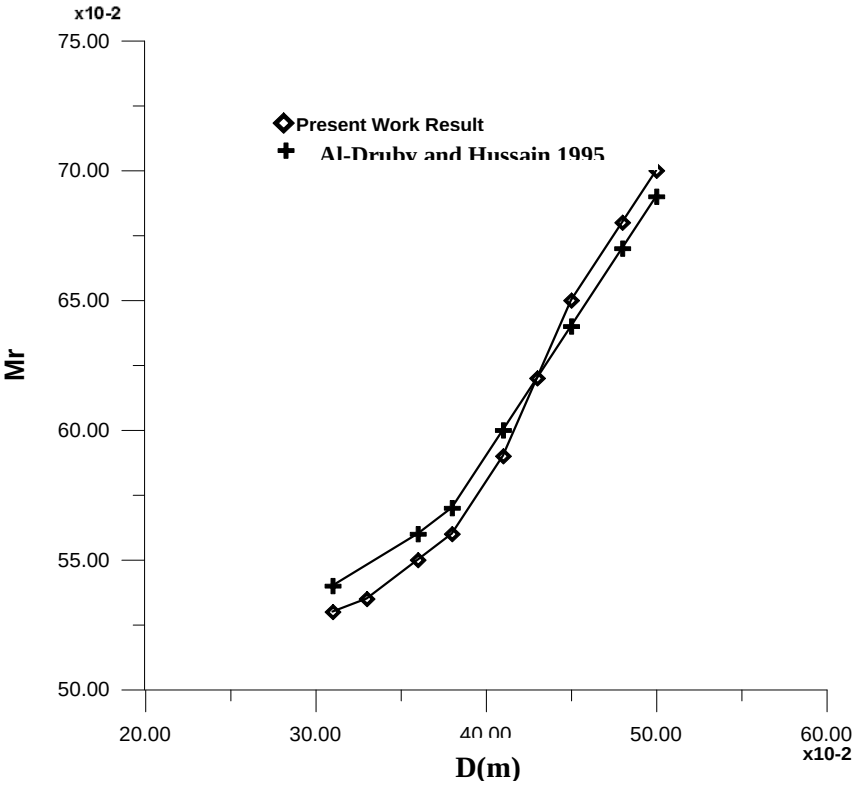

Fig. 5: Mach No. along Blade Length

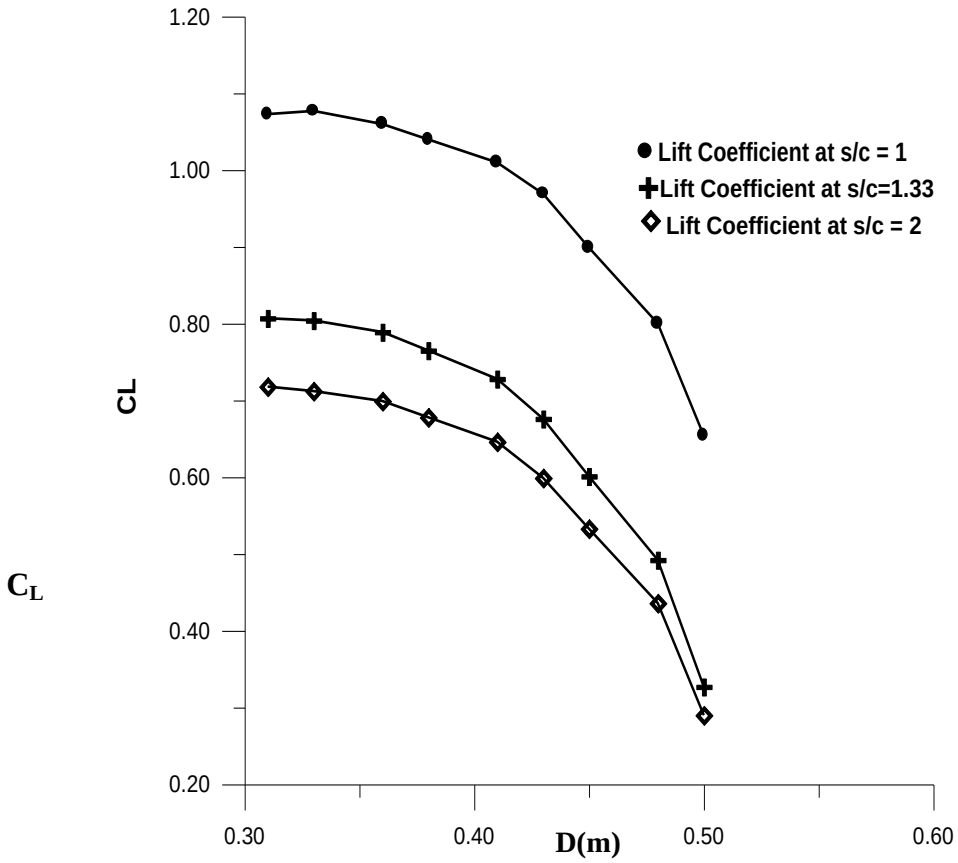

C_L

Fig. 6: Lift Coefficient along Blade Length at Different Solidities

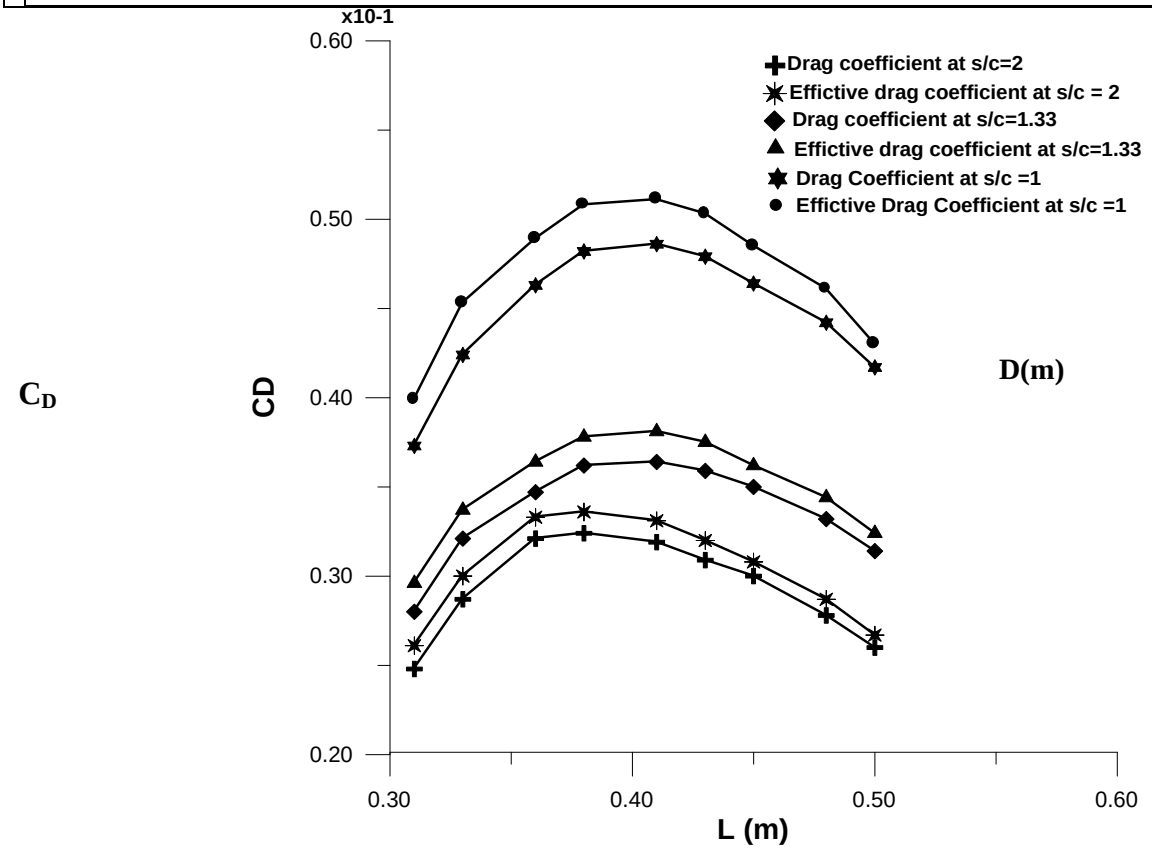

Fig. 7: Drag Coefficient along Blade Length at Different Solidities

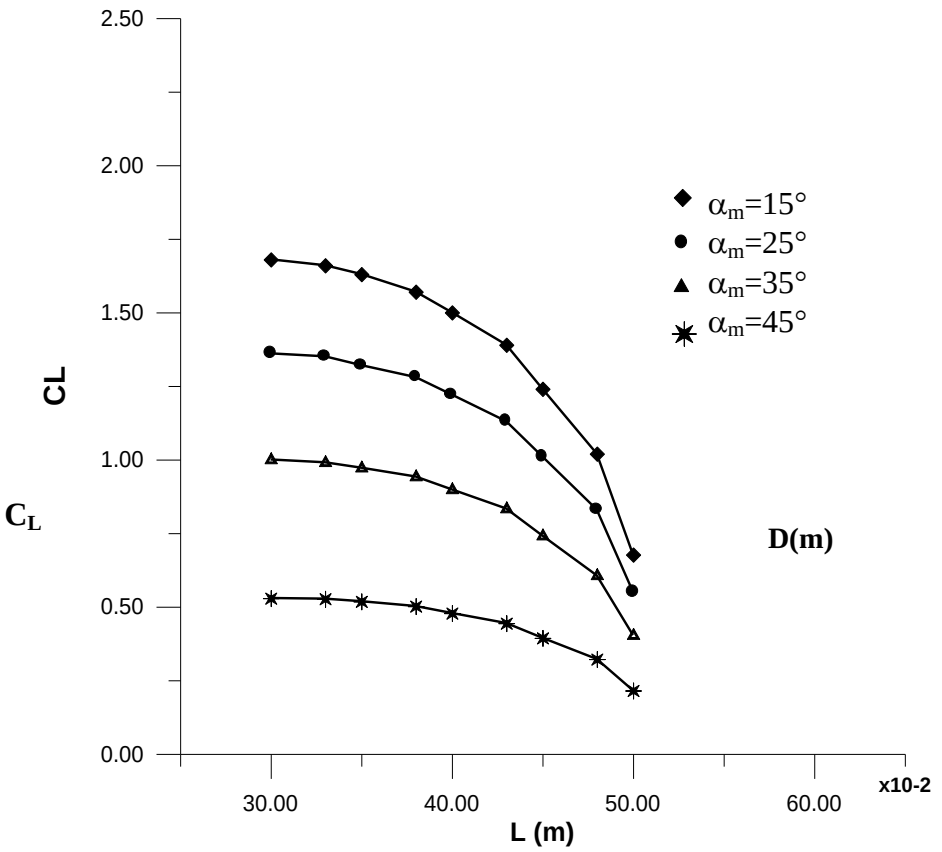

Fig. 8: Lift Coefficient along Blade Length at Different Mean Flow Angle

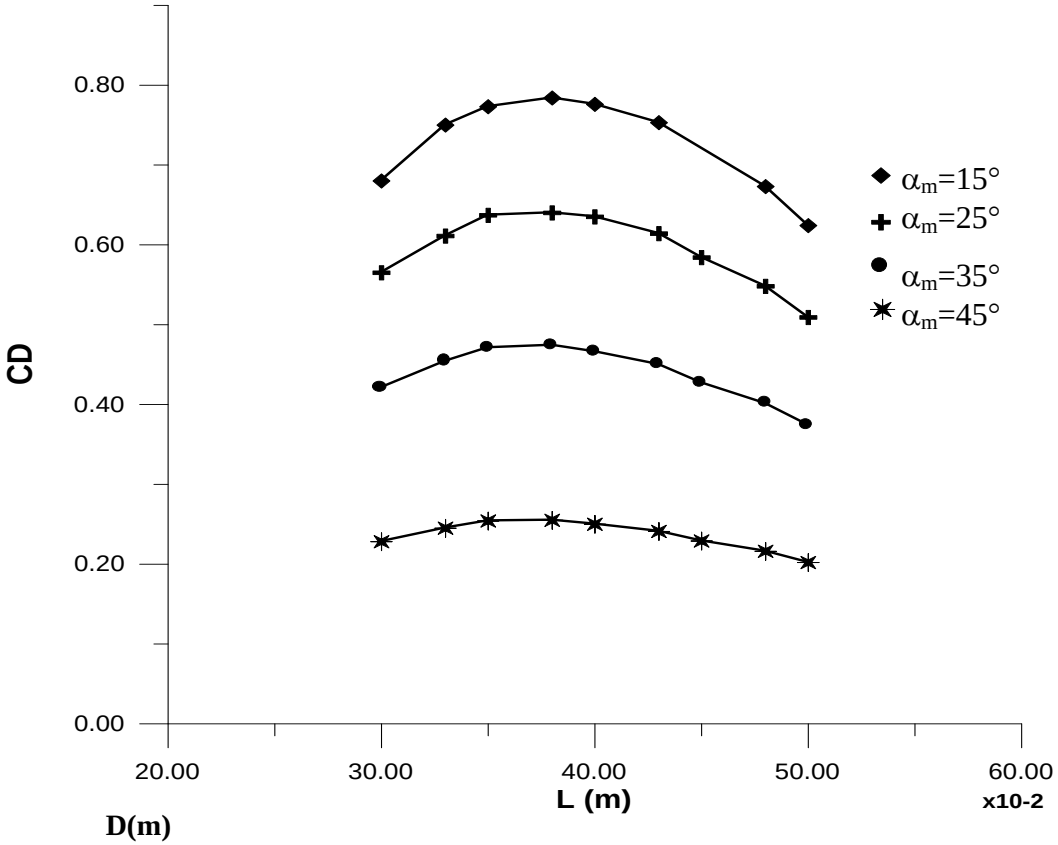

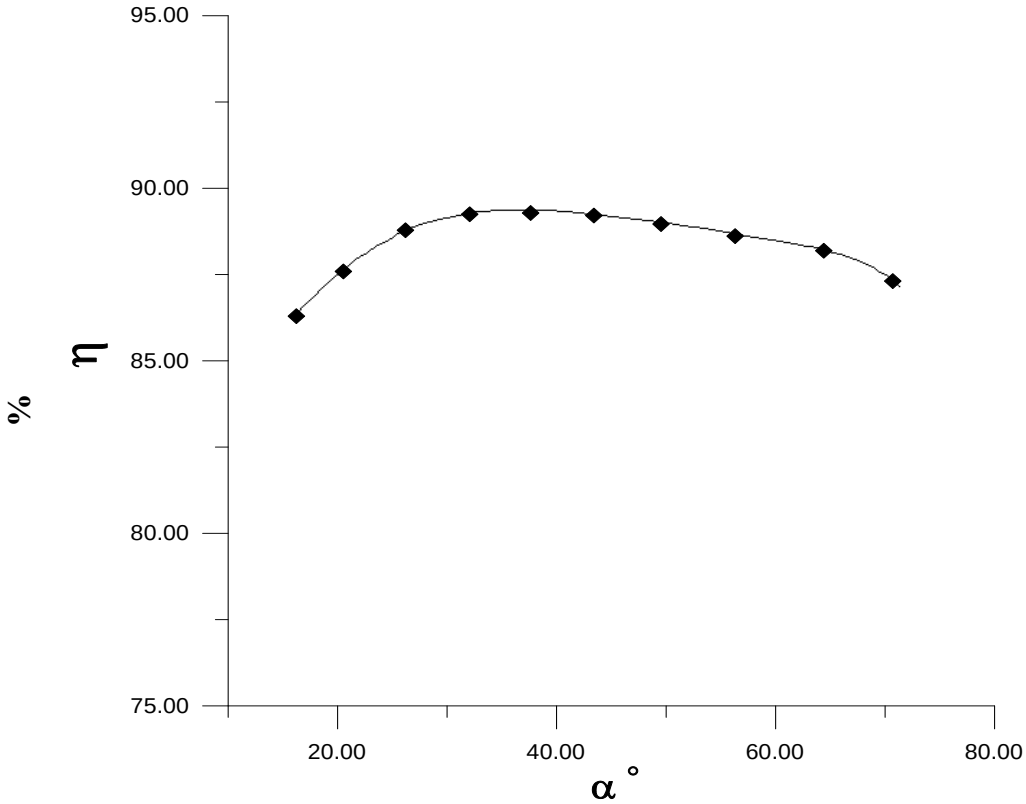

Fig. 10: Cascade Efficiency versus Mean Flow Angle

دراسة عملية لتأثير تثقيب الزعانف على الأداء الحراري للأنابيب المزعنفة حلزونيا

Dr. IhsanY.Hussain
Mech.Eng.Department
University of Baghdad

Dr. Ikhlase M.Fayed
Mech.Eng.Department
University of Technology

Sahra Hassan Ibrahim
Mech.Eng.Department
University of Technology

Dr. Hanna Abdul Hadi
Mech.Eng.Department
University of Technology

الخلاصة

تناول البحث دراسة عملية لتأثير تثقيب الزعانف على الأداء ولقد تمت الدراسة على خمسة نماذج من الأنابيب بقطر(18mm) ومزعنفة حلزونيا بزعانف بارتفاع (12mm) مثقبة من منتصفها بثقوب دائرية بعدد(3,3,6,2 hole /fin) وقطر (3,4,2,3mm) على التوالي حيث تم اختبار كل أنبوب أفقيا عند تعرضه لهواء بسرع قصوى تتراوح بين(m/s 1.5-7.5) ولمدى من أعداد رينولد يتراوح بين ($21.15\times10^3-105.7\times10^3$) وقد درس تأثير تغير قطر الثقوب لعدد ثابت من الثقوب (3 hole/fin) في كل زعنفة و تأثير تغيير عدد الثقوب لقطر ثابت (3mm) على الأداء.وأظهرت النتائج العملية أن عملية تثقيب الزعانف تؤدي إلى زيادة معامل انتقال الحرارة الإجمالي ولجميع الأنابيب المثقبة ولكن نسبة الزيادة تختلف من أنبوب إلى آخر ،و من مقارنة معامل انتقال الحرارة الإجمالي لأنبوب مثقب (بقطر ثقب (3mm),(3 hole/fin)) مع أنبوب غير مثقب الزعانف وجد انه يزداد بنسبة (12.3%) عند السرعة (4.5m/s) وهذه النسبة تستمر بالزيادة لتصل إلى (36%) عند السرعة (7.5 m/s) وعند مقارنة أنبوبين متماثلين بأبعاد الزعانف وبعدد الثقوب في كل زعنفة (3 hole/fin) أن الأنبوب المثقب بقطر صغير (2mm) افضل من الآخر المثقب بقطر (3mm) بنسبة (28%) عند السرعة (7.5 m/s) وانه لقطر ثابت للثقوب (3mm) تؤدي زيادة عدد الثقوب من (2) إلى (3) الى تحسين معامل انتقال الحرارة الإجمالي بنسبة (7.8%) لسرعة (7.5 m/s)كذلك زيادة عدد الثقوب تزيد من معامل انتقال الحرارة الإجمالي اكثر من زيادة قطر الثقوب لمساحة سطحية ثابتة للزعانف (لحالة البحث).

احسان يحيى
اخلاص محمد
هناء عبد الهادي
ساهرة حسن

EXPERIMENTAL STUDY OF FINS PERFORATION EFFECT ON THERMAL PERFORMANCE OF HELICALLY FINNED TUBES

ABSTRACT

The present research includes an experimental study for the effect of fins perforation on the performance of helically finned tubes. The experiments were made on five models of (18 mm) diameter tubes finned spirally with (12mm) high fins perforated with a circular holes , the number of holes was (3-3-6&2 hole /fin) and their diameters were (3,4,2&3mm) respectively .Each tube was tests horizontally by forcing air with(1.5-7.5 m/s) maximum velocity and Reynolds number range ($21.15\times10^3-105.7\times10^3$) on the tube .The effect of number and diameter of holes were studied.The experimental results showed that the fins perforation increase the overall heat transfer coefficient for all perforated fins tubes, but the percentage increase differs from tube to another. From the comparison of overall heat transfer coefficient for perforated finned tube ((3 hole/fin), (3mm) hole diameter) with unperforated finned tube found that it is increased to (12.3%) at air velocity (4.5m/s), this percentage continue with increasing until to reach (36%) at (7.5 m/s). It is found that for two tubes with same fins dimensions and same number of holes (3 hole/fin), the tube with smaller hole (2mm) is better than that of the larger hole (3mm) by (28%) at (7.5 m/s) maximum air velocity, the increase of the number of holes from (2) to (3) for constant hole diameter (3mm) improves the overall heat transfer coefficient by (7.8%) at (7.5 m/s) maximum air velocity .So the increasing of holes number increase the overall heat transfer coefficient more than the increasing of holes diameter for constant fins surface area (for research case).

KEYWORDS: Fins Perforation, Finned Tubes, Helical, Thermal Performance

المقدمـــة

نظـرا لأهميـة المبـادلات الحراريـة ولكثـرة اسـتخدامها بـدأ التوجـه نحـو تحسـين الأداء الحـراري والهيدروليكي لهذه المبادلات الحرارية وقد تم التوصل إلى عدة وسائل لتحسين الأداء ومنها السطوح الممتدة أو الزعانف وتخشين السطح ووسائل تحريك المائع وحلزنة جريان المائع ووسائل الشد السطحي وإضافة مواد محسنة للخواص الحرارية للسوائل وإضافة مواد محسنة للخواص الحرارية للغازات وعملية اهتزاز السطح وغيرها.تعنى الدراسة الحالية بالأنابيب المزعنفة خارجيا التي تستخدم عادة عندما يكون معامل انتقال الحرارة لاحد المائعين اكبر بكثير من المائع الآخر ،كما هو الحال في انتقال الحرارة بين الماء ذو معامل انتقال حرارة عالي تقريباوالهواء **(Kakak, et.al 1981) , (Bell and Mueller 2001)** . قام الباحث **(Abdulah,2000)** بدراسة نظرية لتأثير الثقب على الأداء الحراري للزعانف في حالة انتقال الحرارة بالحمل الحر من سطح زعنفة وقد درس أربعة أنواع من الثقوب الدائري والمربع والمثلث متساوي الأضلاع والمستطيل .وتم التحليل الرياضي لانتقال الحرارة في الزعنفة المثقبة بالاعتماد

على النموذجين أحادي البعد وثنائي البعد وقد قام بحل المعادلات التفاضلية بطريقة العناصر المحددة .ووجد أن التثقيب قد يودي إلى تحسين انتقال الحرارة أو تقليله حسب شكل الثقب وسمك الزعنفة ومعدن الزعانف.

ولقد قدم الباحث **(Zozuly&Khavin,1973)** دراسة عملية لتأثير اضطراب المائع على الأداء الحراري لحزمة من الأنابيب المزعنفة حلزونيا والمرتبة بشكل متعاقب في حالة جريان الهواء عموديا عليها ووجد أن الأداء يتحسن مع زيادة الاضطراب للمائع وكما قارن بين معامل انتقال الحرارة للصفوف المختلفة في الحزمة وقد أجرى تجاربه على حزمة من ستة صفوف من الأنابيب المزعنفة بقطر(22mm) وبارتفاع زعانف(8mm) وبسمك (0.8mm) وبسرعة هواء تتراوح بين(15-5 m/s).

لقد قام الباحثان **(Katz&Beatty,1945)** بدراسة عملية لانتقال الحرارة من مجموعة أنابيب ذات زعانف حلزونية المصنوعة من اصل المعدن وهذه الأنابيب تتضمن عدد زعانف يتراوح بين (157.5-945 fin/m)وبارتفاع زعانف يتراوح بين (1.27-9.652 mm) وقد أجرى مجموعة من القياسات أو البيانات لتقييم أداء هذه الأنابيب مستخدما البخار والهواء والماء كموائع للعمل وقد قام بمقارنة بين النتائج التي حصل عليها ووضع علاقة نظرية لمعامل انتقال الحرارة الإجمالي وقد قارن بين أداء الأنابيب المزعنفة والأنابيب الغير المزعنفة في حالة تعرضها إلى نفس ظروف العمل .

لذلك تناول البحث الحالي دراسة انتقال الحرارة بالحمل القسري من أنابيب مزعنفة حلزونيا منفردة أفقية عند جريان الهواء عموديا عليها .وتتضمن الدراسة الحالية ايجاد معامل انتقال الحرارة الإجمالي لقيم مختلفة من سرعة الهواء ولخمسة نماذج من الأنابيب ذات الزعانف المثقبة بثقوب دائرية لغرض دراسة تأثير عدد وأقطار الثقوب على الأداء الحراري لهذه الأنابيب .

جهاز الاختبار العملي (Experimental Test Rig)

لقد أجريت التجارب العملية على جهاز اختباري يتكون من الأجزاء التالية كما مبين في الشكل(1):

1- دافعة هواء (Blower) أحادية الطور متغيرة السرعة .
2- مجرى هوائي مستطيل المقطع.
3- مسخن حراري(مصنع محليا) لتسخين الماء إلى درجة الحرارة المطلوبة.
4- خزان لتجهيز الماء بتدفق ثابت .
5- مواد عازلة مثل الصوف الزجاجي والفلين لتقليل كمية الحرارة المنتقلة إلى المحيط من سطح المسخن الحراري .

6- مزدوجات حرارية من النوع (T) ومحرار زئبقي لقياس درجة حرارة الماء والهواء الداخل والخارج .

7- ساعة توقيت يدوية

8- دورق زجاجي مدرج لقياس حجم الماء المتدفق.

لقد صنع مجرى هوائي من الخشب المضغوط بطول(3.5 m) وبسمك (1.5cm) ،وهذا المجرى ذات مقطع مستطيل (80 cm ×12.6 cm) ونظرا لعدم توفر خشب بهذه الأبعاد تم تصنيع المجرى من جزأين الأول بطول (2m) والثاني بطول (1.5 m) وقد تم ربطهما بأحكام باستخدام السليكون كمادة لاصقة، وقد تم تصنيع آلية لتبديل الأنابيب في أحد جوانب الجزء الثاني حيث فتحت فيه بوابة بطول (60 cm) وثقبت من مركزها بثقب يساوي قطر الأنبوب الخارجي .

لغرض ربط المجرى الهوائي المستطيل المقطع مع مضخة الهواء الدائرية ذات قطر (12cm) ثم تصنيع ناشر لربط الجزأين من الصفائح المغلونة الخفيفة سمك(1mm) وطول (1m) وذات مقطع مستطيل تكون مساحة مقطع الدخول (12 cm ×12cm) ومساحة الخروج(12.6 cm ×80cm) ،ولضمان انتظام تيار الهواء القادم من المضخة تم وضع مشبك(screen) في بداية الناشر .

لتصنيع الأنابيب المزعنفة موضوع البحث فقد تم استخدام مادة (Carbon steel 0.5%c) لتصنيع الأنابيب أما الزعانف فصنعت من (Nickel steel 0 % Ni) نظرا لتوفرها لدى شركة المعدات الثقيلة (الجهة المصنعة) وقد اختيرت مادة الزعانف بحيث يتناسب مع طريقة تصنيع الأنابيب حيث تم استخدام شريط معدني بعرض(12mm) وبطول (22 m)وبسمك (0.3mm) من المادة المذكورة وبعد أجراء عملية التثقيب بواسطة مثقب ذو مكبس عمودي وقوالب الثقب المطلوب تم تشكيل الشريط لجعله متموجا بواسطة ماكنة تصنيع الأنابيب ليتخذ شكلا قابلا للإحاطة بأنبوب وتتم عملية التصنيع بشد الشريط بعد لحام بدايته على الأنبوب بالأوكسجين وعند تحوير الأنبوب على محور ثابت باستخدام القالب الخاص بالخطوة المطلوبة (5mm) بين الزعانف تم لحام النهاية بنفس الطريقة السابقة وقد تم تصنيع الأنابيب الخمسة بالطريقة السابقة حيث أختلف أنبوب عن الآخر بعدد وقطر الثقوب في الزعانف كما مبين في الجدول (1) الأنابيب الخمسة بطول(1m) وبقطر خارجي (18.375mm) وقطر داخلي (16mm) وبطول مزعنف (78cm) وبعدد زعانف (5 fin/in) والشكل(2) يوضح الأنابيب وترتيب الثقوب في الزعانف.

الجدول (1) مواصفات وأبعاد الأنابيب المصنعة

Tube No.	Fin/in	Hole NO.	Hole Dia.(mm)	dr (mm)	do (mm)	Lf (mm)	T (mm)
1	5	-	–	18	42	12	0.3
2	5	6	2	18	42	12	0.3
3	5	3	3	18	42	12	0.3
4	5	2	3	18	42	12	0.3
5	5	3	4	18	42	12	0.3

– لغرض توفير الماء بدرجة الحرارة المطلوبة للدخول إلى الأنبوب تم تصنيع (مسخن حراري) محلي من النحاس النقي. وهو عبارة عن مبادل حراري مزدوج الأنبوب حيث يتكون من أنبوبين من النحاس النقي الأنبوب الداخلي بقطر داخلي(50mm) وقطر خارجي(54mm) وبسمك حوالي(2mm) وأنبوب خارجي بقطر داخلي(63mm) وقطر خارجي(65mm) وبسمك حوالي(1mm) كل منهما بطول(1m) يحوي بداخله على سلك حراري ذي قدرة kW(5.56)كما هو متوفر محليا وقد تم تثبيت زعانف باللحام الكهربائي على القطر الخارجي للأنبوب الداخلي مما يزيد المساحة السطحية لانتقال الحرارحة واضطراب الماء داخل المبادل .إن هذه الزعانف الحلزونية مصنوعة من شريط نحاسي بارتفاع(4.5mm) مثبتة عن طريق الشد باستخدام قالب معدني خاص على الأنبوب الداخلي ثم لحمت حيث تنتقل الحرارة بالحمل من السلك الحراري وعبرالأنبوب الداخلي بالتوصيل ومنه بالحمل إلى الماء .قد تم استخدام مقاومة متغيرة (30A) لغرض التحكم بالتيار المار خلال سلك المسخن أولا ثم بكمية الحرارة المتولدة فيه ودرجة حرارة الماء الخارج كما في الشكل(3).

لقد تم استخدام العديد من احهزة القياس منها أجهزة قياس درجة الحرارة تم استخدام مزدوج حراري من نوع نحاس – كونستنات (Copper- Constantan) المعروف بنوع(T-type) لقياس درجات الحرارة ويعمل راس المزدوج الحراري الذي هو الجزء الحساس لدرجة الحرارة (Thermocouple Junction) على هيئة اتصال كروي (Spherical Junction)بقطر (0.5mm) وقد تم توصيل المزدوجات الحرارية إلى صندوق توزيع اختباري ومنه إلى المحرار الرقمي (Digital Electronic Thermometer) بواسطة أسلاك توصيل (Compensation wires) وقد دعت الحاجة إلى استخدام مزدوجات حرارية عدد(9) بالإضافة إلى محرار زئبقي وقد وزعت كآلاتي:–

1– قياس درجة حرارة الماء في كل من نقطة الدخول والخروج من الأنبوب المزعنف

2– قياس درجة حرارة الهواء الداخل في نقطة تقع في بداية المجرى الهوائي .

3– قياس درجة حرارة الهواء الخارج ولقد تم اختيار ثلاثة مواقع على طول المجرى الهوائي لغرض تحديد المكان الأفضل لوضع المزدوجات الحرارية اللازمة لقياس درجة حرارة الهواء الخارجي وهي على بعد30 cm و 40cm و50cm من محور

الأنبوب المزعنف وقد اختير الموقع 40cm لكونه متوسط هذين الموقعين تقريبا كما لوحظ من الاختبارات الأولية أن درجة الحرارة تتغير بالاتجاه العمودي على محور المجرى مما دعا إلى استعمال خمسة مزدوجات حرارية لقياس درجة حرارة الهواء وكانت درجة حرارة الهواء الخارج هي معدل هذه الدرجات وقد وضع مزدوجان على عمق (3cm) كما وضع مزدوجان على عمق (5cm) ومزدوج واحد على عمق(6cm) .

ويحسب معدل التدفق الحجمي من خلال قياس الزمن اللازم لتدفق حجم معين من الماء وقد استخدم دورق زجاجي مدرج بحجم 500 $m\ell$ وساعة توقيت يدوية ،وتم قياس سرعة الهواء بتوصيل أنبوبة بيتوت (Pitot – Static tube) إلى مايكرومانومتر رقمي لغرض قياس الفرق بين الضغط السكوني والضغط الكلي بوحدات (mmH_2O) وقد وضعت في مواجهة الجريان وعلى بعد (20cm) من محور الأنبوب المزعنف وفي مركز المجرى الهوائي وقد تم الاعتماد على العلاقة الديناميكة التالية لحساب سرعة الهواء عند الضغط الجوي الاعتيادي.

$$p_{tot} - p_{static} = 0.5\rho_a V_a^{\ 2}$$

$$\left(\frac{H_{tot} - H_{static}}{1000}\right)\rho_w g = 0.5\rho_a V_a^{\ 2}$$

$$V_a = 4.42945\sqrt{\frac{\Delta H(mm)}{\rho_a}} \qquad (m/s)$$

1.حساب معدل تدفق الماء خلال أنبوب الاختبار .

$$m^{\circ}_{wat} = \frac{VOL_{wat}}{time} \times \rho_{wat}$$

كل الخواص الماء عند متوسط درجة حرارته

$$t_{watm} = \frac{t_{wat1} + t_{wat2}}{2}$$

2.حساب كمية الحرارة المفقودة من الماء خلال التبريد في الأنبوب المزعنف.

$$q_{wat} = m^{\circ}_{wat} cp_{wat}(t_{wat1} - t_{wat2})$$

3.حساب كمية الحرارة المنتقلة خلال الأنبوب.

$$q = U_o A_o LMTD$$

حيث أن

$$LMTD = \frac{(T_{wat2} - T_{a1}) - (T_{wat1} - T_{a2})}{Ln\left(\frac{(T_{wat2} - T_{a1})}{(T_{wat1} - T_{a2})}\right)}$$

$$A_o = ((\pi(\pi \times (d_o^2 - d_r^2)N_F) + (\pi \times do \times N_F \times t_F) + \pi \times P_F \times d_r \times N_F)L$$
$$+ \pi \times nh \times t_F \times dh - 2((\pi \times dh^2)/4) \times nh \times N_F$$

4.حساب معامل انتقال الحرارة الإجمالي .(بفرض عدم وجود تسرب حرارة من الأنبوب إلى الجهاز أو المحيط الخارج) .

$$q = q_{wat}$$

$$U_o = \frac{q_{wat}}{A_o \times LMTD}$$

5.حساب معامل انتقال الحرارة لجانب الماء

$$h_i = \frac{k}{d_i} * 0.023\, Re_{wat}^{0.8}\, Pr_{wat}^{0.33}$$

6.حساب معامل انتقال الحرارة لجانب الهواء وبإهمال مقاومة الاتساخ للجانبين .

التجارب العمـلية

لقد تم أجراء نوعين من التجارب في البحث التالي:-

أولا-تجارب أولية : الغرض منها التعرف على دقة أجهزة القياس وأيضا معايرة الأجهزة.

ثانيا-تجارب نهائية: شملت قياس درجات الحرارة للهواء الداخل والخارج والماء الداخل والخارج ومعدل تدفق الماء من الأنابيب ولخمسة سرع للهـواء هي (1,2,3,4,5 m/s) .شملت التجارب على دراسة

I- تأثير تثقيب الزعانف على الأداء الحراري لأنبوب مزعنف حلزونيا.

II- تغير عدد الثقوب على الأداء الحراري لأنبوب مزعنف حلزونيا.

III- تغير قطر الثقوب على الأداء الحراري لأنبوب مزعنف حلزونيا.

وقد كانت هذه الدراسة ضمن برنامج تبعا للخطوات التالية:-

1- تشغيل دافعة الهواء على السرعة الأولى (1 m/s).
2- السماح للماء بالسريان خلال جهاز الاختبار عن طريق فتح صمام خزان الماء كما في الشكل (1).
3- تشغيل المسخن الحراري والتحكم بالمقاومة المتغيرة بتغير فرق الجهد عبر ملف المسخن بعد تثبيت درجة حرارة خروج الماء من المسخن الحراري على درجة الحرارة المطلوبة $50C^{\circ}$ والانتظار لمدة (60 دقيقة) .
4- بعد الوصول إلى حالة الاستقرار بعد حوالي (60) دقيقة تقريبا يتم اخذ القراءات المطلوبة الخاصة بكل أنبوب .
5- تغيير سرعة دفع الهواء ثم الانتظار إلى الوصول إلى حالة الاستقرار واخذ قراءة أخرى وهكذا لخمسة سرع مختلفة.
6- تغيير الأنبوب وإعادة الخطوات (1-5) لكل أنبوب.

مناقشةالنتائج

تناولت الدراسة العملية دراسة الأداء الحراري لأنبوب مزعنف حلزونيا بزعانف(مثقبة وغير مثقبة) كما درس أيضا تأثير تغير عدد وقطر الثقوب للزعانف على معامل الانتقال الحراري الإجمالي ، يبين الشكل (4) مقارنة الأداء الحراري للأنبوب الثالث ذا زعانف مثقبة (قطر(3 mm) وعدد (3) ثقوب) وآخر ذا زعانف غير المثقبة لحالة تغير سرعة الهواء إذ تؤدي زيادة سرعة الهواء إلى زيادة معامل انتقال الحرارة الإجمالي لكلا الأنبوبين ،ولكن الفرق في نسبة الزيادة يكون معدوم في السرعة الواطئة 1.5-3.5) m/s)(ويزداد الفرق في السرعة العالية m/s (3-7.5) إذ تكون نسبة الزيادة للأنبوب المزعنف المثقب (35.6%) بينما تكون النسبة للأنبوب المزعنف غير المثقب (25.9%) وبالرغم من نقصان المساحة السطحية لانتقال الحرارة فان زيادة الاضطرابية الناتجة من تثقيب الزعانف مما يساعد على إعادة تكوين الطبقة المتاخمة الحرارية مما يزيد من معامل انتقال الحرارة الإجمالي،أما تأثير تغير عدد الثقوب على الأداء الحراري لقطر ثقب ثابت فيمكن ملاحظته في الشكل (5) إذ تم مقارنة أنبوبين الثالث والرابع (ثقوب الزعانف متماثلة بالقطر لكلا الأنبوبين ولكنها مختلفة في العدد)، لوحظ أن الأنبوب الرابع ذا ت العدد(2)تعطي زيادة طفيفة في معامل انتقال الحرارة الإجمالي بنسبة (31.6%) أما ذا العدد(3) بنسبة (35.6%) لمدى من سرعة هواء قصوى (3 –7.5 m/s) ، ويبين الشكل (6) تأثير تغير قطر الثقوب على الأداء الحراري لمدى من السرعة الهواء (1.5 –7.5 m/s) حيث قورن الأنبوب الثالث

(قطر(3mm) وعدد (3) ثقوب) مع أنبوب الخامس (قطر(4mm) وعدد (3) ثقوب) ولوحظ أن زيادة سرعة الهواء القصوىm/s (1.5-7.5) تسبب زيادة ملحوظة في معامل انتقال الحرارة الإجمالي للأنبوب الخامس بنسبة(46%) والأنبوب الثالث بنسبة (52%) والناتج عنه زيادة كل من المساحة السطحية للزعانف (الناتج من قطر الثقب القليل) الاضطرابية .

لقد قورن الأنبوب الثاني (قطر(2mm) وعدد (6) ثقوب) مع الأنبوب الثالث (قطر(3mm) وعدد (3) ثقوب) لكونهما متساويان تقريبا في المساحة السطحية الكلية للزعانف. ولوحظ أن معامل انتقال الحرارة الإجمالي يزداد لمدى سرعة الهواء من m/s(1.5-7.5) للأنبوب الثاني بنسبة (49.4%) أما الثالث بنسبة (52%) ولكون معامل انتقال الحرارة الإجمالي للأنبوب الثاني عالي حتى للسرعة الواطئة اقل من(3.5m/s) كما في الشكل (7) إذ انه يزداد بنسبة(20.9%) عند السرعة(m/s 1.5) مقابل(14.3%) عند السرعة (m/s 7.5) عنه للأنبوب الثالث فهو افضل الأنابيب من حيث الأداء الحراري كما في الشكل(8)، ويعزى سبب ذلك إلى أولا الاضطرابات العالية الحاصلة للجريان في الأنبوب الثاني ونظرا لاعتبار الجريان موازي للثقوب فان الضغط على جانبي الزعنفة متساوي لذا لا يتولد جريان ثانوي ولكن في الحقيقة يحصل انحراف لمستوى الثقوب عن مستوى جريان المائع (نتيجة التصنيع) مما يسبب اختلاف الضغط على جانبي الثقوب والمؤدي إلى جريان ثانوي علاوة على تعرض الزعنفة إلى تشوهات سطحية (التموجات) والتي أدت إلى عدم وجود مستوي ثابت للزعنفة وقد تم الحصول على عدد من العلاقات التجريبية بين معامل انتقال الإجمالي وسرعة الهواء القصوى لجميع الأنابيب وكما مبينة في الجدول (2) .

أن الأنابيب متشابه من حيث مادة التصنيع وأبعاد الزعانف وبما أن التدفق للماء الساخن كان تقريبا ثابتا خلال التجربة فان أي زيادة في معامل انتقال الحرارة الإجمالي تكون ناتجة عن زيادة معامل انتقال الحرارة لجانب الهواء.

وتم الوصل الى عدد من الاستنتاجات

1- إن معامل انتقال الحرارة الإجمالي للأنابيب المثقبة الزعانف أعلى من غير المثقبة فهو للأنبوب الثالث يزداد بنسبة(36%) عن قيمته للأنبوب الغير مثقب عند السرعة(7.5m/s).
2- إن تحسين معامل انتقال الحرارة الإجمالي للأنبوب المثقب يتأثر كثيرا بسرعة هواء التبريد حيث يتحسن مع زيادة سرعة الهواء وبنسبة أعلى من غير المثقب .
3- إن تقليل قطر الثقب من(4 mm) إلى (3 mm) ولعدد ثابت (3 hole/fin) من الثقوب تؤدي إلى معامل انتقال حرارة أعلى بنسبة(28.9%) عند السرعة(m/s 7.5) لذلك فان الأقطار الصغيرة للثقب هي الأفضل .

4- لقطر ثابت للثقوب (3mm) تؤدي زيادة عدد الثقوب من (2) إلى (3) إلى تحسن معامل انتقال الحرارة الإجمالي بنسبة (7.8%) لسرعة (7.5 m/s) بنسبة أعلى من تغير القطر لحالة البحث .

5- زيادة عدد الثقوب تزيد من معامل انتقال الحرارة الإجمالي اكثر من زيادة قطر الثقوب لمساحة سطحية ثابتة للزعانف (لحالة البحث).

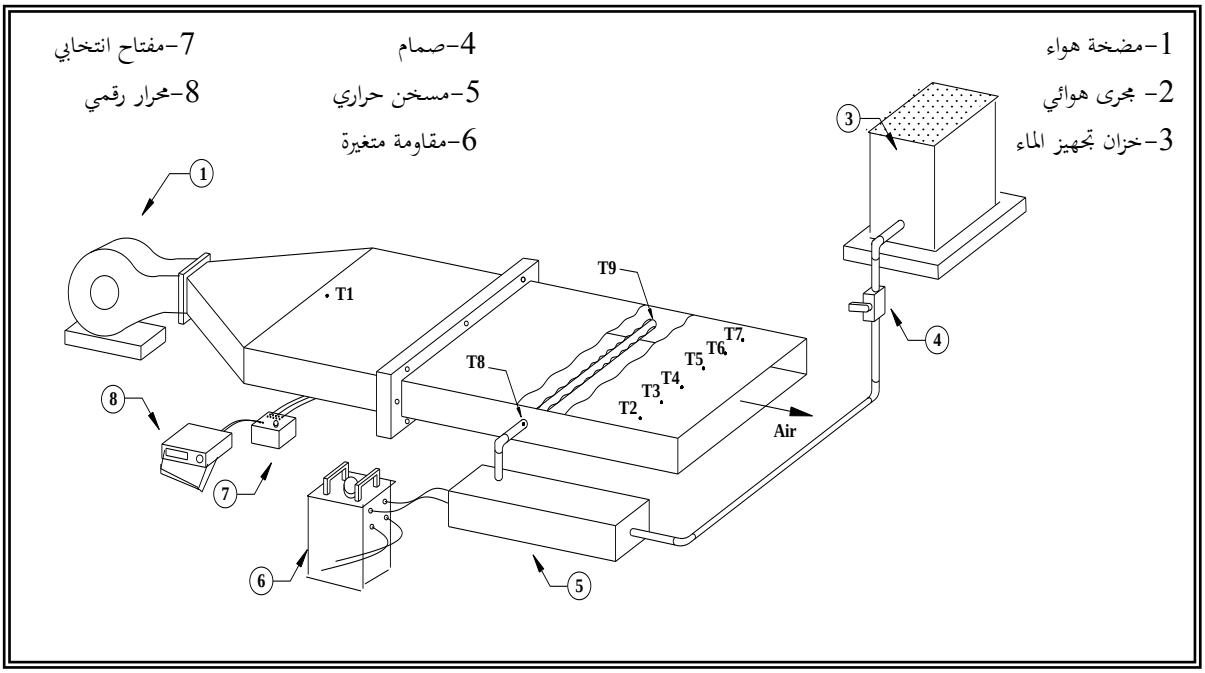

الشكل(1) يبين الجهازالاختباري

متوفر على ا

الشكل (2a) الانبوب الحلزوني المزعنف الغير مثقب

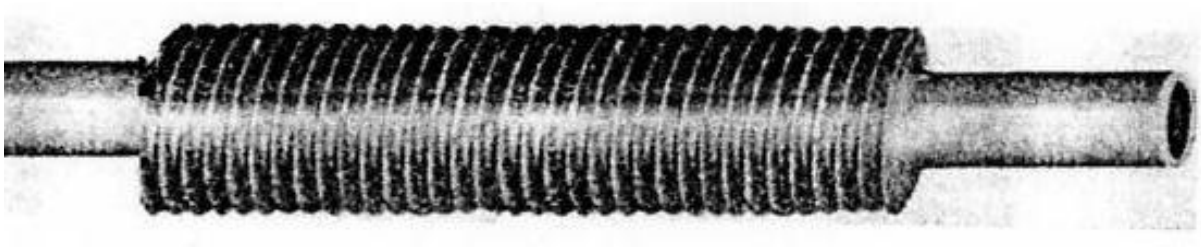

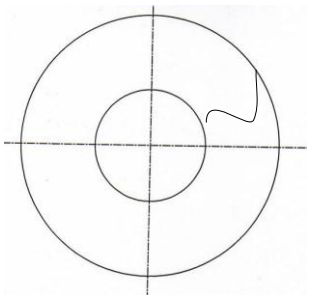

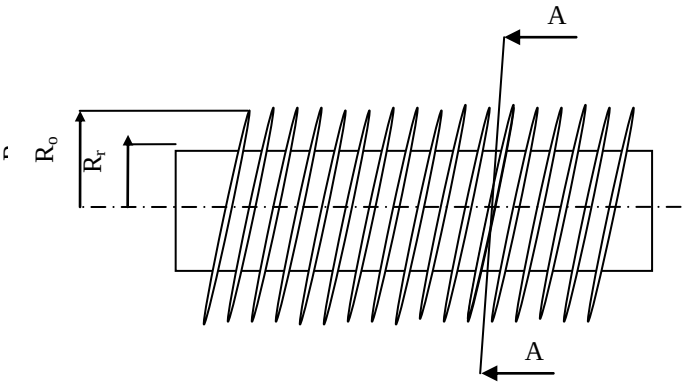

Dimension in (mm)	
dr	18
do	42
t	0.3

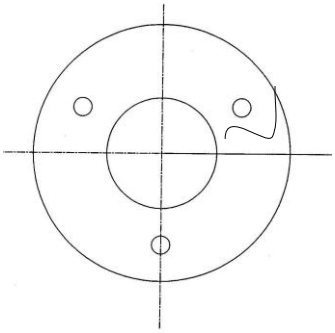

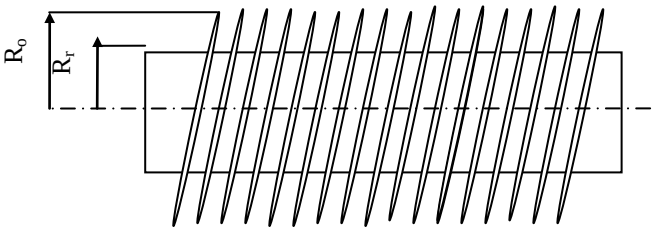

Dimension in (mm)	
dr	18
do	42
t	0.3
dh	3
Nh	3

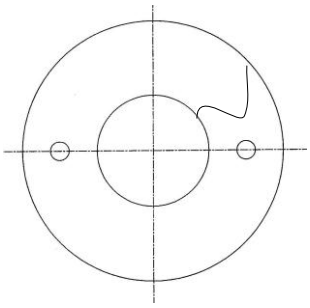

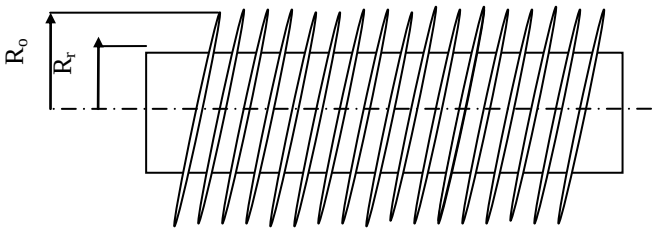

Dimension in (mm)	
dr	18
do	42
t	0.3
dh	3
Nh	2

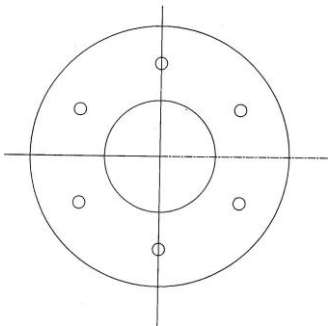

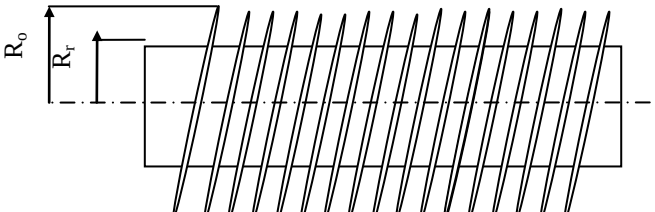

Dimension in (mm)	
dr	18
do	42
t	0.3
dh	2
Nh	6

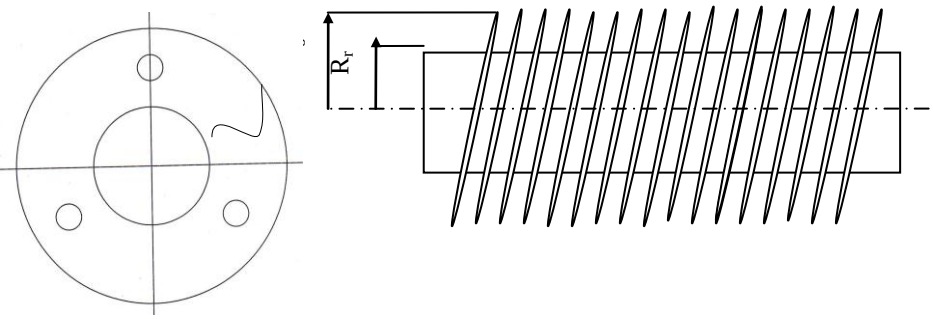

شكل(2) يبين ابعاد الزعانف والثقوب للانابيب الخمسة

1-الأنبوب الخارجي 2- الزعانف الحلزونية 3 -الأنبوب الداخلي 4-القطر الداخلي 5-سلك المسخن 6- عوازل حرارية

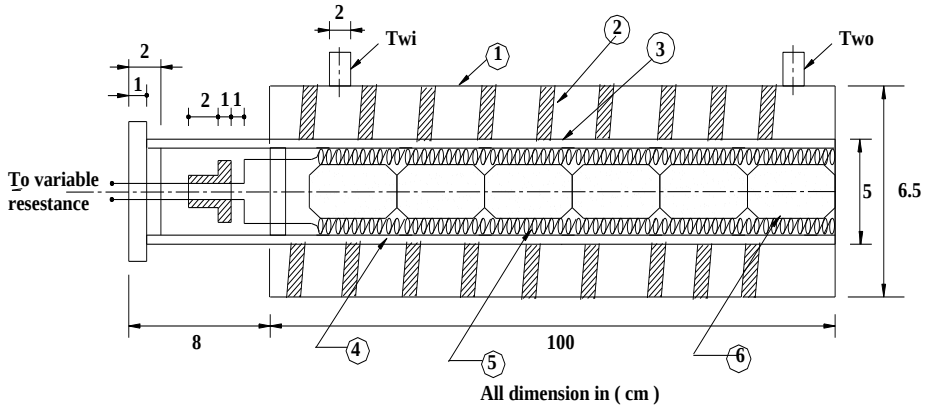

لشكل(3) المسخن الحراري

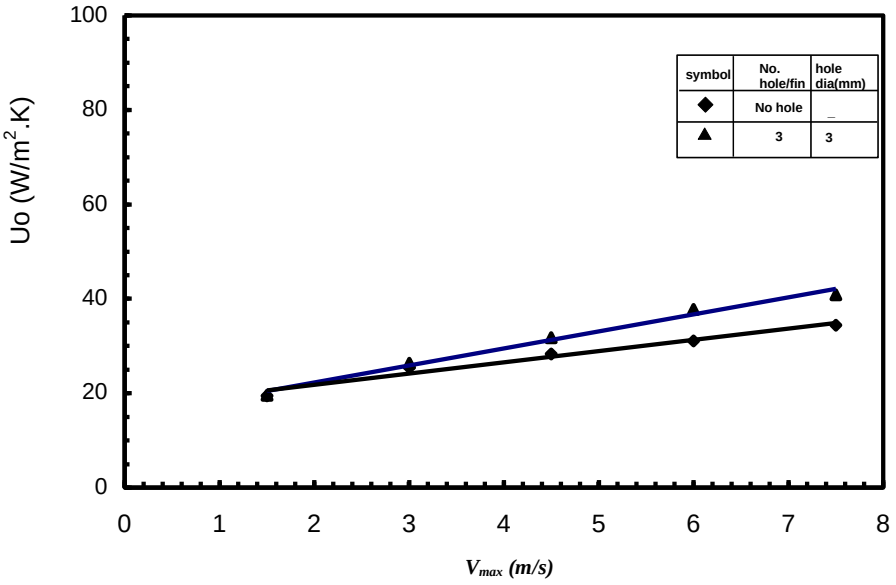

الشكل(4) مقارنة بين معامل انتقال الحرارة الإجمالي لأنبوب مزعنف حلزونيا(مثقب الزعانف وغير مثقب الزعانف)ولمدى من سرعة الهواء

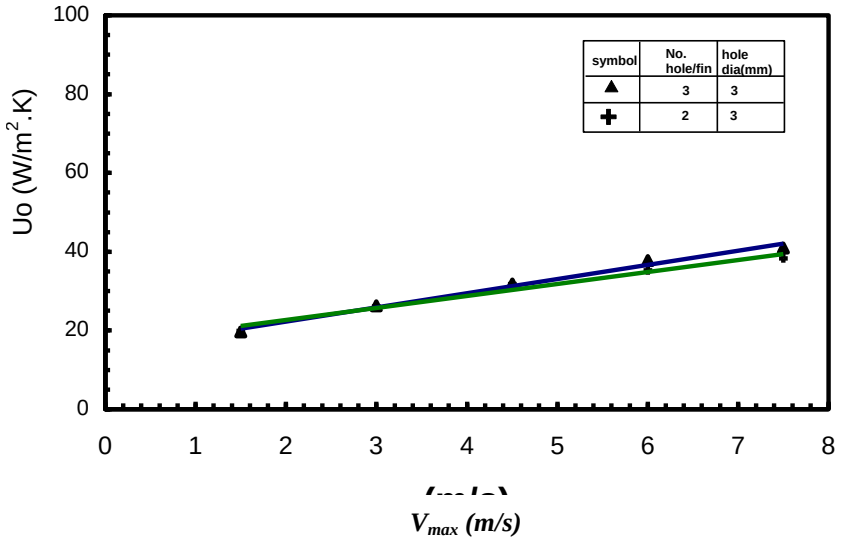

الشكل(5) مقارنة بين معامل انتقال الحرارة الإجمالي لأنبوبين مزعنفين حلزونيا(مثقبين الزعانف بقطر ثقب ثابت وبعدد متغير للثقوب) ولمدى من سرعة الهواء

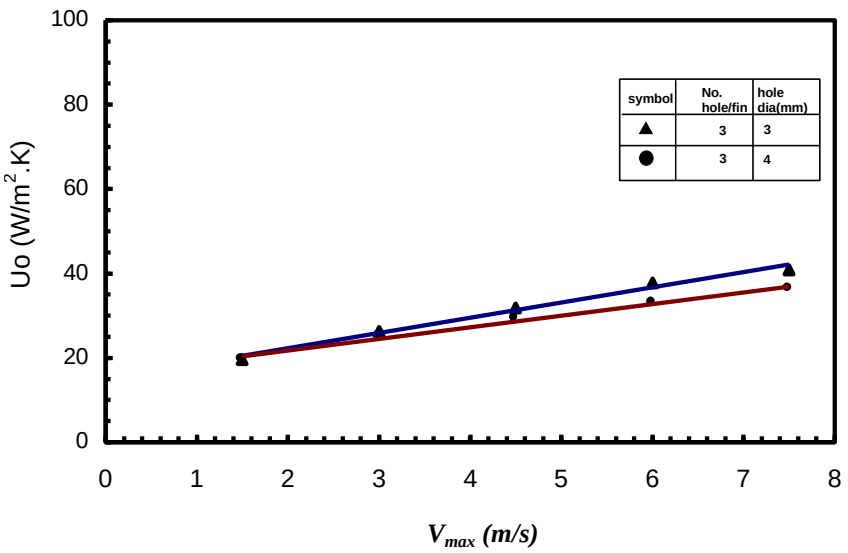

الشكل(6)مقارنة بين معامل انتقال الحرارة الإجمالي لأنبوبين مزعنفين حلزونيا((مثقبين الزعانف بقطر متغير للثقوب وبعدد ثابت) ولمدى من سرعة الهواء

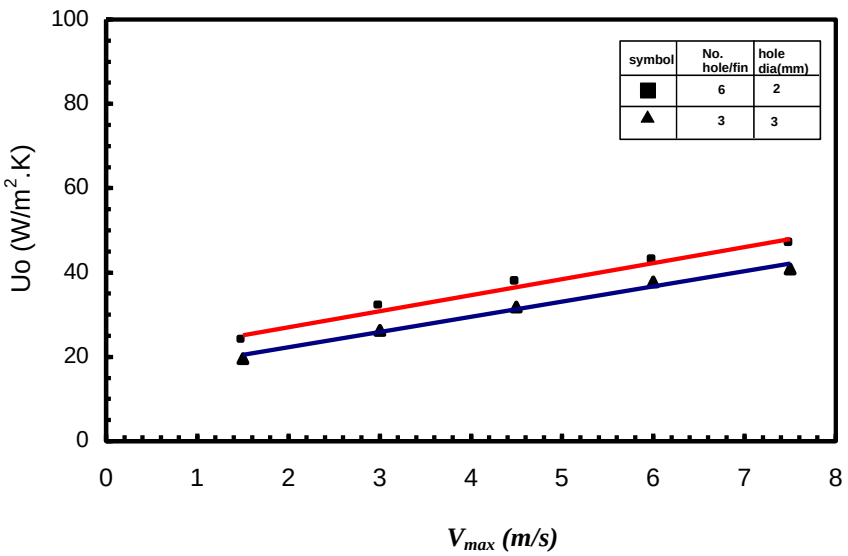

الشكل(7) المقارنة بين معامل انتقال الحرارة الإجمالي لأنبوبين مزعنفين حلزونيا بزعانف ذا مساحة سطحية متساوية ولمدى من سرعة الهواء

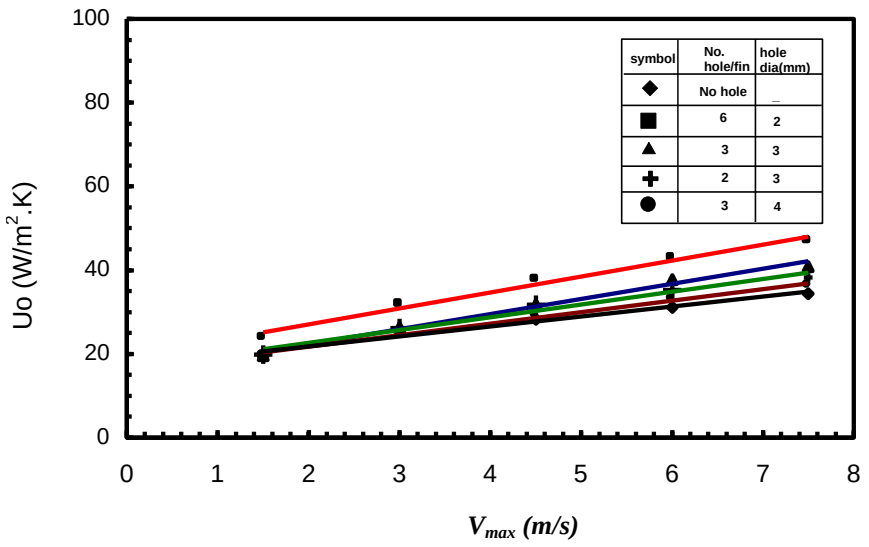

الشكل(8) المقارنة بين معامل انتقال الحرارة الإجمالي للأنابيب

الجدول(2) العلاقات التجريبية للأنابيب الخمسة

Tube No.	Nh	dh (mm)	U_0 (W/m2.K) V_{max}(m/s)
1	0	–	$UO = 2.3741V_{max} + 17.055$
2	6	2	$U_O = 3.8099\ V_{max} + 19.39$
3	3	3	$U_O = 3.6043\ V_{max} + 15.066$
4	2	3	$U_O = 3.0613\ V_{max} + 16.521$
5	3	4	$U_O = 2.76\ V_{max} + 16.2$

REFERENCES

Abdullah ,H. Mousa EL-Eesa ***Enhancement of thermal Performance of Fins Subjected toNautral Convection through Body perforation*** **, PhD. Thesis, Mechanical engineering Department, University of Baghdad,Iraq,2000.**

D.L.Katz, K.O. Beatty, JIR. and A.S Foust, "Heat Transter Through

Tubes with Integral Spiral Fins ''.*Transactions of ASME*. Nov.,pp46-56 1945.

Kakac,S.,et al. ,*Heat exchangers: thermal and hydraulic fundamentals and design* , Hemisphere Publishing Corp., New York,1981.

K.J.Bell and Dr.A.c .Mueller ,*Wolverine Engineering Data* , bookII,P-2, Wolverine tube Inc., Internet, 2001.

N.V.Zozuly A,YU.P.VorobYev and A.A Khavin " Effect of Flow Turbulization on Heat transfer in a finned tube boundle ", *HeatTransfer Soviet Research* , Vol.5, No.1, January– Fberuary, pp154-156,1973.

قائمة الرموز

الرمز	المعنى	الوحدات
D	قطر الانبوب	mm
R	قطر جذر الانبوب المزعنف	mm
Lf	ارتفاع الزعانف	mm
T	سمك الزعانف	mm
Dh	قطر الثقوب	mm
Nh	قطر الثقوب	Hole/fin
U	معامل انتقال الحرارة الإجمالي	$W/m^2.K$
H	معامل انتقال الحرارة	$W/m^2.K$
T	درجة الحرارة	$^\circ C$,K
V	السرعة	m/s
p	الضغط	N/m^2
ρ	الكثافة	kg/m^3
H	الارتفاع	mm
Vol	الحجم	$(m\ell)$
Q	الحمل الحراري	W
LMTD	المتوسط اللوغاريتمي لدرجات الحرارة	K

الرموز السفلية

a يدل على جانب للهواء

r قطر جذر الانبوب المزعنف

wat يدل على جانب للماء

w يدل على الجدار

tot يدل على الكلي

static يدل على الاستاتيكي

max يدل على القيمة العليا

o يدل على للسطح الخارجي

NUMERICAL STUDY OF INCOMPRESSIBLE FLOW AND HEAT TRANSFER IN NON-CIRCULAR DUCTS WITH CUSP CORNERS

Ass. Prof. Dr. Abdulkarim A. Hassan
Energy and Fuel Research Centre
University of Technology
Baghdad - Iraq

Qassim K. Hunaehn
Mechanical Engineering Department
University of Baghdad
Baghdad - Iraq

ABSTRACT

A numerical finite-volume calculation method was used for application to fully-developed flow and heat transfer in straight ducts with 2-Cusp, 3-Cusp and 4-Cusp cross-sectional area. The method was formulated with reference to a non-orthogonal curvilinear coordinate system which was fitted exactly into duct shape. In turbulent flow, the Reynolds stresses were calculated by using the coupled algebraic stress model of Launder and Ying (1973) with a ($k-\varepsilon$) transport model. This turbulent stress model enabled secondary flows to be included in the non-circular duct calculations. In heat transfer solution, three thermal boundary conditions were investigated.Predictions were compared with available numerical and experimental data. The turbulent flow predictions of secondary and axial velocity, wall shear stress and Nusselt number were in reasonable agreement with experiment for the fully-developed flow cases. It is concluded that, although the maximum secondary flow was found to be (1.5%-2.5%) of the mean axial flow, the absence of this flows have significant influence on the flow and heat transfer parameters. Moreover, these flows will increase when the corners of a duct become more acute. Heat transfer results showed that the peripheral temperature variation around the duct has a significant effect on the heat transfer results, and confirmed the inadequacy of the hydraulic radius concept in the cases of the very non-circular ducts when comparison is made with Blasius correlation.

الخلاصة

دراسة عددية باستخدام طريقة الحجوم المحددة تم تطبيقها لحساب الجريان وانتقال الحرارة في أنابيب ذات مقطع غير دائري وتحتوي على زوايا مستدقة.الدراسة اعتمدت على نظام المحاور الغير متعامدة والذي يأخذ شكل مقطع الأنبوب. في الجريان المضطرب, تم حساب اجهادات رينولدز باستخدام نموذج Launder and Ying (1973) مع نموذج $(k-\varepsilon)$, هذا النموذج قادر على حساب الجريان الثانوي الذي يتولد في الأنابيب الغير دائرية المقطع. في حساب انتقال الحرارة, ثلاثة شروط حدية تم تطبيقها. النتائج المستحصلة تم مقارنتها مع نتائج نظرية ومختبرية سابقة. نتائج الجريان المضطرب للسرعة الثانوية والمحورية واجهاد القص ورقم نسلت كانت مطابقة بشكل مقبول مع النتائج المختبرية المتوفرة. لقد تم الاستنتاج أنه رغم ان القيمة القصوى للجريان الثانوي تصل الى(1.5%-2.5%) من معدل الجريان المحوري ,الا أن تأثيره على النتائج واضح, فضلا عن أن هذا الجريان تزداد قوته مع وجود زوايا حادة في مقطع الأنبوب. نتائج أنتقال الحرارة أظهرت أن التغيير المحيطي لدرجة الحرارة حول الأنبوب له تأثير واضح على هذه النتائج وكذلك تبين ضعف مفهوم القطر المكافئ في حالة الانابيب ذوات الزوايا المستدقة عند المقارنة مع علاقة بلسيوس للانبوب الدائري المقطع.

KEYWORDS
non-circular ducts, cusp corners, turbulent flow, secondary flows

INTRUDUCTION

The need for compact flow passages in heat exchangers and other engineering component systems, like, the cooling and heating process in nuclear reactors and all kinds of waste-heat recovery have led to an urgent need for detailed knowledge of flow and heat transfer in non-circular ducts; in particle ducts with cusp corners. Such geometries, i.e. cusp corners, may be found in many applications like tube bundles and the shell and tube which form many types of heat exchangers. Therefore the study of these geometries, for both the flow and heat transfer, is very important in the industrial. This study will provide the require data for behavior of average and local properties for the flow and heat transfer like the friction resistance and the heat transfer coefficient.

For its mathematical simplicity, the fully-developed laminar flow in non-circular ducts has been solved for most practical geometries to investigate the effect of shape on the friction factor by using the hydraulic diameter concept. Examples of these investigations are the work of **(Gunn and Darling 1963)** as they carried out numerical study on fluid energy losses in non-circular conduits, especially sections formed by close packed tube bundles and they also investigated these shapes experimentally. **(Shah and London 1978)** showed that solutions of the governing differential equations have been obtained by both analytical and numerical methods for many non-circular geometries. It was found that non-circular ducts friction factor is always different from that of circular duct. The main reason for this difference is the deformation of the local wall shear stress, which is caused by the duct shape deformation.

A feature of turbulent flow in non-circular ducts which is absent from laminar flow is the “secondary flows” that are generated in the cross-sectional plane. These flows have the effect of transporting some of the core fluid into the corners of the duct, causing the flow to spiral in the axial direction in separate cells located across the cross-section. Although the secondary velocities are relatively weak compared with the main axial flow (about 1%-2.5% of mean axial velocity), but can have significant influence on the flow and heat transfer characteristics. Indeed, the distortions caused to the axial velocity distribution were the main early evidence of the existence of these flows in non-circular ducts.

Experimental work on turbulent flow in non-circular duct geometry is mainly confined to friction factor measurements. Examples of those are, **(Launder and Ying 1973)** for square duct, (Hassan 1984) for isosceles right angle triangular and 4-cusp ducts and **(Rijab et al 1991)** for 3-cusp duct. Previous experimental works showed that any prediction procedure must therefore include secondary flow effects if it is to produce realistic results. An alternative simplified approach was however taken by **(Launder and Ying 1973)** who developed approximate algebraic versions of the Reynolds stress transport equations for the calculation of square duct flow. These were later generalized by **(Gesener and Emery 1976)** who derived an algebraic equation set for the full Reynolds stress tensor. The prediction method of **(Launder and Ying 1973)** has been applied to the axial flow in equilateral triangular and square ducts **(Rapley 1980)**; isosceles right angle triangular and 4-cusp ducts **(Hassan 1984)** and trapezoidal and a wavy ducts **(Rokni and Gatski 1999).**

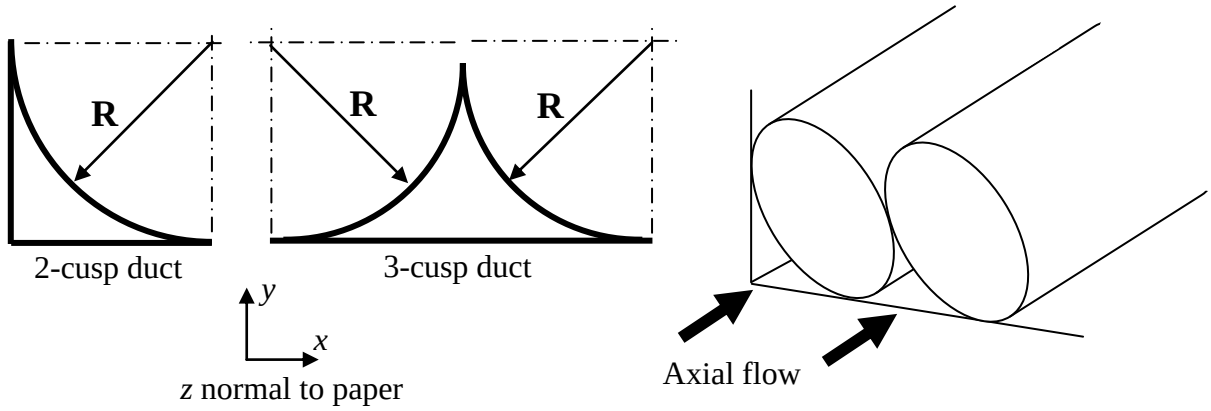

Fig.1: Ducts under consideration

The ducts shown in **Fig.1** are of particular interest because it represents the limiting case of compact rod bundle flows with rods touching with flat plates. Closely spaced rod bundles have important applications in nuclear reactor cores and other compact heat exchangers and, over the years, much effort has gone into methods of prediction **(Hassan 1984)**. However, no calculations of turbulent flow with predicted secondary flow appear to be available for 2-cusp and 3-cusp geometries. Such ducts yield a very non-circular passage shape with curved walls and cusped corners and are thus suitable for the present study. This should provide useful information on local mean flow, secondary flow and turbulence distributions and the problems associated with their prediction generally in this class of duct as well as specifically for the limiting case of rods touching in rod bundle flow.

In the present study, a numerical finite-volume procedure, used for the prediction of fully-developed turbulent flow in straight passages of arbitrary constant cross-section, is applied to 2-cusp and 3-cusp ducts, as shown in **Fig.1**. The method solves the Reynolds, continuity and turbulence transport equations on a non-orthogonal curvilinear grid which is generated numerically to fit the duct cross-section. The Reynolds stresses are calculated with an algebraic stress transport model (ASTM) of **(Launder and Ying 1973)** which links the stresses to mean velocity gradients through the turbulence kinetic energy and its dissipation rate, whose values are obtained by solving their modeled transport equations; i.e. (k-ε) model.

THEORETICAL MODEL

Governing Equations

The Reynolds equation for steady time-averaged incompressible turbulent flow can be written in Cartesian tensor form as **(Hinze 1975):**

$$\frac{\partial(\rho u_i u_j)}{\partial x_i} = -\frac{\partial P}{\partial x_j} + \frac{\partial(\sigma_{ij})}{\partial x_i} \tag{1}$$

and the continuity equation as:

$$\frac{\partial(\rho u_i)}{\partial x_i} = 0 \tag{2}$$

The stress tensor σ_{ij} represents the sum of the viscous and turbulent (Reynolds) stresses, i.e.

$$\sigma_{ij} = \mu\left(\frac{\partial u_i}{\partial x_j} + \frac{\partial u_j}{\partial x_i}\right) - \rho\,\overline{u_i' u_j'} \tag{3}$$

And the energy equation:

$$\frac{\partial}{\partial x_j}\left(\rho u_j T\right) = \frac{\partial}{\partial x_j}\left[\frac{\mu}{\Pr}\frac{\partial T}{\partial x_j}\right] + \frac{\partial}{\partial x_j}\left(-\overline{\rho u_j' t}\right) \tag{4}$$

The terms ($\overline{\rho u_j' t}$) represent the *turbulent heat fluxes.* Simply eddy diffusivity (SED) model based on the Boussinesq approximation is used to provide closure these fluxes, **(Rokni and Gatski 1999).**

$$\overline{\rho u_j' t} = -\frac{\mu_t}{\sigma_T}\frac{\partial T}{\partial x_i} \tag{5}$$

substituting **eq.(5)** into **eq.(4)** gives:

$$\frac{\partial}{\partial x_j}\left(\rho u_j T\right) = \frac{\partial}{\partial x_j}\left[\left(\frac{\mu}{\Pr} + \frac{\mu_t}{\sigma_T}\right)\frac{\partial T}{\partial x_j}\right] \tag{6}$$

Turbulence Modeling

As attention previously, generation of secondary flows by numerical model is an important factor to accurately the prediction of turbulent flow in non-circular passages. A linear eddy-viscosity model (EVM) does not have the ability to predict secondary flows, this being a consequence of the stresses being directly related to co-planar velocity gradients, as with fully-developed laminar flow. This means that a higher order turbulent stress model is needed, which usually entails solving the Reynolds stress transport equations for each stress required. Therefore, the algebraic stress transport model (ASTM) of **(Launder and Ying 1973)** is used in the present study to describe the Reynolds stresses, as:

$$\overline{w'w'} = C_1 k \tag{7}$$

$$\overline{v'v'} = C_3 k - C_2 C_4\left(\frac{k^3}{\varepsilon^2}\right)\left(\frac{\partial w}{\partial y}\right)^2 \tag{8}$$

$$\overline{u'u'} = C_3 k - C_2 C_4\left(\frac{k^3}{\varepsilon^2}\right)\left(\frac{\partial w}{\partial x}\right)^2 \tag{9}$$

$$\overline{u'v'} = \overline{v'u'} = -C_2 C_4\left(\frac{k^3}{\varepsilon^2}\right)\left(\frac{\partial w}{\partial x}\right)\left(\frac{\partial w}{\partial y}\right) \tag{10}$$

$$\overline{u'w'} = -C_4\left(\frac{k^2}{\varepsilon}\right)\left(\frac{\partial w}{\partial x}\right) \tag{11}$$

$$\overline{v'w'} = -C_4\left(\frac{k^2}{\varepsilon}\right)\left(\frac{\partial w}{\partial y}\right) \tag{12}$$

In order to be consistent with the aim of obtaining a prediction procedure for general geometries, no attempt has been made to optimize the empirical constant, whose values have simply been taken from previous studies, **(Launder and Ying 1973)** and **(Rapely 1980)** and may be summaries below:

C_1=0.23,C_2=0.027,C_3=0.562 and C_4=C_μ =0.09

The axial plane shear stresses $\overline{\rho u'w'}$ and $\overline{\rho v'w'}$ are seen from **eq.(11)** and **eq.(12)** to be represented by a gradient diffusion model with an isotropic turbulent viscosity μ_t given by **(Jones and Launder(1972)**:

$$\mu_t = C_\mu \rho \frac{k^2}{\varepsilon} \tag{13}$$

In contrast the cross-plane stresses, which are responsible for secondary flows, are seen from **eqs.(8)-(10)** to depend on strain rates in planes normal to the cross-plane.

The turbulence quantities k and ε, required in the ASTM, were obtained here from the appropriate from of the well-known (k-ε) two equation turbulence model **(Launder and Spalding 1974):**

$$\frac{\partial}{\partial x_j}\left(\rho u_j k\right) = \frac{\partial}{\partial x_j}\left[\left(\mu + \frac{\mu_t}{\sigma_k}\right)\frac{\partial k}{\partial x_j}\right] + G - \rho\varepsilon \tag{14}$$

$$\frac{\partial}{\partial x_j}\left(\rho u_j \varepsilon\right) = \frac{\partial}{\partial x_j}\left[\left(\mu + \frac{\mu_t}{\sigma_\varepsilon}\right)\frac{\partial \varepsilon}{\partial x_j}\right] + \frac{\varepsilon}{k}\left(C_{\varepsilon 1} G - C_{\varepsilon 2}\rho\varepsilon\right) \tag{15}$$

Where σ_k=1.0 and σ_ε=1.2 are the turbulent Prandtl numbers for k andε, respectively, $C_{\varepsilon 1}$=1.55, $C_{\varepsilon 2}$=2.0 and G is the generation rate of turbulence kinetic energy, calculated from **(Hassan 1984);**

$$G \cong \frac{\mu_t}{\rho}\left[\left(\frac{\partial w}{\partial x}\right)^2 + \left(\frac{\partial w}{\partial y}\right)^2\right] \tag{16}$$

Transformation of the Governing Equations

The governing equations can be written in terms of a single general equation for an arbitrary scalar dependent variable as

$$\frac{\partial}{\partial x_j}\left(\rho u_j \phi\right) = \frac{\partial}{\partial x_j}\left[\Gamma\left(\frac{\partial \phi}{\partial x_j}\right)\right] + S_\phi \tag{17}$$

where Γ is an effective diffusion coefficient and S_ϕ is a source term. **Eq.(17)** when cast into general non-orthogonal form with, the aid of the transformation of **(Rhie 1985)** to new independent variables (ζ,,η) and specialized to fully-developed flow in straight passages ($\partial/\partial z$=0 except $\partial P/\partial z$ and $\partial T/\partial z$ **(Kays and Crawford 1993)**), **eqs.(1),(2),(6),(14)** and **(15)** can be written:

u - Momentum: $$\frac{\partial(\rho G_1 u)}{\partial\zeta}+\frac{\partial(\rho G_2 u)}{\partial\eta}=\frac{\partial}{\partial\zeta}\left(\frac{\mu}{J}\alpha\frac{\partial u}{\partial\zeta}\right)+\frac{\partial}{\partial\eta}\left(\frac{\mu}{J}\gamma\frac{\partial u}{\partial\eta}\right)+S_{MX} \quad (18)$$

v - Momentum: $$\frac{\partial(\rho G_1 v)}{\partial\zeta}+\frac{\partial(\rho G_2 v)}{\partial\eta}=\frac{\partial}{\partial\zeta}\left(\frac{\mu}{J}\alpha\frac{\partial v}{\partial\zeta}\right)+\frac{\partial}{\partial\eta}\left(\frac{\mu}{J}\gamma\frac{\partial v}{\partial\eta}\right)+S_{MY} \quad (19)$$

w - Momentum: $$\frac{\partial(\rho G_1 w)}{\partial\zeta}+\frac{\partial(\rho G_2 w)}{\partial\eta}=\frac{\partial}{\partial\zeta}\left(\frac{\mu}{J}\alpha\frac{\partial w}{\partial\zeta}\right)+\frac{\partial}{\partial\eta}\left(\frac{\mu}{J}\gamma\frac{\partial w}{\partial\eta}\right)+S_{MZ} \quad (20)$$

Continuity Equation: $$\frac{\partial(\rho G_1)}{\partial\zeta}+\frac{\partial(\rho G_2)}{\partial\eta}=0 \quad (21)$$

Energy eq.: $$\frac{\partial(\rho G_1 T)}{\partial\zeta}+\frac{\partial(\rho G_2 T)}{\partial\eta}=\frac{\partial}{\partial\zeta}\left[\left(\frac{\mu}{\Pr}+\frac{\mu_t}{\sigma_T}\right)\frac{\alpha}{J}\frac{\partial T}{\partial\zeta}\right]+\frac{\partial}{\partial\eta}\left[\left(\frac{\mu}{\Pr}+\frac{\mu_t}{\sigma_T}\right)\frac{\gamma}{J}\frac{\partial T}{\partial\eta}\right]+S_T \quad (22)$$

k-Equation: $$\frac{\partial(\rho G_1 k)}{\partial\zeta}+\frac{\partial(\rho G_2 k)}{\partial\eta}=\frac{\partial}{\partial\zeta}\left[\left(\mu+\frac{\mu_t}{\sigma_k}\right)\frac{\alpha}{J}\frac{\partial k}{\partial\zeta}\right]+\frac{\partial}{\partial\eta}\left[\left(\mu+\frac{\mu_t}{\sigma_k}\right)\frac{\gamma}{J}\frac{\partial k}{\partial\eta}\right]+S_k \quad (23)$$

ε-Equation: $$\frac{\partial(\rho G_1 \varepsilon)}{\partial\zeta}+\frac{\partial(\rho G_2 \varepsilon)}{\partial\eta}=\frac{\partial}{\partial\zeta}\left[\left(\mu+\frac{\mu_t}{\sigma_\varepsilon}\right)\frac{\alpha}{J}\frac{\partial \varepsilon}{\partial\zeta}\right]+\frac{\partial}{\partial\eta}\left[\left(\mu+\frac{\mu_t}{\sigma_\varepsilon}\right)\frac{\gamma}{J}\frac{\partial \varepsilon}{\partial\eta}\right]+S_\varepsilon$$

(24)

here G_1 and G_2 are contravariant velocities:

$$\left.\begin{aligned} G_1 &= u\frac{\partial y}{\partial\eta}-v\frac{\partial x}{\partial\eta} \\ G_2 &= v\frac{\partial x}{\partial\zeta}-u\frac{\partial y}{\partial\zeta} \end{aligned}\right\} \quad (25)$$

Where J,α,β and γ can be found in **(Karki and Patankar 1989)**. Details of the source term S_ϕ for each equation can be found in **Table 1**. The turbulent stresses appearing in these source terms were calculated with the ASTM **eqs.(8)-(12).**

Table 1: Parameters in the General Transport Equation.

Equation	ϕ	S_ϕ
Continuity	1	0
x-Momentum	u	$-\frac{\partial P}{\partial x}-\frac{\partial}{\partial x}\left(\overline{\rho u'u'}\right)-\frac{\partial}{\partial y}\left(\overline{\rho v'u'}\right)-\frac{\partial}{\partial z}\left(\overline{\rho w'u'}\right)$
y-Momentum	v	$-\frac{\partial P}{\partial y}-\frac{\partial}{\partial x}\left(\overline{\rho u'v'}\right)-\frac{\partial}{\partial y}\left(\overline{\rho v'v'}\right)-\frac{\partial}{\partial z}\left(\overline{\rho w'v'}\right)$
z-Momentum	w	$-\frac{\partial P}{\partial z}-\frac{\partial}{\partial x}\left(\overline{\rho u'w'}\right)-\frac{\partial}{\partial y}\left(\overline{\rho v'w'}\right)-\frac{\partial}{\partial z}\left(\overline{\rho w'w'}\right)$
Energy	T	$\rho\, w\, J\frac{\partial T}{\partial z}$
Turbulent energy	k	$-\rho\varepsilon+G$

Turbulent dissipation	ε	$\frac{\varepsilon}{k}\left(C_1 G - C_2 \rho \varepsilon\right)$

Boundary Conditions

The treatment of solid wall boundaries includes the most difficult part of solving the problem of flow and heat transfer in non-circular duct. The boundary conditions applied around the duct periphery involved the use of wall functions to bridge between the interior solution and wall surfaces. The functions used were conventional and based on the well-known "log-law of the wall" which is written **(Versteeg and Malalasekera 1995)**;

For momentum:
$$\frac{U}{u_\tau} = \frac{1}{\kappa}\ln\left(E\,Y^+\right) \tag{26}$$

where U represents the local resultant velocity and

$$Y^+ = \frac{\rho u_\tau y_n}{\mu} \tag{27}$$

with y_n the distance from the wall along the appropriate coordinate line. u_τ is the local friction velocity taken here as

$$u_\tau = \tau_w / \rho C_\mu^{1/4} k^{1/2} \tag{28}$$

with τ_w the local wall shear stress, κ=0.42 and E=9.025 as in **(Rapley 1980).**

The above relations were used to obtain local wall shear stress for solution of the momentum equations and together with the assumption of local turbulence equilibrium also to obtain relations for the near-wall generation and dissipation of turbulence kinetic energy for solution of the turbulence equations **(Rapley 1980)**.

For energy:
$$T^+ = \sigma_T\left[U^+ + f(\sigma_L/\sigma_T)\right] \tag{29}$$

where T^+ is a non-dimensional temperature defined by**(Versteeg and Malalasekera 1995)**:

$$T^+ = \frac{\rho u_\tau c_P}{q_w}\left(T_w - T_P\right) \tag{30}$$

where T_w is the wall temperature, T_P is the near wall temperature and q_w is the wall heat flux.

and
$$f(\sigma_L/\sigma_T) = 9.24\left[\left(\frac{\sigma_L}{\sigma_T}\right)^{0.75} - 1\right]\times\left\{1 + 0.28\exp\left[-0.007\frac{\sigma_L}{\sigma_T}\right]\right\} \tag{31}$$

as well as, three thermal boundary conditions are applied for heat transfer field as in **(Rapley 1980)**
H1: Constant peripheral temperature and axial heat flux.
H2: Constant peripheral and axial temperature (isothermal wall).
H3: Constant peripheral and axial heat flux.

THE NUMERICAL SOLUTION

The transport equations, i.e. **eq.(18), eq.(19)** and **eq.(20)** for momentum, **eq.(22)** for energy and **eq.(23)** and **eq.(24)** for turbulence, can all be cast into the following common form:

$$\frac{\partial}{\partial\zeta}(\rho\phi G_1)+\frac{\partial}{\partial\eta}(\rho\phi G_2)+\frac{\partial}{\partial z}(\rho\phi G_3)=\frac{\partial}{\partial\zeta}\left(\frac{\Gamma_\phi}{J}\alpha\frac{\partial\phi}{\partial\zeta}\right)+\frac{\partial}{\partial\eta}\left(\frac{\Gamma_\phi}{J}\gamma\frac{\partial\phi}{\partial\eta}\right)+\frac{\partial}{\partial z}\left(J\Gamma_\phi\frac{\partial\phi}{\partial z}\right)+S_{Total} \tag{32}$$

Where ϕ stands for any of the main dependent variables u, v, w, T, k and ε . Γ_ϕ and S_{Total} are respectively the corresponding diffusion term and source, where $S_{Total}=S_N+JS_\phi$, and S_N is the source term arising from the nonorthogonality of the grid system,

$$S_N=-\left[\frac{\partial}{\partial\eta}\left(\frac{\Gamma_\phi}{J}\beta\frac{\partial\phi}{\partial\zeta}\right)+\frac{\partial}{\partial\zeta}\left(\frac{\Gamma_\phi}{J}\beta\frac{\partial\phi}{\partial\eta}\right)\right] \tag{33}$$

and the details of the appropriate Γ_ϕ and S_ϕ for each equation can be found in **Table 1**.

A finite-volume method was used, based on a non-orthogonal grid in the duct cross-plane, **Fig. 2**, and employing a staggered grid arrangement for u and v **(Versteeg and Malalasekera 1995)**.

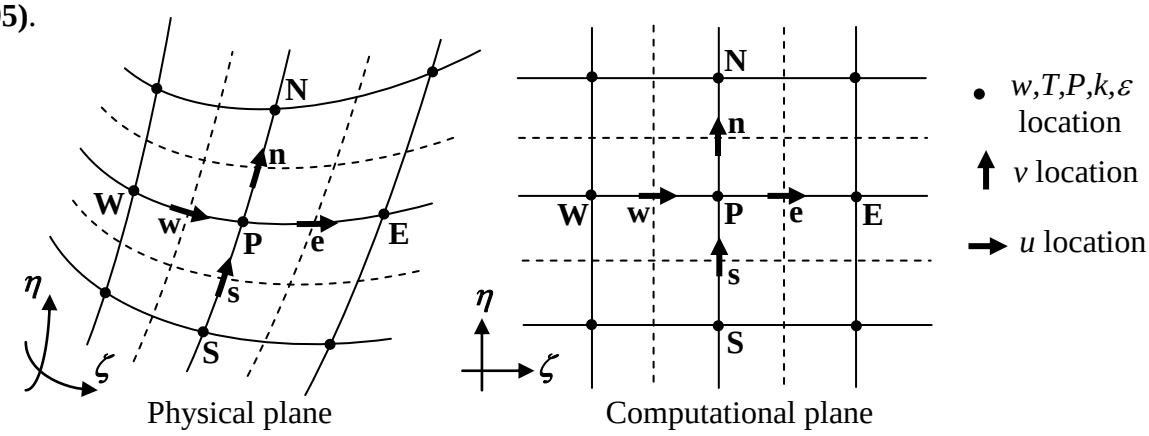

Fig. 2: The cross-plane non-orthogonal curvilinear grid

Integration of each term in **eq. (32)** across the appropriate control volumes led to the final discretized algebraic equation, i.e.

$$(A_P - S_P)\phi_P = A_E\phi_E + A_W\phi_W + A_N\phi_N + A_S\phi_S + S_C \tag{34}$$

where $A_P = A_E + A_W + A_N + A_S$ and S_P and S_C are coefficients of the linearized sources. The A coefficients contain the combined effects of convection and diffusion approximated by a standard hybrid differencing scheme **(Patankar 1980)**. The solution procedure consisted of a repeated outer sequence in which the cross-plane momentum and continuity equations were dealt with by the SIMPLE method of **(Patankar 1980),** and an inner iteration sequence in which the discretized algebraic equations were solved with a conventional line-by-line method based on the well known tri-diagonal matrix algorithm (TDMA). Because of the inherent non-linearity of the discretization equation it is sometimes necessary to slow down the change in ϕ from one iteration to the next, so in the present study, under-relaxation used to avoid divergence to the solution **(Rapley 1980)**. The convergence requirement used was that the sum of the absolute residual sources over the whole field be less than 10^{-3} of reference quantities based on overall mass and momentum flows.

RESULTS AND DISSCUSION

Grid Generation

The non-orthogonal body-fitted curvilinear grid used in the flow and heat transfer predications for 2-Cusp and 3-Cusp ducts was generated numerically by using the most common elliptic partial differential equation, Laplace equation, in the form:

$$\left.\begin{aligned} \frac{\partial^2\zeta}{\partial x^2} + \frac{\partial^2\zeta}{\partial y^2} = 0 \\ \frac{\partial^2\eta}{\partial x^2} + \frac{\partial^2\eta}{\partial y^2} = 0 \end{aligned}\right\} \tag{35}$$

The above were solved by finite differences using central differencing and a similar ADI algorithm to that used in the flow solution. Typical full mesh generated for the present cases shown in **Fig. 3** and **Fig. 4**. Tests with different meshes were used to obtain mean flow solutions that were substantially independent of the mesh and as may be expected, the secondary flow field was found to be more sensitive to mesh changes than mean flow particularly in the regions where nodes became sparse.

The Flow and Heat Transfer Calculations

At first of these calculations, the flow was assumed to be unidirectional flow (without secondary flows). The unidirectional solution severed a number of purposes. The primary purpose was to set it as a first estimate to the solution when the full flow problem is considered. This was found to be very effective in enhancing the stability and convergence rate of the numerical solution. Moreover, the results of the unidirectional solution for the ducts under consideration are compared with these with secondary flow to see the effect of secondary flows on the various parameters. The unidirectional flow is considerably simpler than that with secondary flow, since the mathematical problem is reduced to a one-dimensional problem. It is necessary to solve the axial momentum equation with the ($k-\varepsilon$) turbulence model. The results of this flow will be shown and discussed along with the other results in the following section.

For 2-Cusp duct, the flow in this geometry must represent one of the more severe tests of the present calculation method, particularly in the absence of the smaller acute angle, where the axial velocity, turbulence properties and stresses change rapidly across the narrow duct. A further physical feature of this flow should be the significant damping effect of the walls on turbulence in the acute-angled corner. **Fig. 5** shows the axial velocity plotted at side bisector. The difference between the prediction for unidirectional flow and the real situation is attributed to the influence of the direction of rotation of the secondary flow which caused a reduction of the axial velocity in the side bisector. The effect of Reynolds number on the axial velocity is shown also and as expected, as the flow rate increases the velocity field becomes more full. The predicted secondary velocity vectors in the whole duct geometry are shown in **Fig. 6**. In the symmetry half of the duct, three swirls of secondary flow are predicted with two counter-rotating cells near the acute angle and the other near the right angle. Although there are no theoretical or experimental data available for comparison, the overall pattern seems a logical extrapolation of the isosceles right angle triangular duct flow pattern of **(Hassan 1984)**, and contains the usual features of flow from the core region along corner bisectors into the corners, then returning to the core via the walls and their perpendiculars. The largest secondary velocities are about 1.2% of the mean axial velocity and occur along the corner bisectors and base wall. The effect of secondary flows on the axial velocity contours can be seen in **Fig. 7**.

The predicted wall shearing stress along the curved side and the flat side is plotted in **Fig. 8.** The effect of flow rate and secondary flows is apparent on the distribution of the wall shear stress along the two walls of the duct, and it is similar to that in the axial velocity. The effect of secondary flow in reducing the peripheral variation is evident with reduced shear stress as approach to the center wall. This tendency of secondary flow to make wall shear more uniform is apparent in all previous non-circular passages studied **(Rapley 1980)** and **(Rokni and Gatski 1999)** and can be considered a further characteristic effect of secondary flow on the mean flow.

In heat transfer calculations, the heat transfer was obtained for three thermal boundary conditions, H1, H2 and H3. Details of the treatment of these boundary conditions can be found in **(Rapley 1980).** Air was chosen as a working fluid in these calculations and its properties were taken at bulk temperature of the flow field as in **(Kays and Crawford 1993)**. The local distribution of the heat transfer coefficient for the three boundary conditions, H1, H2 and H3 is presented in **Fig. 9**. The heat transfer coefficient in the case of H3 boundary condition varies steeply in the peripheral direction when compared with that for the other two boundary conditions H1 and H2. This behaviour of the heat transfer coefficient is strongly related to the distribution of the wall temperature in the peripheral direction. The effect of flow rate is presented in **Fig. 9**; therefore as the flow rate increases the profile of the heat transfer coefficient becomes more full. However, the variation of the heat transfer coefficient with the flow rate is very slight for the range of Reynolds numbers in the figure. The effect of the secondary flow is also evident in **Fig. 10** and it is similar to that observed on the local wall shear stress. Therefore, the secondary flow acts to increase the heat transfer coefficient in the corner region and at the same time reduces it in the central region. The mean Nusselt number-Reynolds number characteristics are shown in **Fig. 11**. The relation between the three thermal boundary conditions confirms the previous conclusions from the distributions of heat transfer coefficient. As expected, the predicted results for H1 and H2 are (40%) and (50%) respectively below the pipe flow correlation, whereas the H3 line is about (87%) lower than that of the pipe flow. Moreover, the uniform wall temperature (H1) boundary condition has the maximum value of mean Nusselt number whereas the uniform heat flux case, (H3) is always the smallest. This is caused by the presence of the transverse temperature gradient which is accompanying the H3 boundary condition and does not exist in the H1 boundary condition.

In 3-Cusp duct, **Fig. 12** shows the predicted axial velocity at two sections, the corner and side bisectors; a comparison between the present predictions and experimental data of (Rijab et al 1991), is also made. It is clear that the agreement along the side bisector is very good. Moreover,

the effect of secondary flow is clear also as it tends to make the axial velocity more full near the corner and reduces it near the side bisector. The predicted secondary velocity vectors in the 3-Cusp duct are shown in **Fig. 13**. Although, there is no experimental or theoretical pattern available with which to compare the latter, the three eddies obtained in the symmetry cell are consistent with the equilateral triangular duct case of **(Rapley 1980)** and **(Rokni and Gatski 1999)**, in that flow is from the core region towards the corner along the line of the corner bisecting plane, returning via the walls and wall bisecting planes. The largest secondary velocities were about 1.5% of the mean axial velocity and were located near the wall and along the corner bisector. The axial velocity contours which are presented in **Fig. 14** shows clearly the effect of the secondary flow in convecting the momentum from high momentum central regions towards the low momentum corner regions.

In **Fig. 15** the predicted local wall shear stress is compared with the measurements that made by (Rijab et al 1991). Several indications can be drawn from this figure which confirms those observed earlier in the axial velocity predictions. It is clear that the shear stress decreases near the corners, with higher gradient near the smaller angle. This is due to the laminarization of the flow near the corners. The decrease near the center of the flat is attributed to the existence of the secondary flow, as the secondary flow tends to make wall shear stress more uniform along the section and this similar to the results of **(Hassan 1984)**, in isosceles right angle triangle.

The present calculations for the local distribution of heat transfer coefficient are compared with the experimental measurements of (Rijab et al 1991). The experimental duct had electrically heated walls which were assumed to produce a constant heat flux, H3, boundary condition. This comparison is shown in **Fig. 16** where the present prediction is seen to be in reasonable overall agreement with experiment. The local distribution of heat transfer coefficient for the three boundary conditions H1, H2 and H3 is presented in **Fig. 17**. The present calculations show, however, that the peripheral variation of the heat transfer coefficient in the case of H3 is very steep compared with that of H1 and H2. The main reason is the steep variation of the temperature field in the peripheral direction. The significant effect of secondary flow in making the peripheral variation more uniform is evident from these results. The mean heat transfer coefficient is shown in Nusselt number form in **Fig. 18**. It is apparent from this figure that the difference between H1 and H2 Nusselt number is small. This is expected since the peripheral temperature variations are quite small. On the other hand, the mean Nusselt number for H2 and H3 cases is about 5% and 65% respectively below that of H1; this is caused by the severe wall temperature variations in the peripheral direction in H3 boundary condition.

CONCLUSIONS:

A numerical solution was developed for solving the flow and heat transfer fields in 2-Cusp and 3-Cusp ducts. In flow field, the flow was assumed to be hydrodynamically and thermally fully-developed flow. The secondary flows calculated by using ASTM of **(Launder and Ying1973)**. In heat transfer field, three thermal boundary conditions, H1, H2 and H3 were investigated. The results of the present study were in good agreement with the previous measurements. The following conclusions are indicated from the predictions:

1. In turbulent flow, it is evident that the two-equations ($k-\varepsilon$) model is quite a satisfactory model for turbulent flow in non-circular ducts.

2. The predicted axial velocity and wall shear stress distributions obtained for turbulent flow in corresponding ducts studied were generally found to be flatter than might be expected from the equivalent laminar calculations, taking into account the increased shear due to turbulence. The reason for this was clearly revealed by taking advantage of the facility in the present method of being able to make calculations for the hypothetical situation in which the turbulence secondary flow is suppressed.

3. The algebraic stress transport model (ASTM) of **(Launder and Ying 1973)** have the ability, rather than eddy-viscosity turbulence models, to predicate the secondary flow in straight non-circular ducts.

4. The secondary flows so generated, will distort the mean flow since axial velocity gradients, turbulence kinetic energy and wall shear stress will tend to increase in regions where secondary flow is directed towards the wall, and decrease in regions where it is directed away from the wall. This effect will be seen in axial velocity contours which will bulge into a wall convergence, and in wall shear stresses which will be made more evenly distributed.

5. In turbulent heat transfer, the effect the secondary flow on the local temperature distributions and local heat transfer coefficient was found to be quite significant which indicates the importance of including the secondary flow in the calculations.

REFERENCES

Gunn, D.J. and Darling, M.D. (1963), Fluid Flow and Energy Losses in Non-circular Conduits, Trans. Inst. Chem. Engrs., Vol. 41, pp. 163.

Hassan, A.K.A. (1984), Forced Convection in Isosceles Right Angle Triangular and 4-Cusp Ducts, Ph. D. Thesis, University of Liverpool, U.K.

Hinze, J.O. (1975), Turbulence, McGraw-Hill, New York.

Jones, W.P. and Launder, B.E. (1972), The Prediction of Laminarization with a Two-equation Model of Turbulence, Int. J. Heat Mass Transfers, Vol. 15, pp. 301.

Karki, K. and Patankar, S. (1989), Pressure Based Calculation Procedure for Viscous Flows at All Speeds in Arbitrary Configurations, AIAA Journal, Vol.27, pp. 1167-1174.

Kays, W.M. and Crawford, M.E. (1993), Convective Heat and Mass Transfer, 3rd edition, McGraw-Hill, New York.

Launder, B.E. and Spalding, D.B. (1974), The Numerical Computational of Turbulent Flow, Computer Methods in Applied Mechanics and Engineering, Vol.3, pp. 269-289.

Launder, B.E. and Ying, W.M. (1973), Prediction of Flow and Heat Transfer in Ducts of Square-Section, Proc. I. Mech. E., Vol. 187, pp. 455.

Patankar, S.V. (1980), Numerical Heat Transfer and Fluid Flow, Hemisphere, McGraw-Hill, New York.

Patankar, S.V. and Spalding, D.B. (1972), A Calculation Procedure for Heat Mass and Momentum Transfer in 3D Parabolic Flows, Int. J. Heat Transfer, Vol.15, pp. 1785.

Rapely, C. W. (1980), Fluid and Heat Flow in Tubes of Arbitrary Cross-Section, Ph.D. Thesis, University of London, U.K.

Rhie, C. M. (1985), A Three-Dimensional Passage Flow Analysis Method Aimed at Centrifugal Impellers, Computers and Fluids, Vol. 13, No. 4, pp. 443-460

Rijab, M.S., Hassan, A.K.A. and Muhsen, S.A. (1991), Turbulent Fluid Flow in Three-Cusp Duct,

مجلة الهندسة والتكنولوجيا, المجلد العاشر – العدد السادس (الملحق) ص109.

Rokni, M. and Gatski, T.B. (1999), Predicting Turbulent Convective Heat Transfer in Three-Dimensional Duct Flows, NASA/TM-1999-209843.

Shah, R.K. and London, A.L. (1978), Laminar Flow Forced Convection in Ducts, Advances in Heat Transfer, Academic Press, New York.

Versteeg, H.K. and Malalasekera, W. (1995), An Introduction to Computational Fluid Dynamics, the Finite Volume Method, Longman Scientific and Technical.

NOMENCLATURE

Latin Symbols

A: Coefficient of the discretized equations
C_1, C_2, C_3, C_4: Constants in ASTM
cp : Specific heat at constant pressure , J/(kg.K)
$C_\mu, C_{\varepsilon 1}, C_{\varepsilon 2}$: Constants in ($k-\varepsilon$) turbulence model
D : Diffusion term
E : Logarithmic law constant, equation (3.58)
F : Convection term
g : Metrics tensor element
G : Generation term of the turbulent kinetic energy
$G1, G2, G3$: Contravariant velocity components
h : Heat transfer coefficient, W/(m^2.K)
J : Jacobian of transformation
k : Turbulence kinetic energy, m^2/s^2
Nu : Nusselt number
P : Pressure, N/m^2
q'' : Heat flux, W/m^2
Re : Reynolds number
S_ϕ : Source term of ϕ ,table (3-1)
S_N : Source term due to non-orthogonality, equation (3.40)
S_{Total} : Total source terms
T : Temperature, K
T_b : Bulk (mixed) fluid temperature, K
u, v, w : Cartesian velocity components, m/s
x, y, z : Cartesian coordinate, m
U^+ : Dimensionless velocity, eq. 3.54)
Y^+ : Dimensionless distance from a wall, equation(3.52)

Greek Symbols

α, β, γ : Coordinate transformation parameters, equation(3.29)
δ_{ij} : Kronecker delta
Δ : Grid spacing, m
λ : Under-relaxation factor
ΔV : Elementary volume, m^3
Γ : Diffusion coefficient
ε : Dissipation rate of kinetic energy, N/(s.m^2)
κ : Von Karman constant
μ : Laminar viscosity, kg/(m.s)
μ_e : Effective total viscosity,($\mu+\mu_t$), kg/(m.s)
μ_t : Turbulent viscosity, kg/(m.s)
ν : Kinematics viscosity, m^2/s
ζ, η: Curvilinear coordinates
ρ : Density, kg/m^3
σ_{ij} : Stress tensor, N/m^2
$\sigma_k, \sigma_\varepsilon$: Effective Prandtl numbers
τ_{ij} : Viscous stress tensor, N/m^2

τ_w :Wall shear stress, N/m^2

ϕ :Dependent variable

Subscripts

e,w,n,s :Face of the control volume
E,W,N,S :Neighbor nodes of point p
i,j :Index Notations or coordinate direction identifiers
L :Local value
m :Mean value
MX,MY,MZ :Refers to source term of momentum equation in Cartesian coordinates
nb :Abbreviation of neighboring

Superscripts

* :Guessed quantity or quantity from last iteration
′ :Fluctuating quantity in the time averaging or correction quantity
— :Averaged quantity

Abbreviations

ASTM :Algebraic stress transport model
CFD :Computational Fluid Dynamics
SIMPLE :Semi- Implicit Method for Pressure Linked Equation
TDMA :Tridiagonal Matrix Algorithm

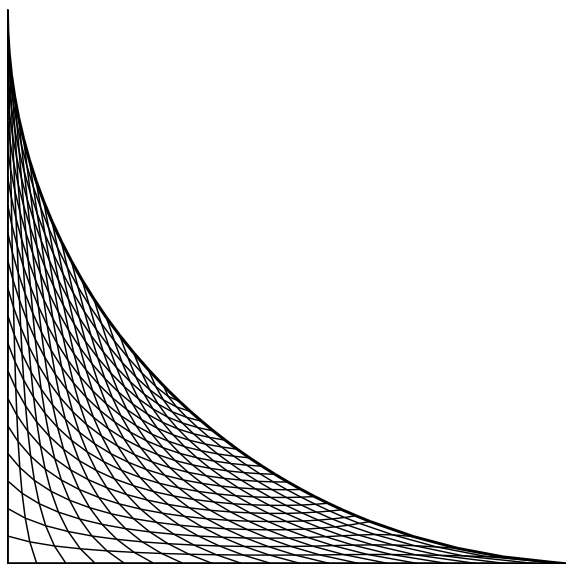

Fig.3: Non-orthogonal curvilinear grid for 2-cusp duct

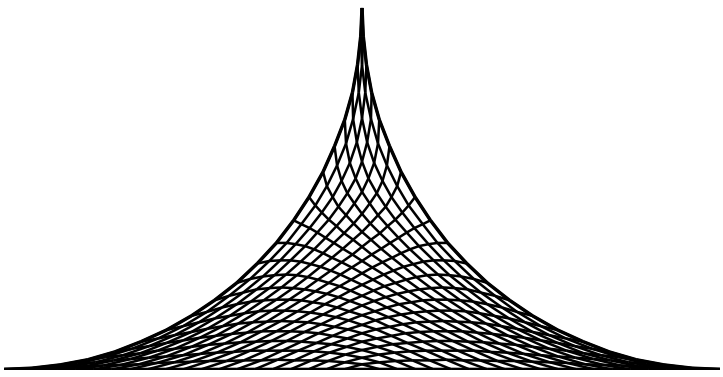

Fig.4: Non-orthogonal curvilinear grid for 3-cusp duct

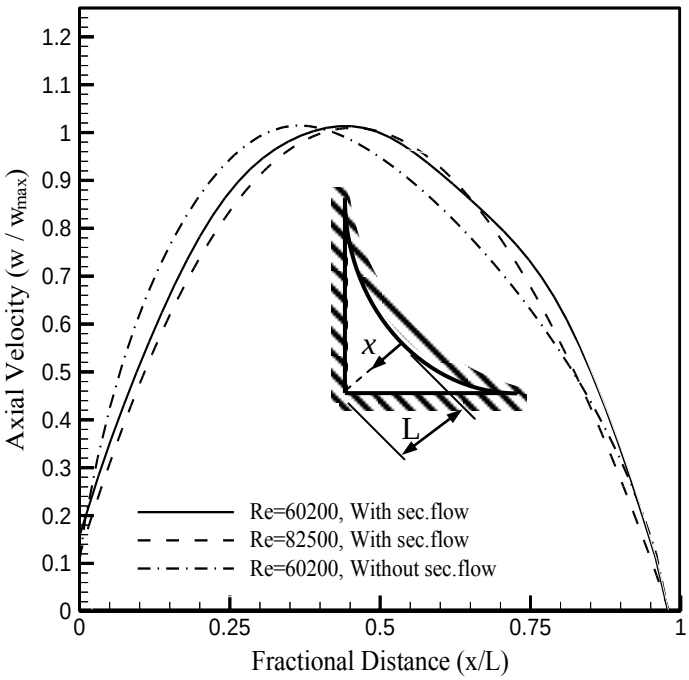

Fig.5: Axial velocity prediction in 2-cusp duct.

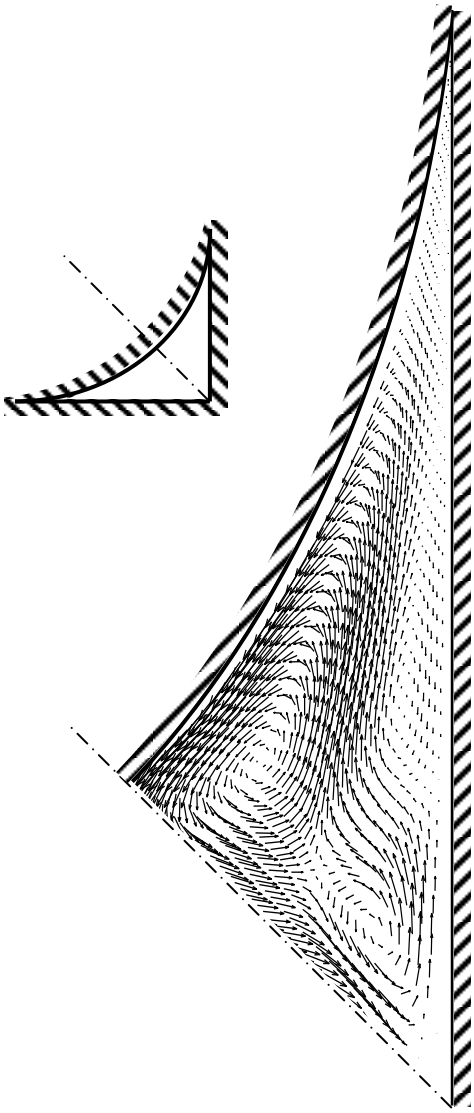

Fig.6: Predicted secondary velocity vectors in 2-cusp duct, Re=60200

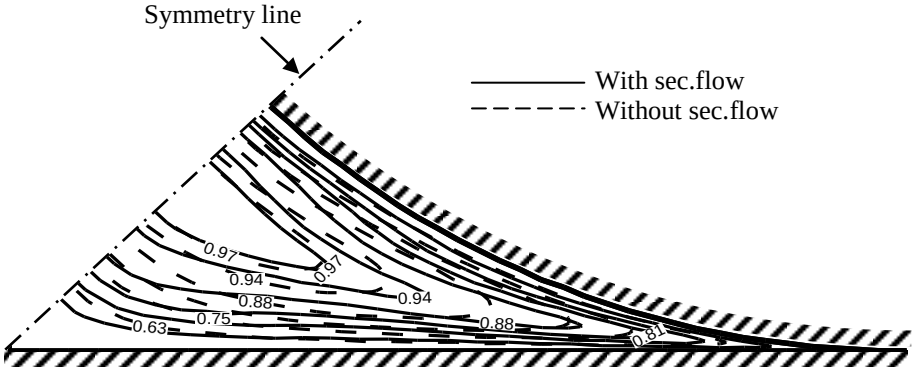

Fig.7: Axial velocity contours in turbulent flow in the 2-cusp duct, Re=60200

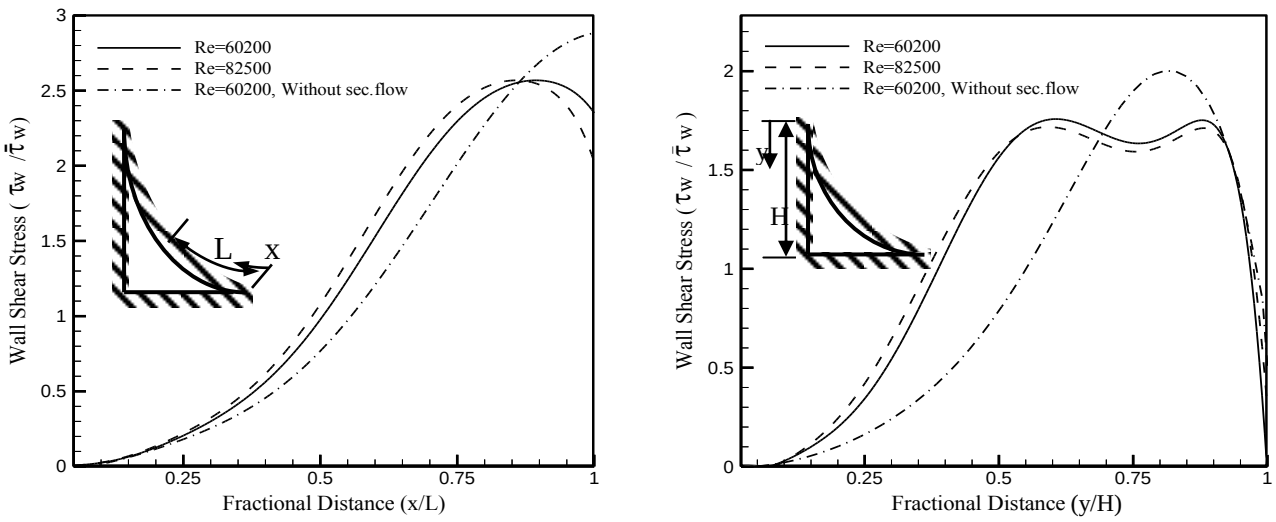

Fig.8: Wall shear stress prediction in turbulent flow in 2-cusp duct

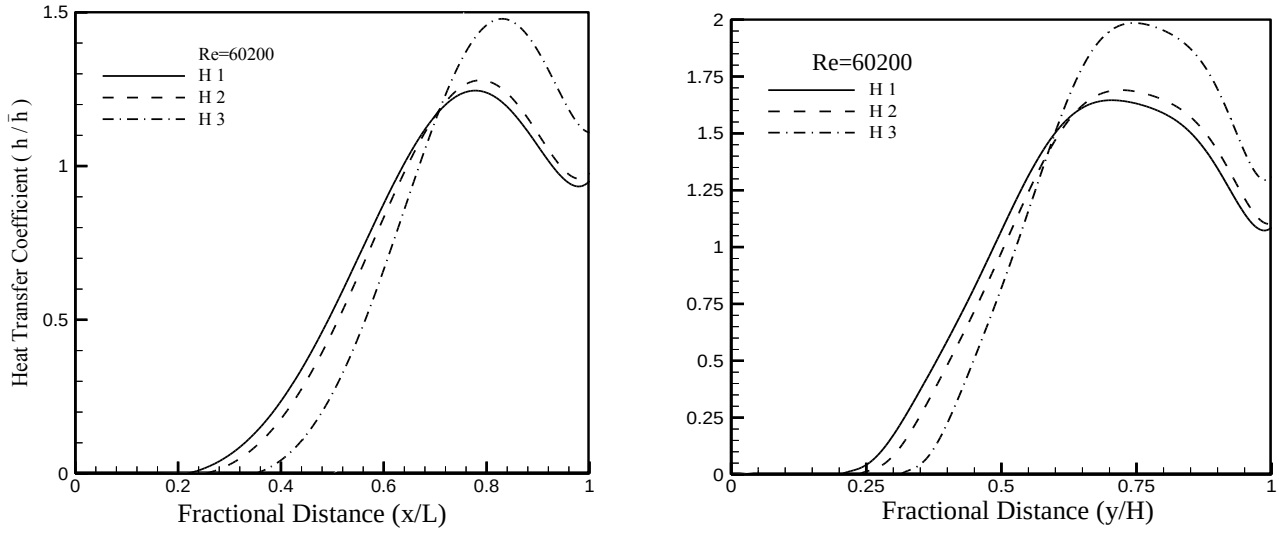

Fig.9: Predicted local distribution of heat transfer coefficient in 2-Cusp duct
(Effect of thermal boundary conditions)

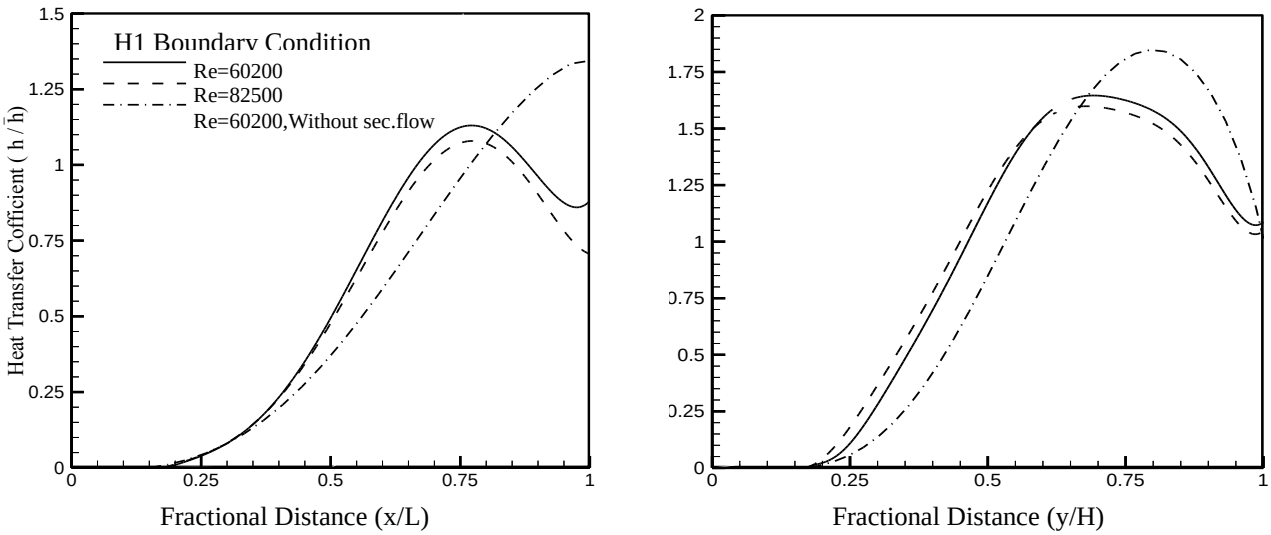

Fig.10: Predicted local distribution of heat transfer coefficient in 2-Cusp duct
(Effect of the secondary flow and the flow rate)

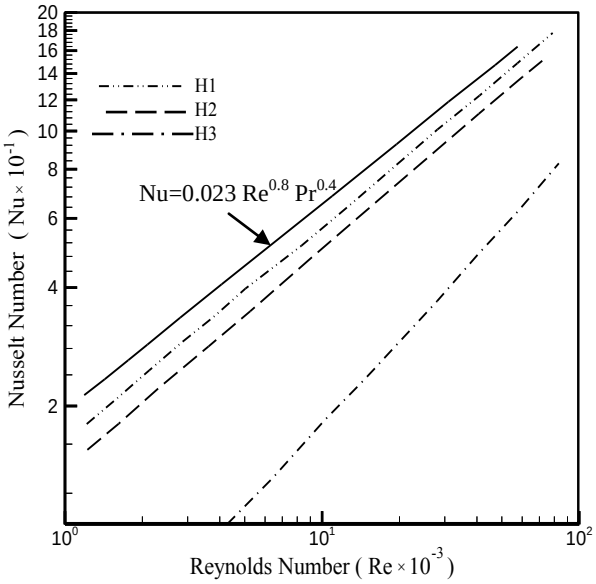

Fig.11: Predicted Nusselt number in 2-cusp Duct.

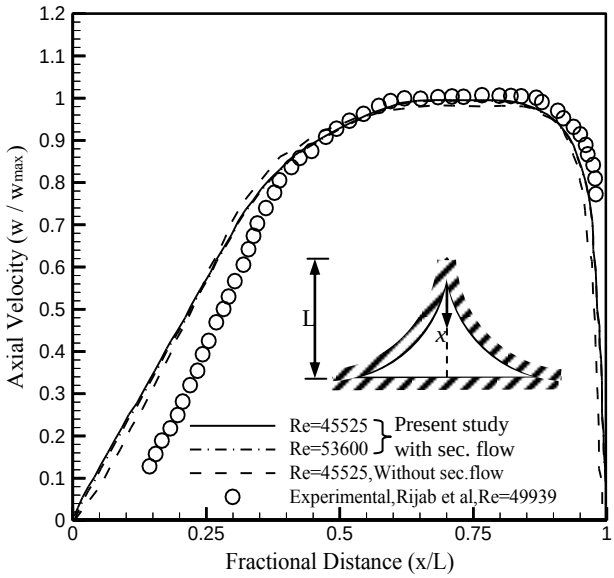

Fig.12-a: Axial velocity in turbulent Flow in 3-cusp duct (corner bisector)

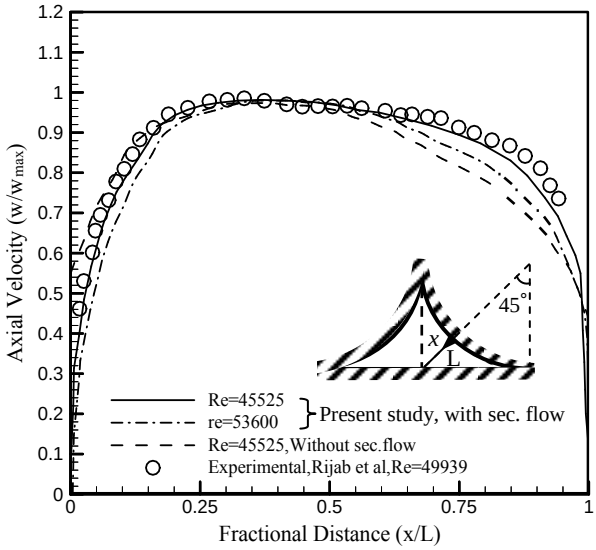

Fig.12-b: Axial velocity in turbulent flow in 3-cusp duct (side bisector)

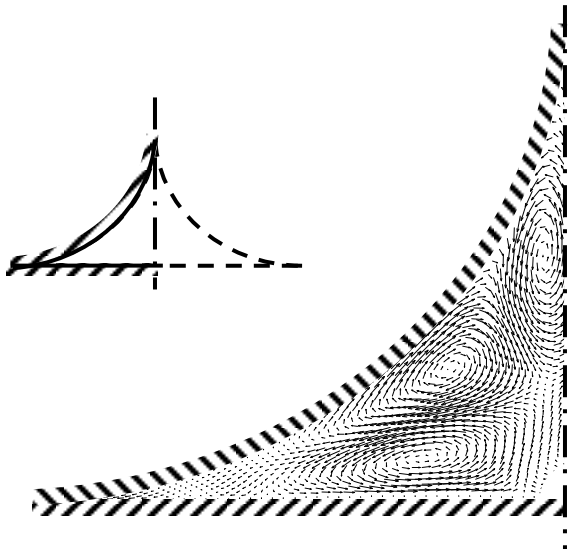

Fig.13: Predicted secondary velocity vectors in 3-cusp duct, Re=45525

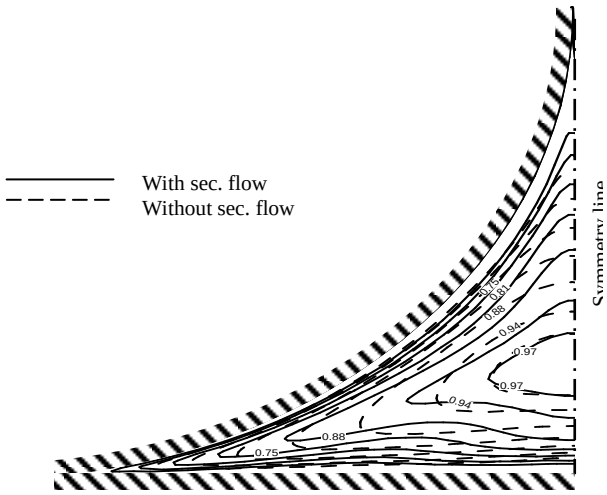

Fig.14: Axial velocity contours in turbulent flow in the 3-cusp duct, Re=45525

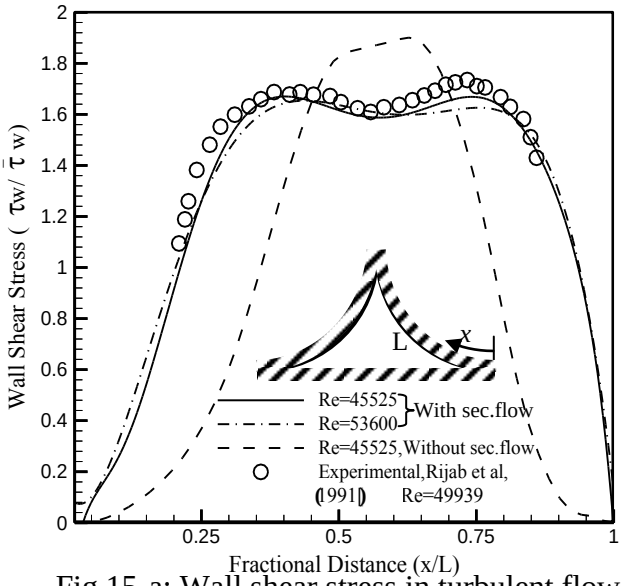

Fig.15-a: Wall shear stress in turbulent flow in 3-cusp duct.

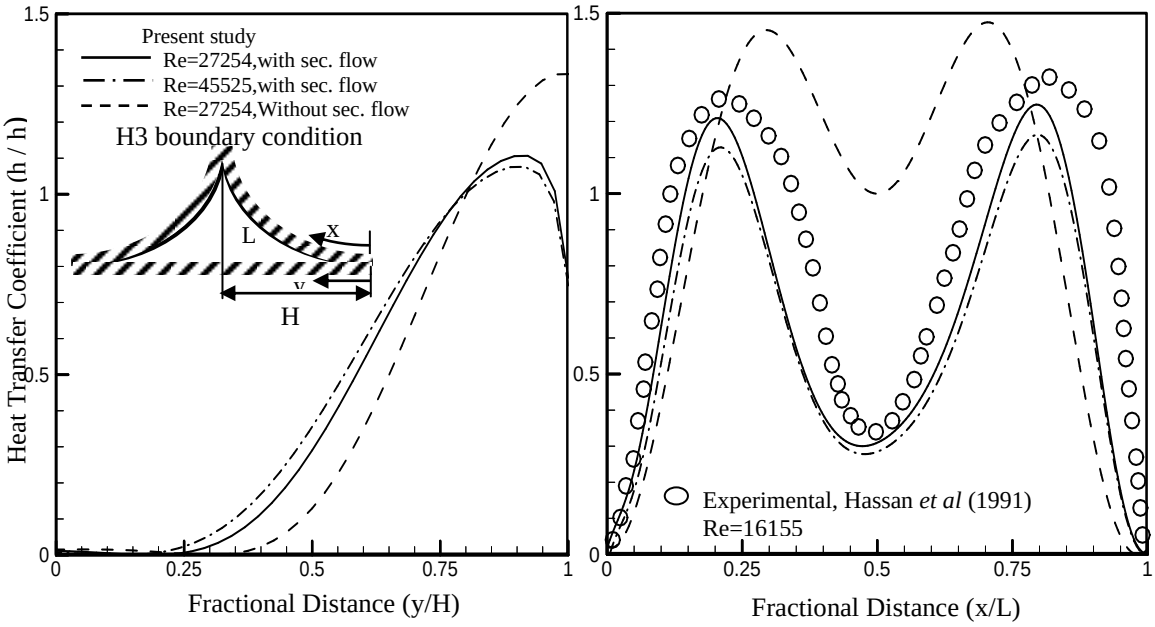

Fig.16: Effect of the secondary flow and the flow rate on the distribution of heat transfer coefficient

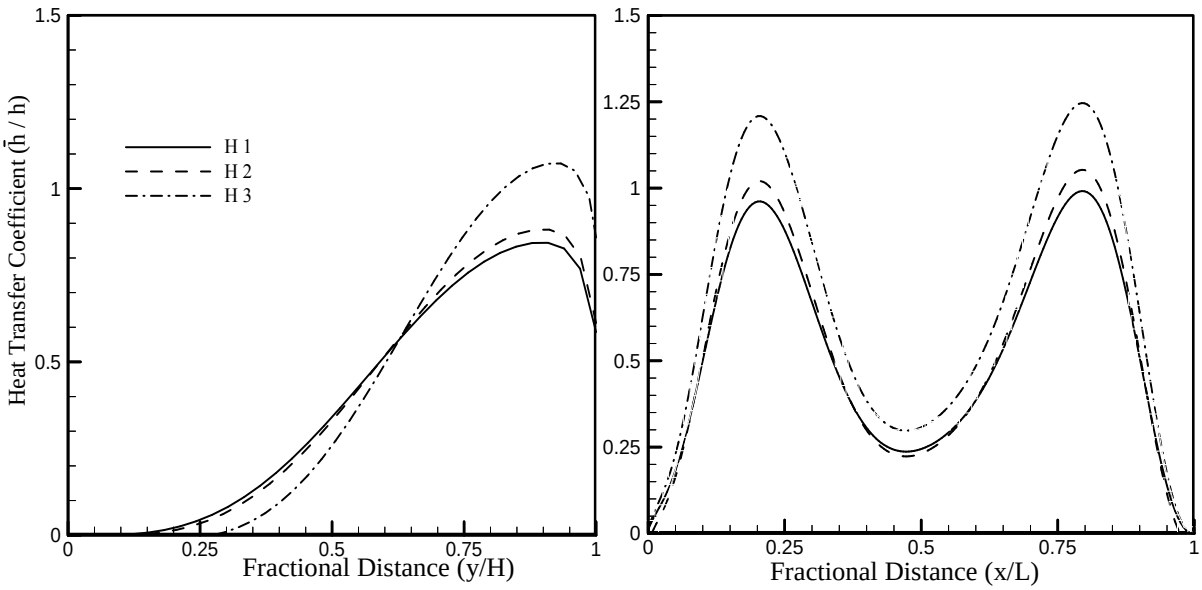

Fig.17: Effect of thermal boundary conditions on the distribution of heat transfer coefficient

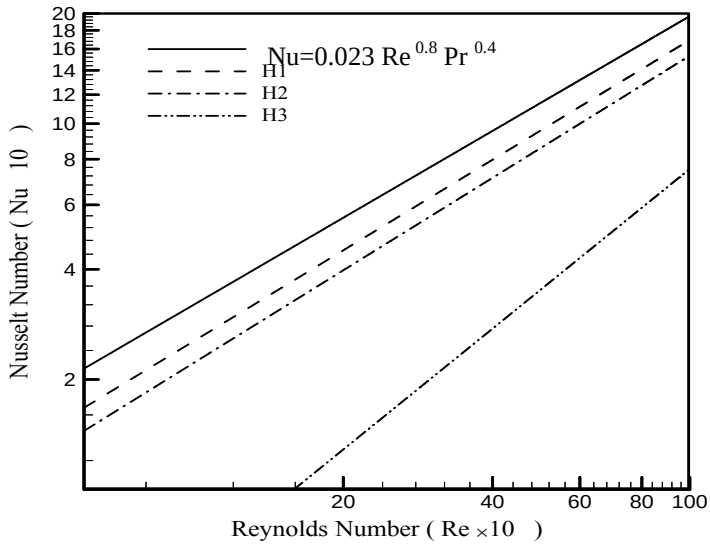

Fig.18: Predicted Nusselt Number in 3-Cusp Duct.

UNSTEADY HYDRODYNAMIC AND THERMAL BOUNDARY LAYERS OVER A FLAT PLATE WITH UNIFORM INJECTION OR SUCTION

Ihsan Y.Hussain
Mech. Engr. Dept.
College of Eng. / University of Baghdad
Baghdad-Iraq

Abdul Wahab A. Taha
Mech. Engr. Dept.
College of Eng. / University of Al-Mustansiriya
Baghdad-Iraq

Ayser M. Fleh
Mech. Engr. Dept.
College of Eng. / University of Baghdad
Baghdad-Iraq

ABSTRACT

A computational algorithm for calculating the unsteady compressible and turbulent hydrodynamic and thermal boundary layers over a porous flat plate with uniform suction or injection is developed in the present work. The mathematical modeling involves the derivation of the governing partial differential equations of the problem. These are the continuity, the momentum, the ($\kappa - \varepsilon$) turbulence model and the energy equations. Besides, the perfect gas law and the Sutherland's law of molecular viscosity are also used. A proper initial and boundary conditions are specified to be used in the solution of the governing equations. A numerical solution of the governing equations is made by using the control volume approach, with non-staggered grid technique and modified SIMPLE algorithm. The numerical solution is capable of calculating the velocity and temperature distributions of the calculation domain, the kinetic energy and dissipation of turbulence, the local and average skin-friction and heat transfer coefficients and Nusselt number, and the hydrodynamic and thermal boundary layers thicknesses. All these parameters are calculated at the transient and steady states. The numerical results show that the developed algorithm is capable of calculating the flow field, properly and accurately. The results show that injection causes slight decrease in the temperature inside the thermal boundary layer, a decrease in skin – friction coefficient, a slight increase in the Nusselt number, a decrease in hydrodynamic boundary layer thickness, an increase in thermal boundary layer thickness and an increase in the time required to reach the steady state. Suction almost causes reverse effects.

الخلاصة

في البحث الحالي، تم التوصل إلى نموذج رياضي عددي لحساب الطبقة المتاخمة الهيدروديناميكية والحرارية العابرة، الانضغاطية والمضطربة على صفيحة مسطحة مسامية مع حقن وسحب بسرعة منتظمة من الصفيحة. يتضمن النموذج الرياضي اشتقاق المعادلات التفاضلية الجزئية للمسألة، والتي هي معادلات الاستمرارية، الزخم، معادلتي نموذج ($\kappa - \varepsilon$) للاضطراب ومعادلة الطاقة. بالإضافة إلى ذلك، تم استخدام معادلة الغاز المثالي وقانون سذرلاند للزوجة الديناميكية. تم تعريف ظروف ابتدائية وحدية مناسبة لاستخدامها في حل المعادلات. تم حل المعادلات عدديا باستخدام تقنية الحجم المحكوم مع شبكة غير مزحفة وطريقة (SIMPEL) المعدلة. للحل العددي القابلية على حساب توزيعات السرع ودرجات الحرارة، الطاقة الحركية والتبدد للاضطراب،

القيم الموقعية والمتوسطة لمعدل الاحتكاك، معامل انتقال الحرارة ورقم نسلت، سمك الطبقة المتاخمة الهيدروديناميكية والحرارية. كل هذه المتغيرات تحسب للحالة العابرة والمستقرة. أظهرت النتائج العددية إن النموذج العددي الذي تم التوصل أليه له القابلية على حساب الجريان بصورة مناسبة ودقيقة. بينت النتائج العددية أن الحقن يسبب انخفاض طفيف في درجة الحرارة داخل الطبقة المتاخمة الحرارية, انخفاض في قيم معامل الاحتكاك, زيادة طفيفة في قيم رقم نسلت, انخفاض في سمك الطبقة المتاخمة الهيدروديناميكية, زيادة في سمك الطبقة المتاخمة الحرارية, وزيادة في الوقت المطلوب للوصول إلى الحالة المستقرة.

KEYWORDS

Boundary Layer, Flat Plate, Unsteady, Hydrodynamic and Thermal, Injection and Suction.

INTRODUCTION:-

The flow and heat transfer inside the boundary layer may be either steady or transient (unsteady) .The most important cases in practical applications are usually steady cases. Nevertheless, there exists some important unsteady applications, such as motion started from rest, periodic motion, accelerated motions, boundary layer behind a moving normal shock wave,…etc. Besides, all processes in nature must pass through a transient period before they attain the steady conditions. Therefore, the calculation of the transient phenomena associated with any process is an important matter. The development of the theory of boundary layer flow in compressible streams was stimulated by the progress in aeronautical engineering and rockets and artificial satellites. When flight velocities of the order of multiples of the velocity of sound are attained, the work of compression and energy dissipation produces considerable increase in temperature and always forces to include thermal boundary layer in the analysis, because the two boundary layers strongly interact with each other. Boundary layers with localized injection and section are frequently found in engineering applications, the configuanation is often found in gas turbine applications, where the aim is to protect the surface from high transfer rates. Other applications have been boundary layer control, drying processes in the chemical industry and more recently, cooling of electronics by means of injections through the printed circuit board. Most of these applications are concerned with injections through a series of small holes. However, many applications also exist (boundary layer control and high efficiency heat exchangers) where the injection is performed through a porous surface. The effects of wall suction or injection have been studied experimentally or numerically, for various flow fields. It has been known that in turbulent boundary layer, uniform blowing from the wall decreases the skin friction and increases the strength of fluctuating quantities, while suction has nearly the opposite effect. However, the increase of turbulent fluctuations from blowing may cause an increase of drag in the downstream due to strong turbulent motion there. In the case of suction, the downstream skin friction may be reduced due to the stabilization of turbulence even through the skin friction increases near the place of suction. The problem was investigated with different approaches. **(Jeongyoung and Haecheon. 1999)** investigated effect of uniform blowing or suction from aspanwise slot on a turbulent layer flow by using the direct numerical simulation technique. **(Per-Age and Anatoli 2000)** examined the effect of localized injection through porous strip on a turbulent boundary layer at zero pressure gradient condition experimentally. **(Park and Sung 2001)** performed study to analyze flow structure behind local suction and blowing in a flat plate turbulent boundary layer. **(Kyoungyoun and Haying 2001)** investigated the effects of local blowing or suction from a span wise on a turbulent boundary layer flow using the direct numerical simulation technique, where three different blowing or suction velocities are imposed on the slot keeping blowing or suction flow rate constant. **(Kyoungyoun and Hynng 2003)** performed direct numerical simulation to analyze the effect of, periodical blowing through a span wise slot on turbulent boundary layer. The present work deals with the calculation of the transient compressible turbulent hydrodynamic and thermal boundary layers over a porous flat plate with uniform suction

or injections see **Fig.1**. It will be assumed that the quantity of fluid removed from the stream is so small that only fluid particles in the immediate neighborhood of the wall are sucked (injected) a way. That is to say the ratio of suction or injection velocity $V_w\ (x)$ to free stream velocity U_∞ is small, say V_w/U_∞ =0.001 to 0.01 the condition of no slip at the wall is retained with suction present, as well as the expression $\tau_w = \mu\left(\frac{\partial u}{\partial y}\right)_0$ for the shearing stress at the wall

MATHEMATICAL MODELIN:-

The usual system of Cartesian coordinates will be adapted, the x-axis being along the wall, and the y-axis being at right angle to it. Suction or injection will be accounted for by prescribing non-zero normal velocity component (V_w) at the wall. In the case of suction Vw<0 and V_w>0 will be used for injection, see Fig (1). Flow and heat transfer with negligible edge effect are assumed (w=0, $\partial(\ )/\partial z = 0$) with uniform suction or injection and negligible axial diffusion ($\partial^2(\ )/\partial x^2 = 0$)

A cording to the previously mentioned assumptions, the governing conservation and constitution laws will be presented here interims of the geometry and coordinates system of **Fig.1** These are the continuity, the momentum, the (K-ε) turbulence model and the energy equations **(Ayser 2005)**:

The continuity equation is

$$\frac{\partial \rho}{\partial \tau} + \frac{\partial}{\partial x}(\rho u) + \frac{\partial}{\partial y}(\rho v) = 0 \qquad (1)$$

The x-direction momentum equations is

$$\rho\left(\frac{\partial u}{\partial \tau} + u\frac{\partial u}{\partial x} + v\frac{\partial u}{\partial y}\right) = -\frac{\partial P}{\partial x} + \frac{\partial}{\partial y}\left(\mu\frac{\partial u}{\partial y}\right) + \frac{\partial}{\partial y}\left(\mu_t\frac{\partial u}{\partial y}\right) \qquad (2)$$

The y-direction momentum equation is;

$$\rho\left(\frac{\partial v}{\partial t} + u\frac{\partial v}{\partial x} + v\frac{\partial v}{\partial y}\right) = -\frac{\partial P}{\partial y} + \frac{\partial}{\partial y}\left(\mu\frac{\partial v}{\partial y}\right) + \frac{\partial}{\partial y}\left(\mu_t\frac{\partial v}{\partial y}\right) \qquad (3)$$

The standard form of (K-ε) model is as follows:-
Turbulence kinetic energy equation;

$$\rho\left(\frac{\partial \kappa}{\partial t} + u\frac{\partial \kappa}{\partial x} + v\frac{\partial \kappa}{\partial y}\right) = \frac{\partial}{\partial y}\left(\frac{\mu_t}{\sigma\kappa}\frac{\partial \kappa}{\partial y}\right) + \mu_t\left(\frac{\partial u}{\partial y}\right)^2 - \rho\varepsilon \qquad (4)$$

And dissipation of turbulence kinetic energy equation;

$$\rho\left(\frac{\partial\varepsilon}{\partial t}+u\frac{\partial\varepsilon}{\partial x}+v\frac{\partial\varepsilon}{\partial y}\right)=\frac{\partial}{\partial y}\left(\frac{\mu_t}{\sigma\varepsilon}\frac{\partial\varepsilon}{\partial y}\right)+\mu_t c_{\varepsilon_1}\frac{\varepsilon}{\kappa}\left(\frac{\partial u}{\partial y}\right)^2-c_{\varepsilon_2}\rho\frac{\varepsilon^2}{\kappa} \tag{5}$$

According to the high Reynolds number (κ-ε) turbulence model the turbulent viscosity μ_t is related to the turbulent kinetic energy (κ) and to the dissipation of turbulent kinetic energy (ε) through the expression;

$$\mu_t = c_\mu \rho\frac{\kappa^2}{\varepsilon} \tag{6}$$

The effective viscosity (μ_{eff}) is related to the turbulent viscosity (μ_t) and to the molecular viscosity (μ) through the relation :-

$$\mu_{eff} = \mu_t + \mu \tag{7}$$

In the above equations, ($c_\mu, c_{\varepsilon_1}, c_{\varepsilon_2}\sigma_k, \sigma_\varepsilon$) are constants at high Reynolds number and the model constants $c_\mu, c_{\varepsilon 1}, c_{\varepsilon 2}$ are set to $c_\mu = 0.09, c_{\varepsilon 1} = 1.44, c_{\varepsilon 2} = 1.92$. Usually, the constants $\sigma_k and \sigma_\varepsilon$ are assigned to $\sigma_k = 1.0 and \sigma_\varepsilon = 1.3$.

The energy equation is;

$$\rho\, cp\left(\frac{\partial T}{\partial t}+u\frac{\partial T}{\partial x}+v\frac{\partial T}{\partial y}\right)=\frac{\partial}{\partial y}\left(k\frac{\partial T}{\partial y}\right)+\frac{\partial}{\partial y}\left(k_t\frac{\partial T}{\partial Y}\right) \tag{8}$$

where;

$$k_t = \frac{\mu_t cp}{\mathrm{P}r_t} \tag{9}$$

For the evaluation of turbulent kinetic energy and dissipation at turbulent Kinetic energy, it is sufficed to fix their values at the near wall node (P) according to the following formula:-

$$\kappa_{\mathrm{P}} = \frac{\tau_\omega}{\rho c_\mu^{1/2}} \tag{10}$$

$$\varepsilon_{\mathrm{P}} = \frac{c_\mu^{3/4}}{V_K y_{\mathrm{P}}}\kappa_{\mathrm{P}}^{3/2} \tag{11}$$

$$y^+ = \frac{\rho y_p c_\mu^{1/4} k_p^{1/2}}{\mu_l} \tag{12}$$

where (y_p)is the normal distance of the near wall node (p) to the solid surface. In the above formula, (k) is the Von Karman constant (0.4187) and (E) is an integration constant that depends on the roughness of the wall. For a smooth wall constant shear stress, (E) has a value of (9.793).

The initial and Boundary conditions for the problem are shown to in **Fig.2**. all the previously discussed differential equations can be conveniently presented in the general form:-

$$\frac{\partial}{\partial t}(\rho\phi)+\frac{\partial}{\partial x}(\rho u\phi)+\frac{\partial}{\partial y}(\rho v\phi)-\frac{\partial}{\partial x}\left[\Gamma_{\phi}\frac{\partial\phi}{\partial x}\right]-\frac{\partial}{\partial y}\left[\Gamma_{\phi}\frac{\partial\phi}{\partial y}\right]=s_{\phi} \qquad (13)$$

In the above equation, ϕ identifies the dependent variables, Γ_{ϕ} is the appropriate exchange coefficient for the variable ϕ, and s_{ϕ} is the source term which includes both the sources of ϕ (positive or negative) and any other terms which cannot find place on the left-hand side of **Eq.(13)**, see **Table .2** .

The derived governing equations and the initial and boundary conditions in **Fig.2** Will be solved numerically by using the control volume approach of **(Patanker 1980)**. The finite difference method (F.D.M.) will be used, and the details of the numerical solution will be described in the next article.

NUMRICAL SOLUTION:-

The general from **Eq.(13)** may be written as;

$$\frac{\partial}{\partial t}(\rho\Phi)+\frac{\partial}{\partial x}\left[\rho u\phi-\Gamma_{\Phi}\frac{d\phi}{dx}\right]+\frac{\partial}{\partial y}\left[\rho v\phi-\Gamma_{\Phi}\frac{d\phi}{dx}\right]=S_{\Phi} \qquad (14)$$

By defining Jas the total flux which consists of convection and diffusion fluxes, or

$$J_x=\rho u\phi-\Gamma\frac{\partial\phi}{\partial x} \qquad (15)$$

$$J_y=\rho v\phi-\Gamma\frac{\partial\phi}{\partial y} \qquad (16)$$

Where J_x and J_Y or the total fluxes through faces normal to the x and y directions respectively with these definitions, **Eq. (14)** can be written

$$\frac{\partial}{\partial t}(\rho\phi)+\frac{\partial J_x}{\partial x}+\frac{\partial J_y}{\partial y}=S_{\Phi} \qquad (17)$$

Eq. (17) was integrated by using the finite volume approach of **(Patenker 1980)**, see **Fig. 3**. The source term has been linerized, and the values at the control volume faces (e, w, n, s) are assumed to be found by linear interpolation (central differences). The resulting final form of the **Eq. (17)** becomes

$$\frac{\left(\rho P\phi_P-\rho P^{\circ}\phi_P\right)\Delta x\Delta y}{\Delta t}+J_e-J_w+J_n-J_S=\left(S_c+S_P\phi_P\right)\Delta x\Delta y \qquad (18)$$

$$a_P\phi_P=a_E\phi_E+a_W\phi_W+a_N\phi_N+a_S\phi_S+b$$

$$a_E=D_eA(P_e)+Max[-F_e,o]$$

$$a_W=D_wA(P_w)+Max[F_w,0] \qquad (19)$$

$$a_N = D_n A(\mathrm{P}_n) + Max[-F_n, 0]$$
$$a_S = D_S A(\mathrm{P}_S) + Max[F_S, 0]$$
$$a_{\mathrm{P}}^{\circ} = \frac{\rho_{\mathrm{P}}^{\circ} \Delta x \Delta y}{\Delta t} \qquad b = S_c \Delta x \Delta y + a_{\mathrm{P}}^{\circ} \phi_{\mathrm{P}}^{\circ} \qquad (20)$$
$$a_{\mathrm{P}} = a_E + a_W + a_N + a_S + a_{\mathrm{P}}^{\circ} - S_{\mathrm{P}} \Delta x \Delta y \qquad (21)$$
$$\phi_e = \phi_E f_e + \phi_p [1 - f_e]$$
$$\phi_w = \phi_W f_w + \phi_p [1 - f_w]$$
$$\phi_n = \phi_N f_n + \phi_p [1 - f_n] \qquad (22)$$
$$\phi s = \phi_S f_s + \phi_p [1 - f_s]$$

Generally

$$a_{\mathrm{P}} \phi_{\mathrm{P}} = \sum_{nb} a_{nb} \phi_{nb} + b \qquad nb = E, W, N, S \qquad (23)$$

where: b = Absolute part of the discretized equation

RESULTS AND DISUSION:-

The investigated case was the flow over a flat plate (1m) length. The height of the calculation domain was taken to be (0.03m), which was twice the boundary layer thickness at the trailing edge. The flow conditions were chosen to ensure that the flow is compressible and turbulent. The free stream pressure and temperature was taken as (101325 pa and 25 $^{\circ}$c). The Mach number was taken as (0.5). Accordingly, the free stream velocity was calculated as (156 m/s). The Reynolds number was calculated to be (1.02E+7). The suction and injection rates were taken as [±0.001 and ±0.0005 (+for injection and – suction)] of the free stream velocity. The wall temperature was taken as (70 $^{\circ}$c).The results will be shown for the solid wall and porous wall with injection and suction, but since the rate of injection and suction were small, their effects are not clear in the figures

Steady State Results:-

Fig.4 to **6** show the velocity profiles with injection or suction. The relative shapes for the velocity profiles are turbulent in these figures. The turbulent profile has apportioned near the wall which is almost linear. This portion is due to a laminar sub layer which hugs the surface very closely. Outside this sublayer the velocity profile is relatively flat in comparison with the laminar profile. It can be concluded from these figures, that injection causes a decrease in boundary layer thickness, while suction causes an increase in boundary layer thickness, and the rate of increase or decrease is proportional to the injection or suction rate, respectively. **Fig.7** to **9** show the temperature distributions inside the thermal boundary-layer with and without injection or suction. The very steep temperature gradient near the wall and the flatness of the profiles indicate clearly the turbulent shape of the profiles. Injection causes a slight decrease in temperature while suction causes reverse effect. **Fig.10** and **11** show the local skin-friction coefficient and the local Nusselt number coefficient respectively, with and without injection or suction. The skin friction coefficient decreases with the flow direction (increasing Rex) due to the decrease of the velocity gradient at the wall, which is caused by the decrease of the velocity of points near the wall due to the increase in resisting viscous forces. This happens for all cases, with and without injection or suction. The injection or suction causes slight difference due to small rates of injection and suction used. But, it can be noticed that injection causes a decrease in (cf_x), while suction causes reverse effect. **Fig.11**

and **13** show the hydrodynamic and thermal boundary-layer growth with and without injection or suction. **Fig.12** shows a decrease in the hydrodynamic boundary-layer thickness with injection. This is so because injection causes an increase in the velocity for points near the wall, which decrease the boundary-layer thickness. The boundary-layer, evidently, begins to grow from zero thickness at the leading edge and continues downstream tending asymptotically to the value given by the equation:-

$$\delta = \frac{0.376x}{\mathrm{Re}_x^{0.2}}$$

Fig.13 indicates an increase in thermal boundary-layer thickness with injection and a decrease with suction.

Transient Results:-

Fig.14 to **16** show the boundary-layer velocity profile history at the trailing edge with and without injection and suction. The time required to reach the steady state is found to be (4.4s) for the solid wall case (V_w=0 m/s). Injection causes an increase of this time to (V_w=0.156m/s). Suction causes reverse effect, that it decreases this time to (2.8s) for (V_w=-0.078m/s) and (1.4s) for (V_w=-0.156m/s). These effects are due to the disturbances caused by injection or suction to or from the boundary-layer. **Fig.17** to **19** show the temperature history across the thermal boundary-layer with and without injection or suction. The temperature profiles consist of linear part near the wall, superimposed on it a parabolic profile due to heat generated by friction. In an analogous way similar to that in **Figs. 14** to **16**, the time required to reach the steady temperature profiles is found to be the (4.2s) for the solid wall (V_w=0), (2.8s) for (V_w=-0.078m/s) and (1s) for (V_w=-0.156m/s). **Fig.20** and **21** show the hydrodynamic and thermal boundary-layers history at the trailing edge. The figures indicate in a very clear picture the effects of injection or suction on the time required to reach the steady state case, which is mentioned and discussed above .The values of this time differ slightly in this case, as shown in **Table.1**. **Fig.22** and **23** show the variation of the average skin friction coefficient and Nusselt number with time. The figures demonstrates the increase of the steady state time with injection and decrease with suction see **Table.2**. **Fig.24** and **25** show the comparison between the empirical and the numerical values of boundary-layer thickness and the local Nusselt number. The maximum relative difference on this line was (18.5%) for the boundary-layer thickness and (26.7%) for the Nusselt number. The minimum relative difference is (1.6%) for the boundary-layer thickness, and (18.28%) for the Nusselt number. The average relative difference is (12.7%) for the boundary layer thickness, and (21.28%) for the Nusselt number.

CONCLUSIONS

Injection causes a slight decrease in the temperature inside the thermal boundary-layer, while suction causes reverse effect. Turbulence kinetic energy level decreases away from the wall region, while effective viscosity level increases away from the walls region. The dissipation rate of turbulence is maximum at points adjacent to the wall surface where the velocity is in the minimum values. The local skin friction coefficient decreases with the flow direction. It can be noticed that injection causes a decrease in local skin friction coefficient while suction causes reverse effect. The local Nusselt number increases with local Reynold number, despite that the local heat transfer coefficient (h_x) decreases with the flow direction due to the increase in the thermal boundary layer

thickness. Injection causes a slight increase in Nusselt number and suction causes reverse effect. The hydrodynamic boundary layer thickness decrease with injection, while thermal boundary layer thickness increases with injection. Injection causes an increase in the time required to reach the steady state, while suction causes a reverse effect.

Table.1: Steady State Time for (δ_h) and (δ_t)

V_w(m/s)	Time	(s)
	δ_h	δ_t
0(solid wall)	4.2	4.2
0.078(injection)	5.5	5.7
0.156(injection)	6.7	6.7
-0.078(suction)	2.7	2.8
-0.156(suction)	1	1

Table.2: Steady State Time for ($\overline{c_f}$) and ($\overline{Nu}$)

V_w(m/s)	Time	(s)
	$\overline{c_f}$	$\overline{Nu}$
0(solid wall)	4.1	3.9
0.078(injection)	5.1	5.5
0.156(injection)	6.4	6.6
-0.078(suction)	2.3	2.5
-0.156(suction)	1.1	2.5

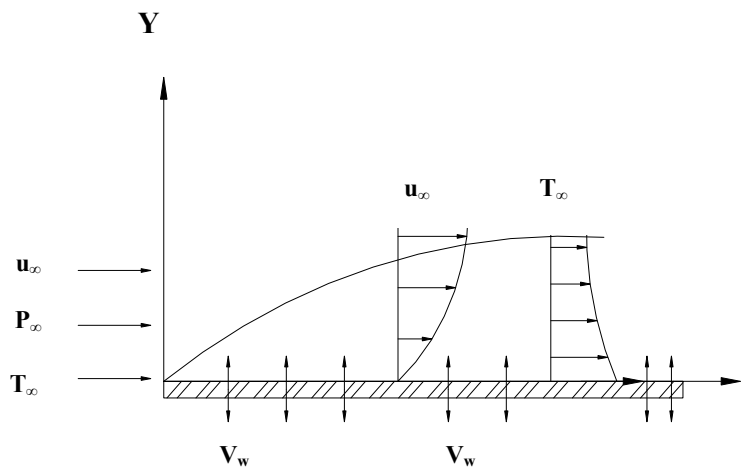

Fig.1: The Problem of the Present Work

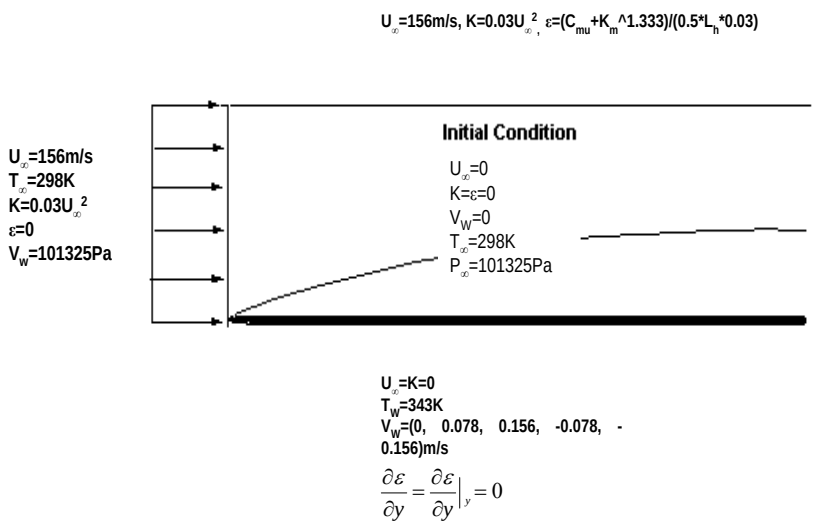

Fig.2: The Initial and Boundary Condition

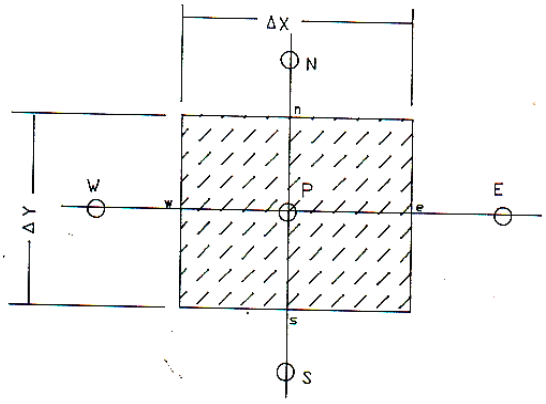

Fig. 3: Control Volume for Tow- Dimensional Case

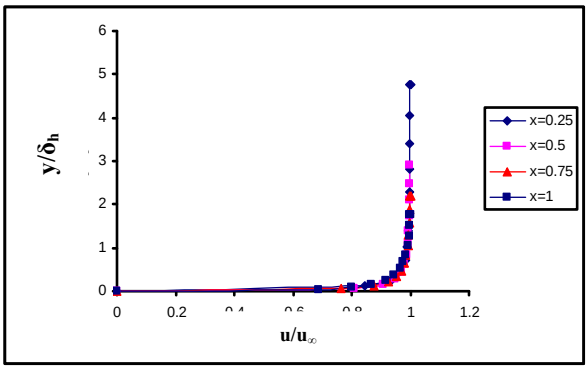

Fig. 4: Boundary-Layer Velocity Profiles (V_w=0m/s)

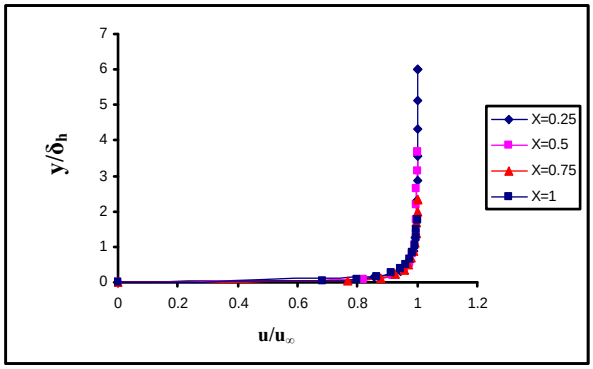

Fig. 5: Boundary-Layer Velocity Profiles (V_w=0.156m/s)

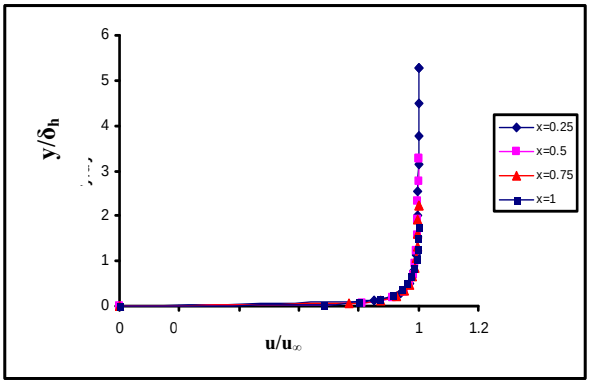

Fig. 6: Boundary-Layer Velocity Profiles (V_w=0.156m/s)

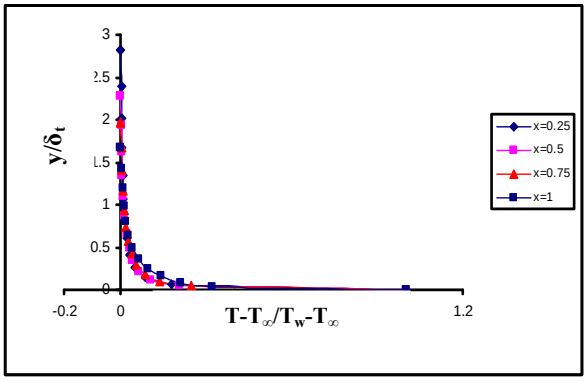

Fig. 7: Thermal Boundary-Layer Temperature Profiles (V_w=0m/s)

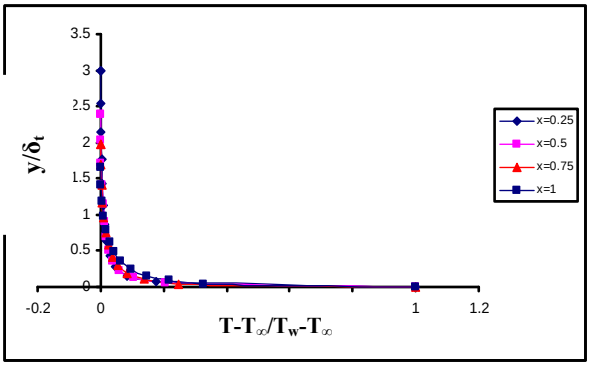

Fig. 8: Thermal Boundary-Layer Temperature Profiles (V_w=0m/s)

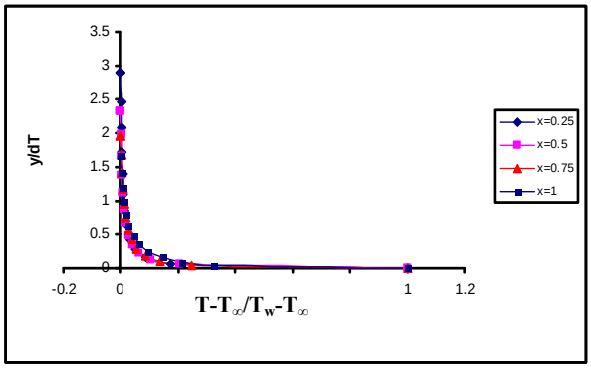

Fig. 9: Thermal Boundary-Layer Temperature Profiles (V_w=0m/s)

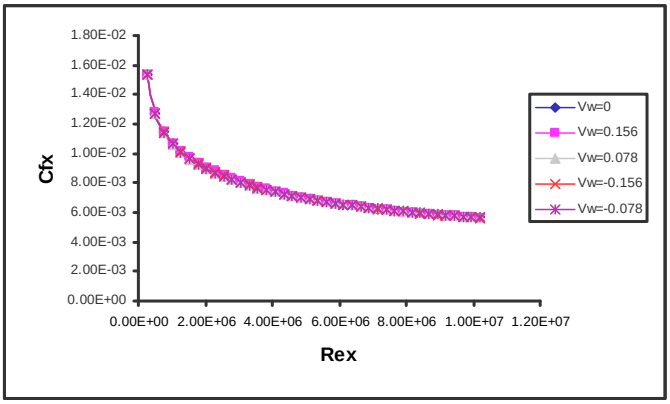

Fig. 10: Local skin Friction Coefficient Variation with Local Reynolds Number

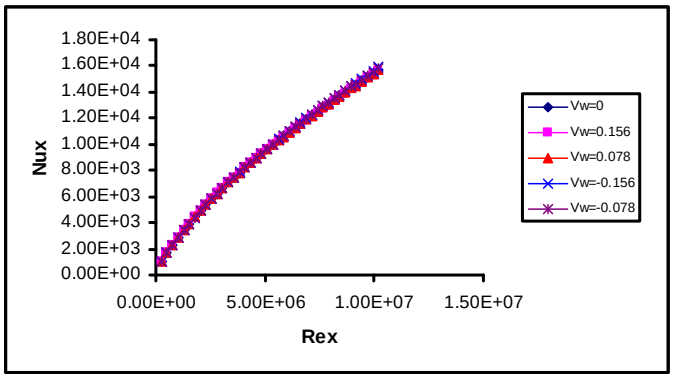

Fig. 11: Local Nusselt Number variation with local Reynolds Number

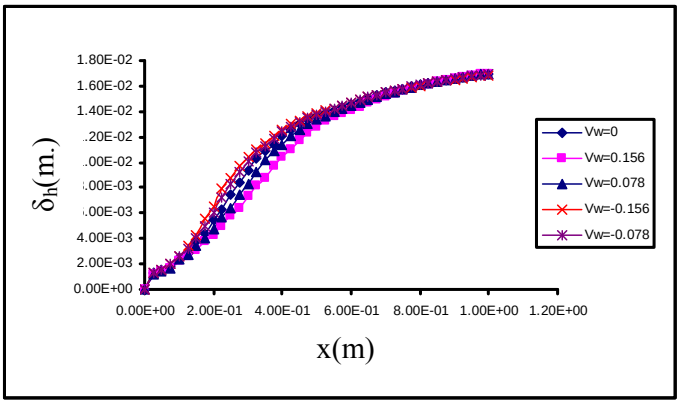

Fig. 12: Hydrodynamic Boundary-Layer Thickness Growth

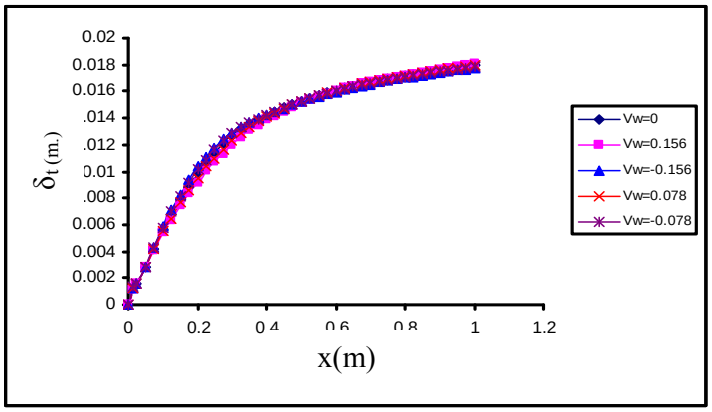

Fig. 13: Thermal Boundary-Layer Thickness Growth

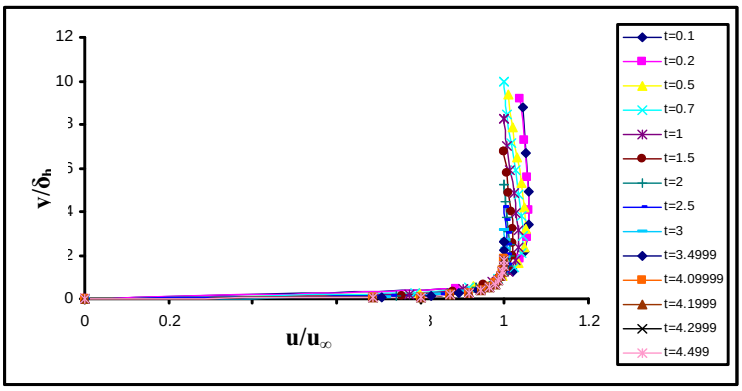

Fig. 14: Boundary-Layer Velocity Profile History at Trailing Edge (V_w=0m/s)

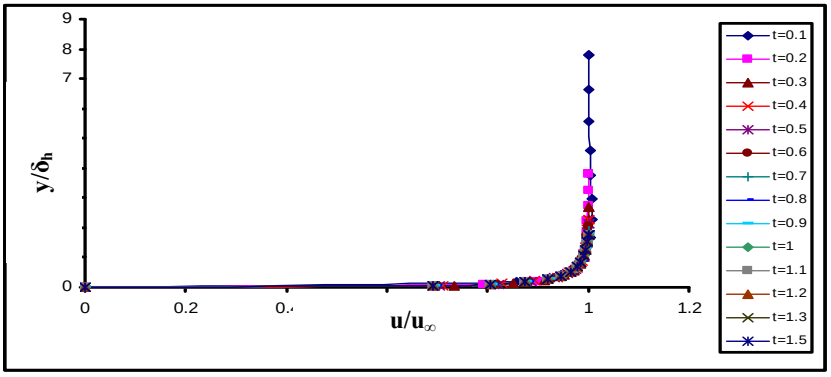

Fig. 15: Boundary-Layer Velocity Profile History at Trailing Edge (V_w=-0.156m/s)

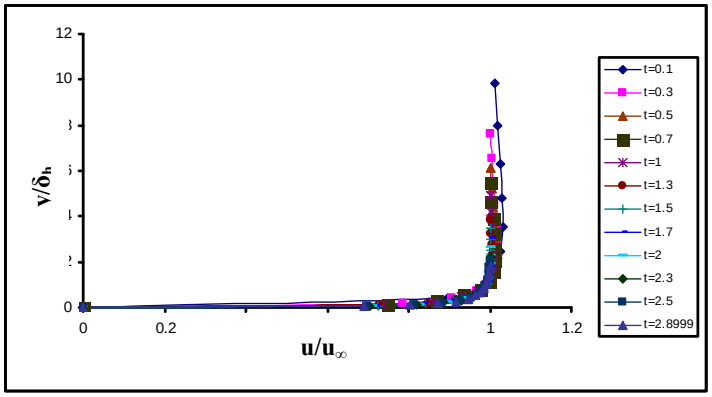

Fig. 16: Boundary-Layer Velocity Profile History at Trailing Edge (V_w=-0.078m/s)

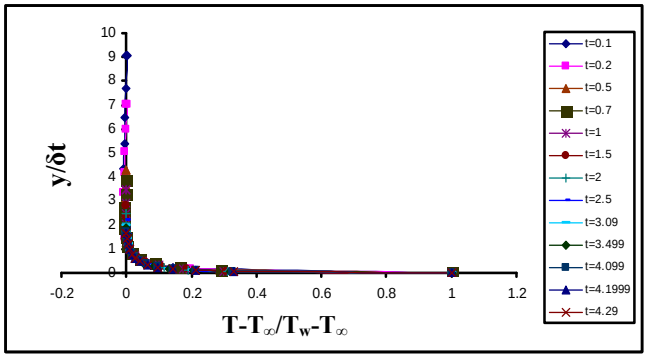

Fig. 17: Boundary-Layer Temperature Profile History at Trailing Edge (V_w=0m/s)

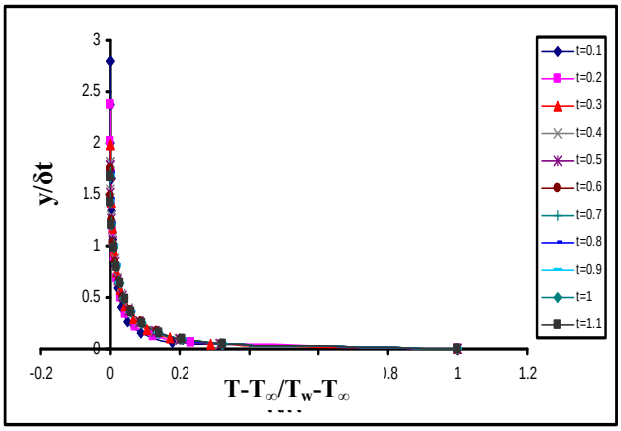

Fig. 18: Boundary-Layer Temperature Profile History at Trailing Edge (V_w=-0.156m/s)

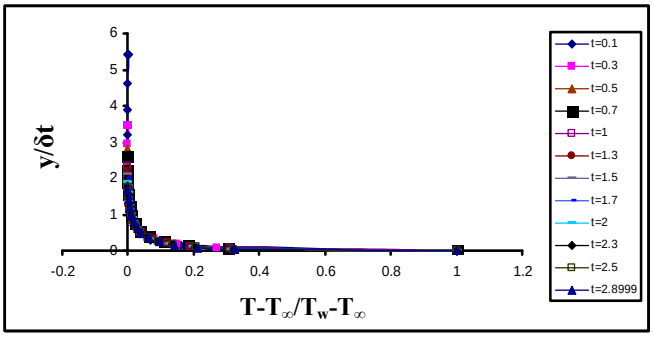

Fig. 19: Boundary-Layer Temperature Profile History at Trailing Edge (V_w=-0.078m/s)

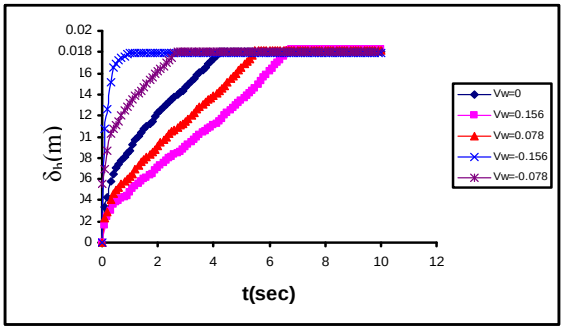

Fig.20: Hydrodynamic Boundary-Layer Variation with Time

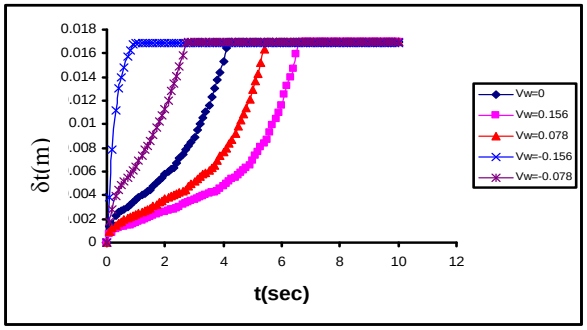

Fig. 21: Temperature Boundary-Layer Variation with Time

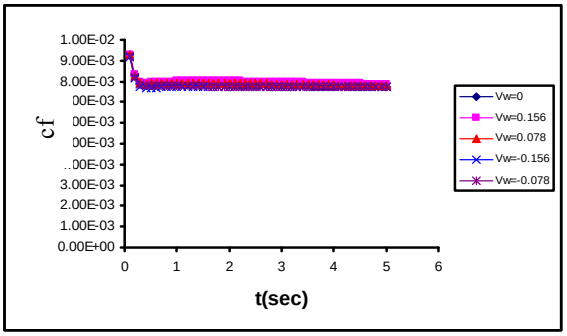

Fig. 22: Mean Skin Friction Variation with Time

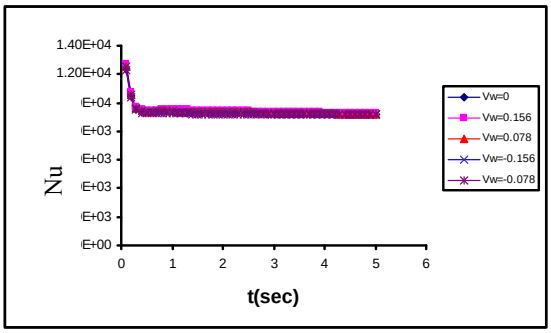

Fig. 23: Mean Nusselt Number Variation with Time

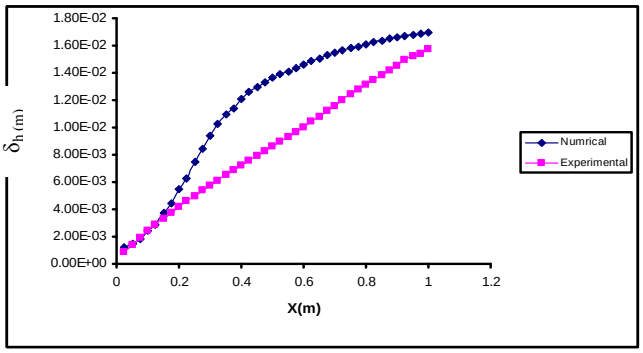

Fig. 24: Comparison of Hydrodynamic Boundary-Layer Results

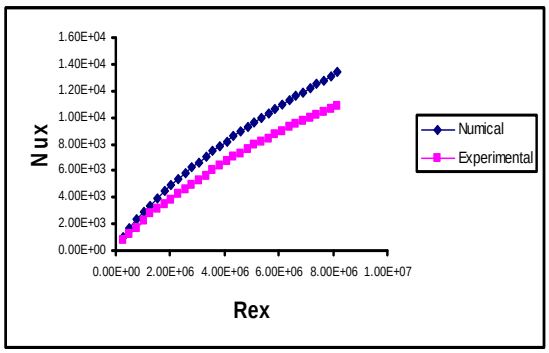

Fig. 25: Comparison of Nusselt Number Results

REFFRENCES

Ayser M. Fleh " Unsteady Hydrodynamic and Thermal Boundary Layers over a Porous Flat Plate", M.Sc. Thesis, Mech. Eng. Dept., University of Al-Mustansirya, 2005

Jeongyoung P. and Haecheon C., "Effects of Uniform or Suction From a Spanwise Slot on a Turbulent Boundary-Layer Flow" J. Physics of Fluids, Vol.11, No. 10, PP. 3095-3105, October (1999).

Kyoungyoun K. and Hyung J. "Assessment of Local Blowing and in a Turbulent Boundary-Layer" Fluid Mechanics Conference Adelaide University, PP. 215-218, December (2001).

Kyoungyoun K. and Hyung J. "Effects of Periodic Blowing from Spanwise Slot on a Turbulent Boundary-Layer" AIAA Journal, Vol.41, No. 10, PP.1916-1924, October (2003).

Nagano Y. and Hishida M., "Improved Form of the $\kappa - \varepsilon$ Model for Wall Turbulent Shear Flows " J. Fluid Mech., Vol.109, PP. 156-160, June (1987).

Nagano Y. and Hishida M., "An Improved $\kappa - \varepsilon$ Model for Boundary Layer Flows " J. Fluid Mech., vol. 112, PP. 33-39, March (1990).

Park, S.H. and Sung, H.J. "Effect of Local Forcing on a Turbulent Boundary Layer" J.Experiments in Fluids, 31, pp 384-393, 2001

Patanker, S.V. " Numerical Heat Transfer and Fluid Flow ", McGraw-Hill Book Company, 1980

Per-Age K. and Anatoli K., "Some Effects of Localized Injection on the Turbulence Structure in a Boundary-layer" J. Physics of Fluids, Vol. 12, No. 11, PP. 2990-2998, November (2000).

NOMENCLATUR

Latin Symbols

Symbol	Description	Units
C_{f_x}	Local Skin-Friction Coefficient	
C_P	Pressure Coefficient, also the Specific Heat at Constant Pressure	J/kg. K
E, W, N, S	Nodal Points Neighbor (Refer to East, West, North and South)	
F	Convective Flux Through a cell Face	m^2/s
J	Flux	$kg/m\ s^2$
K	Thermal Conductivity	W/m. k
K	Kinetic Energy of Turbulence	J
K	Ratio of Specific's Heat, (=1.4 for air)	
M	Molecular Weight	kg/mol
M	Mach number	
Nu	Nusselt Number	
P	Pressure	N/m^2
P	Cell Nodal Point	
Pr	Prandtl Number	
R_e	Reynolds Number	
S	Source Term	
S_R	Sum of Residuals	
T	Temperature	
T_w	the Wall Temperature	
t	Time	sec
U	The Velocity Vector	m/sec
u, v, w	Velocity Components in the x, y and z	m/sec
X, x	X-Coordinate Distance	m
Y, y	Y-Coordinate Distance	m

GREEK SYMBOLS

Symbol	Description	Units
α	Under-relaxation Factor	
ε	Dissipation Rate of Turbulent	
$\Delta X, \Delta Y, \Delta Z$	Cell Distances	
$\delta k, \delta\varepsilon$	Constant in the $K-\varepsilon$ Model	
$\delta x, \delta y$	Half the Cell Distances	
δh	Hydrodynamic Boundary-Layer Thickness	m
δt	Thermal Boundary-Layer Thickness m	
Φ	Dependent Variable in the General Form of Equation	
Γ	Transfer Coefficient	

Γ_{wall}	Diffusion at the Wall	
μ	Laminar Viscosity	kg/m.s
μ_{eff}	Effective Eddy Viscosity	kg/m.s
ρ	Density kg/m^3	
ρ_{sea}	Sea Level Density, (=1.225 Kg/m^3)	kg/m^3
ν	Kinematics Viscosity	m^2/s
$\tau_{w,}\tau_{\circ}$	Wall Shear Stress	N/m^2

SUBSCRIPTS

Symbol	**Description**	**Units**
e, w, n, s	At The Center of The Cell Face	
i, j, k	Coordinate Direction Indices	
nb	Neighbor Points	
o	Initial Value	
P, E, W, N, S	of the Nodal Point	

SUPERSCRIPTS

Symbol	**Description**
o	Old Values
∞	Signifies Free Stream Conditions

MODELLING OF IRAQI GYPSEOUS SOIL BEHAVIOUR UNDER STRESS-FLOW-DISSOLUTION CONDITIONS

Dr. Omar Al-Farouk S. Al-Damluji
Assistant Professor Formerly
Department of Civil Engineering
University of Baghdad

Hayder Mohammed Z. Al-Hassanee
Postgraduate student
Department of Civil Engineering
University of Baghdad

ABSTRACT

Gypseous soils are distributed in many regions in Iraq. Therefore, it is necessary to study the geotechnical properties of such soils due to the possible large damage that may incur structures founded and constructed in or on them. The soil used in this study is from Al-Najef City, Iraq. It is poorly graded sand. It also has a gypsum content of about 28-32%. The mineralogical and chemical properties of the soil are established at first. However, this study is concerned with the dissolution of gypsum and its effect on the soil. The importance of the progress of dissolution is verified through the study of the characteristics of the soil skeleton and the pore fluid. Three differential equations are used to study this effect, namely, *continuity*, *equilibrium* and *dispersion*. They are solved by using the finite element method. In addition, this work uses the hyperbolic stress-strain idealization as a constitutive relationship. Tri-axial (CD) tests are conducted to find the hyperbolic parameters. An experimental setup is modified to find the longitudinal and lateral coefficients of dispersion. One- and two-dimensional problems are solved to study the effect of dissolution. Results reveal high effects of dissolution of gypsum on the settlement, pore water pressure, elastic modulus and Poisson's ratio values. Settlement increases while other parameters (E, B and υ) decrease with increasing dissolution. Furthermore, there is a vast behavioral difference between one and two dimensional problems.

الخلاصة

تنتشر الترب الجبسية في مناطق عديدة من العراق. لذلك من الضروري دراسة الخواص الفيزياوية لهذه الترب بسبب الاضرار المحتملة الكبيرة التي تحدث بالمنشاءآت نتيجة لبناءها عليها او بداخلها. لقد استخدمت تربة من هذا النوع تم جلبها من مدينة النجف في العراق. ان نوع التربة هو رمل متدرج بشكل سيء كما ان لها محتوى من الجبس قدره حوالي 28–32%. لقد تم التحقق من الخواص المعدنية و الكيمياوية للتربة اولاً. بعد ذلك, تتطرق هذه الدراسة الى اذابة الجبس و تأثيره على التربة. لقد تم التحقق من تقادم الاذابة من خلال دراسة خواص الهيكل الصلب و مائع المسام. لقد تم استخدام ثلاثة معادلات تفاضلية لدراسة هذه الظاهرة و هي : الاستمرارية و الاتزان و الانتشار. لقد تم حل هذه المعادلات باستخدام طريقة العناصر المحددة. اضافة الى ذلك, تم استخدام تمثيل اجهاد– انفعال القطع الناقص

كعلاقة تكوينية. لقد تم اجراء فحوص ثلاثية محاور مبزولة لايجاد معاملات علاقة القطع الناقص. لقد تم تعديل جهاز لايجاد معاملي الانتشار الطولي و الجانبي. لقد تم حل مسألتين ببعد واحد و ببعدين لدراسة خواص الاذابة. تظهر النتائج تأثيرات عالية لاذابة الجبس على الهبوط و ضغط الماء المسامي و قيم معاملي المرونة و بويزون. يزداد الهبوط بينما تقل قيم المعاملات الاخرى (معاملي المرونة و التضخم و نسبة بويزون) مع زيادة الاذابة.تظهر الدراسة فرقاَ كبيراَ في الخواص عند دراسة المسألة ببعدين عن البعد الواحد.

KEY WORDS
Gypseous, Dissolution, Dispersion, Finite element, Hyperbolic.

INTRODUCTION

The term "gypsiferous soil" and “gypseous soil” are used to specify the soil that contains gypsum, the first is used by agronomists, while the second is used by civil engineers. Gypsum is present in soils in the form of calcium sulphate dihydrate ($CaSO_4.2H_2O$). A transitional form of calcium sulphate ($CaSO_4.0.5H_2O$) is sometimes found at the soil surface in extremely dry climates (Doner and Lynn, 1977). There is no unique definition for gypseous soils used by civil engineers. It can be stated that a gypseous soil is one in which has a gypsum content enough to change or to affect its engineering properties. Gypseous soils are distributed in many regions in the world including Iraq. They cover about (20٪) of Iraq's area. Gypseous soils in Iraq cover about 7.28٪ of the gypseous soils in the world and 16.2٪ from Asia (FAO, 2001). Many problems relating to construction on gypseous soils were observed. There are three main sources of these problems; first, the *dissolution* and *transportation* of gypsum through soil causes a continuous loss of soil mass and increasing voids. A large reduction in shear strength and an increase in compressibility are the main results of this phenomenon. The second is the variation of shear strength and compressibility characteristics of gypseous soils upon wetting and saturation. The third is the volume change accompanying the dehydration of gypsum or hydration of anhydrite. In the first case, a volume decrease of approximately 39٪ may be reached, while in the second case, the volume may be increased by 63٪)Ismail-1993). The main purpose of this study is to simulate the mechanical behavior of gypseous soils before and during leaching by using the *finite element method* for solving three differential equations, namely, *dispersion* , *flow* and *continuity*. In addition to that, set up experimental facilities which are used for the determination of the dispersive characteristics of gypseous soils (Al-Hassanee, 2004).

LEACHING STRAIN

Consider the element shown in Figure (1) which has a volume (V_o) and the water flows through the element having a velocity (v_i). This element contains some gypsum. Due to flow of water, the gypsum dissolves and causes a decrease in volume: -

$$d_{mass} = dCV_w \quad (1)$$

$$d_{mass} = dC\, v_i\, A\, \Delta t \quad (2)$$

where: -

C: concentration of gypsum in water (mg/l),
t: time (sec),

v_i: velocity (m/sec),
V_w: volume of water (L^3), and

A: area of section (m^2).

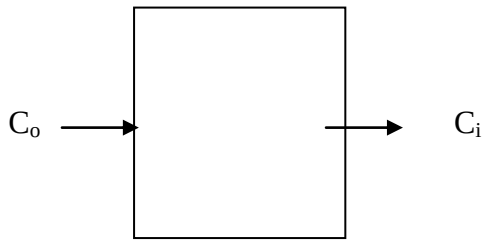

Fig (1) Variation of concentration through element

$$d\,volume = \frac{dC(v_i A \Delta t)}{G_g \gamma_w} \quad (3)$$

where:
G_g: specific gravity of gypsum (with an average value of 2.32),
γ_w : density of water (kg/m^3),

Leaching strain $= dC\left(\frac{v_i A \Delta t}{G_g \gamma_w V_o}\right)$, and (4)

V_o: initial volume of element (L^3).

CONSTITUTIVE EQUATION

The constitutive equation relating effective stress ($\bar{\sigma}$) to the strain of the skeleton is independent of the pore pressure and for a general non- linear material, it can be written in a tangential form thus allowing plasticity, if desired, to be incorporated. If leaching strain is present, the expression is written in a general form as (Lewis and Schrefler, 1987): -

$$d\bar{\sigma} = D_T\left(d\varepsilon - d\varepsilon p - d\varepsilon_m - d\varepsilon_o\right) \quad (5)$$

where:

$$d\varepsilon p = -m\left(\frac{dp}{3K_s}\right) \quad (6)$$

$$d\varepsilon_m = dCV_w G_g \delta_w v_o \quad (7)$$

in which: -

D_T : is the tangent matrix,
m : is equal to unity for the normal stress components and zero for shear stress components,
$d\varepsilon$: the total strain of skeleton,
$d\varepsilon p$: the overall volumetric strain caused by uniform compression of the particles due to the pressure of the pore fluid,
K_s : the bulk modulus of the solid phase,
$d\varepsilon_m$: the strain due to the dissolved mass of calcium sulphate,
$d\varepsilon_o$: represents all other strains not directly associated with stress changes (swelling, thermal, etc.); (Zienkiewicz, 1977), and
dp : is the pore water pressure.

The equilibrium equation relating the total stress (σ) to the body forces (b) and the boundary traction ($\hat{t}$) specified at the boundary (Γ) of the domain (Ω) is formulated in terms of the unknown displacement vector (u). Using the *principle of virtual work*, the general equilibrium statement can be written as (Zienkiewicz, 1977): -

$$\int_\Omega \delta\varepsilon^T \sigma d\Omega - \int_\Omega \delta u^T b d\Omega - \int_\Gamma \delta u^T \hat{t} d\Gamma = 0 \quad (8)$$

Furthermore, upon taking into account the constitutive relationship given by Equation (5) and dividing by dt, the following equation is obtained: -

$$\int_\Omega \delta\varepsilon^T D_T\left(\frac{\partial\varepsilon}{\partial t}\right)d\Omega - \int_\Omega \delta\varepsilon^T m\left(\frac{\partial p}{\partial t}\right)d\Omega + \int_\Omega \delta\varepsilon^T\left(\frac{\partial p}{\partial t}\right)\left(\frac{1}{3K_s}\right)d\Omega -$$

$$\int_\Omega \delta\varepsilon^T D_T\left(\frac{\partial C}{\partial t}\right)\left(\frac{V_w}{G_g \gamma_w V_o}\right)d\Omega - \int_\Omega \delta\varepsilon^T D_T\left(\frac{\partial\varepsilon_o}{\partial t}\right)d\Omega - \left(\frac{df}{dt}\right) = 0 \quad (9)$$

DARCY'S LAW (FLUID PHASE)

The geometrical complexity of a porous medium renders impossible a strict analytical treatment of the fluid velocity within the porous space. To overcome this obstacle, the fictitious seepage velocity (also known as *bulk* or *Darcy's velocity*) is defined as (Lewis and Schrefler, 1987): -

$$q = -\left(\frac{1}{\mu}\right) k \nabla (p + pgh) \tag{10}$$

where:

k : is the absolute permeability matrix of the medium,
μ : the dynamic viscosity of the fluid,
p : the fluid pressure,
ρ : the density of the fluid,
g : the gravitation acceleration, and
h : total head.

CONTINUTY EQUATION

The continuity of flow requires that the following expression is valid (Crichlow, 1977):

Rate of fluid accumulation = $+\nabla(\rho g) = 0$ (11)

which upon combining with Darcy's law given by Equation (10) results in: -

- rate of fluid accumulation = $+\nabla\left\{-\left(\frac{k\rho}{\mu}\right)\nabla(p + \rho gh)\right\} = 0 \cdot$ (12)

There are many factors which contribute to the rate of fluid accumulation and these are enumerated as follows (Lewis et al., 1976): -

a. Rate of change of total strain $\left(\frac{\partial \varepsilon_v}{\partial t}\right) = m^T\left(\frac{\partial \varepsilon}{\partial t}\right)$.

b. Rate of change of the soil volume due to pressure change = $\left(\frac{1-n}{K_s}\right)\left(\frac{\partial p}{\partial t}\right)$.

c. Rate of change of saturation = $n\rho\left(\frac{\partial S}{\partial t}\right)$.

d. Rate of change of fluid density = $nS\left(\frac{\partial \rho}{\partial t}\right)$.

e. Change of soil size due to effective stress change = $\left(\frac{\partial \sigma}{\partial t}\right) - \left(\frac{1}{3K_s}\right) m^T \left(\frac{\partial \sigma}{\partial t}\right)$.

The continuity equation for water, therefore, becomes: -

$$-\nabla^T\{k\nabla(p + \rho gh)\} + \left(m^T - \left(\frac{m^T D_T}{3K_s}\right)\right)\left(\frac{\partial \varepsilon}{\partial t}\right) + \left(\frac{m^T D_T}{3K_s}\right)\left(\frac{\partial C}{\partial t}\right)\left(\frac{V_w}{G_g \gamma_w V_o}\right) +$$

$$\left[\left(\frac{1-n}{K_s}\right) - \left(\frac{1}{3K_s}\right)^2 (m^T D_{Tm})\right]\left(\frac{\partial p}{\partial t}\right) = 0 \tag{13}$$

where:

$$K = k\left(\frac{\rho g}{\mu}\right) \quad (14)$$

and is known as the *coefficient of permeability* or *hydraulic conductivity* matrix whose coefficients have units of length over time.

DERIVATION OF THE ADVECTION-DISPERSION EQUATION

An important relationship in fluid flow is the *principle of conservation of mass*. This principle is a statement of material balance with respect to a volume element fixed in space and may be simply stated as: -

(Rate of Mass Outflow – Rate of Mass Inflow)= (Rate of Change of Mass Inside the volume element). (15)

Applying this principle to the volume element shown in Figure (2) results in: -

$$M_{(X_1+\Delta X_{1/2})} - M_{(X_1-\Delta X_{1/2})} + M_{(X_2+\Delta X_{2/2})} - M_{(X_2-\Delta X_{2/2})} + \quad (16)$$

$$M_{(X_3+\Delta X_{3/2})} - M_{(X_3-\Delta X_{3/2})} = Mp - \frac{\partial M_{VE}}{\partial t}$$

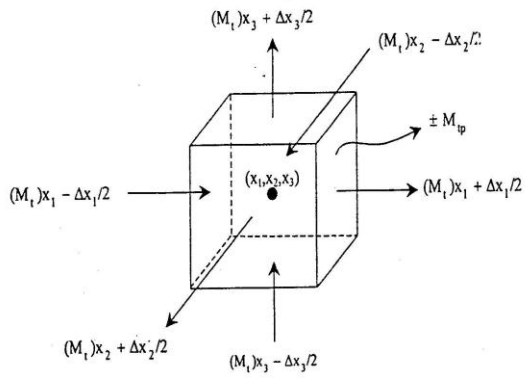

Fig (2)*: Representative elementary volume of porous medium used to develop continuity equation for gypsum in miscible fluid flow*

where: -

$M_{(X_1+\Delta X_{1/2})}$, $M_{(X_2+\Delta X_{2/2})}$, $M_{(X_3+\Delta X_{3/2})}$= rate of mass out–flow across faces $x_1 + \Delta x_{1/2}, x_2 + \Delta x_{2/2}, x_3 + \Delta x_{3/2}$, and

$M_{(X_1-\Delta X_{1/2})}$, $M_{(X_2-\Delta X_{2/2})}$, $M_{(X_3-\Delta X_{3/2})}$= rate of mass in-flow across faces $x_1 - \Delta x_{1/2}, x_2 - \Delta x_{2/2}, x_3 - \Delta x_{3/2}$.

M_{VE} = mass contained inside the volume element,

MP = mass source or sink term which is positive when a sink.

Applying a *Taylor series expansion* about the point X_1, X_2 and X_3, neglecting second and higher order terms and then substituting into Equation (16), the following is obtained after each one of the mass flow rate components is expressed in terms of the fluid density, the dimensions of the volume element and the volume flux:

$$M_{xi} = \rho q_i.\Delta x_i.\ \Delta x_j \quad (17)$$

$$M_{VE} = \rho\Phi S.\Delta x_1.\Delta x_2.\Delta x_3 \quad (18)$$

$$MP = \rho pQ \quad (19)$$

Equation (15) gives:

$$\frac{\partial}{\partial x_1}(\rho q1.\Delta x_2.\Delta x_3)\Delta x_1 + \frac{\partial}{\partial X_2}(\rho q2.\Delta x_1.\Delta x_3)\Delta x_2 + \frac{\partial}{\partial x_3}(\rho q3.\Delta x_1.\Delta x_2)\Delta x_3 = \rho pQ - \frac{\partial}{\partial t}(\rho\Phi S.\Delta x_1.\Delta x_2.\Delta x_3) \quad (20)$$

Reddle and Sunada (1974) used Fick's law for describing diffusion on a microscopic scale in a porous medium. The following is obtained: -

$$\hat{C}\hat{V}_{ti} = \hat{C}V - Dd\hat{T}_{ij}\left(\frac{\hat{C}}{x_j}\right) \tag{21}$$

$\hat{C}$: concentration of tracer (gypsum in our case) in fluid element ,

$\overrightarrow{\hat{V}_t}$: velocity of the tracer in fluid element with respect to a fixed coordinate system,

$\overrightarrow{\hat{V}}$: volumetric velocity of fluid element , and

Dd : is the coefficient of molecular diffusion.

By using macroscopic analysis and assuming isothermal conditions gives (Reddle and Sunada, 1974):

$$\left(\frac{\partial C}{\partial t}\right) = \left(\frac{\rho}{(\rho - \alpha C)}\right)\left(\frac{DD}{\Phi S \Delta x_1 \Delta x_2 \Delta x_3}\right) - V_i\left(\frac{\partial C}{\partial X_i}\right) + (Cp - C)\left(\frac{Q}{\Phi S \Delta x_1 \Delta x_2 \Delta x_3}\right) + \left(\frac{\rho_o C\beta}{(\rho - \alpha C)}\right)\left(\left(\frac{\partial P}{\partial t}\right) + V_i\left(\frac{\partial P}{\partial x_i}\right)\right) \tag{22}$$

where,

β : fluid compressibility,

α : proportionality factor relating C and ρ,

P_o : is the original value of pressure,

ρ_o : is the original value of density,

C_o : is the original value of concentration, and

O : is the original value of the variable (Reddle and Sunada, 1974).

The following assumptions are made for simplifying the dispersion equation: -

1. The volume element is completely saturated with water (S = 1).
2. The porous medium is homogeneous so that the porosity will be independent of position.
3. The density does not vary with concentration ($\alpha = 0$).

Accordingly, Equation (22) becomes:

$$\left(\frac{\partial C}{\partial t}\right) = \left(\frac{\partial}{\partial X_i}\right)\left[\left(D_{ij} + DdT_{ij}\right)\left(\frac{\partial C}{\partial X_i}\right)\right] - V_i\left(\frac{\partial C}{\partial X_i}\right) + (Cp - C)\left(\frac{Q}{\Phi S \Delta x_1 \Delta x_2 \Delta x_3}\right) + C\beta\left(\frac{\partial P}{\partial t}\right) + CV_i\left(\frac{\partial P}{\partial x_i}\right) \tag{23}$$

$$D_{ij} = D_{22}\delta_{ij} + (D_{11} - D_{22})\frac{V_i V_j}{V} \tag{24}$$

Expanding the advection – dispersion equation from equation (24) for a two–dimensional flow, and considering that the transport by molecular diffusion is negligible, the Equation (23) will be as follows: -

$$\left(\frac{\partial C}{\partial t}\right) = D_{11}\left(\frac{\partial C^2}{\partial x^2}\right) + D_{22}\left(\frac{\partial C^2}{\partial y^2}\right) - V_x\left(\frac{\partial C}{\partial x_i}\right) + (Cp - C)\left(\frac{1}{nV_o}\right)(V_x A_y + V_y A_x) + C\beta\left(\frac{\partial P}{\partial t}\right) + CV_i\left(\frac{\partial P}{\partial x_i}\right) \tag{25}$$

FINITE ELEMENT APPLICATION

The fully coupled solution of the one-phase flow (α_1–species) equation in a non-linear porous medium will now be presented in detail. The particular form of the *equilibrium equation* (9), together with the *continuity equation* (13) and the *advection-dispersion equation* (25) represent the governing equations for soil mechanics problems within the lines of Biot's self-consistent theory. The first two mentioned equations are re-written again for the sake of completeness: -

$$\int_{\Omega}\delta\varepsilon^{T}D_{T}\left(\frac{\partial\varepsilon}{\partial t}\right)d\Omega-\int_{\Omega}\delta\varepsilon^{T}m\left(\frac{\partial p}{\partial t}\right)d\Omega+\int_{\Omega}\delta\varepsilon^{T}D_{T}m\left(\frac{\partial p}{\partial t}\right)\left(\frac{1}{3K_{s}}\right)d\Omega-$$
$$\int_{\Omega}\delta\varepsilon^{T}D_{T}\left(\frac{\partial C}{\partial t}\right)\left(\frac{V_{w}}{G_{s}\gamma_{w}V_{o}}\right)d\Omega-\int_{\Omega}\delta\varepsilon^{T}D_{T}\left(\frac{\partial\varepsilon_{o}}{\partial t}\right)d\Omega-\left(\frac{df}{dt}\right)=0 \tag{26}$$

$$\overline{A}=-\nabla^{T}\left\{\frac{k}{\mu}\nabla(P+\rho gh)\right\}+\left(m^{T}-\left(\frac{m^{T}D_{T}}{3K_{s}}\right)\right)\left(\frac{\partial\varepsilon}{\partial t}\right)+$$
$$\left(\frac{m^{T}D_{T}}{3K_{s}}\right)\left(\frac{\partial C}{\partial t}\right)\left(\frac{V_{w}}{G_{g}\gamma_{w}\partial_{o}}\right)+\left[\left(\frac{1-n}{K_{s}}\right)-\left(\frac{1}{3K_{s}}\right)^{2}\left(m^{T}D_{Tm}\right)\right]\left(\frac{\partial p}{\partial t}\right)=0 \tag{27}$$

$$B=-n^{T}\frac{k}{\mu}\nabla(p+\rho gh)-q=0 \tag{28}$$

By using Green's theorem (26) and (27) become (Zienkiewicz, 1977):

$$\int_{\Omega}\left\{\nabla a^{T}\left(\frac{k}{\mu}\right)\nabla(p+\rho gh)+a^{T}\left[m^{T}-\left(\frac{m^{T}D_{T}}{3K_{s}}\right)\left(\frac{\partial\varepsilon}{\partial t}\right)+\left(\frac{m^{T}D_{T}}{3K_{s}}\right)\left(\frac{\partial C}{\partial t}\right)\left(\frac{V_{w}}{G_{s}\gamma_{w}V_{o}}\right)+\right.\right. \tag{29}$$
$$\left.\left.\left[\left(\frac{1-n}{K_{s}}\right)+\left(\frac{n}{K_{w}}\right)-\left(\frac{1}{(3K_{s})^{2}}\right)m^{T}D_{T}m\right]\left(\frac{\partial p}{\partial t}\right)\right]\right\}d\Omega-\int_{\Gamma}\left\{a^{T}n^{T}\left(\frac{k}{\mu}\right)\nabla(p+\rho gh)+b^{T}n^{T}\left(\left(\frac{k}{\mu}\right)\nabla(p+\rho gh)\right)+b^{T}q\right\}d\Gamma=0$$

$$\int_{\Omega}\left\{\nabla a^{T}\left(\frac{k}{\mu}\right)\nabla(p+\rho gh)+a^{T}\left[m^{T}+\left(\frac{n}{K_{w}}\right)\left(\frac{\partial p}{\partial t}\right)\right]\right\}d\Omega-\int_{\Gamma}a^{T}q\,d\Gamma=0 \tag{30}$$

The *Galerkin method* is applied where a = N. The finite element discretization gives the result (Zienkiewicz and Morgan, 1982):

$$\delta u^{T}\left\{\int_{\Omega}B^{T}D_{T}B\,d\Omega\left(\frac{d\overline{u}}{dt}\right)-\int_{\Omega}B^{T}m\overline{N}\,d\Omega\left(\frac{d\overline{p}}{dt}\right)-\int_{\Omega}B^{T}D_{T}\left(\frac{v_{i}A\Delta t}{G_{g}\gamma_{w}V_{o}}\right)N\,d\Omega\left(\frac{d\overline{C}}{dt}\right)-\right.$$
$$\left.\left(\frac{1}{dt}\right)\int_{\Omega}B^{T}D_{T}d\varepsilon_{o}\,d\Omega\right\}-\sigma u^{T}\left\{\int_{\Omega}N^{T}\left(\frac{db}{dt}\right)d\Omega+\int_{\Gamma}N^{T}\left(\frac{dt'}{dt}\right)\right\}=0 \tag{31}$$
$$\int_{\Omega}(\nabla N)^{T}\left(\frac{k}{\mu}\right)\nabla\overline{N}\,d\Omega\overline{p}+\int_{\Omega}N^{T}m^{T}B\,d\Omega\left(\frac{d\overline{u}}{dt}\right)\int_{\Omega}N^{T}\left(\frac{n}{K_{w}}\right)\overline{N}\,d\Omega\left(\frac{dp}{dt}\right)+\int_{\Omega}N^{T}\nabla^{T}\left(\frac{k}{\mu}\right)\nabla\rho gh\,d\Omega\int_{\Gamma}N^{T}q\,d\Gamma=0$$

As for the third differential equation for advection-dispersion (Equation 25), assuming a trial function of the form (Zienkiewicz and Morgan, 1982):

$$C\approx\hat{C}=C_{I}(t)N_{I}(x_{i})P_{I}(t) \tag{32}$$

Applying the weighted residual method with Galerkin's method and integrating the second spatial derivative term by using Green's theorem (Zienkiewicz, 1977), Equation (25) becomes: -

$$\iint\Bigg[\mathrm{Dxx}\left(\frac{\partial N_I}{\partial x}\right)\left(\frac{\partial N_J}{\partial x}\right)C_J+\mathrm{Dyy}\left(\frac{\partial N_I}{\partial y}\right)\left(\frac{\partial N_J}{\partial y}\right)C_J+\mathrm{Vx}N_I\left(\frac{\partial N_J}{\partial x}\right)C_J+$$
$$\mathrm{Vy}N_I\left(\frac{\partial N_J}{\partial x}\right)C_J+N_IN_J\left(\frac{\partial C_J}{\partial t}\right)+C\beta N_IN_J\left(\frac{\partial P_J}{\partial t}\right)+\mathrm{CVx}N_I\left(\frac{\partial N_J}{\partial x}\right)P_J+ \tag{33}$$
$$\mathrm{CVy}N_I\left(\frac{\partial N_J}{\partial y}\right)P_J+\mathrm{NV}_x(\mathrm{Cp}-C)\left(\frac{\mathrm{Ax}}{nV_o}\right)+\mathrm{NV}_y(\mathrm{Cp}-C)\left(\frac{\mathrm{Ay}}{nV_o}\right)\Bigg]dxdy-\int_\Gamma\left[\mathrm{Dxx}\left(\frac{\partial\hat{C}}{\partial x}\right)I_x+\mathrm{Dyy}\left(\frac{\partial\hat{C}}{\partial y}\right)I_y\right]N_Id\Gamma=0$$

The resulting finite element discretization in space of the three above governing equations yields the following system of semi-discrete coupled equations (refer to the appendix for definition of matrices):

$$K\frac{d\bar{u}}{dt}+L\frac{dp}{dt}+UC\frac{d\bar{C}}{dt}=\frac{df}{dt} \tag{34}$$
$$L^T\frac{d\bar{u}}{dt}+S\frac{d\bar{P}}{dt}+HP=F \tag{35}$$
$$CP\frac{d\bar{P}}{dt}+KT\frac{d\bar{C}}{dt}+KD_C+KV_C+PC=F_3 \tag{36}$$

The matrices listed above form the coefficient matrices of the combined equations: -

$$\begin{bmatrix}K & L & UC\\ L^T & S & 0\\ 0 & CP & KT\end{bmatrix}\frac{d}{dt}\begin{Bmatrix}\bar{u}\\ \bar{P}\\ \bar{C}\end{Bmatrix}+\begin{bmatrix}0 & L & 0\\ 0 & H & 0\\ 0 & CP & KD+KV\end{bmatrix}\begin{Bmatrix}\bar{u}\\ \bar{P}\\ \bar{C}\end{Bmatrix}=\begin{Bmatrix}\frac{df}{dt}\\ F\\ F_3\end{Bmatrix} \tag{37}$$

SOLUTION PROCEDURE

The analysis of displacement, fluid flow and dispersion through a deforming porous medium represents a three-degree of freedom field problem. The most obvious solution procedure of the three-coupled semi-discrete Equations (37) developed in the previous section consists of adding the concentration (C) as an additional variable to the existing nodal variable displacement (u) and pressure (P) parameters to solve the system of equations simultaneously. This is usually done by the <u>*monolithic augmentation approach*</u> (Park and Felippa, 1983), first proposed by Lewis and Karahanglu in 1981, but instead of the *advection-dispersion* equation, the *heat flow equation* was used. Following this approach, Equation (37) becomes:

$$\begin{bmatrix}K & L & UC\\ L^T & S+\bar{\alpha}H\Delta_{tk} & 0\\ 0 & CP+\alpha PC\Delta_{tk} & kT+\alpha(KD+KV)\Delta_{tk}\end{bmatrix}_{k,\bar{\alpha}}\begin{Bmatrix}\bar{u}\\ \bar{P}\\ \bar{C}\end{Bmatrix}_{tk+\Delta_{tk}}=$$

$$\begin{bmatrix}K & L & UC\\ L^T & S-(1-\bar{\alpha})H\Delta tk & 0\\ 0 & CP-(1-\bar{\alpha})PC\Delta tk & kT-(1-\bar{\alpha})(KD+KV)\Delta tk\end{bmatrix}_{k,\bar{\alpha}}\begin{Bmatrix}\bar{u}\\ \bar{P}\\ \bar{C}\end{Bmatrix}_{tk}+\begin{Bmatrix}\frac{\partial f}{\partial t}\\ \bar{F}\\ \bar{F}_3\end{Bmatrix}_{k,\bar{\alpha}}\Delta tk \tag{38}$$

The matrices in the above equation need to be evaluated once per time step.

THE HYPERBOLIC MODEL STRESS-STRAIN LAW

Setting out constitutive relations relevant for gypseous soils is still a topic under research. The adoption of the hyperbolic model is an appropriate first step towards this goal, for it is

basically a curve fitting technique of available stress-strain curves from laboratory tested specimens (Majeed, 2000). The hyperbolic stress-strain relationship was first proposed by Kondner (1963), and developed by Duncan and Chang (1970), in an attempt to provide a simple framework encompassing the most important characteristics of soil stress-strain behavior, using the data available from conventional laboratory tests such as the unconsolidated un-drained UU tri-axial compression test or the consolidated drained CD tri-axial compression test. The relationship between stress and strain is assumed to be governed by the generalized Hooke's law of elastic deformations which, for plane strain conditions, may be expressed as follows (Wong an Duncan, 1974):

$$\begin{Bmatrix} \Delta\sigma_x \\ \Delta\sigma_y \\ \Delta\tau_{xy} \\ \Delta\sigma_z \end{Bmatrix} = \frac{E_t}{(1+\upsilon_t)(1-\upsilon_t)} \begin{bmatrix} (1-\upsilon_t) & \upsilon_t & 0 & \upsilon_t \\ \upsilon_t & (1-\upsilon_t) & 0 & \upsilon_t \\ 0 & 0 & \left(\frac{1-2\upsilon_t}{2}\right) & 0 \\ \upsilon_t & \upsilon_t & 0 & 1-\upsilon_t \end{bmatrix} \begin{Bmatrix} \Delta\varepsilon_x \\ \Delta\varepsilon_y \\ \Delta\gamma_{xy} \\ \Delta\varepsilon_z \end{Bmatrix} \tag{39}$$

Kondner (1963), and Kondner and Zelasko (1963) have shown that the stress-strain curves for a number of soils, both clay and sand, could be approximated reasonably accurate by hyperbolas. This hyperbola can be represented by an equation of the form:

$$(\sigma_1 - \sigma_3) = \frac{\varepsilon}{a + b\varepsilon} \tag{40}$$

$$a = \frac{1}{E_i} \tag{41}$$

$$b = \frac{1}{(\sigma_1 - \sigma_3)_{ult}} \tag{42}$$

It may be noted that a and b are, respectively, the intercept and the slope of the best fit resulting straight line. The asymptotic stress value (σ_1-σ_3) may be related to the compression strength, (σ_1-σ_3), by means of a factor R_f as follows:

$$(\sigma_1 - \sigma_3)_f = R_f (\sigma_1 - \sigma_3)_{ult} \tag{43}$$

By expressing the parameters a and b in terms of the initial tangent modulus value and the compressive strength, Equation (40) may be rewritten as:

$$(\sigma_1 - \sigma_3) = \frac{\varepsilon}{\left[\frac{1}{E_i} + \frac{\varepsilon R_f}{(\sigma_1 - \sigma_3)_f}\right]} \tag{44}$$

The variation of E_i and σ3 is represented by an equation of the form (Janbu, 1963):

$$E_i = kP_a \left\{\frac{\sigma_3}{P_a}\right\}^n \tag{45}$$

Equation (45) can also be used for unloading-reloading conditions, but replacing E by E_{ur} and k by $k_{ur.}$ For saturated soils under un-drained conditions, there is no volume change and Poisson's ratio v_i is equal to one-half for any value of confining pressure. For most other soils the value of v_i decreases with confining pressure and this variation of v_i with σ_3 may be expressed by the equation:

$$v_i = G - F\log\left\{\frac{\sigma_3}{P_a}\right\} \tag{46}$$

where:

G: is the value of v_i at a confining pressure of one atmosphere.

F: is the reduction in v_i for a tenfold increase in σ_3.

The instantaneous slope of the curve representing the variation of ε_a and ε_r is υ_t. By differentiating the equation ($\varepsilon_r = \frac{1}{2}(\varepsilon_v - \varepsilon_a)$) with respect to ε_r, substituting Equation (46) and eliminating the strain using Equations (40 to 44), the tangent value of Poisson's ratio may be expressed in terms of the stresses as follows (Majeed, 2000): -

$$\upsilon_t = \frac{G - F\log\left\{\frac{\sigma_3}{P_a}\right\}}{\left[1 - \frac{d(\sigma_1 - \sigma_3)}{AkP_a\left\{\frac{\sigma_3}{P_a}\right\}^n}\right]^2} \qquad (47)$$

where

$$A = \left[1 - \frac{R_f(\sigma_1 - \sigma_3)(1 - \sin\phi)}{2C\cos\phi + 2\sigma_3\sin\phi}\right]$$

DISPERSION TEST

A simplified form of the mass conservation equation was presented in above for the one-dimensional flow through a homogeneous and isotropic porous medium. In order to apply the analysis presented in the derivation of the advection-dispersion equation, it is necessary to have data obtained from one-dimensional flow experiments (Al-Damluji and Al-Rawi, 2005).

The schematic diagram in Figure (3) shows the details of the modified setup. The porous medium box has outer dimensions of (7x30x30) cm. It is made up of 6 mm thick glass sheets and 4mm thick steel sheets where the removable upper cover was manufactured from 1mm thick steel sheets having (3) pores for the outlet water. A matrix of conductivity probes was embedded in the box at various locations to monitor the movement of the gypsum by using an Ohmmeter probe.

Longitudinal dispersion coefficients are determined according to the following equation:

$$D_{11} = 0.5\left\{\frac{t_{84} - t_{16}}{2t_{50}}\right\}v \qquad (48)$$

A plot is made between time and relative concentration $(C-C_o)/(C_{max}-C_o)$. The longitudinal apparent dispersivity (A_{11}) is calculated by plotting the values of (D_{11}) against the corresponding values of (v) on log-log paper, as shown in figure (4a). The best fit equation is:

$$D_{11} = 0.3997\,(v)^{0.904} \qquad (49)$$

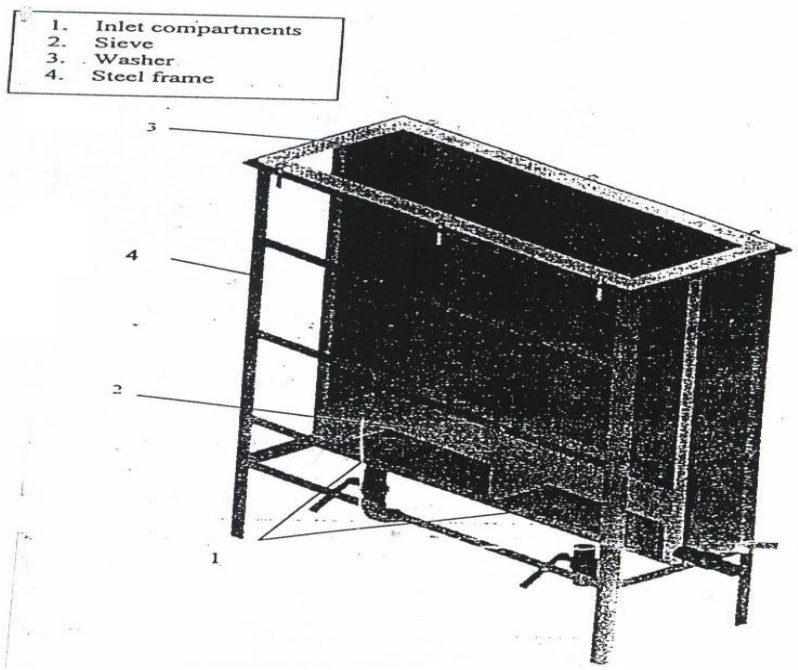

Fig (3) Schematic diagram of the porous medium box

Lateral dispersion coefficients are obtained for various seepage velocities by using the following equation:

$$D_{22} = \frac{V}{L}\left\{\frac{X_{90} - X_{10}}{3.625}\right\}^2 \qquad (51)$$

where;

L = distance from inlet, and

X = lateral distance from 50 % composition point.

The lateral apparent dispersivity (A_{12}) is calculated by plotting the values of (D_{22}) against the corresponding values of (v) on log-log paper, as shown in Figure (4b). The best fit equation is:

$$D_{22} = 0.00255\ (v)^{6.304} \qquad (52)$$

Table (1) Coefficients of longitudinal and lateral dispersions (D_{11} and D_{22})

Velocity (cm/min)		1.51	1.006	0.5033
D_{11} (cm/min)	X=5 cm	0.566	0.403	0.244
	X=15 cm	0.755	0.289	0.1617
	X=25 cm	0.705	0.503	0.236
	Average	0.675	0.398	0.2138
D_{22} (cm/min)		0.0344	0.00225	0.0002

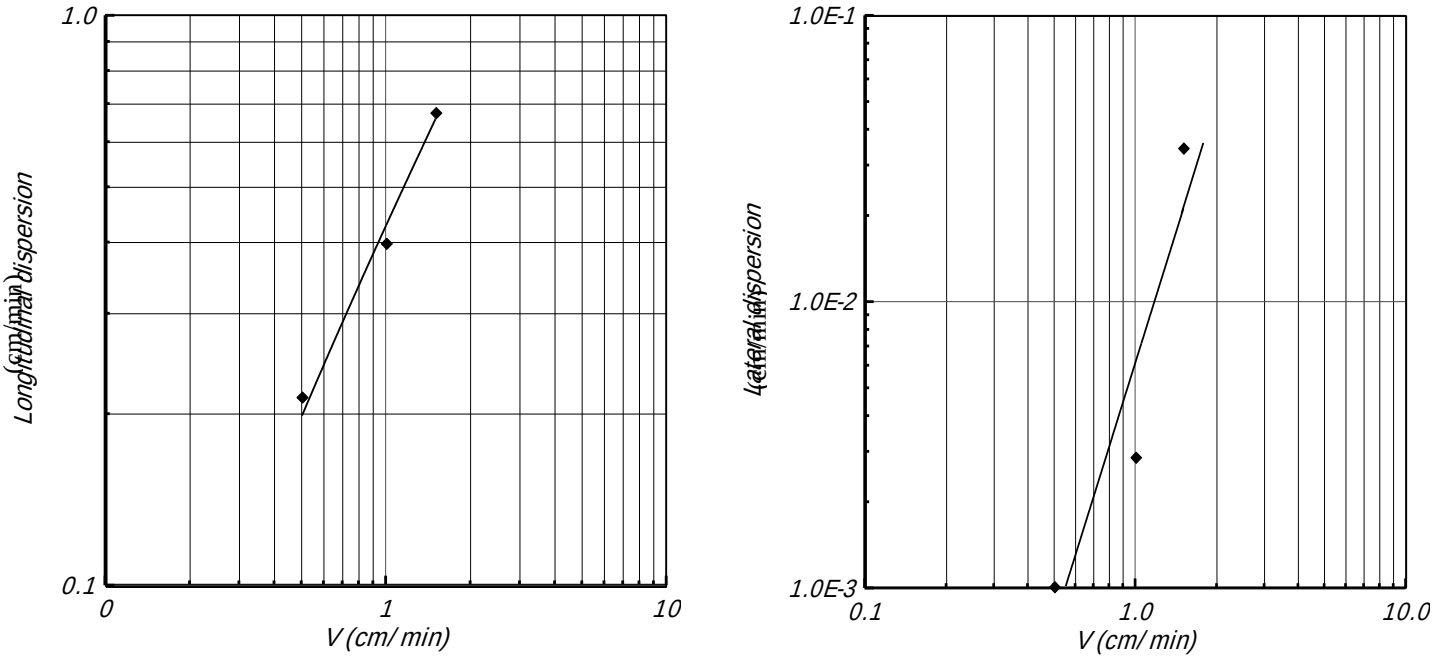

-a- -b-

Fig (4) Longitudinal and lateral dispersive curves for tested soil

pressures, namely 100, 150 and 300kN/m^2. It is worthy to mention that all these tests were

CONSOLIDATED DRAINED TRIAXIAL TEST (CD TEST)

The consolidated drained tri-axial (CD) test was carried out under three different confining conducted in three different stages which are the *saturation*, the *consolidation* and finally the *shearing* stages. Figures (5a, b, c, and d) show the results of the tests.

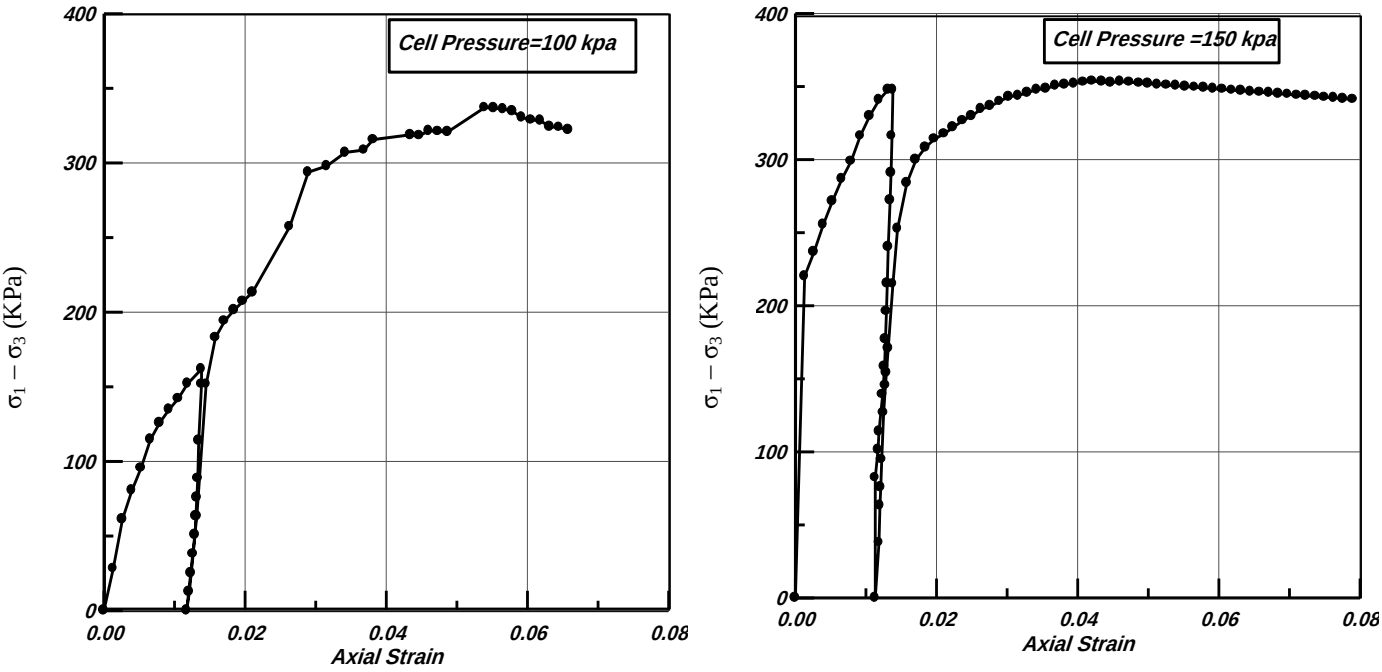

-a- -b-

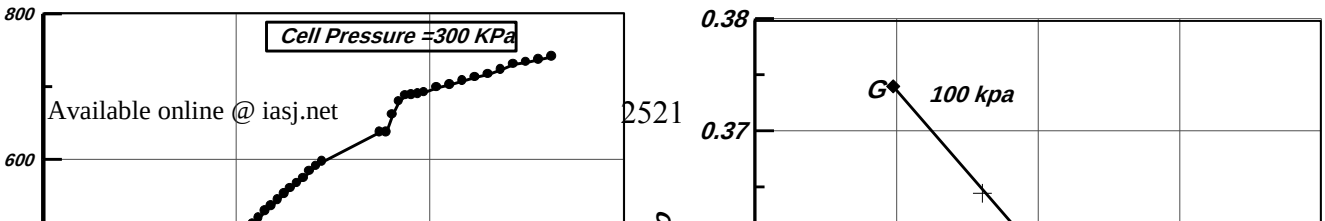

$\sigma_1 - \sigma_3$ (KPa)

Log σ_3/Pa

-c- -d-

Fig (5) Results of drained tri-axial compression (CD) tests under confining stresses of (a)100, (b)150, (c)300kPa, respectively and (d) is the variation of the initial tangent Poisson's ratio with confining stress

Table (2) shows the obtained parameters for the hyperbolic stress-strain relationship. These parameters are used as input data in the developed algorithm. The parameters k, k_{ur} and n from Equation (45), R_f from Equation (43) and G, F and d from Equations (46) and (47) are assumed constant during the dissolution process of gypsum.

Table (2) Parameters of hyperbolic stress-strain relationship

k	k_{ur}	n	Φ	R_f	G	F	D
250	420	3.331	38º.67	0.91	0.374	-0.08	0.0

One Dimensional Problem

The finite element mesh is shown in Figure (6). The width of the mesh is assumed to be equal to 0.5m. An external surface load of 50kN/m2 is assumed to be applied. The time stepping scheme and the material properties for this problem are given in Tables (3) and (4), respectively. There are two cases for this problem with some assumptions:

Case (one): Dissolution of gypsum does not happen in the first problem by assuming $C_o=C_s$. In this case, the developed algorithm solves two equations only, namely, *flow and equilibrium.*

Case (two): Dissolution of gypsum happens by assuming $C_o<C_s$. In this case, the *advection-dispersion* equation is included with the two mentioned in case one equations. Here, C_o will be taken equal to 0.4 gm/l.

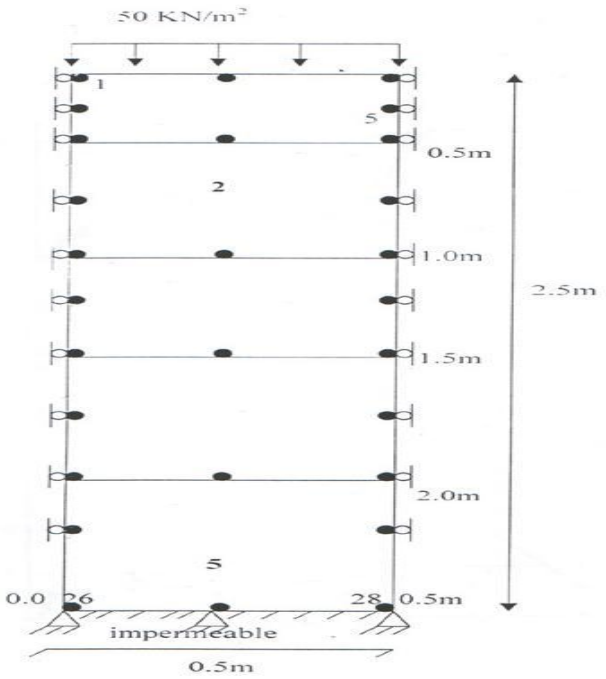

Fig (6) Finite element mesh for the one-dimensional problem

Table (3) Time steps taken for different time values

Time Interval (day)	Number of Time Steps
0.25	8
0.5	8
1.0	104

Figures (7), (8) and (9) show the variation of the elastic modulus, pore water pressure and settlement ratio, respectively at the center of element (1) for cases (one) and (two).

Table (4) Adopted material properties for the one-dimensional problem

The Material properties	Value
Horizontal Coefficient of Permeability, k_h (from tests**)**	2.5 *10^{-5} m/second
Vertical Coefficient of Permeability, k_v (from tests)	2.5 *10^{-5} m/second
Modulus number k (from tests)	250
Modulus number k_{ur} (from tests)	420
Modulus Exponent n (from tests)	3.331
Angle of internal friction Φ (from tests)	38.67°

Failure ratio R_f (from tests)	0.91
Poisson's ratio Parameter G (from tests)	0.374
Poisson's ratio Parameter F(from tests)	-0.08
Poisson's ratio Parameter d (from tests)	0.0
Elastic modulus (initial) (from tests)	23230 KN/m^2
Poisson's ratio (initial) (from tests)	0.37
Surface area of gypsum (Al-Mufty, 1997)	$(3\alpha\ \chi\ \gamma d)/(nr\ Gs\ \gamma w)$
dissolution rate Ḱ (Al-Mufty, 1997)	$(0.15 + 8.6\ v)/10^5$
Longitudinal Dispersion **(**D_{11}) (from tests)	$0.3997\ (v)^{0.904}$
Lateral Dispersion **(**D_{22}) (from tests)	$0.00255\ (v)^{6.304}$
Soil density	18.8 KN/m^2
Cohesion (c) (from tests)	0.0

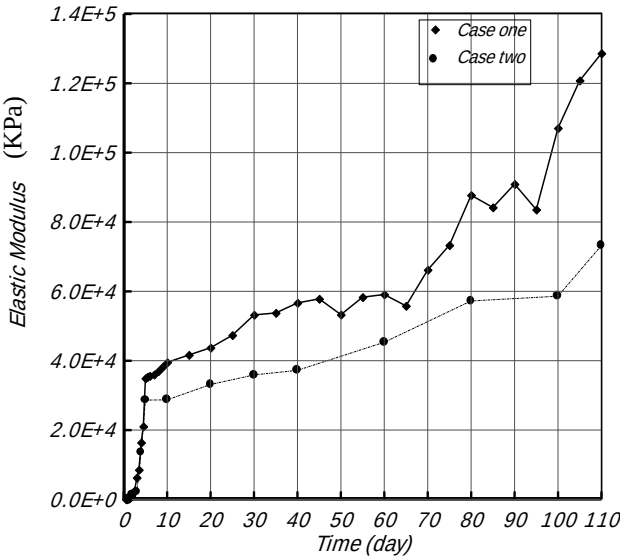

Fig (7) Elasticity modulus-time relation

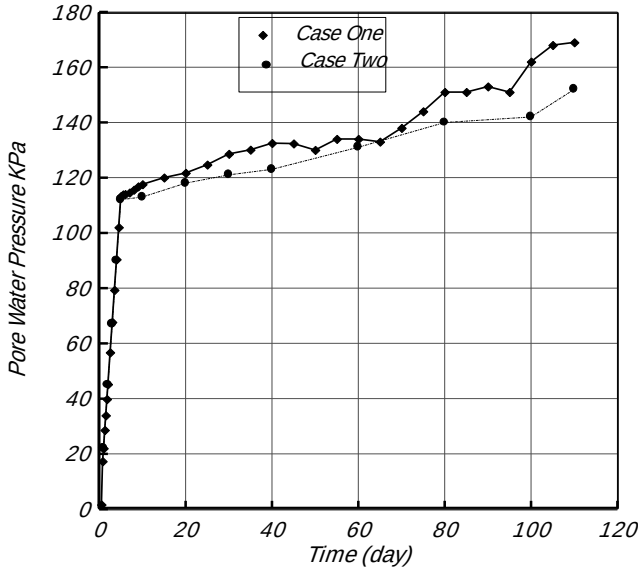

Fig (8) P.W.P.-time relation

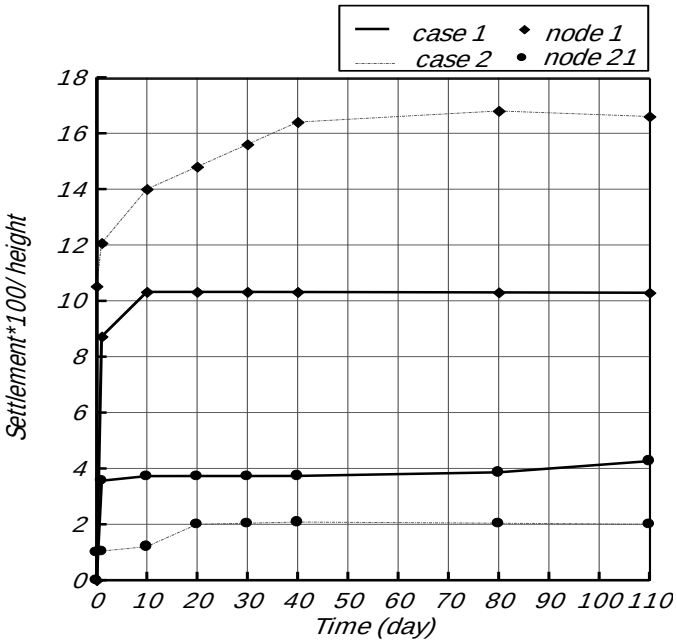

Fig (9) Settlement ratio-time relation

Two Dimensional Problem

Figure (10) shows the finite element mesh. The width of the loaded area B is equal to 9.15m. The applied load is 50kN/m^2.The time stepping scheme and the material properties are the same as those in Tables (3) and (4). Figures (11) and (12) show the results of analysis against time for the elastic modulus and bulk modulus at the center of elements 2, 8, 14, 20, and 26. These results show the variation of values against depth. All the parameters become constant after (5) days of loading and these values are very low when compared to the results of problem one. The values of the elastic modulus are between 500 and 5300 kN/m^2, bulk modulus between 5300 and 22000kN/m^2 and Poisson's ratio between 0.27 and 0.365. Figures (13) and (14) show the variation of pore-water pressure against depth and the settlement against time for cases one and two, respectively.

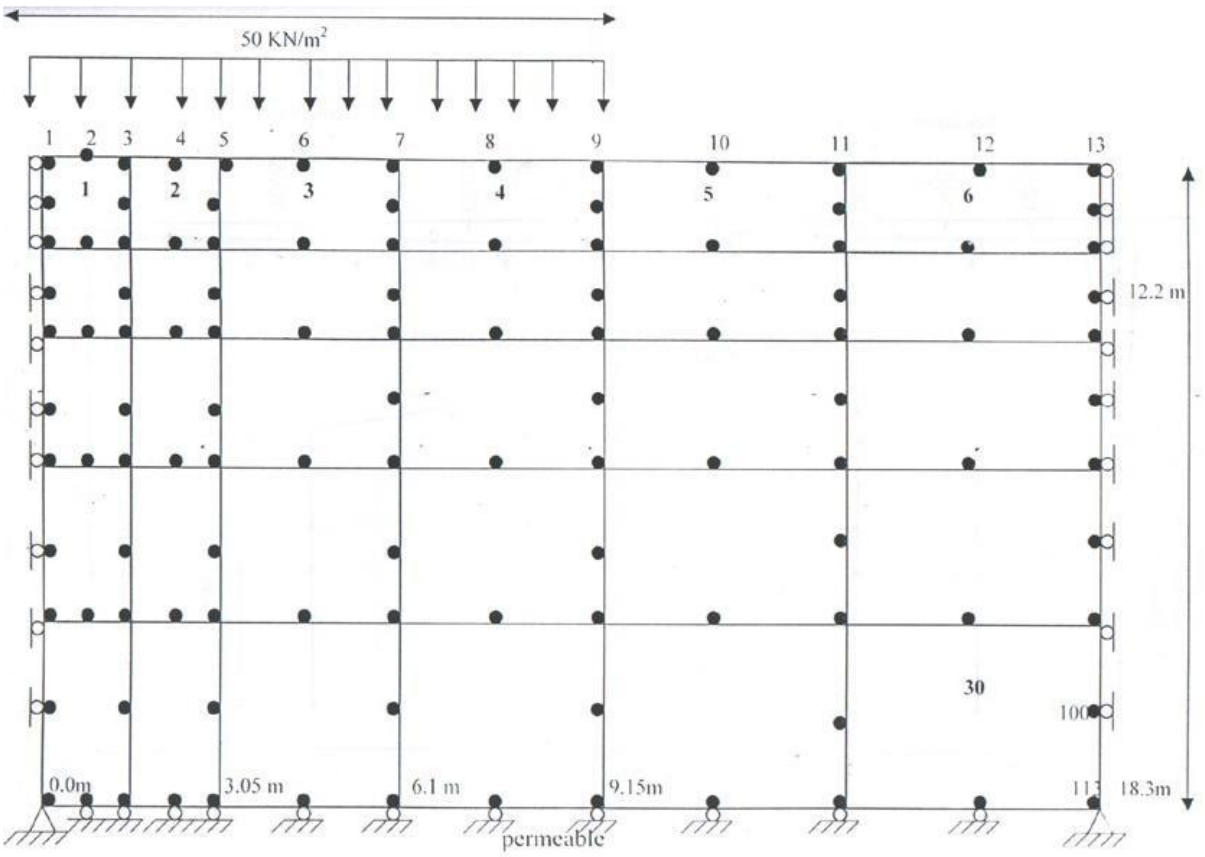

Fig (10) Finite element mesh for the two-dimensional problem

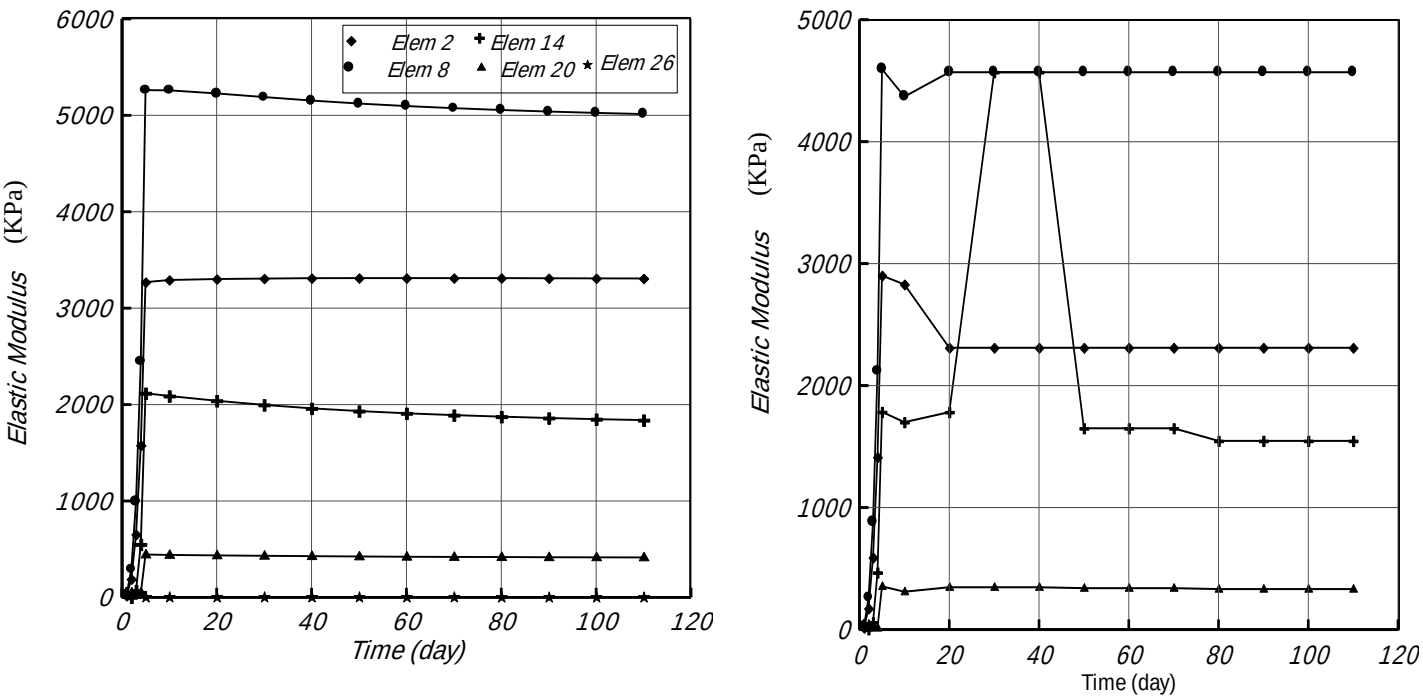

-a- -b-

Fig (11) Variation of elastic modulus with time for (a) case one; and (b) case two

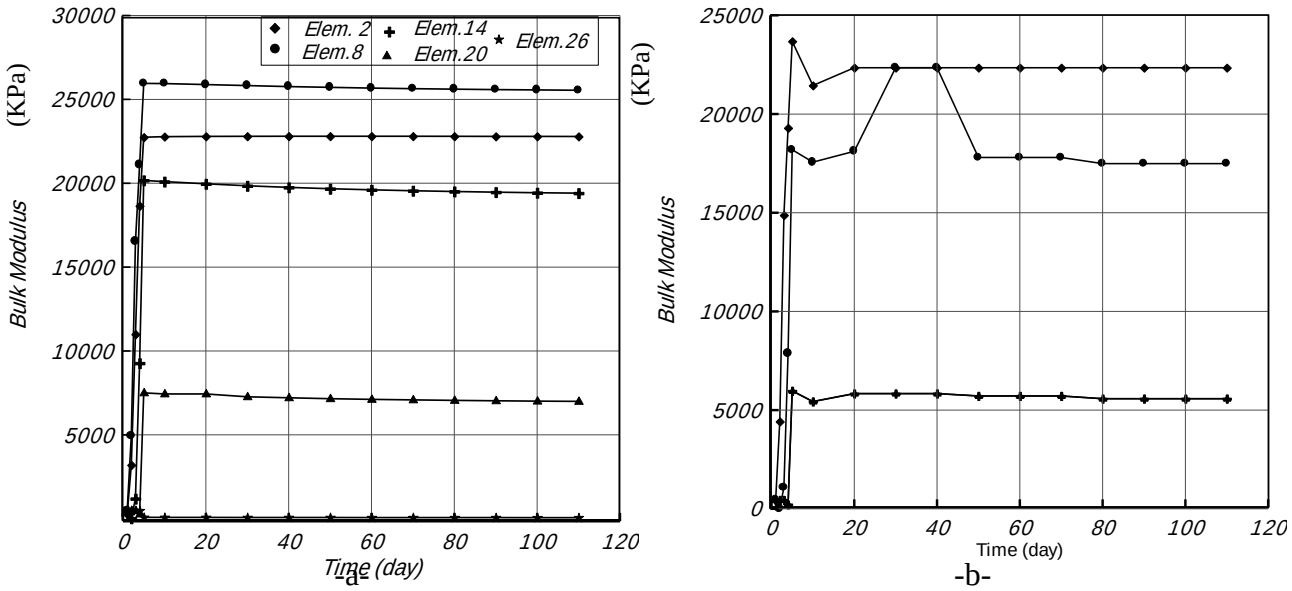

Fig (12) Variation of bulk modulus with time for (a) case one; and (b) case two

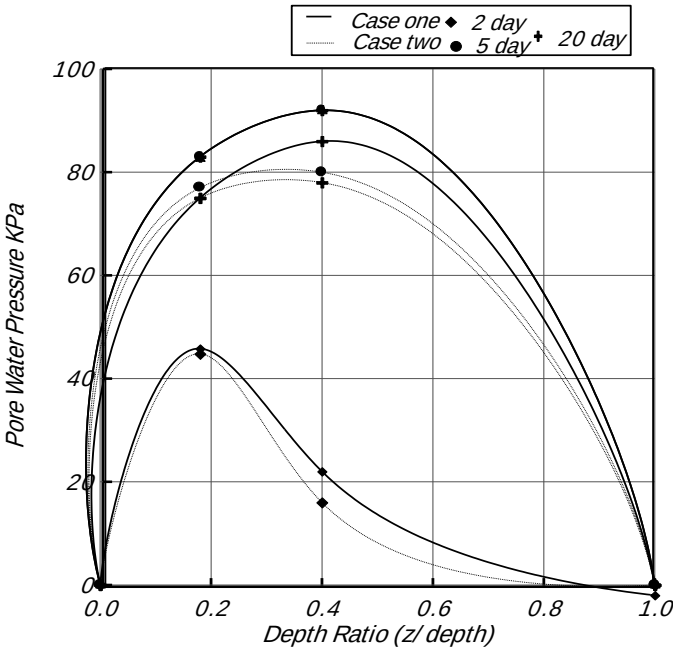

Fig (13) Pore water pressure-depth relation at center of elements 2, 8, 14, 20 and 26

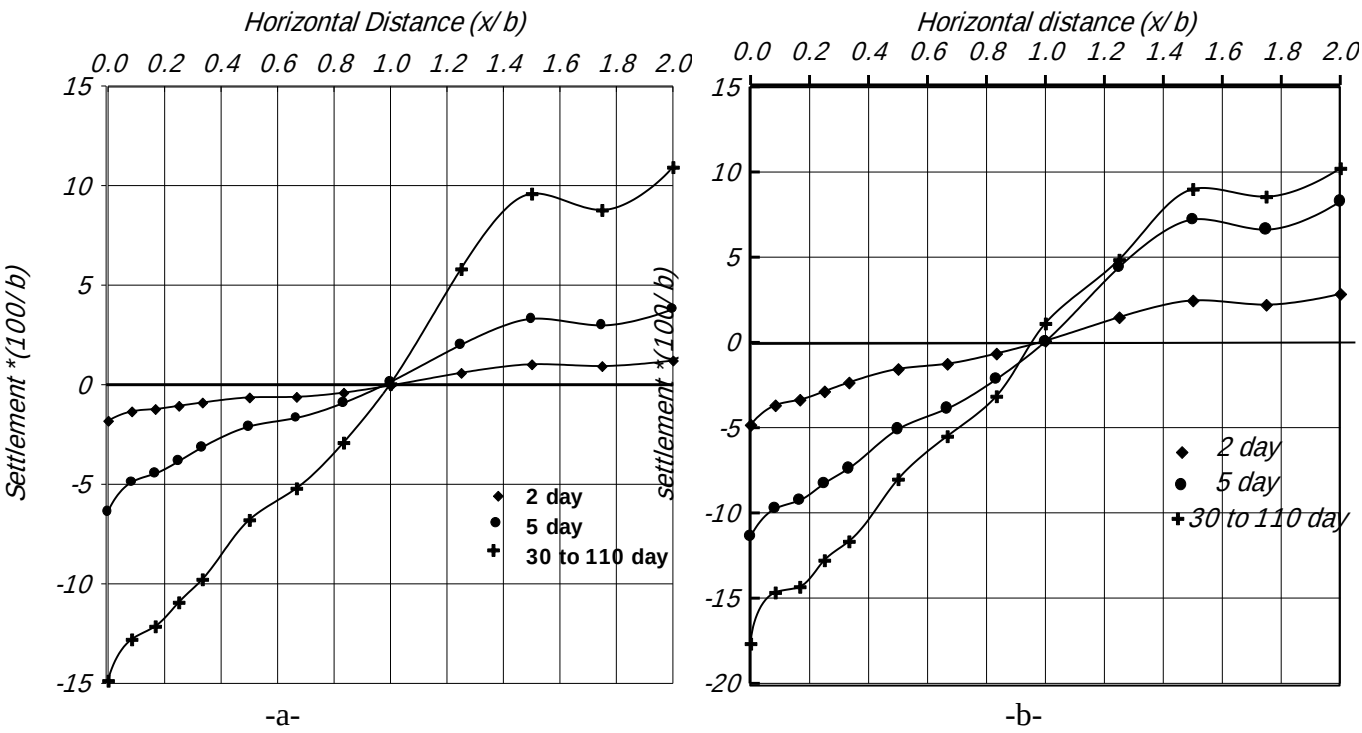

Fig (14) Variation of settlement with time in nodes 1 to 13; (a) case one and (b) case two

CONCLUSIONS

* Results of analysis by using the finite element method show a high effect of dissolution of gypsum on the values of elastic modulus and Poisson's ratio. These parameters and pore water pressures decrease with the increase in dissolution. Dissolution of gypsum is the main reason for this decrease. In addition, there is a high difference in values between the one-dimensional and two-dimensional cases.
* Assuming constant values of hyperbolic stress-strain relationship parameters during the dissolution of gypsum is not correct, because when the content of gypsum varies, some parameters undergo change like specific gravity, density, cohesion and the angle of internal friction. This implies that the values for hyperbolic parameters must vary as the process of dissolution progresses.
* The results of analysis show the soil in a dense state, because the value of the elastic modulus is more than 3000 kN/m^2 and Poisson's ratio more than 0.3. This is similar to laboratory test results.
* The one-dimensional and two-dimensional problems have shown that the dissolution of gypsum decreases with the increase of depth.
* The area of a gypsum particle depends mainly on the diameter. This study assumes that all particles have the same diameter. If the particles considered have varying diameters, then this would have its effect on the results.

Acknowledgement: The authors wish to express their gratefulness to the State Company for Geologic Surveys and Mining, Ministry of Industry of Iraq for the assistance shown without which this research would not have seen light.

Abbreviations:

ASCE = American Society of Civil Engineers.

PWP = pore water pressure.

REFERENCES

- Al-Damluji, O.F. and al-Rawi, M.A. (2005), "Experimental and Numerical Investigations of Dispersion and Transport of Pollutants in an Iraqi Soil", Emirates Journal for Engineering Research, Volume 10, Number 1, Pp 15-25.
- Al-Hassanee, H.M.Z., (2004), "Dissolution and Dispersion Characteristics of Gypseous Soils from Iraq", M.Sc. thesis, Department of Civil Engineering, University of Baghdad.
- Al-Mufty, A.A. (1997), "Effect of Gypsum Dissolution on the Engineering Behavior of Gypseous Soils", Ph.D. Thesis, Department of Civil Engineering, University of Baghdad.
- Al-Rawi, M.A. (2001), "Experimental and Numerical Investigations of Dispersion and Transport of Pollutants in an Iraqi Soil", M.Sc. Thesis, Department of Environmental Engineering, University of Baghdad.
- Bear, J., “Some Experiments in Dispersion”, Journal of Geophysical Research, Vol.66, No.4, 1961, Pp 2455-2467.
- Bear, J. (1972), Dynamics of Fluids in Porous Media, American Elsevier Publishing Company, Inc., New York.
- Bear, J., and Bachmat, Y. (1967), “A Generalized Theory on Hydrodynamic Dispersion in Porous Media’’, I.A.S.H. Symposium, Artificial Discharge and Management of Aquifers, Haifa, IASH72, Pp 7-16.
- Bear, J., and Verruijt, A. (1987), "Modeling Groundwater Flow and Pollution", D. Reidle Publishing Co., Dordrecht, Holland.
- Crichlow, H.B. (1977) “Modern Reservoir Engineering a Simulation Approach”, Prentice-Hall, Englewood Cliffs.
- Doner, H.E. and Lynn, W.C. 1977, "Carbonate, Halide, Sulfate and Sulfide Minerals. In: Minerals in Soil Environments", Ed. by J.B. Weed, Soil Science Society of America, Madison, Wisconsin, Pp 75-98.
- Duncan, J.M. and Chang, C.Y., (1970), "Non-Linear Analysis of Stress and Strain in Soils", Journal of Soil Mechanics and Foundation Division, Proceedings, ASCE, Volume 96, No. SM5, Pp1929-1953.
- FAO Organization Web Site (August, 2001), “Gypsiferous Soils”, State Company for Geological Surveys and Mining, Ministry of Industry, Iraq.
- Ismail, N.F., (1993), “Laboratory and Field Leaching Tests on Coastal Salt-Bearing Soils”, Journal of Geotechnical Engineering, ASCE, Vol. 119, No. 3, Pp 453-470.
- Janbu, N., (!963)
- Majeed, A. H., (2000), “Data Base for Gypseous Soils”, Ph.D. Thesis, Department of Civil Engineering, University of Baghdad.
- Kondner, R.L. (1963), “Hyperbolic Stress-Strain Response of Cohesive Soils”, Journal of Soil Mechanics and Foundation Division, ASCE, Vol. 89, No. SM1, Proc. Paper 3429, Pp 115-143.
- Kondner, R.L and Zelasko, J.S. (1963), “A Hyperbolic Stress-Strain Formulation of Sands”, Proceedings of the 2nd Pan-American Conference on Soil Mechanics and Foundation Engineering, Brazil, Vol.1, Pp 289-324.
- Lewis, R.W. and Karahanoglu, N., (1981), "Simulation of Subsidence in Geothermal Reservoirs", in Numerical Methods in Thermal Problems, Volume II, Ed. Lewis, R.W., Morgan, K. and Schrefler, B.A., Pineridge Press, London, Pp 326-335.

- Lewis, R.W. and Schrefler, B.A., (1987), "The Finite Element Method in the Deformation and Consolidation of Porous Media", John Wiley and Sons Ltd, London.
- Lewis, R.W., Roberts, G.K and Zienkiewicz, O.C. (1976) "A Non Linear Flow Deformation Analysis of Consolidation Problems", Proceedings of the. Second International Conference on Numerical Methods in Geo-mechanics, ASCE, Pp 1106-1118.
- Park, K.C. and Felippa, C.A. (1983) "Partitioned Analysis of Coupled Systems", in Computational Methods for Transient Analysis, Edited by T. Belytschko and T.R.J Hughes, Elsevier Science Publishers, Pp 157-219.
- Reddle, D.L. and Sunada, D,K. (1974), "Numerical Simulation of Dispersion in Groundwater Aquifers", Hydrology Papers, No.41, Colorado State University.
- Wong, K.S. and Duncan, J.M. (1974), "Hyperbolic Stress-Strain Parameters for Non-Linear Finite Element Analysis of Stress and Movements in Soil Masses", Report No. TE-74-3, College of Engineering, University of California, Berkeley, California.
- Zienkiewicz, O.C. (1977) "The Finite Element Method", McGraw-Hill Book Company, London.
- Zienkiewicz, O.C. and Morgan, K. (1982) "Finite Elements and Approximations", John Wiley and Sons. Inc.

List of Symbols:

A : is area of section of flow (m^2).

A_{11} : is the longitudinal apparent dispersivity.
A_{12} : is the lateral apparent dispersivity.
a : is the intercept of the best fit resulting straight line.
b : is the slope of the best fit resulting straight line.
b : are the body forces.
B : is the bulk modulus.
C : is the concentration of gypsum in water (mg/l).
$\hat{C}$: is the concentration of gypsum in the fluid element.
Co : is the original value of concentration.
c : is the cohesion (from tests).
DT : is the tangent matrix.
Dd : is the coefficient of molecular diffusion.
D_{11} : is the longitudinal dispersion **(**D_{11}) (from tests).
D_{22} : is the lateral dispersion **(**D_{22}) (from tests)
dp : is the pore water pressure.
d : is Poisson's ratio Parameter (from tests)
F : is the reduction in Poisson's ratio v_i for a tenfold increase in σ_3 (from tests).
G : is the value of Poisson's ratio v_i at a confining pressure of one atmosphere.
G_g : is the specific gravity of gypsum (usually taken as 2.32).

g : is the gravitational acceleration.

h : is the total head.
Ks : is the bulk modulus of the solid phase.
k : is the absolute permeability matrix of the medium,
k_h : is the horizontal coefficient of permeability, (from tests).
k_v : is the vertical coefficient of permeability, (from tests).
K : is the modulus number (from tests).
k_{ur} : is the modulus number (from tests).
K : is the dissolution rate Ḱ.
L : is the distance from inlet.
M : is the mass.
M_{VE} : is the mass contained inside the volume element.
MP : is the mass source or sink term which is positive when a source and negative when a sink.
m : is equal to unity for the normal stress components and zero for the shear stress components.
n : is the porosity.
n : is the modulus exponent (from tests).
O : is the original value of the variable.
P : is the fluid pressure.
Pa : is the atmospheric pressure.
Po : is the original value of pressure.
R_f : is the failure ratio (from tests).
t : is time (sec).

$\hat{t}$: is the boundary traction ($\hat{t}$) specified at the boundary.

u : is the unknown displacement vector.

υ : is Poisson's ratio.

v_i : is the velocity (m/sec).

V_w : is the volume of water (L^3).

V_o : is the initial volume of element (L^3).

$\overrightarrow{\hat{V}_t}$: is the velocity of the gypsum in the fluid element with respect to a fixed coordinate system.
$\overrightarrow{\hat{V}}$: is the volumetric velocity of the fluid element.

x : is the lateral distance from 50 % composition point.
α : is the proportionality factor relating C and ρ.
β : is the fluid compressibility.
$d\varepsilon$: is the total strain of skeleton.
$d\varepsilon p$: is the overall volumetric strain caused by the uniform compression of the particles due to the pressure of the pore fluid.
$d\varepsilon_m$: the strain due to the dissolved mass of calcium sulphate,

$d\varepsilon_o$: represents all other strains not directly associated with stress changes, e.g. swelling, thermal, …etc.

Φ : is the angle of internal friction (from tests).

Γ : is the boundary.

γ_w : is the density of water (kg/m3).

μ : is the dynamic viscosity of the fluid.

ρ : is the density of the fluid.

ρ_o : is the original value of density.

σ : is the total stress.

Ω : is the domain.

Appendix:

$$K = -\int_{\Omega} B^T D B d\Omega$$

$$L = \int_{\Omega} B^T N d\Omega$$

$$UC = \int_{\Omega} B^T D\left(V_N A_N - V_Y A_Y\right)\left(\frac{\Delta t}{G_g \gamma_w V_o}\right) N d\Omega$$

$$df = -\int_{\Omega} N^T dbd\Omega - \int_{\Gamma} N^T dt' d\Gamma - \int_{\Omega} B^T D d\varepsilon_o d\Omega$$

$$L^T = \int_{\Omega} N^T m^T B d\Omega$$

$$S = -\int_{\Omega} N^T \left(\frac{n}{K_w}\right) N d\Omega$$

$$H = \int_{\Omega} (\nabla N)^T \left(\frac{k}{\mu}\right) \nabla \ddot{N} d\Omega$$

$$F = -\int_{\Gamma} N^T q d\Gamma - \int_{\Omega} (\nabla N)^T \left(\frac{k}{\mu}\right) pgh d\Omega$$

$$CP = \iint CN_I N_J dxdy$$

$$KT = \iint N_I N_J dxdy$$

$$KD = \iint \left\{ Dxx\left(\frac{\partial N_I}{\partial x}\right)\left(\frac{\partial N_J}{\partial x}\right) + Dyy\left(\frac{\partial N_I}{\partial y}\right)\left(\frac{\partial N_J}{\partial y}\right)\right\} dxdy$$

$$KV = \iint \left\{ VxN_I\left(\frac{\partial N_J}{\partial x}\right) + VyN_I\left(\frac{\partial N_J}{\partial y}\right)\right\} dxdy$$

$$PC = \iint \left\{ CVxN_I\left(\frac{\partial N_J}{\partial x}\right) + CVyN_I\left(\frac{\partial N_J}{\partial y}\right)\right\} dxdy$$

$$F_3 = \iint \left\{ NVx(Cp - C)\left(\frac{A_x}{nV_o}\right) + NVy(Cp - C)\left(\frac{A_y}{nV_o}\right)\right\} dxdy$$

EVALUATION OF MATHEMATICAL TECHNIQUES USED FOR PRODUCING DIGITAL ELEVATION MODEL (DEM)

Dr.Hussain Z. Ali
Ministry of Science and Technology (M.O.S.T)
Image Processing/Expert

Mr. Bashar S. Abbas
University of Baghdad
College of Engineering
Department of Surveying

Miss. Afrah M. Daham
University of Baghdad
College of Engineering
Department of Surveying

ABSTRACT

The Digital Elevation Model (DEM) considered a common tool in producing topographic maps, orthophotos and civil engineering projects besides other different engineering applications. As a result many software packages were developed and used to produce DEM from different sources like field surveys, scanned topographic maps and stereo photos exposed from air or space.

This paper is devoted to evaluate the most suitable and accurate interpolation method in producing digital elevation model for the data gathered from existed topographic maps which are also compared with data gathered from field survey. Map scale (1:25000) with contour interval (50m) were chosen in the tests. The accuracy tests based on the National Mapping Accuracy Standards (NMAS) by comparing the result of Root Mean Square Error (RMSE) in elevations with the typical standard deviation (σ_z) proposed by (NMAS) which depends on the scale of maps and contour intervals.

From testing four interpolation techniques ((Kriging, Triangulated Irregular Network (TIN), Inverse Distance Weighting (IDW) and Polynomial)) it was found that kriging is the best method followed by TIN method while IDW method failed in some tests, and the polynomial model failed in all tests.

الخلاصة:

اصبح نموذج الأرتفاع الرقمي (DEM) في الوقت الحاضر شائع الأستعمال في مجال انتاج الخرائط الطبوغرافية ومشاريع الهندسة المدنية هذا وبالاضافة إلى استخدامه بشكل واسع في مجالات اخرى مثل ابراز الأرتفاعات والتخطيط والأستكشافات الجيولوجية والجيوفيزيائية وكنتيجة لذلك فان العديد من البرامج الجاهزة قد تم تطويرها واستخدامها لأنتاج نموذج الارتفاع الرقمي ومن مختلف المصادر مثل المسوحات الأرضية, النماذج المجسمة للصور الجوية والفضائية والخرائط الطبوغرافية الممشطة. وتماشيا مع هذا التوجه فان هذا البحث يتناول استخدام اكثر من طريقة رياضية لأنتاج النموذج وباستخدام برنامج (Autodesk Field Survey) ومن مصدرين مختلفين المصدر الأول هو المسوحات الأرضية للمنطقة سد طق طق لأغراض المقارنة والمصدر الثاني وهو طريقة الخرائط الكنتورية الممشطة (Scanned Contour maps) لمنطقة الدراسة وذات مقياس (1;25000) وبفترة كنتورية مقدارها (50m) وبالأعتماد على نفس البرنامج.

وبعد انتاج النموذج فقد تم فحص الدقة للنماذج والطرق الرياضية و بالأعتماد على معيار دقة الخارطة الوطنية (National Mapping Accuracy Standards (NMAS)) الذي يعتمد على مقياس الخارطة ومقدار الفترة الكنتورية وتم استخراج جذر معدل مربع الخطأ ((Root Mean Square Error (RMSE) لقيم الارتفاع ولكل النماذج وبكل الطرق الرياضية المستخدمة (طريقة الشبكة المثلثية الغير منتظمة (TIN), طريقة ال Kriging, طريقة الوزن بمعكوس المسافات (IDW) و طريقة ال Polynomial) وتم مقارنة الأنحراف المعياري المحسوب(Computed Standard Deviation) مع الأنحراف المعياري النموذجي ((Typical Standard Deviation (σ_z)). وبعد اختبار الدقة فكانت افضل النتائج هي للطريقة ال (Kriging) وتليها طريقة ال (TIN) , اما طريقة ال (IDW) نتائجها كانت مقبولة في بعض الفحوصات وطريقة ال (Polynomial) فنتائجها كانت فاشلة في جميع الفحوصات.

KEY WORD
Digital Elevation Model (DEM), Applications, Interpolation Techniques, Evaluation of Interpolation Techniques.

INTRODUCTION

Digital elevation modeling is one of the modern methods for representing the topographic surface of the terrain, (i.e., how the elevation of the ground surface is changing with position). Traditionally this has been done by contour lines on topographic maps. DEMs have been developed and studied for more than 40 years [Kennie, 1993]. The development has revealed the significance of several main aspects such as data acquisition, interpolation methods, accuracy, computer programs and application, all that will be discussed in this chapter.

For the future, the use of terrain modeling methods will undoubtedly continue to develop and expand, particularly with continued improvements in the price performance ratio of computer systems. National and regional terrain data based on existing topographic maps are now being developed in many parts of the world, and these will play an increasingly important role in terrain visualization during the preliminary planning stage of engineering projects [Anderson, 1998].

The term DEM originally referred to the use of cross sectional height data to describe the terrain. Nowadays, however, the definition is including both grid and non grid data sets. Several other terms are also used to describe the terrain surface. Among the more common are Digital Elevation Model (DEM), Digital Height Model (DHM), Digital Terrain Model (DTM), Digital Ground Model (DGM) and Digital Terrain Elevation Data (DTED) [Kennie, 1993].

THE STUDY AREA:

The study area is described through the following conditions:

- The area is called **(TaqTaq)**, which covers about (12.974km^2), the survey for this area were accomplished by AL-Aali for engineering consultancies by Total Station Topcon, its borders coordinates are shown :

Pt	E (m)	N (m)
1	468460.657	3973469.559
2	464468.958	3973469.559
3	464468.958	3970219.393
4	468460.657	3970219.393

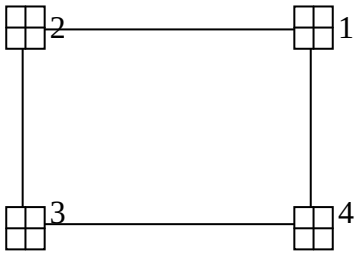

These points help to obtain real-world coordinates, the same tic numbers and locations will be recorded and used for each separate layer of contour lines.The coordinate system of this data set is defined by using the following values which has the following projection data:

Projection	Units	Zone
UTM	Meter	38

This area were covered by a topographic map of a scale 1:25000 with contour interval (50m), It extends between latitude (35° 52' 30"- 36° 00' 00", North) and longitude (44° 30' 00"- 44° 00' 00", East). (See fig.1).

- Valleys and mountains is the most active features of land cover in the region due to high slopes of this region.
- The **Small Zap River** passes through this region.

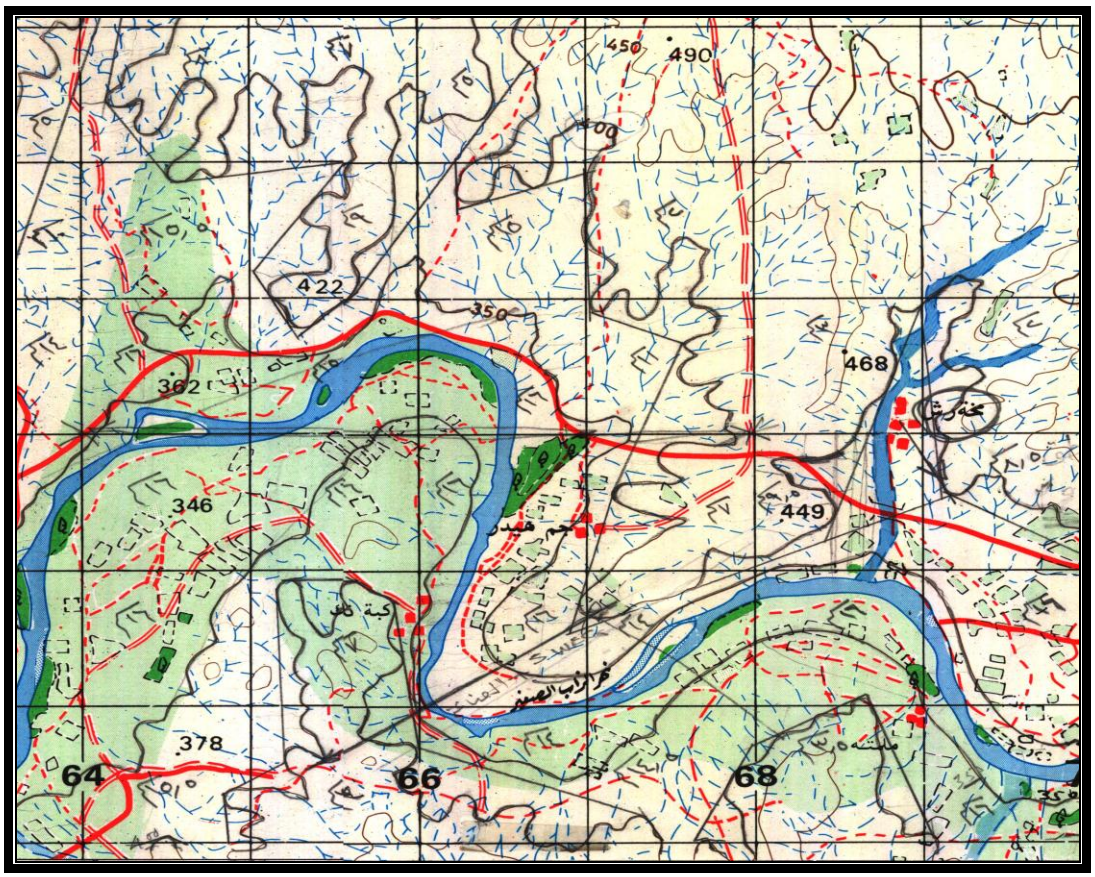

Fig (1): The study area (TaqTaq), (1/25000) scale.

GRIDDING INTERPOLATION ALGORITHM

Gridding produces a regularly spaced array of Z values from irregularly spaced XYZ data. The term "irregularly spaced" implies that the points are randomly distributed over the extent of the map area meaning that the distance between data points is not consistent over the map [Lebrer, 1973]. When the XYZ data is randomly spaced over the map area, there are many "holes" in the distribution of data points.Gridding fills in the holes by extrapolating or interpolating Z values in those locations where no data exists [Surfer, 1995].

- Interpolation**:** the process of estimating the values of an attribute (e.g., elevation) at internal unsampled sites using measurements made at reference points. The interpolation point lies within the range defined by the reference points [Habib, 2003].
- Extrapolation**:** the process of predicting the values of an attribute (e.g., elevation) at external unsampled sites using measurements made at reference points. The extrapolation point lies outside the range defined by the reference points [Habib, 2003].

There are several gridding methods. Each method calculates grid node values using a different algorithm, and can result in a some what different interpretation of input data [Surfer, 1995].

Inverse Distance to a Power Interpolation Method

The Inverse Distance to a Power gridding method is a weighted average interpolator, and can be either an exact or a smoothing interpolator. The Power parameter controls how the weighting factors drop off as distance from a grid node increases. For a larger power, closer data points are given a higher fraction of the overall weight; for a smaller power, the weights are more evenly distributed among the data points.

The weight given to a particular data point when calculating a grid node is proportional to the inverse of the distance to the specified power of the observation from the grid node. When calculating a grid node, the assigned weights are fractions, and the sum of all the weights is equal to 1. When an observation is coincident with a grid node, the observation is given a weight of essentially 1.0, and all other observations are given a weight of almost 0. In other words, the grid node is assigned the value of the coincident observation. This is an exact interpolator [Surfer, 1995].

One of the characteristics of inverse distance is the generation of "bull's-eyes" surrounding the position of observations within the gridded area.

The smoothing parameter can be assigned during inverse distance gridding. If it was greater than zero assures that no one observation is given all the weight at a particular grid node, even if the observation is coincident with the grid node. The smoothing parameter reduces the "bull's-eye" effect by smoothing the interpolated grid.

This method basically depends on estimating the height of the unknown point by computing the distances from this point to the other known points. Weights are proportionally by inverse to distances. Whenever the point being far away, its effect reduce the following equation explain that:

$$Z(X,Y) = \frac{\sum_{i=1}^{n}\left[\frac{Z_i}{d_i^{\,p}}\right]}{\sum_{i=1}^{n}\left[\frac{1}{d_i^{\,p}}\right]} \qquad (1)$$

$$Z(X,Y) = \sum \lambda_i \bullet Z_i \xrightarrow{With} \sum \lambda_i = 1$$

(2)

d_i Is the planimetric distance between the reference point and the ith interpolation point [21].

$$d_i = \sqrt{(X_i - X)^2 + (Y_i - Y)^2} \qquad (3)$$

Z (x,y): is the predicted value at the unsampled location x,y.
n: is the number of measured sample points within the neighborhood defined for x,y.
Z_i: is the observed value at location i.
λ : are the distance-dependent weights associated with each sample point.
d_i: is the distance between the prediction location x,y and the measured location i.
p: is the power parameter that defines the rate of reduction of the weight as distance increases.
We have mention that the weight might be inverse to a distance which rise to the power n, thus n = 1,2,3,4,5,.....

Kriging Interpolation Method

Kriging is a geostatistical gridding method, the geostatistical method is defined as that use spatial coordinates to help in the formulation of models, which are used in the estimation and prediction. In the Geostatistical Analyst: Exploratory and interpolation methods that used information of the spatial coordinates [ESRI, 2001].

Kriging method has proven useful and popular in many fields. This method produces visually appealing contour and surface plots from irregularly spaced data [Ibrahem, 1993]. Kriging attempts to express trends that are suggested in our data, so that, for example, high points might be connected along a ridge, rather than isolated by bull's-eye type contours.

Kriging is a very flexible gridding method. It can be custom fit to a data set by specifying the appropriate variogram model. It incorporates anisotropy and underlying trends in an efficient and natural manner [Habib, 2003].

Kriging is based on the assumption that the parameter being interpolated can be treated as a regionalized variable. A regionalized variable is intermediate between a truly random variable and a completely deterministic variable in that it varies in a continuous manner from one location to the next and therefore points that are near each other have a certain degree of spatial correlation, but points that are widely separated are statistically independent [Habib, 2003]. Kriging is a set of linear regression routines which minimize estimation variance from a predefined covariance model.

This method uses to calculate the auto correlation between the data points and produce a minimum variance estimate. Kriging method produces much more accurate interpolation results than the other methods.

Kriging can be achieved by the following steps:-

- Using the observed height in the Ground Control Points (GCP) to compute experimental covariance function C{d}.
- Choose covariance sample similar to experimental covariance function C{d}.
- Using least square for computing unknowns, which related to function covariance sample.
- Using product equation to interpolate heights.

The kriging interpolation techniques include:-

a. Ordinary Kriging.
b. Simple Kriging.
c. Universal Kriging.

a. Ordinary Kriging: it is presented statistically what can be named Beast Linear Unbiased estimation (**BLUE**) and in this way the summation of weights are one, λ is Lagrange multipliers is a powerful method for finding the maximum and minimum of constrained functions and k is the value of elements equal one, but that mean complex in mathematics

from other side, also the using of this method require solving a huge number of equations [Surfer, 1995]

$$\hat{Z}_p = w^T Z_r and \sum_{i=1}^{n} w_i = 1$$

$$\begin{bmatrix} w_{n\times 1} \\ \lambda \end{bmatrix} = \begin{bmatrix} C\{z_r, z_r\} & K \\ K^T & 0 \end{bmatrix}^{-1}_{(n+1)\times(n+1)} \begin{bmatrix} C\{z_r, z_p\} \\ 1 \end{bmatrix}^{(n+1)\times 1} \tag{4}$$

b. Simple Kriging: Simple kriging is similar to ordinary except that the following equation is not added to the set of equations:

w1 + w2+ w3 = 1 (5)

And the weights do not sum to unity. Simple kriging uses the average of the entire data set while ordinary kriging uses a local average (the average of the scatter points in the kriging subset for a particular interpolation point). As a result, simple kriging can be less accurate than ordinary kriging [Habib, 2003].
Simple kriging is presented statistically what can be named Best Linear Estimation (**BLE**) and next the method interpolation achieve as shown:

Interpolated Height

$$\hat{Z}_p = w^T Z_r$$
$$w_{n\times 1} = \left[C\{z_r, z_r\}\right]^{-1}_{n\times n} \left[C\{z_r, z_p\}\right]_{n\times 1}$$

Quality of the Interpolated Height

$$D\left\{\hat{Z}_p = w^T C\{z_r, z_r\}\right\} w = w^T C\{z_r, z_p\}$$

- Where:

$$C\{z_r, z_r\}_{n\times n} = \begin{bmatrix} C\{0\} & C\{d12\} & C\{d13\} & \cdots & C\{d1n\} \\ C\{d21\} & C\{0\} & C\{d23\} & \cdots & C\{d2n\} \\ C\{d31\} & C\{d32\} & C\{0\} & \cdots & C\{d3n\} \\ \vdots & \vdots & \vdots & \vdots & \vdots \\ C\{dn1\} & C\{dn2\} & C\{dn3\} & \cdots & C\{0\} \end{bmatrix} \tag{6}$$

$$C\{z_r, z_p\}_{n\times 1} = \begin{bmatrix} C\{d_{1p}\} \\ C\{d_{2p}\} \\ C\{d_{3p}\} \\ \vdots \\ C\{d_{np}\} \end{bmatrix} \tag{7}$$

- Note: $C\{d_{ij}\} = C\{d_{ji}\} \Rightarrow C\{z_r, z_r\}$ is symmetric

z_r : vector, its height value of Ground Control Point (GCP).

$C\{z_r, z_r\}$: Covariance between ground control points with each other.

$C\{z_r, z_p\}$: Covariance between ground control points with unknown point.

And it is named $C\{z_r, z_r\}$ and $C\{z_r, z_p\}$ semi-variance.

c. Universal Kriging: One of the assumptions made in kriging is that the data being estimated are stationary. That is, as you move from one region to the next in the scatter point set, the average value of the scatter points is relatively constant. Whenever there is a significant spatial trend in the data values such as a sloping surface or a localized flat region, this assumption is violated. In such cases, the stationary condition can be temporarily imposed on the data by using of a drift term [Surfer, 1995]. The drift is a simple polynomial function that models the average value of the scattered points. The residual is the difference between the drift and the actual values of the scattered points. Since the residuals should be stationary, kriging is performed on the residuals and the interpolated residuals are added to the drift to compute the estimated values. Using a drift this function is often called "universal kriging." the mathematical model of universal kriging is as follow [Habib, 2003]:

$$\begin{bmatrix} \gamma\{d_{11}\} & \gamma\{d_{12}\} & \gamma\{d_{13}\} & \gamma\{d_{14}\} & \gamma\{d_{15}\} & 1 & X_1 & Y_1 \\ \gamma\{d_{21}\} & \gamma\{d_{22}\} & \gamma\{d_{23}\} & \gamma\{d_{24}\} & \gamma\{d_{25}\} & 1 & X_2 & Y_2 \\ \gamma\{d_{32}\} & \gamma\{d_{32}\} & \gamma\{d_{33}\} & \gamma\{d_{34}\} & \gamma\{d_{35}\} & 1 & X_3 & Y_3 \\ \gamma\{d_{41}\} & \gamma\{d_{42}\} & \gamma\{d_{43}\} & \gamma\{d_{44}\} & \gamma\{d_{45}\} & 1 & X_4 & Y_4 \\ \gamma\{d_{51}\} & \gamma\{d_{52}\} & \gamma\{d_{53}\} & \gamma\{d_{54}\} & \gamma\{d_{55}\} & 1 & X_5 & Y_5 \\ 1 & 1 & 1 & 1 & 1 & 0 & 0 & 0 \\ X_1 & X_2 & X_3 & X_4 & X_5 & 0 & 0 & 0 \\ Y_1 & Y_2 & Y_3 & Y_4 & Y_5 & 0 & 0 & 0 \end{bmatrix} \begin{bmatrix} w_1 \\ w_2 \\ w_3 \\ w_4 \\ w_5 \\ \lambda \\ a_1 \\ a_2 \end{bmatrix} = \begin{bmatrix} \gamma\{d_{1p}\} \\ \gamma\{d_{2p}\} \\ \gamma\{d_{3p}\} \\ \gamma\{d_{4p}\} \\ \gamma\{d_{5p}\} \\ 1 \\ X_P \\ Y_P \end{bmatrix} \quad (8)$$

Where:-

λ : is Lagrange multipliers.

a_1 and a_2: the coefficients expressing the trend (two coefficients).

3. Polynomial Regression Interpolation Method

Polynomial Regression is used to define large scale trends and patterns in our data. There are several options can be used to define the type of trend surface. Polynomial Regression is not really an interpolator because it does not attempt to predict unknown Z values [Lebrer, 1973].The form of the 2nd degree polynomial is as follow:

$$Z(X,Y) = a_0 + a_1 X + a_2 Y + a_3 X^2 + a_4 XY + a_5 Y^2$$

(9)

TIN INTERPOLATION ALGORITHM

TINs represent surfaces as contiguous non overlapping triangular faces. A surface value can be estimated for any location by simple or polynomial interpolation of elevations in a triangle. Because elevations are irregularly sampled in a TIN, a variable point density to areas where the terrain changes sharply can be applied, yielding an efficient and accurate surface model [ESRI, 2001].

A TIN preserves the precise location and shape of surface features. Area features such as lakes and islands are represented by a closed set of triangle edges. Linear features such as ridges are represented by a connected set of triangle edges. Mountain peaks are represented by a triangle node.

TINs support a variety of surface analyses such as calculating elevation, slope, and aspect performing volume calculations, and creating profiles on alignments. The disadvantage of TINs is that they are often not readily available and require data collection. TINs are well suited for large-scale mapping applications where positional accuracy and shapes of surface features is important [Surfer, 1995]. The TIN data structure can be used in representing any type of surface accurately. Not only can elevations be interpolated for any location within a TIN, but natural features that form breaks in a surface's slope, such as ridges and streams, can also be stored. After constructing TIN we can interpolated the height of unknown point that its location inside the triangulation network as shown in figure (2) one of the next mathematical techniques could be used [Habib, 2003]:

1.Linear Interpolation.
2.Second Exact Fitted Surface Interpolation.
3.Quintic Interpolation.

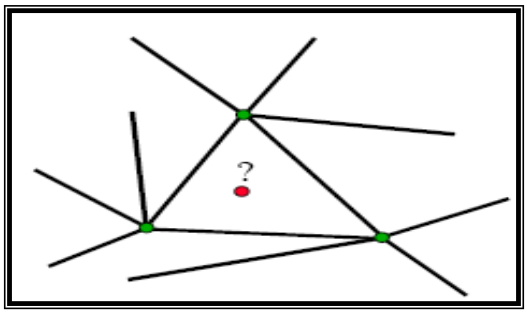

Figure (2): Represent the point unknown elevation [Habib, 2003].

1. Linear Interpolation: it is basically depending on the following equation:

$$Z(X,Y) = a_0 + a_1 X + a_2 Y^2 \tag{10}$$

By known vertices of triangle and by matrix form, so that:

$$I_z = \begin{bmatrix} Z_1 \\ Z_2 \\ Z_3 \end{bmatrix} \mapsto A = \begin{bmatrix} 1 & X_1 & Y_1 \\ 1 & X_2 & Y_2 \\ 1 & X_3 & Y_3 \end{bmatrix} \mapsto x = \begin{bmatrix} a_0 \\ a_1 \\ a_2 \end{bmatrix}$$

$$\begin{bmatrix} Z_1 \\ Z_2 \\ Z_3 \end{bmatrix} = \begin{bmatrix} 1 & X_1 & Y_1 \\ 1 & X_2 & Y_2 \\ 1 & X_3 & Y_3 \end{bmatrix} \begin{bmatrix} a_0 \\ a_1 \\ a_2 \end{bmatrix} \mapsto I_{z_{3\times1}} = A_{3\times3} x_{3\times1} \tag{11}$$

or $\hat{x}_{3\times1} = \left(A^T A\right)^{-1} A^T I_z \quad \hat{x}_{3\times1} = A^{-1} I_z$

Estimate the height at the interpolation point

$$Z(X_P, Y_P) = \begin{bmatrix} 1 & X_P & Y_P \end{bmatrix} \begin{bmatrix} a_0 \\ a_1 \\ a_3 \end{bmatrix}$$

(12)

2. Second Exact Surface: depend on a second degree equation, as shown in equation (13) [Habib, 2003].

$$Z(X,Y) = a_0 + a_1 X + a_2 Y + a_3 X^2 + a_4 XY + a_5 Y^2)$$

(13)

Or in matrix form:-

$$I_z = \begin{bmatrix} Z_1 \\ Z_2 \\ Z_3 \\ Z_4 \\ Z_5 \\ Z_6 \end{bmatrix} \mapsto A = \begin{bmatrix} 1 & X_1 & Y_1 & X_1^2 & X_1Y_1 & Y_1^2 \\ 1 & X_2 & Y_2 & X_2^2 & X_2Y_2 & Y_2^2 \\ 1 & X_3 & Y_3 & X_3^2 & X_3Y_3 & Y_3^2 \\ 1 & X_4 & Y_4 & X_4^2 & X_4Y_4 & Y_4^2 \\ 1 & X_5 & Y_5 & X_5^2 & X_5Y_5 & Y_5^2 \\ 1 & X_6 & Y_6 & X_6^2 & X_6Y_6 & Y_6^2 \end{bmatrix} \mapsto x = \begin{bmatrix} a_0 \\ a_1 \\ a_2 \\ a_3 \\ a_4 \\ a_5 \end{bmatrix} \quad I_{z_{6\times1}} = A_{6\times6} x_{6\times1} \tag{14}$$

$$\hat{x}_{6\times1} = \left(A^T A\right)^{-1} A^T I_z \quad \text{or} \quad \hat{x}_{6\times1} = A^{-1} I_z \tag{15}$$

$$Z(X_P, Y_P) = \begin{bmatrix} 1 & X_P & Y_P & X_P^2 & X_P Y_P & Y_P^2 \end{bmatrix} \begin{bmatrix} a_0 \\ a_1 \\ a_2 \\ a_3 \\ a_4 \\ a_5 \end{bmatrix}. \tag{16}$$

3. Quintic Interpolation: is produces a continuous surface. Considers the surface model to be smooth, that is, the normal to the surface varies continuously within each triangle and between triangles [Habib, 2003]. This smooth characteristic is accomplished by considering the geometry of the neighbouring triangles when interpolating the z value of appoint in a TIN triangle,quintic interpolation depend on a five degree polynomial in x and y as the follow:

$$Z(X,Y) = \sum_{i=0}^{5} \sum_{j=0}^{5-i} a_{ij} X^i Y^j \tag{20}$$

$$Z(X,Y) = a_0 + a_1 X + a_2 Y^2 + a_3 X^2 + a_4 XY + a_5 Y^2 + a_6 X^3 + a_7 x^2 y + a_8 XY^2 + a_9 Y^3$$
$$a_{10} X^4 + a_{11} X^3 Y + a_{12} X^2 Y^2 + a_{13} XY^3 + a_{14} Y^4 + a_{15} X^5 + a_{16} X^4 Y + a_{17} X^3 Y^2 +$$
$$a_{18} X^2 Y^3 + a_{19} XY^4 + a_{20} Y^5$$

Elevation Data Collection

In this work it was depended on collecting the data of elevation from field survey of TaqTaq area, also on the scanned topographic maps by separating the layer of contour lines where the value of the elevation for each line is known, elevation data will be assigned as shown in figure (3).

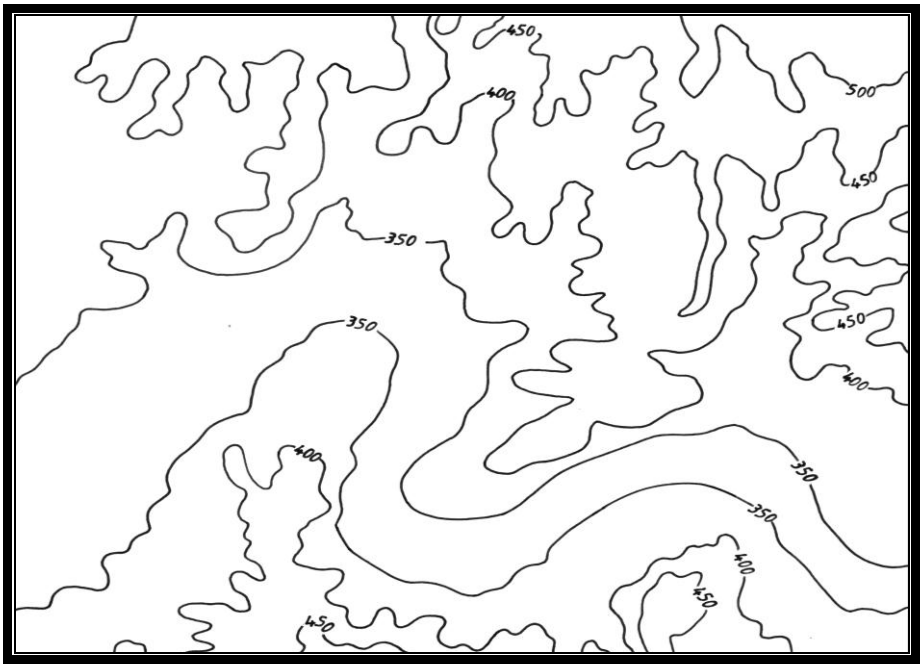

Fig (3): Contour lines of the study area (TaqTaq), from map (1/25000) scale.

Data Modeling

Data Modeling by Using Field Survey

Digital elevation model (DEM) can also be generated from field survey. The accuracy of all field survey method is very high but they are really practical and economical to be implemented over relatively small area of terrain. The field surveys were used here just for compartment purposes with those collected from topographic maps.

The used field survey are for TaqTaq area which is about 32000 surveyed points. The stage of producing the digital elevation model from field survey was the following as:-

The DEM building using the field survey. At first were drawn the points by using (Autodesk field survey) software as shown figure (4), then the points, which are considered in data base and information correlated with digital elevation model, are selected. The model building will be dependent on the triangulation method and gridding method. This means the information that is saved in surface file will be converted to (Triangulated Irregular Network (TIN), Inverse Distance Weighting **(**IDW**)**, Universal Kriging and 2nd polynomial). After that the digital elevation model is displayed as a perspective figure for a three dimensional vision. (See fig. (5), which are plotted by ArcView ver.3.2, (6), (7), and (8)) are illustrate the digital elevation model of the study area (TaqTaq) by using mathematical techniques.

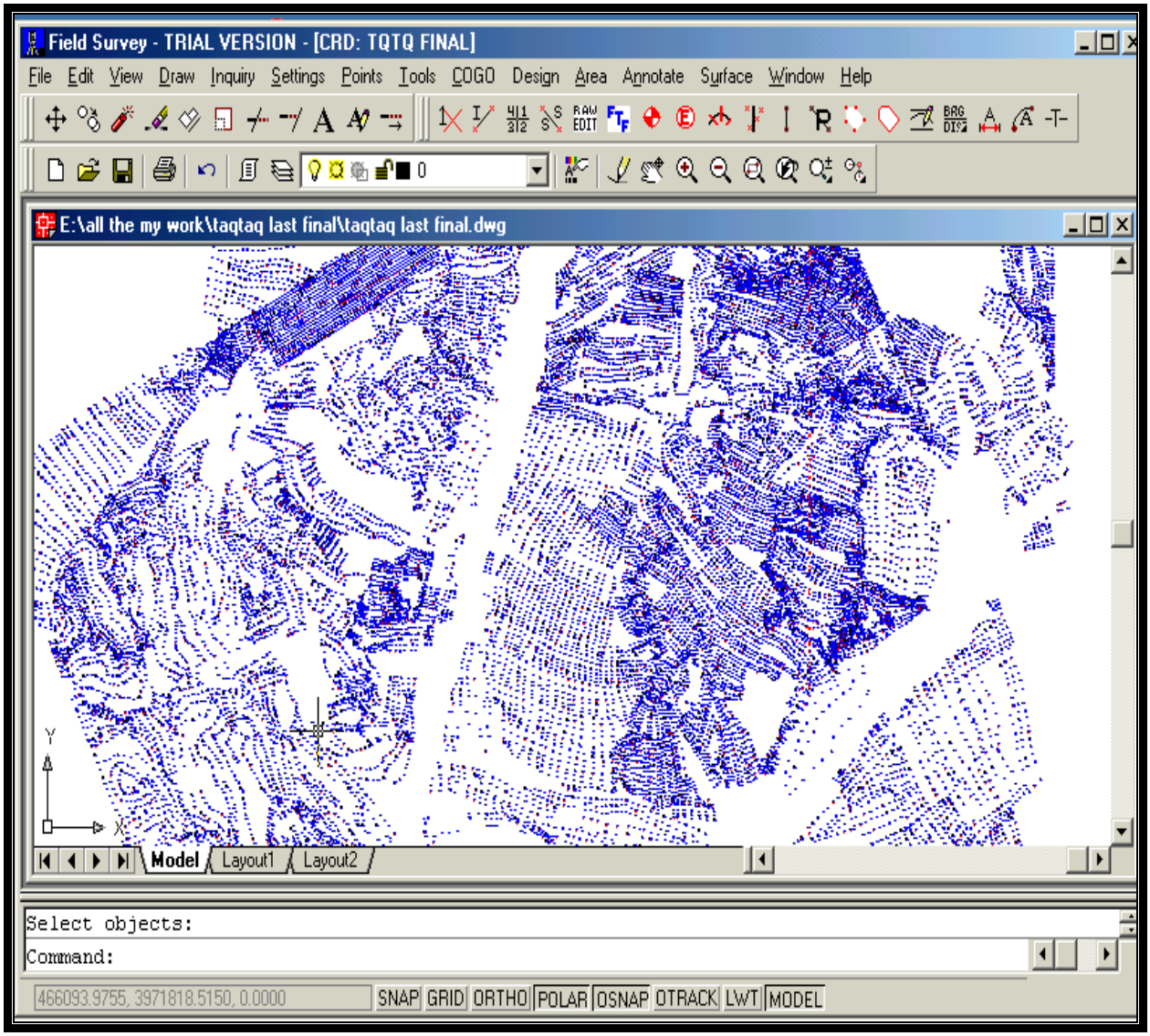

Fig (4): Represent the drawing of the field survey data by using (Autodesk Field Survey) software.

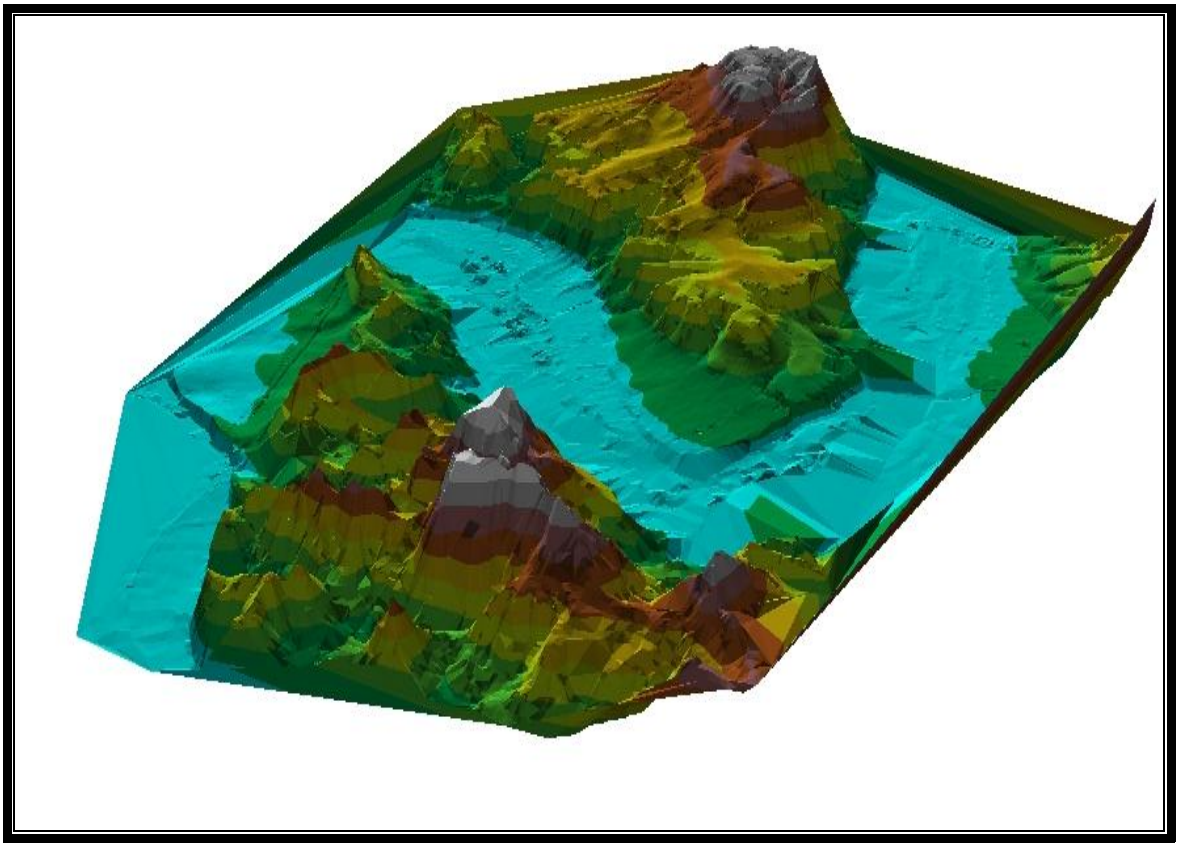

Fig (5): DEM for field survey data of TaqTaq area by (TIN) method.

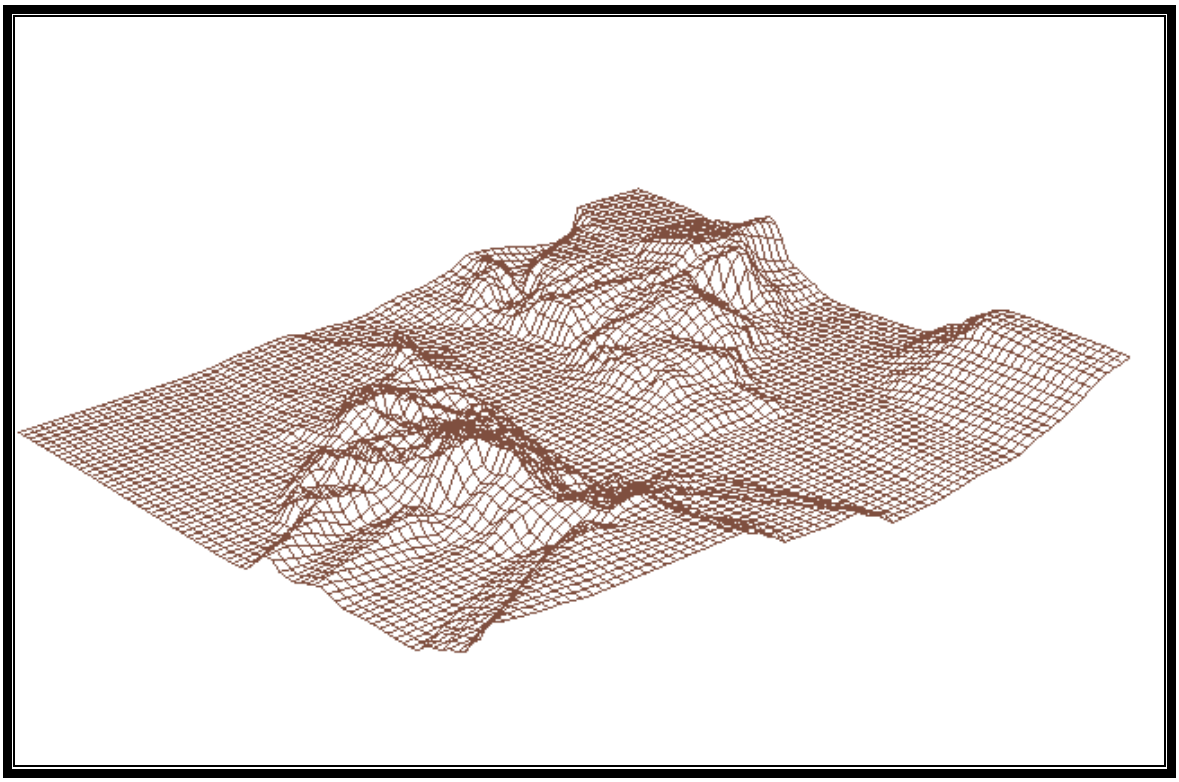

Fig (6): EM for field survey data of TaqTaq area by (Kriging) method.

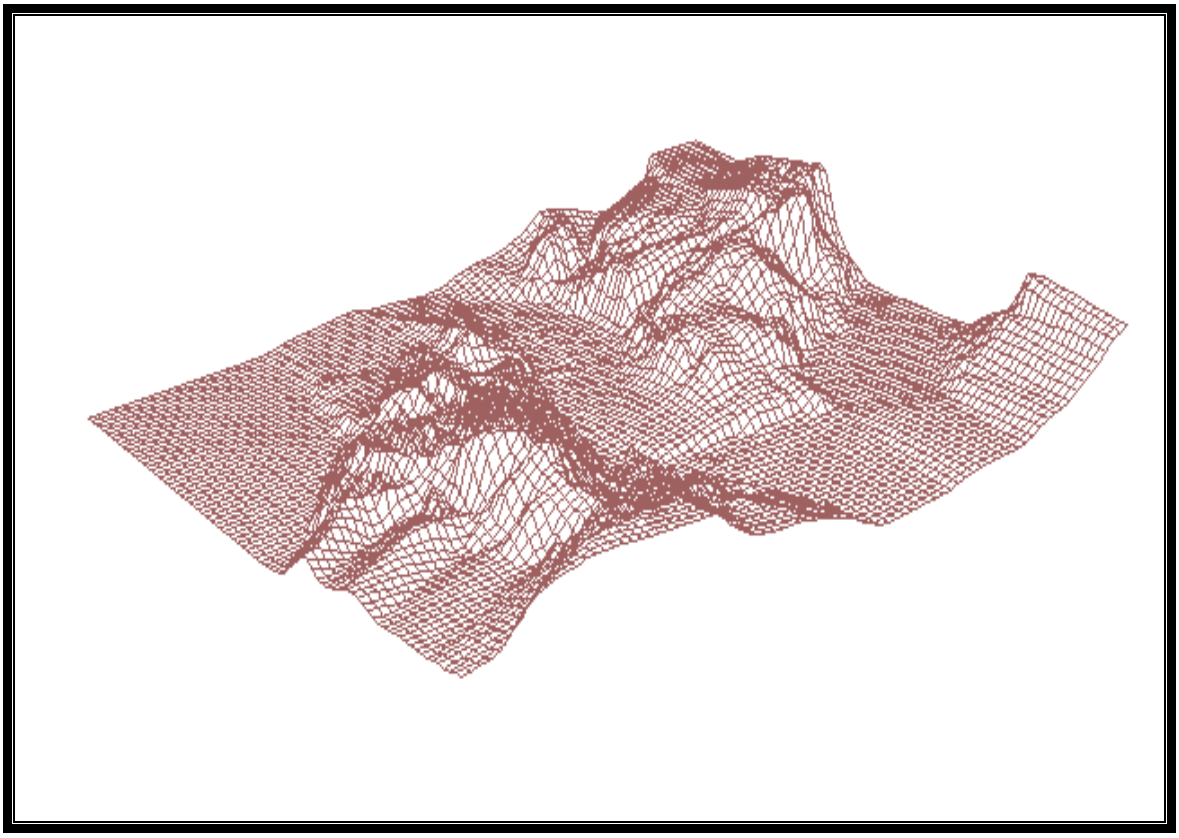

Fig (7): DEM for survey data of TaqTaq area by (IDW) method.

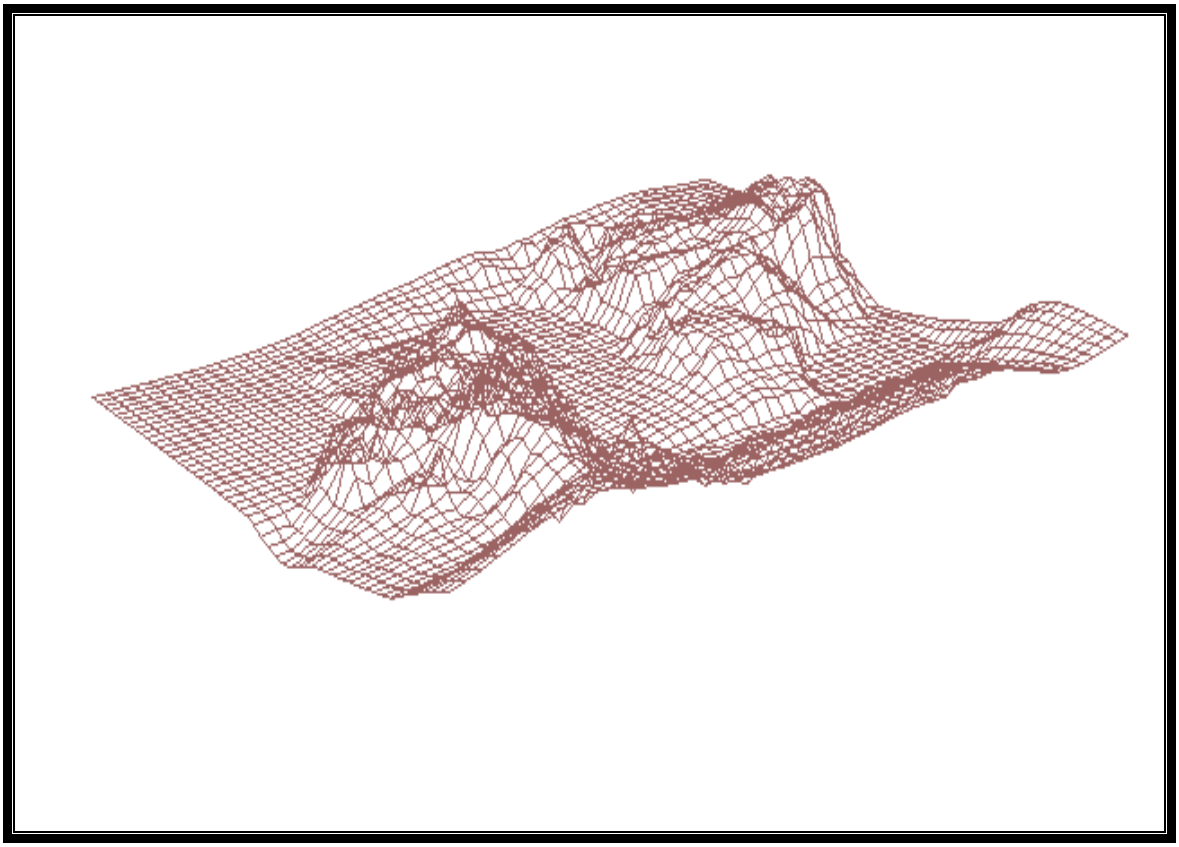

Fig (8): DEM for field survey data of TaqTaq area by (Polynomial) method.

Data Modeling by Using Topographic Map

Digital Elevation Model (DEM) can also be generated from the existing contour map. In this part topographic map with scale (1:25000) have been used to generate the digital elevation model from it. The procedures of DEM generation contain many phases as illustrated below:-

1-Seperate contour lines layer from the study areas topographic maps, by projecting it on a trace paper used for this purpose, with indicating for the value of each line. Understanding this step, with more details can be made from the illustration contour line layer which will be given in figure (3) of the study area known as contour map.

2-Input the contour map to the computer memory. This means a converting a digital form (Raster) by using scanner instrument with a resolution accuracy of about 500dpi, and save it in a special work folder.

3-Convert contour maps from raster format to vector format.By what is called on screen digitizing this operation is fullfilled by using **(Autodesk Field Survey) software**, which shows the contour lines in the first case as separate picture elements (pixles) having a gray-scale value and identified by (sample, line) coordinate format.In the second case, the contour line is identified by a starting point (x_1,y_1) and ending point (x_n,y_n) coordinates. Between these two points there are many points known as (nodes), representing the changing in contour line direction. In this part of scanning and digitizing existing maps, prior to scanning the ground control points or grid points on maps have been fixed on the maps as register points, with known value (Easting, Northing).The values were inserted in the software (Autodesk Field Survey) with scanned maps images to control the coordinates system for DEM as the same as previous model. These control points obtained from the topographic maps of the study areas using a universal transverse meractor (UTM) projection. Each point was chosen in the

topographic maps and the scan images, which should be identified easily, the coordinates of these points for the study area are listed in table:

Table (1): GCP of the Study Area**.**

Point no.	E(m)	N(m)
1	468460.657	3973469.559
2	464468.958	3973469.559
3	464468.958	3970219.393
4	464468.958	3970219.393

4-Errors may result, when the contour lines are drawn. These errors, , are dependent on the region (study area) nature. When some of regions like (taqtaq and halbja) includes high slopes (i.e. very high contour line density), the probability of obtaining errors is increased.
The probable error defined as error resulting from the drawing of the dense contour lines. In addition, the processing includes also the errors in the map obtained as a result of the vectorization. These errors result from the cutting in the lines or the removing of the extra lines. Then reconstruction of contour lines is made in order to be ready for editing and identifying as contour lines having certain height values [Wolf, 1982].
The above processing was done by using **(AutoCAD map, ver. 5.0).** This process is called clean up.
5-DEM building, using the contour maps prepared in the previous steps. At the first step editing the contour lines and giving each contour line its real height value, then select the surface that considered in saving the data and information correlated with DEM building. This model will be depending on the triangulation and gridding method. This means the information that is saved in surface file will be converted to a [“Triangulated Irregular Network" (TIN), "Invese Distance Weighting"(IDW), Kriging and Polynomial]. After that the digital elevation model is displayed as a perspective figure for a three-dimensional vision. As shown figures:-
Figure (9a) which illustrates the digital elevation model produced for the study areas by TIN method.
Figure (9b) which illustrates the digital elevation model produced for the study areas by Kriging method.
Figure (9c) which illustrates the digital elevation model produced for the study areas by IDW method.
Figure (9d) which illustrates the digital elevation model produced for the study areas by Polynomial method.

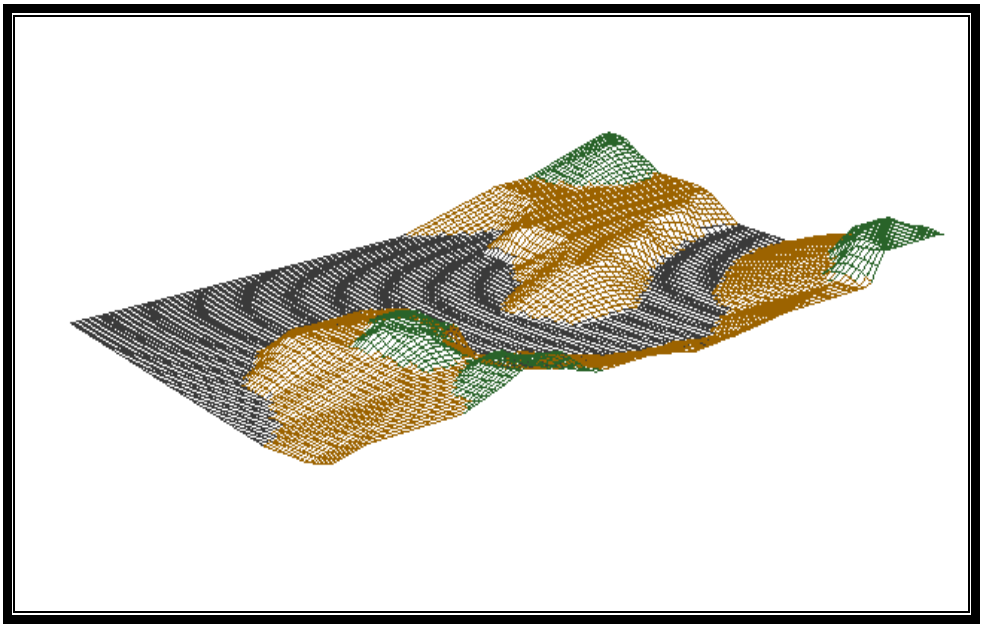

Fig (9a): DEM of the study area (Taq Taq) by TIN method.

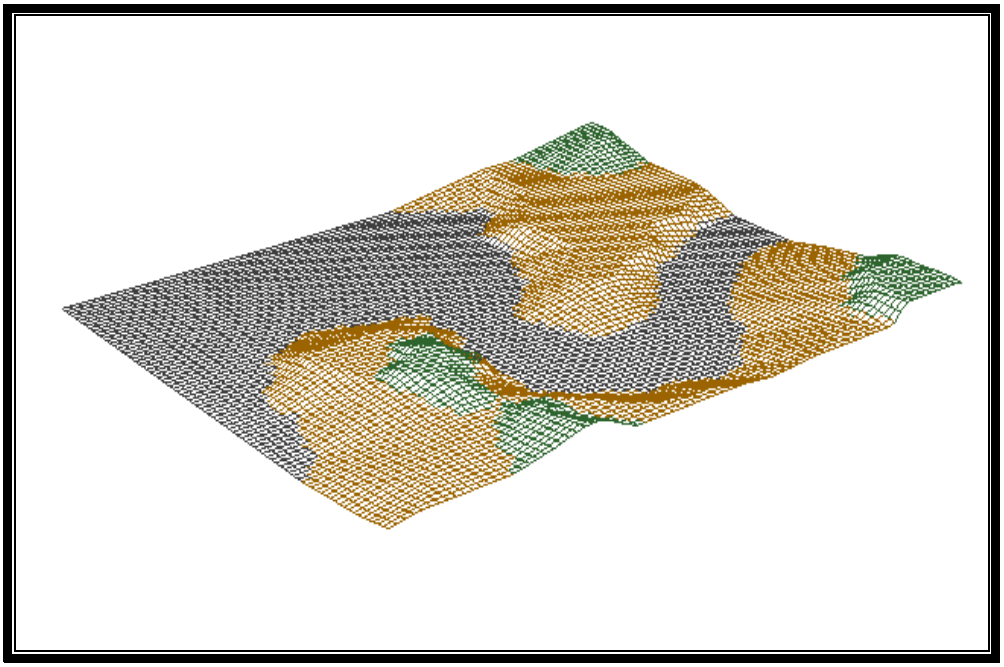

Fig (9b): DEM of the study area (Taq Taq) by Kriging method.

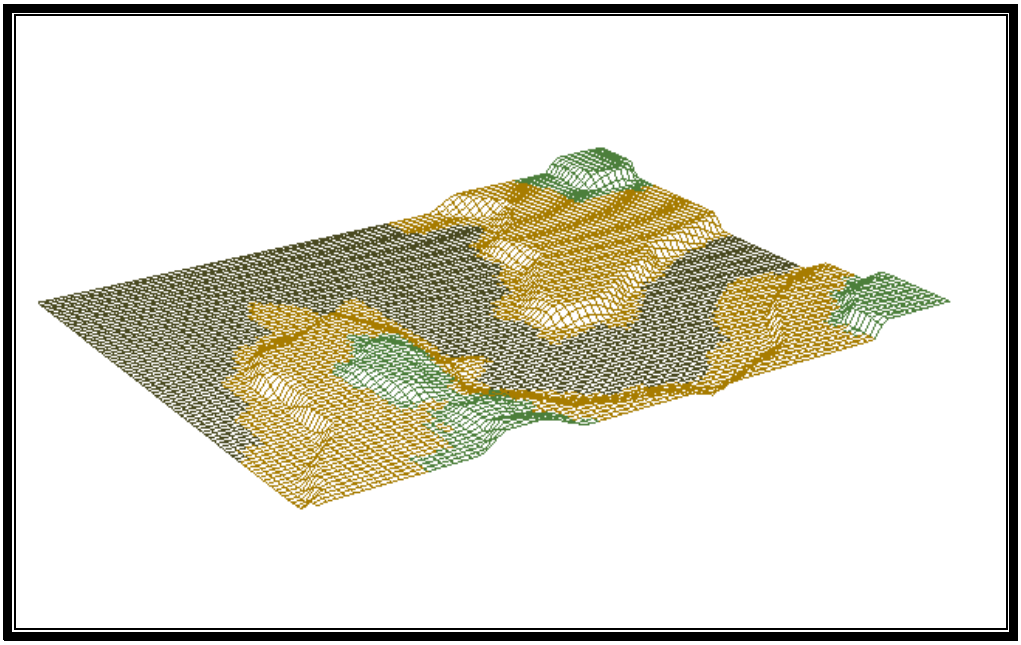

Fig (9c): DEM of the study area (Taq Taq) by IDW method.

Fig (9d): DEM of the study area (Taq Taq) by Polynomial method.

Evaluation of the Mathematical Techniques Accuracy

The Evaluation of Mathematical Techniques Accuracy for the DEM produced from Scanned Topographic Maps

To evaluate the accuracy of the mathematical techniques used for producing the DEM from scanned topographic maps, for study areas, the following procedure should be followed:

After producing the DEM from the scanned topographic maps with various mathematical methods, the models are transferred (Raster Digital Elevation Model) by using the (ERDAS Imagine ver.8.7) software. Figures (10) represent the raster digital elevation model for the study areas.

Thirty random points were chosen on each transferred models and its coordinates were recorded (E, N, Elev.), then simplifying or projecting them in to topographic maps which are related to the same model, using the value of elevation by traditional methods and taking in consideration the distance between the two lines, the point lies between them and the contour interval value, then compute the value of (RMSE) in elevations with the typical standard deviation proposed by National Mapping Accuracy Standard (NMAS) depending on the used map scales and contour intervals, for all models with the mathematical methods.

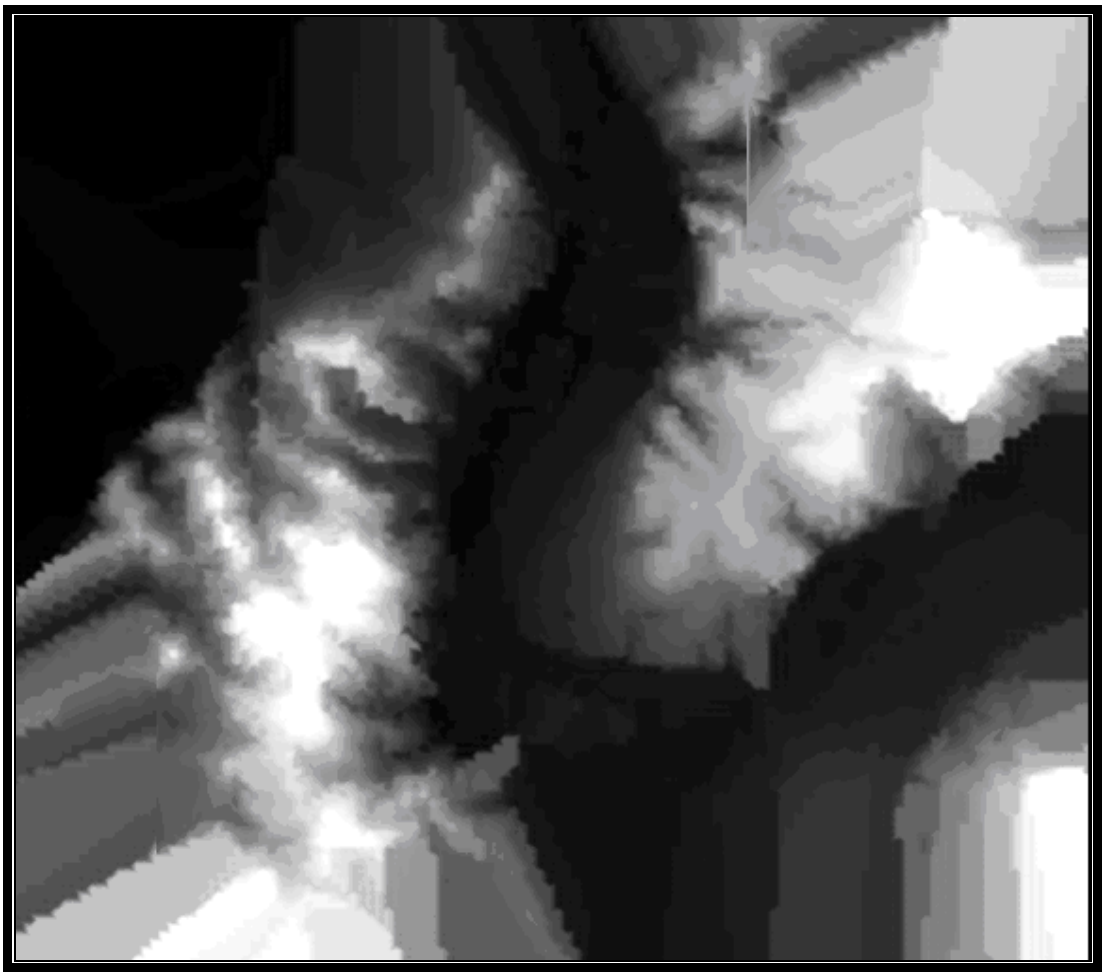

Fig (10): Raster DEM for field survey data of the study area.

The Root Mean Square Error (RMSE) were computed for each mathematical method by equation (21) and the Vertical Map Accuracy Standard (VMAS) also computed as described in section (2.4) for each method and comparative between the computed standard deviation and typical standard deviation as illustrated in table (2) and graphically by figures (11).

$$\sigma_Z = \left[\frac{\sum_{i=1}^{n} \left(\delta_z - \bar{\delta}_z \right)_i^2}{n-1} \right]^{\frac{1}{2}} \tag{21}$$

Table (2): The computed Standard Deviation (σ_z) of DEM for the study areas by using different mathematical techniques.

Case Study. / Methods.	1
TIN	9.694m
Kriging	7.465m
IDW	11.896m
Polynomial	15.146
Vertical Map Accuracy Standard (VMAS)	25m
Typical Standard Deviation	15.2m

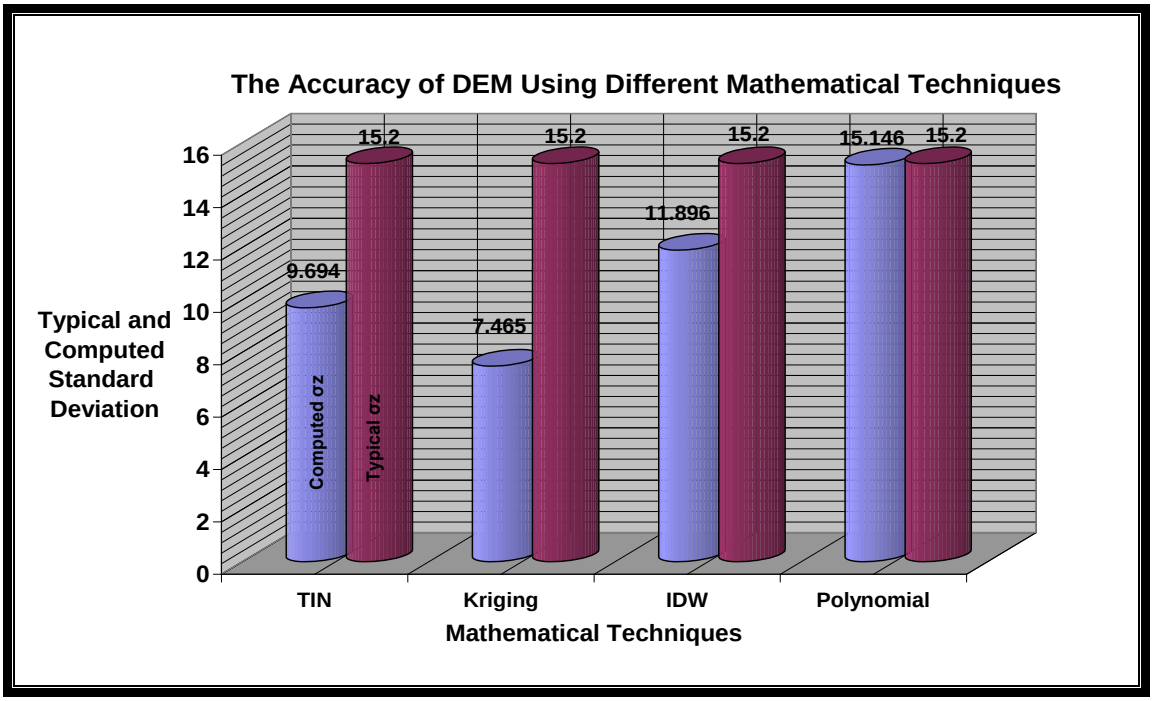

Fig (11): The Accuracy of DEM for the Study area by Using Different Mathematical Techniques Statistically.

The Evaluation of Mathematical Techniques Accuracy for the DEM produced from Field Survey and Topographic Map

To evaluate the mathematical techniques accuracy for the DEM produced from scanned topographic map for TaqTaq area, a compartment have been done by subtracting the produced DEMs from both data types first the evaluation accuracy was made from the model to the map, then an evaluation for the accuracy was made from model to the field survey with many mathematical methods, as follows:-

To examine the accuracy of the model, we consider the layer, of DEM produced from the field survey for TaqTaq area is the main layer which is produced by Universal Kriging method, but the layer of DEM produced from scanned topographic map is the sub-layer produced by the following methods (Universal Kriging, IDW, TIN and Second Degree Polynomial). By using the (Autodesk Field Survey) software, we subtract the main layer from each sub-layer by recalling the two layers and determing them from work file. This process was named (layer subtraction) were results are the differences of elevations (difference in size of cut and fill) see figure (12). Fifty points were selected for checking the accuracy of mathematical methods, in both Digital Elevation Models (DEMs) (main and sub-layer), the difference were computed in (z value), also the value of Root Mean Square Error (RMSE) computed by using a special equation (21).

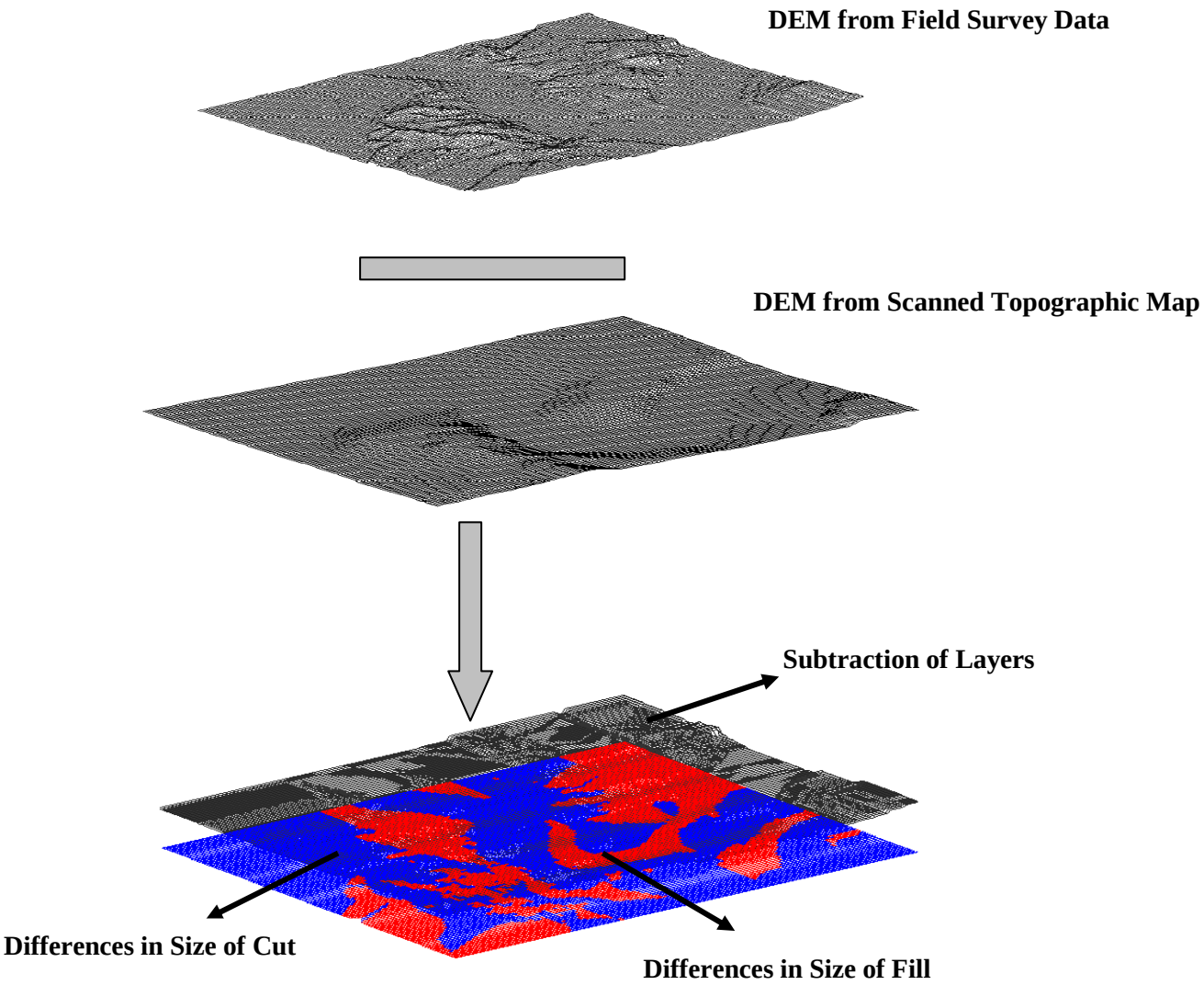

Figure (12): The process of Layers Subtraction by using Autodesk Field Survey software.

Results:

It can be noticed that the differences in elevations values between those obtained from field survey DEM and the obtained one scanned contour map, is within the contour interval limit which is (50m), i.e. this difference is within the acceptable range, but the differences in some

points has exceeded the (50m) contour interval, which caused a "gap" in some areas between the two models.

The reasons why the difference between the points which lies in two models (elevations) exceeds the acceptable range of the contour interval can be caused by one of the following:

1- The scale of the drawing. The larger the scale used the greater the accuracy obtained in line drawing, and hence the greater accuracy in elevation model (DEM). This can be obtained for scales larger than 1/25,000, for e.g. (1/10,000, 1/5,000), and

2- An error has occurred in the drawing of the contour line from aerial photographs in the "gaps" area between the two models.

The Root Mean Square Error (RMSE) were computed for each mathematical technique by equation (21) and also the Vertical Map Accuracy Standard (VMAS) computed. Table (3) summarize the predicted accuracy for all these mathematical methods.

Table (3): The computed standard deviation for the model by using mathematical techniques.

Mathematical Techniques.	σ_z
Triangulated Irregular Network (TIN).	14.439m
Kriging interpolation.	11.849m
Inverse Distance Weighting (IDW).	16.709m
Polynomial interpolation.	17.989m
Vertical Map Accuracy Standard (VMAS)	25m
Typical Standard Deviation	15.2m

A graphical representation of table (3) illustrates the difference in accuracy more as in fig.(13)

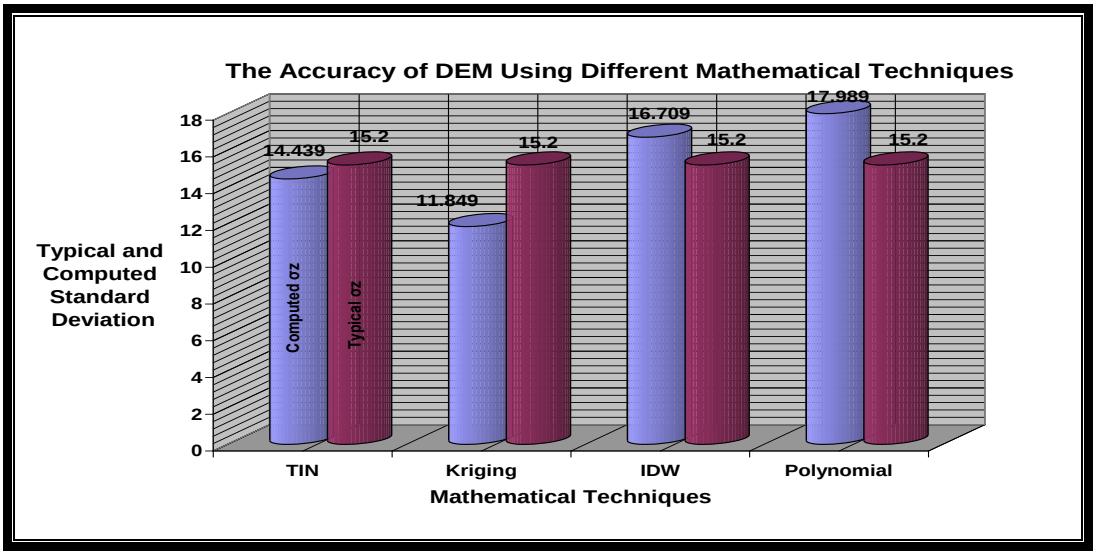

Fig (13): The Accuracy of DEM Using Different Mathematical Techniques Statistically.

Conclusions:

From the results obtained in table (3), the following conclusions extracted:-

1. The DEM's produced by four mathematical methods were compared on the basis of computing the Root Mean Square Error (RMSE). It was found that the best interpolation method is Kriging which gives the best results as illustrated in figure (14).

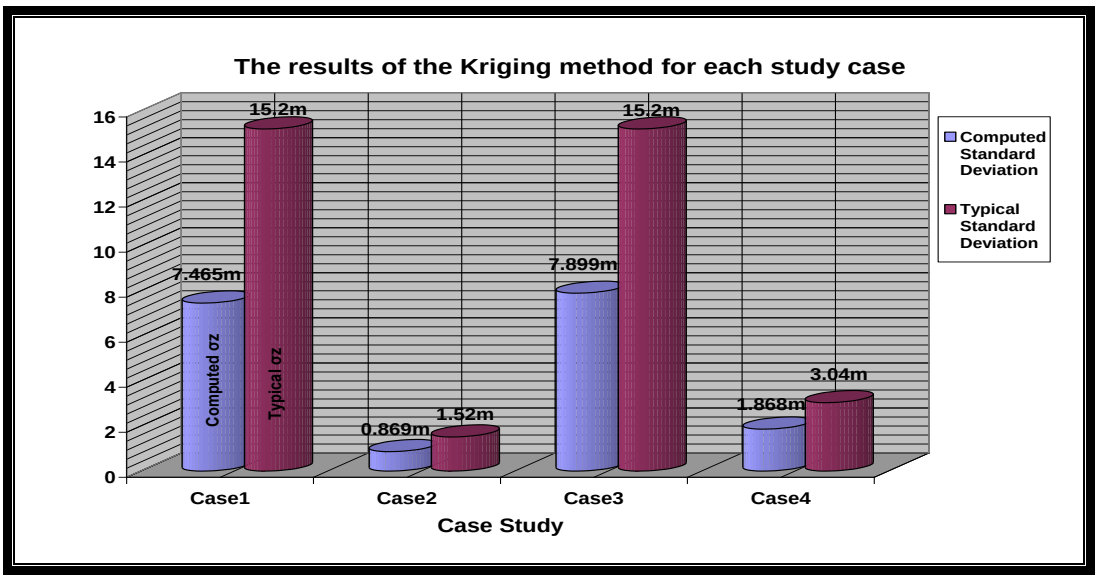

Fig (14): The results of the Kriging method for each study area.

2. The digital elevation model could be produced from scanned topographic maps with acceptable accuracy standards by using suitable interpolation method. It was found that the scale of maps and the contour intervals affect the accuracy besides the interpolation method.

3. When dealing with Raster format DEM it was found that the produced DEMs by mathematical methods is the one produced by Kriging technique which is a model distinguished for its high clarity, it was the reason to produce the photo textured DEM depends on the obtained kriging model.

4. Digital Elevation Models (DEMs) proved the effectiveness of solving many scientific and engineering problems like the intervisibility analysis, terrain analysis, volumetric computations and production of photo-realistic DEMs which is very useful in military applications.

REFERENCES:

Anderson J. M. and Mikhail E. M., **"*Surveying Theory and Practice*"**, 7th edition, University of California Berkeley, pp (792-793), (1998).

ESRI, ***" What is Arc GIS "***, Computer Program, (2001).

Habib, A. ***"Digital Terrain Model***", 2003, http://www.geomatics.ucalgary.ca/~habib/courses/engo573/AKAM-CH-3-1.PDF

Ibrahem, T. A. **"*The Utilization of local resources to develop a geographical information system in survey and route design* "**. M.SC. Thesis, college of engineering, Department of Surveying, Baghdad University, (1993).

Kennie, T.J.M. and Peterie, **"*Engineering Surveying Technology* "**. John wiley and Sons, New York, (1993).

Lebrer, F. **"*Interpolation in Square grid DTM* ",** ITC Journal, No.5, , pp (15-25), (1973).

Surfer(tm) help for Windows Version 6.xx Golden Software Incorporated, 1995 [Help of Surfer Package, (1995)].

ESTIMATION OF EFFICIENCY OF REGENERATED GRANULAR ACTIVATED CARBON BY DIFFERENT METHODS

Prof. Abbas H. Sulaymon
Baghdad university
Eng. college

Ass. Waleed M. Abood
Ass. Head of Eng.
Ministry of industry
Energy & environment research center

ABSTRACT:

In this study regeneration process was carried out for exhausted activated carbon, which has been used for adsorption process of furfural from its solution by three different methods (washing with dilute alcohol ethanol 20%, washing with boiled distilled water at 100C^o؛ and thermal process at (200 – 900) C^o؛. The regenerated activated carbon has been reused in the column system of fixed – bed in order to estimate the adsorption quantities and comparing the value with adsorption quantity of original activated carbon under same condition (furfural with concentration 0.2 kg/m³, bed depth 5 cm, flow rate of liquid 16.16 × 10^{-5} m³/min and particular size of activated carbon (1.5-0.5) mm) in order to estimate the regeneration efficiency for each method which ranged (60-90)%.

الخلاصة:

في هذه الدراسة تمت عملية تنشيط لفحم مستهلك بعد أن تم استخدامه في عملية الامتزاز لمادة الفورفورال من محلوله المائي وتم استخدام ثلاث طرق مختلفة (الغسل بكحول اثيلي مخفف 20% والغسل بماء مقطر مغلي لدرجة 100 م؛ واخيراً عملية الحرارية الجافة بدرجة حرارة متصاعدة من (200-900) م؛ . الفحم المعاد التنشيط تم استخدامه في عملية الامتزاز في عمود ذو حشوة ثابتة لغرض احتساب الكمية الممتزة للمادة ومقارنتها بالقيمة المستحصلة من استخدام فحم غير مستخدم وتحت نفس الظروف (تركيز الفورفورال 0.2 كغم/ م^3 ، عمق الحشوة 5 سم ، معدل جريان 16.16 × 10 $^{-5}$ م^3 / دقيقة و أخيرا حجم الحبيبات للفحم (0.5 – 1.5) ملم لغرض احتساب كفاءة التنشيط لكل طريقة والتي تراوحت من 60-90 %.

KEY WORDS:

Activated carbon, regeneration efficiency, thermal process, adsorption quantity, break point time.

INTRODUCTION:

Activated carbon is used as adsorbent in the process of the adsorption in order to control the odor or amount of organic compound because of its large surface area, it is used as powdered or granular while the last is more useful in the continuous process when waste water is purified by passing through bed of granular activated carbon (Rao1994, Casey 1992). In every small plant, it

may be feasible to use granular carbon for one time but for economical concernment the activated carbon must be regenerated (Culp and Gorden 1971).

Four general methods for reactivation granular carbon are solvent wash, acid or caustic wash, steam reactivation and thermal regeneration (Culp and Gorden 1974). Regeneration efficiency by boiling water method was achieved after 4.5 hr for phenol as (adsorb ate) with activated carbon as (adsorbent) was 90% (Martine and Ng. 1984,1985).

CALCULATION OF REGENERATION EFFICIENCY:

The efficiency of the regerant is judged on the adsorption quantity of activated carbon the efficiency can be calculated by using the following equation of calculation was employed (Martin & Ng. 1984).

$$\text{Regeneration Efficiency (RE \%)} = \frac{q_r}{q_o} \times 100\,\% \qquad \text{.....(1)}$$

Where:
q_o = quantity of solute (adsorb ate) adsorbed per unit weight of adsorbent (original activated carbon) and q_r is quantity of adsorbed solute per unit weight of adsorbent (regenerated carbon) during the passing of solution through fixed – bed column.

$$q_r \,\&\, q_o = \text{س}_{t=0}^{t=t_s} \; [\,(C_o - C\,) / m \;.\; Q\,.t\,] \;\text{.....(2)}$$

EXPERIMENTAL WORK:

The physical properties of Granular activated carbon manufactured by (unicarbo co. Italy) are listed in **table (1).** The exhausted carbon from experiments of fixed – bed column adsorption of furfural. From waste water which was obtained from Al- Dora refinery plant after the stage of primary treatment contaminated with furfural ($C_5H_4O_2$) molecular weight (96.06 gm/mole) (OSHA 2000).

Table (1) properties of activated carbon

Item of analysis	specification
Dimensions (granular)	12 × 40 mesh (0.4- 1.6 mm)
Surface area (m² / kg)	1100 – 1130
Bulk density (kg / m ³)	460 – 480
Ash (%)	5 (max)

REGENERATION OF ACTIVATED CARBON:

Regeneration of exhausted activated carbon was carried out in the laboratory using the following methods (Martine and Ng. 1984, Clup and Gorden 1971).

WASHING WITH ETHANOL 20 %:

50 gm of the exhausted carbon was weight by electric balance (type, mattler, AE200, Swiss) and mixed with 600 ml of (20%) ethanol in Pyrex beaker of 1 liter. Agitating the mixture by using magnetic stirrer (type, prolabo, 2204) at 800rpm for 4 hr at 25 C˚. The washing liquid was changed three times during the process. The mixture was filtered and the activated carbon washed by

distilled water and dried in electrical oven (type, memmert, 8840, West Germany) at 200 C˚ for 3 hr.

WASHING WITH BOILED DISTILLED WATER:

50 gm of exhausted carbon with boiled distilled water in Pyrex beaker of 1 liter and heated at 100 C˚ with agitating at speed 800 rpm for 6 hr with change the boiled distilled water during the process in order to achieve the adsorption of adsorb ate (furfural). The mixture was filtered and the activated carbon was washed by distilled water and dried at electrical oven at 200 C˚ for 3 hr.

THERMAL PROCESS:

50 gm of exhausted activated carbon was washed by distilled water and dried in an oven at 100 C˚ for 1 hr and at 200 C˚ for 2 hr, after that the activated carbon was heated in an electrical furnace (type, Heraeus., Germany) at temp. 600 C˚ for 1.5 hr and the temperature was raised to 900 C˚ for 1.5 hr.

After each experiment the activated carbon was screened to remove the ash and granular with size less than 0.5 mm to be ready for using in adsorption experiment by fixed – bed column.

CONTINUOUS ADSORPTION SYSTEM:

The equipment are shown in **Fig (1)** were used for investigating the adsorption of furfural from the aqueous solution onto (original or regenerated activated carbon) and these equipment are consisted mainly from a vertical Polyvinylchloride (PVC) column fixed – bed with inner diameter 4 cm and 100-cm height, the samples were taken at internal time of 15 min from the bottom of the column. The analysis was carried by calorimetric (type, Jenway, 6030.UK) at wave length 430 nm. (Foste and Lesile 1971). **Table (2)** shows the experiment condition, which were carried out for using original and regenerated activated carbon.

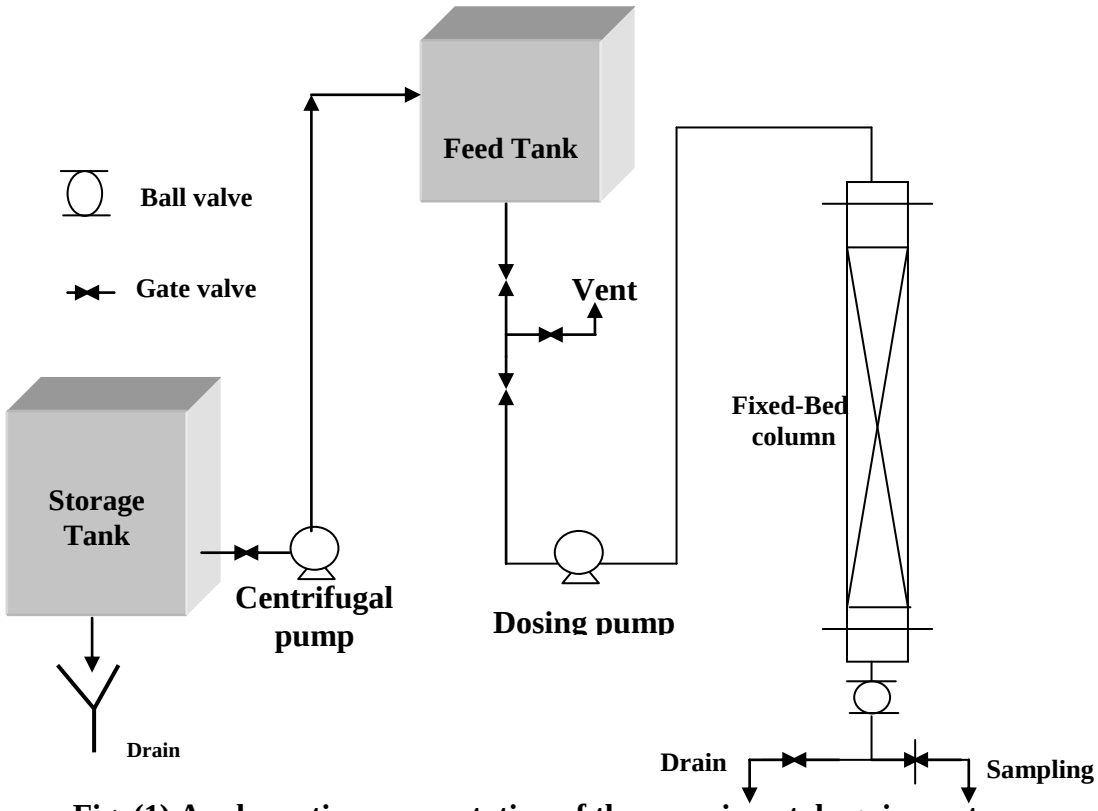

Fig. (1) A schematic representation of the experimental equipment

Table (2) Experiment information data.

experiments	Co (kg/m³) $\times 10^{-3}$	d.p. mm	Q (m³/min) $\times 10^{-5}$	Bed depth cm	Carbon mass in gm
Original gran activated carbon (GAC)	200	0.5 – 1.5	16.16	5	28.9
Regenerated(GAC) by alcohol	200	0.5 – 1.5	16.16	5	28.9
Regenerated(GAC) by boiled distilled water	200	0.5 – 1.5	16.16	5	28.9
Regenerated(GAC) by thermal process	200	0.5 – 1.5	16.16	5	28.9

RESULT AND DISCUSSION:

The break through curve **Fig (2)** showed the time required for break point and **Fig (3)** showed the adsorption quantity vs. time. Both above figures showed that the break point time and total adsorption quantity respectively decrease for regenerated activated compared with the original one **Table (3 and 4).**

Table (3)

Kind of bed	Break point time (min)	Total adsorption quantity (kg/kg)
Original (GAC)	**120**	**23.49**
Reg. (GAC) by alcohol	**35**	**14.3**
Reg. (GAC) by boiled distilled water	**60**	**18.4**
Reg. (GAC) by thermal process	**75**	**21**

Examining **Tables (3 and 4)** it can be seen that the removal of furfural from activated carbon using the washing with dilute alcohol Ethanol 20% is less effective compared with other methods as well as with an undiluted organic with water (Foste and Esile 1971). It is likely that bonding between the organic regenerant and water hinders the regeneration process, and the regeneration efficiency increases with increasing alcohol percent in the solution of regeneration (Martine and Ng 1984).
Using equation (1) to calculate (RE%) of the regenerated (GAC) by dilute ethanol was:
RE % = (14.3 / 23.49) × 100 = 60.80 %
This value of RE % is low compared with other methods, Table (5). This is due to the low solubility of furfural in water at 25 C˚ while its very soluble in pure alcohol (ethanol).
The regeneration by boiled distilled water shows to be an attractive form of regeneration knowing that solubility of furfural in water increases with increasing the temperature (Al-Saady, 2000). This indicates that it is acceptable to use steam in the regeneration in fixed bed adsorbers. The value of RE% by using equation (1) is 78.27%.
Using thermal process indicated that it is more effective process compared with the other methods because the high temperature will let the furfural molecules in the microspores be evaporated but this method leads to high percent of ash as a result of combustion of exhausted (GAC). The value of RE% is 89.4% and percentage of ash was 17%. **Table (5)** shows the efficiencies of the three methods.

Table (5) Regeneration efficiencies

Regenerated GAC	q_o	q_r	RE%
Washing by ethanol 20%.	23.49	14.3	60.8
Washing by boiled distilled water 100 C˚	23.49	18.4	78.27
Thermal process (200-900) C˚	23.49	21	89.4

CONCLUSION:

- Pure organic chemical regenerant, which has high solubility for furfural is more effective in regeneration process than the dilute one.
- Adsorption of furfural onto activated carbon is consider physical adsorption.
- Boiling water proved to be a very successful regenerant due to the process of adsorption is more effective when temperature is increased.
- High temperature of thermal process considered more effective method which help the molecules of adsorb ate release from the micro pores of adsorbent but leads to high percentage of ash formation due to the high temperature of heating.

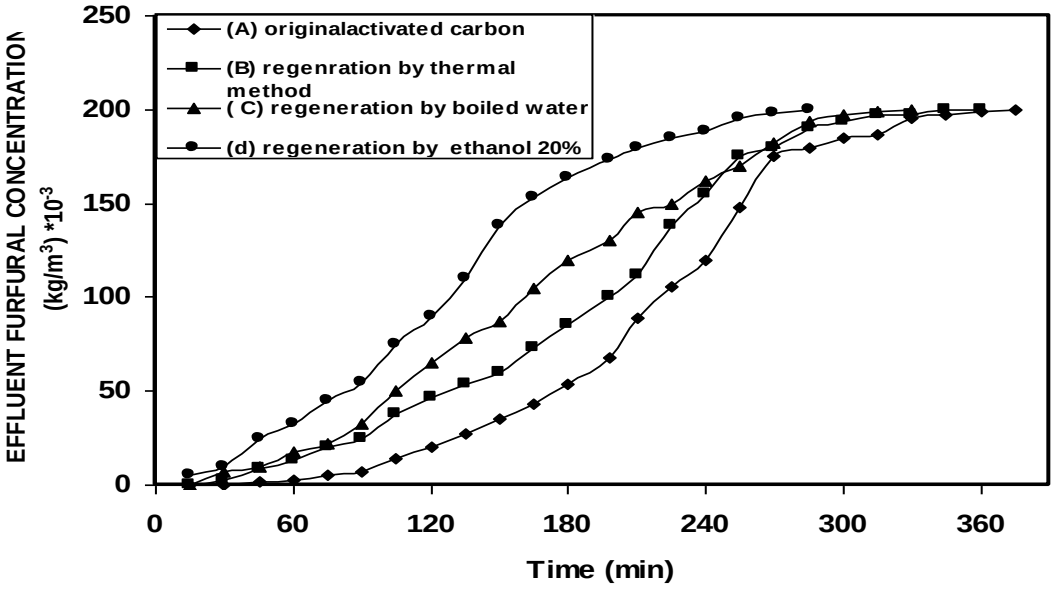

Fig.(2):Break through curves of isotherm adsorption for regenerated activated carbon by different methods comparison with original activated carbon.

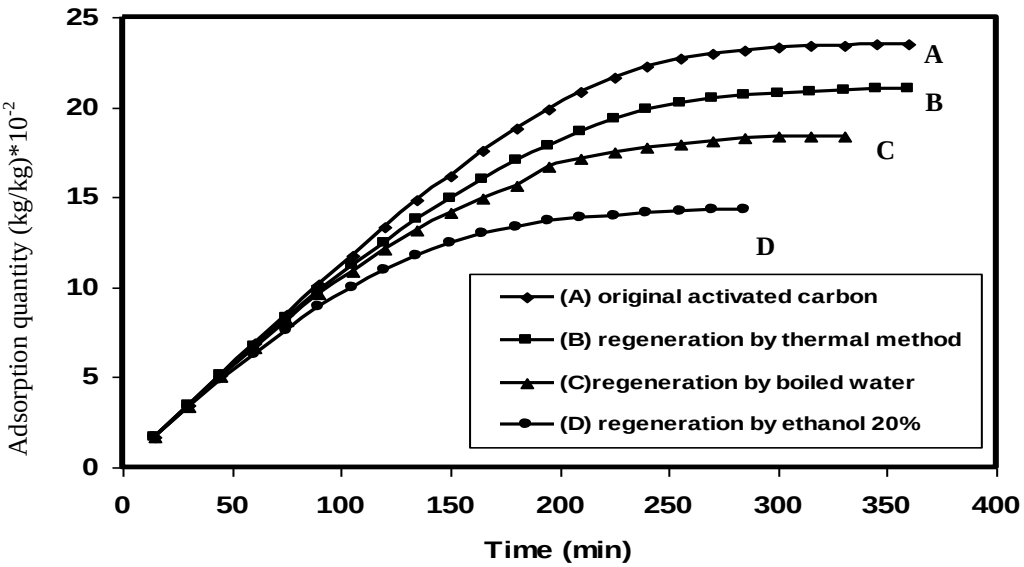

Fig. (3) Adsorption quantities curves of the regenerated activated carbon by different method comparison with original one

Table (4) break through and adsorption rate data for different regeneration methods
Where: C (kg/m^3) X10^{-3} and q (kg/kg)X 10^{-2}

Time min	Original activated carbon		Thermal regeneration		Boiling water method		20%ethanol washing method	
	C	q	C	q	C	q	C	q
15	0	1.72	0	1.72	0	1.72	5	1.69
30	0	3.44	3	3.44	7	3.44	10	3.334
45	2	5.15	9	5.09	10	5.04	25	4.85
60	3	6.85	13	6.708	18	6.617	33	6.3
75	5	8.5	20	8.265	22	8.16	45	7.64
90	7	10.16	25	9.78	33	9.6	55	8.9
105	14	11.78	38	11.18	50	10.9	75	10
120	20	13.32	47	12.5	65	12.07	90	10.95
135	27	14.8	54	13.703	78	13.125	110	11.72
150	35	16.2	60	14.92	87	14.1	138	12.421
165	43	17.56	73	16	105	14.922	153	12.95
180	54	18.8	85	17.01	120	15.614	164	13.36
195	68	19.9	100	17.88	130	16.2	177	13.67
210	89	20.85	112	18.64	140	16.7	180	13.87
225	106	21.65	138	19.33	150	17.133	185	14
240	120	22.3	155	19.87	162	17.46	189	14.13
255	148	22.74	175	20.26	170	17.72	195	14.25
270	175	22.95	180	20.5	182	17.936	198	14.3
285	180	23.12	190	20.67	191	18.126	200	14.3
300	185	23.3	194	20.8	194	18.325		
315	187	23.4	197	20.88	197	18.37		
330	195	23.45	197	21.93	198	18.4		
345	197	23.48	200	21	200	18.4		
360	199	23.49	200	21				
375	200	23.49						

REFERENCES:

- Al- Saady, Niriys H.M, 2000, M.Sc. thesis , Baghdad university, College of Women.
-Carbochem´s report "Activated carbon", June 2004, on www.earochem.com/activatedcarbon101.html..
- Casey T. J., 1992, "Unit treatment processes in water and wastewater engineering", Wiley series New York.
- Clup R. L. and Gordon G. L., 1971, " Advanced wastewater treatment ", New York, CH7-8.
- Clup R. L. and Gordon G. L., 1974, " New concept in water purification", New York, ch. 8.
- Foste R. and Leslie W., 1971, " Encyclopedia of industrial chemical analysis", John Wiely, New York, vol.13, p.232-239.
- Martine R. L., and W. J. Ng., 1984, J. of water Research, vol.. 18, no. 1, p. 59-73.
- Martine R. L., and W. J. Ng., 1985, J. of water Research, vol.. 19, no. 12, p. 1527-1535.
- OSHA, 2000, " Occupational Safety and Health Administration of furfural", U.S. Dep. of labor.
- Rao C. S., 1994, " Environmental Pollution Control Engineering", Wiley Eastern, 2nd, India.

NOMENCLATURE:

C = Concentration of adsorbent at given time (kg / m^3).

C_o = initial concentration of adsorbent (kg/m^3).

d = bed depth (cm).

d_p = diameter of carbon particle (mm).

GAC = granular activated carbon.

m = mass of carbon (gm).

q = flow rate of waste water (m^3/ min).

q_o= adsorption quantity of original GAC.

q_r= adsorption quantity of regenerated GAC.

RE = Regeneration efficiency.

t = time (min).

t_s = time of bed saturation (min) .

NONLINEAR ANALYSIS OF ONE AND TWO DIMENSIONAL CONSOLIDATION PROBLEMS FOR UNBOUNDED SATURATED SOIL MEDIA

N. B. YOUSIF
Al-Nahrain University

S. D. ABDUL-HAMEED
Al-Nahrain University

ABSTRACT

Soil in general is not a linear material, in which the relation between stress and strain is more complicated than the simple, linearly elastic relation. To make accurate deformation analysis of clay deposits, the incremental Biot's theory of consolidation is used together with elasto-viscoplastic constitutive relations based on the critical state concept using the modified Cam-clay model. One and two dimensional consolidation problems were analyzed numerically by the infinite-finite elements. Results show that the proposed method can describe the effect of sample thickness on consolidation phenomena. Also the two dimensional behavior of a clay foundation during the construction of embankment was analyzed.

الخـلاصـــــة

إن التربة وبصورة عامة لا تعتبر كمادة خطية، حيث إن العلاقة بين الإجهاد و الانفعال معقدة جداً مقارنة بالعلاقة الخطية المرنة البسيطة.

لذلك و لغرض الحصول على تحليل دقيق لتشوهات التربة، فقد استعملت نظرية(**Biot's**) للانضمام المتزايد مع علاقات النموذج المرن –اللزج اللدن اعتماداً على مفهوم الحالة الحرجة للتربة و باستخدام النموذج المعروف بـ (**Modified Cam clay**). تم تحليل مسائل الانضمام للتربة ذات البعد الواحد و البعدين عددياً

باستخدام العناصر الغير محددة و المحددة، حيث أظهرت النتائج أن الطريقة المقترحة قادرة على وصف تأثير سمك النموذج على ظاهرة الانضمام، وكذلك تم دراسة سلوكية الأساس الطيني أثناء إنشاء سدة ترابية.

INTRODUCTION

Most work on the analysis of consolidation problems using numerical technique has considered linear elastic behavior of soil. Unfortunately, Terzaghi's consolidation theory does not always describe the relation between excess pore pressure and settlement during consolidation of a clay deposits. Mesri and Choi (1979) reported that the settlement of a soft clay deposits take place with almost constant values of effective stress and pore water pressure. Similar phenomena have been observed for sensitive and aged clays, where this phenomena is due to both time-independent (plastic behavior), and time-dependent (creep) of clay.

In order to make accurate predictions of consolidation problem, it is necessary to use a constitutive model for clay that describes not only in viscid behavior, such as strain hardening, but rate sensitive behavior as well.

In this work, linear elastic Biot's consolidation is modified by extending the media to include infinite domain using an elasto-viscoplastic constitutive relations to model the non-linear soil stress-strain relations; Abdul-Hameed (1998).

CONSTITUTIVE EQUATIONS FOR SATURATED SOIL MEDIA

The general idea of elasto-viscoplastic behavior linking the strains and effective stresses in the soil skeleton are introduced for a general stress state. Perzyna (1966) proposed the following flow rule for viscoplastic deformation in the simple case of an infinitesimal strain field:

$$\dot{\varepsilon}^{vp} = \bar{\gamma}\langle\phi(F)\rangle\frac{\partial F}{\partial \sigma'} \qquad (1)$$

in which $\bar{\gamma}$ is a fluidity parameter controlling the viscoplastic flow rate, $\phi(F)$ represents the strain rate effect on the yielding of the material, and defined as:

$$\rangle\phi(F)\langle = \begin{Bmatrix} 0 & F < 0 \\ \phi(F) & F \geq 0 \end{Bmatrix} \tag{2}$$

The functional form of $\phi(F)$ is given by Zienkiewicz et al. (1975) as follows:

$$\phi(F) = \left(\frac{F}{F_o}\right)^N \tag{3}$$

where F_o the yield value is in uni-axial stress and N is an exponent, which is simply used equal to unity.

The function F is an appropriate yield function. The mechanical behavior of clays can be described by the modified Cam-clay model (Roscoe and Burland, 1968). The yield surface of this model is an ellipse in **p-q** plot as shown in Fig. (1), and mathematically is expressed as:

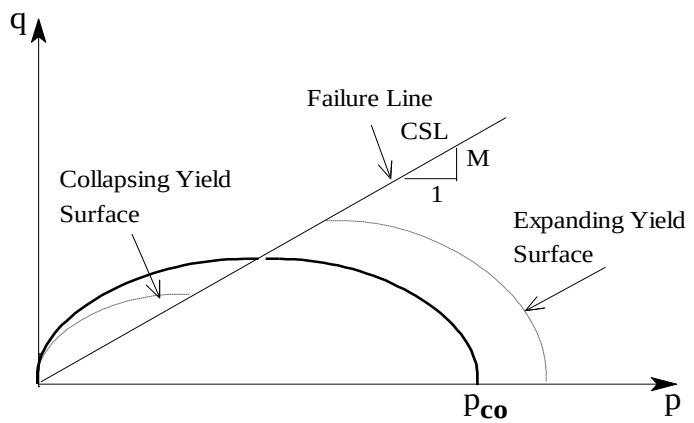

Fig. (1) Modified Cam-Clay Model in The Space of The Two Stress Invariants P and q.

$$F = \frac{q^2}{M_{c.s}^2} + p^2 - p.p_c\left(\varepsilon_{vp}^v\right) \tag{4}$$

where **p, q, p_c,** and $\mathbf{M_{c.s}}$ are respectively the mean effective stress, the deviator stress and are related to the stress invariants as given in **[**Appendix **A],** the current diameter of

the ellipse (yield surface) in p-direction and is analogous to a pre-consolidation pressure and the value of the stress ratio (**q/p**) at the critical state conditions; $\mathbf{M_{c.s}}$ is related to the angle of internal friction ϕ obtained from tri-axial compression test by:

$$M_{c.s} = \frac{6.\sin\phi}{3-\sin\phi}.g(\theta) \tag{5}$$

The shape of the failure surface in the deviatoric π- plane can be made to coincide with Mohr-Coulomb principles with a smooth variation (Yousif, 1984):

$$g(\phi) = \frac{2K}{(1+K)-(1-K).\sin 3\theta} \tag{6}$$

In which θ is the Lode angle defined in the deviatoric plane (Yousif, 1984):

$$K = \frac{3-\sin\phi}{3+\sin\phi} \tag{7}$$

When yielding occurs, the yield surface will expand or contract as the soil hardens or softens as shown in Fig. (1). The initial size of the ellipse is governed by the maximum pre-consolidation pressure ($\mathbf{p_{co}}$) to which the soil has previously been subjected during its past history. The change in the current value of the hardening parameter (**pc**) is related to the viscoplastic volumetric strain increment through the following equation:

$$\Delta p_c = \frac{\lambda-\kappa}{1+e_o}.p_{co}.\Delta\varepsilon_{vp}^{v} \tag{8}$$

where $\mathbf{e_o}$ is the initial void ratio, **λ** is the slope of the normal consolidation line in **e-ln p** space, and **κ** is the slope of swelling and recompression line in **e-ln p** plot as shown in Fig.(2).

CONSOLIDATION ANALYSIS BY THE FINITE ELEMENT METHOD

The consolidation problem may be discretized using finite elements. A pore pressure degree of freedom is added to the usual displacement degree of

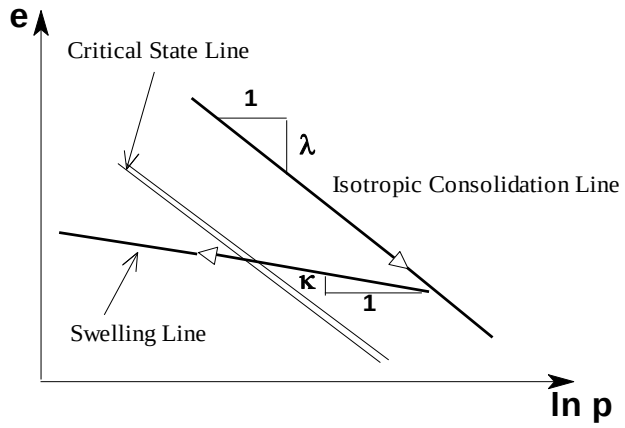

Fig. (2) Consolidation and Swelling Lines in e-ln p plot.

Freedom at the corner nodal points only. The spatial integrations may then be performed using Gaussian quadrature, and a time marching process is used to perform the time integration.

Shape functions {N} and $\{N_p\}$ are used to relate the continuous values of displacements u, and pore pressure p to the to the nodal values u^n , and p^n as follows (Zienkiewic , 1977) :

$$\left.\begin{aligned}\{u\} &= \{N\}^T.\{u^n\}\\ \{p\} &= \{N_p\}^T\{p^n\}\end{aligned}\right\} \tag{9}$$

The coupled equations for an element may be written in matrix form as [detailed of which are given by Yousif (1984) and Abdul-hameed (1998)]:

$$\begin{bmatrix} K_T & L \\ L^T & -0.5\Delta t.H \end{bmatrix}\begin{Bmatrix} du^n \\ dp^n \end{Bmatrix} = \begin{Bmatrix} df + C \\ 0 \end{Bmatrix} \tag{10}$$

In which the gravity load $\overline{F}$ is set equal to zero.

Where the element stiffness matrix $[K_T]$ is given in the usual way by:

$$[K_T] = \int_v B^T.D.B.dv \tag{11}$$

In which D is the elasticity matrix either for plane strain or axi-symmetric conditions. The matrix [L] couples the stiffness equations with those of fluid flow and is given as:

$$[L] = \int_v B^T.m.N_p^T.dv \tag{12}$$

Where

$$m^T = \begin{pmatrix} 1 & 1 & 0 & 1 \end{pmatrix} \tag{13}$$

The fluid flow [H] matrix is given by:

$$[H] = \int_v \left(\nabla N_p^T\right)^T \frac{\{k\}}{\gamma_w} \nabla N_p^T.dv \tag{14}$$

Where {k} is the permeability matrix, ∇ is the del-operator defined as:

$$\nabla^T = \begin{pmatrix} \frac{\partial}{\partial x} & \frac{\partial}{\partial y} & \frac{\partial}{\partial z} \end{pmatrix} \tag{15}$$

{df} is the incremental load vector, due to boundary or body force loading and is given as:

$$df = \int_v N^T.db.dv + \int_s N^T.dt.ds \tag{16}$$

Where b and t are body forces and boundary tractions respectively. And finally, C is the additional load vector due to viscoplastic flow or stress relaxation and is given as:

$$[C] = \int_v B^T.D.\dot{\varepsilon}^{vp}.\Delta t_n.dv \tag{17}$$

The symmetry of the final formulation is assumed providing K_T is symmetric as in the case of using associated plasticity theory. For a specified time step Δt, and prescribed

incremental loadings, the unknown increments of displacements $u^n(\Delta t)$ and pore pressure $p^n(\Delta t)$, can be obtained.

COMPOSITE INFINITE ELEMENT FOR CONSOLIDATION PROBLEMS

This type of element can be formulated to show the different types of decay rates applied for the field variables. For consolidation problems the decay rate applied can be obtained from the available analytical solutions.

Solutions for the instantaneous loading condition at ($t=0^+$) and at the end of consolidation ($t=\infty$) responses indicate that the vertical displacement at the surface of the half-space decays approximately in inverse proportion to the radial distance from loaded area.

The element with a (1/r) order decay rate was found to yield the most accurate solutions for various consolidation problems, Selvadurai and Gopal (1986).

Hence, the same type of decay rate (1/r) is employed in this research work to develop the composite infinite element used for consolidation problems. Five-nodded infinite element was shown in Fig. (3), represent an infinite medium in the ξ-direction. This element is a combination of five-nodded infinite element which representing quadratic variation for the displacement field and a two-nodded super parametric infinite element which is representing a linear variation for the pore pressure field.

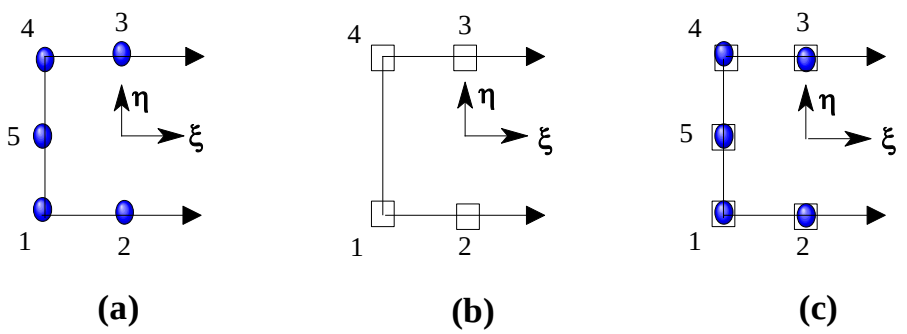

Fig.(3) Composite Infinite Element;
One)Five-Nodded Element for Displacement;
Two)Two-Nodded Super parametric Element for Pore Pressure; and
Three)Superposed Element [After Selvadurai and Rajagopal (1989)].

The pore pressure shape functions for the two-nodded super parametric element are obtained directly from those of the four-nodded linear quadrilateral element. Node 2 and 3 of this element are used only for mapping and are not used for interpolation.

Displacement shape functions for the five-nodded element are obtained from those of the eight-nodded quadratic element. Mapping and element shape functions can be found in Abdul-Hameed (1998).

The requirements for completeness and monotonic convergence are satisfied by these elements and therefore, the mapping is independent of the choice of the coordinate system.

The implementation of the infinite element required the following modifications:

* The jacobian is formulated on the basis of the singular mapping functions.
* The interpolation is carried on the basis of the variable at two or five nodes as indicated in Fig. (3).
* The mapping functions referring to the particular geometry of infinite elements is that the nodded coordinates of outer nodes (2 & 3) shown in Fig. (3 c) are taken twice as those of the corresponding inner nodes (1 & 4).

NUMERICAL APPLICATION

The coupled field equations presented by Eq. (11) have been incorporated into a finite element program called **"EVPCON" written in FORTRAN 77,** developed for this study to analyze one and two dimensional consolidation problems.

One-Dimensional Consolidation Analysis

An external uniform surface load (**T = 100 kN/m^2**) is applied to a clay layer and drainage is allowed to occur in the vertical direction only. The finite element mesh used in this analysis is shown in Fig. (4). The material properties needed for the nonlinear modified Cam-clay model are listed in Table (1). Euler's time integration scheme is used to calculate the viscoplastic strain increments.

The predicted settlements and pore pressure are presented for different values of over consolidation ratios in Figs. (5) And (6) for sample thickness of H=5cm. The pore pressure distribution are non-dimensionalized with respect to the initial pore pressure (p =T00), and settlements with respect to the final settlement (S∞) predicted by Terzaghi's classical solution. The non-dimensional time factor Tv was used as the abscissa.

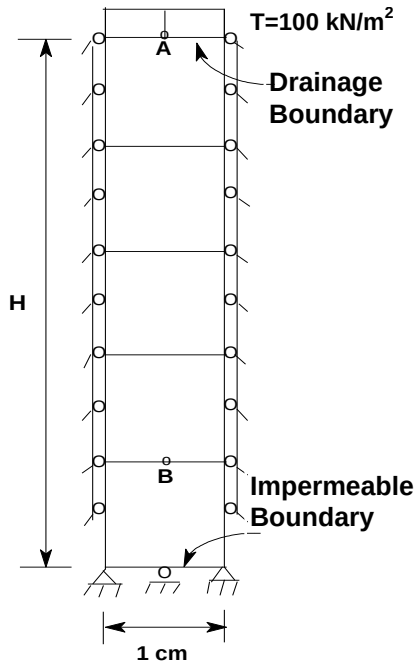

Fig. (4) Finite Element Mesh and Boundary Conditions for 1-D Nonlinear Consolidation.

Table (1) Material Properties Used for 1-D Consolidation Analysis

Material Properties	Soil
Young's Modulus, E′ (kN/m^2)	10000
Poisson's Ratio, ν′	0.333
Coefficient of Permeability, k (m/day)	$1*10^{-4}$
Fluidity Parameter, $\bar{\gamma}$ (day^{-1})	$8.64*10^{-5}$
Initial Void Ratio, e_o	1.5
Slope of Normal Consolidation Line, λ	0.231
Slope of Swelling Line, κ	0.05
Angle of Internal Friction, ϕ′	22
Initial Vertical Effective Stress, σ'_{yo} (kN/m^2)	200

The inclusion of the viscoplasticity effects decreases the magnitude of dissipation of pore pressure for Tv between 0.03 and 0.5. Therefore, the predicted pore pressure is higher than those predicted by the elastic analysis.

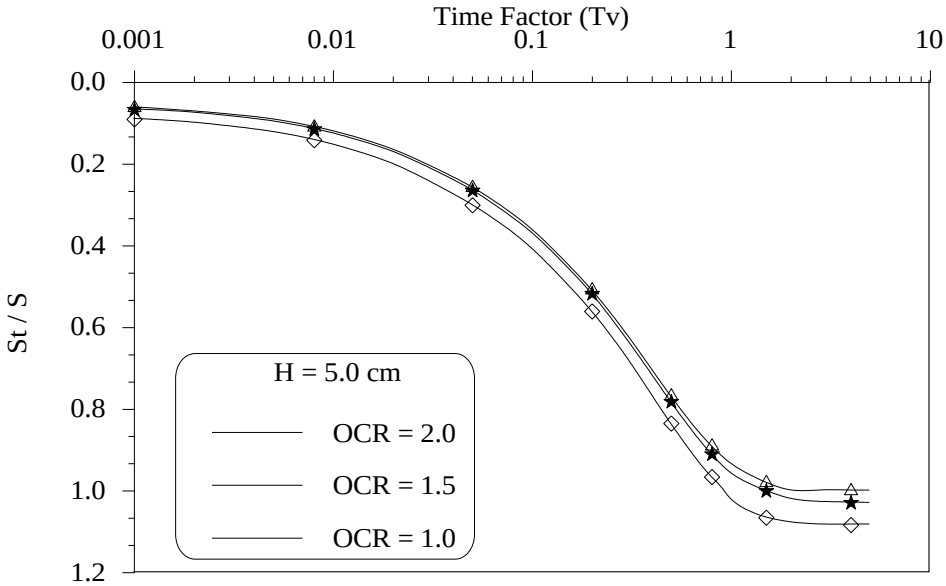

Fig. (5) One-Dimensional Consolidation; Surface Settlements versus Time Factor at (node A) for Different OCR.

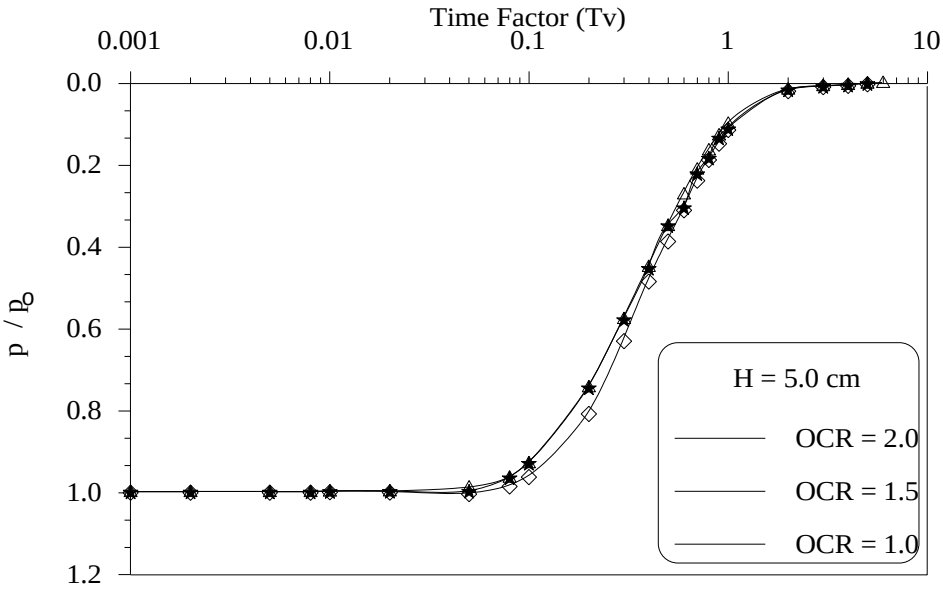

Fig. (6) One-Dimensional Consolidation; Pore Pressure versus Time Factor at (node B) for Different OCR.

When (OCR=2). Similarly the predicted settlements are higher than those predicted by the elastic theory. Figures (5) and (6) also show the effect of using different over consolidation ratio (OCR) on the predicted results. As (OCR) values increase the behavior is approaching that of the elastic solution obtained by Terzaghi's theory. For

(OCR) equal 2 elastic behaviors is predicted within the yield surface as the state of stress approaches the yield point viscoplastic is predicted till the end of consolidation. For (OCR) equal 1 non-linear analysis is predicted immediately upon loading.

Figure (7) shows the predicted vertical settlement-time curves for clay layer of (OCR=1) but of different heights, in which the effect of drainage path has been investigated.

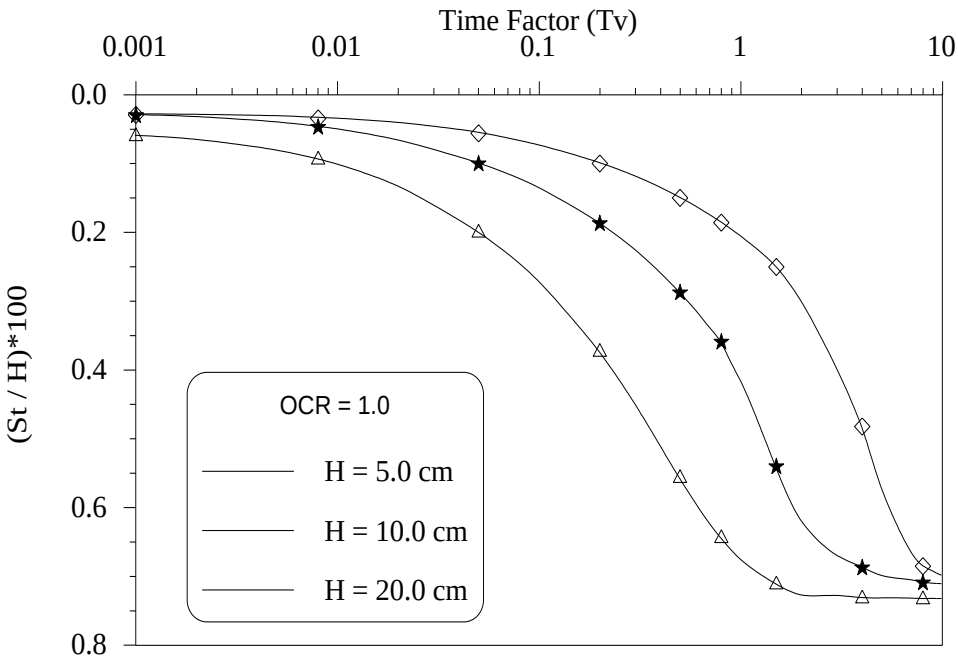

Fig.(7) One-Dimensional Consolidation; Surface Settlements Versus Time Factor at (node A) for Different OCR.

The predicted viscoplastic strain for the cases investigated was found to be proportional inversely to soil thickness. This behavior is experimentally supported by Aboshi (1973), who carried out several one-dimensional consolidation tests with different specimen heights on clay exhibiting creep settlement, it was found that the viscoplastic volumetric strain rate ($\dot{\varepsilon}^{VP}$) for the thick sample is lower than that of the thin sample.

Two-Dimensional Consolidation Analysis

The response of clay foundation during the construction of embankment has been investegated by Tavenas and Leroueil (1980). They reported that none of the existing

analytical methods can describe field data. Oka et al. (1986) were the first who tried to account for this behavior using elasto-viscoplastic constitutive equations based on Cam-clay model and Biot's consolidation theory.

The construction of a similar embankment is analyzed numerically using the developed elasto-viscoplastic constitutive equations and Biot's consolidation theory under plane strain conditions. The infinite-finite elements idealization and boundary conditions are shown in Fig. (8). The material properties used for the nonlinear visco-plastic using the modified Cam clay model are listed in Table (2). The rate of loading required by the analysis is taken equal to 2 kN/m^2/day**.** The calculations were stopped at 100 days at the end of construction.

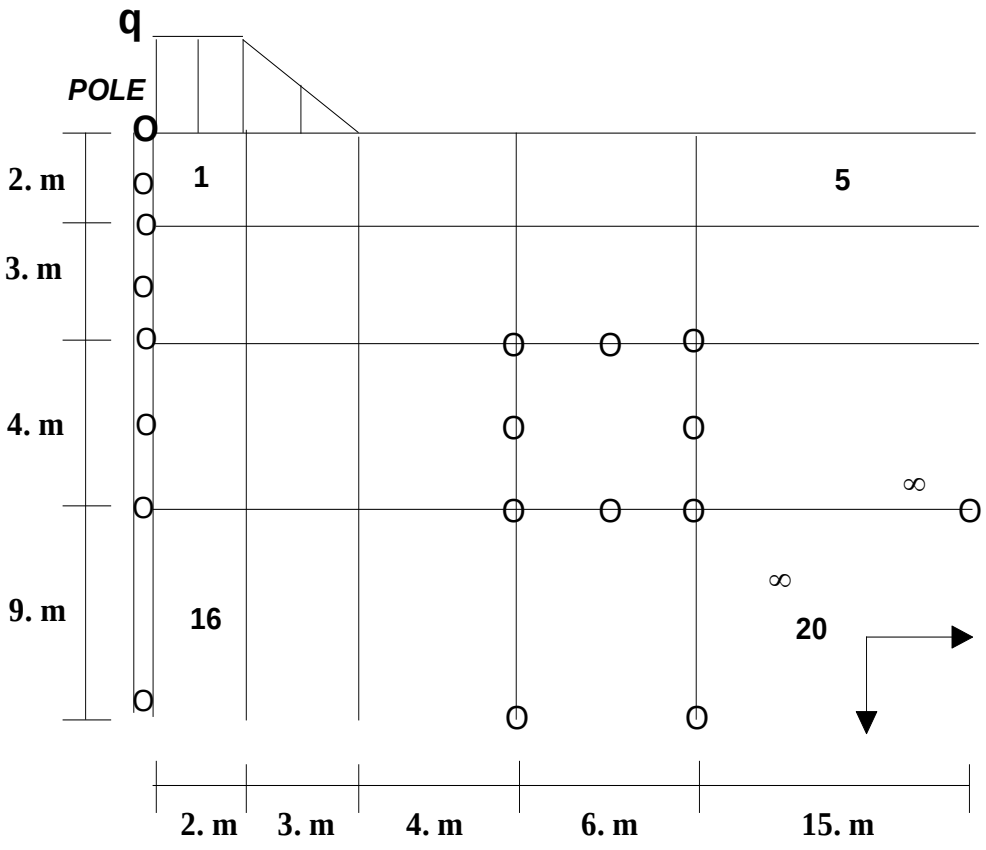

Fig. (8) Infinite-Finite Elements Mesh and Boundary Conditions.

Table (2) Material Properties Used for 2-D Consolidation Analysis

Material Properties	Soil
Young's Modulus, E′ (kN/m^2)	5350
Poisson's Ratio, ν′	0.333
Coefficient of Permeability, k (m/day)	$1*10^{-5}$
Fluidity Parameter, $\bar{\gamma}$ (day^{-1})	$8.64*10^{-8}$
Initial Void Ratio, e_o	1.5
Slope of Normal Consolidation Line, λ	0.231
Slope of Swelling Line, κ	0.05
Angle of Internal Friction, ϕ′	22
Initial Vertical Effective Stress, σ'_{yo} (kN/m^2)	100

Figure (9), shows the settlement-time profile predicted at the center line elements and immediately below the embankment. Figures (10) and (11), show the distribution of excess pore pressure and lateral displacement versus depth build up during construction. Both lateral displacement and pore pressure are at maximum values between 2 to 5 m depth as shown.

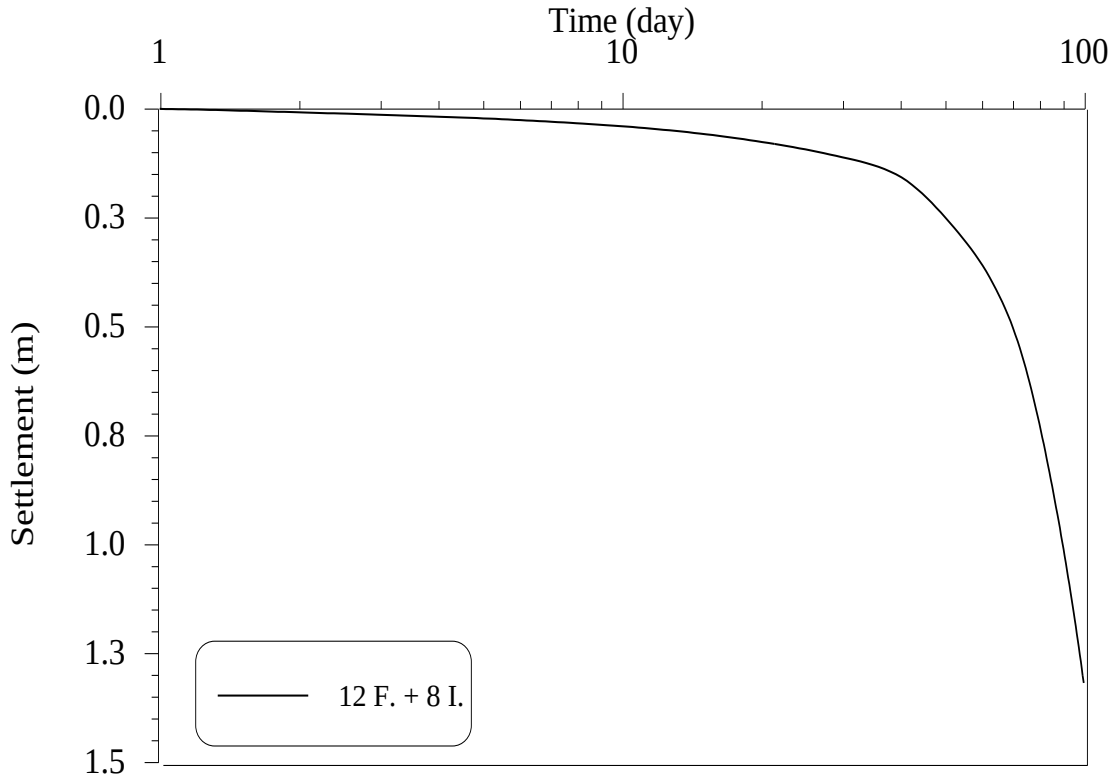

Fig. (9) Settlement-Time profile Center Line Elements.

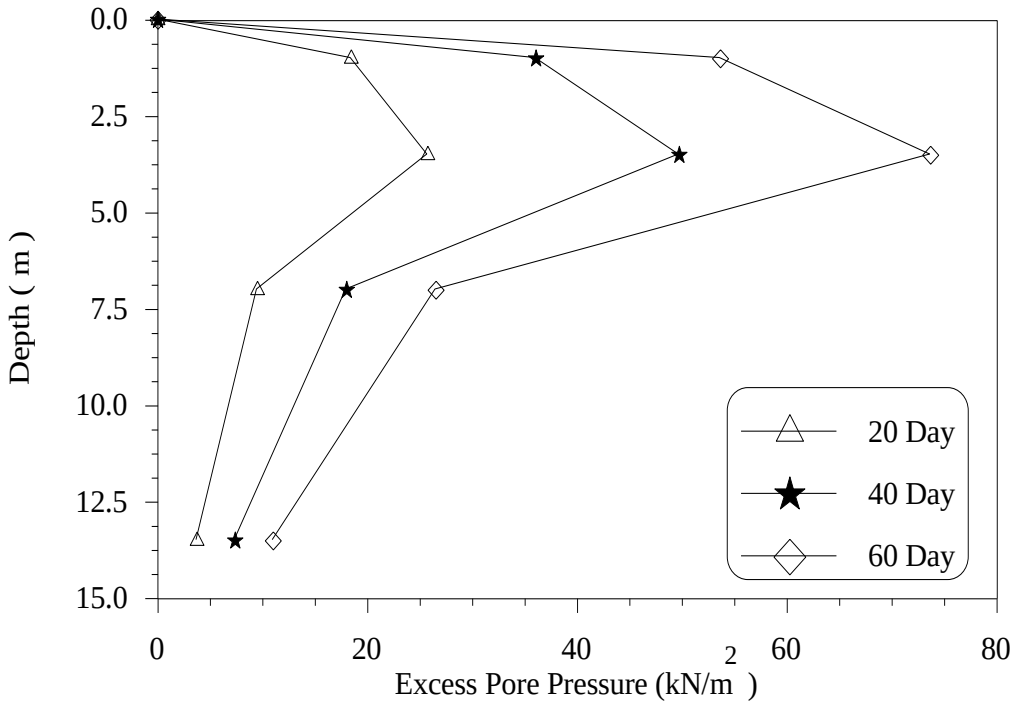

Fig. (10) Distribution of Excess Pore Pressure at Center of the First Column of the Elements versus Depth.

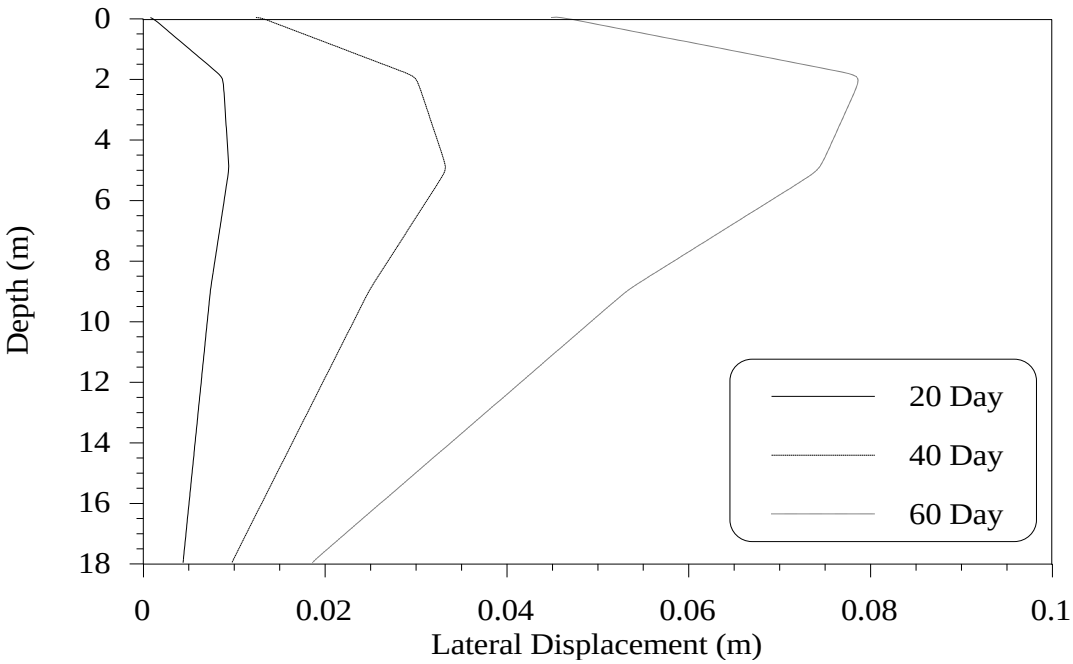

Fig. (11) Distribution of Lateral Displacement with Depth at Embankment Toe.

The relation between excess pore pressure and total vertical stress increment $\Delta\sigma_v$ of element 1 is shown in Fig. (12). As shown the ratio $p/\Delta\sigma_v$ is almost equal to 0.8 during early construction, thereafter the ratio increases to 1.0.

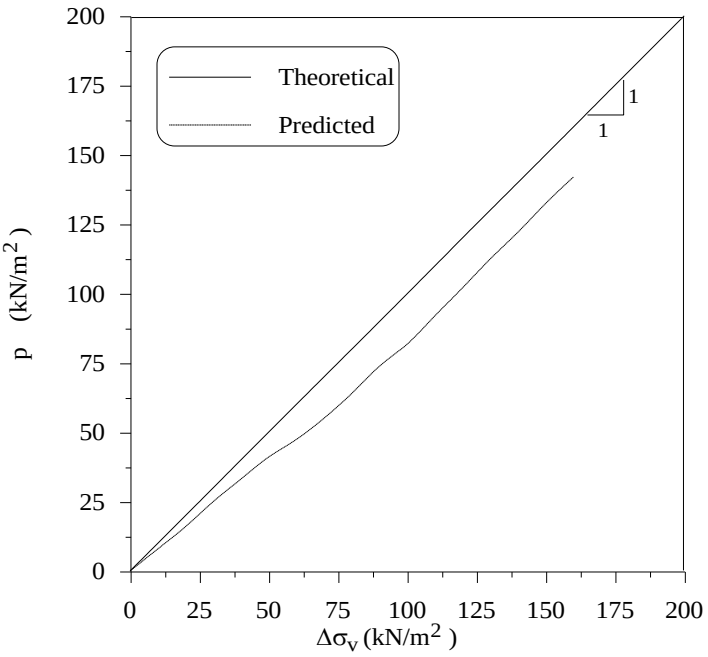

Fig. (12) Excess Pore Pressure versus Total Vertical Stress for Element1.

The trends of predicted behavior agree well with the field observation reported by Tavenas and Leroueil (1980). They related it to the fact that as natural clay is initially over consolidated, the rate of pore pressure dissipation is high at beginning of construction and $p/\Delta\sigma_v$ is smaller than unity, and as construction advances, pore pressure increment becomes equal to embankment load due to passage of clay to the state of normally consolidated, and the behavior is totally nonlinear.

SUMMARY AND CONCLUSIONS

The main conclusions obtained from these analyses can be summarized as follows:

1. The effect of using different over consolidation ratio (OCR) on the predicted clay behavior was examined, in which the elastic behavior was obtained when (OCR) equal 2, while the nonlinear behavior was predicted immediately upon loading when (OCR) is equal to 1.

2. The inclusion of viscoplastic flow decreases the amount of dissipation of pore pressure for the time factor Tv between 0.03 to 0.5.
3. The developed visco-plastic model can describe the effect of the length of the drainage path on the consolidation settlement. Where, the viscoplastic volumetric strain rate for the thick sample is found to be less than that of the thin sample.
4. The behavior of clay foundation during embankment construction was simulated using the developed model. From the distributions of excess pore pressure at center line element and lateral displacement at toe versus depth, maximum values are found at depths between 2 to 5 m. Also, the rate of pore pressure dissipation is high at beginning of construction and ($p/\Delta\sigma_v$) is smaller than unity, and as construction advances this rate becomes equal to embankment load. This behavior is related to the passage of clay to state of normally consolidated from the state of over consolidated.
5. A numerical difficulty encountered in all analyses carried is in the choice of the fluidity parameter $\bar{\gamma}$. The predicted results were very sensitive and a value between 10^{-8} - 10^{-12} per second was used.

APPENDIX A

The state of effective stress of a soil continuum needed for the modified Cam clay model are the mean effective stress and the deviatoric stress respectively:

$$\left.\begin{aligned} P &= \frac{1}{3}\left(\sigma_1+\sigma_2+\sigma_3\right) \\ q &= \sqrt{3}\left(\frac{1}{2}S_{ij}S_{ij}\right)^{\frac{1}{2}} \end{aligned}\right\} \qquad \text{(A-1)}$$

Where σ_1, σ_2 and σ_3 are the three principal stresses and S_{ij} is the deviatoric stress as:

$$S_{ij} = \sigma_{ij} - \frac{1}{3}.\delta_{ij}.\sigma_{kk} \qquad \text{(A-2)}$$

Here σ_{ij} is the stress tensor, δ_{ij} is the kronecker delta.

REFERENCES

* Abdul-Hameed, S.D., "**Elasto-Viscoplastic Analysis of Unbounded Saturated Soil Media**," M.Sc. Thesis, Department of Civil Engineering, Saddam University, Iraq, 1998.

* Aboshi, H., "**An Experimental Investigation on The similitude of consolidation of Clay Including Secondary Creep Settlement**," Proc. 8th ICSMFE, 4 (3), pp. 88, 1973.

* Mesri, G., and Choi, Y.K., "**Excess Pore Water Pressure during Consolidation**," Proc. 6th Asian Regional Conf. on Soil Mech. and Found. Eng., 1, pp. 151-154, 1979.

* Oka, F., Adachi, T., and Okano, Y., "**Two-Dimensional Consolidation Analysis Using an Elasto-Viscoplastic Constitutive Equation**," Int. J. Num. and Analyt. Meth. Geomech., Vol. 10, No. 1, pp. 1-16, 1986.

* Perzyna, P., "**Fundamental Problems in Viscoplasticity**," Adv. Appl. Mech., Vol. 9, pp. 243-277, 1966.

* Roscoe, H.K., and Burland, J.B., "**On the Generalized Stress-Strain Behavior of Wet Clay**," Engineering Plasticity, (Heyman, J., and Leckie, F.A. Ed.), Cambridge: Cambridge University Press, pp. 535-609, 1968.

* Selvadurai, A.P.S., and Gopal, K.R., "**Consolidation Analysis of the Screw Plate Test**," Proc. 39th, Canadian Geotech. Conf., Ottawa, Canada, pp. 167-178, 1986.

* Selvadurai, A.P.S., and Rajagopal, K., "**Composite Infinite Element for Modeling Unbounded Saturated-Soil Media**," J., Geomech. Eng., Vol. 115, No. 11, pp. 1633-1646, November, 1989.

* Simoni, L., and Schrefler, B.A., "**Mapped Infinite Elements in Soil Consolidation**," Int. J. Num. Meth. Eng., Vol. 24, No. 3, pp. 513-527, 1987.

* Tavenas, F., and Leroueil, S., "**The Behavior of Embankments Clay Foundations**," Canadian Geoth. J., Vol. 17, No. 2, pp. 236-260, 1980.

* Yousif, N.B., "**Finite Element Analysis of Some Time Dependent Construction Problems in Geotechnical Engineering**," Ph.D. Thesis, State University of New York at Buffalo, New York, 1984.

* Zienkiewicz, O.C., Humpheson, C., and, Lewis, R.W., "**Associated and Non - Associated Visco - Plasticity and Plasticity in Soil Mechcanics**," Geotechnique, Vol. 25, No. 4, pp. 671-689, 1975.

* Zienkiewicz, O.C., "**The Finite Element Method**," 3rd edition, McGraw-Hill, London, 1977.

AN INDIRECT ROTOR-FLUX-ORIENTED CONTROL OF A TWO-PHASE INDUCTION MOTOR DRIVE

Turki K. Hassan
Dept. of Elect. College of Engineering University of Al-Mustansirayh

ABSTRACT

A vector control is proposed for a two phase induction motor drive . The motor is driven by H-bridge current-regulated pulsewidth modulated voltage source inverter. The vector control is based upon rotor field orientation concepts that have been adopted for this type of machine. Simulation results are provided to illustrate the system operation and the MATLAB/SIMULINK has been used for simulation**.**

الخلاصة

يتناول هذا البحث مقترح باستخدام سيطرة الموجه في مسوق المحرك الحثي ثنائي الطور حيث يستخدم مبدل نوع قنطرة H والمسيطر عليه بطريقة تضمين عرض النبضة نوع تنظيم التيار. سيطرة الموجه تستند على مبادئ اعتبار فيض الدوار كمحور والتي تم استخدامها لهذا النوع من المكائن.تم ايجاد نتائج المحاكاة باستخدام *MATLAB/SIMULINK* لتوضيح عمل المنظومة .

KEY WORDS

Two phase induction motor, indirect rotor-flux-oriented control.

INTRODUCTION

Control systems utilize the fractional-horsepower size electromagnetic components as motors and sensors to measure speed and position of controlled elements. A two phase induction motor is used as a control motor, and is suitable for control systems up to a few hundred watts.

The two phase induction motor has two-phase windings located in stator slots ,which are displaced from each other by 90° electrical degrees. One winding is always supplied and is called the excitation(or main) winding. The control signal is applied to the other winding (called control or auxiliary winding) , such that with no control signal the motor must be at standstill.

In order to develop a torque the two windings voltages must be shifted in time-phase. The motor operates from a single-phase supply and utilize a phase-splitting

capacitor to develop a rotating field in the air gap. However , due to an elliptical rotating field, a pulsating torque that causes higher noise than a three-phase induction motor.

In recent years various schemes have been proposed for inverter-driven two phase induction motor. In references (1, 2) square voltage waveforms with quadrate phase shift are supplied to the two-phase windings of a two phase induction motor driven by an inverter. Though this drive is simple and cheap, the control range of speed is limited and the harmonic content of the output is high. In references (3, 4) phase-difference angle control of a two-phase induction motor is used which can extend the speed control range without a substantial increase in cost of the drive . However , under phase –difference angle control , the torque pulsation still exists. In reference (5) space-vector pulse width-modulation (SVPWM) inverter is proposed for constant-power operation of a two phase induction motor . Though with this scheme a smooth torque is obtained ,the drive can not suitable for constant torque with variable speed applications which are needed highly in industry. Also the dynamic response of the speed is very slow and the system has no ability to reject the disturbances in the load torque , system parameters and the dc power supply , since the system is an open loop system.

This paper introduces a variable speed drive for a two phase induction motor .A current-regulated pulsewidth modulated two phase voltage-source inverter is designed as a balanced two phase supply for the motor. A vector control method and the rotor field orientation concepts have been adopted for this type of machine to obtain closed loop speed control drive system like a separately excited dc motor drive.

Simulation results are presented to demonstrate the main characteristics of the proposed drive system, and the MATLAB/SIMULNK has been used to perform the simulation studies.

MACHINE MODEL

The simplified representation for the 2-phase machine is shown in Fig.1 .When a stator winding is distributed for the purpose of producing a sinusoidal MMF wave in space , it is convenient to consider the winding as an equivalent single coil and express the mutual coupling between it and an equivalent rotor coil as a sinusoidal function of the angular displacement between their magnetic axes.

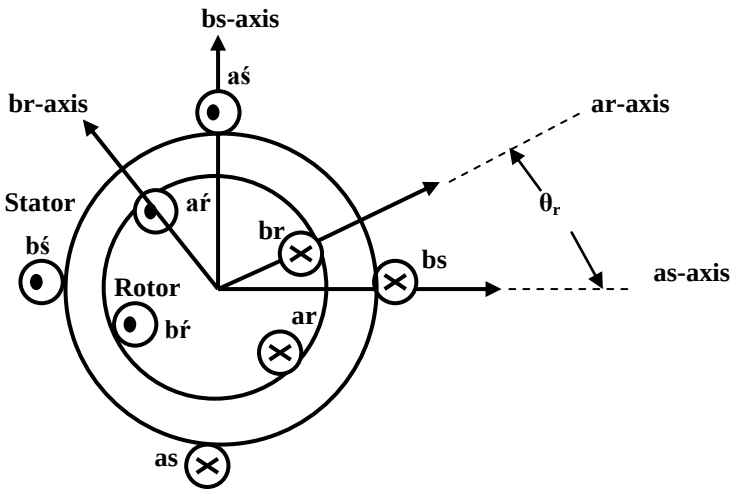

Fig.1 A 2-phase Symmetrical Machine .

If the induction machine has either a squirrel-cage rotor or a coil-wound rotor with the same number of phases as the stator, the rotor can be considered as having equivalent coils (shown in Fig.1). The stator windings are identical ,i.e. ,both windings have an identical number of effective turns N_s , identical resistance r_s ,identical leakage inductance L_{ls} ,and self inductance L_s. Similarly rotor windings are identical which have the same effective turns N_r ,resistance r_r ,leakage inductance L_{lr} , and self inductance L_r.

The voltage equations for the stator phases are written

$$v_{as} = p\lambda_{as} + r_s i_{as} \tag{1}$$

$$v_{bs} = p\lambda_{bs} + r_s i_{bs} \tag{2}$$

In the case of the rotor phases

$$v_{ar} = p\lambda_{ar} + r_r i_{ar} \tag{3}$$

$$v_{br} = p\lambda_{br} + r_r i_{br} \tag{4}$$

For induction motor with squirrel cage rotor $v_{ar}=0$,$v_{br}=0$,therefore equation 3 and equation 4 can be written

$$0 = p\lambda_{ar} + r_r i_{ar} \tag{5}$$

$$0 = p\lambda_{br} + r_r i_{br} \tag{6}$$

Where λ is the total flux-linkages of a particular winding , and p is the operator d/dt .

Figure 2 shows the angular relation of the stator and rotor axes of a 2-phase machine with the third set which is an orthogonal set (d-q axis) . It is clear that as-bs set is fixed in the stator . The ar-br set is fixed in the rotor and hence rotates at an electrical angular velocity of ω_r

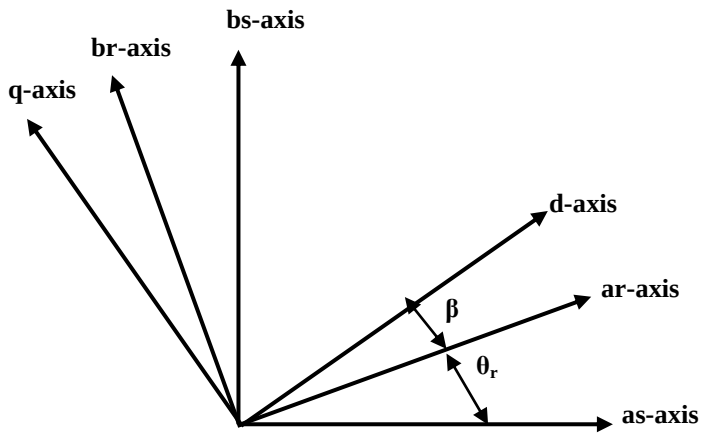

Fig.2 Axes of 2 pole 2 phase symmetrical machine

The equations of transformations which can be correlated to the angular relation of the axes in Fig.2 , are

Stator

$$f_{ds} = f_{as}\cos\theta + f_{bs}\sin\theta \tag{7}$$

$$f_{qs} = f_{bs}\cos\theta - f_{as}\sin\theta \tag{8}$$

Rotor

$$f_{dr} = f_{ar}\cos\beta + f_{br}\sin\beta \tag{9}$$

$$f_{qr} = f_{br}\cos\beta - f_{ar}\sin\beta \tag{10}$$

Where

$$\theta = \beta + \theta_r \tag{11}$$

In these equations the variable f can represent either voltage , current , or flux-linkage .If the transformation equations are used to transform the voltages , currents , and flux-linkages of both the stator and the rotor to the arbitrary reference frame (d-q axis) ,with the rotor variables are referred to the stator windings and with the self-inductances separated into leakage inductance component and a magnetizing inductance component, the following equations are obtained [6],[7] :

$$v_{ds} = p\lambda_{ds} - \omega\lambda_{qs} + r_s i_{ds} \tag{12}$$

$$v_{qs} = p\lambda_{qs} + \omega\lambda_{ds} + r_s i_{qs} \tag{13}$$

$$0 = p\lambda_{dr}' - (\omega - \omega_r)\lambda_{qr}' + r_r' i_{dr}' \quad (14)$$

$$0 = p\lambda_{qr}' + (\omega - \omega_r)\lambda_{dr}' + r_r' i_{qr}' \quad (15)$$

Where

$$\lambda_{ds} = L_{ls} i_{ds} + M(i_{ds} + i_{dr}') \quad (16)$$

$$\lambda_{qs} = L_{ls} i_{qs} + M(i_{qs} + i_{qr}') \quad (17)$$

$$\lambda_{dr}' = L_{lr}' i_{dr}' + M(i_{dr}' + i_{ds}) \quad (18)$$

$$\lambda_{qr}' = L_{lr}' i_{qr}' + M(i_{qr}' + i_{qs}) \quad (19)$$

$$\omega = p\theta \quad (20)$$

$$\omega - \omega_r = p\beta \quad (21)$$

For the 2-phase machine ,

$$L_{ls} = L_s - L_{ms} \quad (22)$$

$$L_{lr}' = L_r' - L_{ms} \quad (23)$$

$$M = L_{ms} \quad (24)$$

$$L_{ms} = \frac{N_s}{N_r} L_{sr} \quad (25)$$

L_{sr} is the mutual inductance between stator and rotor. N_s and N_r are the effective turns of a stator and rotor phase winding respectively. The primes are used to denote rotor quantities referred to the stator windings.

It is clear that the voltage equations (12) to (15) of the symmetrical induction machine may be expressed in any reference frame by setting the speed of the arbitrary reference frame , ω , equal to the speed of the desired reference speed. For example , the voltage equations expressed in the stationary reference frame may be obtained by setting ω to zero . For a reference frame fixed in the rotor ω is set equal to the electrical angular velocity of the rotor , ω_r . The voltage equations in the synchronously rotating reference frame are obtained by setting ω equal to the electrical angular velocity of the fundamental frequency component of the applied stator voltages ω_e .

An expression for the instantaneous electromagnetic torque can be obtained by applying the principle of virtual displacement [7] .This expression is

$$T_e = (\frac{P}{2})(\lambda_{qr}{}' i_{dr}{}' - \lambda_{dr}{}' i_{qr}{}') \tag{26}$$

Where P is the number of poles .

In order to obtain the dynamic characteristics , it is necessary to relate torque and speed , and the relation can be expressed as

$$T_e = (\frac{2}{P})Jp\omega_r + (\frac{2}{P})B\omega_r + T_l \tag{27}$$

Where T_l is load torque , J is the moment of inertia , and B is the friction constant **.**

INDIRECT ROTOR-FLUX ORIENTATION

The indirect rotor-flux oriented controller is derived from the dynamic equations of the machine in the synchronously rotating reference frame , i.e., $\omega=\omega_e$. The rotor voltage equations of the two phase induction motor in synchronously rotating reference frame are given by

$$0 = r_r{}' i_{dr}{}' - \omega_{sl}\lambda_{qr}{}' + p\lambda_{dr}{}' \tag{28}$$

$$0 = r_r{}' i_{qr}{}' + \omega_{sl}\lambda_{dr}{}' + p\lambda_{qr}{}' \tag{29}$$

Where

$$\omega_{sl} = \omega_e - \omega_r \tag{30}$$

$$\lambda_{dr}{}' = L_{lr}{}' i_{dr}{}' + M(i_{dr}{}' + i_{ds}) \tag{31}$$

$$\lambda_{qr}{}' = L_{lr}{}' i_{qr}{}' + M(i_{qr}{}' + i_{qs}) \tag{32}$$

Where ω_{sl} is the slip frequency in rad/sec .

The fluxes and currents in the above equations are represented in the synchronously rotating reference frame . In the vector control strategies , the ac motors are controlled like separately excited dc motors which have independent channels for the flux and torque control . In order to link the d-axis of the reference frame to the rotor flux vector , the q –component of this flux has to be equal to zero [8]

$$\lambda_{qr}{}' = 0 \tag{33}$$

$$\lambda_r{}' = \lambda_{dr}{}' \tag{34}$$

Substituting (33) ,(34) in (28) ,(29) ,(31) and (32) causes the new rotor flux and voltage equations

$$r_r' i_{dr}' + p\lambda_r' = 0 \tag{35}$$

$$r_r' i_{qr}' + \omega_{sl}\lambda_r' = 0 \tag{36}$$

$$\lambda_r' = L_r' i_{dr}' + M i_{ds} \tag{37}$$

$$L_r' i_{qr}' + M i_{qs} = 0 \tag{38}$$

Where

$$L_r' = L_{lr}' + M \tag{39}$$

The rotor currents in terms of the stator currents are derived from equations (37) and (38) as

$$i_{dr}' = \frac{\lambda_r' - M i_{ds}}{L_r'} \tag{40}$$

$$i_{qr}' = -\frac{M i_{qs}}{L_r'} \tag{41}$$

The rotor flux in term of the stator current i_{ds} can be obtained by substituting equation (40) in equation (35) as

$$\lambda_r' = \frac{M i_{ds}}{1 + s\tau_r} \tag{42}$$

Where s is the laplace transform (s=p) and τ_r is the rotor time constant which is

$$\tau_r = \frac{L_r'}{r_r'} \tag{43}$$

Substituting (33) ,(34) and (41) in (26) cause the new electromagnetic torque equation to be

$$T_e = \left(\frac{P}{2}\right)\frac{M}{L_r'}\lambda_r' i_{qs} \tag{44}$$

Equation (44) indicates that the developed torque depends on the rotor flux and quadrature-axis component of the stator current (i_{qs}) . The torque variation is proportional to the variation of I_{qs} when the rotor flux is controlled as a constant and the behavior of the two phase induction motor becomes like a separately excited dc motor . Equations (36) and (41) are used to derive a formula for slip frequency ω_{sl} in terms of i_{qs} and $\lambda_r^{/}$ as

$$\omega_{sl} = \frac{M i_{qs}}{\tau_r \lambda_r^{/}} \tag{45}$$

For the indirect rotor-flux orientation , the rotor flux position required for coordinates transformation is generated from the rotor speed ω_r and the slip frequency ω_{sl} as

$$\theta_e = \int (\omega_{sl} + \omega_r) dt \tag{46}$$

IMPLEMENTATION OF INDIRECT ROTOR- FLUX-ORIENTED CONTROL SCHEME

The block diagram that is shown in figure (3) represents the indirect rotor flux-oriented control scheme for two phase induction motor drive . The dc supply voltage is converted to balanced two phases supply through H-bridge inverter [2],[4] which is consisted of four insulated gate bipolar transistors (IGBT) . Fig. 4 shows the H-bridge inverter and the way of connecting the two phase windings . This is a cheaper method because it uses only four semiconductor switches . Fig. 4 also shows that two capacitors are connected in series in the dc link to form a midpoint that is connected to neutral point N . In practice , two large resistors are also needed in parallel with the capacitors to balance the voltage of the capacitors.

The output of the inverter is applied to the stator windings of the motor. Motor ratings and its parameters are given in Appendix. The rotor speed ω_m is sensed and compared with the reference speed ω_m^* and the error is converted to the reference torque T_e^* using proportional-integral controller (P-I controller). The reference quadrature-axis stator current i_{qs}^*(torque current) and the slip frequency ω_{sl} are calculated in terms of the reference torque and the rotor flux using equation (44) and equation (45) respectively.

For the indirect rotor-flux-oriented control, the rotor flux position (angle) is calculated using equation (46). The stator currents i_{as} and i_{bs} are measured and converted to the direct-axis component i_{ds} and quadrature-axis component i_{qs} of the stator current using the equations (7) and (8) of transformation from stationary reference frame to the synchronously rotating reference frame (Park transformation) .

The rotor flux referred to stator ($\lambda_r^{/}$) is calculated in term of direct-axis component of stator current (i_{ds}) using equation (42) .The drive has rotor-flux control loop. The rotor flux command ($\lambda_r^{/*}$) is constant and the drive operates in the constant-torque region. The P-I controller is used for the rotor flux loop and the output of the controller represents the reference direct-axis component of stator current (i_{ds}^*).

The currents i_{ds}^* and i_{qs}^* are reference command currents for the current-regulated pulse width modulation (CRPWM) block that will force motor stator currents to follow these reference currents .There are two P-I controllers in the CRPWM block which convert the current errors between the references and feedback into reference magnet and torque voltages .These voltages are transformed to stationary reference frame using inverse park transformation and then converted to motor terminal voltages by using sinusoidal pulsewidth modulation [9] .

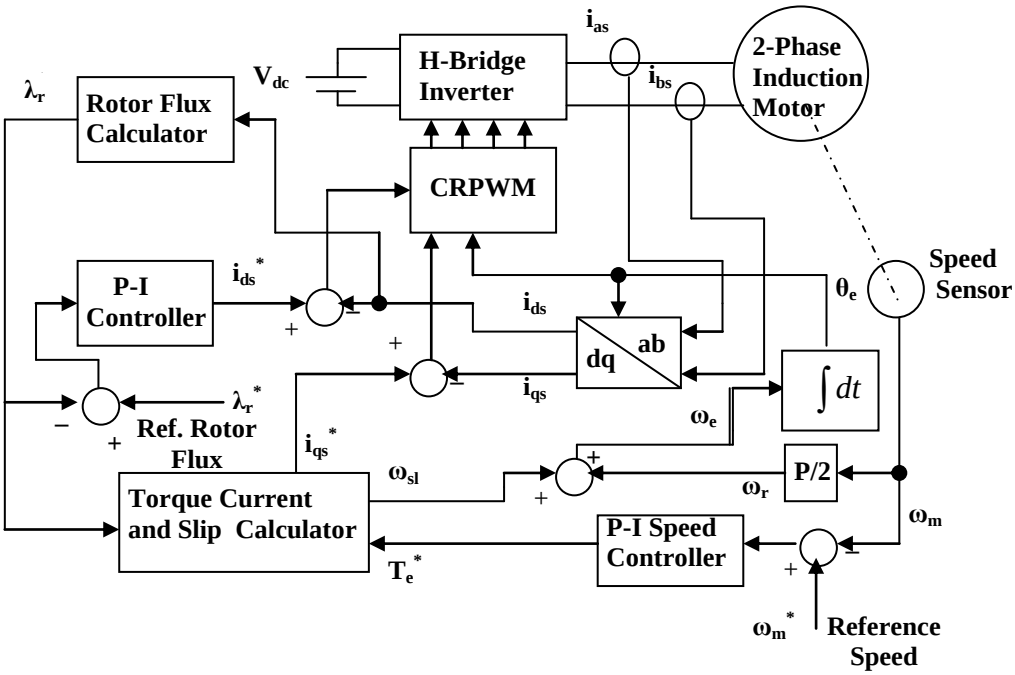

Fig.3 Block diagram of the indirect rotor- flux-oriented control of a two phase induction motor drive

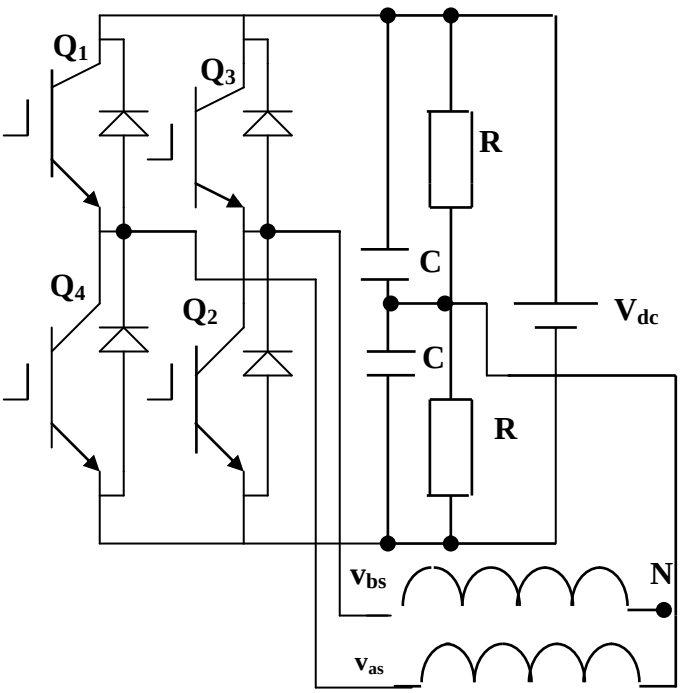

Fig.4 H-bridge inverter with phases connection

RESULTS

Digital simulations were carried out to simulate the control responses of the indirect rotor-flux-oriented control scheme using MATLAB/SIMULINK . The simulations set up such that the drive system is tested with low and high values of a step reference speed command ,also the system is tested with load and with no load for each reference speed command.

Fig.5 and Fig.6 show the simulated values of the rotor speed and the two- phase stator currents of the motor respectively. A step reference speed command of 30 rad/sec value is applied with no load torque .The rotor speed tracks the reference speed at steady state with small overshoot (approximately 1 rad/sec). The stator currents are balanced and each is limited to a maximum value of 12 A at starting in order to protect the semiconductor switching devices of the inverter from high current. The outputs of the speed controller and flux controller are provided with limiters to prevent stator currents from exceeding permissible value. The stator currents drop to a low no load of (2A) value when the speed reaches the steady state.

Fig.7 and Fig.8 represent the rotor speed and stator currents respectively for the same step reference speed command (30 rad/sec) with applied load of 4 Nm.The rotor speed response is similar with the case of no load (Fig.5).The stator currents are raised to a value of 4.5 A (maximum value) proportional to the applied load .

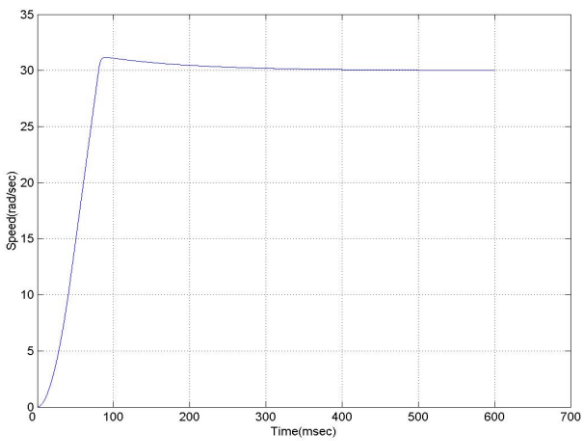

Fig.5 Rotor speed for reference value of 30 rad/sec With no load

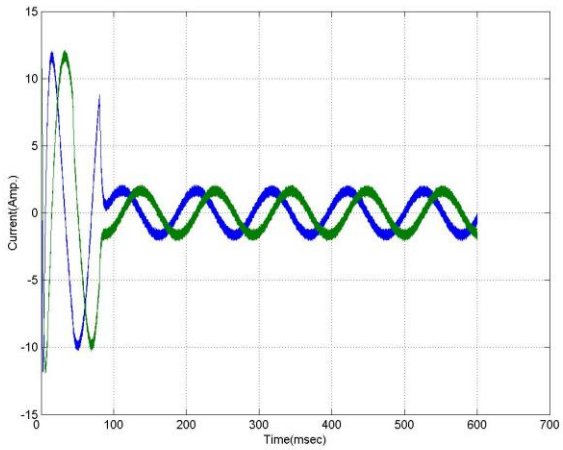

Fig.6 Two phase stator currents for reference value of 30 rad/sec With no load

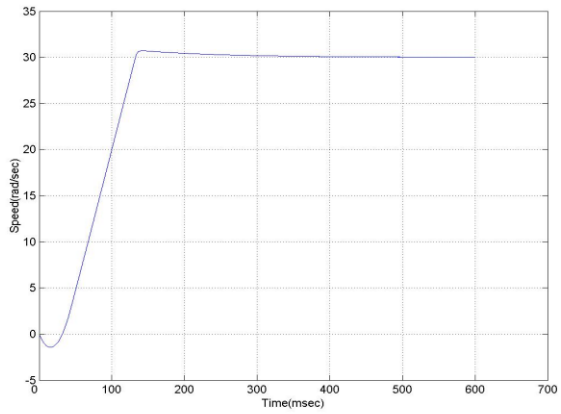

Fig.7 Rotor speed for reference value of 30 rad/sec With load value of 4 Nm

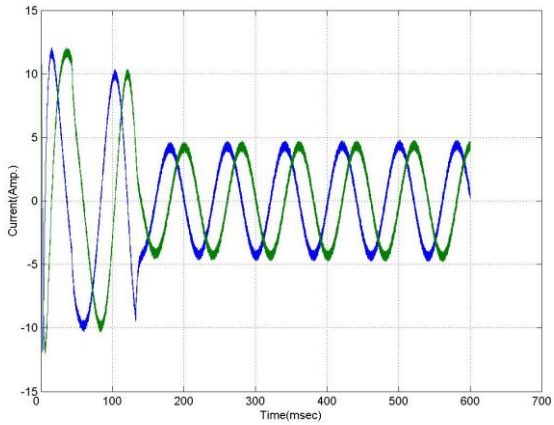

Fig.8 Two phase stator currents for reference value of 30 rad/sec with load value of 4 Nm

The drive system is tested at speed near the rated speed by applying a step reference speed command value of 130 rad/sec. Fig.9 shows the rotor speed which tracks the reference speed at steady state. Fig.10 shows the two phase stator currents with small no load value at steady state. Fig.11 and Fig.12 represent the rotor speed and stator currents for the case of 4 Nm applied load and reference speed of 130 rad/sec.

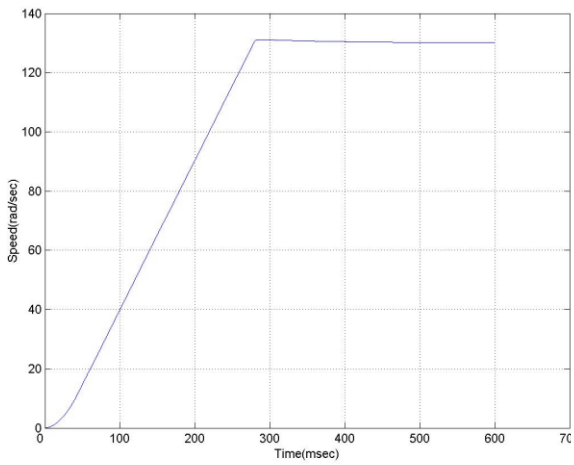

Fig.9 Rotor speed for reference value of 130 rad/sec With no load

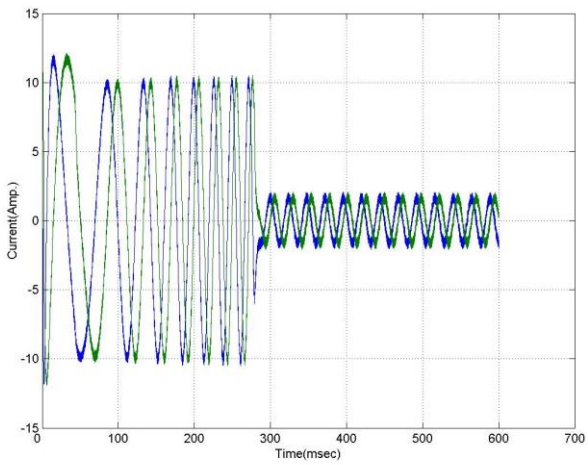

Fig.10 Two phase stator currents for reference value of 130 rad/sec with no load

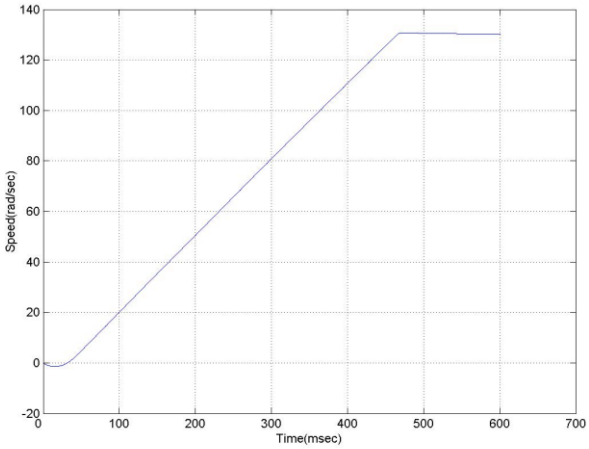

Fig.11 Rotor speed for reference value of 130 rad/sec With load value of 4 Nm

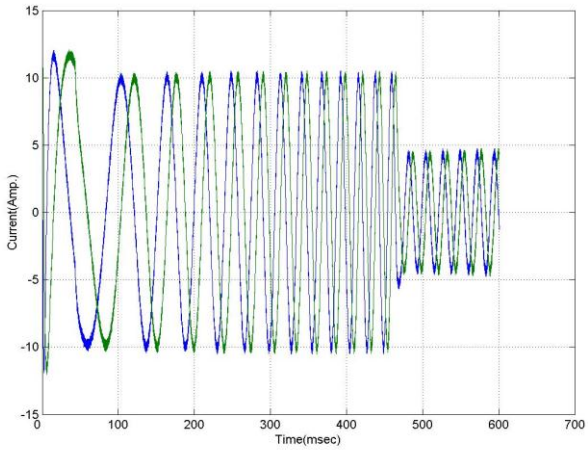

Fig.12 Two phase stator currents for reference value of 130 with load value of 4 Nm

To investigate the robustness of the proposed drive system, we analyzed the speed response and the stator currents of the motor to step change in load torque. Fig.13 and Fig.14 show the rotor speed and the stator currents when the motor is started by applying a step reference speed of 30 rad/sec with no load torque. After 0.35 sec, a step load torque of 4 Nm value is applied .Avery small dip in speed (approximately 0.5 rad/sec) occurs and the speed returns to its original value after 0.15 sec .The stator currents increases to a value of 4.5 A (maximum value) at the instant of applying the load .

Fig.15 and Fig.16 represent the rotor speed and stator currents for the case of starting the motor with applied load of 4 Nm and reference speed value of 30 rad/sec . After 0.35 sec a load is removed ,a small rise in speed occurs which decay to zero after 0.15 sec .The stator currents is reduced to its no load value at the instant of removing the load. Figs. 17-20 are similar to Figs. 13-16 but with 130 rad/sec reference value in order to verify the robustness at high speed .

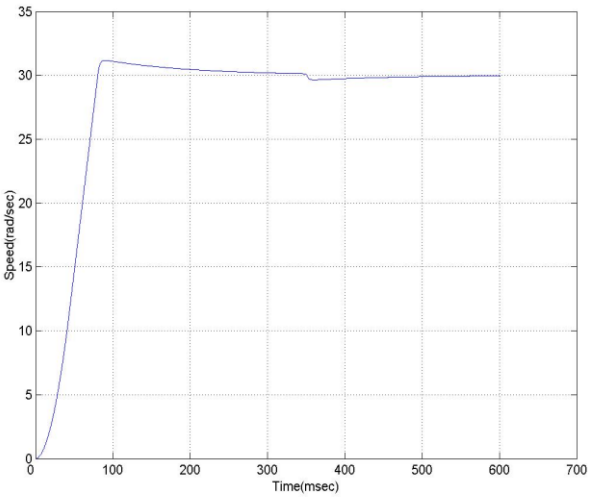

Fig.13 Rotor speed for reference value of 30 rad/sec with no load .After 0.35sec load torque of 4 Nm value is applied

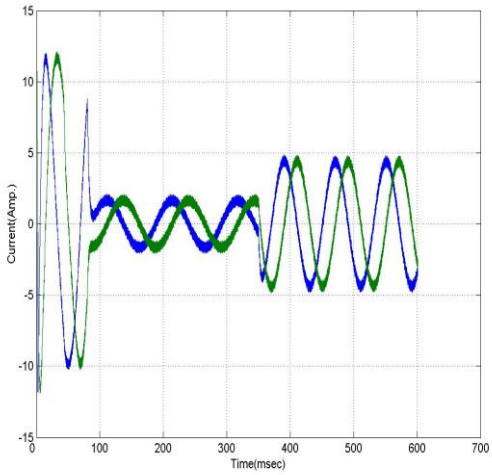

Fig.14 Stator currents for reference value of 30 rad/sec with no load.After 0.35sec load torque of 4 Nm value is applied

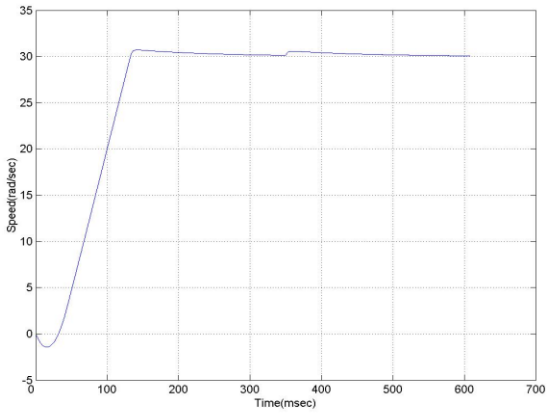

Fig.15 Rotor speed for reference value of 30 rad/sec with 4 Nm load. After 0.35 sec the load torque is removed

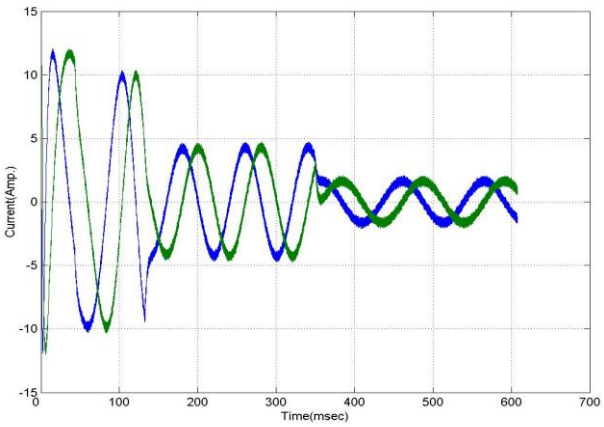

Fig.16 Stator currents for reference of 30 rad/sec with 4 Nm load. After 0.35 sec the load is removed

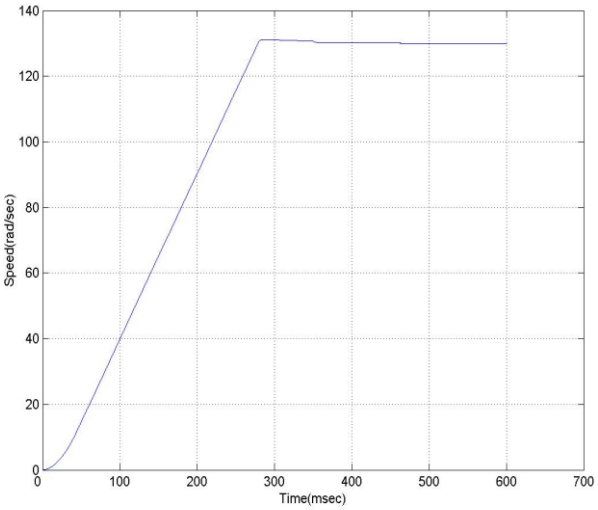

Fig.17 Rotor speed for reference value of 130 rad/sec with no load .After 0.35 sec the load torque of 4 Nm value is applied

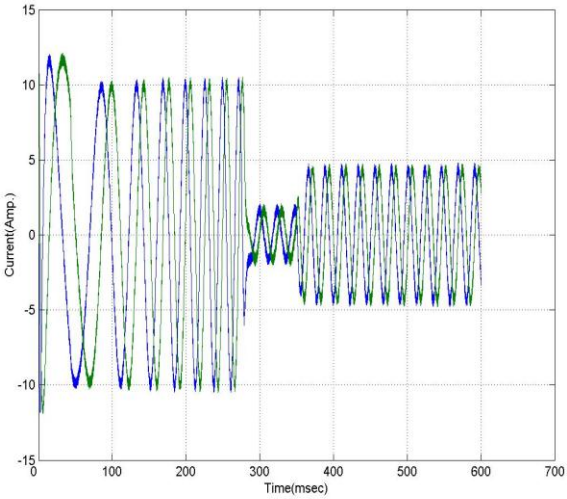

Fig.18 Stator currents for reference value of 130 rad/sec with no load. After 0.35 sec the load torque of 4 Nm value is applied

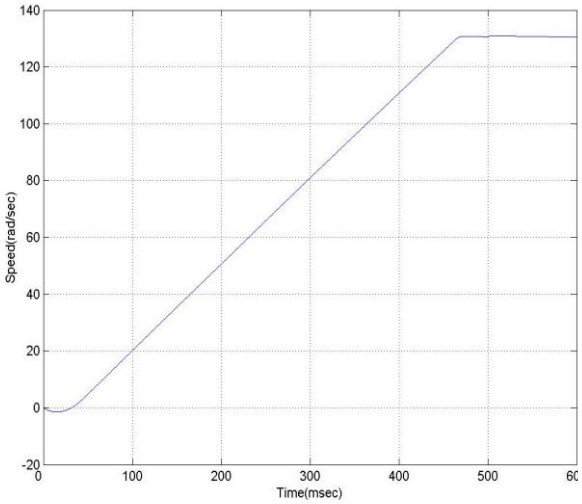

Fig.19 Rotor speed for reference value of 130 rad/sec with 4 Nm load .After 0.5 sec the load torque is removed

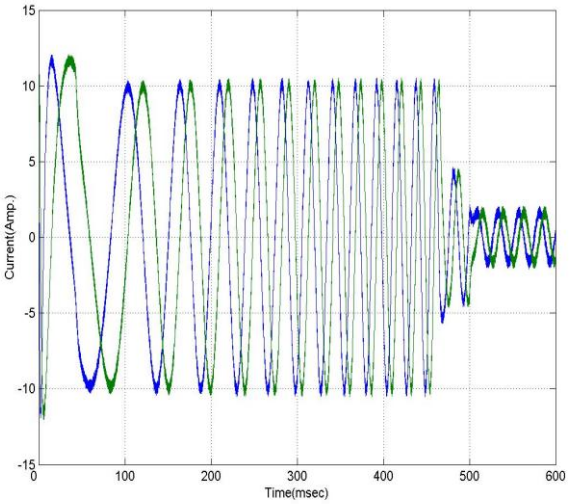

Fig.20 Stator currents for reference value of 130 rad/sec with 4 Nm load .After 0.5 sec the load torque is removed

Figs 21-23 show the rotor speed ,stator currents and rotor flux respectively .The motor is started with 30 rad/sec reference speed and no load torque. After 0.3 sec the reference speed is increased to 130 rad/sec. The rotor speed tracks the reference speed at steady state for each step. The rotor flux tracks the reference of 0.5 Wb value and independent upon the speed command.

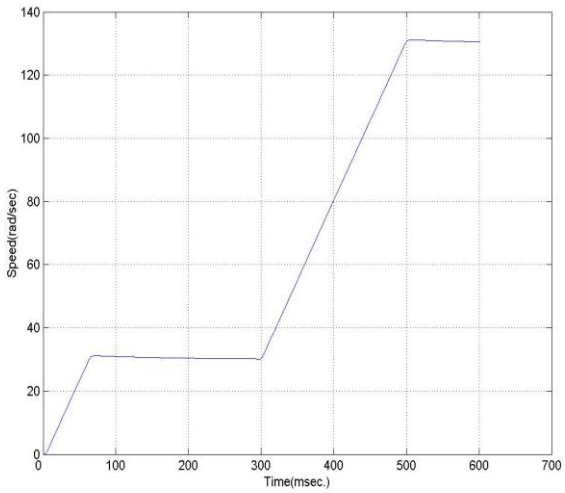

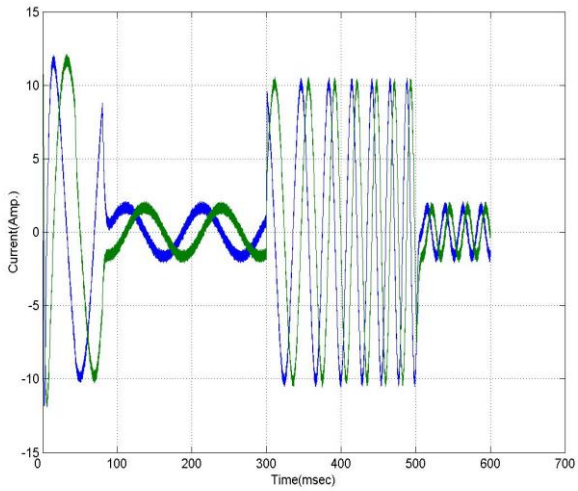

Fig.21 Rotor speed for reference value of 30 rad/sec with no load. After 0.3 sec the reference is increased to 130 rad/sec

Fig.22 Stator currents for reference value of 30 rad/sec with no load. After 0.3 sec the reference is increased to 130 rad/sec

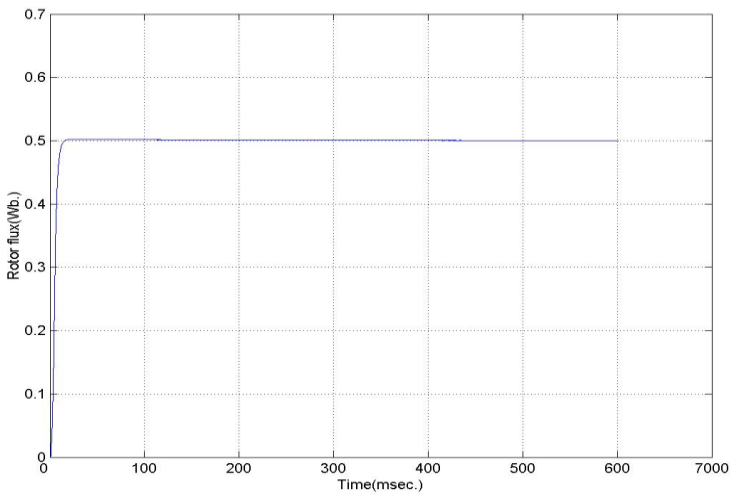

Fig.23 Rotor flux for reference flux value of 0.5 Wb

CONCLUSIONS

This paper has discussed the indirect rotor-flux-oriented control scheme for two phase induction motor. The modeling approach proposed made it possible to adapt some high performance control for use with a two phase motor drive system. Simulation tests were considered satisfactory and have confirmed the claimed features.

In spite of being more complex than other strategies, like the standard V/Hz , the use of indirect rotor-flux- oriented control may not result in additional cost in terms of data processing. This is due to the innovations of microelectronics that increase the capability of processing information and reducing cost and power consumption of the integrated circuits.

Based on simulation results , the following conclusions are made:

1. The rotor speed can be varied from zero up to rated value.
2. Balanced sinusoidal currents are obtained due to sinusoidal pulse width modulation.
3. The drive system is robust against the variation of the load torque. Small dip in speed occurs when a step of load torque is applied ,this dip decays to zero after short time (approximately 150 msec.).. Small rise in speed occurs when the load is removed .This rise decays to zero after short time (approximately 150 msec.).

The proposed drive system can be experimentally built with digital signal processing board for fast calculations of control algorithms in real time. Also the H-bridge inverter with IGBT transistors can be built to convert the dc voltage in to two phase balanced supply using sinusoidal PWM.

APPENDIX

The specifications of two phase motor that is used for simulation are: 1hp, 2Φ, 110 V, four poles and the parameters of the motor are:

$M = 308.4mH$, $L_{lr}' = 10.1mH$

$L_{ls} = 10.1mH$

$r_s = 3.2\Omega$, $r_r' = 2.4\Omega$

$J = 0.02$ kg.m^2 , $B = 2.945\times10^{-4}$ kg.m^2/sec

REFERENCES

1. L. M. C. Mhango and R. Perryman, "Analysis and simulation of a high-speed two-phase AC drive for aerospace applications," Proc. IEE-Elect. Power Applicat., vol. 144, no. 2, pp. 149-157. Mar. 1997.

2. I. R. Smith, D. Creighton, and L. M. C. Mhango, "Analysis and performance of a novel two- phase drive for fan and water-pumping applications," IEEE Trans. Ind. Electron., vol. 36, pp. 530-538, Nov. 1989.

3. D. Jang and G. Cha, "Phase-difference control of 2-phase inverter-fed induction motor," in Conf. Rec. IEEE-IAS Annu. Meeting, 1989, pp.377-383.

4. Do- Hyun and J. S. Won," Voltage, frequency and phase-difference angle control of PWM inverters-fed two-phase induction motors," IEEE Trans. Power Electronics, vol. 9 pp. 377-383, July 1994.

5. M. A. Jabbar, Ashwin M. Khambadkone, and Zhang Yanfeng," Space-vector modulation in a two-phase induction motor drive for constant-power operation," IEEE Trans. Industrial Electronics, Vol. 51, No. 5, pp. 1081-1088, October 2004.

6. P. C. Krause, O. Wasynczuk, and S. D. Studhoff, " Analysis of Electric machinery," Piscataway, NJ: IEEE Press, 1995.

7. P. C. Krause, and C. H. Thomas," Simulation of symmetrical induction machinery," IEEE Trans. Power Apparatus and Systems, Vol. PAS-84, No. 11, pp. 1038-1052, November 1965.

8. Rik W. De Doncker, Francesco Profumo, Michele Pastorelli, and Paolo Ferraris, " Comparison of universal field oriented (UFO) controllers in different reference frames," IEEE Trans. Power Electronics, Vol. 10, No. 2, pp. 205-213, March 1995.

9. J. Holtz," Pulsewidth modulation for electric power conversion," Proc. IEEE, Vol. 82, No. 8, pp. 1194-1214, Aug. 1994.